DYNA

Journal of theFacultad de Minas, Universidad Nacional de Colombia - Medellin Campus
DYNA 91 (232), April - June, 2024 - ISSN 0012-7353

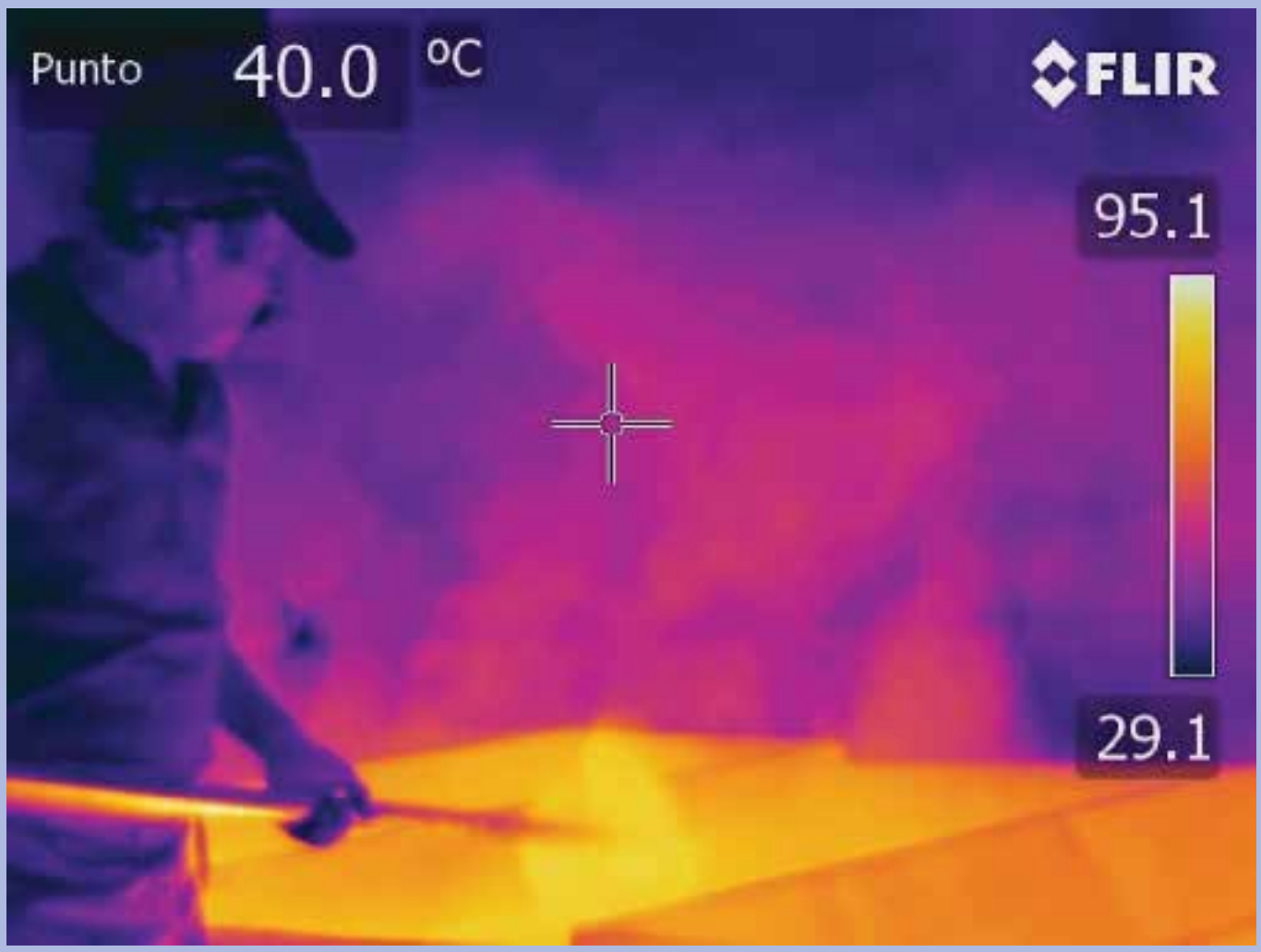

Facultad de Minas
Sede Medellín

UNIVERSIDAD
NACIONAL
DE COLOMBIA

DYNA
http://dyna.medellin.unal.edu.co/

DYNA is an international journal published by the Facultad de Minas, Universidad Nacional de Colombia, Medellín Campus since 1933. DYNA publishes peer-reviewed scientific articles covering all aspects of engineering. Our objective is the dissemination of original, useful and relevant research presenting new knowledge about theoretical or practical aspects of methodologies and methods used in engineering or leading to improvements in professional practices. All conclusions presented in the articles must be based on the current state-of-the-art and supported by a rigorous analysis and a balanced appraisal. The journal publishes scientific and technological research articles, review articles and case studies.

DYNA publishes articles in the following areas:

Organizational Engineering
Civil Engineering
Materials and Mines Engineering
Geosciences and the Environment
Systems and Informatics
Chemistry and Petroleum
Mechatronics
Bio-engineering
Other areas related to engineering

Publication Information

DYNA (ISSN 0012-73533, Printed; 2346-2183, online).
Is published by the Facultad de Minas, Universidad Nacional de Colombia, with a quarterly periodicity (January - March, April - June, July - September and October - December).
Circulation License Resolution 000584 de 1976 from the Ministry of the Government.

Contact information:
Web page: https://revistas.unal.edu.co/index.php/dyna
E-mail: dyna@unal.edu.co
Mail address:
Revista DYNA
Facultad de Minas
Universidad Nacional de Colombia - Medellín Campus
Carrera 80 No. 65-223 Bloque M9 - Of.:107
Telephone: (574) (604) 4255343
Medellín - Colombia

Notice
All statements, methods, instructions and ideas are only responsibility of the authors and not necessarily represent the view of the Universidad Nacional de Colombia. The publisher does not accept responsibility for any injury and/or damage for the use of the content of this journal.
The concepts and opinions expressed in the articles are the exclusive responsibility of the authors.

Institutional Exchange Request
DYNA may be requested as an institutional exchange through the e-mail: canjebib_med@unal.edu.co or to the postal address:

Biblioteca Central “Efe Gómez”
Universidad Nacional de Colombia, Sede Medellín
Calle 59A No 63-20
Teléfono: (574) (604) 430 97 86
Medellín - Colombia

Indexing and Databases

DYNA is admitted in:

The National System of Indexation and Homologation of Specialized Journals CT+I-PUBLINDEX, Category C

Science Citation Index Expanded
SCImago Journal & Country Rank - SJR
SCOPUS
SciELO Scientific Electronic Library Online
Chemical Abstract - CAS
Scientific Electronic Library on Line - SciELO
GEOREF
PERIÓDICA Data Base
Latindex
Actualidad Iberoaméricana
Redalyc - Scientific Information System
Directory of Open Acces Journals - DOAJ
PASCAL
CAPES
UN Digital Library - SINAB
EBSCO Host Research Databases

Publisher’s Office
Luz Alexandra Montoya Restrepo, Director
Mónica del Pilar Rada T., Editorial Coordinator
Catalina Cardona A., Editorial Assistant
Manuela González C., Editorial Assistant

Todograficas Ltda., Diagramming

Reduced Postal Fee
Tarifa Postal Reducida # 2014-287 4-72.
La Red Postal de Colombia, expires Dec. 31st, 2024

UNIVERSIDAD
NACIONAL
DE COLOMBIA

DYNA

DYNA
http://dyna.medellin.unal.edu.co/

Universidad Nacional de Colombia

DYNA
http://dyna.medellin.unal.edu.co/

Universidad Nacional de Colombia

Journal DYNA, 91 (232), April - June, 2024. Medellín. ISSN 0012-7353 Printed, ISSN 2346-2183 Online

CONTENTS

DYNA
http://dyna.medellin.unal.edu.co/

Universidad Nacional de Colombia

Our Cover
Adaptative comfort modeling for a typical non-centrifugal cane sugar processing facility

Authors
Giovanni Andrés Cortés-Tovar, Robinson Osorio-Hernández & Jairo Alexander Osorio-Saráz

DYNA
http://dyna.medellin.unal.edu.co/

Universidad Nacional de Colombia

Revista DYNA, 91 (232), Abril - Junio. Medellín. ISSN 0012-7353 Printed, ISSN 2346-2183 Online

CONTENIDO

DYNA
http://dyna.medellin.unal.edu.co/

Universidad Nacional de Colombia

Nuestra carátula
Modelamiento de confort adaptativo para un trapiche panelero

Autores
Giovanni Andrés Cortés-Tovar, Robinson Osorio-Hernández & Jairo Alexander Osorio-Saráz

DYNA
http://dyna.medellin.unal.edu.co/

UNIVERSIDAD NACIONAL DE COLOMBIA

Phytoremediation of Methylene Blue and Congo Red by duckweed (*Lemna minor*)

Flor Y. Ramírez-Castillo [a], Diana E. Guillén-Padilla [a], Cristian I. Méndez-Sandate [a], Alma L. Guerrero-Barrera [b*] & Francisco J. Avelar-González [c]

[a] *Laboratorio de Biología Celular y Tisular, Centro de Ciencias Básicas, Universidad Autónoma de Aguascalientes, Aguascalientes, México. flor.ramirez@edu.uaa.mx, guillendiana2018@gmail.com, cristianivmesa@gmail.com*
[b] *Laboratorio de Biología Celular y Tisular, Departamento de Morfología, Centro de Ciencias Básicas, Universidad Autónoma de Aguascalientes. Aguascalientes, México. alguerre@correo.uaa.mx, lilian.guerrero@edu.uaa.mx, *Correspondence author*
[c] *Laboratorio de Estudios Ambientales, Departamento de Fisiología y Farmacología, Centro de Ciencias Básicas, Universidad Autónoma de Aguascalientes. Aguascalientes, México. javier.avelar@edu.uaa.mx*

Received: September 1st, 2023. Received in revised form: February 28th, 2024. Accepted: March 8th, 2024.

Abstract
Synthetic colorants are widely used globally by different industries for the dyeing process. However, these chemicals pollute the environment and affect human health by causing allergies, hives, dermatitis, and cancer. This study aims to compare the effectiveness of duckweed (*Lemna minor*) in the removal of the Methylene Blue (MB) and Congo red (CR) dyes at different concentrations (1 mg/L, 5 mg/L, 10 mg/L, and 15 mg/L). Absorbance values were determined at 665 nm for MB and 497 nm for CR after 96 hours. The results show higher removal of MB compared to CR for all concentrations (95.49 % vs. 59.32%, 1 mg/L; 97.24% vs. 39.43%, 5mg/L; 91.30% vs 28.47%, 10mg/L; y 85.42% vs 20.27%, 15mg/L). The removal of MB was observed after 30 min of contact with duckweed, while the removal of CR was observed after 24 hours in all concentrations.

Keywords: Methylene blue; Congo Red; phytoremediation*; Lemna minor*; duckweed; textile dyes.

Fitorremediación de Azul de Metileno y Rojo Congo por lenteja de agua (Lemna minor)

Resumen
Los colorantes sintéticos son altamente utilizados a nivel global por distintas industrias para el proceso de tinción. Sin embargo, estos químicos son altamente contaminantes para el ambiente y afectan la salud humana provocando alergias, urticaria, dermatitis y cáncer. Este estudio tiene como objetivo comparar la efectividad de la lenteja de agua (*Lemna minor*) en la remoción de los colorantes azul de metileno (AM) y rojo Congo (RC), a distintas concentraciones (1mg/L, 5mg/L, 10 mg/L y 15 mg/L). Los valores de absorbancia fueron determinados a 665 nm para AM y 497 nm para RC. Los resultados muestran que el porcentaje de remoción de AM fue mayor que el de CR (95.49 % vs 59.32%, 1 mg/L; 97.24% vs 39.43%, 5mg/L; 91.30% vs 28.47%, 10mg/L; y 85.42% vs 20.27%, 15mg/L). La remoción del AM se observó a los 30 minutos de contacto, mientras que el RC redujo la absorbancia a partir de las 24 horas.

Palabras clave: Azul de metileno; Rojo Congo; fitorremediación; *Lemna minor*; lenteja de agua; colorantes textiles.

1 Introduction

Dyes are compounds widely used for coloring products in several industries, including textiles, cosmetics, leather tanning, and pigmentation [1]. In the textile industry, the synthetic dyes have greater use. These chemicals are generally discharged before treatment as wastewater effluent into water bodies such as stream water, lakes, ponds, and rivers, thus creating a significant water pollution problem [1-3].

Due to their chemical structure, dyes have high stability

How to cite: Ramírez-Castillo, F.Y., Guillén-Padilla, D.E., Méndez-Sandate,C.I., Guerrero-Barrera, A.L. and Avelar-González, F.J., Phytoremediation of Methylene Blue and Congo Red by duckweed (Lemna minor). DYNA, 91(232), pp. 9-15, April - June, 2024.

and resistance to bio-, photo-, and thermo-degradation [4]. Therefore, they tend to persist in the environment, creating problems for the water bodies by colored water, increasing biochemical and chemical oxygen demand, increasing suspended solids, impairing photosynthesis, and inhibiting plant growth [3]. In addition, microorganisms that inhabit aquatic environments could cause direct destruction or inhibit their catalyzing capacity [5,6]. Likewise, synthetic dyes can also cause human health problems such as allergy, rhinitis, asthma, dermatitis, skin and eye irritation, problems with the central nervous system, cancer, and mutation [7,3].

Several physicochemical methods for removing dyes from water sources include adsorption, photocatalysis, advanced oxidation, precipitation, ion exchange, membrane filtration, coagulation, and solvent extraction [8-10].

Phytoremediation is an alternative technology for removing contaminants in water, soil, sediments, and air [11]. These techniques are considered low-impact, environmentally friendly, cost-effective, and easy-to-use methods since they are driven by solar energy and use the capacity of plants, their roots, and microorganisms associated with them to absorb, filter, precipitate, metabolize, and compartmentalize or sequester organic and inorganic pollutants [10-13].

Lemna minor, from the *Lemnaceae* family, commonly known as duckweeds, is one of the most used aquatic plants for bioremediation of aquatic environments with multiple contaminants, such as nitrogen, ammonia, phosphates, total solids, organic compounds, heavy metals, drugs, and synthetic dyes [14]. *L. minor* is a free-floating macrophyte found in freshwater bodies and sewage waters. Due to their rapid vegetative propagation, fastest growth rates, ability to accumulate large amounts of biomass in a short period, easy of harvestable, and great adaptability to diverse environmental factors such as different range of temperature and pH, as well as their tolerance to several pollutants, these aquatic plants have a great potential for phytoremediation [14,15].

Several studies have reported the ability of duckweed for phytoremediation of methylene blue dye [16-18]. However, little is known about the phytoremediation potential for more diverse dyes, such as Congo Red [2,7,19]. This study aims to investigate the removal potential of duckweed (*L. minor*) for the removal of two dyes with different chemical structures, methylene blue (triaryl methane dye, ionic dye) and Congo Red (diazo dye, anionic dye) in aqueous solution. The effect of contact time was also studied to optimize the phytoremediation process.

2 Methods

2.1 Plant cultivation

L. minor was collected from ponds at San Francisco de los Romo, Aguascalientes, Mexico, during June 2023. The plants were gently washed with tap water to remove unwanted impurities. Subsequently, the plants were kept in distilled water for 2 h. Before the experimentation, the plants were maintained using Hoagland´s modified nutrient solution at 27 ± 30ºC for 15 days. All the plants used were healthy (intense lemon green color without root detachment).

2.2 Decolorization of Methylene blue and Congo Red assays

Methylene blue (triethylmethane dye, MB [$C_{16}H_{18}N_3SCl.3H_2O$; PM 372.90 gr/mol] and Congo Red (diazo dye [$C_{32}H_{22}N_6Na_2O_6S_2$; PM 696.7 gr/mol] were used as contaminants to be removed (Fig. 1). The initial pH of the colored solution was 6.9 to 7.2. The initial temperature ranged from 26.6ºC to 27.2ºC. During the treatment time intervals, absorbance and concentration of dyes were calculated using a UV/Vis spectrophotometer at a wavelength of 665 nm for methylene blue and 497 nm for Congo Red [17].

The decolorization test were carried out in 250 ml flasks containing 100 ml of colored solutions of MB and CR at concentration of 1 mg/L, 5 mg/L, 10 mg/L, and 15 mg/L. Four grams of *L. minor* was exposed to water contaminated with MB and CR at room temperature (24ºC ± 4ºC) under white lamp light at 10,000 to 25,000 lux meters [17]. For the trial, it was ensured that all plants roots reached the bottom of the beaker during the test to increase root sorption capacity and rhizosphere clearance mechanisms [22].

Samples of 2 ml of colored water were collected at 0, 30, 60, 90, 120, and 180 min; and 24, 48, 72 and 96 hours. Absorbance values were measured at each set point. All measurements were performed in triplicate. The removal of both dyes was evaluated by absorbance in terms of decolorization. The percentage of discoloration was calculated based on the following equation [23]:

$$Decolorization\ (\%) = \left(1 - \frac{At}{Ao}\right) \times 100$$

Where "A_0" describes the absorbance of the colored solution at time zero (before treatment), and "A_t" represents the absorbance measured after exposure to the colored solutions at time "t."

2.3. Statistical analysis

The results of the experiments were analyzed by one-way ANOVA with the Turkey-Kramer multiple comparison test using the GrapPad Prisms 8.0.2 program. The results were considered statistically significant with $p \leq 0.05$. Data are presented as the mean and standard deviation of three replicates.

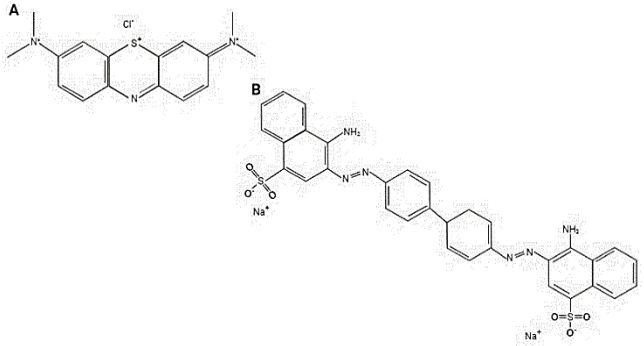

Figure 1. Chemical structure of A) Methylene blue (MB) and B) Congo Red (CR). The images were created using BioRender.com on-line tool (https://app.biorender.com/).
Source: adapted from the literature [20,21].

3 Results and discussion

The results of the effect of the exposure time and the initial concentration of MB and CR solutions on the absorbance of both dyes are presented in Fig. 2. For both colored solutions, a reduction of the absorbance was observed (Fig. 2A and 2B). The removal time was much shorter for the MB than the CR since the decrease of MB was observed after 30 minutes of the assay for all concentrations tested. Meanwhile, CR did not show any significant reduction in the first 180 minutes of the experiment for all concentrations, including the minor concentration of 1 mg/L (Fig. 2A).

Fig. 3 illustrates the maximum reduction of CR and MB over 96 hours with set points every 24 hours. Figure 3B indicates that the maximum reduction for CR was achieved at the 24-hour mark, and no further significant reduction was observed. On the other hand, Figure 3A shows that MB exhibited a more significant removal at 24 hours, which continued to be observable until 72 hours, including the highest concentration tested of 15 mg/L of dye. At 96 hours, a slight increase in the absorbance was seen in all concentrations except for the lowest concentration of 1 mg/L of MB.

Notably, when we compared the reduction between the 30-min mark vs. 180-min mark, a significant reduction of the MB dye was observed for all concentrations, with the percentage of decolorization of 63.74% vs. 80.73%, $p<0.01$ (1 mg/L, respectively), 28.67% vs. 73.05%, $p < 0.001$ (5 mg/L, respectively), 16.79% vs. 48.08%, $p < 0.001$(10 mg/L, respectively), and 5.32% vs. 34.77%, $p < 0.001$ (15 mg/L, respectively). In contrast, when we compared the reduction between the 30-min mark and 180-min mark on CR dye, we found the best percentage of remotion for the most concentrated solution of 15 mg/L of CR dye with a reduction of 9.97% at 30-min vs. 17.06% at 180-min with significant differences between both time marks ($p < 0.001$, Fig. 4B). Non-significant differences were found for all other concentrations.

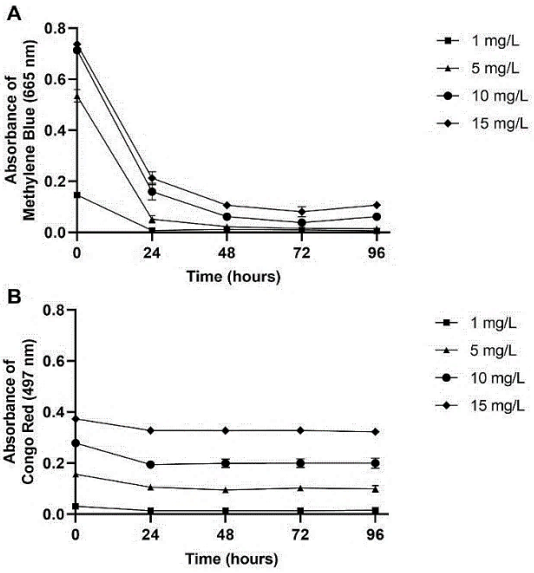

Figure 3. The absorbance of methylene blue (MB, A) and Congo red (CR, B) at concentrations of 1 mg/L, 5 mg/L, 10 mg/L, and 15 mg/L of dye, after treatment with L. minor for 24, 48, 72 and 96 hours. The values are presented as the average of the triplicate ± standard deviation. MB was measured at 665 nm and CR at 497 nm.
Source Self-made image.

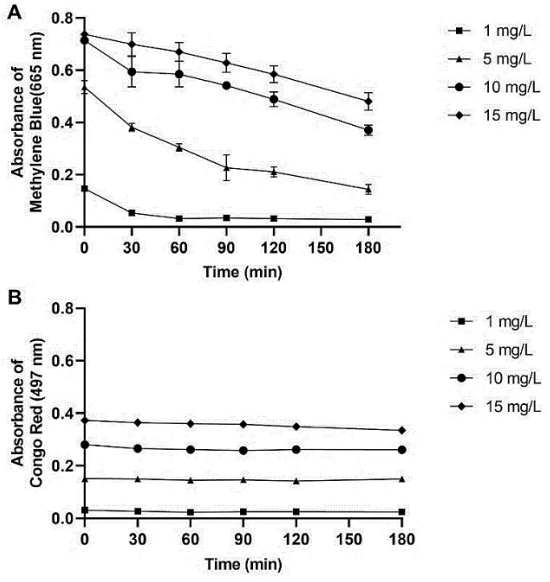

Figure 2. The absorbance of methylene blue (MB, A) and Congo red (CR) at concentrations of 1 mg/L, 5 mg/L, 10 mg/L, and 15 mg/L of dye, after treatment with *L. minor* for 30, 60, 90 and 180 min. The values are presented as the average of the triplicate ± standard deviation. MB was measured at 665 nm and CR at 497 nm.
Source: Self-mage image.

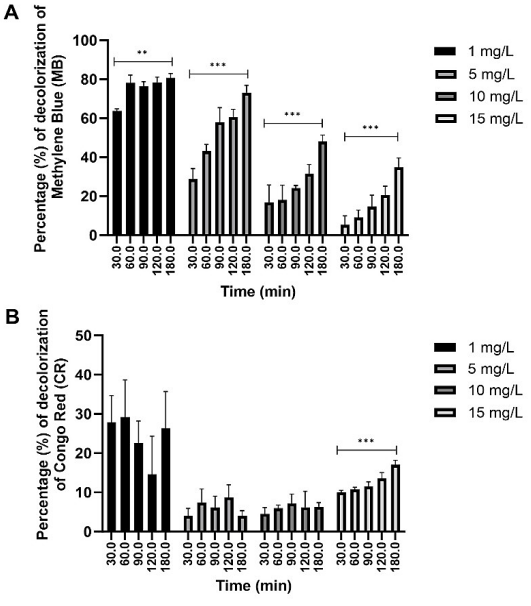

Figure 4. Percentage removal in terms of decolorization of methylene blue (MB, A) and Congo red (CR, B) dyes at concentrations of 1 mg/L, 5 mg/L, 10 mg/L, and 15 mg/L of dye after treatment with L. minor for 30, 60, 90, 120 and 180 minutes. Values are presented as the average of triplicate.
Source: Self-made image.

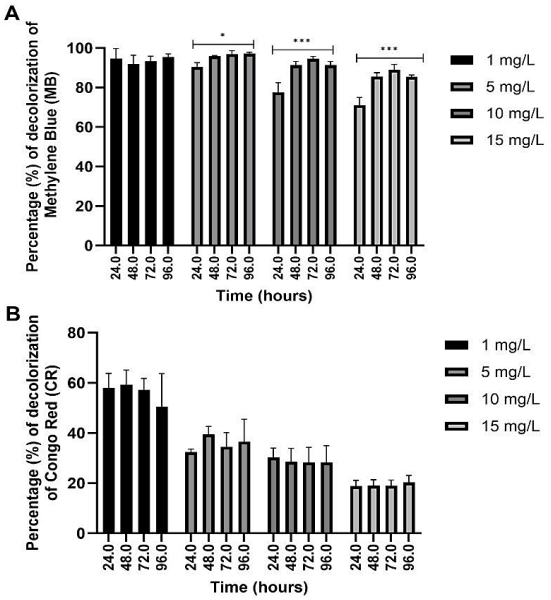

Figure 5. Percentage removal of methylene blue (A, C) and Congo red (B, D) dyes at concentrations of 1 mg/L, 5 mg/L, 10 mg/L, and 15 mg/L of dye after treatment with L. minor for 180 minutes (A, B) and 96 hours (C, D). Values are presented as the average of triplicate. Source: Self-made image.

The maximum removal efficiency of the MB dye at the lowest concentration of 1 mg/mL was reached in the full contact time of 96 hours, with percentages of decolorization of 95.49%. However, no significant differences were found in the 24-hour and 96-hour mark at this concentration (Tabl. 5A). Taking as reference the 96 hours, we found a significant difference among this set point and 24 hours, with the percentage of decolorization of MB of 97.26% vs. 90.35%, $p < 0.05$ on the concentration of 5 mg/L of dye (96-hour vs 24-hour, respectively), of 77.58% vs. 91.31%, $p < 0.001$ for 10 mg/L of dye (respectively), and of 71.13% vs. 85.43%, $p < 0.001$ for 15 mg/L of dye (respectively). However, non-significant differences were found between 48- and 72-hours vs. 96-hours of treatment (Fig. 5A).

Compared with previous studies where removal percentages of MB were 80.56% at 24 hours at a concentration of 50 mg/L [16] and 98% at a concentration of 15 mg/L [23], we observed a lower percentage of efficiency (71.13%, Fig. 5A) in the same exposure time (24 h). This could be explained by the amount of biomass used since in Can-Terzi et al. [24], 4.9 gr of the plant was used, while our study used only 4 gr. In addition, pH and temperature variations also modify the percentage of remotion of pollutants. This agrees with Torbati et al. [25], who evaluated the ability of duckweed to decolorize the acid dye Bordeaux B (ABB and aminoazo benzene dye) and determined that increasing the plant's temperature and weight, increases the efficiency of dye removal. In addition, the quantity of the biomass is of great importance since it has been found that the mechanisms of remotion are related to biosorption [24] and phytoadsorption through electrostatic interactions, hydrogen bonds, as well as degradation by desulfurization and denitrification processes [16,26]. Therefore, the greater the amount of plant present, the greater the sorption surface are disponible for the dye molecules [27]. However, in lower concentrations of 1 mg/L and 5 mg/L we achieve 94.59% and 90.4% of removal at 24 h (Fig. 5A).

Similar to the results obtained by Reema et al. [28] and Khataee et al. [27] that determined a removal percentage higher than 80% for MB after three days of contact, we observer a removal percentage of 88.93% of MB in 72 h at concentration of 15 mg/L (Fig. 5A). The MB-colored solution in lower concentrations of 1 and 5 mg/L reduced almost the maximum percentage of dye at 24 hours (94.59% and 90.41%, respectively); thus, no significant differences were observed between 24 and 96 hours of contact with ducked for the lower concentration tested (95.49%, Fig. 5A). On the contrary, the solutions with the highest concentration (10 and 15 mg/L) were significantly reduced at 96 hours compared to the contact time of 24 hours ($p < 0.001$, Fig. 5A). Therefore, the higher the concentration of MB, the longer contact time was required to increase the percentage of efficiency in the removal of the colored solution.

Regarding Congo Red (CR) dye, within the first 180 min of contact with duckweed, the removal percentage in terms of decolorization was 26.35% (1 mg/L), 4.04% (5 mg/L), 6.32% (10 mg/L) and 17.07% (15 mg/L), respectively (Fig. 4B). Likewise, the maximum decolorization of CR was performed at different set points for different concentrations. At 1 mg/L and 5mg/L of CR dye, maximal decolorization was found at 48 hours (59.32 %, and 39.43%, respectively); at 10 mg/L was found at 24 hours (30.27%), and at 15 mg/L was achieved at 96 hours (20.27%). Nevertheless, non-significant differences were found among all-time marks after 48 hours (Fig. 5B). This agrees with the survey by Kaur et al. [2], which determined that the contact time for maximum decolorization was 40 hours for the CR dye using *the Trachyspermum ammi* plant. In contrast with our study, Mahajan et al., [19] found a maximal removal percentage of 95% of CR dye solution at 24 hours using *Chara vulgaris*, however, these differences could be explained by the amount of algae used (5 g), the temperature (33ºC), the pH of 7, and different species used.

Notably, the decolorization rate of both MB and CR dyes decreases as the concentration of dye increases. This might be due to the high concentration of the dye molecule in the solution blocking the pores on the root surface and the rate of decolorization decrease [2]. Moreover, the toxic effects of the dye could be affecting the metabolic activity of the plant [29]. Indeed, previous studies have found that exposure to CR inhibits plant growth, decreasing biomass percentage and chlorophyll a biosynthesis [30]. On the other hand, the rapid adsorption in the initial phase of the experiment is caused by the large amount of dye particles in the solution and the large number of free sites available in the plant for the adsorption process [3].

In the CR dye assay, a significant reduction in absorbance was observed at 24 and 48 h, while after 72 h, an increase in absorbance was noticed (Fig. 3B and 5B). We observed that certain plants begin to die after 48 h (results not shown). Thus, previously adsorbed dye is released from the dead plants into the colored solution [31]. In addition, the difference between the removal percentage achieved for MB

vs CR and the removal time can be influenced by the chemical structure of both dyes. CR is an anionic dye and a more complex structure with higher molecular weight than MB, which is, in contrast, an ionic dye. Therefore, duckweed can potentially remove ionic dyes better than anionic ones. A study that compares the remotion process of MB vs. CR using *T. ammi* has also shown a better remotion for MB (99% or removal) compared to CR (91% of removal) [2]. Likewise, it seems that the sorption mechanisms of both dyes are different since we noticed that the root in the treatment with MB was colored after a few minutes of contact time and depleted about 72 hours; meanwhile, for the CR, the root remained attached to the frond, and it is the frond that is colored by the dye (data not show). Further studies will focus on the mechanisms of Congo Red removal by duckweed.

Other strategies for removing CR from wastewater include the use of adsorbents. This adsorbent comprises the use of *Azolla filiculoides* that removes 95% of CR dye in optimal conditions [32], *Vernonia amygalina* leaf powder with an adsorption capacity of 57.47 mg/g at pH 8 [33], nylon fiber waste with the removal of 95% for CR concentration of 400 mg/L at pH 6 [34], fly ash (waste material within SiO_2, Al_2O_3, Fe_2O_3, Na_2O, MgO and K_2O as constituents) within an adsorption capacity of 22.12 mg/g [35], hydrochard and MgAl layered double hydroxide (HC-MgAlLDH) nanocomposite with a removal capacity of 348.78 mg/g of CR [36], natural clay glauconite (a heterogeneous phyllosilicate mineral) activated with 2M NaOH with removal efficiency ~77% [37], metal-organic frameworks such as zeolitic imidazolate framework-8 with an adsorption capacity of 1250 mg/g [38], activated carbon, among others. However, even when adsorbents have taken a great interest due to the large quantities of available adsorbents and high adsorption capacity [39], some of these treatments, such as activated carbon, alumina, and silica gel, fly ash and zeolites require regeneration or disposal of adsorbents, thus limiting their application [24,33].

Furthermore, although phytoremediation is a promising method for dye removal, managing the plant biomass produced after the remediation process is crucial to avoid converting it into secondary pollution through post-mortem decomposition. Unfortunately, there is limited research on post-remediation management [40]. Simple harvesting will reduce the re-entry of pollutants by up to 75% [41]. Song et al. [40] demonstrated that it is possible to re-use remediation plant biomass (*Pharagmites australis* and *Typha angustifolia*) as a friendly fertilizer. It has also been suggested to use phytoremediation biomass for energy generation by incineration [42] or by production of bio-ethanol [43]. Nowadays, composting, leachate compaction, combustion, gasification, pyrolysis, torrefaction, and metal recovery are used for phytoremediation biomass management. The extraction and recovery of metalloids and metals from contaminated biomass is considered as a valuable bio-product [44].

Among dyes, Torbarti et al. [26] have shown that *L. minor* possessed reasonable reusability in the repetitive decolorization operation of triarylmethane dye with biodegradation in eight intermediate compounds, which could convert into the CO_2 and water (deep oxidation). Can-Terzi et al. [24] propose that the phytoremediation biomass of MB could be used as fertilizer since their desorption showed that MB that was removed by *L. minor* has remained within the plant structure and adhered into the functional groups of the plant. The authors also propose the use of *L. minor* biomass as biofuel production. Imron et al. [31] showed that rhizobacteria on *L. minor* could degrade MB into CO_2, water, and other intermediate products that will be adsorbed by *L. minor* onto leaves [31]. However, post-phytoremediation biomass treatment may be an essential issue to address.

4 Conclusion

The results demonstrate the ability of duckweed (*Lemna minor*) for the removal of Methylene Blue (MB) and Congo Red (CR) dyes in aqueous solutions. Duckweed has a higher percentage of efficiency in removing the Methylene Blue (95.49%, 1 mg/L; 97.24%, 5 mg/L; 91.30%, 10 mg/L; and 85.42%, 15 mg/L) compared to Congo Red dye (59.32%, 1 mg/L; 39.43%, 5 mg/L; 28.47%, 10 mg/L; and 20.27%, 15 mg/L) at al concentrations tested. Duckweed (*L. minor*) can reduce a percentage of ~90% of MB in less than 24 hours, while it reduces rates to ~ 20% of CR dye in the same contact period. Future studies will focus on exploring the mechanisms of adsorption and the toxicity of Congo Red in *L. minor*.

References

[1] Garg, S., and Roy, A. Chapter 18. Phytoremediation: an alternative approach for removal of dyes. In: Biotechnological Strategies for Promoting Invigorating Environs. Phytoremediation. Editor(s): Bhat, R.A., Policarpo-Tonelli, F.M., Dar, G.H., and Hakeem, K., Academic Press, 2022, pp. 369-386. DOI: https://doi.org/10.1016/B978-0-323-89874-4.00005-4.

[2] Kaur, N., Kaushal, J., and Mahahan, P., Phytoremediation of methylene blue dye (triarylmethane) and Congo red (azo) by *T. ammi* L.: Kinetic studies. Int. J. Environ. Sci. Technol, 21, pp. 1697-1714, 2023. DOI: https://doi.org/10.1007/s13762-023-05037-x

[3] Al-Tohamy, R., Ali, S.S., Li, F., Okasha, K.M., Mahmoud, Y.A.G., Elsamahy, T., Jio, H., Fu, Y., and Sun, J., A critical review on the treatment of dye-containing wastewater: ecotoxicological and health concerns of textile dyes and possible remediation approaches for environmental safety. Ecotoxicology and Environmental Safety, 231, art. 113160, 2022. DOI: https://doi.org/10.1016/j.ecoenv.2021.113160

[4] Moulay, A., and Abdelilah, C., Electrochemical studies of adsorption of paraquat onto $Ca_{10}(PO_4)_6(OH)_2$ from aqueous solution, Leonardo Jour. Sci. [online]. 12, pp. 25-34, 2008, Available at: https://www.semanticscholar.org/paper/Electrochemical-Studies-of-Adsorption-of-Paraquat-Chtaini/18011cbefcfa217892dd7b24f6cbbc661a51f2bb

[5] Mehdi, S., Halimah, M., Nashriyah, M., and Ismail, B.S., Adsorption and desorption of paraquat in two Malaysian agricultural soils, Am. Euras. J. Sustain. Agri, 3(3), pp. 555-560, 2009, DOI: https://doi.org/10.1007/s10661-010-1565-6

[6] Tan, I.A.W., Ahmad, A.L., and Hameed, B.H., Adsorption of basic dye on high surface area activated carbon prepared from coconut husk: equilibrium, kinetic and thermodynamic studies, J. Hazard. Mater, 154(1-3), pp. 337-346, 2008. DOI: https://doi.org/10.1016/j.jhazmat.2007.10.031

[7] Somasekhara, R., Sivarama, K.L., and Varada, R.A., The use of an agricultural waste material, Jujuba seeds for the removal of anionic dye (Congo red) from aqueous medium, J. Hazard. Mater, (203-204), pp. 118-127, 2012. DOI: https://doi.org/10.1016/j.jhazmat.2011.11.083

[8] Ali, N., Zada, A., Zahid, M., Ismail, A., Rafiq, M., Riaz, A., and Khan, A., Enhanced photodegradation of methylene blue with alkaline and transition-metal ferrite nanophotocatalysts under direct sun light irradiation. Journal of the Chinese Chemical Society, 66(4), pp. 402-408, 2018. DOI: https://doi.org/10.1002/jccs.201800213

[9] Kang, Y.G., Yoon, H., Lee, C.S., Kim, E.J., and Chang, Y.S., Advanced oxidation and adsorptive bubble 611 separation of dyes using MnO_2-coated Fe_3O_4 nanocomposite, Water research, 151, pp. 413-422, 2019. DOI: https://doi.org/10.1016/j.watres.2018.12.038

[10] Ullah, A., Farooq, M., Nadeem, F., Rehman, A., Hussain, M., Nawaz, A., and Naveed, M., Zinc application in combination with zinc solubilizing *Enterobacter* sp. improved productivity, profitability, zinc efficiency, and quality of desi chickpea. Journal of Soil Science and Plant Nutrition, 20(4), pp. 2133-2144, 2020. DOI: https://doi.org/10.1007/s42729-020-00281-3

[11] Khandare, R.V., and Govindwar, S.P., Phytoremediation of textile dyes and effluents: current scenario and future prospects. Biotechnology Advances, 33(8), pp. 1697-1714, 2015. DOI: https://doi.org/10.1016/j.biotechadv.2015.09.003

[12] Yan, A., Wang, Y., Tan, S.N., Mohd, Yusof, M.L., Ghosh, S., and Chen., Phytoremediation: a promising approach for revegetation of heavy metal-polluted land. Front, Plant Sci, 11, art. 359, 2022. DOI: https://doi.org/10.3389/fpls.2020.00359

[13] Noor, I., Sohail, H., Sun, J., Nawaz, M.A., Li, G., Hasanuzzaman, M., and Liu, J., Heavy metal and metalloid toxicity in horticultural plants: tolerance mechanism and remediation strategies, Chemosphere, 303, art. 135196, 2022. DOI: https://doi.org/10.1016/j.chemosphere.2022.135196

[14] Zhou, Y., Stepanenko, A., Kishchenko, O., Xu, J., and Borisjuk, N., Duckweeds for phytoremediation of polluted water, Plants, 12(3), art. 589, 2023. DOI: https://doi.org/10.3390/plants12030589

[15] Kaur L., and Kanwar, N., Duckweed: a model for phytoremediation technology, Holistic Approach Environ, 12(1), pp. 39-58, 2022. DOI: https://doi.org/10.33765/thate.12.1.4

[16] Imron, M.F., Kurniawan, S.B., Soegianto, A., and Wahyudianto, F.E., Phytoremediation of methylene blue using duckweed (*Lemna minor*), Heliyon, 5(8), art. 2206, 2019. DOI: https://doi.org/10.1016/j.heliyon.2019.e02206

[17] Al-Baldawi, I.A., Abdullah, S.R.S., Anuar, N., and Hasan, H.A., Phytotransformation of methylene blue from water using aquatic plant (*Azolla pinnata*). Environ. Technol. Innov. 11, pp. 15-22, 2018. DOI: https://doi.org/10.1016/j.eti.2018.03.009

[18] Wibowo, Y.G., Syahnur, M.T., Al-Azizah, P.S., Gintha, D.A., and Gifta-Lululangi, B.R., Phytoremediation of high concentration of ionic dyes using aquatic plant (*Lemna minor*): a potential eco-friendly solution for wastewater treatment, Environmental Nanotechnology, Monitoring & Management. 20, art. 100849, 2023. DOI: https://doi.org/10.1016/j.enmm.2023.100849

[19] Mahajan P., and Kaushal J., Degradation of Congo Red Dye in Aqueous Solution by Using Phytoremediation Potential of Chara Vulgaris. Chitkara Chemistry Review. 1(1), pp. 67-75, 2013. DOI: https://doi.org/10.15415/ccr.2013.11005.

[20] National Center for Biotechnology Information. PubChem Compound Summary for CID 6099, Methylene Blue. [online]. 2024. [Retrieved March 5th of 2024]. Available at: https://pubchem.ncbi.nlm.nih.gov/compound/Methylene-Blue.

[21] National Center for Biotechnology Information. PubChem Compound Summary for CID 11313, Congo red. [online]. 2024. [Retrieved March 5th of 2024]. Available at: https://pubchem.ncbi.nlm.nih.gov/compound/Congo-red.

[22] Almuktar, S.A.A.A.N., Abed, S.N., and Scholz, M., Wetlands for wastewater treatment and subsequent recycling of treated effluent: a review, Environ. Scie. Pollut. Res, 23, pp. 23595-23623, 2018. DOI: https://doi.org/10.1007/s11356-018-2629-3

[23] Al Farraj, D.A., Elshikh, M.S., Al Khylaifi, M.M., Hadibarata, T., Yunirato, A., and Syafiuddin, A., Biotransformation and detoxification of antraquione dye green 3 using halophilic *Hortaea* sp., Int. Biodeterior. Biodegrad., 140, pp. 72-77, 2019. DOI: https://doi.org/10.1016/j.ibiod.2019.03.011

[24] Can-Terzi, B., Goren, A.Y., Okten, H.E., and Sofuoglu, S.C., Biosorption of methylene blue from water by live *Lemna minor*, Environmental Technology & Innovation., 22, pp. 101432, 2021. DOI: https://doi.org/10.1016/j.eti.2021.101432

[25] Torbati, S., Toxicological risks of Acid Bordeaux B on duckweed and the plant potential for effective remediation of dye-polluted waters. Environ. Sci. Pollut. Res., 26, pp. 27699–27711, 2019. DOI: https://doi.org/10.1007/s11356-019-05898-1

[26] Torbati, S., Feasibility and assessment of the phytoremediation potential of duckweed for triarylmethane dye degradation with the emphasis on some physiological responses and effect of operational parameters., Turk. J. Biol., 39(3), pp. 438–446, 2015. DOI: https://doi.org/10.3906/biy-1411-23

[27] Khataee, A.R., Movafeghi, A., Torbati, S., Salehi-Lisar, S.Y., and Zarei, M., Phytoremediation potential of duckweed (*Lemna minor* L.) in degradation of C.I. Acid Blue 92: artificial neural network modeling., Ecotoxicol. Environ. Saf., 80, pp. 291–298, 2012. DOI: https://doi.org/10.1016/j.ecoenv.2012.03.021

[28] Reema, R.M., Saravanan, P., Kumar, M.D., and Renganathan, S., Accumulation of methylene blue dye by growing *Lemna minor*. Separ. Sci. Technol., 46(6), pp. 1052–1058, 2011. DOI: https://doi.org/10.1080/01496395.2010.528503

[29] Kabra, A.N., Khandare, R.V., Kurade, M.B., and Govindwar, S.P., Phytoremediation of a sulphonated azo dye Green HE4B by Glandularia pulchella (Sweet) Tronc. (Moss Verbena), Environmental Science and Pollution Research, 18(8), pp. 1360-1373, 2011. DOI: https://doi.org/10.1007/s11356-011-0491-7

[30] Adomas, B., Sikorski, Ł., Bęś, A., and Warmiński, K., Exposure of *Lemna minor* L. to gentian violet or Congo red is associated with changes in the biosynthesis pathway of biogenic amines. Chemosphere, 254, art. 126752, 2020. DOI: https://doi.org/10.1016/j.chemosphere.2020.126752

[31] Imron, M.F., Ananta, A.R., Ramadhani, I.S., Kurniawan, S.B., and Sheikh-Abdullah, S.R., Potential of *Lemna minor* for removal of methylene blue in aqueous solution: Kinetics, adsorption mechanism, and degradation pathway, Environmental Technology & Innovation, 24, art. 101921, 2021. DOI: https://doi.org/10.1016/j.eti.2021.101921

[32] Sundararaman, S., Senthil Kumar, P., Deivasigamani, P., Jagadeesan, A.K., Devaerakkam, M., Al-Hashimi, A., and Choi, D., Assessing the Plant Phytoremediation Efficacy for *Azolla filiculoides* in the Treatment of Textile Effluent and Redemption of Congo Red Dye onto *Azolla* Biomass. Sustainability, 13, art. 9588, 2021. DOI: https://doi.org/10.3390/su13179588

[33] Zewde, D., and Geremew, B., Removal of Congo red using Vernonia amygdalina leaf powder: optimization, isotherms, kinetics, and thermodynamics studies, Environmental Pollutants and Bioavailability, 34(1), pp. 88-101, 2022. https://doi.org/10.1080/26395940.2022.2051751

[34] Hamad, K.H., Yasser, A.M., Nabil, R., Tarek, R., Hesham, E., El-Telbany, A., Saeed, A., Selim, S.E., and Abdelhamid, A.E., Nylon fiber waste as a prominent adsorbent for Congo red dye removal. Sci Rep, 14, art. 1088, 2024. DOI: https://doi.org/10.1038/s41598-023-51105-0

[35] Harja, M., Buema, G., and Bucur, D., Recent advances in removal of Congo Red dye by adsorption using an industrial waste. Sci Rep, 12, art. 6087, 2022. DOI: https://doi.org/10.1038/s41598-022-10093-3

[36] Huang, Y., Yin, W., Zhao, T.L., Liu, M., Yao, Q.Z., and Zhou, G.T., Efficient removal of Congo Red, Methylene Blue and Pb(II) by Hydrochar-MgAlLDH nanocomposite: synthesis, performance and mechanism, Nanomaterials (Basel), 13(7), art. 1145, 2023. https://doi.org/10.3390/nano13071145

[37] Hamd, A., Salah, D., Alyafei, H.F., Soliman, N.K., El-Reedy, A.A.M., Elzanaty, A.M., Al-Saeedi, S.I., Al-Ghamdi, A., Shaban, M., El-Sayed, R., and Ahmed, S.A., NaOH-activated natural glauconite for low-cost adsorption of Congo Red dye. Water, 15, art. 3753, 2023. DOI: https://doi.org/10.3390/w15213753

[38] Jiang, C., Fu, B., Cai, H., art. Cai, T., Efficient adsorptive removal of Congo red from aqueous solution by synthesized zeolitic imidazolate framework-8, Chemical Speciation & Bioavailability, 28, pp. 1-4, pp. 199-208, 2016. DOI: https://doi.org/10.1080/09542299.2016.1224983

[39] Habiba, U., Siddique, T.A., Joo, T.C., Salleh, A., Ang, B.C., and Afifi, A.M., Synthesis of chitosan/polyvinyl alcohol/zeolite composite for removal of methyl orange, Congo Red and chromium(VI) by

flocculation/adsorption, Carbohyd. Polym, 157, pp. 1568–1576, 2017. https://doi.org/10.1016/j.carbpol.2016.11.037
[40] Song, U., and Park, H., Importance of biomass management acts and policies after phytoremediation. J. Ecology Environ., 41, art. 13, 2017. DOI: https://doi.org/10.1186/s41610-017-0033-4
[41] Asaeda, T., Trung, V.K., and Manatunge, J., Modeling the effects of macrophyte growth and decomposition on the nutrient budget in shallow lakes. Aquatic Botany, 68, pp. 217–237, 2000. DOI: https://doi.org/10.1016/S0304-3770(00)00123-6
[42] Brooks, R.R., Chambers, M.F., Nicks, L.J., and Robinson, B.H., Phytomining. Trends in Plant Science, 3, pp. 359–362, 1998. DOI: https://doi.org/10.1016/S1360-1385(98)01283-7
[43] Banuelos, G.S., Phyto-products may be essential for sustainability and implementation of phytoremediation. Environmental Pollution, 144, pp. 19–23, 2006. DOI: https://doi.org/ 10.1016/j.envpol.2006.01.015
[44] Khan, A.H.A., Kiyani, A., Santiago-Herrera, M., Ibáñez, J., Yousaf, S., Iqbal, M., Martel-Martín, S., and Barros, R., Sustainability of phytoremediation: post-harvest stratagems and economic opportunities for the produced metals contaminated biomass. Journal of Environmental Management, 326(Pt B), 116700, 2023. DOI: https://doi.org/10.1016/j.jenvman.2022.116700

A.L. Guerrero-Barrera, received a Dr. in Cellular Biology and a MSc. in Cellular Biology from CINVESTAV-IPN. PhD in Cellular Biology, Institute of Biotechnology of the UNAM. Publication of 73 scientific articles. Member of the National System of Researchers (SNI) Level II. Direction of 22 doctoral, 4 master's, and 33 undergraduate theses. UAA. Full-Time Research Professor since 2001. Visiting Professor at the University of Cergy Pontoise, France 2017. Sabbatical stay at Faculty of Veterinary Medicine, University of Montreal 2009. Participant in the "Researchers with Commercial Success" program, CONACYT-INFOTEC 2014, Leaders in Innovation Scholarship Program. Royal Academy of Engineering and Isis Group Oxford 2015 and "Researchers with commercial success," CONACYT-INFOTEC 2015.
ORCID: 0000-0002-0952-8544

F.J. Avelar-González, received a Dr. in Biotechnology from CINVESTAV-IPN. He is a BSc. Eng. in Biochemical Engineer who graduated from the Autonomous University of Aguascalientes, Mexico and has a MSc. in Biotechnology from CINVESTAV-IPN. He is a member of the National System of Researchers (SNI), Level I, and a full-time research professor at the Autonomous University of Aguascalientes.
ORCID: 0000-0002-0777-9243

F.Y. Ramírez-Castillo, is a BSc. Eng. in Biochemical Engineer and Dr. in Biological Sciences from the Autonomous University of Aguascalientes, Mexico. She has published 12 indexed articles on the detection of pathogens in water, antimicrobial resistance, and the detection of pathogens in respiratory diseases. She carried out a research stay at the Université de Montréal focused on the pathogenesis and antimicrobial resistance of *E. coli*, molecular diagnostic techniques of pathogens in aquatic environments, antimicrobial resistance, urinary tract infections, and respiratory infections, and studies of contamination in surface waters. She is a member of the National System of Researchers (SNI), Level I
ORCID: 0000-0003-1707-2441.

D.E. Guillén-Padilla, is a BSc. in Biological Pharmaceutical Chemist from the Autonomous University of Aguascalientes, Mexico. She is currently working on a project for the molecular characterization of clinical isolates of *P. aeruginosa* resistant to quinolones, where the presence or absence of genes that code for resistance to this antibiotic, mediated by plasmids or present in a determining region, is evaluated. Likewise, it participated in the phytoremediation mini-project, where the ability of the aquatic plant *Lemna minor* to remove dyes present in water contaminated with said dyes was evaluated.
ORCID: 0009-0000-3585-9681

C.I. Méndez Sandate, Bachelor´s degree in Biological Pharmaceutical Chemist at the Autonomous University of Aguascalientes, Mexico. The thesis project is "Evaluation of the phytotoxicity of the antibiotic enrofloxacin in the floating aquatic plant *Lemna minor* (duckweed). Likewise, he participated in the phytoremediation mini-project, where the ability of the aquatic plant *Lemna minor* to remove the methylene blue and Congo red dyes present in the aqueous solution was evaluated.
ORCID: 0009-0004-7637-4794

DYNA
http://dyna.medellin.unal.edu.co/

UNIVERSIDAD NACIONAL DE COLOMBIA

Adaptative comfort modeling for a typical non-centrifugal cane sugar processing facility

Giovanni Andrés Cortés-Tovar [a], Robinson Osorio-Hernández [a] & Jairo Alexander Osorio-Saráz [b]

[a] *Universidad Nacional de Colombia, Sede Bogotá, Facultad de Ingeniería, Bogotá, Colombia. gacortest@unal.edu.co, rosorioh@unal.edu.co*
[b] *Universidad Nacional de Colombia, Sede Medellín, Facultad de Ciencias Agrarias, Medellín, Colombia. aosorio@unal.edu.co*

Received: January 24th, 2024. Received in revised form: February 29th, 2024. Accepted: March 11th, 2024.

Abstract
The production of non-centrifuged cane sugar in Colombia takes place in post-harvest facilities that generate significant heat and steam resulting from the evaporation of cane juices during the process. This study aimed to improve the comfort conditions of a facility of this type in the municipality of Pacho, Cundinamarca, Colombia, through bioclimatic simulation, where the enclosure on the walls and the lantern window were modified. The evaluation of adaptative thermal comfort revealed that configurations with open perimeter and lantern window demonstrated the best bioclimatic behavior. This is attributed to the increased ventilation area and chimney effect, which optimizes the transfer of heat and mass. Likewise, it was observed that there is a generalized behavior of thermal discomfort for workers in the thermal zone of the oven, due to the high emissions of heat and steam in this specific area.

Keywords: thermal stress; computer simulation; natural ventilation; thermal load; panela.

Modelamiento de confort adaptativo para un trapiche panelero

Resumen
La producción de azúcar de caña no centrifugada, en Colombia se realiza en instalaciones de poscosecha que generan alta cantidad de calor y vapor, producto de la evaporación de los jugos de caña del proceso. Este estudio tuvo como objetivo mejorar las condiciones de confort de una instalación de este tipo en el municipio de Pacho, Cundinamarca, Colombia, a través de simulación bioclimática, donde se modificó el cerramiento en las paredes y en la ventana cenital. Se evalúo el confort térmico adaptativo, donde el mejor comportamiento bioclimático se presentó en las configuraciones con perímetro abierto y ventana cenital, esto debido a que una mayor área de ventilación y efecto chimenea optimizan la transferencia de calor y masa; así mismo, se observó que hay un comportamiento generalizado de incomodidad térmica para los trabajadores en la zona térmica hornilla, debido a las altas emisiones de calor y vapor en esta zona.

Palabras clave: estrés térmico; simulación computacional; ventilación natural; carga térmica; panela.

1 Introduction

The production of non-centrifuged cane sugar (NCS), as defined by FAO [1] and referred to as "panela" in Colombia [2], involves the extraction, purification and concentration of sugar cane juices [3]. This traditional agroindustry holds significant importance in the rural sector of Colombia [4].

Colombia is the second world producer of NCS with 14.9% after India [5,6], and has the highest per capita consumption of panela, with 24 kg/person/year [7]. According to [8] more than 350,000 families participate in cultivation.

The processing and preparation of NCS in Colombia primarly occurs in traditional buildings called trapiches [9], and industrially in NCS honey plants. This activity is carried out one or two days every two or three weeks, when there is enough cane to process. As a result, most of the time workers work in the crops, and adapt better to external conditions than to the environment inside of the agroindustrial facilities.

Workers in this agroindustry generally undertake physically demanding tasks in conditions characterized by high relative humidity (often exceeding 80%), and elevated temperatures inside [10] (Fig. 1). Such working conditions can affect the health and performance of operators [11,12].

How to cite: Cortés-Tovar, G.A., Osorio-Hernández, R. and Osorio-Saráz, J.A., Adaptative comfort modeling for a typical non-centrifugal cane sugar processing facility. DYNA, 91(232), pp. 16-22, April - June, 2024.

a) b)

Figure 1. Exposure of workers to high humidity and temperature conditions in the Pacho Panela installation, a) RGB image, b) thermal image.
Source: Own elaboration

Industrial and agroindustrial workers are at risk of heat stress-related illnesses due to equipment emitting thermal radiation such as ovens and evaporators within facilities [13], psychological effects, reduced productivity, and increased incident rate [14–16].

In order to mitigate this type of adverse situations, bioclimatic architecture offers solutions focusing on suitable environmental conditions for occupants [17], emphasizing parameters of comfort, energy savings and environmental protection [18]. One of the most used bioclimatic and energy simulation tools is the free EnergyPlus™ software [19-21].

Comfort is defined as the mental condition expressing satisfaction with the environment [22], Thermal comfort is influenced by physical parameters such as dry bulb temperature, relative humidity, Average Radiant Temperature, and Air Velocity, and physiological and behavioral factors [23,24]. These factors can affect health, work productivity, and learning ability [25,26].

The adaptive comfort model is based on the principle that people tend to adapt physiologically and behaviorally to restore comfort if a change causes thermal discomfort [27,28]. According to [29] adaptive models show high potential for application in latitudes near the equator; Furthermore, the percentage of hours in which it is possible to use natural ventilation in regions close to the equator is between 50 and 90% of the hours of the year, unlike other regions where the use of natural ventilation is limited by season changes.

The adaptive thermal comfort model included in the ASHRAE 55 standard emerged as a method for buildings with natural ventilation [30,31]. Two ranges are established according to the percentage of occupant acceptability, 80% corresponding to a temperature interval of ± 3.5°C for a typical application and 90% corresponding to a temperature interval of ± 2.5°C [32].

For a healthy work environment, the Colombian Ministry of Labor and Social Security recommends an air temperature between 14°C and 25°C, with relative humidity between 30% and 70% [33].

Currently, no reported studies have evaluated adaptive thermal comfort in agroindustrial plants for the preparation of NCS. Therefore, this study aimed to assess adaptive thermal comfort for workers in a traditional NCS production facility through computational simulation. It also seeks to evaluate different envelope configurations to improve the bioclimatic environment for workers.

2 Material and methods

This study was carried out at the NSC PachoPanela post-harvest facility situated in the municipality of Pacho, Cundinamarca, Colombia (N05°10'59"; W074°09'31", 1858 masl). The average temperature in this region is 20°C [34] and the monthly production of NSC ranges between 1 and 1.5 tons.

The simulation and analysis were conducted throughout the entire year, using an EPW (Energy Plus Weather) climate file. This approach aimed to observe the behavior within the facility over time, considering the daily climatic variations during activities such as grinding, evaporation of juices in the oven and other processes. The different activities and thermal zones inside the facility are show in Table 1.

The geometry of the installation was created using the SketchUp® program, and the Open Studio plugin (Fig. 2), which generated idf type files. The dimensions of this building are 20.30 m wide x 23.50 m long, with an average height of 4.10 m for the cane thermal zones, transit area, boiler, and molding. The oven thermal zone has a height of 6.50 m, and the roof is gabled in galvanized sheet with a slope of 35%.

Table 1.
Activities carried out at the facility during the preparation of NCS.

Thermal zone	Activity	People	Work hours
Cane area	Collection of sugar cane bagasse	1	24
	Grinding and extraction of cane juice	1	24
	Cane grinding	1	24
Transit area	Preparation of work - Intermittent traffic of workers during the work day	1	24
Furnace area	Oven management	1	13
	Removal of floating material from the juice.	1	13
	Evaporation of cane juices	1	13
Boiler area	Boiler feed	1	13
Molding	Molding and packaging	2	13

Source: Own elaboration

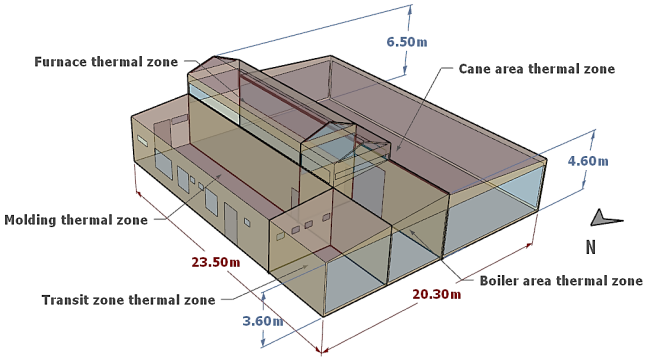

Figure 2. Geometry and thermal zones inside the facility.
Source: Own elaboration

Table 2.
Thermal properties of materials.

Material	λ	P	C
	W m^{-1} °K^{-1}	kg m^{-3}	kJ kg^{-1} °K^{-1}
Brick	1.05	1800	1.00
Wall ceramics	1.05	2000	0.92
Floor ceramics	1.05	2000	0.92
Galvanised steel	55	7800	0.42
Fibercement	0.65	1600	0.84
Clay	0.90	1500	0.92
Wood	0.15	600	1.34
Concrete	1.75	2200	1.00
Mortar	1.15	2000	1.00

λ: Thermal conductivity, ρ: density, C: Specific heat.
Source: Obtained from NBR-15220, (2005) [37] and LabEEE, (2015) [38].

Table 3.
Equipments power and metabolic rates for activities.

Thermal zone	Area	Lightning	Mill motor	Oven	Metabolic Rate
	m^2	W m^{-2}	W	W	W
Cane area	236	0.51	5965.6	-	568
Furnace	73	1.03	-	552706	520
Transit area	29	0.51	-	-	632
Molding	94	3.67	-	-	520
Boiler area	45	1.00	-	-	632

Source: Own elaboration

In each of the three critical work areas (furnace, cane area and molding), an Extech Rth10 humidity and temperature datalogger was installed, brand humidity and temperature dataloggers were installed, with a temperature range of -40 to 70°C, precision of ± 1 °C, relative humidity scale: 0 to 100% RH, with a resolution of 0.1°C, 0.1 HR.

The facility has a gable roof with galvanized zinc tiles, structural masonry walls, and concrete floor. The thermal properties of the composite materials were calculated [35], utilizing the simplified layer method [36]. Table 2 show the thermal properties of the construction materials.

To establish boundary conditions, it is necessary to calculate the heat generated within the construction. This encompasses the heat produced by machines, cooking processes, lighting, and human metabolism.

Table 3 presents the power values for lights, machines, and equipment (boiler), along with the metabolic rates per body surface area of the workers. It is noteworthy that a height of 1.6m^2 was considered [39].

The internal environment of the facility was simulated throughout the year considering various configurations for openings in the perimeter walls and open or closed lantern windows. This aimed to assess the impact of ventilation area variations within the facility. Considering that the

Table 4.
Modeled treatments.

Treatments	Perimeter Enclosure			Lantern Window	
	Open	Solid Brick	Perforated Brick	Open	Closed
T1	X			X	
T2	X				X
T3		X		X	
T4			X	X	

Source: Own elaboration

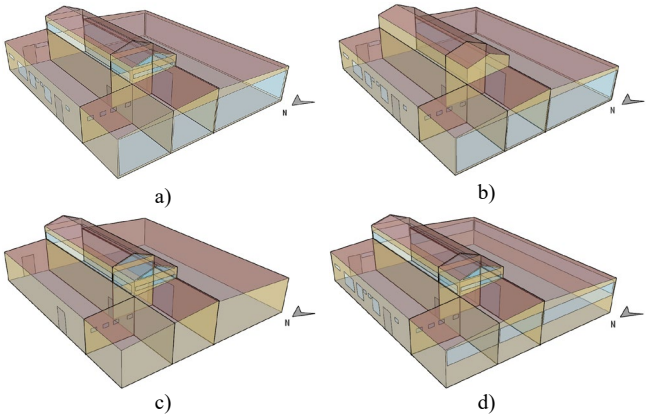

Figure 3. Simulated treatments, a) T1; b) T2 c) T3; d) T14.
Source: Own elaboration

Table 5.
Coefficient A values as a function of air speed.

V_a (m s^{-1})	< 0.2	0.2 - 0.6	0.6 - 1.0
A	0.5	0.6	0.7

Source: Obtained from ASHRAE Standard 55, (2017) [27].

installation's roof is currently made of zinc tile, the model with this roof and characteristics served as the control treatment (T1: installation without perimeter enclosure - open overhead window - zinc tile). The modeled treatments are outlined in Table 4 and Fig. 3.

For this study, the adaptive comfort model proposed by [27], using the eq. (1) to find the value of the operative temperature (T_o).

$$T_o = A \cdot T_a + (1 - A) \cdot MRT \quad (1)$$

Where T_o: operative temperature (°C), T_a: average temperature of the previous month or of the season (°C), A: coefficient as a function of air speed (Table 5), MRT: mean radiant temperature (°C).

The MRT is determined using eq. (2) [39], with the black globe temperature (T_g) and dry bulb temperature (T_{db}).

$$MRT = \sqrt[4]{(T_g + 273)^4 + 0.4 \cdot 10^8 \cdot \sqrt[4]{|T_g - T_{db}|} \cdot (T_g - T_{db})} - 273 \quad (2)$$

Eq. (3) [40] allows us to estimate the black globe temperature from the dry bulb temperature.

$$T_g = -0.9387 + 0.8562 \cdot T_{db} + 0.0162 \cdot {T_{db}}^2 \quad (3)$$

Operating temperature includes MRT, which in this case helps to size the radiant thermal effect of the oven and the ceiling.

The operating temperature represents the climatic conditions to which occupants are relatively adapted and is graphically depicted as the neutral line [27]. Two levels of thermal comfort are established based on the occupant's percentage of acceptability. A comfort band is specified for 80% and 90% acceptability range [41] to operationalize an adaptive equation. Finally, results of the

simulations carried out for each of the four treatments were compared.

The average daily operating temperature for each of the five thermal zones was considered as a variable (T_{oad}). The T_{oad} results were compared with the T_o graphically equivalent to the neutral line, along with the acceptability range of 80% and 90%, for the four treatments.

The agreement between the measured field values and those described by the EnergyPlus™ model (with Treatment 1) was evaluated using the normal mean square error (NMSE) calculated by eq. 4, recommended by the ASTM for the evaluation of indoor air quality models [42].

$$NMSE = \frac{1}{n}\sum_{i=1}^{n}\frac{(Y_{pi} - Y_{mi})^2}{Y_{pi}Y_{mi}} \quad (4)$$

Where $NMSE$: normal mean square error, Y_{pi}: predicted value, Y_{mi}: measured value, n: data number.

A total 151 temperature and relative humidity data were used for the furnace thermal zone, 278 for the cane thermal zone, and 145 data for the Molding thermal zone. The varying data numbers are different in each thermal zone because the activities have different time durations. Values with an NMSE less than 0.25 are accepted as good indicators of agreement. As this value approaches zero, the agreement between the measured and predicted values is greater [42].

Furthermore, a statistical analysis of means was carried out using the Tukey test ($P < 0.05$), to assess if there is a statistical difference between the different treatments or envelope configurations.

3 Results and discussion

Table 6 presents the comparison and validation result through NMSE between the data obtained from the computational model and the experimental data of the control treatment (T1), for the variables temperature and relative humidity. NMSE values < 0.25 show good agreement between the model results and the real data, which means it can represent the actual bioclimatic conditions of the facility, and it is used to accurately predict the environmental behavior of the facility inside.

Table 6.
Comparison of experimental and simulated temperature and relative humidity data.

Thermal zone			Average	NMSE
Furnace	T (°C)	S	25.08 +/- 3.91	
		M	24.90 +/- 3.31	0.00754
	RH (%)	S	73.54 +/- 14.94	
		M	80.17 +/- 8.80	0.03398
Cane area	T (°C)	S	23.02 +/- 3.29	
		M	25.57 +/- 3.93	0.03606
	RH (%)	S	76.44 +/- 13.77	
		M	80.23 +/- 7.91	0.03398
Molding	T (°C)	S	24.74 +/- 2.84	
		M	25.82 +/- 2.97	0.01510
	RH (%)	S	77.60 +/-12.22	
		M	78.69 +/-8.29	0.04726

T: temperature, RH: relative humidity S: simulation, M: measurement.
Source: Own elaboration

Table 7.
Percentage of mean operating temperature data below the upper limit of acceptability 80%.

	T1	T2	T3	T4
Boiler area	87.4	88.5	57.8	85.2
Transit area	99.2	98.4	67.9	95.9
Furnace	0.0	0.0	0.0	0.0
Molding	92.9	90.4	89.3	90.2
Cane area	90.4	83.6	36.4	88.5

Source: Own elaboration

Table 7 shows the percentage of daily mean operating temperature points above and below the 80% upper limit of acceptability for the four treatments, obtained from the simulation.

Table 7 illustrates that a high percentage of data in the four treatments falls within the acceptability range for comfort in the thermal zones: boiler area, transit area, molding and cane area. Treatments with open perimeter exhibit better comfort conditions, while the closed perimeter of solid brick (T3) shows the least favorable performance. In the furnace area thermal zone for all treatments, data surpass the upper limit of acceptability of 80% [32], indicating thermal stress.

Fig. 4 graphically depicts the behavior of operating temperature over time for the 4 treatments, where most of the thermal zones offer comfort to the occupants for the majority of the time; with the treatment with open perimeter and lantern window (T1) providing the best conditions, followed by T2, attributed to a greater natural ventilation area. Special attention must be given to the hygrothermal conditions of workers in the furnace area. Additionally, there is a need to evaluate or improve the design of this area to mitigate heat stress.

As the T_o is contingent on MRT and the average air temperature within each thermal zone, when the perimeter walls are closed (T3), the transfer of energy and mass to the outside decreases. Consequently, the temperature and vapor concentration generated, arising from the evaporation of cane juices from the process, increase a lees favorable condition for the comfort of workers [24].

Similarly, for T4, the reduction in the percentage of days with T_{oad}within the comfort range for the four thermal zones (excluding the furnace thermal zone), results from reduced ventilation caused by the perforated brick enclosure. Despite this, it exhibits more favorable conditions compared to T3.

Table 8 shows means tests for T_{oad} in the five thermal zones across the four treatments, over a one-year period. The reference point considered the average of the values of the upper limit of acceptability (80%) of the comfort band, which is 26.80°C, across all twelve months of the year.

Across all treatments, the thermal zone of the oven exceeds the maximum limit of 26.80°C due to the presence of the oven and the hot vapors of the cane juice. Consequently, this zone does not provide comfortable conditions for workers. The highest value is observed in T2 with a value of 36.28°C. This could be attributed to the closed lantern window in this treatment, which reduces its natural ventilation area compared to T1, and the limited effectiveness of the chimney effect [43], essential for the transfer of energy and vapor mass.

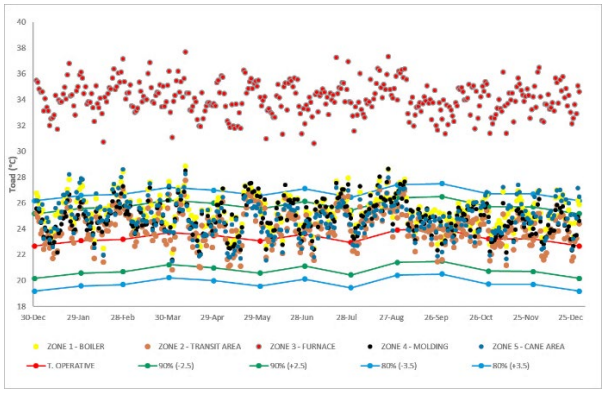

a)

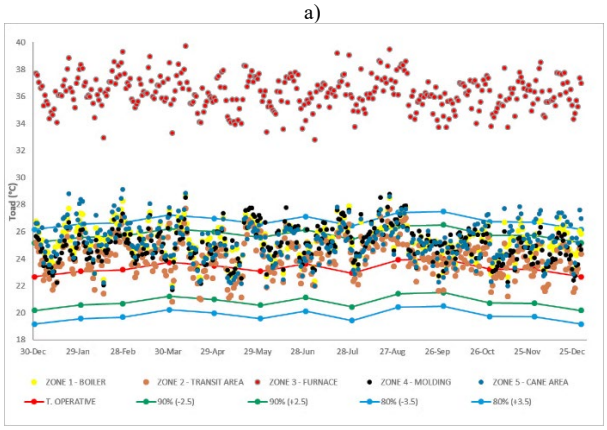

b)

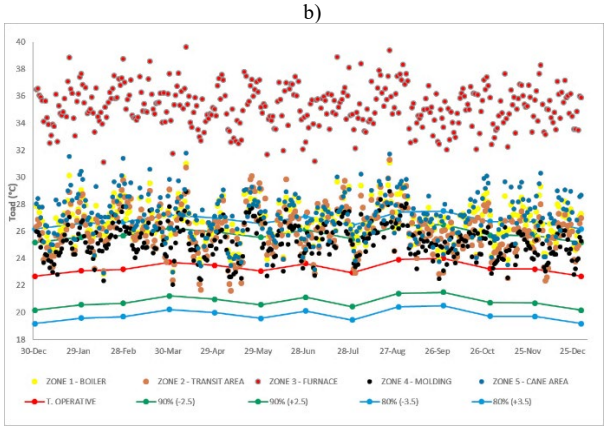

c)

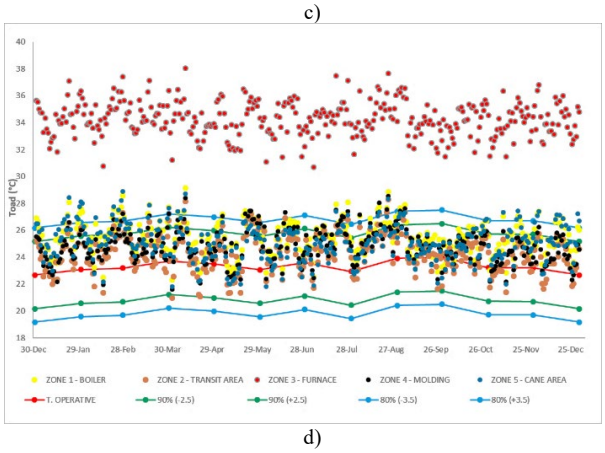

d)

Figure 4. T_{oad} in time compared with the values of T_o during the twelve months of the year in a) T1, b) T2, c) T3 y d) T4.
Source: Own elaboration

Table 8.
Tukey test for T_{oad} in the different treatments.

Zona térmica	n	T1	T2	T3	T4
Boiler area	365	25.30a +/- 1.23	25.22a +/- 1.23	26.67b +/- 1.43	25.44a +/- 1.23
Transit area	365	24.09c +/- 1.33	24.11c +/- 1.33	26.11bd +/- 1.68	24.32c +/- 1.36
Furnace	365	34.09e +/- 1.26	36.28f +/- 1.23	35.24g +/- 1.50	34.26e +/- 1.29
Molding	365	24.85ac +/- 1.28	25.04a +/- 1.31	25.19a +/- 1.27	24.82ac +/-1.27
Cane area	365	24.85ac +/- 1.39	25.29a +/- 1.42	27.07h +/- 1.65	25.07a +/- 1.38

Groups sharing the same letter indicate no significant statistical difference, as determined by the Tukey test with a value of P <0.001 and F = 3803.098.
Source: Own elaboration

To improve thermal comfort in the oven thermal zone, Studies have shown that reducing exposure duration is one way to protect employees against infrared radiation and high temperatures, wearing specialist clothes, such as aluminized garments, and appropriate eye protection, such as infrared-filtered glasses, can help prevent injuries or lessen their severity [44,45].

The values of T3 in general are higher, due to the perimeter enclosure. This treatment stands out as the only one where the cane area thermal zone falls outside average comfort conditions, and the boiler area hovers close to the upper limit of 80%.

As the natural ventilation area of the building decreases, the transfer of energy and vapor mass is reduced. Taking the above into account, heat and mass transfer is more effective in T1.

4 Conclusions

The architectural configuration that presented the best bioclimatic conditions in terms of operating temperature was observed in treatments with open perimeter walls. The best being the one that featuring open lantern window, confirming the importance of the natural ventilation area and the combination of dynamic and thermal ventilation for the rapid evacuation of heat and steam in such installations.

A consistent trend of thermal discomfort among workers in the furnace thermal zone was noted, attributed to the high emissions of heat and steam in the non-centrifuged cane sugar manufacturing process, which suggests that this space should be redesigned to provide a more suitable environment for operators working in this area.

Workers experienced comfortable conditions inside the facilities throughout the year, with the exception of the thermal zone of the furnace.

Acknowledgements

The authors express their gratitude to the Universidad Nacional de Colombia, and to the panela producers, especially the producers of the municipality of Pacho, Cundinamarca, in the “PachoPanela” mill, for their support and for granting permission to gather and utilize information essential for the preparation of this research.

References

[1] Jaffé, W.R., Nutritional and functional components of non centrifugal cane sugar: a compilation of the data from the analytical literature, Journal of Food Composition and Analysis, 43, pp. 194–202, 2015. DOI: https://doi.org/10.1016/j.jfca.2015.06.007.

[2] García, J.M., Narváez, P.C., Heredia, F.J., Orjuela, Á., and Osorio, C., Physicochemical and sensory (aroma and colour) characterisation of a non-centrifugal cane sugar ("panela") beverage, Food Chemistry, 228, pp. 7–13, 2017. DOI: https://doi.org/10.1016/j.foodchem.2017.01.134.

[3] Gutiérrez-Mosquera, L.F., Arias-Giraldo, S., and Ceballos-Peñaloza, A.M., Energy and productivity yield assessment of a traditional furnace for noncentrifugal brown sugar (panela) production, International Journal of Chemical Engineering, 2018, art. 6841975, 2018. DOI: https://doi.org/10.1155/2018/6841975.

[4] Ramírez-Gil, J.G., Characterization of traditional production systems of sugarcane for panela and some prospects for improving their sustainability, Revista Facultad Nacional de Agronomia Medellin, 70(1), pp. 8045–8055, 2017. DOI: https://doi.org/10.15446/rfna.v70n1.61763.

[5] Volverás-Mambuscay, B., González-Chavarro, C.F., Huertas, B., Kopp-Sanabria, E., and Ramírez-Durán, J., Effect of the organic and mineral fertilizer on the performance of sugarcane yield in Nariño, Colombia, Agronomy Mesoamerican, 31(3), pp. 547–565, 2020. DOI: https://doi.org/10.15517/AM.V31I3.37334.

[6] Alarcón, A.L., Palacios, L.M., Osorio, C., César Narváez, P., Heredia, F.J., Orjuela, A., and Hernanz, D., Chemical characteristics and colorimetric properties of non-centrifugal cane sugar ("panela") obtained via different processing technologies, Food Chemistry, 340(August 2020), art. 128183, 2021. DOI: https://doi.org/10.1016/j.foodchem.2020.128183.

[7] Andrade, M., Johanna, M., Torres, G., y Nelson, E., La panela del Catatumbo, una alternativa agroindustrial con perfil Internacional, Revista Espacios [Online]. 41(25), pp. 159–170, 2020. [date of reference December 15th of 2021]. Available at: http://sistemasblandosxd.revistaespacios.com/a20v41n25/a20v41n25p13.pdf

[8] Duarte-Muñoz, M., Torres-González, M.J., Salazar-Beleño, A.M., Carreño-Castaño, L.A., and Pacheco-Valderrama, M.M., Análisis de la situación actual de la industria de transformación de la caña de azúcar en Santander, CITECSA [Online]. 14(23), pp. 31–51, 2022. [date of reference May 08th of 2023]. Available at: https://revistas.unipaz.edu.co/index.php/revcitecsa/article/view/313

[9] Ministerio de la Protección Social de Colombia – MinSalud. Resolución Numero 779 de 2006, del 17 de marzo. Por la cual se establece el reglamento técnico sobre los requisitos sanitarios que se deben cumplir en la producción y comercialización de la panela para consumo humano y se dictan otras disposiciones. Diario Oficial de la República de Colombia N° 46.223 del 17 de marzo de 2006, 2006.

[10] Torres, H.A. y Osorio, R., Evaluación de las condiciones de secado del bagazo usado como combustible en trapiche panelero en el municipio de Nocaima Cundinamarca, en: Congreso Colombiano de Estudiantes de Ingeniería Agrícola CEIA 2020 - Innovación y desarrollo avanzando hacia una agricultura sostenible Bogotá, Colombia, 2020, 28 P.

[11] Amaro, A.L.N., Junior, T.Y., Yanagi, S. de N.M., Ferraz, G.A.E.S., and Campos, A.T., Climate change and rural workers thermal comfort: historical and future impacts, Engenharia Agricola, 38(2), pp. 173–179, 2018. DOI: https://doi.org/10.1590/1809-4430-Eng.Agric.v38n2p173-179/2018.

[12] Habib, R.R., El-Haddad, N.W., Halwani, D.A., Elzein, K., and Hojeij, S., Heat stress-related symptoms among bakery workers in Lebanon: a national cross-sectional study, Inquiry (United States), 58, 2021. DOI: https://doi.org/10.1177/00469580211990517.

[13] Occupational Safety and Health Administration – OSHA, Overview: working in outdoor and indoor heat environments [Online], 2021. [date of reference January 25th of 2022]. Available at: https://www.osha.gov/heat-exposure

[14] Bolghanabadi, S., Ganjali, A., and Ghalehaskar, S., Investigation of thermal exposure in traditional neyshabur bakeries using heat strain and physiological indices, MethodsX, 6(February), pp. 355–359, 2019. DOI: https://doi.org/10.1016/j.mex.2019.02.003.

[15] Instituto Sindical de Trabajo Ambiente y Salud de España – ISTA, Exposición laboral a estrés térmico por calor y sus efectos en la salud. ¿Qué hay que saber? [Online], QAR Comunicación SA, 2019. [date of reference January 25th of 2022]. Available at: https://istas.net/sites/default/files/2019-04/Guia%20EstresTermico%20por%20exposicion%20a%20calor_0.pdf

[16] Roelofs, C., Without warning: worker deaths from heat 2014–2016, New Solutions, 28(2), pp. 344–357, 2018. DOI: https://doi.org/10.1177/1048291118777874.

[17] Dacanal, C., Luz, S.doN., Turco, S.H.N., and Vasconcelos, O.C.d.M., Diagnosis and recommendations for the bioclimatic design of grape packing houses in hot and dry climate, Engenharia Agricola, 38(1), pp. 1–6, 2018. DOI: https://doi.org/10.1590/1809-4430-Eng.Agric.v38n1p1-6/2018.

[18] Chen-Austin, M., Castillo, M., De Mendes Da Silva, Á., and Mora, D., Numerical assessment of bioclimatic architecture strategies for buildings design in tropical climates: a case of study in Panama, E3S Web of Conferences, 197, pp. 1–10, 2020. DOI: https://doi.org/10.1051/e3sconf/202019702006.

[19] Chong, A., Gu, Y., and Jia, H. Calibrating building energy simulation models: A review of the basics to guide future work, Energy and Buildings, 253, art. 111533, 2021. DOI: https://doi.org/10.1016/j.enbuild.2021.111533.

[20] Banihashemi, F., Weber, M., and Lang, W., Model order reduction of building energy simulation models using a convolutional neural network autoencoder, Building and Environment, 207(PB), art. 108498, 2022. DOI: https://doi.org/10.1016/j.buildenv.2021.108498.

[21] Osorio, R.H., Tinôco, I.deF.F., Carlo, J.C., Saraz, J.A.O., and Torres, I.D.A., Bioclimatic analysis of three buildings for wet processing of coffee in Colombia, Revista Facultad Nacional de Agronomia Medellin, 71(3), pp. 8609–8616, 2018. DOI: https://doi.org/10.15446/rfnam.v71n3.64566.

[22] Gao, N., Shao, W., Rahaman, M.S., Zhai, J., David, K., and Salim, F.D., Transfer learning for thermal comfort prediction in multiple cities, Building and Environment, 195(November 2020), art. 107725, 2021. DOI: https://doi.org/10.1016/j.buildenv.2021.107725.

[23] Geng, Y., Ji, W., Lin, B., and Zhu, Y., The impact of thermal environment on occupant IEQ perception and productivity, Building and Environment, 121, pp. 158–167, 2017. DOI: https://doi.org/10.1016/j.buildenv.2017.05.022.

[24] Ma, N., Aviv, D., Guo, H., and Braham, W.W., Measuring the right factors: a review of variables and models for thermal comfort and indoor air quality, Renewable and Sustainable Energy Reviews, 135(August 2020), art. 110436, 2021. DOI: https://doi.org/10.1016/j.rser.2020.110436.

[25] Zhang, S. and Lin, Z., Standard effective temperature based adaptive-rational thermal comfort model, Applied Energy, 264(February), art. 114723, 2020. DOI: https://doi.org/10.1016/j.apenergy.2020.114723.

[26] Hong, T., Kim, J., and Lee, M., Integrated task performance score for the building occupants based on the CO_2 concentration and indoor climate factors changes, Applied Energy, 228(April), pp. 1707–1713, 2018. DOI: https://doi.org/10.1016/j.apenergy.2018.07.063.

[27] ASHRAE. Definitions. Section 3. In: Standard 55 Thermal Environmental Conditions for Human Occupancy. Atlanta, Ga American Society of Heating Refrigerating, and Air Conditioning Engineers, Inc. 2017.

[28] Humphreys, M.A. and Fergus, N.J., Principles of adaptive thermal comfort, in: Sustainable houses and living in the hot-humid climates of Asia, Kubota, T., Rijal, H.B., and Takaguchi, H., Eds., Singapore: Springer Singapore, 2018, pp. 103–113. DOI: https://doi.org/10.1007/978-981-10-8465-2_10.

[29] Bienvenido-Huertas, D., Pulido-Arcas, J.A., Rubio-Bellido, C., and Pérez-Fargallo, A., Influence of future climate changes scenarios on the feasibility of the adaptive comfort model in Japan, Sustainable Cities and Society, 61(June), art. 102303, 2020. DOI: https://doi.org/10.1016/j.scs.2020.102303.

[30] De Dear, R.J., Xiong, J., Kim, J., and Cao, B., A review of adaptive thermal comfort research since 1998, Energy and Buildings, 214, art. 109893, 2020. DOI: https://doi.org/10.1016/j.enbuild.2020.109893.

[31] Hellwig, R.T., Teli, D., Schweiker, M., Choi, J.H., Lee, M.C.J., Mora, R., Rawal, R., Wang, Z., and Al-Atrash, F., A framework for adopting

adaptive thermal comfort principles in design and operation of buildings, Energy and Buildings, 205, art. 109476, 2019. DOI: https://doi.org/10.1016/j.enbuild.2019.109476.
[32] Ferrari, S. and Zanotto, V., Adaptive comfort: analysis and application of the main indices, Building and Environment, 49(1), pp. 25–32, 2012. DOI: https://doi.org/10.1016/j.buildenv.2011.08.022.
[33] Ministerio de Trabajo y Seguridad Social de Colombia. Resolución 2400 de 1979. Por el cual se establecen disposiciones sobre vivienda, higiene y seguridad industrial en los establecimientos de trabajo [Online], 1979 [date of reference October 15th of 2021]. Available at: https://www.alcaldiabogota.gov.co/sisjur/normas/Norma1.jsp?i=53565
[34] IDEAM Atlas Climatológico de Colombia. [Online]. [date of reference June 15th of 2021]. Available at: http://atlas.ideam.gov.co/visorAtlasClimatologico.html
[35] Instituto Nacional de Metrologia Qualidade e Tecnologia - anexo Geral V - Catálogo de Propriedades Térmicas de Paredes, Coberturas e Vidros - Portaria no. 50, de 01 de Fevereiro de 2013 [Online], 2013 [date of reference May 15th of 2021]. Available at: https://www.inmetro.gov.br/consumidor/produtospbe/regulamentos/anexov.pdf
[36] Osorio, R.H., Guerra, L.M.G., Tinôco, I.deF.F., Saraz, J.A.O., and Aristizábal, I.D.T., Simulation of a thermal environment in two buildings for the wet processing of coffee, DYNA, 82(194), pp. 214–220, 2015. DOI: https://doi.org/10.15446/dyna.v82n194.49526.
[37] Associação Brasileira de Normas Técnicas – ABNT, Desempenho térmico de edificações - parte 2: métodos de cálculo da transmitância térmica, da capacidade térmica, do atraso térmico e do fator de calor solar de elementos e componentes de edificações. NBR15220-2, 2005.
[38] Laboratório de Eficiência Energética em Edificações – LabEEE, Florianópolis Universidade Fed. St. Catarina Sd Homepage Laboratório Pesqui. [Online]. 2021. [date of reference May 25th of 2021]. Available: http://www.labeee.ufsc.br
[39] Lamberts, R., and Dutra, L., Eficiência Energética na Arquitetura, 3rd ed. ELETROBRAS/PROCEL, Brazil, 2014.
[40] Abreu, P.G.de, Abreu, V.M.N., Franciscon, L., Coldebella, A., and Amaral, A.G., Estimativa da temperatura de globo negro a partir da temperatura de bulbo seco, Revista Engenharia na Agricultura, 19(6), pp. 557–563, 2011. DOI: https://doi.org/10.13083/reveng.v19i6.273.
[41] Williamson, T., and Daniel, L., A new adaptive thermal comfort model for homes in temperate climates of Australia, Energy and Buildings, 210, art. 109728, 2020. DOI: https://doi.org/10.1016/j.enbuild.2019.109728.
[42] ASTM, American Society for Testing and Materials, Standard Guide for Statistical Evaluation of Indoor Air Quality Models (D5157-91) [Online]. 2002. [date of reference December 15th of 2021]. Available at: http://sistemasblandosxd.revistaespacios.com/a20v41n25/a20v41n25p13.pdf
[43] Baêta, F.C. and Souza, C.F., Ambiência em edificações rurais, 2nd ed. Editora UFV, 2010.
[44] Guerra-García, L.M., Ferreira-Tinôco, I.deF., Osorio-Saraz, J.A., and Osorio-Hernández, R., Thermal comfort in buildings for wet processing of coffee, Revista de Arquitectura (Bogotá), 21(1), pp. 101–111, 2019. DOI: https://doi.org/https://doi.org/10.14718/RevArq.2019.21.2.2597.
[45] Almoosa, A., Asal, A., Atif, M., and Ayachit, S., Occupational eye injury: the neglected role of eye protection, Bahrain Medical Bulletin, 39(2), pp. 82–84, 2017. DOI: https://doi.org/10.12816/0047525.

G.A. Cortés-Tovar, received the BSc. Eng. in Agricultural Engineering in 2010, BSc. Eng. in Civil Engineering in 2013 and MSc. in Construction in 2022, all of them at the National University of Colombia - Bogotá. He has worked in research carried out at Agrosavia between 2010 and 2012, and since 2013 in the execution of engineering projects, carrying out project coordination, cost control, consulting, construction supervision, and in research projects. His research interests include: sustainable buildings, bioclimatic simulation, building energy, environmental comfort and construction materials. He is currently an occasional professor at the Department of Civil and Agricultural Engineering, Faculty of Engineering, at the National University of Colombia - Bogotá.
ORCID: 0000-0001-7141-8218

R. Osorio-Hernandez, received the BSc. Eng. in Agricultural Engineering in 2006 from the Universidad Nacional de Colombia - Medellin, the MSc. degree in 2012, and the PhD degree in Agricultural Engineering from the Universidade Federal de Viçosa – Brazil in 2016. His research areas include: bioclimatic simulation, rural buildings, postharvest, and energy in agriculture. Currently he works in the Universidad Nacional de Colombia - Bogotá, as associate professor in the Department of Civil and Agricultural Engineering.
ORCID: 0000-0002-8698-7234

J.A. Osorio-Saraz, received the BSc. Eng. in Agricultural Engineering in 1998 from the Universidad Nacional de Colombia - Medellin, is Sp in Environmental Legislation in 2001 from the Universidad de Medellin, MSc. degree in Materials Engineering in 2006 from the Universidad Nacional de Colombia – Medellin, PhD. degree in Agricultural Engineering in 2010, from the Universidade Federal de Viçosa – Brazil. Since 2003 Dr. Osorio is professor at the Universidad Nacional de Colombia - Medellin, teaching and rural constructions, computational modeling for livestock housing, air quality and animal welfare.
ORCID: 0000-0002-4358-3600

DYNA
http://dyna.medellin.unal.edu.co/

UNIVERSIDAD NACIONAL DE COLOMBIA

The impact of nanotechnology in achieving sustainable design

Mohamed Saied Ahmed [a], Henar Aboelmaged Kalefa [b] & Hisham Sameh Hussein [a]

[a] Department of Architectural Engineering, Faculty of Engineering, Cairo University, Giza, Egypt. Mkaseem162@gmail.com, drheshamsameh@gmail.com
[b] Assistant Professor, Department of Architectural Engineering, Vice Dean of the Faculty of Engineering, 6th October University, Giza, Egypt. Henar.eng@o6u.edu.eg

Received: August 18th, 2023. Received in revised form: February 27th, 2024. Accepted: March 13th, 2024.

Abstract
In light of the current energy crisis affecting the world, as it constitutes a great economic burden, and with the increase in consumption of natural environment resources, the environment has been negatively affected, which has had a negative impact on human health. Therefore, the problem is summarized in how to achieve environmental sustainability in architecture using nanotechnology. The research used the descriptive analytical approach: the theoretical study presents the concept of sustainability, sustainable design, nanotechnology, nanomaterials, applications of nanotechnology in the field of architecture. An analytical study of one of the existing administrative buildings that achieved sustainability without the use of nanomaterials. Practical study: an applied experiment for one of the thermal insulation nanomaterials, based on the study and attempts to reach accurate results. The practical experience has proven good results in achieving thermal insulation and access to thermal comfort in case of use of nanomaterials in buildings.

Keywords: sustainable design; nanotechnology; nano applications in architecture; energy consumption.

El impacto de la nanotecnología en la consecución de un diseño sostenible

Resumen
A la luz de la actual crisis energética que afecta al mundo, ya que constituye una gran carga económica, y con el aumento del consumo de recursos naturales, el medio ambiente se ha visto afectado negativamente, lo que ha tenido un impacto negativo en la salud humana. Por lo tanto, el problema se resume en cómo lograr la sostenibilidad ambiental en la arquitectura utilizando la nanotecnología. La investigación utilizó el enfoque analítico descriptivo. El estudio teórico presenta el concepto de sostenibilidad, diseño sostenible, nanotecnología, nano materiales. Un estudio analítico de uno de los edificios administrativos existentes que logró la sostenibilidad sin el uso de nano materiales. Estudio práctico: Un experimento aplicado para uno de los nano materiales de aislamiento térmico, basado en el estudio y los intentos de alcanzar resultados precisos La experiencia práctica ha demostrado buenos resultados en el logro del aislamiento térmico y el acceso al confort térmico en caso de uso de nano materiales en los edificios.

Palabras clave: diseño sostenible; nanotecnología; nano aplicaciones en arquitectura; consumo de energía.

1 Introduction

In recent years, a significant impact has emerged from man's exploitation of resources, which hurts the surrounding environment in attempts to repair the resulting damage back the Interest in the concept of sustainability [1,2].

1.1 Overview of studies of previous studies

1.1.1 Architectural studies Adam Ritchie, Randall Thomas 2009

We can design an environmental building with environmentally friendly specifications, such as achieving natural ventilation, and natural lighting, introducing high technology to reduce the heat load on the building and the city, and other things that must be followed when designing buildings, that is, to be environmentally friendly [3].

1.1.2 Architectural study Cama – 2013

She explained the importance of combining the elements of LEED and eco-friendly design. An environment that consumes less energy and adopts the use of technologies associated with instincts helps to feel comfortable and work better [4].

How to cite: Ahmed, M.S., Khalifa, H.A. and Hussein, H.S., The impact of nanotechnology in achieving sustainable design. DYNA, 91(232), pp. 23-32, April - June, 2024.

1.1.3 Architect's studies 2015-Connelly & Dunier & Daniels

The importance of using green walls in architecture, especially interior architecture, as the basic elements for environmentally friendly design, and the importance of having interior architecture live through elements and ideas that depend on integrating architecture with sustainability. [5].

1.2 The concept of sustainability

Linguistic meaning: The origin of the word sustainability sustainer returns. To the origins of the Latin came from term uphold to attribution from below The community starts the foundation From the bottom in construction by its present and future occupants According to the Greek concept [6].

Sustainability: It is the exploitation of resources in the best available ways and capabilities, whether human, material, or natural, in an effective and balanced manner in the environment and urbanization to ensure continued performance without wasting the gains of future generations. [7].

The concept of sustainability at the World Conference on Development and Environment: She is filling the needs of human beings in the present without affecting future generations to meet their needs in the future.

Sustainability is indicative of maintaining operations that are specifically, permanently, and continuously different, as the world progresses and adverse effects on the environment such as global warming. [8].

Sustainability relates to several areas, including economic, social, institutional, and environmental in society, and is considered a means of organizing activities to make society, individuals, and the economy able to meet their needs and correspondence and express their extreme [9].

The most comprehensive definition of sustainability: Sustainable development: is a simple thought, balancing the economic, social and urban objectives of the environment with existing possibilities, and combining two basic principles; They are meeting the needs of the present generation and not infringing on future generations' access to their future requirements; Using natural sources without residues, protecting the natural ocean [10].

1.3 Sustainable design

- It is a design philosophy that seeks to improve the quality of the natural environment and minimize damage to the maximum extent possible in all áreas [11].
- It is a trend in the design of physical and environmental objects and services to comply with the requirements and themes of Sustainability and reducing negative damage to the environment.
- Sustainable design is the term that represents the intelligent application of sustainability principles in engineering and design. These principles apply to architecture and design.
- Maybe identification " sustainable " that is a term used to describe the use of sustainability principles in the design and development of architecture, industry, and various fields.
- It is possible to combine sustainable design and architecture through coordination between the design of buildings and the surrounding environment in a regular relationship in a manner that depends on the design integrated with nature from the environmental perspective and the least exploitation of resources and achieve the greatest benefit to achieve sustainability, which is what results in the concept of environmentally friendly architecture.

1.4 Environmentally friendly architecture

The process of designing buildings in a manner that respects the environment and reduces its energy, materials, and resources while reducing the effects of build on the environment and organizing no harmony with nature.

Principles of environmentally friendly architecture: The building is designed to achieve sustainability in the environment, taking into account all the resources contained in the building, whether materials or energy, to contribute to the needs of the building's users.

1. Energy conservation
2. Climate adaptation
3. Minimize the use of new resources
4. Respect the site
5. Respect for workers and users
6. Overall design
7. Good design

2 Materials and methods

2.1 General principles for designing environmentally friendly buildings

1. Preserving the general health of the population, the surroundings, and the globe unsatisfied in general.
2. Conservation of energy, water, and natural resources.
3. Realization of the concept of sustainability in the building economy in the construction and maintenance of these housing.
4. The use of materials that do not have a negative impact on the environment in their production, whether they are used, maintained, or disposed of.
5. Waste disposal in a way that does not have a negative impact on the environment, and waste treatment to serve the ecosystem [12].
6. Cost saving through recycling and energy production.

2.2 Sustainable building evaluation systems

1. **LEED**: Leadership in energy and Environmental Design Green Building Rating system.
2. **BREEAM**: The Building Research Establishment Environmental Assessment Method.
3. **Green Globes:** Building Environmental Assessment.

Table 1.
Shows the relative weights of the different evaluation systems

Evaluation system	Site sustainability	Energy efficiency	Water efficiency	Materials and resources	Indoor environmental quality
LEED	20%	25%	8%	19%	22%
BREEAM	10%	19%	6%	12.5%	15 %
Green Globes	11.5%	38%	8.5%	10%	20%
CASBEE	15 %	20%	2%	15%	20%
Estidama	6.7%	25%	24%	16%	21%
GPRS	5%	25%	35%	10%	10%

Source: Authers.2024

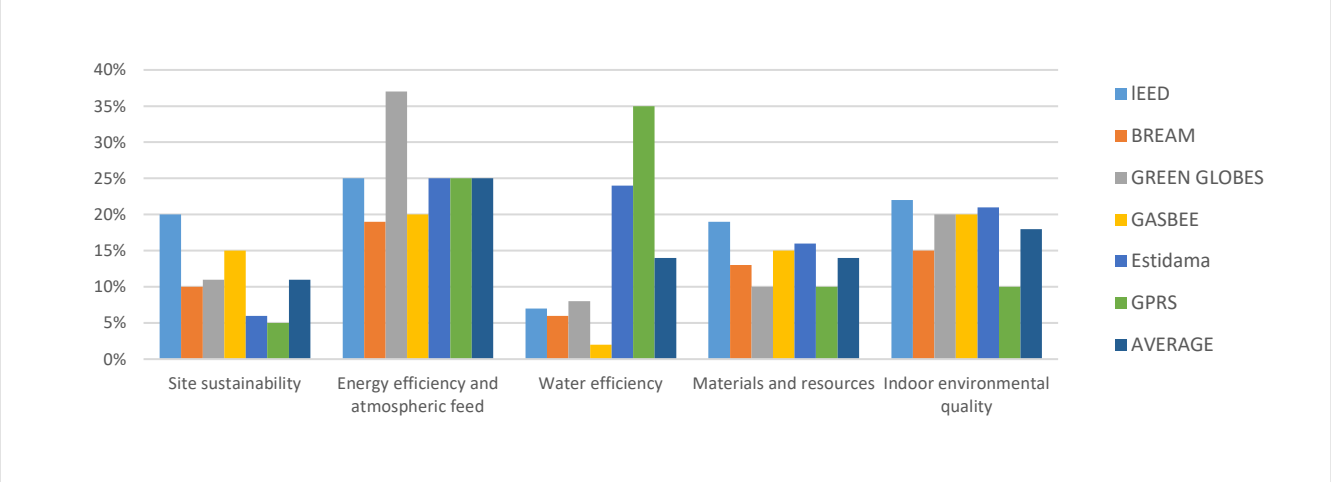

Figure 1. Shows the relative weights of the different evaluation systems.
Source: https://www.wbdg.org/design-objectives/sustainable

1. **CASBEE:** Comprehensive Aassessment System for Building Environmental Efficiency.
2. **GPRS:** The Egyption Green Rating.
3. **Estidama**

When studying the building evaluation systems, it was found that they agree with the basic criteria that must be available in buildings in order to achieve the concept of sustainable buildings: (location — energy efficiency — water efficiency — materials and resources — indoor environment quality) which it becomes clear that: Energy efficiency comes in the first place with the highest relative weights as the in Table 1 and Fig. 1 shows.

It is also followed by the quality of the internal environment in most evaluation systems. Materials and resources follow it. It was found that the water efficiency contradicts the global and local systems in terms of proportions; we find that the global systems gave it.

An evaluation of no more than 8.5%, while the regional systems gave it about 24%, while the local system gave it 35%. The sustainability of the site came at the last level.

From the foregoing, it is clear to us: that the whole world is moving towards the rationalization of energy and water for resources; to improve the indoor environment.

Nanotechnology has shown a tremendous breakthrough in improving the properties of materials and adjusting them to meet the requirements of the environment and achieving sustainability in all fields, especially in architecture, and shows through its impact on buildings to become sustainable and environmentally friendly, so we will expand the search for nanotechnology and its impact to achieve sustainability and its impact on the cost [14].

2.3 Nanotechnology

Nanomaterials:

They are very small particles with two dimensions at the bottom, containing structural components that are smaller than 1 micrometer in one of their dimensions. These materials enable us to provide solutions.

It is a modern technology that has great effects on many sciences and industries, as it adds more applications and functions than its traditional counterparts, and it reduces cost and energy consumption that controlling these properties in creating new materials to complex problems in several areas, including the problems of buildings and facilities.[15].

Goals of green nanotechnology:

1. Producing nanomaterials without harming the environment or human health, and providing solutions to environmental problems in general, and architecture in particular, by integrating the principles of green chemistry. Chemical Green with nanomaterials used in buildings, and making its products non-toxic ingredients. Using less energy, renewable inputs where possible, and using sustainable thinking in the life cycle

in all stages of designing nanomaterials, and making them have the least impact on the environment. [16].

2. It includes products that benefit both the natural and the built environment, either directly or indirectly, and have the ability to clean hazardous waste sites, desalinate water, or treat pollutants.

The impact of nanotechnology :

Nano technique depends on her job of re-ranking atoms materials and of course, whenever the arrangement atomic to the article changes its characteristics resulting in Limit big with development in the properties of materials, nanomaterials showed a significant impact on the materials [17] used in construction as Table 2 show.

Research and studies have proven that traditional buildings have a significant impact on pollution and increased energy consumption, which affects the environment clearly, Fig. 2 shows the impact section built on the environment in the United States of America as indicated by Fig 2.

We find that building nanomaterials and finishes significantly reduce the resulting pollution and contribute clearly to reducing energy consumption. We will address this through the analysis and application of nanomaterials and study their impact on achieving sustainability.

Table 2.
Area the impact of nanotechnology on buildings

Nanotechnology in Architecture	Materials	**Structural materials**	**Non-structural materials Glass**
		Concrete	Glass
		Steel	Plastic
		Wood	Drywall
		New Materials	Roofing
	Protection	Filtration, Air purification Indoor air quality - Outdoor air purification	
		Coatings Self-cleaning - Antibacterial	
		Solar Energy	Reduction of Energy consumption: Lighting; Insulation; VIPS-Aerogel-Thin-film; PCMS
		Electronics / Sensors	
		Energy Production	

Source: Ahmed, Yousra Abdel-Aziz Fadl, Mona Mostafa El-Taher. Concepts and applications of sustainability in residential areas. Sudan University of Science and Technology, 2016.

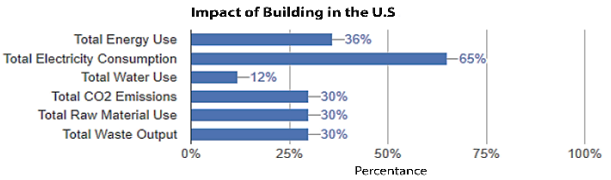

Figure 2. Shows impact of build on the environment USA
Source: [13] https://www.wbdg.org/design-objectives/sustainable

Table 3
The criteria and points of sustainability assessment show the buildings of the study cases.

Evaluation score	Evaluation points	Sustainability standards	
	The basic building system is energy efficient. Reducing emissions of carbon compounds and polluting gases. Reliance on renewable energy. the total	Energy and atmosphere 25%	Environmental criteria 82.5%
	Reliance on recyclable materials. Reuse of resources. Reliance on locally manufactured materials Use of materials with lower emissions the total	Building materials and resources 14%	
	Ventilation quality. Reducing the use of chemicals and sources of pollution Use daylight for flats Thermal comfort the total	Indoor environmental quality 18%	
	Water treatment technologies Waste water recycling Reduce water use the total	Water efficiency 14%	
	No negative impact on the external environment Waste management Rain water management the total	Site sustainability 11.5%	
	Rational consumption of ores and materials Reduce energy cost Reduce maintenance costs. Increasing the life span of the building the total	Standards economical 10%	
	Observance of aesthetic standards Provide convenience to the user Compatibility with modern architecture the total	The standards the social 7.5%	
	Total summation		

Source: Authors.2024

2.4 Analytical studies

Study methodology:

The research aims to: Clarify the impact and effectiveness of the integration of nanotechnology with sustainable architecture.

The application of green Nano architecture in buildings, which in turn leads to raising the efficiency and sustainability of buildings, through an analytical study of some proposed buildings that represent the architecture of the future, taking into account the principles of sustainable design using green nanotechnology.

Analysis and evaluation of selected projects through several points:

1. Building site.
2. Building activity.
3. Description of the building.
4. used nano applications.
5. Investigation unless Sustainability.
6. Evaluate the building using evaluation criteria.

Sustainability Assessment Criteria and Points Study Case Buildings

The Table 3 is the main table based on which the analysis and evaluation of the buildings selected.

Evaluation method:

Buildings will be evaluated with a sign indicating the average percentage to achieve each of the assessment points drawn from the building's description. The conclusion of the average percentage achievement of each standard; access to the final valuation of the building, according to Table 4.

Tablet 4.
Indcates levels of assessment of study case buildings

Unavailable	Weak	Good	Very good	Scales
—	○	◑	●	Code
0 %	1: 30%	30: 60%	60: 90%	Class

Source: Authors.2024.

A sustainable building without the use of nanomaterials

Bahrain Tower-Abu Dhabi

Building analysis:

Building site: Abu Dhabi city.

Construction activity: Administrative building.

Construction activity: Administrative building.

Architect: Aedas Architec.

Category: A building with a sustainable design without the use of nanotechnology.

Description of the building: Each tower contains 29 floors.

The first contains the headquarters of the Abu Dhabi Investment Council, and the second contains the main offices of Al Hilal Bank.

The designer was inspired by the design of the towers from the traditional "mashrabiya" that adorned the windows of traditional Arab houses since the century the14 as Fig. 3 shows.

This clever, geometric design of the mashrabiya provides both shade and privacy, while at the same time allowing for an enclosure external all the time.

Figure 3. Shows Bahrain Towers in Abu Dhabi.
Source: https://content.iospress.com/articles/journal-of-facade-design-and-engineering/fde0040

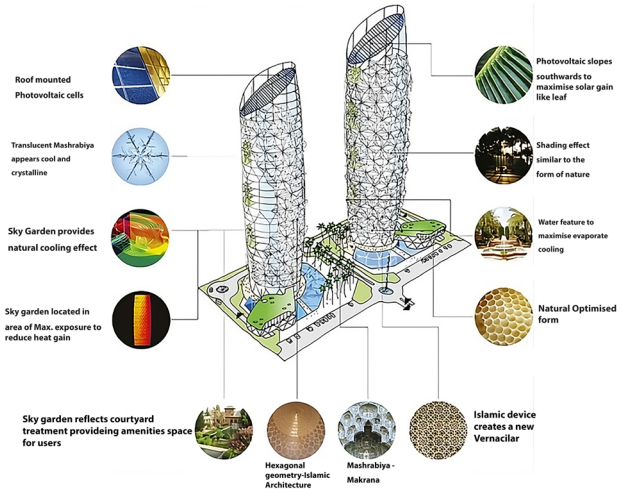

Figure 4: Demonstrates a dynamic Mashrabiya - inspired by the past is an adaptive natural system -Bahrain Towers in Abu Dhabi.
Source: https://content.iospress.com/articles/journal-of-facade-design-and-engineering/fde0040

- The external façade consists of 2,000 elements, all of which resemble the cells of palm tres as Fig. 5 shows.
- This dynamic mashrabiya opens and closes depending on the movement of the sun; which helps reduce heat inside the tower by 50% almost, thus saving a lot of electrical energy consumed by the air conditioner in the hot weather.

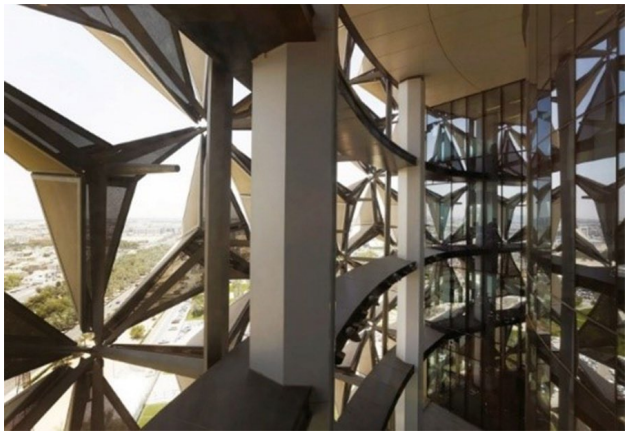

Figure 5: Shows the shape of the mashrabiya from the outside and the inside Source: https://content.iospress.com/articles/journal-of-facade-design-and-engineering/fde0040.

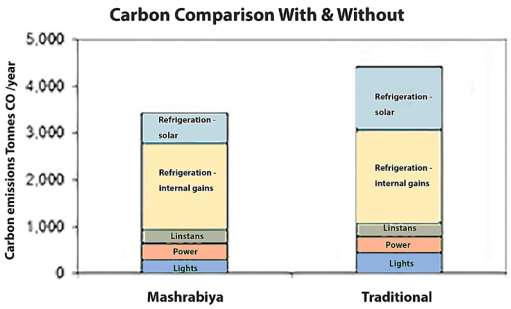

Figure 6. It shows a comparison between the percentage of carbon emissions and waste in the traditional case and the case of using the mashrabiya. Source: MUTEB ALAYAFI, Ahmed Mostafa. "Trends and challenges of smart facades technologies in buildings and the reality of their application in Saudi Arabia (Riyadh as a model) JES. Journal of Engineering Sciences, 50, 5, 2022, 263-283. DOI: 10.21608/jesaun.2022.136177.1134

Table 5.
The evaluation criteria and points are recommended for a Sustainability Bahrain Towers building–Abu Dhabi, Source: researche

Evaluation score	Evaluation points	Sustainability standards	
●	The basic building system is energy efficient.		
◑	Reducing emissions of carbon compounds and polluting gases.	Energy and atmosphere 25%	
◑	Reliance on renewable energy.		
◑	The total		
○	Reliance on recyclable materials.		
○	Reuse of resources.		
○	Reliance on locally manufactured materials	Building materials and resources 14%	
◑	Use of materials with lower emissions		
○	The total		
◑	Ventilation quality.		
◑	Reducing the use of chemicals and sources of pollution		
●	Use daylight for flats	Indoor environmental quality 18%	
●	Thermal comfort		
●	The total		
—	— Water treatment technologies		
—	Waste water recycling	Water efficiency 14%	
—	Reduce water use		
○	The total		
◑	No negative impact on the external environment		
○	Waste management	Site sustainability 11.5%	
—	Rainwater management		
○	the total		
◑	Rational consumption of ores and materials		
●	Reduce energy cost		
○	Reduce maintenance costs.	Standards economical 10%	
○	Increasing the life span of the building		
○	The total		
●	Observance of aesthetic standards		
●	Provide convenience to the user		
●	Compatibility with modern architecture	The standards the social 7.5%	
●	The total		
◑	**Total summation**		

Environmental criteria 82.5%

Source: Authors 2024.

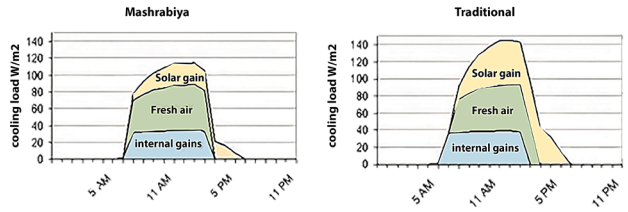

Figure 7. It shows a comparison between cooling in the traditional case and in the case of using the Mashrabiya.
Source: MUTEB ALAYAFI, Ahmed Mostafa. "Trends and challenges of smart facades technologies in buildings and the reality of their application in Saudi Arabia (Riyadh as a model) JES. Journal of Engineering Sciences, 50, 5, 2022, 263-283. DOI: 10.21608/jesaun.2022.136177.1134.

- The ability to provide shade for the building prompted the architects to dispense with the dark glass that obscures external light in all areas at times, and this.
- Worked to save the electricity consumed by lighting during the day.
- It will use a group of Solar panels on the roof to heat the water as Fig. 4 explain.

Nanotechnologies used:
There is no use of nanotechnologies.

Achievements the sustainability: The use of natural materials helped reduce material waste where the Reach rate waste to 30% about buildings, but the team managed the design from scale down level Waste by a large percentage where it came from 3% to 5% in this project as Fig. 6 shows.

Office workspaces have been isolated from the rest of the building, as the use of mashrabia has reduced the energy consumption of those spaces from both lighting loads and cooling loads by up to 50% which has helped to maintain thermal comfort within the building as Fig. 7 shows.

Use solar panels to participate in getting energy in the building, which is used for several purposes, including heating water.

Building evaluation criteria and points: The Table 5 is the main table to evaluation of the building.

<u>Commercial Bank headquarters–Comers Bank Headquarters - Germany</u>:

Building analysis:
Building site: Germany.
Construction activity: Office administrative building.
Architectural: a company Foster + Partners.
Category: A building with a sustainable design without the use of nanotechnology as Fig. 8 shows.

Description of the building: The horizontal projection of the tower in the form of a triangle contains three pillars; they are the office floors and a "trunk" formed by the full-height central courtyard a Fig. 9 shows.

- It applied the idea of gardens in the sky, and these gardens graduated in a spiral form along the tower.
- The gardens will be used to provide natural air to offices overlooking the central courtyard.

The gardens have trees from different vegetation areas, and the type of plants depends on the orientation of the garden where there are 5 gardens in each building.

Figure 8. Building Commercial Bank headquarters- Germany.
Source: Saad Fadi, Adel Al-Kurdi, Commercial Bank headquarters as one of the sustainable buildings, Arab Journal for Scientific Publishing, fourth issue, 2018.

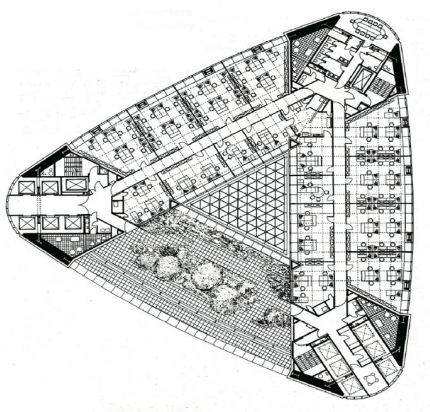

Figure 9. Shows a horizontal projection of the Commercial Bank - Germany
Source: Manghutay, Jalil Ghazaei. "The Design of Administrative Building Based on Climate Considerations: A Case Study in Khuzestan Engineering Systems Buildings." *European Online Journal of Natural and Social Sciences* 4 (2015): 397-407.

Figure 10. It shows the ventilation and lighting openings of the tower, the commercial headquarters bank –in Germany.
Source: Saad Fadi, Adel Al-Kurdi, Commercial Bank headquarters as one of the sustainable buildings, Arab Journal for Scientific Publishing, fourth issue, 2018.

- Building composed of 53 floors It is the tallest building in Europe.
- The design of the building was based on natural ventilation, with the use of mechanical assistance from air conditioners,

used only in harsh conditions. Ventilation and natural lighting are achieved through existing windows located in the perimeter of the building and are controlled using a central computer [22] as Fig. 10 shows.

Principles of green architecture realized in the building: The building was outstanding by applying the principles of green architecture.

1. The building was adopted in its design So that it responds to the direction of wind and solar energy, to ensure optimal ventilation and benefit from the maximum amount of daylight.
2. The triangle shape and central courtyard are designed to help create an area of negative pressure, which drives natural ventilation through the building.
3. The building is designed to be naturally ventilated for 60% of the year, with "sky gardens" allowing natural ventilation during seasons. This approach was expected to reduce energy consumption by up to 50% [23].
4. Provide cooling by cooled ceilings, while heating from ambient heat. The windows are connected to a system BMS to ensure that mechanical ventilation only operates when windows are closed. Where artificial lighting was connected to motion sensors and timers.
5. All wood used in the building is from managed sources. Facilities were provided to separate operational waste and compost waste.
6. Building performance: Studies have shown that the tower actually consumes 20% less energy than expected, and there has been an annual decrease in energy consumption. This is because building users have extended the period of natural ventilation to 85% compared to the 60% designed for i. [24].

Nanotechnologies used: It does not use nanotechnology.

Building Evaluation criteria and points: The Table 6 is the main table to evaluation of the building.

Table 6.
Showing the sustainability evaluation criteria and points of the headquarters building of the Commercial Bank – Germany.

Evaluation score	Evaluation points	Sustainability standards	
◑	The basic building system is energy efficient.	Energy and atmosphere 25%	Environmental criteria 82.5%
●	Reducing emissions of carbon compounds and polluting gases.		
●	Reliance on renewable energy.		
●	The total		
◑	Reliance on recyclable materials.	Building materials and resources 14%	
◑	Reuse of resources.		
○	Reliance on locally manufactured materials		
◑	Use of materials with lower emissions		
◑	The total		
●	Ventilation quality.	Indoor environmental quality 18%	
●	Reducing the use of chemicals and sources of pollution		
●	Use daylight for flats		
◑	Thermal comfort		
●	The total		
○	Water treatment technologies	Water efficiency 14%	
◑	Waste water recycling		
○	Reduce water use		
○	The total		
●	No negative impact on the external environment	Site sustainability 11.5%	
●	Waste management		
◑	Rainwater management		
●	The total		
●	Rational consumption of ores and materials	Standards economical 10%	
●	Reduce energy cost		
◑	Reduce maintenance costs.		
◑	Increasing the life span of the building		
◑	The total		
●	Observance of aesthetic standards	The standards the social 7.5%	
◑	Provide convenience to the user		
●	Compatibility with modern architecture		
●	The total		
◑	**Total summation**		

Source: Authers.2022.

So, the administrative buildings (the subject of the study) that achieve sustainability take a good evaluation in reaching a clean environment with less pollution and achieving comfort for users. Through study and research, we seek to increase production and save energy consumption in accordance with the aforementioned criteria.

As a result, and with the completion of research and studies that appeared recently and were conducted on nanomaterials, which showed their impact on architecture and construction significantly, some materials were tested in the laboratory and applied practically to see the extent of their impact on buildings and their impact on the surrounding environment to prove the validity of the hypothesis search.

Practical experience

Elements of the experiment:

Building bricks - Source of light and heat– Tin oxide nano powder – Resinous substance – Thermal imaging camera.

Experience Goal:

The main objective is to reach a highly transparent heat-insulating material and to conduct the tests necessary to ensure its health and to convert it into liquid material to facilitate its painting on the walls and to study its impact.

Equipment needed for the experiment:

1. Processing of brick molds and start making layers of whiteness (oysters) and paste (such as a founding plate) before placing the final paint of the material as Fig. 11 show.
2. The paint material was prepared in the laboratory by mixing both tin oxide powder and the resin using laboratory mixing devices, and making sure that the powder dissolved completely and turned into a liquid substance that is easy to Paint.
3. Ensure that the surface used to apply the material is clean to ensure correct results.

Steps of the experiment:

1. It was Applied a layer of insulating material for the external faces of the simulation room wall.
2. Using an ordinary lamp as a source of light and heat (simulated natural heat source).
3. Use the heat source to expose the external destination of the room for 6 hours continuously to ensure exposure to a large amount of heat.
4. Using a thermometer to measure from the heat emitted from the used source, measuring the temperature of the destination exposed to the source, and measuring the internal temperature of the wall as Fig. 12 shows.

Figure 11. Explain the stages of preparing the templates used in the experiment.
Source: Authors 2024.

The result of the experiment:

After several experiments and in different ways to use the material and paint it on the model used, and when measuring, it was found that there is a difference in degrees Celsius between the inside and the outside Fig. 13 shows the method of measuring temperature so, it can be used as a heat-insulating paint material, and it achieves good results in reducing energy consumption and achieving thermal comfort. Therefore, it can be used in the exterior paints of the building to give the highest thermal efficiency.

Figure 12. Shows exposing a room sample to lamp heat
Source: Authers .2024

Figure 13. Demonstrates the method of measuring temperature by practical experiment
Source: Authors .2024

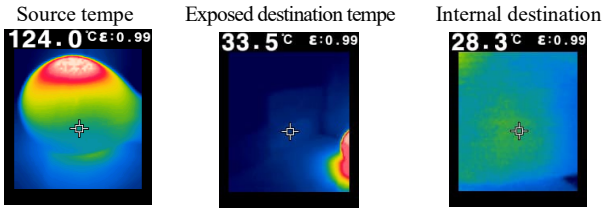

Figure 14: Show the temperature measurements resulting from the experiment.
Source: Authors 2024.

Measurements obtained from the experiment:

The temperatures were measured in the experiment as in Fig. 14. And by analyzing and studying the aforementioned buildings in

the research, when applying the heat insulating material (the subject of the experiment) on the external aspects of the building, it is expected to reduce the amount of heat entering and improve the internal environment of the building by 5.15%, according to the results of the preliminary experiment that was proven according to the mathematical equations calculated from the average temperatures external and internal / number of hours %, which helps greatly in reducing energy consumption in the building.

3 Results and discussions

Therefore, administrative buildings (the subject of the study) that achieve sustainability using nanomaterials are the best ever at reaching a pristine environment with less pollution and convenience for users, helping to increase production and save energy consumption.

The analytical study, according to the proposed assessment of sustainability criteria, showed that nanomaterials greatly improved the property of the building, giving an excellent assessment according to the standards, but that the building used for conventional materials that can preserve the environment has achieved a good assessment according to the standards, which demonstrates the validity of the research hypothesis.

4 Conclusion

Through a theoretical and analytical study of previous buildings, we have come up with:

1. Nanotechnology can be used to develop green architecture avoiding its side effects sunless human and environment; to achieve an integrated framework Sustainability from design, through the use of these materials in construction, to the safe disposal of Nano waste.
2. Nanotechnology has succeeded in showing impressive results practically and theoretically in achieving the principles of sustainability in buildings especially in the field of energy efficiency, material resource utilization, and air purification.
3. Nanotechnology is characterized by adding new properties to materials that help raise energy efficiency and extend the life span of the virtual building. It also works to increase durability and contributes significantly to the application of sustainable design principles.
4. The use of nanotechnology applications in the design process is a radical change in architectural thought, and it helps in the development of architecture and its compatibility with the requirements of the environment significantly.
5. Paying attention to the design of buildings using materials that preserve the health of the users of the building and achieving the concept of sustainability and economy in construction and maintenance.
6. The costs allocated to the building can be saved by recycling some materials or elements and increasing energy production instead of consuming it.

References

[1] Yeang, K., Designing with Nature: the ecological basis for architectural design; McGraw-Hill, NY, USA, 1995.

[2] Abel, C., Architecture & Identity: towards a global eco-culture. Architectural Press, 1997.

[3] Ritchie, A., and Thomas, R., Sustainable urban design: an environmental approach, Taylor & Francis Group, 2009, pp.42-55.

[4] Cama, R., Nature-based design: the new green, Herman Miller, Inc, 2013, pp. 5-6.

[5] Daniels, M., Dunier, D., and Connelley, M., How to use green walls in biophilic design, CitiesAlive, New York City, 2015, 22 P.

[6] WordNet. A Lexical Database for English. [online]. Available at: https://wordnet.princeton.edu/

[7] Adam R., and Randall T., Sustainable urban design: an environmental approach, Taylor, Francis Group, 2009. 22 P.

[8] United Nations, Report of the World Commission on Environment and Development, General Assembly Resolution, 1987, pp. 42-187.

[9] Ahmed, Y.A.-A.F., and Mona, M. El-T., Concepts and applications of sustainability in residential areas. Sudan University of Science and Technology, Sudan, 2016.

[10] Genders S., Transitional Strategies for the Twenty-First Century, UNESCO, UNESCO Publishing Center, Cairo, 1992

[11] Mclennan, J.F., The philosophy of sustainable design - Ecotone - Kansas City Missouri, USA, 2004, 4 P.,

[12] Mohamed, A.S.Y., Nano-Innovation in Construction. A New Era of Sustainability. 2015 International Conference on Environment and Civil Engineering-ICEACE'2015, 2015. DOI: https://doi.org/10.15242/IAE.IAE0415416

[13] WBDG – Whole Building Desing Guide. Sustainable the WBDG Sustainable Committee. OVERVIEW. [online]. Available at: https://www.wbdg.org/design-objectives/sustainable

[14] Moslim, Science Nanotechnology: Nanotechnology and Nano science 2022.

[15] Ramadan, A., et al, The formation of ecological alive interior architecture. Breakout design for workplaces – Case Study, Journal of Engineering and Sustainable Development, 23(2), art. 0015, 2019. DOI: https://doi.org/10.31272/jeasd.23.2.15

[16] Allah, S.A.M.I.H., Towards smart and sustainable architecture using nanotechnology, University of Benghazi, Benghazi, Libya, 2019. ICTS24632019-AC4026

[17] Hashem, E.M., The role of nanotechnology in improving product properties and increasing their shelf life, Journal of Architecture, Arts and Alasania, 8(3-7), pp. 166-186, 2023. DOI: https://doi.org/10.21608/MJAF.2021.65029.2238

[18] Abdulmajid, K., and Ethan, K., Innovations in Dynamic Architecture, Journal of Facade Design and Engineering,3(2), pp. 185-221, 2015. DOI: https://doi.org/10.3233/FDE-150040.

[19] Muteb, A., and Ahmed, M., Trends and challenges of smart facades technologies in buildings and the reality of their application in Saudi Arabia (Riyadh as a model). JES. Journal of Engineering Sciences, 50(5), pp. 263-283, 2022. DOI: https://doi.org/10.21608/jesaun.2022.136177.1134

[20] Al-Kurdi, S.F.A., Commercial Bank headquarters as one of the sustainable buildings, Arab Journal for Scientific Publishing, 4, 2018.

[21] Manghutay, J.G., The design of administrative building based on climate considerations: a case study in Khuzestan Engineering Systems Buildings. European Online Journal of Natural and Social Sciences, 4, pp. 397-407, 2015.

[22] Desing City, Bloomberg headquarters designed by Foster + Partners sets a new standard in sustainable office design. [online]. Available at: https://designcitylab.com/post/architecture/bloomberg-headquarters-designed-by-foster-partners-sets-a-new-standard-in-sustainable-office-design

[23] Arch Daily, Bloomberg's European HQ / Foster + Partners. [online]. Available at: https://www.archdaily.com/882263/bloombergs-european-hq-foster-plus-partners

[24] Architects' Journal. Building study: Foster ramps it up at Bloomberg, [online]. 2017. Available at: https://www.architectsjournal.co.uk/buildings/building-study-foster-ramps-it-up-at-bloomberg

M.S. Ahmed, is a BSc. in Fine Arts, Department of Architecture, Helwan University in 2016, and holds a MSc. in Raising the efficiency of administrative buildings through nanotechnology applications within the framework of sustainability, from Cairo University, Sp. in Building Technology in 2020, and a Dr. student in the Department of Architectural Engineering, Cairo University.
ORCID: 0009-0001-0326-0532

H.A. Kalefa, is Associated professor at Faculty of Engineering in 6 October University, Egypt.
ORCID: 0009-0009-4220-3205

H.S. Hussin, is a Professor of Architecture at Department of Architectural Engineering at Faculty of Engineering, Cairo University.
ORCID: 0009-0007-1499-2695

DYNA
http://dyna.medellin.unal.edu.co/

UNIVERSIDAD NACIONAL DE COLOMBIA

Influence of input variables on the unitary deformation experienced in pipes subjected to the action of lateral loads

Julián Francisco Gamba-Gómez [a], Yaneth Pineda-Triana [a], Daniel Mauricio Bermúdez-Rincón [a] & Osmar Albert Gamba-Gómez [b]

[a] *Facultad de Ingeniería, Universidad Pedagógica y Tecnológica de Colombia, Tunja, Colombia. julian.gamba@uptc.edu.co, yaneth.pineda@uptc.edu.co, daniel.burmudez01@uptc.edu.co*
[b] *Facultad de Ciencias y Tecnología, Universidad Santo Tomas, Bogotá, Colombia. osmar.gamba@usta.edu.co*

Received: October 6th, 2023. Received in revised form: February 9th, 2024. Accepted: March 14th, 2024.

Abstract
The hydrocarbon transportation industry uses extensive pipeline networks subject to complex loading conditions. The finite element analysis (FEA) has proven to be effective in simulating the deformation behavior in these pipelines, which assists in the assessment of their integrity and risks. In this work, a model developed using finite elements is proposed to analyze the behavior of API 5L Gr B carbon steel pipes, subject to internal pressure and lateral loads. The model is validated through uniaxial tensile and four-point bending tests. In addition, parametric analysis is carried out considering variables such as diameter, lateral load, and distance between supports. The objective is to identify which one of these variables has the most influence in the unit strain. The results indicate that the unit strain obtained from the numerical model agrees with the experimental tests. Furthermore, it is concluded that the diameter is the influential parameter.

Keywords: pipelines; bending moment; risk assessment; integrity pipeline.

Influencia de las variables de entrada en la deformación unitaria evidenciada en tuberías sometidas a la acción de cargas laterales

Resumen
La industria del transporte de hidrocarburos utiliza extensas redes de tuberías sometidas a condiciones de carga complejas. El análisis por elementos finitos ha demostrado ser efectivo para simular el comportamiento de deformación en estas tuberías, lo que ayuda en la evaluación de su integridad y riesgos. En este trabajo, se propone un modelo desarrollado mediante elementos finitos para analizar el comportamiento de tuberías de acero al carbono API 5L Gr B, sujetas a presión interna y cargas laterales. El modelo se valida mediante pruebas experimentales de tensión y flexión de cuatro puntos. Además, se realiza análisis paramétrico considerando variables como diámetro, la carga lateral y distancia entre soportes. El objetivo es identificar cuál de estas variables influye más en la deformación unitaria. Los resultados indican que la deformación unitaria obtenida del modelo numérico concuerda con las pruebas experimentales. Además, se concluye que el diámetro es el parámetro influyente.

Palabras clave: tuberías de transporte; momento flector; evaluación de riesgo; integridad de tuberías.

1 Introduction

Hydrocarbon transportation pipelines are one of the most economical means used to carry out this type of activities [1] (ASME, 2010). Due to the flexibility during the construction process, it is common to manufacture transportation networks that extend over large lengths [2] (Ellenberger, 2010), crossing different geographies during its transit that can range from flat terrain to undulating and high mountain terrain. Due to the heterogeneity in geography, it is common for lines to be subjected to complex vertical, lateral, and axial load conditions added to the internal pressure used for transportation [3] (Ozkan & Mohareb, 2009), these loads can generate unplanned deformations in the pipes. It is estimated that about 23% of the failures that have occurred in pipelines in the United States in the last 20 years are associated with these types of loads [4] (Ahn et al., 2016).

How to cite: Gamba-Gomez, J.F., Pineda-Triana, Y., Bermudez-Rincon, D.M. and Gamba-Gomez, O.A., Influence of input variables on the unitary deformation experienced in pipes subjected to the action of lateral loads. DYNA, 91(232), pp. 33-40, April - June, 2024.

The application of lateral and axial loads in pipes can generate local collapse of the structure [5] (Bazhenov et al., 2016), this behavior depending on the characteristics of the phenomenon and the function for which the component is intended, can compromise its structural capacity (Li et al., 2017), generating damage such as wrinkles, ovals, and cracks among others [6] (Antaki, 2005).

It has been shown that the diameter and magnitude of the applied load are some of the parameters that influence the result of strain and stress experienced by the material [3] (Ozkan et al., n.d.), these parameters being of interest for the operation, design and integrity management [1] (ASME, 2010) sites in which environmental conditions occur that facilitate the application of external loads.

The finite element technique (FEA) in which plastic behaviors of the material are included is suitable for simulating pipes subjected to various loading situations [7] (Cai et al., 2018), it is important to emphasize that when large deformations occur, the material hardening model must consider strain hardening [4] (Ahn et al., 2016), whether general or local.

The present work proposes a numerical model based on the finite element technique, which considers non-linear behaviors in terms of material, geometry, and contacts. The objective of the analysis focuses on taking as input parameters the diameter of the pipe, the magnitude of the applied load and the distance between supports and evaluating which of them has the greatest impact on the unit strain results obtained.

The proposed FEA model is validated through uniaxial tension and four-point bending results. The identification of the relevance of parameters is carried out through the development of an experimental design, based on the response surface technique, which takes as input data the results obtained from the FEA model for the sample points defined in the experimental design.

2 Materials and methods

For the development of the FEA model, the ANSYS v 2023 R2 software in its academic version was used. The developed model uses 3D type elements to perform the discretization, considering nonlinearities of the material type, contacts, and geometry, in order to reduce the computational cost of the solution, it was contemplated to evaluate a quarter of the geometry, including symmetry conditions in the X and Z axes for this purpose. As strategies for stabilization and convergence of the solution, low-stiffness springs were included and the number of loading steps and substeps was adjusted [8] (Nazemi, 2009).

2.1 Finite element model

The developed FEA model considers the geometry used during a four-point bending test [16], including the pipe under analysis, a set of rollers that supports the pipe and another that applies the load. The length of the pipe considered was 6 times the diameter of the pipe, with a view to avoid the end effect.

For the discretization of the model, solid elements of the SOLID 186 type [9] (ANSYS, 2022b) were used. These elements allow six degrees of freedom and within their formulation they consider the effects of nonlinearities associated with material, contacts, and geometry.

The numerical model developed considered a mapped type of mesh with refinements in the load application zones and boundary conditions. The mesh used included a total of 24,884 nodes associated with 4,364 elements. In order to guarantee the results obtained are independent of the discretization used, skeweness was used as a metric, obtaining values of 0.004826 m the worst case.

2.2 Loading and boundary conditions

The load application was carried out through two steps (Li et al, 2017) (Wang et al, 2021) [10,11], the first step considers the application of a pressure of 8.27 Mpa on the internal face of the pipe , together with the displacement in the -Y direction of the load application roller, the second step considers the application of a displacement in the +Y direction of the load application roller, which frees the pipe from the action of the lateral load.

As a boundary condition, a Fixed support type constraint [12] (ANSYS, 2022a) was applied to the load support roller. This condition does not allow the displacement or rotation of any degree of freedom. The constraint remained constant during the two load application steps (Shuai et al, 2020) [13]. In order to facilitate the convergence of the model, low stiffness springs were included during all load application steps.

2.3 Material parameters

The material used considers the properties of an API 5L Gr B steel, under a multilinear type of isotropic hardening model [14] (Kamaya, 2014), the stress-strain data considered were taken from tests of tension carried out on specimens made of this material. To assure the behavior of the material fits the input data, tests were carried out in the software considering the same geometry of the tension test (Tee, 2020) [15].

2.4 Model Calibration

Model validation was carried out using the results of a four-point bending test, the geometry considered for the development of the tests [16] is presented in Fig 1. The simulation point selected to validate the model corresponded to a pipe diameter of 0.1016 m, lateral displacement of 0.09 m, distance between supports of 0.6 m, thickness of 0.003048 m, and API 5L Gr B carbon steel, the axial deformation at the point indicated in Fig 2 was considered as the output variable. The selection of the values for the validation point considered the ease of acquiring the material for the manufacture of the specimens, characteristics of the equipment available in the laboratory and typical configurations found in hydrocarbon distribution networks.

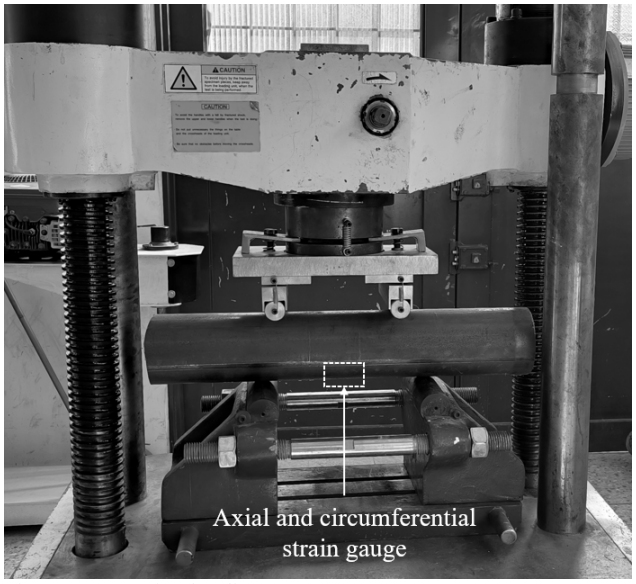

Figure 1. Four points bending-test
Source: The author

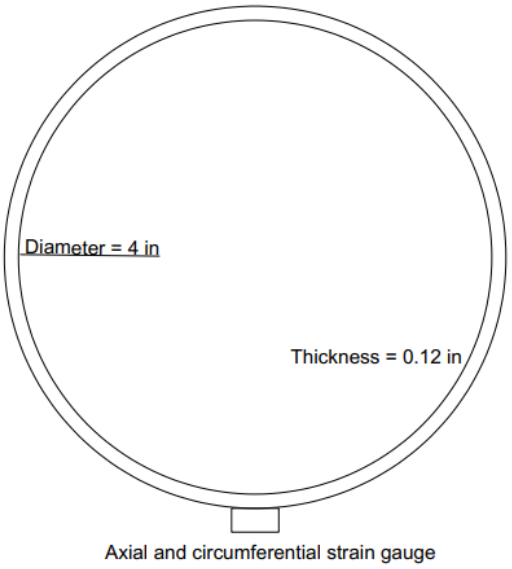

Figure 2. Deformation measurment configuration
Source: The author

The output graphs are expressed in terms of lateral displacement vs evidenced deformation, in each of the positions described in Fig 2.

The deformation measurements were carried out using a deformation measurement device, the assembly was built with two (2) type K strain gauges, one for the measurement of the circumferential strain and another for the measurement of the axial strain, as presented in the Figs. 2, 3.

The electronic device for measuring deformation includes a Wheaston bridge, coupled to a Raspberry 4.0 card to capture, store, and process the information coming from the gauges. This information is stored and presented through an interface developed in Python. The developed scheme is presented in Figs. 3 and 4.

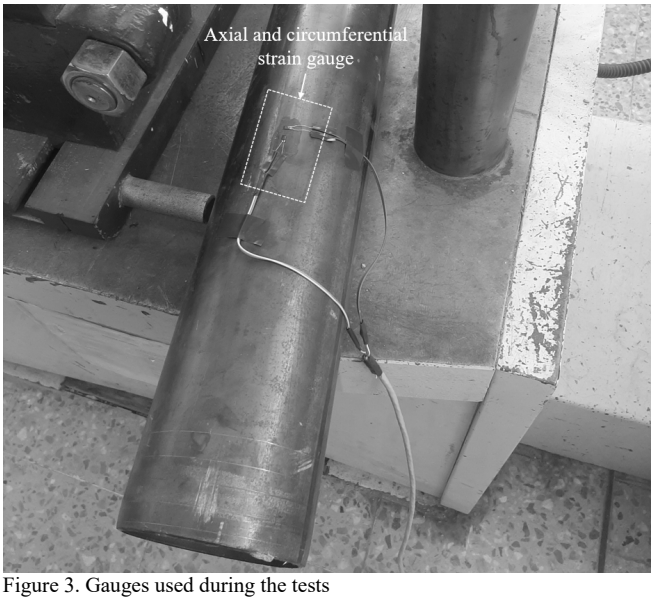

Figure 3. Gauges used during the tests
Source: The author

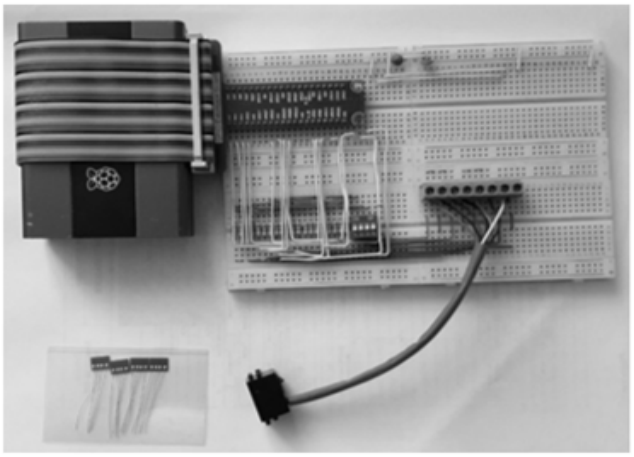

Figure 4. Electronic Setup to obtained signal from sensors
Source: The author

The measuring device was calibrated through tension tests carried out on a Shimadzu UH500 KNI universal machine, in which a flat probe 40 cm long, 2 cm wide and 0.30 cm thick and a load application speed of 5 mm/minute were placed [17]. A strain gauge was placed in the specimen to measure the deformation in the direction of load application in parallel with the extensometer Shimadzu TYPE STRAIN SG 50 – 50. To have additional data to perform the numerical validation of the model, the test described above was developed using a numerical model, in which the geometry was developed and meshed using the same type of solid elements and considering the same material model, graphs of the test setup and its numerical equivalent are presented in Fig 5.

From the graphs obtained, it can be seen how the results obtained from the numerical model are consistent with those reported in the experimental test, which allows the validation of the developed model.

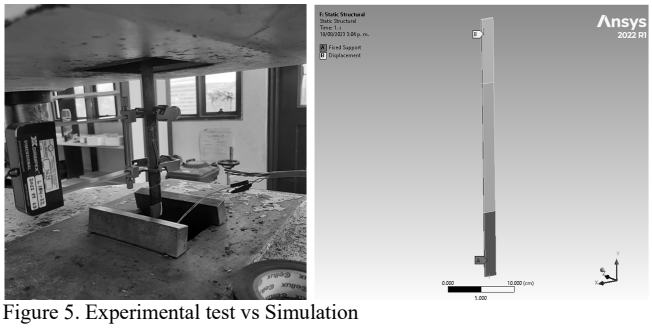

Figure 5. Experimental test vs Simulation
Source: The author

Table 1.
Experimental design range.

Diameter V1 [m]	0.0508	0.1016	0.2032
Lateral Distance V2 [m]	0.03	0.06	0.09
Axial Distance V3 [m]	0.3	0.45	0.6

Source: The author

2.5 Experiment design

In order to analyze which of the geometric parameters is most relevant when bending deformation phenomena occur, the following variables of interest were selected for the present study: magnitude of the applied lateral load, distance between the supports and diameter of the pipe. From these variables, an experimental design of the response surface type was carried out, having the values described in Table 1 for each of the variables.

The ranges of the variables presented were selected to obtain output data that are in the plastic zone of the material, without reaching the ultimate breaking stress, this so that the output data can be used to make comparisons with real pipeline operation cases. In addition to this, there was a maximum distance of 10 cm as a restriction for lateral displacement, due to the support available for the execution of the four-point bending test.

3 Results

3.1 Model validation

The model validation results are presented for the tensile test and the result of the four-point bending test.

3.1.1 Tensile test results

The Fig 6 shows the deformation results obtained for the tension test and the respective numerical model. The graph shows how the two results present similar linear behaviors. It is important to indicate that a slight difference is seen in the results of stress in the area close to the yield stress, this is because the model considers the local plasticization phenomenon that can occur once the proportional limit is exceeded, forming transient Luder's bands [18].

The curve presented in Figure 6 was constructed from the displacement and force data measured in the universal machine, as described in eq. (1)(2), these values are transformed into true stress and deformation according to eqs. (3)(4).

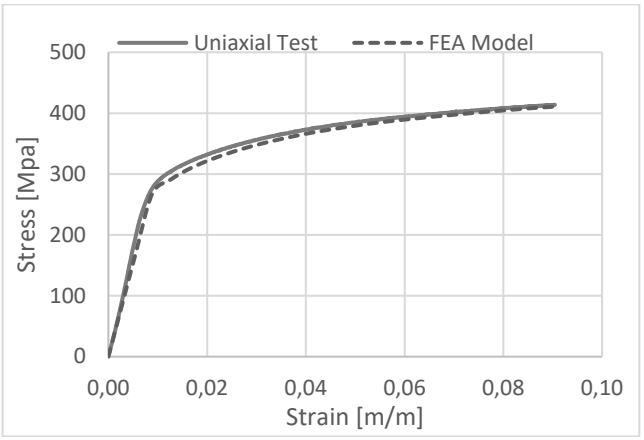

Figure 6. Deformation Test vs Numerical Model
Source: The author

$$\sigma_{Eng} = \frac{F}{A_{Ini}} \quad (1)$$

$$\varepsilon_{Eng} = \frac{\Delta L}{L_{Ini}} \quad (2)$$

$$\sigma_{real} = \sigma_{Eng} * \left(1 + \varepsilon_{Eng}\right) \quad (3)$$

$$\epsilon_{real} = ln\left(1 + \varepsilon_{Eng}\right) \quad (4)$$

Where σ_{Eng}, ε_{Eng} correspond to the engineering stress and deformation, σ_{real} and ϵ_{real} correspond to the real stress and deformation.as well as A_{Ini} and L_{Ini} correspond to the area and initial lengths of the specimens.

In the case of the numerical model developed using the finite element technique, it calculates the displacements according to eq. (5)

$$F = K * u \quad (5)$$

Where F corresponds to the external force matrix, K to the global stiffness matrix of the structure and u corresponds to the nodal displacement matrix. For cases in which there are non-linearities; Whether geometric, contact or material, the stiffness matrix is not constant and varies with displacement, the solution of this type of systems is obtained through an iterative series of linear approximations.

3.1.2 Four-point bending test results

The Fig 7 presents the configuration of the numerical model, loads and restrictions, and Fig. 8 describes the location of the point for deformation measurement.

The comparison between the results of the numerical model and those obtained from the experimental setup are presented in Fig. 9. In the case of the experimental results, the curve presented was constructed from the data of lateral displacement vs longitudinal deformation measured by the strain gauges, these same quantities were taken from the numerical model. It is important to mention that the quantities described were selected, taking into account that they are the primary data obtained from the sensors installed during the test execution.

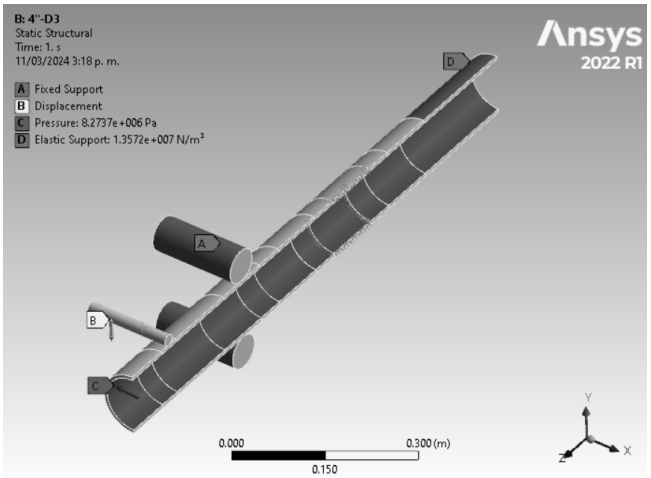

Figure 7. Numerical model configuration
Source: The author

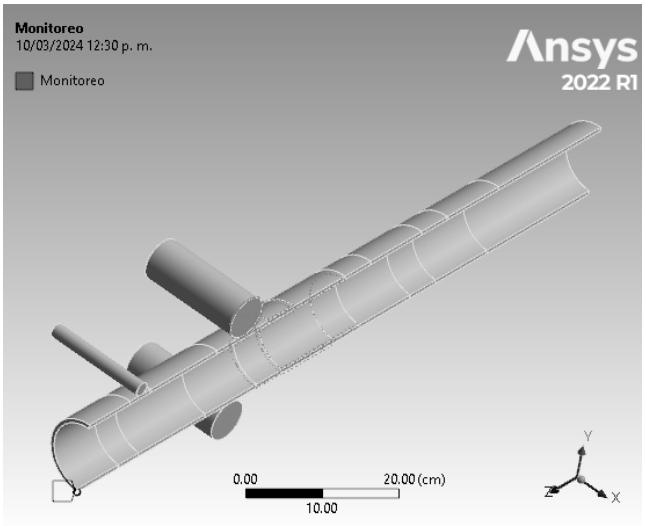

Figure 8. Deformation measurement point
Source: The author

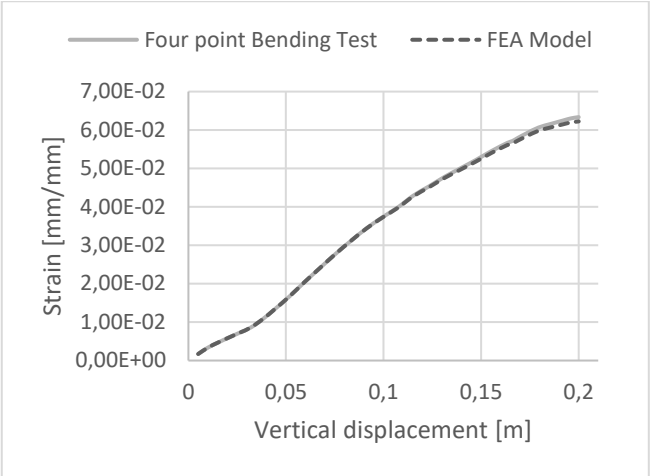

Figure 9. Unitary Deformation
Source: The author

From the results obtained, a similar behavior can be seen in both cases. This observation allows us to corroborate the coherence between the results, thereby validating the behavior of the numerical model [23-25]. During the development of the analysis, it was evident that the maximum error does not exceed 7% and this is in the middle region of the plasticity zone, the difference between the numerical values and the experimental ones in this zone can be associated with the capacity of deformation of the adhesive used to fix the gauges to the base metal [21], which can have a lower deformation rate than that of the base metal, especially for considerable deformations.

3.2 Experimental design results

The results obtained from the FEA numerical model for the four-point bending test, considering the variables, ranges and nomenclature defined in Table 1, are presented in Table 2 in terms of strain (E1) and principal stress (S1). From the data presented, it can be seen the ultimate tensile strength of the material was not exceeded considering the limit values defined in API 5L for a Gr B steel [20] (API, 2013).

When verifying the results presented in Table 2, it can be seen how the highest stress results are presented for diameters of 0.0508 m, with values close to 339.8 Mpa, this value is above the yield point of the material (248 Mpa) [20] (API,2013) but well below the ultimate tensile strength of the material (415 Mpa)[20](API,2013), for the case of 0.1016 m the stress is reduced on average by about 10%, presenting a similar behavior with respect to the yield limits and ultimate strength described. Finally, the lowest stress occurred for diameters of 0.2032 m which the average value is very close to the yield limit of the material. The stress and deformation results presented correspond to real values.

Table 2.
Principal Strain and Stress.

V1 [m]	V2 [m]	V3 [m]	E1 [m/m]	S1 [MPa]
0.0508	0.03	0.3	1.67E-03	333.7
0.0508	0.03	0.45	1.66E-03	332.5
0.0508	0.03	0.6	1.64E-03	327.6
0.0508	0.06	0.3	1.69E-03	338.1
0.0508	0.06	0.45	1.70E-03	339.0
0.0508	0.06	0.6	1.68E-03	336.6
0.0508	0.09	0.3	1.67E-03	333.7
0.0508	0.09	0.45	1.70E-03	339.7
0.0508	0.09	0.6	1.70E-03	339.8
0.1016	0.03	0.3	1.43E-03	285.4
0.1016	0.03	0.45	1.61E-03	321.7
0.1016	0.03	0.6	1.65E-03	329.3
0.1016	0.06	0.3	1.51E-03	301.1
0.1016	0.06	0.45	1.67E-03	333.9
0.1016	0.06	0.6	1.71E-03	341.9
0.1016	0.09	0.3	1.52E-03	304.7
0.1016	0.09	0.45	1.66E-03	332.4
0.1016	0.09	0.6	1.72E-03	344.4
0.2032	0.03	0.3	3.11E-04	62.2
0.2032	0.03	0.45	5.45E-04	109.0
0.2032	0.03	0.6	7.49E-04	149.8
0.2032	0.06	0.3	1.02E-03	204.5
0.2032	0.06	0.45	1.25E-03	250.8
0.2032	0.06	0.6	1.39E-03	278.6
0.2032	0.09	0.3	1.49E-03	297.8
0.2032	0.09	0.45	1.62E-03	323.7
0.2032	0.09	0.6	1.66E-03	331.9

Source: The author

Table 3.
ANOVA results

Source	DF	Adj SS	Adj MS	F-Value	P-Value
Model	6	0.000003	0.000001	44.58	0
Linear	3	0.000003	0.000001	69.41	0
V1[m]	1	0.000002	0.000002	125.97	0
V2[m]	1	0.000001	0.000001	69.23	0
V3[m]	1	0	0	13.02	0.002
2-Way Int	3	0.000001	0	25.92	0
V1[m]*V2[m]	1	0.000001	0.000001	71.66	0
V1[m]*V3[m]	1	0	0	5.76	0.026
V2[m]*V3[m]	1	0	0	0.34	0.567
Error	20	0	0		
Total	26	0.000004			

Source: The author

To establish in greater detail, the relevance of the factors considered together with their interaction, ANOVA analysis was carried out on the results obtained. The analysis data are presented in Table 3, having a significance level of the test of 0.05.

For the data presented, the quantity Adj SS corresponds to the sum of squares, Adj MS corresponds to the sum of the mean square, F-Value corresponds to the statistic of a Fisher test, understood as the variance between the measurement of the samples/variation within of the samples and P-Value corresponds to the probability of obtaining a value equal to or greater than the one observed [22].

From the data presented in Fig. 9 and Table 3, it can be seen the parameter that has the greatest relevance on the principal strain value obtained is the diameter of the pipe. Likewise, it was evident that the interaction between the diameter and the magnitude of the lateral displacement is the second most relevant factor the lateral displacement as the third factor and distance between supports as fourth factor. It is important to mention that both the interaction and the magnitude of the lateral displacement have similar orders of magnitude. Finally, the combination of diameter/distance between supports is the interaction with the least relevance, the interaction between the magnitude of the lateral load and the distance between supports has no significant relevance in the strain result.

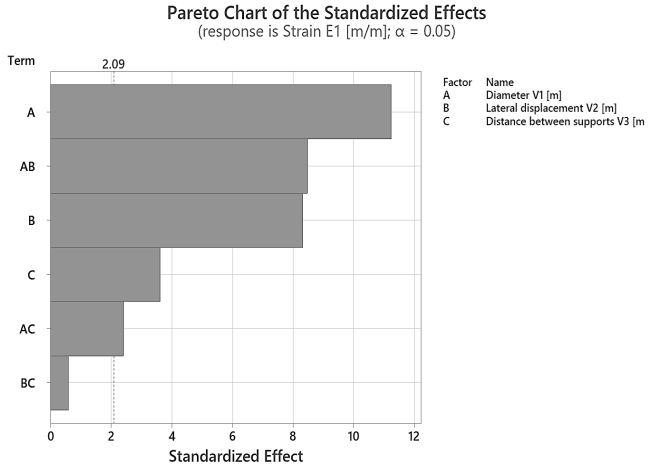

Figure 9. ANOVA results
Source: The author

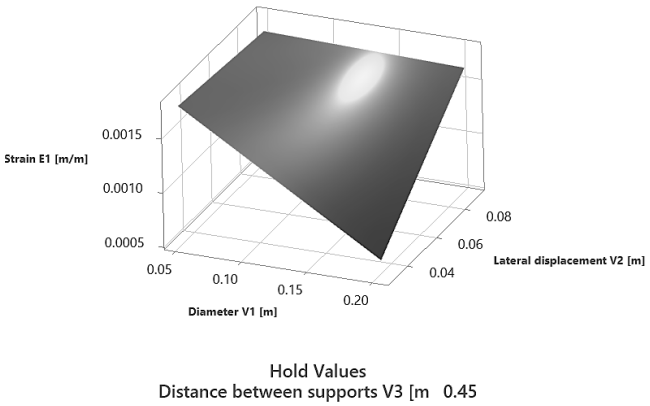

Figure 10. Strain as diameter and lateral displacement
Source: The author

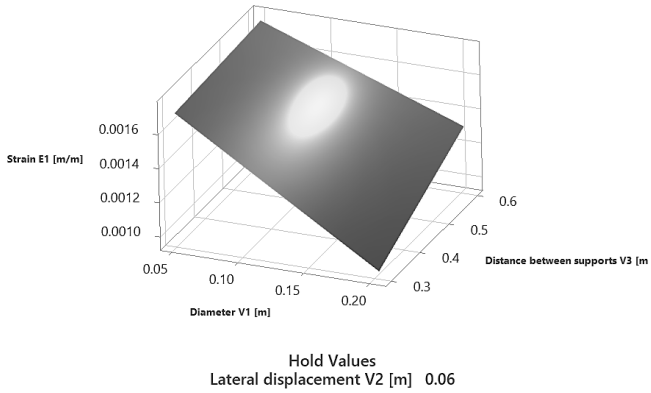

Figure 11. Strain as function of diameter and lateral desplacement
Source: The author

The Fig. 10 shows the response surface obtained for the strain as a function of the diameter of the pipe and the magnitude of the lateral displacement. In the Figure it can be seen how the lowest strain values are obtained for larger diameters and low magnitudes of lateral displacement, the magnitude of the strain increases as the diameter decreases and the lateral displacement increases, the influence on the strain result being more representative for increases in diameter. Likewise, a quadratic behavior can be seen in the strain result as the two parameters increase simultaneously.

Regarding the behavior of the effort when the diameter of the pipe and the distance between supports are taken as input parameters, the response surface obtained is presented in Fig. 11, a linear behavior in the growth of the effort was evident as the diameter decreases and the distance between supports increases, the interaction between the two input parameters exhibits linear behavior for the entire range of values considered.

Finally, the behavior of the principal strain as a function of the lateral displacement and the distance between supports is presented in T 12, in which linear increases in the strain can be seen as the input parameters are varied. In this case, it is important to mention that the relevance of the interaction between the input parameters is not significant.

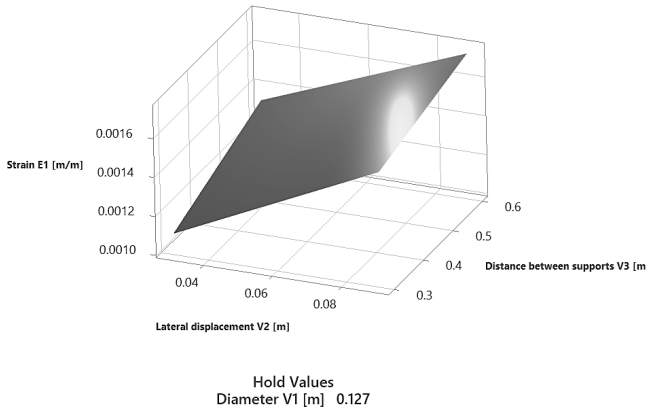

Figure 12. Stress as function supports and lateral displacement
Source: The author

4 Conclusions

The present analysis studies the influence of factors such as the diameter of the pipe, the magnitude of the applied transverse load and the distance between supports on the level of strain that can be evidenced in a pipe. A numerical model was developed using the finite element technique to analyze the phenomenon; the results were validated through experimental uniaxial tension and four-point bending tests. Finally, on the validated model, an experimental design of the response surface type was defined, in which each of the input variables were varied in three ranges and the results were obtained in terms of principal stress and strain, the most relevant conclusions are presented below.

The results obtained from the numerical model developed using 3D solid elements to discretize the geometry are in good agreement with the results obtained for both the uniaxial tension test and the four-point bending test. This allows the technique to be used to analyze the behavior that a pipe can experience when it is subjected to bending moments.

Of the variables considered, the diameter is the one that has the greatest relevance when a pipe is subjected to a lateral load, in the same way the magnitude of lateral displacement is the second independent variable that influences the result of strain obtained, finally the distance between supports is the last variable with significant relevance to the strain result obtained.

Regarding the interactions between the variables, it was evident that the interaction between the diameter of the pipe/magnitude of the lateral displacement is the most relevant, exhibiting a quadratic growth in the strain as the diameter decreases and the lateral load increases simultaneously. The second interaction of relevance is the one that occurs when the diameter and distance between supports vary simultaneously; however, this effect is low and is very close to the limit of significance. Finally, the interaction between the magnitude of the lateral displacement and the distance between supports does not have significant relevance in the strain result obtained.

Regarding the measurement of deformation using strain gauges, it was evident that in general terms these allow for an adequate measurement; it is important to take care of the effect of temperature on this type of device since it can significantly impact the result obtained.

References

[1] ASME, Pipeline Integrity Assurance-A Practical Approach, [Online]. 2010. Available at: https://www.copyright.com
[2] Phillip, J., Ellenberger, Piping and pipeline calculations manual: construction, design, fabrication, and examination. Butterworth-Heinemann/Elsevier, 2010.
[3] Ozkan, I.F., Mohareb, M. and Asce, M., Testing and Analysis of Steel Pipes under Bending, Tension, and Internal Pressure, Journal of Structural Engineering, 135(2), art. 9445, 2009. DOI: https://doi.org/10.1061/(ASCE)0733-9445(2009)135:2(187).
[4] Ahn, K., Lim, I.G., Yoon, J., and Huh, H., A simplified prediction method for the local buckling load of cylindrical tubes, International Journal of Precision Engineering and Manufacturing, 17(9), pp. 1149–1156, 2016. DOI: https://doi.org/10.1007/s12541-016-0139-0.
[5] Bazhenov, V.A., Luk'yanchenko, O.O., Kostina, O.V., and Gerashchenko, O.V., Nonlinear bending stability of a long flexible cylindrical shell with geometrical imperfections. Strength of Materials, 48(2), pp. 308–314, 2016, DOI: https://doi.org/10.1007/s11223-016-9766-z.
[6] Antaki, G.A., Fitness-for-service and integrity of piping, vessels, and tanks: ASME code simplifed. McGraw-Hill, USA, 2005.
[7] Cai, J., Jiang, X., Lodewijks, G., Pei, Z., and Wu, W., Residual ultimate strength of seamless metallic pipelines under a bending moment-a numerical investigation, Ocean Engineering, 164, pp. 148–159, 2018. DOI: https://doi.org/10.1016/j.oceaneng.2018.06.044.
[8] Nazemi, N., Behavior of X60 Line Pipe under Combined Axial and Transverse Loads with Internal Pressure, 2009. [Online]. Available at: https://scholar.uwindsor.ca/etd
[9] ANSYS, Element Reference, 2022. [Online]. Available at: http://www.ansys.com
[10] Li, Y., Shuai, J., Jin, Z.L., Zhao, Y.T., and Xu, K., Local buckling failure analysis of high-strength pipelines, Pet Sci, 14(3), pp. 549–559, 2017. DOI: https://doi.org/10.1007/s12182-017-0172-3.
[11] Wang, J., Shuai, Y., He, R., Dou, X., Zhang, P., and Feng, C., Ultimate strain capacity assessment of local buckling of pipelines with kinked dents subjected to bending loads. Thin-Walled Structures, 169, 2021. DOI: https://doi.org/10.1016/j.tws.2021.108369.
[12] ANSYS, Basic Analysis Guide, 2022. [Online]. Available at: http://www.ansys.com
[13] Shuai, Y. et al., Local buckling failure analysis of high strength pipelines containing a plain dent under bending moment, J Nat Gas Sci Eng, 77, 2020, DOI: https://doi.org/10.1016/j.jngse.2020.103266.
[14] Kamaya, M., Ramberg-Osgood type stress-strain curve estimation using yield and ultimate strengths for failure assessments, International Journal of Pressure Vessels and Piping, 137, pp. 1–12, 2014. DOI: https://doi.org/10.1016/j.ijpvp.2015.04.001.
[15] Tee, K.F., and Wordu, A.H., Burst strength analysis of pressurized steel pipelines with corrosion and gouge defects, Eng Fail Anal, 108, 2020 DOI: https://doi.org/10.1016/j.engfailanal.2019.104347.
[16] NACE, Standard Test Method - Four-Point Bend Testing of Materials for Oil and Gas Applications, 2016.
[17] ASTM E 8M, Standard Test Methods for Tension Testing of Metallic Materials, 2001.
[18] Han, J., Lu, Ch., Wu, B., Li, J., Li, H., Lu, Y., and Gao, Q., Innovative analysis of Luders band behaviour in X80 pipeline steel Materials Science & Engineering A, A683, pp. 123-128, 2017. DOI: https://doi.org/10.1016/j.msea.2016.12.008
[19] Urriolagoitia-Sosa, G., Durodola, J.F., Lopez-Castro, A., and Fellows, N.A., A method for the simultaneous derivation of tensile and compressive behaviour of materials under Bauschinger effect using bend tests, Journal of Mechanical Engineering Science, 220(10), pp. 1509-1518, 2006. DOI: https://doi.org/10.1243/09544062JMES180
[20] API Specification 5L, Specification for line pipe, 2013.
[21] Keil, S., Technology and practical use of strain gages, Publisher: Ernst & Sohn a Wiley Brand, 2017.
[22] Montgomery, D.C., Design and analysis of experiments, Wiley, USA, 2020.

[23] Shuai, Y. Wang, X-H., Cheng, Y.F., Buckling resistance of an X80 steel pipeline at corrosion defect under bending moment. J. Nat Gas Sci Eng, 93, art. 104016, 2021. DOI: https://doi.org/10.1016/j.jngse.2021.104016
[24] Wang, J. et al., Ultimate strain capacity assessment of local buckling of pipelines with kinked dents subjected to bending loads. J. Thin-Walled Structures, 169, art. 108369, 2021. DOI: https://doi.org/10.1016/j.tws.2021.108369
[25] Jindra, D. et al., Experimental and numerical simulation of a three-point bending test of a stainless-steel beam. J. Transportation Research Procedia, 55, pp. 1114-1121 2021. DOI: https://doi.org/10.1016/j.trpro.2021.07.183

J.F. Gamba-Gomez, received the BSc. Eng in Electromechanical Engineering in 2010, Postgraduate in Structural Numerical Analysis using the finite element method in 2019 from the ESSS, Postgraduate in numerical analysis of flows using CFD in 2020 from the ESSS and MBA Sp. in Business Intelligence and Big Data in 2020 from the European Postgraduate Institute. From 2012 to date she has worked as a stress and mechanical integrity analyst for different industries in the Oil & Gas sector. His research interests include: Structural simulation using finite elements; transient analysis using explicit dynamics; behavior of materials and analysis of technological risks in the operation of facilities used for the transportation of hydrocarbons.
ORCID: 0009-0008-8123-8147

Y. Pineda-Triana, received the BSc. Eng in Metallurgical Engineering in 1991, a Sp. in Industrial Radiography in 1993 from the Universidad Pedagógica y Tecnológica de Colombia and a Dr. in Mechanical and Materials Engineering from the Universidad Politécnica de Valencia, Spain. Currently, she is a full professor in the Engineering Metallurgical School at pregraduate and postgraduate level, Facultad de Ingeniería, Universidad Pedagógica y Tecnológica de Colombia. His research interests include: composites (laminates, reinforced plastics, synthetic and natural fibers); coatings and films; ceramics; mechanical engineering; process engineering.
ORCID: 0000-0002-5561-9412

D.M. Bermúdez-Rincón, received the BSc. Eng in Mechanical Engineering Engineer in 2015, from the Libre University. Bogotá, Colombia. Sp. in Integrity and Corrosion Management in 2019 from the Universidad Pedagógica y Tecnológica de Colombia, Tunja, Colombia. Since 2015 he has worked for companies in the Oil and Gas sector. He is currently a master's student in Integrity and Corrosion Management at the Universidad Pedagógica y Tecnológica de Colombia. His research interests include: simulation; modeling; mechanical integrity and risk analysis for hydrocarbon transportation pipelines
ORCID: 0009-0003-6045-7096

O.A. Gamba-Gómez, received the BSc. Eng in Civil Engineering in 2009 and a MSc. in Metallurgy and Materials Science in 2020, both from the Universidad Pedagógica y Tecnológica de Colombia, Tunja, Colombia. From 2010 to 2013 he worked in the private sector in the civil works sector, since the end of 2014 he has been working for the Universidad Pedagógica y Tecnológica de Colombia as an operative technician for the materials and structures laboratory, he was a professor for the civil engineering school in 2016, 2017 and 2021 in the undergraduate modality, he has also been a professor for the Specialization program in Construction Pathology at the Universidad Santo Tomas since 2022. His research interests include: new materials; mechanical testing; dynamic testing; advanced concrete design.
ORCID: 0000-0002-2124-5723

DYNA
http://dyna.medellin.unal.edu.co/

UNIVERSIDAD NACIONAL DE COLOMBIA

Postural physical burden of street vendors in Boyacá, Colombia

María Nubia Molano-Sotaquira, Fabian Alfredo Torres-Sandoval & Carlos Alfredo Millán-Pérez

Universidad Pedagógica y Tecnológica de Colombia, Tunja, Colombia. maria.molano07@uptc.edu.co, fabian.torres01@uptc.edu.co, carlos.millan@uptc.edu.co

Received: January 24th, 2024. Received in revised form: March 12th, 2024. Accepted: March 21th, 2024.

Abstract

It was performed an observational study of transversal cut with a descriptive approach with the objective of evaluating the postural physical burden of fruits and vegetables street vendors in Boyacá, Colombia through the ergonomic assessment method REBA. The chosen population of the study was fifteen workers from a street vendors association in Sogamoso city. The results show that the vendors have a high and very high risk of generating musculoskeletal disorders due to the postural burden they are exposed to. Some recommendations were made to decrease the physical burden based on four strategic angles: education, social responsibility, self-learning and engineering control at workplaces. This brings to the conclusion that the problematic perceived in this population of workers from the informal sector is similar to the one seen in other regions and countries; it is recommended the active participation for developing policies that allow to improve their work conditions and life quality.

Keywords: postural physical burden; ergonomic assessment method; informal labor; musculoskeletal disorders; street vendors.

Carga física postural en vendedores ambulantes de Boyacá, Colombia

Resumen

Se realizó un estudio observacional de corte transversal con enfoque descriptivo con el objetivo de evaluar la carga física postural en vendedores ambulantes de frutas y verduras en Boyacá, Colombia a través del método de evaluación ergonómica REBA. La población del estudio correspondió a quince trabajadores de una asociación de vendedores ambulantes de la ciudad de Sogamoso. Los resultados muestran que los vendedores tienen un riesgo alto y muy alto de generar trastornos musculo esqueléticos por la carga postural a la que están expuestos. Se presentaron recomendaciones para disminuir la carga física desde cuatro líneas estratégicas: capacitación, responsabilidad social, autoaprendizaje y control de ingeniería en los puestos de trabajo. Se concluye que la problemática identificada en esta población trabajadora del sector informal es similar a la presentada en otras regiones y países; se recomienda la participación en la construcción de políticas que permitan mejorar sus condiciones laborales y calidad de vida.

Palabras clave: carga física postural; método de evaluación ergonómica; trabajo informal; trastornos músculo esqueléticos; vendedores ambulantes.

1. Introduction

Below there are mentioned the most relevant aspects of the previously addressed topics for the development of this research work.

1.1 Informal labor and decent labor

In Latin America and the Caribbean, the labor scope is marked by the uncertainty of people belonging to the working population, given that unemployment is increasing and the quality in job offers is getting worse. The social uneasiness shows the lack of decent labor, related to the few opportunities to access to a decent work, fair payment, social protection and occupational rights. The unemployment rate in the region tends to increase, registering less growth in paid employment and a deceleration in the registered employment, being both formal labor indicators. Whereas, there was an increase in self-employment, which suggests a higher tendency to the informal labor [1].

How to cite: Molano-Sotaquira, M.N., Torres-Sandoval, F.A. and Millán-Pérez, C.A., Postural physical burden of street vendors in Boyacá, Colombia. DYNA, 91(232), pp. 41-48, April - June, 2024.

After the pandemic the decent work deficit has increased and so the historic levels of inequality in Latin America and the Caribbean, being one of the most affected regions worldwide. In 2021 the rate of unemployment in the region increased to 11% and in Colombia the increase was higher getting close to 16%. During this year the informal labor leaded the employment recovery contributing with almost 70% of the new jobs. Nevertheless, the link between labor informality, low incomes and inequality became more evident. Additionally, the informal workers have been deeply affected by the deduction of employment and incomes [2].

In Colombia the informal sector is constituted by enterprises that do not have commercial register before the Chamber of Commerce and neither are they classified as quasi-partnerships for not having a complete or simplified accountability that allows them to separate their outcomes, this also includes the enterprises without accountability of their workers. Between September of 2022 and February of 2023, the informal occupation was 58,1% on average [3,4].

In this way, the goal of decent labor since the beginning has been to link the economic social development with people´s occupational rights. According to the principles of decent labor, the labor is not merchandising and all human beings have the right to material welfare and spiritual development in conditions of freedom, dignity, economic security and equality [5].

For these reasons, the National Government committed, through the article 74 of the Law 1753 of 2015 under the coordination of the Ministry of Labor, to adopt the national policy of decent labor, this policy is currently being processed and it seeks the creation of employment, the labor formality, el social dialogue, the occupational rights guarantee and the protection to workers in public and private sectors throughout the country [6].

1.2 Risk factors and musculoskeletal disorders associated to physical burden

The musculoskeletal disorders (MSDs) are currently considered as one of the most important health problems in labor affecting all the economic sectors. The movement repetitiveness, the excessive use of strength, the inadequate postures and the weight lifting are the main cause of damages in the musculoskeletal system [7]. The MSDs represent an important workload for the world´s economy and health, being the low-back pain one of the most frequent causes of disability in the majority of countries [8].

In Colombia, according to a study which analyzed the constant of accidentality and occupational illness between 1994 and 2016, it was identified that the most frequent diagnoses of occupational illness during 2002 were MSDs, where 20% corresponded to a carpal tunnel syndrome and 18% to lumbosacral spine disorders. This situation was evidenced again in 2011, where 40% of pathologies corresponded to a carpal tunnel syndrome, followed by less than 10% of non-specified low-back pain [9].

According to the third National Health and Work Conditions Survey performed in 2021, in Colombia the percentual distribution of occupational dangers in workplaces shows the physical burden with the highest percentages; among them hands and/or arms repetitive movements (73.58 %), tasks requiring to hold still during all or great part of the working hours (70.06 %) and biomechanical danger with the possibility of causing pain (57.81 %) [10].

In a bibliometric analysis performed in different countries around the world about work and occupational health in informal workers during 2010-2016, in which Colombia contributed with the biggest amount of scientific production, it was found that within informal labor the activities of street sales and waste recovery stand out. Amongst the identified risks with the highest frequency there could be found biomechanical aspects of physical burden such as repetitive movements, body postures and overexertion due to burden manipulation. The body sections with the biggest affectation were the upper limbs, the back and the neck among others with musculoskeletal affectations mainly. In terms of labor characteristics, it is pointed out the lack of affiliation to social security, long working days and rights violation [11].

According to a study developed by the Social Protection Ministry in 2008 about the health and work conditions of workers from the informal sector in twenty states of the country, it was found that the informal commerce sector is related to the diverse health problems and unsafe work environment. Among the priority risk factors identified it was found that 47,2% of workers perform strained postures or movements [12].

1.3 Ergonomics and physical burden

The ergonomics allows to apply theories and design methods to optimize the human welfare and the productive systems development. The domain areas of ergonomics cover the physical, cognitive and organizational aspects of human being related to work. Within the physical ergonomics it is analyzed the human biomechanics in relation to physical activity, covering aspects such as the postures, the manual manipulation of burden and the repetitive movements, among others [13].

Fernández [14] describes the work of physical burden as the group of physical requirements to the ones the worker is exposed. It is measured through physiologic indicators and it can be manifested in the short term as a work accident or in the long term as an occupational illness.

In relation to human posture, it can be defined as a sequential and automatic process that allows the permanent global positioning of the body axis in relation to the movement of the center of mass on a base of support, allowing the motor act to respond to a particular environment [15].

The work postures generate dynamic and static burdens in the musculoskeletal system of a person. During the static work the blood circulation and the muscle metabolism decrease, reducing the efficiency of muscular performance. Being exposed to a continuous or frequent static burden generates local muscular contraction and, consequently, fatigue, which may produce disorders in the muscular system [16].

The Technical Note for Prevention N° 452 indicates that the postural burden can be reduced by improving the tasks, the work conditions and increasing the functional capacity of the workers´ musculoskeletal system [16]. For the estimate of physical burden, the ergonomic assessment methods allow to identify and estimate the risk factors present at the workplaces [17].

1.4 Street vendors association

The Street vendors association in this case of study is located in the city of Sogamoso, Boyacá and it has as its main goal the development of activities related to street sales (stationary and traveling) aiming to satisfy the needs of commercialization of products from the shopping basket and to acquire economic resources for the subsistence of its fifteen associated members.

The association is a small enterprise and it has registered its economic activity before the Chamber of Commerce, publicly proving its activity as informal merchants. In a preliminary observation done to the vendors from the association, it could be established that the risk they are exposed the most due to physical burden are the inadequate postures, given the unfavorable conditions in which this population perform their work.

According to the Decree number 487 of 2021 [18] in which it is established the statute for the use of public space in the territory of Sogamoso, the informal street vendors offer their goods or services by going around the routes and other public spaces.

2 Methodology

It was performed an observational study of transversal cut with a descriptive approach, with the objective of evaluating the postural physical burden of fruits and vegetables street vendors in Boyacá, Colombia through the ergonomic assessment method REBA.

2.1 Population

The population for the study corresponds to the fifteen vendors from the association, from whom, in its entirety, it was collected the necessary data for the development of the investigation.

2.2 Collection and data analysis strategies

The collection and data analysis were performed in three stages:

2.2.1 Stage 1

In the first stage, an initial description of the workplaces of the vendors from the association was done, these merchants used carts as the principal tool for transporting and selling their products, from which some aspects were described such as the number of wheels, the space they take, the materials they are built with and its weight.

Then, it was done a description of the sales activity, for this, it was presented the different tasks done in a working day and aspects such as the number of baskets filled with products which are transported by cart, the baskets' weight, the distance from the storage cellar to the point of sale and the number of hours with higher sales.

After that, it was performed a sociodemographic characterization of the workers, for which a questionnaire was used in which data was collected about age, gender, number of children, the existence of any kind of disability, social stratum, marital status, educational level, number of people they are in charge of, the time destined to street sales, days of the week they work, as well as the hours they work every day and the laterality.

Finally, it was determined the perception of musculoskeletal symptoms in the vendors, for this the Nordic questionnaire [19] was used, which allowed to collect data about the presence of corporal pain, the body sections with symptomatology (arms, wrists, legs, neck, torso), the perception of symptomatology (muscle cramps, pain, mobility loss, stiffness) and the pain frequency.

2.2.2 Stage 2

The second stage was focused on developing an assessment of the postural physical burden in the vendors from the association through the ergonomic assessment method named REBA (Rapid Entire Body Assessment), which allows to estimate the strained postures in upper limbs.

To select this ergonomic assessment method an observation of the vendors´ sales activity was done; where it was identified as principal risk factor the postural burden being the most frequent among other biomechanical risk factors such as the repetitive movements and manual manipulation of de burdens.

2.2.3 Stage 3

In this stage the recommendations for the reduction of the postural physical burden were set. For this, initially the risk factors that generated the highest rates in the application of the assessment method REBA were identified. Then, it was performed a revision of different documents such as articles, norms and guides about the recommendations for the reduction of the physical burden. Finally, the recommendations most in line with the problem and the context analyzed were selected.

2.3 Ergonomic assessment method REBA

The Method REBA allows to estimate the strained postures that present a high frequency in the tasks and that involve the upper limbs mainly. The method divides the body in two groups: group A, where torso and neck movements are estimated as well as the leg positioning, additionally it is estimated the relation burden/strength. In the group B the arms positioning and forearms and wrists movements are estimated, additionally it is estimated the grip, with the aid of Tables 1 and 2 [20].

Table 1.
Group A

Neck													
		1				2				3			
Legs		1	2	3	4	1	2	3	4	1	2	3	4
Torso	1	1	2	3	4	1	2	3	4	3	3	5	6
	2	2	3	4	5	3	4	5	6	4	5	6	7
	3	2	4	5	6	4	5	6	7	5	6	7	8
	4	3	5	6	7	5	6	7	8	6	7	8	9
	5	4	6	7	8	6	7	8	9	7	8	9	9
Burden / Strength													
0			1		2			+ 1					
< 5 kg			5 - 10kg		10kg			Quick or abrupt installation					

Source: [20]

Table 2.
Gruup B

Forearm							
		1			2		
Wrist		1	2	3	1	2	3
Arm	1	1	2	2	1	2	3
	2	1	2	3	2	3	4
	3	3	4	5	4	5	5
	4	4	5	5	5	6	7
	5	6	7	8	7	8	8
	6	7	8	8	8	9	9
Grip							
0 - Good		**1 - Regular**		**2 - Bad**		**3 - Unacceptable**	
Good grip and grip force		Acceptable grip		Possible but not acceptable		Uncomfortable, no hand grip	

Source: [20]

Table 3.
Combination groups A and B

		Score B											
		1	2	3	4	5	6	7	8	9	10	11	12
Score A	1	1	1	1	2	3	3	4	5	6	7	7	7
	2	1	2	2	3	4	4	5	6	6	7	7	8
	3	2	3	3	3	4	5	6	7	7	8	8	8
	4	3	4	4	4	5	6	7	8	8	9	9	9
	5	4	4	4	5	6	7	8	8	9	9	9	9
	6	6	6	6	7	8	8	9	9	10	10	10	10
	7	7	7	7	8	9	9	9	10	10	11	11	11
	8	8	8	8	9	10	10	10	10	10	11	11	11
	9	9	9	9	10	10	10	11	11	11	12	12	12
	10	10	10	10	11	11	11	11	12	12	12	12	12
	11	11	11	11	11	12	12	12	12	12	12	12	12
	12	12	12	12	12	12	12	12	12	12	12	12	12
Task	1	One or more static body parts											
	1	Repetitive movements											
	1	Unstable postures											

Source: [20]

Afterwards, the estimates from groups A and B are combined and it is added the estimate of additional aspects such as static postures and repetitive movements with the aid of Table 3, which allows to obtain a final score final from the task assessment.

Next, with the final score it is determined the level of action and risk and the necessary intervention through the Table 4.

Table 4.
Determination of risk level

Action level	Score	Risk Level	Intervention
0	1	Imperceptible	Not necessary
1	2 to 3	Low	May be necessary
2	4 to 7	Medium	Necessary
3	8 to 10	High	Necessary soon
4	1 to 15	Very high	Immediate action

Source: [20]

Table 5.
Description of workplaces

Workplace	Wheels	Area m^2	Structural material	Roof material	Weight Kg
1	2	1	Steel	Polyester	200
2	3	1,4	Steel	vinyl canvas	400
3	4	1,26	Steel	vinyl canvas	250
4	4	0,9	Steel and wood	vinyl canvas	150
5	4	1,4	Wood	vinyl canvas	250
6	3	1,26	Steel and wood	vinyl canvas	250
7	3	0,8	Steel and wood	vinyl canvas	175
8	3	0,8	Steel	vinyl canvas	275
9	3	0,8	Steel and wood	vinyl canvas	250
10	3	1	Wood	vinyl canvas	275
11	3	1,1	Wood	Polyester	300
12	3	0,72	Wood	Polyester	300
13	3	0,72	Steel	vinyl canvas	100
14	4	1,2	Steel	vinyl canvas	250
15	4	1,2	Steel	vinyl canvas	250

Source: The authors.

3 Results and discussion

3.1 Description of workplaces

The carts are presented as the main tool used by vendors for transportation and sales.

According to the Table 5, the carts have from 2 to 4 wheels, they occupy an area of 0,72 to 1,4 m2 and the materials used for its structure building are wood and steel and for the roof it is used polyester and vinyl canvas.

3.2 Description of the fruits and vegetables street sales activity

The activity can be divided into the following tasks:

- Getting the cart ready
- Putting the baskets with product on the cart
- Transporting the cart from the cellar to the point of sales
- Organizing the products on the cart
- Packing the products in plastic bags
- Selling the products
- Transporting the cart from the point of sales to the cellar

Below, in the Table 6, there are presented aspects that describe the street sales activity.

According to the Table 6, from 5 to 20 baskets are transported by carts, having a weight from 20 to 30 Kgs. The distance from the cellar to the points of sales is from 1,28 to 1,98 Kms.

In geographical terms there is a concentration of Street vendor activity mainly in the central zone of the city of Sogamoso, located in strategic points of mobility such as the corners of streets, taking the space of the sideways. The cellar is located in the reseller's marketplace, in the northwest zone of the city.

Table 6.
Description of the sale activity

Vendor	Baskets transported daily	Basket' weight (Kg)	Distance from the cellar to the point of sale (Km)	Number hours with higher sales
1	6	25	1,28	2
2	7	20	1,79	3,5
3	15	25	1,28	2
4	5	22,5	1,33	1
5	11	20	1,28	2
6	9	25	1,33	2
7	6	25	1,86	3
8	20	20	1,6	3,5
9	12	25	1,98	3
10	15	25	1,6	2
11	17	25	1,44	3
12	17	30	1,37	3
13	8	20	1,6	2
14	9	25	1,6	2
15	11	25	1,69	3
Average	11,20	23,83	1,54	2,47

Source: The authors.

Table 7.
Sociodemographic profile of vendors from the association

Categorie	Variable	%
Age (years)	18 – 29	14%
	30 – 39	13%
	40 – 49	40%
	50 – 59	20%
	>60	13%
Gender	Female	80%
	Male	20%
Number of children	1– 3	54%
	4– 6	33%
	>7	13%
Disability population	Yes	20%
	No	80%
Social stratum	1	7%
	2	93%
Marital status	Married	28%
	Free Union	36%
	Single	29%
	Divorced	7%
Educational level	Primary	40%
	Secondary	53%
	Technical	7%
Number of people they are in charge of	1	10%
	2	20%
	3	40%
	4	30%
Time destined to street sales	1 to 10 years	13%
	11 to 20 years	20%
	More than 20 years	67%
Days of the week they work	5 days	6%
	6 days	47%
	7 days	47%
Hours they work every day	1 to 8 hours	33%
	9 to 11 hours	47%
	12 hours or more	20%
Laterality	Right	80%
	Left	20%

Source: The authors.

3.3 Sociodemographic profile of vendors from the association

Some of the most important aspects that can be observed in the Table 7, are that 40% of vendors are between 40 to 49 years old, 80% are women, all of them are from the social strata 1 and 2, 53% have completed high school, 67% have been working in the same area for more than 20 years and 47% work during 9 to 11 hours per day.

3.4 Perception of the symptoms associated to musculoskeletal disorders

In the Table 8 there are presented the categories and variables that were considered in perception of symptoms, referred by the surveyed workers and associated people as musculoskeletal disorders.

It was found that the body sections where the symptomatology is presented more frequently are neck and torso, the most frequent symptomatology is pain and it mainly appears when they finish the working day. These results are similar to the ones found in other research works worldwide [11], where it was also found the symptomatology in neck and torso of workers from the informal sector as well as pain as the most frequent symptom related to physical burden [8,10].

3.5 Assessment of the postural physical burden in vendors from the association through the ergonomic assessment method REBA

Below, in the Table 9 it is presented the estimate for the different body sections gathered in the groups A and B, the score increases in relation to the pain that represents each posture adopted by the vendors.

Table 8.
Perception of the symptoms associated to musculoskeletal disorders

Categories	Variable	%
Body pain	Yes	87%
	No	13%
Body sections with symptomatology	Arms	4%
	Wrists	13%
	Legs	13%
	Neck	30%
	Torso	27%
	None	13%
Perception of symptomatology	Muscle cramps	7%
	Pain	27%
	Mobility loss	20%
	Stiffness	33%
	None	13%
Pain frequency	Finish the working day	40%
	Permanently	27%
	During the work day	13%
	None	13%
	Only at night	7%

Source: The authors.

Table 9.
Application of the REBA method

Vendor		1	2	3	4	5	6	7	8	9	10	11	12	13	14	15
Group A	Torso	4	4	4	3	4	4	3	4	3	3	4	3	4	4	4
	Neck	2	2	2	2	2	2	2	2	1	2	2	2	2	2	2
	Legs	2	1	2	2	2	2	3	2	2	1	1	1	3	2	1
	Total	6	5	6	5	6	6	6	6	4	4	5	4	7	6	5
Group B	Arms	3	2	2	2	2	5	5	4	3	4	3	3	3	4	3
	Forearms	1	1	1	1	2	1	1	1	1	2	1	1	1	1	2
	Wrists	2	3	2	2	3	2	3	2	3	2	2	2	2	2	2
	Total	4	3	2	2	4	7	8	5	5	6	4	4	4	5	4
Group C	Strength exerted	2	2	2	2	2	2	2	2	2	2	2	2	2	2	2
	Total group A	8	7	8	7	8	8	8	7	6	6	7	6	9	8	7
	Grip type	1	1	2	2	2	2	1	2	1	1	0	1	0	1	2
	Total group B	5	4	4	4	6	9	9	8	6	7	4	6	4	6	6
	Total group C	10	8	9	7	10	10	10	10	8	9	8	8	10	10	9
Muscular activity	One or more static body parts	1	1	1	1	1	1	1	1	1	1	1	1	1	1	1
	Repetitive movements	1	2	1	1	1	1	1	1	1	1	1	1	1	1	1
	Unstable postures	1	0	0	1	1	0	0	0	0	0	0	0	1	0	0
Final score		13	10	11	10	13	12	12	12	10	11	10	10	13	12	11

Source: The authors.

According to the Table 10, it is found that the body section with the highest score was the torso, followed by the arms and the neck, these results are related to the perception of symptoms where the neck and the torso showed the most frequent symptomatology. The latter is similar to what was found in other research works developed at national and international level [11], where the affectations in the back and the neck in workers from the informal sector were the most representative.

The results from the ergonomic assessment show that the vendors have a high and very high risk of generating any kind of musculoskeletal disorder due to the postural physical burden they are exposed to. In a similar way to other research [11,12] performed at a national and international level, it can be identified in the informal workers a high physical burden generated by inadequate postures, together with excessive use of strength and repetitive movements that may generate MSDs.

3.6 Recommendations for reducing the postural physical burden

The recommendations are organized in four strategic angles: education, social responsibility, self-learning and engineering control at workplaces:

Table 10.
Interpretation of risk level

Vendor	Final score	Risk		
		Level	Risk	Action
1	13	4	Very high	Immediate action
2	10	3	High	Necessary soon
3	11	4	Very high	Immediate action
4	10	3	High	Necessary soon
5	13	4	Very high	Immediate action
6	12	4	Very high	Immediate action
7	12	4	Very high	Immediate action
8	12	4	Very high	Immediate action
9	10	3	High	Necessary soon
10	11	4	Very high	Immediate action
11	10	3	High	Necessary soon
12	10	3	High	Necessary soon
13	13	4	Very high	Immediate action
14	12	4	Very high	Immediate action
15	11	4	Very high	Immediate action

Source: The authors.

3.6.1 Education

It is suggested to begin with a feedback where the vendors from the association realize the inadequate postures they are currently adopting, the additional risk factors that were identified, the risk they are exposed to and the possible affectations these postures can generate in their health.

Then, information can be shared through lectures about postural hygiene, looking for a good positioning in the comfort angles from their different body sections.

Likewise, recommendations can be given about the importance of postural change, the use of comfortable and safe clothing to work, the use of elements for resting as chairs, the correct positioning of the lower limbs on the ground, the task rotation, the implementation of adequate postures for the manual manipulation of burdens, the maximum allowed weight to manipulate and the adequate shape that the handles should have.

3.6.2 Social responsiblity

The Ministry of Labor in Colombia establishes through the article 5 of the Law 1988 of August 2nd, 2019 [21] the guidelines for the elaboration of the public policy of informal vendors and in the Resolution number 1213 of 23 June 2020 [22] the methodologic structure and the deadlines for its creation in the different territorial collectivities around the country. Hence, it corresponds to the Municipal Administration of Sogamoso, the creation and implementation of this public policy. For its creation, in the system of agents, there should be included the different informal vendors organizations.

The purpose of the public policy is to seek strategies that provide solutions to different situations of vulnerability in the sector and thus increase the capacities and opportunities towards conditions of fairness and equity, diminishing the levels of poverty and inequality. Based on this, it is recommended for the association to actively participate in the creation process of this public activity.

3.6.3 Self-learning

It is recommended the implementation of a self-assessment and self-care tool that allows the worker, through simple questions or images, to identify possible musculoskeletal symptoms in his different body sections and eventually provide recommendations of postural hygiene.

3.6.4 Engineering control at workplaces

It is suggested to adapt the current workplaces or to replace them for newer ones that help to solve the identified issue. Some of the new features proposed for the workplaces are:

- Steering and brake system with the intention of reducing the transportation effort.
- Gyratory chair that allows to reduce torso rotations, with backrest and adjustable height.
- The reach to different components must be at a short or medium distance to the vendors avoiding positions out of comfort angles.
- Four-wheel mobility, seeking better stability and burden distribution in the product transportation.
- Separated compartments for product exhibition that allow better organization and avoid the products for sale to be mixed among themselves.
- Unfolding roof that covers the workplace and the vendor.
- The use of light materials such as polymers and aluminum, with the intention to reduce the total weight of the workplace.
- General dimensions according to the daily sales volume, seeking to avoid over dimensioning which represents a higher total weight of the workplace.

4. Conclusions

The results of the study show that 73 % of the workers have a very high risk of generating MDSs due to postural physical burden they are exposed to, which means that an immediate intervention must be done to improve their work conditions.

The identified issue in this work population from the informal sector is similar to the one presented in other regions and countries; it is recommended to look for support from the government and participate in the development of policies that favor the improvement of their work conditions and quality of life.

In terms of the work conditions of the street vendors, it was evidenced a high physical burden with higher exposition to risk in group A (torso, neck and legs) according to the assessment of the method REBA, which includes inadequate postures together with repetitive movements and manual manipulation of burden.

Similar to other regions and countries, the street vendors from the association in Sogamoso lack affiliation to social security within the contributive regiment, besides, they lack affiliation to retirement pensions and occupational risks, with the future implications that this issue has for their quality of life and the one of their families.

The street vendors from the association, having to work in public space, are exposed to other risks of biological, chemical, climatic and physical kind as well as insecurity, among others, that must be investigated and assessed in further research aiming for an integral solution to this issue.

It is necessary to coordinate work groups between the association and the territorial entity (Municipality de Sogamoso, Boyacá) to manage the given recommendations for decreasing the postural physical burden.

References

[1] Organización Internacional del Trabajo. Panorama Laboral América Latina y el Caribe 2019. Oficina Regional de la OIT para América Latina y el Caribe, Lima, Perú, 2019, 152 P.

[2] Maurizio, R., Empleo e informalidad en América Latina y el Caribe: una recuperación insuficiente y desigual, Organización internacional del Trabajo, Ginebra, Suiza, 2021, 54 P.

[3] Departamento Administrativo Nacional de Estadística. Boletín Técnico Gran Encuesta Integrada de Hogares (GEIH) septiembre – noviembre 2022, Bogotá, Colombia, 2022, 16 P.

[4] Departamento Administrativo Nacional de Estadística. Boletín Técnico Gran Encuesta Integrada de Hogares (GEIH) diciembre 2022 – febrero 2023, Bogotá, Colombia, 2023, 16 P.

[5] Somavía, J., El trabajo decente. Una lucha por la dignidad humana, Organización internacional del Trabajo, Santiago, Chile, 2014, 766 P.

[6] Ley No. 1753, Artículo 74. Por el cual se expide el plan nacional de desarrollo 2022- 2026 Colombia potencia mundial de la vida. Congreso de Colombia, Bogotá, Colombia, 19 de mayo de 2023.

[7] Morales, L., Ramón, M., Collantes, S. y Aldás, D., Riesgo ergonómico por levantamiento de cargas: caso de estudio talleres de mantenimiento vehicular de maquinaria pesada. Revista Científica y Tecnológica UPSE, 6(1), pp. 17-26, 2019. DOI: https://doi.org/10.26423/rctu.v6i1.328

[8] Ibarra-Villanueva, C. y Astudillo-Cornejo, P. Factores de riesgo biomecánico lumbar por manejo manual de cargas en el reparto de productos cárnicos. Arch Prev Riesgos Labor, 24(4), pp. 342–354, 2021. DOI: https://doi.org/10.12961/aprl.2021.24.04.02

[9] Álvarez, S., Palencia, F. y Riaño-Casallas, M., Comportamiento de la accidentalidad y enfermedad laboral en Colombia 1994 – 2016. Rev la Asoc Española Espec en Med del Trab., [En línea]. 28(1), pp. 10-19, 2019. Disponible en: https://scielo.isciii.es/pdf/medtra/v28n1/1132-6255-medtra-28-01-10.pdf

[10] Ministerio de Trabajo y Organización Iberoamericana de Seguridad Social. Tercera Encuesta Nacional de Condiciones de Seguridad y Salud en el Trabajo en el Sistema General de Riesgos Laborales, Bogotá, Colombia, 2021, 590 P.

[11] Puentes-León, K.J., Rincón-Bayona, L.Y. y Puentes-Suárez, A., Análisis bibliométrico sobre trabajo y salud laboral en trabajadores informales, 2010-2016. Rev. Fac. Nac. Salud Pública, 36(3), pp. 71-89, 2018. DOI: https://doi.org/10.17533/udea.rfnsp.v36n3a08

[12] Ministerio de la Protección Social. Diagnostico nacional de las condiciones de salud y trabajo de las personas ocupadas en el sector informal de la economía de 20 departamentos de Colombia y propuesta de monitoreo de estas condiciones, 2008, 142 P.

[13] Rincón, O., Ergonomía y procesos de diseño: consideraciones metodológicas para el desarrollo de sistemas y productos, 1ra ed., Pontificia Universidad Javeriana, Bogotá, Colombia, 2010, 24 P.

[14] Instituto Nacional de Seguridad e Higiene en el Trabajo (España). NTP 177: la carga física de trabajo: definición y evaluación. Barcelona, España, 1986, 9 P.

[15] Orozco, R.A., Conceptos generales para la descripción y evaluación de los riesgos por carga física, 1ra ed., Universidad del Rosario, Bogotá, Colombia, 2012, 31 P.

[16] Instituto Nacional de Seguridad e Higiene en el Trabajo (España). NTP 452: evaluación de las condiciones de trabajo: carga postural. Barcelona, España, 1997, 9 P.

[17] Instituto Nacional de Seguridad e Higiene en el Trabajo (España). NTP 451: evaluación de las condiciones de trabajo: métodos generales. Barcelona, España, 1997, 6 P.

[18] Decreto No. 487. Por medio del cual se modifica el Decreto 242 de 2006 que adoptó el Estatuto del Espacio Público para el Municipio de Sogamoso. Alcaldía del Municipio de Sogamoso, Sogamoso, Colombia, 2021.
[19] Kuorinka, I., Jonsson, B., Kilbom, A., Vinterberg, H. Biering-Sørensen, F. Andersson, G., and Jørgensen, K., Standardised Nordic questionnaires for the analysis of musculoskeletal symptoms. Applied Ergonomics, 18(3), pp. 233-237, 1987. DOI: https://doi.org/10.1016/0003-6870(87)90010-X
[20] Instituto Nacional de Seguridad e Higiene en el Trabajo (España). NTP 601: evaluación de las condiciones de trabajo: carga postural: método REBA (Rapid Entire Body Assessment). Barcelona, España, 2001. 7 P.
[21] Ley No. 1988. Por la cual se establecen los lineamientos para la formulación, implementación y evaluación de una política pública de los vendedores informales y se dictan otras disposiciones. Congreso de la República de Colombia, Bogotá, Colombia, 02 de agosto de 2019.
[22] Resolución No. 1213. Por medio de la cual se reglamentan los plazos y la metodología para la elaboración de la política pública de vendedores informales de que trata la Ley 1988 de 2019. Ministerio de Trabajo de Colombia. Bogotá, Colombia, 23 de junio de 2020.

M.N. Molano-Sotaquira, is BSc. in Public Administrator from the Escuela Superior de Administración Pública (ESAP). MSc. in Occupational Safety and Health (OSH) from the Universidad Pedagógica y Tecnológica de Colombia. Coordinator of social projects and external advisor to private entities on auditing and implementation of OSH management systems at the Municipal Administration of Firavitoba. Her areas of interest are: OSH, management systems and social management.
ORCID: 0009-0001-0458-7270

F.A. Torres-Sandoval, is BSc. in Industrial Designer from the Universidad Pedagógica y Tecnológica de Colombia (UPTC). Sp in Ergonomics from the Universidad El Bosque, Colombia. MSc. in Occupational Safety and Health (OSH) from the UPTC. Researcher in the Grupo de Investigación en Diseño Taller 11 in the Ergonomics and Design line. Professor at the Industrial Design School and OSH Master's program at the UPTC. His areas of interest are: OSH, Ergonomics and Design.
ORCID: 0000-0002-3766-1027

C.A. Millan-Pérez, is BSc. in Public Administrator from the Escuela Superior de Administración Pública (ESAP), Colombia. MSc. in Administration from the Universidad Pedagógica y Tecnológica de Colombia. Data analyst of the Contraventions Subdirectorate at the Secretaría Distrital de Movilidad. His areas of interest are: Occupational Health and Safety, Project Management, Legislation and Big Data.
ORCID: 0000-0002-2531-9902

DYNA
http://dyna.medellin.unal.edu.co/

UNIVERSIDAD NACIONAL DE COLOMBIA

Dashboard for assessing patient flow management in hospital institutions

Yasniel Sánchez-Suárez [a], Verenice Sánchez-Castillo [b] & Carlos Alberto Gómez-Cano [c]

[a] *Facultad de Ingeniería Industrial, Universidad de Matanzas, Matanzas, Cuba. yasnielsanchez9707@gmail.com*
[b] *Facultad de Ingeniería, Universidad de la Amazonia, Florencia, Colombia. ve.sanchez@udla.edu.co*
[c] *Dirección de Investigaciones, Corporación Unificada Nacional de Educación Superior, Florencia, Colombia. carlos_gomezca@cun.edu.co*

Received: September 22th, 2023. Received in revised form: April 1st, 2024. Accepted: April 4th, 2024.

Abstract
Proactive control of hospital processes significantly influences patient performance and satisfaction. The objective of the research is to develop a dashboard for the evaluation of patient flow management in hospital institutions. Descriptive quantitative study was developed and previous methodologies were analyzed. A procedure was developed for the preparation of a dashboard for the evaluation of patient flow management in hospital institutions, structured in five stages and nine steps, including procedures for the identification of key variables and aggregation of indicators. A dashboard was prepared for the General Surgery service of a Clinical Surgical Teaching Hospital, which is composed of 18 indicators, 6 synthetic indexes and an integral indicator. The integral indicator obtained a value of 0.79 (4), which shows the effectiveness of the actions implemented during the deployment of the improvement model. Among the positive implications for health managers is the possibility of monitoring strategies with a process vision.

Keywords: management control; patient flow; hospital management; indicators; dashboard.

Tablero de control para evaluar la gestión de los flujos de pacientes en instituciones hospitalarias

Resumen
El control proactivo de los procesos hospitalarios influye de forma significativa en el rendimiento y satisfacción de los pacientes. El objetivo de la investigación es desarrollar un tablero de control para la evaluación de la gestión del flujo de pacientes en instituciones hospitalarias. Se desarrolló un estudio cuantitativo descriptivo y se analizaron metodologías precedentes. Se elaboró un proceder para la confección de un tablero de control para la evaluación de la gestión de los flujos de pacientes en instituciones hospitalarias, estructurado en cinco etapas y nueve pasos, incluye procedimientos para la identificación de variables clave y agregación de indicadores. Se confeccionó un tablero de control para el servicio de Cirugía General de un hospital Clínico Quirúrgico Docente, que está compuesto por 18 indicadores, 6 índices sintéticos y un indicador integral. El indicador integral obtuvo un valor de 0,79 (4), lo que es muestra de la eficacia de las acciones implementadas durante el despliegue del modelo de mejora. Entre las implicaciones positivas para los gestores sanitarios está la posibilidad de monitorear las estrategias con una visión de proceso.

Palabras clave: control de gestión; flujo de pacientes; gestión hospitalaria; indicadores; tablero de control.

1 Introduction

Hospital management has evolved from the traditional vision to a process approach with greater patient participation in care, an element that marks a before and after in the development of the quality of health services [1,2]. This management should be developed according to the characteristics of its environment and patients who demand these services, by considering parameters of flow, rhythm and evolution of the care network, with responses in accordance with the care model, flexible, timely and effective [3].

How to cite: Sánchez-Suárez, Y., Sánchez-Castillo, V. and Gómez-Cano, C.A., Dashboard for assessing patient flow management in hospital institutions. DYNA, 91(232), pp. 49-57, April - June, 2024.

Hospital services must be planned [4], organized [5], managed [6] and controlled [7], in order to increase their performance. Among the tools widely used in the sector is management control. Hospital management control helps to understand the conditions of the institution and its processes in terms of meeting strategic goals [8,9].

The balanced scorecard is emerging as a proactive management tool that takes a strategic approach to management [10,11], its deployment generally contemplates the following perspectives: financial, customer, internal processes, and learning and growth [12].

For the operational control of processes, dashboard have been created to monitor the specific management [13]. They are of great importance in the management of patient flows by allowing operational decisions to be made in order to optimize patient trajectories through a healthcare organization, it also allows a diagnosis of the behavior of patient flow management, as an alternative to those proposed in other studies [14].

Patient flow refers to the movement of patients through care areas in order to receive treatment [15]. Its management is holistic in nature, as it influences the entire system [16], it takes into account the patient's criteria regarding the perceived quality during its trajectory [17], and it is influenced by efficient capacity planning based on flow demand forecasting [18]. The main objectives of its management are: reducing patient waiting time, reducing hospital stay, optimizing capacity, improving patient satisfaction and hospital performance [19].

Duarte Forero et al [20] identifies three main flows to the hospital service:

- Elective patients flow, usually transiting through departments or external services (outpatient).
- Urgent patient flow, usually presented by on-call or emergency services.
- Patients flow referred to inpatient services from other levels of care.

Different analysis and improvement tools have been used for patient flow management, among them mathematical modeling, which requires a correct characterization [21] and classification of patients [3]. Discrete event simulation models [22-24], system dynamics [25], agent-based simulation [26], queuing theory [27], Markov and compartmental models [28,29] have been developed.

These models make it possible to optimize hospital capacity and align strategies based on the results obtained and the improvements modeled [30], elements that in turn optimize the use of resources, minimize waste and optimize processes by parallel activities [31].

An analysis of patient flow management methodologies (Table 1) summarizes the main elements:

- Among the tools most commonly addressed in the methodologies are discrete event simulation and linear, integer and dynamic programming.
- Lean manufacturing has been developed to eliminate all those activities that do not generate value to patient treatment.
- Capacity scheduling in hospital systems and its influence on resource optimization.
- They use isolated indicators to evaluate the management of patient flows but there is no evidence of the conception of an integral indicator that contemplates all the variables that influence patient flows.

Table 1.
Analysis of methodological procedures for the patient flows management.

Tool/ Author	Medina León et al [32]	Gartner and Kolisch [33]	Pellizarri [34]	Armony et al [35]	Mathews and Long [36]	Chen et al [37]	Andersen et al [38]	Blouin Delisle et al [39]	Duarte Forero & Camacho [20] Oliveros	Vali et al [40]
Linear programming		X				X	X			X
Operations management			X							
Exploratory data analysis				X						
Queuing theory				X	X					
Simulation	X				X	X	X		X	
Discrete programming		X								
Lean manufacturing			X					X		
Resource allocation					X	X				
Capacity planning						X				
Markov models							X			
Indicators									X	
System dynamics									X	
Total	**1**	**2**	**2**	**2**	**3**	**4**	**3**	**1**	**3**	**1**

Source: Own elaboration.

The hospital taken as a reference for the application of the research is a second level hospital, Teaching Surgical Clinic, which has a well-structured strategic planning, but there have been problems in the fulfillment of goals and objectives that influence its evaluation in terms of compliance with specific quality standards. Based on interviews with managers (representatives of key result areas), there is evidence of the need for alignment between the strategic and operational levels, through the monitoring of specific indicators in each of the services.

On the other hand, a review of the audit reports reveals problems due to patient dissatisfaction, functional focus in the management of activities and lack of motivation among the staff, an element that arouses the interest of the evaluators and the institution's quality personnel.

Based on brainstorming in the boards of directors, the need to proactively control critical control points in the hospital's services is identified, through a management approach to patient flows focused on their trajectory as an element that influences performance and patient satisfaction.

Consequently, the objective of the research is to develop a dashboard for the evaluation of patient flow management in hospital institutions.

2 Methodology

Methodologies for the construction of Balanced Scorecard (BSC) and Dashboard have been developed and

adapted to the characteristics of production and service systems [41]. Hospitals are increasingly using indicators to measure the performance of their processes [42].

Methodologies that have focused on the conception of a dashboard for monitoring indicators and consider patient flows as a variable of importance and impact on hospital performance are taken as a reference:

- Sexton et al [43] proposes a patient dashboard in the electronic medical record for use during communication between nurses in an operating room. Although the methodology focuses on the patient and the optimization of length of stay, it does not take into account transfers and the management of interactions with other processes present in the patient's trajectory.
- Alhabib et al [44] implements a dashboard for measuring the satisfaction of emergency employees, with the objective of evaluating the elements used in the service. The dashboard does not focus on patient journey management. The importance of specialist criteria in future design and implementation is highlighted.
- Kenigsberg et al [45] developed an internal dashboard to facilitate visualization and quick reviews of automated weekly vaccine safety surveillance big data. They include a set of variables to group key indicators, they do not show how to group those variables into synthetic and comprehensive indices.
- Cinelli et al [46] designed a dashboard to track licensing requirements and Drug Enforcement Administration requirements, the dashboard decreases patient wait times. Although it improves indicators related to patient flows, it does not focus on internal indicators that influence service performance.
- Franklin et al [11] propose a methodology that focuses on timely and efficient care in the emergency department, takes into account individual characteristics, although they consider variables such as flow coordinators to reduce the length of stay of patients, implement a prototype of a performance panel to monitor operational indicators in real time.

Although the methodologies show the potential of dashboard for monitoring indicators and improving process performance, they do not focus on a methodological procedure for their preparation. Based on the gaps found, a procedure is proposed for the construction of a dashboard to evaluate the performance of patient flows in the process under study, in addition to allowing the detection of gaps and deviations. It is structured in five stages and nine steps (Fig. 1).

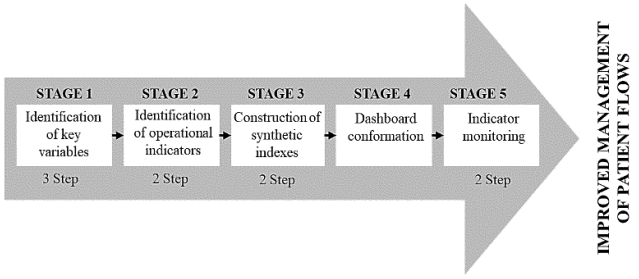

Figure 1. Procedure for the preparation of the dashboard.
Source: Own elaboration.

It is focused on the monitoring of operational indicators of hospital services, in such a way as to allow the heads of services to monitor the related key indicators and their alignment with the strategic indicators at the institutional level, an element that is in line with other telemedicine and health monitoring research [47].

The methodology is of a descriptive quantitative type, and its application was carried out in the General Surgery service, in a second level hospital (Clinical Surgical Teaching Hospital), from June to December 2022.

2.1 Description of the procedure

2.1.1 Stage 1. Identification of key variables

Objective: to identify variables that define the behavior of patient flows in the selected services.

Step 1. Identification and selection of variables

Based on a systematic review of the literature, variables used in research to characterize the management of patient flows are identified, listed and refined according to the specific characteristics of each department. The selection should consider those variables with the highest frequency of occurrence, which should be clearly and precisely defined.

Step 2. Variable consultation with experts

The variables previously identified in the literature should be presented to the experts and specialists of the service, so that they can validate the variables by consensus. The experts may add or delete any of the variables previously found.

Step 3. Definition of the objectives of the variables

When defining the objectives for key variables, the institution's specific goals and objectives must be taken into account to ensure management alignment.

2.1.2 Stage 2. Identification of operational indicators

Objective: to identify operational indicators that describe the behavior of key service variables.

Step 4. Selection of indicators

This research uses the procedure proposed by Hernández Nariño and Marqués León [48], which consists of five steps: collecting indicators used in the process, by specialists, and in the literature, reducing the list of indicators, selecting the indicators.

Step 5. Association of indicators with key variables

For their relationship, it should be taken into account that the indicator and the variables have the same management objective and goal, and that the set of indicators as a whole should represent the key variable.

2.1.3 Stage 3. Construction of synthetic indexes

Objective: to assign a weight to the key variables defined in the management of the service's patient flows.

Step 6. Calculation of mathematical coefficients

The coefficients for each of the variables make it possible to give them a priority in management. The Analytical Hierarchical Process (AHP) is developed in the research. For its deployment, subjective evaluations of the experts are needed regarding the relative importance of each of the indicators of the variable, the levels of consistency are evaluated from the consistency index that must have values lower than 0.10.

Step 7. Formation and calculation of the quantitative index

The proposed integral index was calculated arithmetically, using an additive function, which compares the maximum level reached by each of the synthetic indexes with that of the service at the time of measurement. Eq. (1) was used for the calculation.

$$IIFP = \frac{\sum_{j=1}^{Q} P_j * V_j}{5 \sum_{1}^{Q} V_j} \quad (1)$$

Where:

- IIFP: Comprehensive Patient Flow Index.
- Pj: score of the j-th indicator.
- Vj: relative weight of the j-th indicator.
- Q: number of indicators to be included in the index.

For the evaluation of the proposed integral indicator, a rating scale is proposed (Fig. 2). The scale takes values from 1 to 5, based on the analysis of the behavior of previous indicators studied. In the normalization of the indicator, the desired value or purpose, the ranges for each purpose and the indicator's score on the scale should be made clear. Hernández Nariño [49] and Ramos Castro [50] were used as a reference. The scale can be improved according to the characteristics of the services studied.

2.1.4 Stage 4. Dashboard conformation

Objective: to propose a software tool that makes the calculation of indicators and their analysis proactively feasible.

With the indicators classified and validated by the experts, we proceeded to build the dashboard. The dashboard will show an operational view of the management of flows, and should be easy to interpret by specialists and managers, and practical to ensure the familiarization of personnel with it in short periods of time. It should include the institution's logo, a tab to identify the selected service or object of analysis, pivot tables and graphs to be selected according to the specific context.

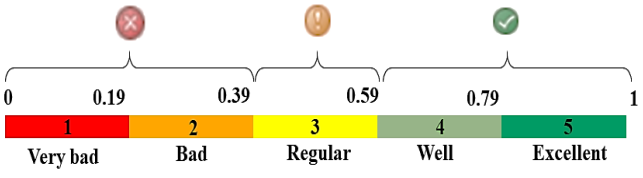

Figure 2. Synthetic and comprehensive index valuation scale.
Source: Own elaboration.

2.1.5 Stage 5. Indicators monitoring

Objective: to monitor the behavior over time of the indicators on the dashboard.

The follow-up allows management to proactively analyze the negative behavior of the indicators with respect to the target values and take measures to channel them to the desired goals. The dashboard should also be designed to ensure the best alignment with the organization's strategy.

Step 8. Search for causes of poor performance of the integral indicator

Here the integral indicator is disaggregated to its minimum expression (synthetic indicators and indicators), with the objective of identifying cause-effect relationships.

Step 9. Reduction of failures during the implementation of corrective actions

Some of the techniques that can be used for the initial collection of existing problems are: interview, observation, survey, document review, the Delphi Method and the multi-attribute and multi-criteria methods, which will be selected according to the specific conditions of each process and according to the scope of the corrective action. For the reduction of the list of failures in the research, the Kendall's coefficient method is used.

3 Discussion of results

The following results were obtained from the application of the proposed procedure for the preparation of a dashboard to evaluate the patient flows management in hospital institutions.

3.1 Stage 1. Identification of key variables

Step 1. Identification and selection of variables

From the analysis of 27 methodologies focused on patient flow management, seven variables were identified: sequence of activities (74.1 %), focus on the trajectory (88.9 %), system capacity (92.6 %), service demand (77.8 %), computerization (55.6 %), personnel qualification (59.3 %) and contingency policy (7.4 %). The variables with the highest frequency of occurrence were the first six, since contingency policies only appeared in two studies, with special relevance in the Covid-19 period. The research considers the rest of the variables identified as cross-cutting.

Step 2. Variable consultation with experts

At a working meeting, the variables were presented to the experts, who considered them valid for characterizing patient flows in hospital institutions.

Step 3. Definition of the objectives of the variables

Table 2 shows the objective of each key variable identified.

3.2 Stage 2. Identification of operational indicators

Step 4. Selection of indicators

From the literature review, 27 indicators were initially identified; the specialists recommended including three indicators related to the process; the Delphi method was used to reduce the list of indicators and 18 indicators were selected.

Table 2
Key variables objectives.

Variable	Objective
Activity sequence	Develop actions to carry out activities in a logical and orderly manner.
Focus on trajectory	Ensure the continuous nature of patient flow with a focus on trajectory.
System capacity	To guarantee the availability of resources based on the quality of medical actions in hospital institutions.
Service demand	To quantify the amount of medical care provided to a population by one or more providers over a period of time.
Informatization	Computerize hospital processes for effective decision making.
Personnel qualification	Strengthen the qualification of health personnel in order to improve the quality of care.

Source: Own elaboration.

Table 3
List of indicators and key variables.

Code	Key Variable	Code	Indicator selected
IS-SA	Activity sequence	SA-01	Average waiting time for medical discharge
		SA-02	Number of interruptions
IS-ET	Focus on trajectory	ET-03	Average waiting time per medical procedure
		ET-04	Waiting time for diagnostic support activities
		ET-05	Average waiting time per nursing procedure
		ET-06	Unambiguous patient identification
IS-CS	System capacity	CS-07	Bed occupancy rate
		CS-08	Average length of hospital stay
		CS-09	Emergency waiting time
		CS-10	Operating room availability
IS-DS	Service demand	DS-11	External customer satisfaction
		DS-12	Percentage of outpatient surgeries
		DS-13	Number of patients on surgical waiting list
IS-I	Informatization	I-14	Capacity of computerization systems
		I-15	Total hospital services computerized
IS-CP	Personnel qualification	CP-16	Internal customer satisfaction
		CP-17	Medication error rate
		CP-18	Adverse event rate related to patient misidentification.

Source: Own elaboration.

Step 5. Association of indicators with the key variables
Table 3 shows the grouping of indicators by key variable.

3.3. Stage 3. Construction of synthetic indexes

Step 6. Calculation of mathematical coefficients
The Hierarchical Analytical Process was applied by means of joint elaboration among the experts, who issued their criteria with respect to the paired comparisons that allow quantifying the role played by each indicator in the corresponding synthetic indexes. Table 4 shows an example of the weights for each synthetic indicator by key variable that make up the integral indicator of patient flows, with a consistency index of 3.4 % below 10 %, which shows the consensus among the experts.

Table 4
Weights for comprehensive patient flow index.

Criterion (indicator)	Weight (W)	Standard deviation (±)
Activity sequence	14,0 %	5,0 %
Focus on trajectory	20,8 %	4,4 %
System capacity	25,3 %	8,0 %
Service demand	25,3 %	8,0 %
Informatization	6,3 %	1,8 %
Personnel qualification	8,3 %	2,0 %

Source: Own elaboration.

Step 7. Formation and calculation of the quantitative index
From the analysis of the baseline measurement, it is concluded that the management of patient flows in the General Surgery service is good with an evaluation of 0.79 (4), which is a sample of the effectiveness of the actions implemented during the deployment of the model for improvement. However, out of the 18 indicators defined, 2 are evaluated as poor (11.11 %), 6 have a regular performance (33.33 %) and 10 are evaluated as good (55.56 %). None of the indicators was evaluated as excellent or very bad.

3.4 Stage 4. Dashboard conformation

A dashboard was designed (Fig. 3), the purpose values of the indicators are based on the flow of emergencies to the General Surgery service, and it acts as a traffic light, alerting with colors: red (bad or terrible behavior), green (good or excellent behavior) and yellow (regular behavior).

3.5 Stage 5. Indicators monitoring

Step 8. Search for causes of poor performance of the integral indicator
In order to search for the causes of poor performance of the integral indicator, an analysis of performance drivers was performed (Fig. 4).

Step 9. Reduction of failures during the implementation of corrective actions

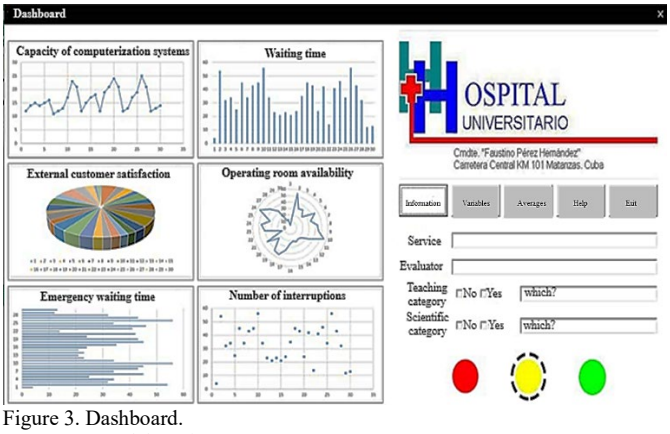

Figure 3. Dashboard.
Source: Own elaboration.

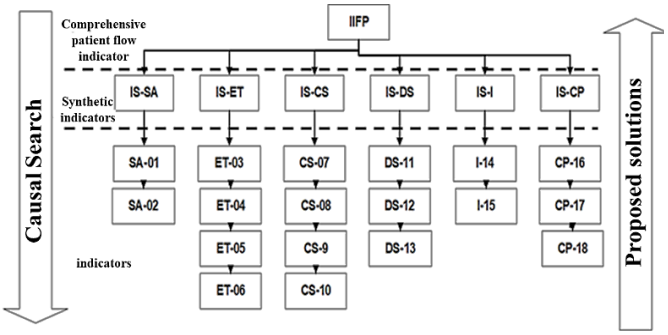

Figure 4. Analysis of performance inducers.
Source: Own elaboration.

Table 5
Failures identified during the implementation of improvements.

Key Variables	Identified faults
Activity sequence	✓ Deficiencies in medical records ✓ Need for a signage system in the hospital ✓ Interruptions in diagnosis-related activities or processes in elective patient flows ✓ Long waiting times for patients waiting for discharge.
Focus on trajectory	✓ Information and actions are not linked. ✓ Patient identification is not done correctly at admission.
System capacity	✓ Operations suspended due to lack of medical supplies. ✓ Deficiencies in medical supplies planning ✓ Scarce bed availability ✓ Unavailability of operating rooms
Service demand	✓ Dissatisfaction of patient escorts ✓ Low levels of planning of outpatient surgeries
Informatization	✓ Low levels of computerization ✓ Low levels of computer literacy of health care personnel to operate complex software ✓ Insufficient capacity of hospital systems
Personnel qualification	✓ Actions resulting in dissatisfaction with working conditions ✓ Shortages of medical staff related to anesthesiology services

Source: Own elaboration.

Based on the monitoring of the proposed indicators, a set of failures were identified during the execution of the improvement solutions (Table 5), which serve as a starting point for identifying the root causes of the negative behavior of the indicators.

To reduce the list and identify the main failures or deficiencies identified during the execution of the improvement proposal, the Kendall method was used, which allowed prioritizing seven failures that represent 38.89 % of the total identified, these are:

1. Deficiencies in medical records
2. Long waiting times for patients waiting to be discharged.
3. Patient identification is not done correctly at admission.
4. Scarce bed availability
5. Dissatisfaction of those accompanying patients.
6. Low levels of computerization
7. Shortage of medical personnel related to anesthesiology services.

Currently, with the development of information and communication technologies, institutions are seeking alternatives to improve their processes in order to generate competitive advantages [51], in this context, innovation plays a fundamental role in rethinking and restructuring ways of managing processes [52] and constitutes an alternative for health risk management [53].

The use of indicators to measure the performance of processes has made it posible to reduce subjetive decisions on improvement and to align strategies more and more with the visión, misión and organizational objectives [54], an element that is supported by García Peña et al [55] who emphasize the importance of monitoring indicators in management.

In correspondence with research, González López-Valcárcel and Ortún [56] show the importance of digital technologies and their influence on agile decision making in health services, in addition to reflecting the potential for integration and care coordination. On the other hand, Chen et al [57] demonstrated its usefulness in increasing hospital throughput by reducing patient waiting times between treatment stages. Artificial intelligence tools have also been developed to organize the high volumes of data generated by these control tools [58], an element that becomes an improvement opportunity for the proposed dashboard.

Esquer Rochin et al [59] it evidences the usefulness of dashboard in the understanding and implementation of improvement solutions. This research also provides a procedure for the creation of an integral indicator and analysis of inducers that allow the behavior of indicators to be channeled.

4 Conclusions

Six key variables were identified for the management of patient flows in hospital institutions, to which operational indicators were associated to support the proactive management of the process with a focus on the patient's trajectory and were aggregated in an additive function with the objective of creating a comprehensive indicator that allows the evaluation of management and the implementation of improvement solutions in hospital services.

A dashboard was created and a methodological procedure was proposed for its conception, which is flexible before future redesigns during the implementation process. It functions as a traffic light in the event of deviations from the values proposed in the synthetic indicators, and a root cause analysis was proposed to support the identification of root causes, which facilitates the work of specialists in decision-making.

The indicators were applied in the General Surgery service and a value of 0.79 (4) was obtained for the integral indicator, which indicates that the management of patient flows is good, and that the actions carried out to improve the trajectory and coordination of activities in a proactive manner have a tendency towards efficiency; however, of the 18 indicators, 2 are evaluated as bad, representing 11.11% of the total, 6 have a regular performance (33.33%) and 10 are evaluated as good (55.56%), while none was evaluated as excellent or very bad (55.56%), while none was evaluated as excellent or very bad (55.56%). 11 % of the total, 6 have a regular performance (33.33 %) and 10 are evaluated as good (55.56 %), while none was evaluated as excellent or very bad.

Among the limitations of the present study is that the dashboard only allows evaluating the management of emergency patient flows in hospital institutions, identifying as a gap the need to adjust the target values of the indicators identified in terms of elective patient flows, the research does not explicitly show how to align the dashboard with other strategic evaluation instruments of the institution. It was also considered important in future redesigns of the dashboard to insert indicators such as the occupancy rate (percent of total occupied beds) and the turnover interval (time elapsed between the discharge of a patient and the admission of another patient in the same bed).

Among the positive implications of the proposed dashboard for health managers is that it allows the tracking of indicators and historical studies related to the management of patient flows with a focus on the trajectory, allows monitoring and comparing strategies with a process vision among the different departments, allows evaluating the current state of management and its alignment with the objectives and goals of the institutional strategic planning, and facilitates decision making and reduces management errors.

4.1 Future research

In future research, it is recommended to redesign the dashboard, based on the improvement of the IIFP, with the possibility of using other management indicators related to the particularities of each of the hospital services, the different clinical management variables that influence patient flows and the purpose values for the evaluation of the indicators based on elective patient flows. In addition, to develop studies of control limits per variable for each of the indicators associated with these variables, which will make it possible to increase the precision of the scale of evaluation of the indicators and consequently readjust the measurements of the synthetic and IIFP.

References

[1] Jabalera, M., Pons, M., Gómez, E., and del Castillo, M., Hacia la excelencia en gestión hospitalaria. Un modelo de gestión estratégica, Journal of Healthcare Quality Research, 34(3), pp. 148-153, 2019. DOI: https://doi.org/10.1016/j.jhqr.2019.02.005

[2] Adriana-Roussel, P., Impacto de un modelo de gestión de la calidad de un servicio de inmunización del Hospital de Alta Complejidad. El Cruce, Salud, Ciencia y Tecnología, 2(44), pp. 1-14, 2022. DOI: https://doi.org/10.56294/saludcyt202244

[3] Sánchez-Suárez, Y., Instrumento metodológico para la gestión de flujos de pacientes de instituciones hospitalaria, PhD Thesis, Facultad de Ciencias Técnicas, Universidad de Matanzas, Matanzas, Cuba, 2023.

[4] Bouckaert, N., Van den Heede, K., and Van de Voorde, C., Improving the forecasting of hospital services: a comparison between projections and actual utilization of hospital services, Health Policy, 122(7), pp. 728-736, 2018. DOI: https://doi.org/10.1016/j.healthpol.2018.05.010

[5] Herlina, Madjid, M., Rusman, A.D.P., Sari, R.W., Noer, N.B., and Rivai, F., The application of the fast method needed in improving hospital services, Enfermería Clínica, 30, pp. 240-243, 2020. DOI: https://doi.org/10.1016/j.enfcli.2020.06.055

[6] Aluvalu, R., Mudrakola, S., Maheswari, U., Kaladevi, A.C., Sandhya, M.V.S., and Rohith-Bhat, C., The novel emergency hospital services for patients using digital twins, Microprocessors and Microsystems, 98, art. 104794, 2023. DOI: https://doi.org/10.1016/j.micpro.2023.104794

[7] Bahalkeh, E., Chiam, T.C., and Yih, Y., An interpretable clustering classification approach for assessing and adjusting hospital service lines, Healthcare Analytics, 4, art. 100255, 2023. DOI: https://doi.org/10.1016/j.health.2023.100255

[8] Georgescu, I., Management control literature and French public hospitals, Health Policy, 111(3), pp. 324-327, 2013. DOI: https://doi.org/10.1016/j.healthpol.2013.06.014

[9] Acero-Moreno, A.M., Ordoñez-Paredes, B.A., Toloza-Guardias, H.P., and Vega-Palmera, B., Análisis estratégico para la empresa Imbocar, seccional Valledupar – Colombia. Región Científica, 2(1), art. 202395, 2023. DOI: https://doi.org/10.58763/rc202395

[10] Fatima, T., and Elbanna, S., Advancing sustainable performance management in the hospitality industry: a novel framework based on a health-inclusive balanced scorecard, Tourism Management Perspectives, 48, art. 101141, 2023. DOI: https://doi.org/10.1016/j.tmp.2023.101141

[11] Franklin, A., Gantela, S., Shifarraw, S., Johnson, T.R., Robinson, D.J., King, B.R., Mehta, A.M., Maddow, C.L., Hoot, N.R., Nguyen, V., Rubio, A., Zhang, J., and Okafor, N.G., Dashboard visualizations: supporting real-time throughput decision-making, Journal of Biomedical Informatics, 71, pp. 211-221, 2017. DOI: https://doi.org/10.1016/j.jbi.2017.05.024

[12] Peralta-Llivipuma, M.R., Erazo-Álvarez, J.C., and Narváez-Zurita, C.I., Cuadro de mando integral, enfoque estratégico al proceso administrativo y educativo, Visionario Digital, 3(2.2), pp. 120-144, 2019. DOI: https://doi.org/10.33262/visionariodigital.v3i2.2.627

[13] Sakly, H., and Ben-Jeddou, K., Development and implementation of dashboard in the Pharmacy Department at University Hospital, Le Pharmacien Clinicien, 57(1), pp. 6-15, 2022. DOI: https://doi.org/10.1016/j.phclin.2021.09.002

[14] Sánchez-Suárez, Y., Marqués-León, M., Hernández-Nariño, A., y Suárez-Pérez, M.M., Metodología para el diagnóstico de la gestión de trayectorias de pacientes en hospitales, Región Científica, 2(2), art. 2023115, 2023. DOI: https://doi.org/10.58763/rc2023115.

[15] Torres-Moreno, G.C., y Velasco-Peñaloza, J.C., Aplicación de la metodología BMP e instrumentos Lean para evaluación del flujo de pacientes en el área de servicios quirúrgicos. Estudio de caso: hospitales de alta complejidad, Tesis de grado, Ingeniería Industrial, Universidad Santo Tomás, Colombia, 2020.

[16] Manning, L., and Islam, S., A systematic review to identify the challenges to achieving effective patient flow in public hospitals, Int J Health Plann Mgmt, 38(3), pp. 805-828, 2023. DOI: https://doi.org/10.1002/hpm.3626

[17] Castillo, C.Y., Patient's perception of the quality of care in the Ambulatory Surgery Unit of the Polyclinic Hospital of the western area of the Metropolitan Area of Buenos Aires, Salud, Ciencia y Tecnología, 3, art. 504, 2023. DOI: https://doi.org/10.56294/saludcyt2023504.

[18] Lees-Deutsch, L., and Robinson, J., A systematic review of criteria-led patient discharge, J Nurs Care Qual, 34(2), pp. 121-126, 2019. DOI: https://doi.org/10.1097/NCQ0000000000000356

[19] Alhaider, A., Lau, N., Davenport, P., and Morris, M., Distributed situation awareness: a health-system approach to assessing and designing patient flow management, Ergonomics, 63(6), pp. 682-709, 2020. DOI: https://doi.org/10.1080/00140139.2020.1755061

[20] Duarte-Forero, E.L., y Camacho-Oliveros, M.Á., Planeación de la capacidad hospitalaria: un enfoque desde el flujo de pacientes con Dinámica de Sistemas, INGE CUC, 16(1), pp. 217-233, 2020. DOI: https://doi.org/10.17981/ingecuc.16.1.2020.16

[21] Broggi, L., Kemmerer, J., Bandriwskyj, C., Fernández, A., Gangoni, C., and Laura, V.H., Characterization of patients and measures implemented during the pandemic in a high complexity hospital in Argentina: an analysis from a nursing perspective, Salud, Ciencia Y Tecnología, 3, art. 513, 2023. DOI: https://doi.org/10.56294/saludcyt2023513

[22] Tamburis, O., and Esposito, C., Process mining as support to simulation modeling: a hospital-based case study, Simulation Modelling Practice and Theory, 104, art. 102149, 2020. DOI: https://doi.org/10.1016/j.simpat.2020.102149

[23] Homavazir, Z., Nagappan, B., and Singh, A., Exploring the contribution of engineering in enhancing workflow and efficiency in

nursing. Salud, Ciencia y Tecnología, 3(459), pp. 1-9, 2023. DOI: https://doi.org/10.56294/saludcyt2023459

[24] Sánchez-Suárez, Y., Sánchez-Castillo, V., y Gómez-Cano, C.A., Modelo para la gestión de flujos de pacientes, validado en un servicio de cirugía general. Revista Cubana de Medicina Militar [Online]. 53(1), art. 024022338, 2024. [date of reference March 4th of 2024]. Available at: https://revmedmilitar.sld.cu/index.php/mil/article/download/22338/2477

[25] Keshtkar, L., Rashwan, W., Abo-Hamad, W., and Arisha, A., A hybrid system dynamics, discrete event simulation and data envelopment analysis to investigate boarding patients in acute hospitals, Operations Research for Health Care, 26, art. 100266, 2020. DOI: https://doi.org/10.1016/j.orhc.2020.100266

[26] Saeedian, M., Sepehri, M.M., Jalalimanesh, A., and Shadpour, P., Operating room orchestration by using agent-based simulation, Perioperative Care and Operating Room Management, 15, art. 100074, 2019. DOI: https://doi.org/10.1016/j.pcorm.2019.100074

[27] Tyagi, M., Tyagi, P.K., Singh, S., Sathpathy, S., Kant, S., Gupta, S.K., and Singh, R., Impact of application of queuing theory on operational efficiency of patient registration, Medical Journal Armed Forces India, 79(3), pp. 300-308, 2023. DOI: https://doi.org/10.1016/j.mjafi.2021.06.028

[28] Ludbrook, G.L., and Leaman, E., Cost-Effectiveness in perioperative care: application of Markov modeling to pathways of perioperative care, Value in Health, 25(2), pp. 215-221, 2022. DOI: https://doi.org/10.1016/j.jval.2021.07.018

[29] Belciug, S., and Gorunescu, F., A hybrid genetic algorithm-queuing multi-compartment model for optimizing inpatient bed occupancy and associated costs, Artificial Intelligence in Medicine, 68, pp. 59-69, 2016. DOI: https://doi.org/10.1016/j.artmed.2016.03.001

[30] Dauncey, S.J., Kelly, P.A., Baykov, D., Skeldon, A.C., and Whyte, M.B., Rhythmicity of patient flow in an acute medical unit: relationship to hospital occupancy, 7-day working and the effect of COVID-19. QJM: monthly journal of the Association of Physicians, 114(11), pp. 773-779, 2022. DOI: https://doi.org/10.1093/qjmed/hcaa334

[31] Berg, E., Weightman, A.T., and Druga, D.A., Emergency department operations II: patient flow. Emergency Medicine Clinics of North America, 38(2), pp. 323-337, 2020. DOI: https://doi.org/10.1016/j.emc.2020.01.002

[32] Medina-León, S.V., Medina-Palomera, A., y González-Ángeles, Á., Reducir tiempos de espera de pacientes en el departamento de emergencias de un hospital utilizando simulación. Industrial Data [Online]. 13(1), pp. 67-76, 2010. [date of reference September 15th of 2023]. Available at: http://www.redalyc.org/articulo.oa?id=81619989010

[33] Gartner, D., and Kolisch, R., Scheduling the hospital-wide flow of elective patients, European Journal of Operational Research, 233(3), pp. 689-699, 2014. DOI: https://doi.org/10.1016/j.ejor.2013.08.026

[34] Pellizarri, M., La mejora del flujo de pacientes a través del hospital. Revista ITAES [Online]. 17(1), pp. 11-18, 2015. [date of reference September 15th of 2023]. Available at: https://studylib.es/doc/7753042/la-mejora-del-flujo-de-pacientes-a-trav%C3%A9s-del-hospital

[35] Armony, M., Israelit, S., Mandelbaum, A., Marmor, Y.N., Tseytlin, Y., and Yom-Tov, G.B., On patient flow in hospitals: a data-based queueingscience perspective. Stochastic Systems, 5(1), pp. 146-194, 2015. DOI: https://doi.org/10.1287/14-SSY153

[36] Mathews, K.S., and Long, E.F., A conceptual framework for improving critical care patient flow and bed use. Ann Am Thorac Soc, 12(6), pp. 886-894, 2015. DOI: https://doi.org/10.1513/AnnalsATS.201409-419OC

[37] Chen, X., Wang, L., Dingand, J., and Thomas, N., Patient flow scheduling and capacity planning in a smart hospital environment, IEEE Access, 4, pp. 135-148, 2016. DOI: https://doi.org/10.1109/ACCESS.2015.2509013

[38] Andersen, A.R., Nielsen, B.F., Reinhardt, L.B., and Stidsen, T.R., Staff optimization for time-dependent acute patient flow, European Journal of Operational Research, 272(1), pp. 94-105, 2019. DOI: https://doi.org/10.1016/j.ejor.2018.06.015.

[39] Blouin Delisle, C.H., Drolet, R., Hains, M., Tailleur, L., Allaire, N., Coulombe, M., and Vézo, A., Improving interprofessional approach using a collaborative lean methodology in two geriatric care units for a better patient flow, Journal of Interprofessional Education and Practice, 19, pp., 2020. DOI: https://doi.org/10.1016/j.xjep.2020.100332

[40] Vali, M., Salimifard, K., Gandomi, A.H., and Chaussalet, T.J., Application of job shop scheduling approach in green patient flow optimization using a hybrid swarm intelligence, Computers & Industrial Engineering, 172, art. e108603, 2022. DOI: https://doi.org/10.1016/j.cie.2022.108603

[41] Suárez-Gargallo, C., and Zaragoza-Sáez, P., A comprehensive bibliometric study of the balanced scorecard, Evaluation and Program Planning, 97, art. 102256, 2023. DOI: https://doi.org/10.1016/j.evalprogplan.2023.102256

[42] Sánchez-Suárez, Y., Trujillo-García, L., Marqués-León, M., y Santos-Pérez, O., Los indicadores de gestión hospitalarias en tiempos de Covid 19. Visionario Digital, 5(4), pp. 58-77, 2021. https://doi.org/10.33262/visionariodigital.v5i4.1901

[43] Sexton, P., Whiteman, K., George, E.L., Fanning, M., and Stephens, K., Improving PACU throughput using an electronic dashboard: a quality improvement initiative. Journal of PeriAnesthesia Nursing, 37(5), pp. 613-619, 2022. DOI: https://doi.org/10.1016/j.jopan.2021.11.005

[44] Alhabib, D., Alumarn, A., and Alrayes, S., Emergency room visualization dashboard user satisfaction in Saudi Arabia, Informatics in Medicine Unlocked, 21, art. 100493, 2020. DOI: https://doi.org/10.1016/j.imu.2020.100493

[45] Kenigsberg, T.Y.A., Hause, A.M., McNeil, M.M., Nelson, J.C., Ann Shoup, J., Goddard, K., Lou, Y., Hanson, K.E., Glenn, S.C., and Weintraub, E.S., Dashboard development for near real-time visualization of COVID-19 vaccine safety surveillance data in the Vaccine Safety Datalink, Vaccine, 40(22), pp. 3064-3071, 2022. DOI: https://doi.org/10.1016/j.vaccine.2022.04.010

[46] Cinelli, C., Somsen, D., Quinn, A., Horn, N., and Murray, R., Implementation of an electronic dashboard for reporting and tracking of health care professional requirements, Journal of the American College of Radiology, 18(1 Part A), pp. 75-78, 2021. DOI: https://doi.org/10.1016/j.jacr.2020.09.021

[47] Castillo, V.S., Cano, C.A.G., and Gonzalez-Argote, J., Telemedicine and health applications for health monitoring in rural communities in Colombia: a systematic review. EAI Endorsed Transactions on Pervasive Health and Technology, 9(1), pp. 1-17, 2023. DOI: https://doi.org/10.4108/eetpht.9.3400

[48] Hernández-Nariño, A., y Marqués-León, M., Procedimiento de determinación de indicadores. Aplicación a un proceso del Hospital "Mario Muñoz Monroy, Jornada Científica del Hospital "Mario Muñoz Monroy", Matanzas, Cuba, 2006.

[49] Hernández-Nariño, A., Contribución a la gestión y mejora de procesos en instalaciones hospitalarias del territorio matancero, PhD Thesis, Departamento de Ingeniería Industrial, Universidad de Matanzas "Camilo Cienfuegos", Matanzas, Cuba, 2010.

[50] Ramos-Castro, G., Gestión del desempeño del Sistema de Ciencia e Innovación enfocado a los procesos académicos en Salud, PhD Thesis, Departamento de Ingeniería Industrial, Universidad de Matanzas, Matanzas, Cuba, 2022.

[51] Afanador-Cubillos, N., Historia de la producción y sus retos en la era actual, Región Científica, 2(1), art. 202315, 2023. DOI: https://doi.org/10.58763/rc202315

[52] Machuca-Contreras, F., Canova-Barrios, C., y Fabián-Castro, M., Una aproximación a los conceptos de innovación radical, incremental y disruptiva en las organizaciones, Región Científica, 2(1), art. 202324, 2023. DOI: https://doi.org/10.58763/rc202324

[53] Cano, C.A.G., Castillo, V.S., Losada, Y.B., and Monje, M.A.B., Analysis of the risks associated with the provision of services in respiratory diseases ward during the COVID 19 pandemic at the Hospital Maria Inmaculada, Salud, Ciencia y Tecnologia, 2, art. 123, 2022. DOI: https://doi.org/10.56294/saludcyt2022123

[54] Gonzales-Centon, J.M., Chávez-Cubas, W., Berrio-Huillcacuri, J., and Santos-Maldonado, A.B., El crecimiento empresarial y su relación en la rentabilidad de una MYPE del rubro comercial en Arequipa, Perú, Región Científica, 2(1), art. 202387, 2023. DOI: https://doi.org/10.58763/rc202387

[55] García-Peña, M., López-Ocmin, L.S., y Romero-Carazas, R., Control interno de inventario y la gestión de resultados de un emporio

comercial de la región de San Martín - Perú. Región Científica, 2(1), art. 202392, 2023. DOI: https://doi.org/10.58763/rc202392
[56] González-López-Valcárcel, B., and Ortún, V., Reconstrucción del sistema sanitario: gobernanza, organización y digitalización. Informe SESPAS 2022, Gaceta Sanitaria, 36, pp. S44-S50, 2022. DOI: https://doi.org/10.1016/j.gaceta.2022.02.010
[57] Chen, H.-F., Hou, Y.-H., and Chang, R.-E., Application of the balanced scorecard to an academic medical center in Taiwan: the effect of warning systems on improvement of hospital performance, Journal of the Chinese Medical Association, 75(10), pp. 530-535, 2012. DOI: https://doi.org/10.1016/j.jcma.2012.07.007
[58] Mejías, M., Guarate-Coronado, Y.C., and Jiménez-Peralta, A.L., Inteligencia artificial en el campo de la enfermería: implicaciones en la asistencia, administración y educación, Salud, Ciencia y Tecnología, 2(88), pp. 1-7, 2022. DOI: https://doi.org/10.56294/saludcyt202288
[59] Esquer-Rochin, M.A., Gutierrez-Garcia, J.O., Rosales, J.-H., and Rodriguez, L.-F., Design and evaluation of a dashboard to support the comprehension of the progression of patients with dementia in day centers. International Journal of Medical Informatics, 156, art. 104617, 2021 DOI: https://doi.org/10.1016/j.ijmedinf.2021.104617

Y. Sánchez-Suárez, is BSc. Eng. in Industrial Engineering, in 2021, MSc. of Business Administration in 2023, and PhD. in Science, Industrial Technical Engineering all of them from the University of Matanzas, Matanzas, Cuba. He is currently a trainee in the Quality Department of the University of Matanzas. His main research interests include operations management, management, business, supply chain management and hospital management.
ORCID: 0000-0003-1095-1865.

V. Sánchez-Castillo, is BSc. Eng. in Agroecological Engineer from the Universidad de la Amazonia, Colombia. MSc. in Regional Studies in Environment and Development from the Universidad Iberoamericana de Puebla, Mexico. PhD. in Anthropology from the Universidad del Cauca, Colombia. Professor linked to the Universidad de la Amazonia. Associate Researcher at Minciencias. Director of the GIADER Research Group, category A in Minciencias-Colombia.
ORCID: 0000-0002-3669-3123.

C.A. Gómez-Cano, is BSc. in Public Accountant from Universidad de la Amazonia. Public Administrator from Escuela Superior de Administración Pública – ESAP. Business Administrator from Corporación Unificada Nacional de Educación Superior - CUN. Sp. in Pedagogy from the Universidad de la Amazonia, Colombia. Sp. in Public Management from the Escuela Superior de Administración Pública - ESAP. MSc. in Education Sciences from the Universidad de la Amazonia, Colombia MSc. in Management and Evaluation of Investment Projects from the Universidad Externado de Colombia, Bogotá, Colombia. Associate Researcher of the Ministry of Science, Technology and Innovation of Colombia. Professor and Researcher linked to the School of Administrative Sciences of the Corporación Unificada Nacional de Educación Superior - CUN, regional Caquetá.
ORCID: 0000-0003-0425-7201.

DYNA
http://dyna.medellin.unal.edu.co/

UNIVERSIDAD NACIONAL DE COLOMBIA

Probabilistic Weibull reliability of a shaft design subjected to bending and torsion stress

Manuel Baro [a] & Manuel R. Piña-Monarrez [b]

[a] *Tecnológico Nacional de México, Campus Nuevo Casas Grandes, Nuevo Casas Grandes, México. mbaro@itsncg.edu.mx*
[b] *Industrial and Manufacturing Department of the Engineering and Technological Institute, Universidad Autónoma de Ciudad Juárez, Cd. Juárez, México. Manuel.pina@uacj.mx*

Received: September 30th, 2023. Received in revised form: March 18th, 2024. Accepted: April 8th, 2024.

Abstract
The circular shaft serves as the axis of rotation for the components. It is subjected to flexion and tearing, indicating that fatigue is the mode of failure. The range of stresses resulting from the mean and alternating loads determines the occurrence of fatigue failure. The deterministic fatigue analysis, calculated using the stress average obtained from SN curves, can only represent the mean life. This is because the stress range is not a single number, and therefore it cannot provide the reliability level for the stress. The study employs the Weibull distribution to estimate loads and parameters for a probabilistic shaft design under bending and torsion. The minimum strength is assessed using corresponding stress analysis to determine the reliability index for the designed shaft.

Keywords: probabilistic design; Weibull distribution; reliability; stress-strength.

Confiabilidad probabilística Weibull en el diseño de un eje sometido a esfuerzos de flexión y torsión

Resumen
El eje circular sirve de eje de rotación de los componentes. Está sometido a flexión y desgarro, lo que indica que el modo de fallo es la fatiga. El rango de tensiones resultante de las cargas medias y alternas determina la aparición del fallo por fatiga. El análisis determinista de la fatiga, calculado a partir de la tensión media obtenida de las curvas SN, sólo puede representar la vida media. Esto se debe a que el rango de tensiones no es un número único y, por lo tanto, no puede proporcionar el nivel de fiabilidad de la tensión. El estudio emplea la distribución de Weibull para estimar las cargas y los parámetros de un diseño probabilístico de un eje sometido a flexión y torsión. La resistencia mínima se evalúa mediante el correspondiente análisis de tensiones para determinar el índice de fiabilidad del eje diseñado.

Palabras clave: diseño probabilístico; distribución de Weibull; fiabilidad; tensión-resistencia.

1 Introduction

A shaft is a spinning, often circular cross-section that is used in a variety of applications to convey power and rotational motion [1]. The main goal of a shaft design is to make them safe and to continuously enhance this goal, engineers focus on increasing their dependability and efficiency [2]. The shaft design is considered to be a typical mechanical engineering issue in which the effect of the uncertainty, i.e., environment or usage circumstances and material strength qualities, is to try to reduce this uncertainty by applying safety factors [3].

In general, a shaft failure results from bending stress perpendicular to the shaft axis, and the shaft fracture resulting from torsional stress most frequently disposed at a 45° angle to the shaft axis [4], i.e. the stresses acting on the shaft is the σ_x, σ_y and τ_{xy} [5]. Bending and torsion imply that the failure mode of shafts is by fatigue. Then, when shafts are exposed to alternating strains over extended periods, fatigue develops.

How to cite: Baro, M. and Piña-Monarrez, M.R., Probabilistic weibull reliability of a shaft design subjected to bending and torsion stress. DYNA, 91(232), pp. 58-65, April - June, 2024.

To estimate shaft fatigue time, statistical models are crucial since the fatigue behavior of shafts under cyclic stress is random [6]. The Weibull distribution, on the other hand, is the distribution that, using the weakest link concept, could be one of the best predictors of fatigue life [7]. The Weibull distribution is a natural distribution for forecasting lifespan as a result. Moreover, as the Weibull model for fatigue estimate effectively predicts life, it should be utilized to forecast the fatigue SN reliability R(t) [8]. The Weibull distribution has the property of lognormal distribution. This shows that the shape parameters have not changed even though the position and scale parameters have changed [9]. i.e. $X_i \sim W(\beta, \eta, \gamma) \rightarrow \min(X_1, X_2, \ldots X_m) \sim W(\beta, \eta, \gamma_m^{-1/\beta})$. In that case, at least one data set is also Weibull distributed. Based on these facts, we present a probabilistic Weibull model analysis of shaft designs under bending and torsional loading to predict the lifetime SN number [10]. The Weibull distribution withstand stress analysis is then used to calculate the reliability R(t) of the shaft under variable stress [11].

2 Fatigue

Fatigue occurs when a material is subjected to cyclic loads below the threshold at which failure can occur [12]. The cumulative and irreversible nature of damage caused by fatigue processes and the fact that failures often occur suddenly make it difficult to detect incremental changes in material behavior over time [13]. The material behavior under this type of load is different from that under static load materials that can withstand large static loads and can fail at lower loads when repeated many times. Fatigue failure is caused by repeated loading. It is reported that 90% of all devastation is caused by it. On the other hand, fatigue is affected by three basic factors [14].

The three most important factors that affect fatigue are: many cycles, a wide range of applied loads, and high maximum stresses (bending and torsion). There is no universal theory to explain how materials behave under fatigue and cyclic loading, making material fatigue and damaging formation a complex process [15]. By measuring the fatigue life of a component under a given load cycle sequence, fatigue analysis aims to predict fatigue life in actual operation. Fatigue prediction techniques often fall into two categories [16]. The first focuses on predicting crack initiation using a combination of damage as a function of component stress [17]. The second approach is based on the mechanism of continuous fatigue life by calculating damage cycles [18]. According to the deterministic point of view, there are three main ways used in design to identify a cyclically loaded component that would fail over time [19]. In general, the life forecast of sensitive to fatigue parts is based on the safe-life approach [20]. These three methods are linear elastic fracture mechanics, stress-life method, and strain-life method. The purpose of these techniques is to predict N, cycles to failure at a given stress level [21]. This error cycle is categorized as follows: $1 N \leq 10^3$ the cycles as low-cycle fatigue, whereas high-cycle fatigue is $N > 10^3$ cycles [22].

This deterministic method of fatigue calculations is used by most contemporary fatigue standards (ASTM E606/E606M). Due to the use of deterministic algorithms, fatigue estimation always produces the same result given an input [23]. The random nature of fatigue and deterministic fatigue techniques that use characteristic values and high safety factors to explain are fraught with uncertainty [24]. As the issue of fatigue assessment is so complicated and has not yet been properly resolved, probabilistic approaches are required for accurate damage prediction, constructive design, and fatigue risk analysis [25]. Therefore, it is essential to evaluate and predict the fatigue life of elements using mathematical and probabilistic models [1]. Therefore, according to the weakest-link principle, the survival probability of a uniformly loaded volume $V(0)$ is given by all probabilities $m = \frac{V_0}{dV}$ volume elements survive [26].

$$Q_s = 1 - p = \prod_{i=1}^{m}(1 - dP) = (1 - \lambda(s)dV)^m \quad (1)$$

And introducing $V_0 = mdV$ in eq. (2)

$$Q_s = \left(1 - \frac{\lambda(S)V_0}{m}\right)^{\frac{m}{\lambda(s)dV}\lambda(s)dV} \quad (2)$$

As both m and dV rise indefinitely, Eq. (3) transforms into an exponential function, as shown by

$$Q_s = e^{-(\lambda(s)V_0)} \quad (3)$$

2.1 Fatigue Failure Mode for Shafts

A rotating part that conveys power or motion is called a shaft. Typically, its cross-section is round. It provides an axis of rotation or oscillation for a variety of parts, such as cranks, pulleys, and gears. Shafts are designed to transmit motion, so they must be subjected to bending, axial rotation, and torsional loads to transmit motion [27]. Torque is transferred from input to output by torsional stress. The shaft component transmits torque xy. At stable operating levels, the torque is often fairly constant and the outer surface experiences a maximum shear stress due to torsion [28]. A given load element alternates between compression and tension with each rotation of the shaft, so that a constant bending moment applied to the rotating shaft produces a reversible moment in rotation. For deterministic methods of fatigue analysis, the axial stress is lower than the bending stress [29]. Thus, a shaft's failure mechanism is due to fatigue when it is subject to alternating loads over time. The cumulative damage from each cycle approaches a tipping point, leading to failure [30]. As a result, unlike most failure types, fatigue causes failure at loads much below the maximum value. As a result, fatigue is probabilistic rather than deterministic. The ASTM acknowledges that the Weibull distribution is the function that may estimate the life of fatigue [31]. Hence, the mean stress and the alternating stress may be determined using Mohr circle based on the bending stress x, the axial stress y, and the torsion stress xy data. As a result, according to, the values of the Weibull distribution may be approximated

using the principal stresses σ_1 and σ_2 [32].

The foundation of the Mohr circle and the formulation of the maximum stress estimation are described in the next section.

2.2 Generalities of Mohr Circle

The Mohr circle, which was found by Culmann (1866) and explored in detail by Mohr (1882), is a graphical representation of the aforementioned stress connections [33].

$$Cos^2\theta = \frac{1+\cos 2\theta}{2} \tag{4}$$

$$Sen^2\theta = \frac{1-\cos 2\theta}{2} \tag{5}$$

Think about the stressed-out plane condition, where only σ_x, σ_y and τ_{xy} act. Assume that we are aware of these coordinate stresses. Finding the stress state in rotating configurations is the goal in this situation. i.e., determine the major stressors σ_1, σ_2 [34]. Let be θ the angle where the main stresses are operating between the original coordinate system and the rotated system e.g. σ_1, σ_2 and τ_{max} [35]. Based on the normal stresses σ_x, σ_y and τ_{xy}, the major stressors are predicted [36].

The trigonometric double angle is used to mathematically justify the Mohr circle method. i.e.

$$\sigma_x{}' = \sigma_x \cos^2\theta + \sigma_y sen^2\theta + 2\tau_{xy} sin\theta cos\theta\ 0$$

$$\sigma_y{}' = \sigma_x \operatorname{sen}^2\theta + \sigma_y \cos^2\theta - \tau_{xy} sin\theta cos\theta$$

$$\tau_{xy} = (\sigma_y - \sigma_x) sin\theta\, cos\,\theta + \tau_{xy}(cos^2\theta - sen^2\theta) \tag{6}$$

The Mohr circle is a tool that makes it easier to see how rotating the axis affects the stresses and the second-rank tensor [37]. A rotation does not occur for a $xy = 0$, which implies that the stresses produced in the normal plane are acting equally in the normal plane [38]. Nevertheless, as the main stresses are occurring on the rotational plane if $xy \neq 0$, then the Weibull distribution should be utilized rather than the normal distribution [39].

The necessary equations for the estimation of the main stresses as well as the angle of action are presented below.

Maximum stress

$$\sigma_1 = \frac{\sigma_X + \sigma_y}{2} + \sqrt{\left(\frac{\sigma_X + \sigma_y}{2}\right)^2 + \tau_{xy}^2} \tag{7}$$

Minimum stress

$$\sigma_2 = \frac{\sigma_X + \sigma_y}{2} - \sqrt{\left(\frac{\sigma_X + \sigma_y}{2}\right)^2 + \tau_{xy}^2} \tag{8}$$

Mohr circle center

$$\mu = \frac{\sigma_x + \sigma_y}{2} = \frac{\sigma_1 + \sigma_2}{2} \tag{9}$$

Maximum shear stress (ratio)

$$\tau_{max} = \sqrt{\left(\frac{\sigma_X + \sigma_y}{2}\right)^2 + \tau_{xy}^2} = \frac{\sigma_1 - \sigma_2}{2} \tag{10}$$

Principal angle

$$\theta_p = \frac{\tan^{-1}\left(\frac{2\tau_{xy}}{\sigma_x - \sigma_y}\right)}{2} \tag{11}$$

Shear angle θ_s

$$\theta_s = \frac{\tan^{-1}\left(\frac{\sigma_x - \sigma_y}{2\tau_{xy}}\right)}{2} \tag{12}$$

Thus, depending on the strength of the material, the maximum shear stress theory and the deformation energy theory provide a safe state S y and the safety factor S f.

$$DE = \sqrt{\sigma_x^2 - \sigma_x\sigma_Y + \sigma_y^2} < S_y/S_f \tag{13}$$

And the maximum stress is.

$$\sigma_{max} = S_y/S_f \tag{14}$$

The parameters of the Weibull distribution can be obtained entirely from the primary stresses using the Mohr circle-Weibull relation [40]. However, this fatigue failure prediction method does not consider stress as a random variable [41].

3 Weibull Distribution

In this section, the Weibull model used in fatigue analysis is presented along with the theoretical basis and characterization definitions. Due to its versatility, the Weibull distribution is often used in reliability and service life studies [42]. Depending on the value of the Weibull parameter, the Weibull distribution can be used to describe different life behaviors. The values of the shape and scale parameters have a strong influence on the distribution characteristics [43]. The probability density function of the Weibull distribution is given by.

$$f(t) = \frac{\beta}{\eta}\left(\frac{t}{\eta}\right)^{\beta-1} exp^{-\left(\frac{t}{\eta}\right)^{\beta}} \tag{15}$$

The Weibull distribution cumulative and reliability functions are

$$F(t) = 1 - exp^{-\left(\frac{t}{\eta}\right)^{\beta}} \tag{16}$$

$$R(t) = exp^{-\left(\frac{t}{\eta}\right)^{\beta}} \tag{17}$$

The linear form of Eq. (17) is given by.

$$\ln\left(-\ln\left(1 - F(t_i)\right)\right) = -\beta \ln\eta + \beta \ln t_i\ =$$

$$Y_i = \beta[-\ln(\eta) + \ln(t_i)] \tag{18}$$

Or equivalently is given by

$$Y_i = b_0 + \beta X_i \tag{19}$$

Where $Y_i = \ln(-\ln(1 - F(t_i))) = -\beta \ln(\eta)$, and $x_i = \ln(t_i)$, $F(t_i)$. The median rank is given by.

$$F(t_i) = \frac{1 - 0.3}{n + 0.4} \tag{20}$$

The sample n is determined by the reliability R(t).

$$n = \frac{-1}{\ln(R(t))} \tag{21}$$

The mean μ_y and the standard deviation σ_y of the vector Y are

$$\mu_y = \sum_{i=1}^{n} \frac{Y_i}{n} \tag{22}$$

$$\sigma_y = \sqrt{\sum_{i=1}^{n} \frac{Y_i}{n} \left(\frac{Y_i - \mu_y}{n - 1}\right)^2} \tag{23}$$

4 Weibull Distribution Properties

Concerning to location and scale transformation the Weibull distribution is stable, which is the first of two crucial Weibull distribution characteristics for fatigue lifetime prediction.

$$X \sim W(\beta, \eta, \gamma) \leftrightarrow \frac{X - a}{b} \sim W\frac{\gamma - a}{b}, \frac{\eta}{b}, \beta \tag{24}$$

This implies that while the shape parameters are kept unchanged, the transformation constants a and b are given new scale and position parameters in relation to their former values. In other words, assuming the scale and position parameters stay the same, the converted variable is likewise a Weibull random variable. Their resilience to the most straightforward random variable manipulations, $X_i = 12, \ldots, m,$ demonstrates their independence and uniform distribution.

$$X_i \sim W(\beta, \eta, \gamma) \rightarrow \min(X_1, X_2, \ldots, X_m) \sim W(\gamma, \eta_m^{-\frac{1}{\beta}}, \beta) \tag{25}$$

This shows that a random variable's distribution is the same as a collection of independently distributed random variables if it is a Weibull variable. There is a minimum with a collection of identical random values X_i through X_m that are independently distributed and have a common $Cdf\ F(x)$.

$$F_{min}(x) = 1 - [1 - F(x)]^m \tag{26}$$

$$F_{min}(x) = 1 - \left\{1 - \left(1 - exp\left[-\left(\frac{x-\lambda}{\gamma}\right)^{\beta}\right]\right)\right\}^m = 1 - exp\left[-\left(\frac{x-\lambda}{\gamma m^{-\frac{1}{\beta}}}\right)^{\beta}\right] \tag{27}$$

5 Fundaments of the Fatigue Weibull Model

The Weibull model is used for fatigue life of constant cycle components based on the following principles:

According to the weakest link theory, the fatigue of a longitudinal member is equal to the minimum fatigue of its components.

$$F_{min}(x) = F_{nl}(x) = 1 - [1 - F_l(x)]^n \tag{28}$$

The second fundament is stability, which means that the selected distribution family must hold for different lengths, it is to say, a parametric family of $cdfs$ is used to represent the cdf for fatigue of a longitudinal element of length l, according to Eq. (18) the element must be

$$F(x; \beta(nl), \eta(nl), \gamma(nl)) = 1 - [1 - (29)\, F((x; \beta(nl), \eta(nl), \gamma(nl))]^n \tag{29}$$

The Weibull distribution was the only distribution that could satisfy this functional equation.

A third concept, known as limit behavior, is that in extreme cases where the component size of an element tends to zero or the number of components tends to infinity, the distribution function is asymptotic and the distribution in the independent case are the Weibull and Gumbel distributions.

$$\begin{aligned} \text{Lim}\, f(x) &= \lim [\beta, \eta, \gamma(1 \\ &\quad - exp^{\eta x})^{\beta - 1} exp\{\beta, \eta \\ &\quad - \gamma(exp^{\eta x} - 1)^{\beta}] \\ &= \beta, \eta, \gamma * 1 \end{aligned} \tag{30}$$

$$\begin{aligned} \text{Lim}\, f(x) &= \lim_{0 \to \infty} [\beta, \eta, \gamma(1 - e^{\eta x})^{\beta - 1} e\{\beta, \eta \\ &\quad - \gamma(e^{\eta x} - 1)^{\beta}] \\ &= \beta, \eta, \gamma * 1^{\beta - 1} * 0 \end{aligned} \tag{31}$$

The approach to fully estimate the Weibull distribution parameters directly from the primary stresses [39].

6 Estimation of Weibull Parameters by Method

Step 1:
Choose reliability level.

Step 2:
Using the $R(t)$ indices from step 1, compute the corresponding n values in equation (20). As a result, use the F_{ti} values from equation (20) and the mean and standard values. to calculate the appropriate element Y_i. Deviation from equations (22) and (23).

Step 3:
Perform a stress analysis to determine the maximum and

minimum primary stress and calculate the ratio. $\sigma_1; \sigma_2$.

Step 4.

By utilizing the Weibull distribution's initial shape parameter value, $\ln(t_{io}) = \frac{Y_i}{\beta}$ it is

$$\beta = \frac{-4\mu_y}{\ln\left(\frac{\sigma_1}{\sigma_2}\right)} \tag{32}$$

Estimate standardized logarithms ($\ln(t_{oi})$) elements, and calculate the initial μ_{og}, μ_o and the $g(x)$ values are given by.

$$\mu_{og} = \sum_{i=1}^{n} \frac{\ln(t_{oi})}{n} = \frac{\mu_y}{\beta} \tag{33}$$

$$\mu_o = \sum_{i=1}^{n} \frac{t_{oi}}{n} \tag{34}$$

$$g(x) = \sum_{i=1}^{n} \frac{Y_i}{n} = \exp(\mu_{og}) \tag{35}$$

Step 5.

Determine the corresponding β value given by

$$\beta = \frac{-4\mu_y}{\ln\left(\frac{\sigma_1}{\sigma_2}\right) * (0.9947)} \tag{36}$$

Step 6.

With the principal stresses σ_1 and σ_2, estimate the mean μ. Then, based on the Mohr circle estimation μ and the estimated t_{oi} mean value μ_o of step 5, determine the corresponding scale η parameter of the Weibull distribution as

$$\eta = \frac{\mu}{\mu_o} \tag{37}$$

The β value of step 5 and the η value of step 6 corresponds to the Weibull parameters that represents the observed stresses σ_1 and σ_2 values.

Finally, given that stress behavior is typically viewed as falling below a log-normal distribution provided by

$$f(t) = \frac{1}{t\sigma_g\sqrt{2\pi}} \exp\left\{-\left(\frac{ln\,(t_i - \mu_g}{2\sigma_g}\right)^2\right\} \tag{38}$$

With log-mean μ_g and log-standard deviation σ_g parameters, thereby because both μ_g and σ_g [44] the log-normal distribution's parameter connection in terms of β and η is given by

$$\beta = \frac{\sigma_y}{\sigma_g} \tag{39}$$

$$\eta = \exp\left\{\mu_g - \frac{\mu_y}{\beta}\right\} \tag{40}$$

Where μ_y and σ_y from Equation (22) mean and standard deviation, respectively (23). Then the negative μ_g and the standard deviation is given by

$$\sigma_g = \frac{\sigma_y}{\beta} \tag{41}$$

$$\mu_g = \ln(\eta) + \frac{\mu_y}{\beta} \tag{42}$$

In the next part, the approach is now applied, and the results are compared to those of the deterministic method.

7 Weibull Shaft Lifetime Application

The used data to run the numerical application are an alternator rotor is supported by the shaft in Fig. 1. It is constructed from AISI 4340 steel that has been heating treated, ground, and given a Brinell hardness range of 323–370. (R, 35 to 40). The shaft will experience an axial force from the rotor of up to $130\ MPa$ and a maximum bending stress of $607\ MPa$. The predicted dependability is $R(t) = 95\%$, and the shaft will rotate at a speed of $12000\ rpm$. Tensile yield, the properties of the material, correspond to a material with a 277 Brinell hardness, Sy, and ultimate strength, Sut, with $Sy = 113Mpa$ and $Sut = 128Mp$, respectively (see Figs. 1 and 2) [45].

This suggests that if the system is in equilibrium, the total sum of all forces and moments must equal zero.

8 Parameters of the Design Shaft

Step 1. The desired reliability index according to the data is 95%, however, to have an integer n value the reliability level to use will be equal to $R(t) = 0.9535$.

Step 2. By using Eq. (31) the n value is estimated as follows:

$$n = \frac{-1}{\ln(0.9535)} = 21$$

Then, using Eq. (31) according to the n value estimated, the corresponding $F(ti)$ elements, and Yi elements, in the same way, the μ_y and σ_y values are given in Table 1.

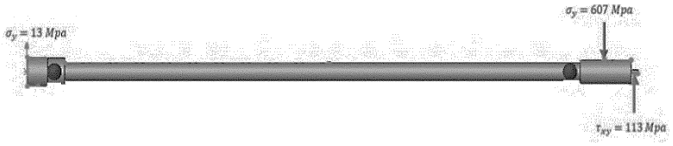

Figure 1. Shaft
Source: The authors

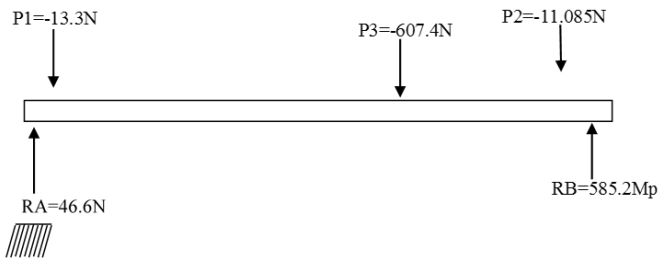

Figure 2. Free-Body diagram
Source: The authors

Table 1.
Weibull $\beta = 3.710802$ and $\eta = 409.156$
Example of a table.

n	$F(t_i)$	Y_i	$\ln(t_{oi})$	t_{oi}	n	$F(t_i)$	Y_i	$\ln(t_{oi})$	t_{oi}
1	0.03271	-3.403483	-1.7148667	0.1799877	12	0.546729	-0.234122	-0.117964	0.888728
2	0.079439	-2.491662	-1.2554397	0.2849505	13	0.593458	-0.105285	-0.0530486	0.948334
3	0.126168	-2.003463	-1.0094577	0.3644166	14	0.640187	0.021928	0.0110488	1.01111
4	0.172897	-1.661646	-0.8372308	0.4329077	15	0.686916	0.149526	0.0753395	1.0782502
5	0.219626	-1.394398	-0.7025764	0.4953075	16	0.733645	0.279845	0.1410017	1.1514266
6	0.266355	-1.172054	-0.5905467	0.5540243	17	0.780374	0.415962	0.2095851	1.2331664
7	0.313084	-0.979381	-0.4934674	0.6105058	18	0.827103	0.562502	0.2834202	1.3276629
8	0.359813	-0.807447	-0.4068375	0.6657524	19	0.873832	0.727616	0.3666139	1.4428407
9	0.406542	-0.650492	-0.3277546	0.7205398	20	0.920561	0.929311	0.4682391	1.5971792
10	0.453271	-0.504509	-0.2542	0.7755367	21	0.96729	1.22966	0.6195719	1.8581324
11	0.5	-0.366513	-0.1846699	0.8313787		$\mu_y=$	-0.545624	$\mu_{oi}=$ -0.274916	$\mu_o=$ 0.878673
						$\sigma_y=$	1.1751169	$\sigma_{oi}=$ 0.5920901	$\sigma_o=$ 0.4454875

Source: The authors

Determinant of the stresses is given by.

$$Det = 78910 - 12769 = 66141$$

corresponding geometric mean is

$$g(x) = \sqrt{66141} = 257.178926\ Mpa.$$

the arithmetic mean is given by

$$\mu = \frac{607 + 130}{2} = 368.5\ Mpa.$$

The eigenvalues are given by $\lambda = \mu \pm \sqrt{\mu^2 - g(x)^2}$

$\sigma_1 = \mu + \sqrt{368.5Mpa^2 - 257.1789Mpa^2}$ *=345.6443Mpa*

$\sigma_2 = \mu - \sqrt{368.5Mpa^2 - 257.1789Mpa^2}$ *=191.3557Mpa.*

The angle acting on this system is given by Eq. (25), this is equivalent to

$$\theta = \tan^{-1}\left(\frac{257.178926Mpa}{345.6443Mpa}\right) = 36.6513352$$

In such a way the principal stresses σ_1 and σ_2 are equal to *345.6443Mpa, and 191.3557Mpa,* respectively.

Determine the value of β of the Weibull distribution as

$$\beta = \frac{-4(-0.54562)}{\ln\left(\frac{345.6443Mpa}{191.3557Mpa}\right) * (0.9947)} = 3.71080171$$

The scale value η of the Weibull distribution is determined as

$$\eta = \frac{368.5Mpa}{0.900634} = 409.1562166$$

The parameter that represents the Weibull distribution family is given by $W{\sim}(\beta = 3.71080717, \eta = 409.1562166)$. Then, these Weibull parameters are the stress distribution parameters (see Table 1).

9 Estimation of strength parameters and its corresponding reliability

The basis of the investigation is the initial stress intensity ratio from the Weibull analysis. This gives the minimum material strength and maximum principal stress at which failure occurs. After that, the procedure will be explained.

Step 1.
Determine the principal stresses.
In this case the principal stresses are $\sigma_1 = 345.6443Mpa.$ and $\sigma_2 = 191.3557Mpa.$

Step 2.
Used the estimated Weibull parameters.

$$\eta = 409.1562166 \quad \text{and} \quad \beta = 3.71080171$$

Step 3.
Estimate the value of g_x

$$g_x = \sqrt{345.6443 * 191.3557} = 257.17894$$

Step 4.
Select the reliability level and using the corresponding β value estimate the values of t_{oi}.
If the desired reliability is 95% and $\beta = 3.71080171$ then.

$$t_{oi} = (-\ln(R(t))^{\frac{1}{\beta}} \tag{43}$$

$$t_{oi} = (-\ln(0.95)^{\frac{1}{3.71}} = 0.44906317$$

Step 5.
Estimate the minimum strength.

$$Strength_{min} = \eta * t_{oi} \tag{44}$$

$$Strength_{min} = 409 * 0.4490 = 183.7368904$$

Step 6.
Estimate the minimum strength average.

$$Strength_{min} = \mu_{min} - \sigma_{min} \quad (45)$$

$$\mu_{min} = Strength_{min}/0.90 \quad (46)$$

$$\mu_{min} = \frac{183.7368904}{0.90} = 204.1521004$$

$$Strength_{min} = 409 * 0.4490 = 183.7368904$$

Step 7.
Determine t_o

$$t_o = \sqrt{\sigma_2/\sigma_1} \quad (47)$$

$$t_o = \sqrt{191.3557/345.644} = 0.744056972$$

Step 8.
Estimate $Strength_{min}$ with

$$Strength_{min} = 1/\eta^{1/\beta} \quad (48)$$

$$Strength_{min} = 1/409.156216^{1/3.71} = 0.19769094$$

Step 9.
Determine the scale parameter as

$$\eta = \frac{Strength_{min}}{((-\ln(R(t))^{\frac{1}{\beta}})} \quad (49)$$

$$\eta = \frac{183.7368904}{((-\ln(0.95)^{\frac{1}{3.71}})} = 409.1560003$$

Step 10.
Estimate the corresponding design reliability using equation 17.

$$Strength_{min} = \eta * t_{oi} \text{ and } strength_{max} = \eta/t_{oi} \quad (50)$$

$$Strength_{min} = 409.1562166 * 0.744056972 = 304.4351375$$

$$R(t) = exp^{-\left(\frac{409.156}{304.435}\right)^{3.71}} = 0.949944802$$

As can be seen, the reliability of the design for the diameter and the used material corresponds to 95% and the estimated Weibull family for both stress and resistance represents the fatigue behavior completely.

10 Conclusion

By predicting the primary stresses and the lowest and average loads, the probabilistic design for the analysis of the chosen element can be estimated, in this case, an axis, and first, evaluate the validity of the design for the stress and load. It is also feasible to identify the associated loads for the resistance and the accompanying Weibull parameters using the estimated Weibull distribution parameters. This allows for the calculation of the dependability of the resistance, which accurately depicts the resistance distribution. It is feasible to construct appropriate decision-making for the type of stress and resistance by determining the related distributions, as shown in this study.

References

[1] Khan, A., Das, A., and Bhaskar, A.S., Prediction of fatigue life of glass-vinyl-ester-polyurethane sandwich structure using mathematical model. In: Pal, S., Roy, D., Sinha, S.K. (eds), Processing and Characterization of Materials. Springer Proceedings in Materials, 13, Springer, Singapore. 2021. DOI: https://doi.org/10.1007/978-981-16-3937-1_24

[2] Ebrahimi, A., Effect analysis of RAMS parameter in design & operation of DP system in floating offshroe structure, Royal Institute of Technology, October, 2010.

[3] Rao, B.C., Revisiting classical design in engineering from a perspective of frugality, Heliyon, 3(5), art. e00299, 2017. DOI: https://doi.org/10.1016/j.heliyon.2017.e00299.

[4] Xu, Z., Cui, Y., Li, B., Liu, K., Shi, F., and Cao, P., Impact analysis of initial cracks angle on fatigue failure of flange shafts. Coatings, 12(2), 2022. DOI: https://doi.org/10.3390/coatings12020276

[5] Rexnord Industries G.G., LLC, Gears-Shafts-Bearings-Seals, Failure Analysis Installation & Maintenance, 2(August), 1978, 20 P.

[6] Korczewski, Z. and Marszałkowski, K., Energy analysis of the propulsion shaft fatigue process in a rotating mechanical system. Part III dimensional analysis. Polish Maritime Research, 28(2), pp. 72–77, 2021. DOI: https://doi.org/10.2478/pomr-2021-0023.

[7] Barraza-Contreras, J.M., Piña-Monarrez, M.R., and Molina, A., Fatigue-life prediction of mechanical element by using the Weibull distribution, Applied Sciences (Switzerland), 10(18), art. 6384, 2020. DOI: https://doi.org/10.3390/APP10186384.

[8] Zhao, Y.X., and Liu, H.B., Weibull modeling of the probabilistic S-N curves for rolling contact fatigue, Int J Fatigue, 66, pp. 47–54, 2014. DOI: https://doi.org/10.1016/j.ijfatigue.2014.03.008.

[9] Taketomi, N., Yamamoto, K., Chesneau, C., and Emura, T., Parametric distributions for survival and reliability analyses, a review and historical sketch, Mathematics, 10(20),art. 10203907, 2022. DOI: https://doi.org/10.3390/math10203907.

[10] Matsuda, S. and Ogi, K., Effect analysis of loading rate on relationship between strength and flaw size of ceramics using probabilistic model on the basis of SCG concept, Transactions of the JSME (in Japanese), 83(847), pp. 16-00369-16–00369, 2017. DOI: https://doi.org/10.1299/transjsme.16-00369.

[11] Baro-Tijerina, M., Piña-Monárrez, M.R., and Villa-Covarrubias, B., Stress-strength weibull analysis with different shape parameter β and probabilistic safety factor, DYNA (Colombia), 87(215), pp. 28–33, 2020. DOI: https://doi.org/10.15446/dyna.v87n215.84909.

[12] Aaronson, L.S., Defining and measuring fatigue. Journal of Nursing Scholarship, 31(1), pp. 45–50, 1999. DOI: https://doi.org/10.1111/j.1547-5069.1999.tb00420.x.

[13] Ma, X., Yang, F., Li, J., Xue, Y., and Guan, Z., Fatigue life assessment method of in-service mechanical structure. Advances in Mechanical Engineering, 13(2), pp. 1–9, 2021. DOI: https://doi.org/10.1177/1687814021996524.

[14] Khalaf, M.R. and Al-Ahmed, A.H.A., Effect of large openings on the behavior of reinforced concrete continuous deep beams under static and repeated load. E3S Web of Conferences, 318, pp. 3–10, 2021. DOI: https://doi.org/10.1051/e3sconf/202131803012.

[15] Hosseini, S.M., Azadi, M., Ghasemi-Ghalebahman, A., and Jafari, S.M., Data analysis of striation spacing, lifetime, and crack length in crankshaft ductile cast iron under cyclic bending loading through high-cycle fatigue regime, Data Brief, 45(December), art. 108666, 2022. DOI: https://doi.org/10.1016/j.dib.2022.108666.

[16] Kashyzadeh, K.R., Souri, K., Bayat, A.G., Jabalbarez, R.S, and Ahmad, M., Fatigue life analysis of automotive cast iron knuckle under constant and variable amplitude loading conditions. Applied Mechanics, 3(2), pp. 517–532, 2022. DOI: https://doi.org/10.3390/applmech3020030.

[17] Liu, B., Sun, Y., Wang, J., and Zhang, G., Characteristic analysis of crack initiation and crack damage stress of sandstone and mudstone under low-temperature condition. Journal of Cold Regions Engineering, 34(3), art. 0225, 2020. DOI: https://doi.org/10.1061/(asce)cr.1943-5495.0000225.
[18] Kim, H.S., A practical procedure for predicting the remaining fatigue life at an arbitrary stress ratio, Journal of Composites Science, 6(6), art. 60170, 2022. DOI: https://doi.org/10.3390/jcs6060170.
[19] Kim, J., Anterior cruciate ligament microfatigue damage detected by collagen autofluorescence in situ. J Exp Orthop, 9(1), art. 74, 2022. DOI: https://doi.org/10.1186/s40634-022-00507-6.
[20] Chen, M., Xiong, X., Zhuang, W., and Zeng, F., Fatigue life analysis of automotive glass regulator based on ABAQUS and FE-SAFE. IOP Conf Ser Earth Environ Sci, 571(1), art. 012109, 2020. DOI: https://doi.org/10.1088/1755-1315/571/1/012109.
[21] Alamnie, M.M., and Endalemaw, Y., Fatigue life analysis of rail-welds using linear elastic fracture mechanics, ISEC 2019 - 10th International Structural Engineering and Construction Conference (July), 2019. DOI: https://doi.org/10.14455/isec.res.2019.197.
[22] Wang, S., Tang, S., He, C., and Wang, Q., Cyclic deformation and fatigue failure mechanisms of thermoplastic polyurethane in high cycle fatigue, Polymers (Basel), 15(4), art. 5040899, 2023. DOI: https://doi.org/10.3390/polym15040899.
[23] Chai, Y., Gao, W., Ankay, B., Li, F., and Zhang, C., Aeroelastic analysis and flutter control of wings and panels: a review. International Journal of Mechanical System Dynamics, 1(1), pp. 5–34, 2021. DOI: https://doi.org/10.1002/msd2.12015.
[24] Guo, F., Hu, F., Wu, S., He, F., Liu, J., and Wu, X., System dynamics in structural strength and vibration fatigue life assessment of the swing bar for high-speed maglev train. International Journal of Mechanical System Dynamics, 2(2), pp. 178–189, 2022. DOI: https://doi.org/10.1002/msd2.12045.
[25] Schneider, J., and Haindl, H., Mechanic treatment of fastener holes: the influence of compressive residual stress on the corrosion behaviour of aluminium alloys, Materials and Corrosion, 59(9), pp. 753–761, 2008. DOI: https://doi.org/10.1002/maco.200804149.
[26] Hirschberg, V., Wilhelm, M., and Rodriguez, D., Cumulative nonlinearity as a parameter to quantify mechanical fatigue. Fatigue Fract Eng Mater Struct, 43(2), pp. 265–276, 2020. DOI: https://doi.org/10.1111/ffe.13120.
[27] Hahn, S., Feldmeth, S., and Bauer, F., Assessment of the lubricity of grease-sealing rotary shaft seals based on grease properties. Chem Eng Technol, 46(1), pp. 53–60, 2023. DOI: https://doi.org/10.1002/ceat.202200382.
[28] Patel, N., Mohebbi, A., Jan, C.D., and Guo, J., Maximum shear-stress method for stable channel design. Guo, 146(12), art. 01827, 2020. DOI: https://doi.org/10.1061/(asce)hy.1943-7900.0001827.
[29] Turbucz, M., and Fayad, J., Can semirigid fixation of the rostral instrumented segments prevent proximal junctional kyphosis in the case of long thoracolumbar fusions? A finite element study, SPIN (March), art. 22931, 2023. DOI: https://doi.org/10.3171/2023.1.SPINE22931.
[30] Joun, M.S., Ji, S.M., Chung, W.J., Cho, G.S., and Lee, K.H., A new general fatigue limit diagram and its application of predicting die fatigue life during cold forging, Materials, 15(79, pp. 1–17, 2022. DOI: https://doi.org/10.3390/ma15072351.
[31] Wang, Y., and Peng, Z., Fatigue life prediction method of mechanical parts based on Weibull distribution. IOP Conf Ser Mater Sci Eng, 782(2), art. 022068, 2020, DOI: https://doi.org/10.1088/1757-899X/782/2/022068.
[32] Pawliczek, R., and Rozumek, D., Limited stress surface model for bending and torsion fatigue loading with the mean load value, Materials, 14(22), art. 227023, 2021. DOI: https://doi.org/10.3390/ma14227023.
[33] Parry, Mohr's Circles, Stress Paths, and Geotechnics. New York, USA, 2004.
[34] Stresses, P., Stress, Strain, Mohr' s Circle, 2014, pp. 1–7.
[35] Narayan, K., Behdinan, K., and Vanderpol, P., An equivalent uniaxial fatigue stress model for analyzing landing gear fuse pins, Strength of Materials, 38(3), pp. 278–288, 2006. DOI: https://doi.org/10.1007/s11223-006-0041-6.
[36] Pelleg, J., Mechanical Properties of Materials, Vol. 190, Springer, 2012, 645 P. DOI: https://doi.org/10.1007/978-94-007-4342-7.
[37] Wang, Z., Sun, G., Wang, W., and Zhang, M., Application for surveillance video with tensor factorization in machine learning. SSRN Electronic Journal (February), art. 4218404, 2022. DOI: https://doi.org/10.2139/ssrn.4218404.
[38] Taniguchi, Y., Takizawa, K., Otoguro, Y., and Tezduyar, T.E., A hyperelastic extended Kirchhoff–Love shell model with out-of-plane normal stress: I. Out-of-plane deformation, Comput Mech, 70(2), pp. 247–280, 2022. DOI: https://doi.org/10.1007/s00466-022-02166-x.
[39] Piña-Monarrez, M.R., Weibull stress distribution for static mechanical stress and its stress/strength analysis. Qual Reliab Eng Int, 34(May), pp. 229–244, 2017. DOI: https://doi.org/10.1002/qre.2251.
[40] Li, L., Cao, H., Guan, J., He, S., Niu, L., and Liu, H., A three-parameter Weibull distribution method to determine the fracture property of PMMA Bone Cement, Polymers (Basel), 14(17), pp. 1–17, 2022. DOI: https://doi.org/10.3390/polym14173589.
[41] Menan, F., P-a A., and François, M., The stress-strength interference method applied to fatigue design: the independence of the random variables, Procedia Eng., 133(December), pp. 746–757, 2015. DOI: https://doi.org/10.1016/j.proeng.2015.12.656.
[42] Sugito, P M.A., Ispriyanti, D., and Dewi, L.N., Analysis of geometric and Weibull queuing model. Case study: customer service and electronic ID card recording counters at Dispendukcapil of Semarang City. Journal of Physics: Conference Series, 1943(1), art. 012151, 2021. DOI: https://doi.org/10.1088/1742-6596/1943/1/012151.
[43] Khan, M.G.M. and Ahmed, M.R., Bayesian method for estimating Weibull parameters for wind resource assessment in the Equatorial region: a comparison between two-parameter and three-parameter Weibull distributions, Wind Energy Science, 8, pp. 1277–1298, 2023. DOI: https://doi.org/10.5194/wes-8-1277-2023
[44] Piña-Monarrez, M.R. and Ortiz-Yañez, J.F., Weibull and lognormal Taguchi analysis using multiple linear regression. Reliability Engineering & System Safety, 144, pp. 244–253, 2015. DOI: https://doi.org/10.1016/j.ress.2015.08.004.
[45] Juvinall, R.C., and Saunders, H., Fundamentals of Machine Component Design. J. Mech., Trans., and Automation, 105(4), pp. 607-607, 2012. DOI: https://doi.org/10.1115/1.3258522.

M. Baro-Tijerina, is a researcher-professor in the Industrial and Manufacturing Department at the Technological Institute of Nuevo Casas Grandes, Mexico, He completed his BSc. Eng. in Industrial and System from the ITSNCG. MSc. in Industrial Engineering from the Universidad Autónoma de Ciudad Juárez, México, getting the highest mark. By last he completed his Technology PhD in 2020. Also getting the highest mark. Contact al164467@alumnos.uacj.mx.
ORCID: 0000-0003-1665-8379

M.R. Piña-Monárrez, is a researcher-professor in the Industrial and Manufacturing Department at the Autonomous University of Ciudad Juárez, México. PhD. in Science in Industrial Engineering in 2006 from the Instituto Tecnológico de Ciudad Juárez, México. He had conducted research on system design methods including robust design, reliability and multivariate process control. He is member of the National Research System (SNI), of the National Council of Science and Technology (CONACYT) in México.
ORCID: 0000-0002-2243-3400

DYNA
http://dyna.medellin.unal.edu.co/

UNIVERSIDAD NACIONAL DE COLOMBIA

A reliability model for non-isothermal isotropic damages

Allan Jonathan da Silva & Felipe do Carmo Amorim

Centro Federal de Educação Tecnológica Celso Suckow da Fonseca (CEFET/RJ), Itaguaí, Rio de Janeiro, Brasil. allan.jonathan@cefet-rj.br, felipe.amorim@cefet-rj.br

Received: September 27th, 2023. Received in revised form: April 2nd, 2024. Accepted: April 8th, 2024.

Abstract
This study introduces a novel lifetime distribution originating from the Neyman Type A distribution. We built a Neyman Type A counting process and developed a survival function. Some statistical properties of the new distribution were presented, such as the resulting humped hazard function and its convergence. An accelerated test model structure with Arrhenius law was specified, and the effects of different accelerating stresses were analyzed. The hazard function implied by the model is inversely proportional to the stress, which results in interesting features and provides an efficient approach to describe the lifespan phenomena of some engineering metals and bulbs under low temperatures. The estimation of parameters of the accelerated model by maximum likelihood, mean time to failure, and expected number of failures are discussed in the numerical experiments.

Keywords: reliability; Neyman type A distribution; accelerated life tests.

Un modelo de confiabilidad para daños isotrópicos no isotérmicos

Resumen
Este artículo presenta una nueva distribución de vida útil que se origina a partir de la distribución de Neyman Tipo A. Construimos el proceso de conteo de Neyman Tipo A y desarrollamos la función de supervivencia. Se presentan algunas propiedades estadísticas de la nueva distribución, como la función de riesgo resultante en forma de joroba y su convergencia. Se especifica una estructura de modelo de prueba acelerada con la ley de Arrhenius, y se analizan los efectos de diferentes tensiones acelerantes. La función de riesgo implicada por el modelo es inversamente proporcional al estrés, lo que resulta en características interesantes: el modelo proporciona un enfoque eficiente para describir los fenómenos de vida útil de algunos metales de ingeniería y bombillas a bajas temperaturas. Se discute la estimación de parámetros del modelo acelerado mediante máxima verosimilitud, el tiempo medio hasta la falla y el número esperado de fallas en experimentos numéricos.

Palabras clave: confiabilidad; distribución de Neyman tipo A; pruebas de vida aceleradas.

1 Introduction

Understanding how components and systems age is of academic and industrial interest. The development of the lifetime distribution is the core of reliability engineering and related areas. From statistical distributions, many important concepts such as the hazard function, mean time to failure, probability of failure, and mean residual life can be obtained. There is a vast amount of modern literature supporting the component's lifetime. The reliability engineering basics can be found in [1,2]. The accelerated life test models can be found in [3]. Many recent books discuss warranty policies, such as [4-9] discussed maintenance policies, costs associated with imperfect repairs, and maintenance optimization with variable recovery factors, respectively.

Many models discuss the lifetime data distributions. Classical exponential, Weibull, and lognormal distributions have been extensively studied. These models can derive various hazard functions. [3] also found many life-stress relationships, such as Arrhenius and inverse power laws, to address the accelerated life test problem. In this context, physical laws are merged with statistical distributions to describe the failure behavior in distinct stress scenarios. In general, the higher the stress level, the lower the product performance and mean time to failure. Arrhenius's law, for example, inversely relates the lifespan to thermal stress. The inverse-power law is the same for non-thermal stresses, such

How to cite: da Silva, A.J. and Amorim, F.C., A reliability model for non-isothermal isotropic damages. DYNA, 91(232), pp. 66-76, April - June, 2024.

as voltage or vibration. The Eyring model is typically used for temperature- or humidity-accelerated stresses [3].

Nonetheless, some types of failure occur in lower-temperature environments. Cold weather tends to wear fluorescent bulbs and shorten their lifespans. Steels suffer from low temperature brittle fatigue. Aircraft and chemical processing equipment are required to operate at low temperatures, and the behavior of metals needs to be considered. Jae Myung Lee, the Guest Editor of the Special Issue "Low-Temperature Behavior of Metals" of the Metals journal, stated in [10]: "*Many engineering metals become brittle at low temperatures so that the structures fabricated using these materials may fracture or fail unexpectedly when subjected to stress levels at which the performance may be satisfactory under normal temperatures.*"

In general, the increase in the tensile and yield strengths at low temperatures is characteristic of metals. Extremely low temperatures may reduce the toughness. The transition temperature at which brittle fracture occurs is lowered by a series of characteristics, such as a decrease in the carbon content or grain size and an increase in the nickel or manganese content [11].

Notably, the behavior of metals at low temperatures is not limited to traditional crystalline metals. Brittle metallic glasses, such as Mg-based bulk metallic glasses, can also exhibit brittle behavior at low temperatures. However, even in these brittle glasses, there are indications of a "ductile" fracture mechanism, as observed through the presence of a dimple structure at the fracture surface [11].

The development of special materials that are resistant to low temperatures to store and transport hydrogen, for example, is a matter of concern. Many studies have discussed low-temperature embrittlement and fracture of metals, such as [12-17] showed that the impact toughness of locomotive wheel steel at $-60°$ test temperature has decreased three times in relation to temperatures from $-20°$ to $20°$. In the investigation of a Pb-free circuit board applied for space exploration by [18], it was shown that the ball grid array solder joint changed from ductile to brittle over the range of $-70°$ to $-80°$.

This study's novel application of a new probability distribution in reliability modeling is contextualized within the broader field of material failure analysis under extreme conditions such as low temperatures. Recent studies, such as [19], have explored superposition-based predictions of creep in polymer films at cryogenic temperatures, emphasizing the need for predictive models in environments where traditional testing is challenging. Similarly, [20] investigated the strain-hardening behavior of AISI 304 stainless steel at varying temperatures, highlighting the influence of temperature on the mechanical properties and fracture morphology. [21] discussed the computational limitations of the five main creep failure models. Furthermore, research by [22-24] has delved into the complexities of material behaviors under stress and temperature variations, revealing intricate patterns of mechanical response and failure mechanisms that are crucial for advanced engineering applications. Our model extends these discussions by providing a robust statistical framework that captures the risk failure behaviors of metallic materials at low temperatures, offering significant insights compared to existing methods. By integrating the principles observed in these studies, our approach enhances the predictive accuracy of material failure models, facilitating a more reliable design and assessment of materials for low-temperature applications.

This study aims to introduce a novel approach in reliability engineering by adapting the Neyman Type A distribution to analyze material failures under low-temperature conditions, a prevalent scenario in engineering applications. Unlike classical physico-statistical distributions such as Weibull and log-normal distributions, which primarily focus on high-stress behaviors, the Neyman Type A distribution provides a unique and robust tool for understanding and predicting failure behaviors in cold environments where materials, especially metals, exhibit brittle fractures and low-temperature fatigue. This work pioneered the use of the Neyman Type A distribution in reliability engineering, offering new insights into the failure behavior of metals in cold climates and establishing a new life-stress relationship. The chosen distribution not only captures the nuances of temperature-dependent failure rates but also features a distinctive hump-shaped hazard function that accurately defines the probability of early failures. Unlike other common distributions, it stabilizes at a non-zero constant failure rate, thus providing a strong justification for its specific application in studying metallic material failures.

The remainder of this paper is organized as follows. Section 2 defines the discrete process and introduces the counting process derived from the Neyman type-A distribution. Section 3 considers the properties of the new lifetime distribution, such as the hazard function and its maximum-likelihood estimators. A life stress model is introduced in Section 4, the properties of the new distribution are discussed, and simulations are performed. Finally, Section 5 concludes the study and discusses future work.

2 Neyman type A distribution

Consider a Poisson distribution for which the Poisson parameter $\Theta=\phi\theta$, where ϕ is a constant, and θ has a Poisson distribution with parameter λ. The outcome distribution is known as Neyman type A probability distribution [25]. This probability distribution has found applications in a diverse range of areas, ranging from biological systems [26] to the modeling of natural disasters [27]. A detailed discussion of the mixture distributions can be found in [28].

The characteristic function of the Neyman type A (NTA) probability distribution is given by

$$\hat{f}(u;\lambda,\phi) = \mathrm{e}^{\left[\lambda\left(\mathrm{e}^{\phi\left(\mathrm{e}^{iu}-1\right)}-1\right)\right]}. \tag{1}$$

The cumulant generating function of (1) is given by

$$h(u) = \left[\lambda\left(\mathrm{e}^{\phi\left(\mathrm{e}^{iu}-1\right)}-1\right)\right] \tag{2}$$

and the cumulants

$$\begin{gathered} c_1 = \lambda\phi,\ c_2 = \lambda\phi(1+\phi), \\ c_4 = \lambda\phi(1+7\phi+6\phi^2+\phi^3), \end{gathered} \tag{3}$$

calculated according to [29].

The approximation given by the COS method in [30] is particularly useful when the probability mass function is difficult to manipulate, its cumulative function has no analytical solution, and/or the function itself does not exist in an explicit form. In such cases, we may resort to the Fourier cosine series given that we know the corresponding characteristic function.

Figs. 1 and 2 depict the approximation of the Neyman type-A probability function via the Fourier Series. The local peaks at 0,25,50,76,103,129,153 and 173 for the parameters $\lambda = 7$ and $\phi = 25$ which highlight the multimodality of the distribution, were discussed by [31].

An advantage of the solution via Fourier series is that the distribution is well approximated with a finite number of cosine terms, in contrast to Neyman's type-A analytical probability mass function given by

$$\mathbb{P}\{X = x\} = \frac{\mathrm{e}^{-\lambda}\phi^x}{x!}\sum_{j=0}^{\infty}\frac{\left(\lambda \mathrm{e}^{-\phi}\right)^j j^x}{j!},\ x = 0,1,\ldots, \tag{4}$$

which has an infinite sum for each x and a factorial function. The latter is a computational challenge for large values of x. For example, the reliability of redundant equipment, desired in terms of the probability of r or fewer failures for a fixed period of time, is given by

$$R(t) = \sum_{x=0}^{r}\mathbb{P}\{X = x\} = \sum_{x=0}^{r}\left[\frac{\mathrm{e}^{-\lambda}\phi^x}{x!}\sum_{j=0}^{\infty}\frac{\left(\lambda \mathrm{e}^{-\phi}\right)^j j^x}{j!}\right], \tag{5}$$

which inherits the computational challenges of Eq. (4).

Definition 1. The counting process N(t) derived from the NTA distribution has a probability distribution given by

$$\mathbb{P}\{N(t) = x\} = \frac{\mathrm{e}^{-\lambda t}(\phi t)^x}{x!}\sum_{j=0}^{\infty}\frac{\left(\lambda t \mathrm{e}^{-(\phi t)}\right)^j j^x}{j!},\ x = 0,1\ldots \tag{6}$$

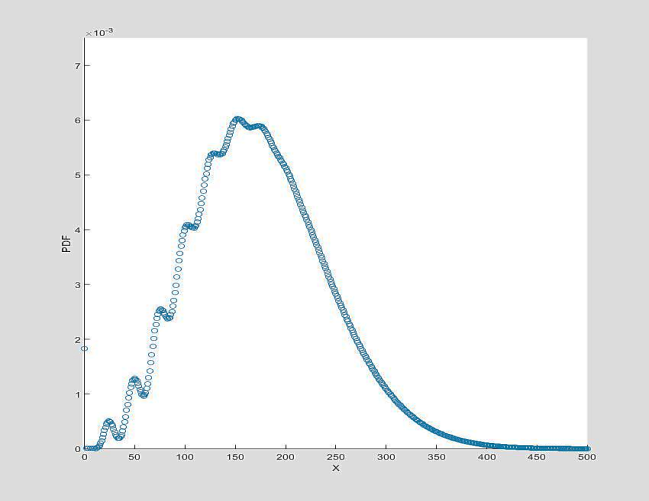

Figure 1. Neyman type A probability mass function.
Source: Authors.

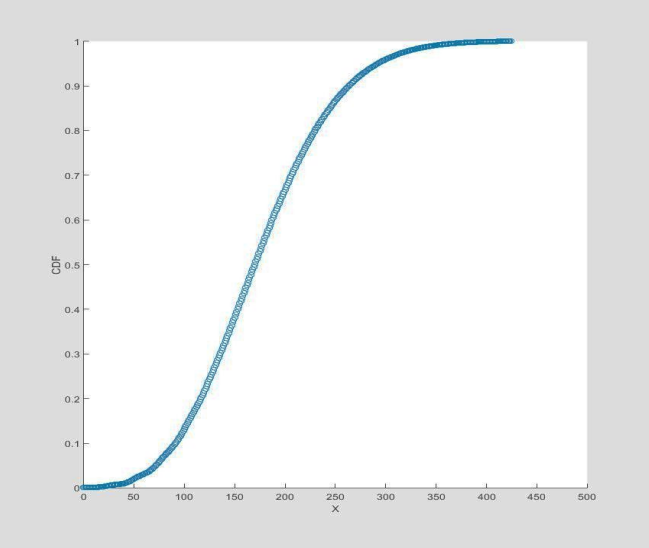

Figure 2. Neyman type A probability cumulative distribution.
Source: Authors.

In other words, for fixed parameters λ and ϕ, the probability of random variable N(t) being equal to x at time t is given by (6). Note that, as shown in [25], for the discrete random variable, $\mathbb{P}\{N(0) = 0\} = 1$.

3 Neyman type A Reliability function

This section proposes closed-form expressions of the reliability model derived from the Neyman type A counting process, their derived functions and associated properties, and the maximum likelihood estimators.

Theorem 1. The reliability (survival probability) function derived from the NTA counting process (6) is governed by:

$$R(t) = \mathrm{e}^{-\lambda t + \lambda t \mathrm{e}^{-\phi t}}. \tag{7}$$

Proof. The probability of no arrival until time t is

$$\begin{aligned}\mathbb{P}\{N(t) = 0\} &= \frac{\mathrm{e}^{-\lambda t}(\phi t)^0}{0!}\sum_{j=0}^{\infty}\frac{\left(\lambda t \mathrm{e}^{-(\phi t)}\right)^j j^0}{j!} \\ &= \mathrm{e}^{-\lambda t + \lambda t \mathrm{e}^{-\phi t}} = R(t).\end{aligned} \tag{8}$$

Eq. (8) provides the reliability function obtained from the NTA counting process. Note that $R(0) = 1$ and

$$\begin{aligned}&\lim_{t\to\infty}\mathrm{e}^{-\lambda t + \lambda t \mathrm{e}^{-\phi t}} \\ &= \lim_{t\to\infty}\mathrm{e}^{-\lambda t}\mathrm{e}^{\lambda t \mathrm{e}^{-\phi t}} \\ &= \lim_{t\to\infty}\frac{\mathrm{e}^{\lambda t \mathrm{e}^{-\phi t}}}{\mathrm{e}^{\lambda t}} \\ &= \lim_{t\to\infty}\frac{\mathrm{e}^{\frac{\lambda t}{\mathrm{e}^{\phi t}}}}{\mathrm{e}^{\lambda t}} \\ &= \frac{\lim_{t\to\infty}\mathrm{e}^{\frac{\lambda t}{\mathrm{e}^{\phi t}}}}{\lim_{t\to\infty}\mathrm{e}^{\lambda t}} = \frac{\mathrm{e}^0}{\infty} = \frac{1}{0} = 0,\end{aligned} \tag{9}$$

which agrees with the reliability axioms.

Corollary 1. If the reliability function is given by

$$R(t) = \mathrm{e}^{-\lambda t+\lambda t\mathrm{e}^{-\phi t}}, \tag{10}$$

then, its associated probability density function is given by

$$f(t) = \lambda\left(\mathrm{e}^{\phi t} + \phi t - 1\right)\mathrm{e}^{-\lambda t-\phi t+\lambda t\mathrm{e}^{-\phi t}}. \tag{11}$$

Consequently, the hazard rate is given by

$$h(t) = \lambda\left(\mathrm{e}^{\phi t} + \phi t - 1\right)\mathrm{e}^{-\phi t} \tag{12}$$

Proof. Let

$$R(t) = \mathrm{e}^{-\lambda t+\lambda t\mathrm{e}^{-\phi t}}. \tag{13}$$

The cumulative distribution function is given by $F(t) = 1 - R(t)$. Therefore, the probability density function is given by

$$\begin{aligned}\frac{dF(t)}{dt} &= \frac{d(1-R(t))}{dt}\\ &= \frac{d\left(1-\mathrm{e}^{-\lambda t+\lambda t\mathrm{e}^{-\phi t}}\right)}{dt}\\ &= \lambda\left(\mathrm{e}^{\phi t} + \phi t - 1\right)\mathrm{e}^{-\lambda t-\phi t+\lambda t\mathrm{e}^{-\phi t}} = f(t).\end{aligned} \tag{14}$$

The hazard rate is simply given by

$$\begin{aligned}h(t) &= \frac{f(t)}{R(t)}\\ &= \frac{\lambda\left(\mathrm{e}^{\phi t} + \phi t - 1\right)\mathrm{e}^{-\lambda t-\phi t+\lambda t\mathrm{e}^{-\phi t}}}{\mathrm{e}^{-\lambda t+\lambda t\mathrm{e}^{-\phi t}}}\\ &= \lambda\left(\mathrm{e}^{\phi t} + \phi t - 1\right)\mathrm{e}^{-\phi t}\end{aligned} \tag{15}$$

The hump-shaped behavior of the hazard function is similar to that implied by the lognormal distribution. It initially increases, reaches a maximum, and then decreases toward a constant value. The following two corollaries clarify this issue.

Corollary 2. The NTA hazard function (12) is a humped model.

Proof. Note that the derivative of the hazard function given by

$$\frac{\partial h(t)}{\partial t} = \lambda\mathrm{e}^{-\phi t}\left(f\mathrm{e}^{\phi t} + \phi\right) - \phi\lambda\mathrm{e}^{-\phi t}\cdot\left(\mathrm{e}^{\phi t} + \phi t - 1\right) \tag{16}$$

8 da Silva and Amorim

finds root at $t^* = \frac{2}{\phi}$. Since that $\lambda > 0$, and

$$\frac{\partial^2 h(t)}{\partial t^2} = \phi^2\lambda(\phi t - 3)\left(\mathrm{e}^{-\phi t}\right) \tag{17}$$

we have that

$$\frac{\partial^2 h(t^*)}{\partial t^2} = -\phi^2\lambda\mathrm{e}^{-2}. \tag{18}$$

So, the NTA hazard function finds its maximum at t^*.

Corollary 3. The NTA hazard function converges to λ in the long run.

Proof. If the hazard function is given by

$$h(t) = \lambda\left(\mathrm{e}^{\phi t} + \phi t - 1\right)\mathrm{e}^{-\phi t}, \tag{19}$$

then

$$\begin{aligned}&\lim_{t\to\infty}\lambda\left(\mathrm{e}^{\phi t} + \phi t - 1\right)\mathrm{e}^{-\phi t}\\ &\lambda\lim_{t\to\infty}\left(\mathrm{e}^{\phi t} + \phi t - 1\right)\mathrm{e}^{-\phi t}\\ &\lambda\lim_{t\to\infty}\left(1 + \phi t\mathrm{e}^{-\phi t} - \mathrm{e}^{-\phi t}\right)\\ &\lambda\left(\lim_{t\to\infty}1 + \lim_{t\to\infty}\phi t\mathrm{e}^{-\phi t} - \lim_{t\to\infty}\mathrm{e}^{-\phi t}\right)\\ &\lambda\left(1\lim_{t\to\infty}1 + 0\lim_{t\to\infty}\phi t\mathrm{e}^{-\phi t} - 0\lim_{t\to\infty}\mathrm{e}^{-\phi t}\right) = \lambda\end{aligned} \tag{20}$$

Fig. 3 depicts the probability density, Fig. 4 shows the reliability, and Fig. 5 shows the hazard rate functions. We may note an increasing hazard rate up to a certain point in time, namely $\frac{2}{\phi}$, where the function starts to decrease and stabilizes at a constant rate. In the short term, the model may characterize early failures and burn-in testing times. In the long run, the hazard function behaves similar to the hazard function of the exponential distribution.

Corollary 4. The mean time to failure (MTTF) given by

$$MTTF = \int_0^\infty sf(s)ds = \int_0^\infty R(s)ds \tag{21}$$

is not analytically available.

Proof. Note that

$$\begin{aligned}\text{MTTF} &= \int_0^\infty sf(s)ds\\ &= \int_0^\infty s\lambda\left(\mathrm{e}^{\phi t} + \phi t - 1\right)\mathrm{e}^{-\lambda t-\phi t+\lambda t\mathrm{e}^{-\phi t}}ds\end{aligned} \tag{22}$$

And

$$\begin{aligned}\text{MTTF} &= \int_0^\infty R(s)ds\\ &= \int_0^\infty \mathrm{e}^{-\lambda t+\lambda t\mathrm{e}^{-\phi t}}ds\end{aligned} \tag{23}$$

Have no antiderivative. Another consequence of Corollary 4 is that the moment-generating function is not available analytically.

Corollary 5. The maximum likelihood estimators of the NTA reliability parameters are given by

$$\lambda = -\frac{n}{\sum_{i=1}^n t_i\mathrm{e}^{-\phi t_i} - t_i}. \tag{24}$$

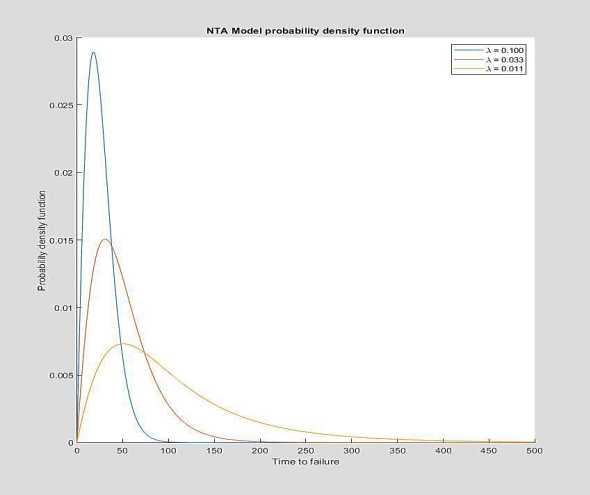

Figure 3: Neyman type A probability density functions.
Source: Authors.

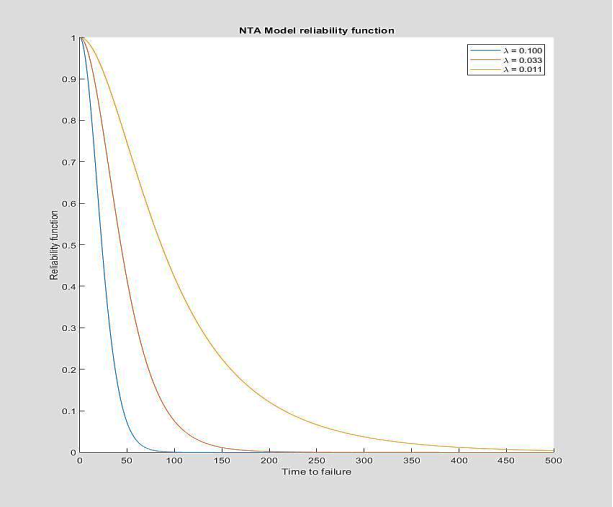

Figure 4 Neyman type A reliability functions.
Source: Authors.

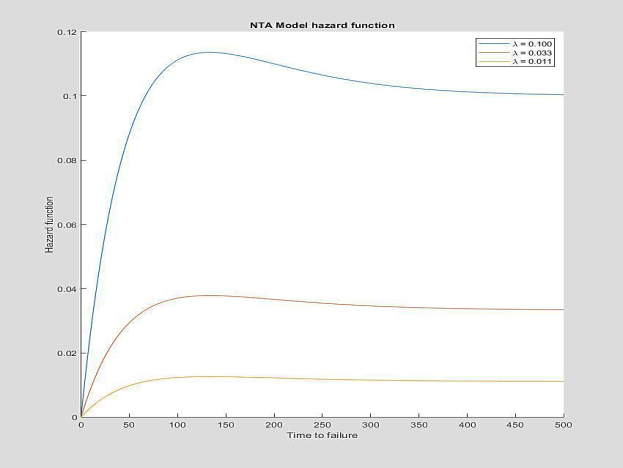

Figure 5: Neyman type A hazard rate functions.
Source: Authors.

And

$$\sum_{i=1}^{n} \frac{t_i e^{\phi t_i} + t_i}{e^{\phi t_i} + \phi t_i - 1} - \sum_{i=1}^{n} \lambda t_i^2 + e^{-\phi t_i} + t_i = 0. \tag{25}$$

An estimator for ϕ is not analytically available. Its approximation is given by the numerical solution of nonlinear equation (25).

Proof. Given a random sample $t_1, t_2, \ldots, t_n$, the maximum likelihood estimators of the NTA lifetime density function with parameters (λ, ϕ) are obtained by finding $\frac{\partial \mathcal{L}}{\partial \lambda} = 0$ and $\frac{\partial \mathcal{L}}{\partial \phi} = 0$ [32]. Then, the likelihood function for n non-censored data points is given by

$$L = \prod_{i=1}^{n} \lambda\left(e^{\phi t_i} + \phi t_i - 1\right) e^{-\lambda t_i - \phi t_i + \lambda t_i e^{-\phi t_i}}. \tag{26}$$

We have that

$$L = \lambda^n \prod_{i=1}^{n} \left(e^{\phi t_i} + \phi t_i - 1\right) e^{-\lambda t_i - \phi t_i + \lambda t_i e^{-\phi t_i}} \tag{27}$$

Putting $\mathcal{L} = \ln(L)$, then,

$$\begin{aligned} \mathcal{L} = n \ln \lambda + \sum_{i=1}^{n} \ln\left(e^{\phi t_i} + \phi t_i - 1\right) \\ + \sum_{i=1}^{n} \lambda t_i e^{-\phi t_i} - \lambda t_i - \phi t_i \end{aligned} \tag{28}$$

Finding the extreme points of 27] we have

$$\frac{\partial \mathcal{L}}{\partial \lambda} = \frac{n}{\lambda} - \sum_{i=1}^{n} t_i e^{-\phi t_i} - t_i = 0. \tag{29}$$

So, the maximum likelihood estimator for the parameter λ is given by

$$\lambda = -\frac{n}{\sum_{i=1}^{n} t_i e^{-\phi t_i} - t_i}. \tag{30}$$

Following from (27) we have

$$\frac{\partial \mathcal{L}}{\partial \phi} = \sum_{i=1}^{n} \frac{t_i e^{\phi t_i} + t_i}{e^{\phi t_i} + \phi t_i - 1} - \sum_{i=1}^{n} \lambda t_i^2 + e^{-\phi t_i} + t_i = 0. \tag{31}$$

Note that estimator (31) for ϕ is not available analytically. By substituting (30) into (31), the approximation for ϕ is given by the numerical solution of the following nonlinear equation:

$$\begin{aligned} \sum_{i=1}^{n} \frac{t_i e^{\phi t_i} + t_i}{e^{\phi t_i} + \phi t_i - 1} + \\ \sum_{i=1}^{n} \left(\frac{n}{\sum_{i=1}^{n} t_i e^{-\phi t_i} - t_i}\right) t_i^2 - e^{-\phi t_i} - t_i = 0. \end{aligned} \tag{32}$$

Suppose the failure times of a product follow the NTA distribution with parameters $\phi = 0.015$. In addition, we consider that the manufacturer's cost c_0 for the given product equals unity. The warranty cost for renewing the free replacement warranty for a period of W is given by

$$\mathbb{E}[C(W)] = \frac{c_0 F(W)}{1 - F(W)} = \frac{c_0\left(1 - \mathrm{e}^{-\lambda W + \lambda W \mathrm{e}^{-\phi W}}\right)}{\mathrm{e}^{-\lambda W + \lambda W \mathrm{e}^{-\phi W}}}. \quad (33)$$

Fig. 6 depicts the warranty cost for a renewing free replacement warranty [4] for various warranty periods by varying parameter λ. As predicted, the value of λ that produces the lowest reliability or largest hazard function, as illustrated in Fig.6, produces the highest warranty costs.

4 Arrhenius-NTA model for accelerated tests

Let a quantifiable life measure G implied by the Arrhenius law be given by

$$G(V) = C\mathrm{e}^{\frac{B}{V}}. \quad (34)$$

The Arrhenius relationship is a physics-based model derived for the temperature life dependence, V, in Kelvin. It is a widely used model to relate the product life and temperature [3]. In Equation (34), C is a nonthermal constant that depends on geometry, size, fabrication, and other factors. It is determined experimentally, and deals with the frequency of molecules that collide in the correct orientation to initiate a chemical reaction. Parameter B is the relationship between the activation energy and Boltzmann Constant. The activation energy deals with the magnitude of the effect of the stress on the component. The details can be found in [3] and [1].

Let the probability density function of life data be given by (11). Let the inverse scale parameter λ be equal to the quantifiable life measure of Arrhenius law. Setting $G(V) = \lambda$ we have the Arrhenius-NTA probability density function:

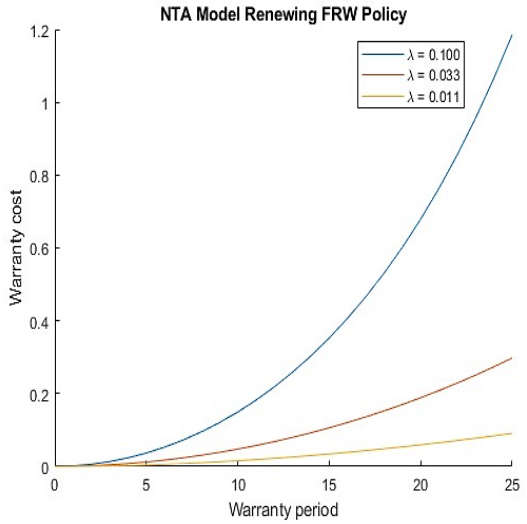

Figure 6. Hazard function.
Source: Authors.

$$f(t,V) = C\mathrm{e}^{\frac{B}{V}}\left(\mathrm{e}^{\phi t} + \phi t - 1\right)\mathrm{e}^{-C\mathrm{e}^{\frac{B}{V}}t - \phi t + C\mathrm{e}^{B}t\mathrm{e}^{-\phi t}}. \quad (35)$$

The probability density function (35) has the following important characteristics: It is shown that the model is qualitatively suitable for investigating the fluorescent bulb lifespan in cold weather, the toughness of steels, and the Ductile to Brittle Transition Temperature. We have that

$$R(t,V) = \mathrm{e}^{-C\mathrm{e}^{\frac{B}{V}}t + C\mathrm{e}^{\frac{B}{V}}t\mathrm{e}^{-\phi t}}, \quad (36)$$

and

$$h(t,V) = C(\mathrm{e}^{\varphi t} + \varphi t - 1)\mathrm{e}^{\frac{B}{V} - \varphi t}. \quad (37)$$

The probability density functions 35, 46, and 37 are depicted in Figs. 7, 8 and 9 for the parameters $C = 0.0002, B = 1000$ and $\phi = 0.0025$. Note that in the brittle fatigue of metals for a fixed mechanical load, the lower the temperature, the higher is the chance of failure. The resulting positive slope of the short end of the hazard function describes the gradual decrease in load resistance well.

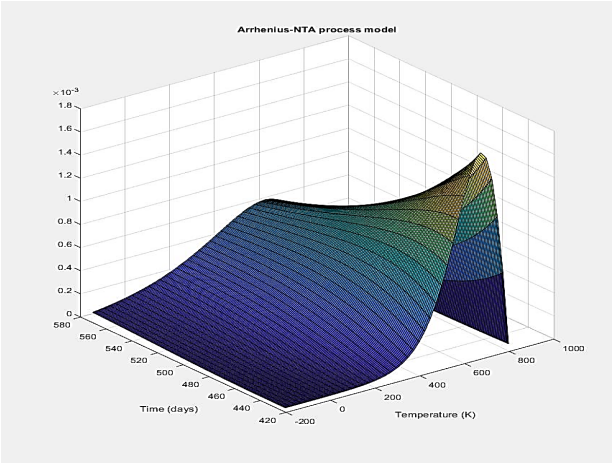

Figure 7. Probability density function.
Source: Authors.

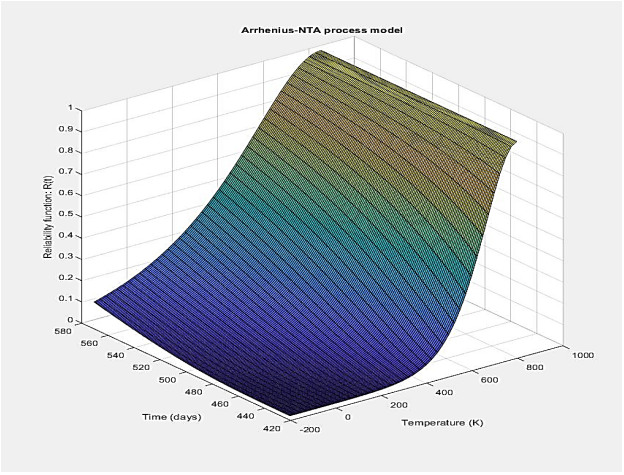

Figure 8. Reliability function.
Source: Authors.

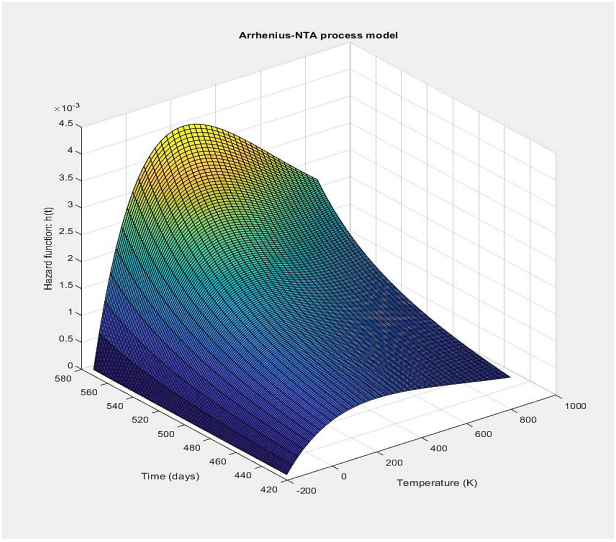

Figure 9. Hazard function.
Source: Authors.

The hazard function inherits the NTA model hump-shaped properties.

Corollary 6. The Arrhenius-NTA hazard function (37) is a humped model.

Proof. Note that the derivative of the hazard function given by:

$$\frac{\partial h(t,V)}{\partial t} = -C\phi(\phi t - 2)\mathrm{e}^{\frac{B}{V}-\phi t} \tag{38}$$

finds root at $t^* = \frac{2}{\phi}$. Since that $\lambda > 0$, and

$$\frac{\partial^2 h(t,V)}{\partial t^2} = C\phi^2(\phi t - 3)\mathrm{e}^{\frac{B}{V}-\phi t}, \tag{39}$$

we have that

$$\frac{\partial^2 h(t^*,V)}{\partial t^2} = -C\phi^2\lambda\mathrm{e}^{\frac{B}{V}-2}. \tag{40}$$

So, the Arrhenius-NTA hazard function finds its maximum at t^*.

Corollary 7. The Arrhenius-NTA hazard function (37) increases as the stress V decreases.

Proof. If the hazard function is given by

$$h(t,V) = C(\mathrm{e}^{\varphi t} + \varphi t - 1)\mathrm{e}^{\frac{B}{V}-\varphi t}, \tag{41}$$

then

$$\begin{aligned} &\lim_{V\to 0} C(\mathrm{e}^{\varphi t} + \varphi t - 1)\mathrm{e}^{\frac{B}{V}}\mathrm{e}^{-\varphi t} \\ &C(\mathrm{e}^{\varphi t} + \varphi t - 1)\mathrm{e}^{-\varphi t}\lim_{V\to 0}\mathrm{e}^{\frac{B}{V}} \\ &C(\mathrm{e}^{\varphi t} + \varphi t - 1)\mathrm{e}^{-\varphi t}\lim_{V\to 0}\mathrm{e}^{\frac{B}{V}} = \infty \end{aligned} \tag{42}$$

Corollary 7 shows that the hazard function of the Arrhenius-NTA model is inversely proportional to stress. This is precisely the behavior of metallic materials. In general, the increase in the tensile and yield strengths at low temperatures is characteristic of metals. However, it is important to note that it is not claimed here that every metallic material can be fitted better by the Arrhenius-NTA reliability distribution. The modeling gain must be tested in each case.

Corollary 8. The Arrhenius-NTA hazard function converges to $C\mathrm{e}^{\frac{B}{V}}$ in the long run. Proof. If the hazard function is given by:

$$h(t,V) = C(\mathrm{e}^{\varphi t} + \varphi t - 1)\mathrm{e}^{\frac{B}{V}-\varphi t}, \tag{43}$$

then

$$\begin{aligned} &\lim_{t\to\infty} C\mathrm{e}^{\frac{B}{V}}(\mathrm{e}^{\varphi t} + \varphi t - 1)\mathrm{e}^{-\varphi t} \\ &C\mathrm{e}^{\frac{B}{V}}\lim_{t\to\infty}(\mathrm{e}^{\varphi t} + \varphi t - 1)\mathrm{e}^{-\varphi t} \\ &C\mathrm{e}^{\frac{B}{V}}\lim_{t\to\infty}\left(1 + \phi t\mathrm{e}^{-\phi t} - \mathrm{e}^{-\phi t}\right) \\ &C\mathrm{e}^{\frac{B}{V}}\left(\lim_{t\to\infty} 1 + \lim_{t\to\infty}\phi t\mathrm{e}^{-\phi t} - \lim_{t\to\infty}\mathrm{e}^{-\phi t}\right) \\ &C\mathrm{e}^{\frac{B}{V}}\left(1\lim_{t\to\infty} 1 + 0\lim_{t\to\infty}\phi t\mathrm{e}^{-\phi t} - 0\lim_{t\to\infty}\mathrm{e}^{-\phi t}\right) = C\mathrm{e}^{\frac{B}{V}} \end{aligned} \tag{44}$$

As in Corollary 4, the MTTF of the Arrhenius-NTA is not analytically available. Figs. 10 and 11 show the numerically solved mean time to failure (MTTF) of the Arrhnenius-NTA model.

The solution can be obtained by

$$MTTF = \int_0^\infty sC\mathrm{e}^{\frac{B}{V}}\big(\mathrm{e}^{\phi s} + \phi s - 1\big)\mathrm{e}^{-C\mathrm{e}^{\frac{B}{V}}s-\phi s+C\mathrm{e}^{\frac{B}{V}}s\mathrm{e}^{-\phi s}}ds \tag{45}$$

Or

$$MTTF = \int_0^\infty \mathrm{e}^{-C\mathrm{e}^{\frac{B}{V}}s+C\mathrm{e}^{\frac{B}{V}}s\mathrm{e}^{-\phi s}}ds, \tag{46}$$

which is the expected value of the random variable t or integration through the entire domain of the survival function. The MTTF can also be achieved through simulation, as introduced in the next section. It was shown that lower temperatures and higher activation energies decreased the MTTF of the component under test. A large activation energy indicates that stress has a substantial effect on MTTF.

Lower values of C and ϕ had a greater influence on the effect of temperature on the life of the component. When fixed, the parameters were $C = 0.002$ and $\phi = 0.0025$.

Corollary 9. The maximum likelihood estimators of the Arrhenius-NTA reliability parameters are given by:

$$C = -\frac{\sum_{i=1}^n \mathrm{e}^{\phi t_i}}{\sum_{i=1}^n t\mathrm{e}^{\phi t_i+\frac{B}{V}} - \mathrm{e}^{\frac{B}{V}}t_i}, \tag{47}$$

$$\frac{\partial \mathcal{L}}{\partial B} = \sum_{i=1}^n \frac{Ct_i\mathrm{e}^{\frac{B}{V}-\phi t_i}}{V} - \frac{Ct_i\mathrm{e}^{\frac{B}{V}}}{V} + \frac{n}{V} \tag{48}$$

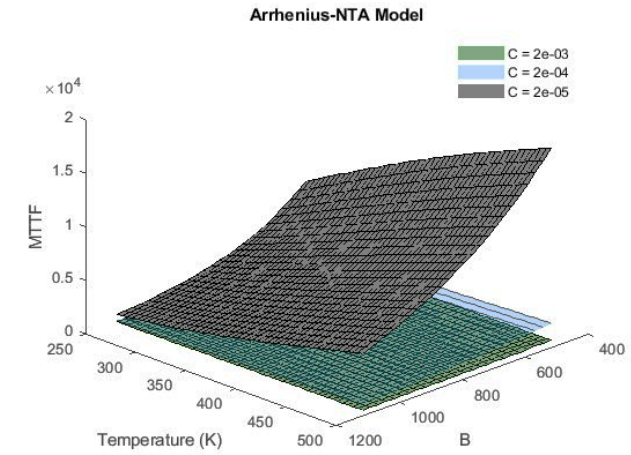

Figure 10. Mean time to failure varying parameter C.
Source: Authors.

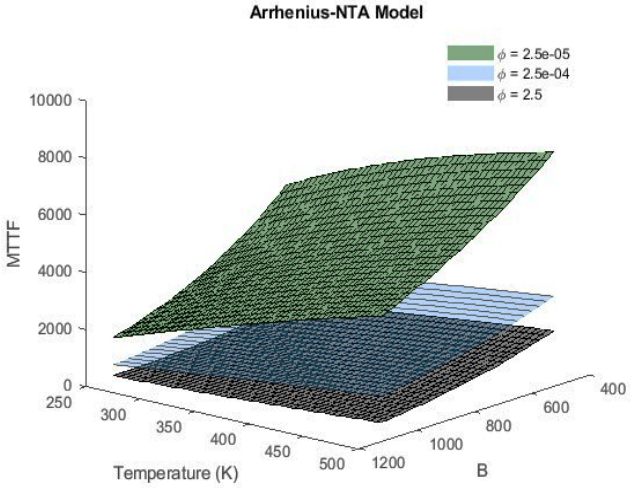

Figure 11. Mean time to failure varying parameter ϕ.
Source: Authors.

and

$$\frac{\partial \mathcal{L}}{\partial \phi} = \sum_{i=1}^{n} - Ct_i^2 \mathrm{e}^{\frac{B}{V} - t_i\varphi} + \frac{t_i \mathrm{e}^{t_i\varphi} + t_i}{\mathrm{e}^{t_i\varphi} + t_i\varphi - 1} - t_i = 0. \quad (49)$$

Estimators for B and ϕ are not analytically available. Their approximations are given by the numerical solution of the nonlinear Equations 48) and (49), respectively.

Proof. Given a random sample $t_1, t_2, \ldots, t_n$, the maximum likelihood estimators of the Arrhenius-NTA lifetime density function with parameters (C, B, ϕ) are obtained by finding $\frac{\partial \mathcal{L}}{\partial C} = 0, \frac{\partial \mathcal{L}}{\partial B} = 0$ and $\frac{\partial \mathcal{L}}{\partial \phi} = 0$ [32]. Then, the likelihood function for n non-censored data points is given by

$$L = \prod_{i=1}^{n} C\mathrm{e}^{\frac{B}{V}} \left(\mathrm{e}^{\phi t_i} + \phi t_i - 1\right) \mathrm{e}^{-C\mathrm{e}^{\frac{B}{V}} t_i - \phi t_i + C\mathrm{e}^{\frac{B}{V}} t_i \mathrm{e}^{-\phi t_i}}. \quad (50)$$

We have that

$$L = \left(C\mathrm{e}^{\frac{B}{V}}\right)^n \prod_{i=1}^{n} \left(\mathrm{e}^{\phi t_i} + \phi t_i - 1\right) \mathrm{e}^{-C\mathrm{e}^{\frac{B}{V}} t_i - \phi t_i + C\mathrm{e}^{\frac{B}{V}} t_i \mathrm{e}^{-\phi t_i}}$$

$$\mathcal{L} = \ln(L) = n \ln\left(C\mathrm{e}^{\frac{B}{V}}\right) + \sum_{i=1}^{n} \ln\left(\mathrm{e}^{\phi t_i} + \phi t_i - 1\right) + \sum_{i=1}^{n} \left(C\mathrm{e}^{\frac{B}{V}}\right) t_i \mathrm{e}^{-\phi t_i} - \left(C\mathrm{e}^{\frac{B}{V}}\right) t_i - \phi t_i \quad (51)$$

Finding the extreme points of (51) in terms of C we have

$$\frac{\partial \mathcal{L}}{\partial C} = \frac{n}{C} + \sum_{i=1}^{n} t_i \mathrm{e}^{\frac{B}{V} - \phi t} - \mathrm{e}^{\frac{B}{V}} t_i = 0. \quad (52)$$

So, the maximum likelihood estimator for the parameter C is given by

$$C = -\frac{n}{\sum_{i=1}^{n} t_i \mathrm{e}^{\frac{B}{V} - \phi t_i} - \mathrm{e}^{\frac{B}{V}} t_i}. \quad (53)$$

Finding the extreme points of (51) in terms of B we have

$$\frac{\partial \mathcal{L}}{\partial B} = \frac{n}{V} + \sum_{i=1}^{n} \frac{Ct_i \mathrm{e}^{\frac{B}{V} - \phi t_i}}{V} - \frac{Ct_i \mathrm{e}^{\frac{B}{V}}}{V} = 0. \quad (54)$$

Finding the extreme points of (51) in terms of ϕ we have

$$\frac{\partial \mathcal{L}}{\partial \phi} = \sum_{i=1}^{n} - Ct_i^2 \mathrm{e}^{\frac{B}{V} - t_i\varphi} + \frac{t_i \mathrm{e}^{t_i\varphi} + t_i}{\mathrm{e}^{t_i\varphi} + t_i\varphi - 1} - t_i = 0. \quad (55)$$

Note that estimators (54) for B and (55) for ϕ are not analytically available.

4.1 Simulation

In the following tables, we present the estimated parameters and value of the log-likelihood function. Notably, the relative error decreased as the sample size increased. The true parameters are by *V=300, C=0.0002, B=1000* and $\phi = 0.0025$. The expected number of failures in an interval of time is calculated using the renewal process, which is associated with the distribution function $F(t) = 1 - R(t).M(t)$ given by

$$M(t) = F(t) + \int_0^t \left[\sum_{r=1}^{\infty} F_r(t-x)\right] f(x)dx, \quad (56)$$

is called the renewal function, and was discussed by [1]. The function $M(t)$ is difficult to obtain in analytical form, but an efficient numerical approximation can be found in [33].

Table 1.
MLE estimators for $n = 30$.

Parameter	Estimation	Relative Error
C	0.000028665638	0.856
B	1437	0.437
ϕ	0.006615886708	1.646
$\mathcal{L}$	200.57	0.0046

Source: Authors.

Table 2.
MLE estimators for *n=300*

Parameter	Estimated	Relative Error
C	0.000250776105	0.253
B	1335	0.335
ϕ	0.000420982926	0.831
$\mathcal{L}$	1939	0.0032

Source: Authors.

Table 3.
MLE estimators for $n = 900$.

Parameter	Estimated	Relative Error
C	0.000204747157	0.023
B	1163	0.163
ϕ	0.001189293500	0.524
$\mathcal{L}$	5792	0.0015

Source: Authors.

As shown in Tables 4 and 5, the expected number of failures in $t \in (0,1000)$ for a set of selected temperatures and parameter B of the Arrhenius-NTA model (35). The base parameters are $V = 300, B = 1000$ and $\phi = 0.0025$. It is clear that, confirming the above results, the expected number of failures increased as V decreased. The opposite was true for parameter B.

The approximation of the renewal function is particularly useful for calculating the warranty costs and maintenance policies.

Table 4.
Expected number of failures for $t = 1000$.

Temperature (K)	$M(t)$
250	4.73
300	3.07
350	2.19
400	1.67

Source: Authors.

4.2 Application procedure

This procedure outlines the application of the Neyman Type A reliability model to analyze the failure of metallic materials under low-temperature conditions. The model is particularly useful for understanding and predicting the failure behavior of metals subjected to extreme thermal stresses.

Table 5.
Expected number of failures for $t = 1000$.

Parameter B	$M(t)$
700	1.469
800	1.904
900	2.434
1000	3.071

Source: Authors.

- Identify the parameters: The fundamental parameters for this model include the operating temperature and fixed applied mechanical stress.
- The experimental failure data of the material were collected at various temperatures to capture the variation in the failure rate with temperature.
- Apply the Neyman Type A distribution to the collected data to estimate the model parameters and the material survival function using the maximum likelihood estimators given by Equations (47), (48), and (49).
- The estimated survival function (36) was used to predict the reliability of the material under defined operational conditions.
- Equations (45) or (46) were used to estimate the mean time to failure.

To validate the model, a comparison of the reliability predictions with the actual failure data obtained under controlled operational conditions must be conducted as well as a sensitivity analysis to understand the impact of each parameter on the model and refine the application procedure based on these insights.

5 Discussion

The application of the Neyman Type A distribution is especially pertinent in engineering contexts where material failures at low temperatures are critical. This scenario is often encountered in metallic structures and components used in extremely cold environments such as polar regions, aerospace applications, and equipment employed in low-temperature chemical processes. These conditions are noteworthy for inducing brittleness and fatigue in metals, phenomena that occur when materials are exposed to temperatures below their ductile–brittle transition point. In such scenarios, conventional failure characteristics observed at normal or elevated temperatures do not apply, rendering traditional reliability analyses insufficient.

With its ability to model failure behaviors in multimodal distributions, the Neyman Type A distribution is a valuable

statistical tool for predicting the reliability of these materials under reduced thermal stress conditions. For instance, aircrafts operating at high altitudes encounter extremely low temperatures that can compromise the integrity of metallic components, necessitating a reliability model that can adequately predict the likelihood of failure. Similarly, in polar regions, engineering structures and equipment must withstand not only intense cold, but also significant temperature variations, which can adversely affect their performance and durability.

The implementation of a model based on the Neyman Type A distribution in engineering projects allows designers and engineers to conduct more refined and accurate assessments of the reliability and performance of materials and components under low-temperature conditions. By integrating this model into the design processes, it is possible to simulate the failure behavior of materials over time and under various environmental stress conditions, leading to improvements in material selection, structural design, and maintenance strategies. By quantifying the failure risk more accurately, engineers can optimize the design to withstand adverse conditions and enhance the safety and efficiency. Furthermore, the model can be employed to develop accelerated testing plans, helping to identify weaknesses in engineering designs and ensuring that selected materials meet the durability and reliability requirements before large-scale implementation. This not only extends the lifespan of components, but also reduces maintenance and replacement costs, significantly contributing to the sustainability and economic efficiency of engineering projects.

Therefore, the selection of the Neyman Type A distribution for this study is grounded in the necessity of a statistical model that can accurately reflect the peculiarities of failures at low temperatures, allowing for a more precise and reliable analysis of the lifespan and failure behavior of metallic materials in these demanding contexts.

6 Conclusion

In this study, we introduced a novel statistical model utilizing the Neyman Type A distribution for reliability analysis, specifically tailored to address the challenges of modeling material failures at low temperatures. The development of the model was driven by the need to understand and predict the brittle fracture of metals under cold conditions, a scenario that is often overlooked in conventional reliability engineering. Through our research, we have not only demonstrated the humped behavior of the hazard function and its convergence to a constant rate λ, but also highlighted the utility of the model in accurately describing the inversely proportional relationship between failure risk and stress. This unique characteristic underscores the significance of the model in engineering applications in which low-temperature performance is critical.

Our findings align closely with the initial objectives of this study, providing a robust framework for analyzing the reliability of materials in environments subjected to thermal stress. The predictive capacity of the model for early failure and its behavior under varying stress conditions offers substantial advancement in the field of reliability engineering. Future research directions include testing the model against alternative stress scenarios, conducting sensitivity analyses of the parameters, and validating the model with experimental data to enhance its comparability with the existing models. Additionally, exploring the interaction between mechanical load and temperature in a nonthermal life-stress relationship model presents an exciting avenue for extending the applicability of our work. This study not only fills a gap in the existing literature, but also sets the stage for more comprehensive and accurate reliability assessments in engineering disciplines concerned with low-temperature material performance.

References

[1] Elsayed, E.A., Reliability Engineering, Wiley Series in Systems Engineering and Management, 3rd Ed., Wiley. 2021. DOI: https://doi.org/10.1002/9781119665946.

[2] Deshpande, J.V. and Purohit, S.G., Lifetime data: statistical models and methods, Series on quality, reliability and engineering statistics, World Scientific. 2005. DOI: https://doi.org/10.1142/5988.

[3] Nelson, W., Accelerated testing: statistical models, test plans, and data analyses, 2nd Ed., John Wiley & Sons, 2004.

[4] Wallace, R., Blischke, M., Rezau-Karim, D.N.P.M., Warranty data collection and analysis, Springer Series in Reliability Engineering, Springer, 2011. DOI: https://doi.org/10.1007/978-0-85729-647-4.

[5] Rahman, A., and Chattopadhyay, G., Long term warranty and after sales: service concept, policies and cost models, Springer Briefs in Applied Sciences and Technology, Springer, 2015. DOI: https://doi.org/10.1007/978-3-319-16271-3.

[6] Murthy, D.N.P., and Jack, N., Extended warranties, maintenance Service and lease contracts: modeling and analysis for decision-making, Springer Series in Reliability Engineering, Springer, 2014. DOI: https://doi.org/10.1007/978-1-4471-6440-1.

[7] Smith, R., and Mobley, R.K., Rules of thumb for maintenance and reliability engineers, Elsevier, 2008.

[8] da Silva, A.J., Maintenance policy costs considering imperfect repairs. Reliability: Theory & Applications. 1(72), pp. 564-574, 2023. DOI: https://doi.org/10.24412/1932-2321-2023-172-564-574

[9] de Souza, F.L.C., da Silva, A.J., Statistical learning for maintenance optimization: modeling the hazard function with variable recovery factors. Revista de Gestão e Secretariado, 15(2), art. e3478, 2024. DOI: https://doi.org/10.7769/gesec.v15i2.3478

[10] Lee, J.M., Special issue: Low-temperature behavior of metals, Metals 12(4), 2022.

[11] Xi, X., Zhao, D.Q., Pan, M.X., Wang, W., Wu, Y., and Lewandowski, J.J., Fracture of brittle metallic glasses: Brittleness or plasticity. 2005. DOI: https://doi.org/10.1103/PhysRevLett.94.125510

[12] Lancaster, J., Chapter 4 - The technical background, in: Lancaster, J., ed., Engineering Catastrophes, 3rd Ed., Woodhead Publishing, 2005, pp. 139-189. DOI: https://doi.org/10.1533/9781845690816.

[13] Chernov, V., Kardashev, B., and Moroz, K., Low-temperature embrittlement and fracture of metals with different crystal lattices dislocation mechanisms, Nuclear Materials and Energy 9, 496-501. 2016. DOI: https://doi.org/10.1016/j.nme.2016.02.002.

[14] Sallaba, F., Rolof, F., Ehlers, S., Walters, C.L., and Braun, M., Relation between the fatigue and fracture ductile-brittle transition in s500 welded steel joints, Metals 12(3), art. 305, 2022. DOI: https://doi.org/10.3390/met12030385

[15] Park, J.Y., Kim, B.K., Nam, D.G., and Kim, M.H., Effect of nickel contents on fatigue crack growth rate and fracture toughness for nickel alloy steels, Metals 12(2), art. 173, 2022. DOI: https://doi.org/10.3390/met12020173

[16] Mulford, R.A., Grain-boundary embrittlement of ni and ni alloys, in C. Briant and Banerji, S., Ed., Embrittlement of Engineering Alloys, Vol. 25 of Treatise on Materials Science & Technology, Elsevier, pp. 1-19. 1983. DOI: https://doi.org/10.1557/S0883769400069001.

[17] Lepov, V., Grigoriev, A., Achikasova, V., and Lepova, K., Cold resistance of materials as an integrity factor of railway transport in the

extreme environment, in Procedia Structural Integrity: 1st International Conference on Integrity and Lifetime in Extreme Environment, Vol. 20, 2019, pp. 57-62. DOI: https://doi.org/10.1016/j.prostr.2019.12.116.
[18] Li, Y., Fu, G., Wan, B., Jiang, M., Zhang, W., and Yan, X., Failure analysis of sac305 ball grid array solder joint at extremely cryogenic temperature, Applied Sciencies 10, 2020. DOI: https://doi.org/10.3390/app10061951.
[19] Bo-Bonning, C., Blackburn, J., Stretz, H.A., Wilson, C.D., Johnson, W.R., Superposition-based predictions of creep for polymer films at cryogenic temperatures, Cryogenics, 104, art. 102979, 2019. DOI: https://doi.org/10.1016/j.cryogenics.2019.102979.
[20] Soares, G.C., Rodrigues, M.C.M., and Santos, L.deA., Influence of temperature on mechanical properties, fracture morphology and strain hardening behavior of a 304 stainless steel. Materials Research, 20, pp. 141–151, 2017. DOI: https://doi.org/10.1590/1980-5373-MR-2016-0932
[21] Mohsin-Sattar, A.R., Othman, S., Kamaruddin, M.A., and Rashid, K., Limitations on the computational analysis of creep failure models: a review. Engineering Failure Analysis, 134, art. 105968 2022. DOI: https://doi.org/10.1016/j.engfailanal.2021.105968.
[22] Hossain, M.A., and Stewart, C.M., A probabilistic creep model incorporating test condition, initial damage, and material property uncertainty. International Journal of Pressure Vessels and Piping. 193, art. 104446, 2021. DOI: https://doi.org/10.1016/j.ijpvp.2021.104446.
[23] Chandra, K., Kain, V., Bhutani, V., Raja, V.S., Tewari, R., Dey, G.K., and Chakravartty, J.K., Low temperature thermal aging of austenitic stainless-steel welds: kinetics and effects on mechanical properties. DOI: https://doi.org/10.1016/j.msea.2011.11.055
[24] Run-Zi, W., Hang-Hang G., Shun-Peng Z., Kai-Shang L., Ji W., Xiao-Wei W., Miura, H., Xian-Cheng Z., and Shan-Tung T., A data-driven roadmap for creep-fatigue reliability assessment and its implementation in low-pressure turbine disk at elevated temperatures. Reliability Engineering & System Safety, 225, art. 108523, 2022. DOI: https://doi.org/10.1016/j.ress.2022.108523.
[25] Neyman, J., On a new class of contagious distributions applicable in entomology and bacteriology, Ann. Math. Stat 10, pp. 35-57, 1939. DOI: https://doi.org/10.1214/aoms/1177732245.
[26] Martin, D.C., and Katti, S.K., Approximations to the neyman type a distribution for practical problems, Biometrics 18(3), pp. 354-364, 1962. DOI: https://doi.org/10.2307/2527477.
[27] Ozel, G., and Turkan, S., Neyman type a distribution for the natural disasters and related casualties in Turkey, Journal of Data Science 13(3), pp. 533-550, 2022. DOI: https://doi.org/10.6339/JDS.201507_13(3).0007.
[28] Johnson, N.L., Kemp, A.W., and Kotz, S., Univariate discrete distributions, Wiley Series in Probability and Statistics, 3rd Ed., Wiley. 2005. DOI: https://doi.org/10.1002/0471715816.
[29] Fang, F., and Oosterlee, C.W., A novel pricing method for European options based on Fourier-cosine series expansions, SIAM Journal on Scientific Computing 31(2), pp. 826-848, 2009. DOI: https://doi.org/10.1137/080718061.
[30] da Silva, A.J., Baczynski, J., and Vicente, J.V.M., Recovering probability functions with Fourier series. Pesquisa Operacional, 43, art. 7882 2023. DOI: https://doi.org/10.1590/0101-7438.2023.043.00267882
[31] Shenton, L.R. and Bowman, K.O., Remarks on large sample estimators for some discrete distributions, technometrics, Technometrics 9(4), pp. 587-598,1967. DOI: https://doi.org/10.2307/1266197.
[32] Fisher, R.A., On the mathematical foundations of theoretical statistics, Philosophical Transactions of the Royal Society of London 222, pp. 309-368, 1922. DOI: https://doi.org/10.1098/rsta.1922.0009.
[33] Sasongko, L. and Mahatma, T., The estimation of renewal functions using the mean value theorem for integrals (mevti) method. d'CARTESIAN 5, pp. 111-120, 2016. DOI: https://doi.org/10.35799/dc.5.2.2016.14984.

A.J. Da Silva, received the BSc. Eng. in Production Engineering from the Catholical University of Petropolis (UCP), Petropolis, Rio de Janeiro - Brazil, in 2012. MSc. and PhD. in Computational Modeling from the National Laboratory for Scientifical Computing (LNCC), Petropolis, Rio de Janeiro - Brazil, in 2015 and 2021, respectively. Since 2016, he has been a Professor with the Production Engineering Department, CEFET/RJ, Itaguai, Rio de Janeiro - Brazil. His research interests include numerical methods, stochastic processes, reinforcement learning, reliability engineering, and quantitative finance applications.
ORCID: 0000-0001-9763-6395

F.DoC. Amorim, holds a BSc in 2013, MSc. In 2015, and PhD. In 2018, in Mechanical Engineering from the Fluminense Federal University (UFF), Brazil. He is a Sp. in Radiological Protection and Safety of Radioactive Sources in 2018, from the Institute of Radioprotection and Dosimetry (IRD/CNEN) in partnership with the International Atomic Energy Agency (IAEA). Currently, he is a professor at the Federal Center for Technological Education Celso Suckow da Fonseca (Cefet/RJ), working in the Department of Mechanical Engineering and in the Graduate Program in Mechanical Engineering and Materials Technology (PPEMM). He has experience in the field of mechanical engineering, with an emphasis on solid, elastic, and plastic body mechanics, focusing mainly on the following topics: industrial maintenance, structural integrity, mechanical behavior of materials, mechanics of composite materials, and polymers. Hewas awarded the Young Scientist of Our State (JCNE) - FAPERJ - 2022. He currently serves as the Coordinator of the Coordination of Research and Technological Studies (COPET) at Cefet/RJ.
ORCID: 0000-0001-6658-0106

DYNA
http://dyna.medellin.unal.edu.co/

UNIVERSIDAD NACIONAL DE COLOMBIA

Evaluation and improvement process in quality of service: case studies of restaurants in Manabí

Yanelis Ramos-Alfonso [a], Angelica Beatriz Ruiz-Cedeño [b], Aracelys Sánchez-Briones [b] & Neyfe Sablón-Cossio [c]

[a] Facultad de Ciencias Matemáticas Físicas y Químicas. Universidad Técnica de Manabí, Manabí, Ecuador. yanelis.ramos@utm.edu.ec
[b] Facultad de Ciencias Administrativas y Económicas. Universidad Técnica de Manabí, Manabí, Ecuador. angelica.ruiz@utm.edu.ec, yenniz.sanchez@utm.edu.ec
[C] Facultad de Posgrado. Universidad Técnica de Manabí, Manabí, Ecuador. neyfe.sablon@utm.edu.ec

Received: February 6th, 2024. Received in revised form: March 21th, 2024. Accepted: April 18th, 2024.

Abstract
The objective of this research is to evaluate the quality of restaurant services of Manabí, a local offer of Ecuador; as a basis for systematic improvement. Through a descriptive, non-experimental and cross-sectional study; Difference 5 of the Servqual Model was contextualized, adding the aspects of convenience of schedules, attractiveness and understanding of the menu, value for money; among others; which integrated with improvement tools through time study, constitutes the main contribution of the study. Its application in two Manabí restaurants allowed the validation of the usefulness of the proposed instrument for the evaluation and improvement of the quality of restaurants in the Manabí context. In the case of a traditional restaurant, a reduction in service times was achieved by determining effective service standards during peak hours; In the modern one, the need for differentiation strategies based on age is established.

Keywords: Servqual model; quality of services; restaurants, time study.

Proceso de evaluación y mejora en la calidad del servicio: caso de estudio restaurantes en Manabí

Resumen
El objetivo de esta investigación es evaluar la calidad de los servicios en la restauración manabita, autóctona oferta del Ecuador; como base para la mejora sistemática. Mediante un estudio descriptivo, no experimental y transversal; se contextualizó la diferencia 5 del Modelo Servqual, añadiendo los aspectos de conveniencia de horarios, atractivo y comprensión de la carta-menú, relación calidad-precio; entre otros; lo que, integrado con herramientas de mejora mediante el estudio de tiempos, constituye el aporte principal del estudio. La aplicación en dos restaurantes manabitas permitió la validación de la utilidad del instrumento propuesto para la evaluación y mejora de la calidad de la restauración en el contexto manabita. En el caso de un restaurante tradicional se logró la disminución de los tiempos de atención por la determinación de normas de servicio efectivas en horarios pico; en el moderno se establece la necesidad de estrategias de diferenciación en torno a la edad.

Palabras clave: modelo Servqual; calidad de los servicios; restaurantes; estudio de tiempos.

1 Introduction

In Latin America, some countries have sought to position themselves as tourist destinations, using gastronomy as a channel for cultural expression and take advantage of natural resources. Ecuador has an autochthonous and varied gastronomy that makes both national and foreign consumers feel attracted to try it, and this experience is enriched by an adequate service culture.

The cuisine of the Manabí province is one of the most recognized and widely-known of Ecuador. Some dishes stand out, such as: plantain empanadas, stuffed with cheese or beef and prepared according to traditional custom; seco de gallina criolla, encebollado, tortillas de maíz, corviche, ceviche, among others.

How to cite: Ramos-Alfonso, Y., Ruiz-Cedeño, A.B., Sánchez-Briones, A., and Sablón-Cossio, N., Evaluation and improvement process in quality of service: case studies of restaurants in Manabí. DYNA, 91(232), pp. 77-85, April - June, 2024.

These dishes can be enjoyed by national and foreign customers in restaurants located in the coastal area, on the highways and in the cities themselves. These restaurants may have different kinds of infrastructure and amenities, some more rustic and simple and some more modern-looking; However, the expectations regarding the quality of the food and the service are similar.

Manabitan cuisine is recognized for its exquisite flavors and traditional methods of preparation, which transcend the national gastronomy; however, some research, such as that of Castro-Farías [1], suggests that average levels of satisfaction are influenced by aspects such as: opening hours, menu comprehensibility, service culture and value for money. That is why it is necessary to evaluate the perceived quality of instruments appropriate to these expectations, in a context where administrative decisions are often made empirically.

It is of vital importance to define and validate instruments that allow the evaluation of the quality of these catering services, as a way to establish actions that move these institutions towards constant improvement.

Process reengineering can be a great competitive advantage for companies, given that, redesigning processes to obtain improvements may increase performance and even reduce costs, if done properly [1]. The first step to improve food service processes is to evaluate them from the customer's perspective.

Zeithaml et al. [2] defined perceived quality as: "the difference between the perceptions of the customer and the perceived quality of the service". This definition is the basis for the development of its main proposal: The Servqual Model.

The 1991 version of said instrument, establishes 5 parameters and 22 questions, as shown in Fig. 1. The dimensions are [3]:

- Reliability: refers to the ability to execute the promised service reliably and carefully. That is, that the company fulfills its promises, on deliveries, service provision, problem solving and pricing.
- Responsiveness: This is the willingness to assist users and to provide them with prompt and adequate service. It refers to attentiveness and promptness in dealing with requests, answering customer questions and complaints, and solving problems.

Table 1.
Servqul Applications & Service Process Improvement Tools

BR	Sector	Comments
[4]	Guarantee Court	The highest levels of expectations were found in the dimensions of reliability, security and tangible aspects; for which the main dissatisfactions are identified.
[5]	Hospital registration and check-in process	Considers integrating patient satisfaction with process improvement tools (Lean principles, VSM: Value Stream Map), which reduced complaints by 40%.
[6]	Pizzeria Establishment	Reliability and tangibility were affected variables, caused essentially by the lack of technologies with which to provide the service.
[7]	Restaurants	The authors used an instrument in order to adapt Servqual in restaurants with the variables: internal service quality, market orientation and organizational citizenship behavior.
[8]	TAST Steakhouse in Taiwan	Studies the importance and attributes of cognitive satisfaction with service quality.
[9]	National Parks	These authors propose that service quality is understood as the discrepancies between expectations and perceptions, and that specific factors are defined on the basis of each area of interest.
[10]	Telecommunications	The components of logistics, reliability, responsiveness, security and comprehension are used.
[11]	General model for services	This model uses terms such as performance measurement and service industry, combining the benefits of Servqual with RDM, balanced scorecard, etc.
[12]	Banking sector	This work recognizes the Servqual model as the basis on which other work has been developed, validating a contextualization of it.
[13]	Higher education	This study links constant improvement with the evaluation of service quality using the Servqual model, adjusted for training programs.
[14]	Water and sewer company	These authors contextualize Servqual and integrate it into the quality deployment diagram (QDF) in order to better understand customer needs.
[15]	Banking sector	This work contextualizes Servqual by employing a conclusive statistical analysis.
[16]	Public hospital	These authors propose a model that prioritizes the attributes of the quality of services, based on the Servqual scale, which is contextualized
[17]	Hospital de especialidades	This work uses the modified Servqual model, considering aspects related to recreation and sports, to promote health tourism in a general sense.
[18]	Hospitals	The Servqual model is integrated with the Saaty analytical hierarchy (AHP) in order to classify corporate hospitals.
[19]	Pharmaceutical studies	This work deals with the question of whether Servqual or Servperf (satisfaction versus performance) is most appropriate. It was discovered that, in the studied context, satisfaction is more predictable, unlike that which had occurred in other work by the same authors.
[20]	Users of cloud service platforms	These authors contextualize and perform convergent validity tests in order to establish the consistency of the modified Servqual scale.
[21]	Restaurants	The value of empathy is shown.
[22]	Restaurants and hospitality	These authors employ a simulation to analyze the differences in the service provided by robots and human personnel by using from Servqual.
[23]	Filipino fast-food restaurant	This work establishes that food safety is an important attribute as regards satisfaction.
[24]	General	These authors state that multiplicative models predict service quality and customer satisfaction better than additive models.
[25]	Restaurants	Servqual is integrated with with a Petri net in order to improve response capacity in a Colombian restaurant.
[26]	Restaurants in the non-state sector	The evaluation of service quality is integrated with improvement tools such as timing, process simulation, and six sigma methodologies.

Source: Own elaboration

- Assurance: It is the knowledge and attentiveness of employees and their ability to inspire credibility and trust.
- Empathy: Refers to the level of individualized attention offered by companies to their customers. It should be conveyed through personalized service or service tailored to the customer's taste.
- Tangible elements: It refers to the appearance, aesthetics and material amenities, such as infrastructure, equipment, resources, personnel, etc., that are the most important elements of a company's business.

It is important to pair the evaluation of perceived quality through the Servqual Model with other process improvement tools because the end goal is to obtain actual significant changes in the service.

Table 1 shows applications of Servqual in various services, and its integration with other tools that allow the improvement of these service processes.

The versatility of the Sevqual model and its wide use for the evaluation of the quality of services of diverse nature, including catering, can be appreciated. Nonetheless, variations can be observed in the making and application of surveys, depending on the context and the number of items.

Another aspect to consider in the previous review, there is a tendency to analyze the incidence of sociodemographic variables such as sex, age and purchasing power, as well as the close relationship between evaluation, diagnosis and orientation of service quality improvement programs.

Furthermore, Wu et al. [8]; Jasmon A., et al. [11]; Franceschini et al. [14]; Parrado- Hernández et al. [26] and Causado-Rodríguez et al. [25] all integrate the Servqual Model with tools for process improvement. These tools are based on: the study and measurement of work (timing), simulation, six sigmas, Lean and VSM principles, and are focused on improving the response capacity in the cycle of the services studied. The above establishes the usefulness of Servqual for the evaluation of the quality of services and its integration with tools for process improvement.

In restaurant services, other models related to the Servqual scale have been developed, among which we can mention:

DINESERV: Instrument proposed by Stevens et al. [27] for measuring service quality in restaurants. It is based on the SERVQUAL model; It proposes 5 categories, it establishes 29 elements, including aspects related to hygiene, the menu, among others.

Servperf Model establishes the evaluation only of perceptions [28].

Tangserv adds tangible and social elements through three parameters: Layout and design, in relation to factors such as interior decoration and furnishings; product and service, considering the presentation and variety of food; and environmental and social, including music and temperature.

Campoverde-Aguirre, et.al, [29]; they state that this model is questionable because of its unclear methodology. Given the limitations, DINESCAPE proposes a scale of six factors: aesthetics of the facilities, environment, lighting, service product, design, and social factors.

It is proposed by [29] that this model offers a reliable statistical analysis, although only focusing in the inner processes of the restaurant. These authors propose a contextualization for the measurement of the quality of service in gastronomic fairs through four categories: reliability, tangibility, sensitivity and adequacy.

The above models constitute contextualization of Servqual for the evaluation of the quality of service in gastronomy and catering. However, they must be adjusted to the quality characteristics valued by customers in different contexts.

According to the problem stated above, it is necessary to establish questions concerning: How to evaluate and improve the quality of restaurant services in the Manabí province, which attributes require most attention and what tools can be used to improve service processes.

1.1 Objective

The objective of this study to evaluate the quality of services, using a valid and contextualized instrument for restaurants in Manabi, as a basis on which to improve service processes.

2 Methodology

The research had a quantitative, cross-sectional, non-experimental, descriptive, and correlational approach; using the survey as a technique for collecting information, applied to two case studies of the Manabi restaurant sector.

The study was carried out by developing the following procedure (Fig. 1). The first step of the procedure was established on the adequacy of the measurement instrument (Difference 5 of the modified Servqual Model) and its validation in the restaurants that were studied. The remaining steps could be replicated in other restaurants in Manabí and in general, under the principles of flexibility and relevance.

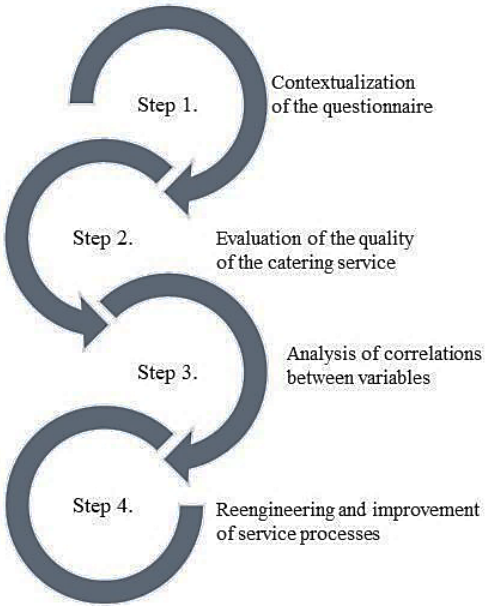

Figure 1. Procedure used to evaluate and improve the quality of restaurant services.
Source: Own elaboration

Step 1. Contextualization of the questionnaire

The questionnaire employed in the survey was developed with the help of 9 specialists in gastronomic service management who had specific training in the area, had worked for more than 5 years in the Manabí restaurant sector and that had done studies in the area of service quality. The above was corroborated by the coefficient k=½(kc+ka), where kc represents a measure of knowledge of the topic being researched and ka is a measure of the sources of argumentation of potential experts [30].

The dimensions and questions of the Servqual model were listed, adding DINESERV AND DINESCAPE; the specialists were subjected to a first round of questions to add other variables (items) to those established by models to evaluate the quality of the restaurant service.

A survey was subsequently applied to these specialists, who were asked to evaluate a list of possible questions and weigh the importance of each one for the evaluation of the corresponding dimension. Agreement in expert judgment was established using a non-parametric Kendall test. The demonstrated consensus of the experts established the inclusion of those questions that attained median values in the "important" and "very important" categories.

After establishing validity by means of expert judgment, the internal consistency of the instrument was analyzed using Cronbach's alpha and the principal components analysis, which had to have favorable values for values greater than 0.7 in the first case, and 0.6 in the case of KMO. The scale used included five categories: Much less than expected, less than expected, equal to expected, more than expected and much more than expected.

The total list was submitted to the judgment of the experts who, by means of coincident judgments, were supported by the Kendall test
(Table 2) with an asymptotic Sig of 0.00. They chose the median values in the categories of "important and very important". A total of 17 questions were chosen.

The questionnaire, with 17 questions, was applied as a pilot test to 100 clients, considering a scale of 5 levels from "much less than expected" as the lowest, to "much more than expected" the highest, which allows to establish a difference in the customer's mind between expectations and perceptions.

This analysis allowed the improvement of the formulation of some questions for a better understanding in the Manabí context. Then, the sample for finite populations was obtained, with a sampling error of 4.96% for a total of 290 valid questionnaires applied in the month of March 2023, in consideration of an average monthly visit of 1000 clients.

An exploratory factor analysis was carried out, which allowed us to reduce and better interpret the quality

Table 2.
Kendall non-parametric test values.

N	9
Kendall's W [a]	.522
Chi-Square	112,833
Df	24
Asymp. Next.	,000

Source: Own elaboration

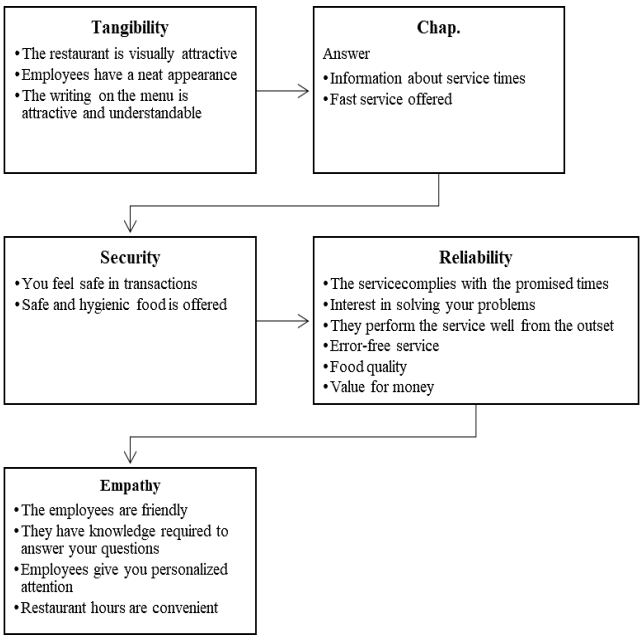

Figure 2. Established questions and dimensions
Source: Own elaboration

dimensions of the services evaluated. Subsequently, a confirmatory factor analysis showed a Kaiser-Meyer-Olkin Measure value of 0.759, with a significance of 0.000 and a determinant close to, but not equal to zero, which indicates no presence of an identity matrix. Additionally, the internal consistency of the instrument was validated and yielded a Cronbach's alpha value of 0.937, thus denoting the one-dimensionality of the variable studied. Finally, the 5 dimensions and 17 questions included are shown in Fig. 2.

Highlights include additions to the original Servqual Model:

- The menu is attractive and understandable
- Restaurant hours are convenient
- Safe and hygienic food is offered
- The quality of the food
- The quality-price ratio

Step 2. Evaluation of the quality of the catering service

The study was carried out in two restaurants that represent the context of manabitan cuisine and culture, and that have been in business for more than 5 years. These have achieved the loyalty of a group of customers and have improved their market shares since their launch, and this was the reason for selecting them. In both cases, the sampling used was for convenience, in the month of March 2023, the surveys were applied in person to customers.

Case 1 corresponds to a restaurant located in the city of Chone that offers traditional dishes. It serves approximately one thousand customers per month, which made it possible to establish a sample of 290 customers for the survey. This allowed statistical inference by segments, based on a sampling error of 4.96%.

Case 2 is located in the city of Portoviejo, the capital of Manabí, and specializes in American and Argentine cuts of

meat. In their promotional messages they state: "To cross our doors is to begin a culinary, visual and sensory journey, where we share our experiences collected from around the world." It has 1200 reservations per month, which required a sample of 292 in order to obtain conclusive results with a confidence level of 95 % and a sampling error of 5%.

In order to interpret the results, the measures of central tendency (median and mean) were analyzed for each question and parameter. Deficiencies were identified as those responses that attained average values below 3, which corresponded to a failure to meet expectations. The frequencies of responses were analyzed for those cases in which it was difficult to attain unsatisfactory measures of central tendency.

Step 3. Analysis of correlations between variables

Non-parametric tests were carried out in order to establish the relationships between sociodemographic variables. In the case of sex, the Mann-Whitney U was used to establish two categories. However, 4 ranges were established for age and it was, therefore, analyzed using the Kruskal-Wallis H. The perceived quality values of the cases studied were also compared.

The analyses are carried out by applying the following twelfth hypothesis:

H0: There is homogeneity between groups.

H_1: There are differences between groups.

Critical region: Sig. Asymptotic ≤ 0.05 Rejection of null hypothesis.

Step 4. Reengineering and improvement of service processes

The authors Chica-Castro and Solís-Ferrer [31] proposed a general methodology based on the identification of processes, along with their strengths and weaknesses, through a diagnosis and redesign that allows the operation of the system to be optimized.

Using this idea as a basis, the proposal is to start from the flow cycle of the service process, establishing the critical activities according to what was stated by the customer, listing the possible solutions, and applying the engineering tools that would contribute to dealing with them. We also propose the use of timing as an important time study technique for the standardization and regulation of work, thus allowing the establishment of optimal personnel needs based on the number of visitors and peaks in demand for the service.

In order to carry out timing in the restaurant, the tables were established as the unit of observation, based on which service times (Th) and independent times (Te) were established, and in which the person offering the service does not intervene, such as consuming the food [29].

The service standard was established as:

Ns = (Th+Te)/Th

Ns: Service standard

Th: Serving time

Te: Independent time

The necessary observations were determined by establishing

Formula:

$$n = (\frac{ts}{k\underline{x}})^2 \quad (1)$$

where:

-t (probability of occurrence),

-s (standard deviation),

-k (margin of error),

-x (average or average of the cycle times in each of the stages of the process).

3 Results

Step 1 was developed by establishing the questionnaire for the evaluation of the quality of services in the context of Manabí restaurants.

Table 3 shows the analysis of the measure of central tendency (mean) for both cases, per question and per parameter.

Table 3.
Central tendency values by items and dimensions.

Questions/Case study	Attributes	CASE 1: Traditional Restaurant		CASE 2: Modern Restaurant	
		Half	Great average	Half	Great average
The restaurant is visually attractive	Tangibility	3.89		4.6	
Employees have a neat appearance	Tangibility	3.84	**3.86**	4.4	**4.53**
The writing on the menu is attractive and understandable	Tangibility	3.84		4.6	
The service complies with the promised times	Reliability	2.77		4.6	
Interest in solving your problems	Reliability	2.72		4.93	
They perform the service well from the outset	Reliability	3.31	**3.14**	4.6	**4.62**
Error-free service	Reliability	3.31		4.6	
Food quality	*Reliability	3.31		4.53	
Value for money	*Reliability	3.41		4.46	
Information about service times	Chap. Ans.	2.57	**2.52**	4.66	**4.63**
Fast service offered	*Chap. Ans.	2.46		4.6	
You feel safe in transactions	Security	3.26	**3.26**	4.6	**4.6**
Safe and hygienic food is offered	Security	3.84		4.73	
The employees are friendly	Empathy	3.31		4.53	
They have knowledge required to answer your questions	Empathy	2.67	**2.9**	4.73	**4.71**
Employees give you personalized attention	Empathy	2.52		4.8	
Restaurant hours are convenient	*Empathy	3.1		4.8	
Overall Average		**3.14**		**4.73**	

Source: Own elaboration

As can be seen, the average satisfaction in the first case (traditional restaurant) is 3.14, i.e. a level of satisfaction of 62.8%; lower than in the second case (modern restaurant), which has an average of 4.73, representing 94.6% satisfaction according to the scale used.

Case 1 shows dissatisfaction in responsiveness and empathy, although the remaining parameters and questions show median values of 3 for the most part, which corresponds to the average value of the scale. Tangibility stands out as the most highly rated parameter, which suggests that the market segment in this type of service is not so demanding with regard to tangible aspects.

Contrasting with this result is case 2, where all the dimensions show general satisfaction, with tangibility being the least valued, specifically the cleanliness of the employees. Likewise, value for money, friendliness of employees, speed of service, and that the service is done right the first time. It is worth mentioning that the prices of the products in this case are high in comparison with other similar businesses, so the client has a high expectation in relation to the aforementioned aspects, in that order.

Gender does not affect the overall mean of satisfaction; the asymptotic sigma higher than 0.05 in both cases, evidences that men and women have similar behaviors in their level of satisfaction (Table 4).

Similarly, the Kruskal-Wallis nonparametric H test was performed (Table 5) to analyze the differences between groups according to age. It is established that there are differences between the groups in case 2 (modern restaurant), but not in the first case.

The 19 to 34 and 34 to 50 age groups have average satisfaction values of 4.7 and 4.75, respectively, while clients in the 51 to 65 range have an average value of 4.46, which shows that the service has more favorable characteristics for younger clients. Changes are needed to improve the perceived quality in age groups over 50, especially considering that this is the most lucrative segment.

In the step of Reengineering and improvement of service processes, a partial result related to case 1 is presented, this being the one that showed the greatest weaknesses associated essentially with responsiveness and empathy. The process

Table 4.
Analysis of group differences by sex.

	General average	General average
U de Mann-Whitney	22	47,5
W de Wilcoxon	50	113,5
Z	-0,704	-0,162
Asymptotic sig.(bilateral)	0,482	0,871
Exact significance [2*(one-sided sig.)].	0,536[b]	0,882[b]
	Case 2	**Case 1**

Source: Own elaboration

Table 5.
Analysis of group differences in terms of age.

	General average	General average
Kruskal-Wallis H	7,778	1,468
gl	2	3
Asymptotic sig.	0,02	0,69
	Case 2	**Case 1**

Source: Own elaboration

Table 6.
Average durations per activity in timekeeping at the table.

No.	Activity	Classification	Duration
1	Take order and take to kitchen	Th	5 min
2	Wait for service	Te	15 min
3	Brings order	Th	6 min
4	Consume service	Te	20 min
5	Brings bill	Th	7 min
6	Wait for change	Te	7 min
7	Brings change and collects service	Th	15 min

Source: Own elaboration

begins with the arrival of the customer, checking the menu, taking of the order, consumption, payment and removal from the table, removal of the customer.

The unit of observation was the table, for the timing, we started with 5 initial observations, which according to the average values showed the need for a total of 12. F 6 shows the summary of the approximate times of the activities of the table service cycle.

Serving time: 1: 5 min; 3: 6 min; 5: 7 min; 7: 15 min.

Independent time: 2: 15 min; 4: 20 min; 6: 7 min.
Average Th = (5+6+7+15)/4 = 8.25 min.
Te average = (15+20+7)/3 = 10.66 min.
Ns=(Th+Te)/Th = (8,25+10,66)/8,25 = 2,29

It is established that each employee can serve 2.29 tables, which can be rounded to 2 assuming that the employee will have limited time, but should strive to provide empathetic and time-efficient service. In this restaurant, the service standard was 4 tables per employee, double the recommended number. Based on this study, two employees were added at peak demand times, established between 12:00 and 14:00 pm, to speed up service. In addition, classes on good service practices were given, and the collection activity was automated through the acquisition of computer equipment, which improved response times, reducing waiting times from 22 to 15 minutes on average.

4 Discussion

The findings obtained herein generally coincide with those of Mu et al. [33], who stated that: “it is necessary that the organization adopt a culture of total quality, in such a way that from the leader to the lowest level employee provide their services with quality for the sake of customer service” (p. 13), given the deviations found regarding the need to offer a better service as regards friendliness, response times, the employees’ appearance and their interest in dealing with each customer’s particular needs.

The established questionnaire considers 17 questions and 5 parameters, in relation to the 5 parameters and 22 questions of the Servqual. Some were added, such as the menu is attractive and comprehensible, safe and hygienic food is offered, coinciding with the DINESERV model, the quality of the food, such as Stevens, et. al, [27], adding restaurant hours and the quality-price.

Therefore, the essential contribution of the proposal in the

integration and adaptation for the proposal of an instrument contextualized to the restaurant sector of Manabí is established.

The usefulness of the Sevqual model has been established with regard to its validity for the evaluation of and improvement to the quality of Manabí restaurant service processes. In addition, there is also the usefulness of employing a differential scale, which reduces efforts related to the application of a single questionnaire. The authors Ramos-Farroñán, et.al, [28] applied the Servperf Model to a touristic restaurant, but dealt only with perceptions. In the case described herein, a single instrument is used to measure both perceptions and expectations. Likewise, the neatness of employees could be identified as a variable with some level of affectation, denoting the value that customers place on this tangible aspect in modern restaurants, and influenced precisely by the high expectations of knowledgeable clients with experience of international cuisine.

The findings also coincide with those of Fuentes-Gómez et al. [34], who identified shortcomings in temperatures (food quality), variables that also appear in both pieces of research, thus corroborating the importance of including this important tangible in the assessment of the perceived quality in restaurant services.

The authors Corrêa de Melo and Dumke de Medeiros [6], allude to the shortcomings of the service in a pizzeria owing to poor technologies and in which customers expressed dissatisfaction with the fulfillment of the promised times, along with the tangible aspects, which corroborates what was found in Case 1 (traditional restaurant). This was used as the basis on which to make improvements as regards times through the use of process reengineering by shortening cycle times and automation.

Process reengineering can be tailored to the conditions of each institution, and in the case of restaurants, the study of time, the establishment of process standards and service norms, and structural improvements to the process, can contribute to efficiency as regards the reduction of cycle times, and greater customer satisfaction. This aspect was addressed by Abarca-Sánchez & Ramos-Alfonso [35] through the use of timing for increased productivity and reduced cycle times in a condensed milk packaging company. The study and measurement of work continues to be a useful tool for the standardization of and improvement to both manufacturing and service processes [36].

In summary, the methodological and practical usefulness of the procedure developed for the systematic evaluation of the perceived quality in Manabí cuisine is highlighted by the use of a validated scale that is easy to understand for users, composed of 17 questions to be answered by means of a differential scale that establishes from much less than expected, to more than expected. making it simple to compare expectations and perceptions with a single app. Added to this is the integration with the study of times for the establishment of standards of care that favor both good customer service and the well-being of workers, by managing with appropriate work standards at a normal work pace, an element also addressed by [29], as an essential aspect of the improvement of the catering service.

5 Conclusions

This paper shows a proposal for a procedure for the evaluation of and improvement to quality in two restaurants in Manabí, which offer modern versus traditional cuisine. This procedure establishes the use of the Servqual Model for the evaluation of the quality of the restaurant services in the cases studied, and time study tools, such as timing, in order to improve the performance of the processes and customer satisfaction by shortening attention times. It could be replicated in similar institutions, under the principles of flexibility and relevance.

The Servqual Model has again been validated, this time in the context of restaurants in Manabí, using expert judgement and the internal consistency of the scale used, which in this case corresponds to a differential that allows the contrast of expectations and perceptions through the application of a single instrument. 16 questions were established, to which others were added such as: the attractiveness of the menu, the quality of the food, value for money and the convenience of the schedules.

The evaluation of the questionnaire in two restaurants that are representative of traditional Manabí cuisine (Case 1) versus modern cuisine (Case 2), showed that there were lower satisfaction values for the former, essentially as regards the capacity for response and empathy, denoted as empiricism in activity. In the second case, meanwhile, although to a lesser extent, an impact on tangibility was established. This made it possible to infer the demanding expectations that the visiting market segment has. In this case, it was possible to confirm the need to develop strategies that would be more appropriate for people over 50 years of age.

The evaluation of the quality of the service showed the guiding elements of improvement, which allowed the reengineering of the service process in Case 1, from the establishment of a work organization standards service (2 tables per employee during peak demand hours), which allowed a reduction in cycle times. This is an example of the usefulness of integrating work study and measurement tools in the context of evaluating and improving the quality of services.

In future research it will be necessary to expand on the integration of the Servqual model (with regard to all its differences) with other process improvement tools, such as simulation, six sigmas, plant designs, and the quality deployment diagram in order to develop the best solutions by which to improve quality tailored to services of a different nature.

References

[1] Castro-Farías, K.V., Análisis de la satisfacción de los clientes del restaurante Choclo Loco en Manta. Tesis de grado de Ingeniería Comercial. Universidad Laica Eloy Alfaro de Manabí. [en línea]. 2018. Disponible en: https://repositorio.uleam.edu.ec/bitstream/123456789/1006/1/ULEAM-ADM-0026.pdf

[2] Zeithaml, V.A., Berry, L., and Parasuraman, A., Las consecuencias conductuales de la calidad del servicio. Diario de Marketing, 60(2), pp. 31-46, 1996.

[3] Castillo-Zamora L.V., Modelo SERVQUAL de la calidad de servicio y la satisfacción del usuario externo en el centro de rehabilitación en sustancias psicoactivas del Hospital Hermilio Valdizán, Lima. Tesis Maestría en Gestión de los Servicios de la Salud, [en línea]. 2018. https://repositorio.ucv.edu.pe/bitstream/handle/20.500.12692/31268/Castillo_ZL.pdf?sequence=1&isAllowed=y

[4] Ganga-Contreras, F., Alarcón-Henríquez, N. y Pedraja-Rejas, L., Medición de calidad de servicio mediante el modelo SERVQUAL: el caso del Juzgado de Garantía de la ciudad de Puerto Montt - Chile. Ingeniare. Revista Chilena de Ingeniería, 27(4), pp. 668-681, 2019. DOI: https://doi.org/10.4067/S0718-33052019000400668

[5] Nino, V., Martínez, K.J., Gómez, K., and Claudio, D., Improving the registration process in a healthcare facility with lean principles. Journal of Industrial Engineering and Management, 14(3), pp. 538-551, 2021. DOI: https://doi.org/10.3926/jiem.3432

[6] Corrêa de Melo, C. e Dumke de Medeiros, D., Aplicação do modelo servqual modificado para avaliação da qualidade dos serviços prestados pelos estabelecimentos de pizzaria. Xl Encontro nacional de engenharia de produção. "Contribuições da Engenharia de Produção para a Gestão de Operações Energéticas Sustentáveis". Iguaçu, Paraná, Brasil, 2020.

[7] Gjurašić, M., Internal service quality in hotel industry – conceptualization and measurement. Tourism and Hospitality Management, 25(1), pp. 227-237, [online]. 2019. Available at: https://hrcak.srce.hr/220336

[8] Wu, T.H., Weng, S.J., Lin, Y.T., Kim, S.H., and Gotcher, D., Investigating the importance and cognitive satisfaction attributes of service quality in restaurant business - A case study of TASTy steakhouse in Taiwan. Journal of Foodservice Business Research, 23(4), pp. 263-284, 2020. DOI: https://doi.org/10.1080/15378020.2020.1749799.

[9] Valčić, I., and Marković, S., Service quality measurement in national parks in the Republic of Croatia: application of modified ecoserv model. Tourism and Hospitality Management, 25(2), pp. 435-438, 2019.

[10] Torieh, A.M., Measuring the gap between perceptions and expectations using SERVQUAL an applied study on telecommunication services in KSA (Mobily telecommunication company). Scientific Journal of King Faisal University, 21(1), pp. 259-285, 2020. DOI: https://doi.org/10.37575/h/edu/1609

[11] Jasmon, A., Dean, W.F., and Maarof, F., Effectual performance management model for the service industry. Business transformation through innovation and knowledge management: an academic perspective. In: Proceedings of the 14th International Business Information Management Association Conference, IBIMA, 2, 2010, pp. 1174-1186.

[12] Sureshchandar, G.S., Rajendran, C., and Anantharaman, R.N., Determinants of customer-perceived service quality: a confirmatory factor analysis approach. Journal of Services Marketing, 16(1), pp. 9-34, 2002. DOI: https://doi.org/10.1108/08876040210419398.

[13] Tóth, Z.E., and Surman, V., Listening to the voice of students, developing a service quality measuring and evaluating framework for a special course. International Journal of Quality and Service Sciences, 11(4), pp. 455-472, 2019. DOI: https://doi.org/10.1108/IJQSS-02-2019-0025.

[14] Franceschini, F., Galetto, M. y Turina, E., Calidad del servicio de agua y alcantarillado: propuesta de una nueva herramienta de monitoreo multicuestionario. Gestión de Recursos Hídricos 24(12), pp. 3033-3050, 2010. DOI: https://doi.org/10.1007/s11269-010-9593-0

[15] Zaheer, A., Structure equation modeling (SEM) approach for evaluating and analyzing the effect of IT-based services in banking sector on customer service quality (SEVQUAL). International Journal of Advanced and Applied Sciences, 10(2), pp. 147-155, 2023. DOI: https://doi.org/10.21833/ijaas.2023.02.018.

[16] Altuntas, S., Dereli, T., and Erdoğan, Z., Evaluation of service quality using SERVQUAL scale and machine learning algorithms: a case study in health care. Kybernetes, 51(2), pp. 846-875, 2022. DOI: https://doi.org/10.1108/K-10-2020-0649.

[17] Markovic, S., Loncaric, D., and Loncaric, D., Service quality and customer satisfaction in the health care industry - Towards health tourism market. Tourism and Hospitality Management, 20(2), pp. 155-170, 2014.

[18] Khan A.M.R, Prasad, P.N., and Rajamanoharane, Sw., Service quality performance measurement management in corporate hospitals using analytical hierarchy process. International Journal of Manufacturing Technology and Management, 26(1-4), pp. 196-212, 2012. DOI: https://doi.org/10.1504/IJMTM.2012.051434

[19] Mandal, K., and Gupta, H., Gap versus performance-based measure of pharmaceutical education service quality: an empirical comparison. Indian. J. Pharm. Educ. Res., 53(3), pp. 421-34, 2019. DOI: https://doi.org/10.5530/ijper.53.3.75

[20] Boakye, K.G., Natesan, P., and Prybutok, V.R., A correlated uniqueness model of service quality measurement among users of cloud-based service platforms. Journal of Retailing and Consumer Services, 55, art. 102098, 2020. DOI: https://doi.org/10.1016/j.jretconser.2020.102098.

[21] Baluyot, M.B., and Pampolina, A.C., Exploring the relationship of service quality on customer's delight in selected restaurant of laguna, Philippines. Estudios de Economia Aplicada, 39(12), art. 6024, 2021. DOI: https://doi.org/10.25115/eea.v39i12.6024.

[22] Zhang, S., Hu, Z., Li, X., and Ren, A., The impact of service principal (service robot vs. human staff) on service quality: the mediating role of service principal attribute. Journal of Hospitality and Tourism Management, 52, pp. 170-183, 2022. DOI: https://doi.org/10.1016/j.jhtm.2022.06.014.

[23] Ong, A.K.S., Prasetyo, Y.T., Mariñas, K.A., Perez, J.P.A., Persada, S.F., Nadlifatin, R., Chuenyindee, T., and Buaphiban, T., Factors affecting customer satisfaction in fast food restaurant "Jollibee" during the COVID-19 Pandemic. Sustainability (Switzerland), 14(22), art. 15477, 2022. DOI: https://doi.org/10.3390/su142215477.

[24] Park, S.J., Yi, Y., and Lee, Y.R., Multiplicative versus additive models in measuring service quality. Total Quality Management and Business Excellence, 34(15-16), pp. 2105-2123, 2023. DOI: https://doi.org/10.1080/14783363.2023.2229272.

[25] Causado-Rodríguez, E., Charris, A.N. y Guerrero, E.A. Mejora continua de la atención al cliente a través de ServQual y Red Petri en restaurante Santa Marta - Colombia. Información Tecnológica, 30(2), pp. 73-84, 2019. DOI: https://doi.org/10.4067/S0718-07642019000200073

[26] Parrado-Hernández, C.A., Pérez de Armas. M., Barrera-García, A., Procedimiento para la mejora de la calidad en restaurantes del sector no estatal. Desarrollo Sustentable, Negocios, Emprendimiento y Educación, 4(34), pp. 28-47, 2022.

[27] Stevens, P., Knutson, B., and Patton, M., Dineserv: A Tool for Measuring Service Quality in Restaurants. Cornell Hotel and Restaurant Administration Quarterly, 36, pp. 56-60, 1995. DOI: https://doi.org/10.1177/001088049503600226

[28] Ramos-Farroñán, E.V., Mogollón-García, F.S., Santur-Manuel, L., and Cherre-Morán, I., El modelo Servperf como herramienta de evaluación de la calidad de servicio en una empresa. Universidad y Sociedad, 12(2), pp. 417-423, 2020, https://rus.ucf.edu.cu/index.php/rus/article/view/1538

[29] Campoverde-Aguirre, R, Carvache-Franco, M, Carvache-Franco, W. y Almeida-Cabrera, M., Análisis de la calidad del servicio en festivales gastronómicos. Sostenibilidad, 14(21), art. 14605, 2022. DOI: https://doi.org/10.3390/su142114605

[30] Herrera-Masó, J.R., Calero-Ricardo, J.L., González-Rangel, M.Á., Collazo-Ramos, M.I. y Travieso-González, Y., El método de consulta a expertos en tres niveles de validación. Revista Habanera de Ciencias Médicas, [en línea]. 21(1), art. e4711. 2022. Disponible en: https://revhabanera.sld.cu/index.php/rhab/article/view/4711

[31] Chica-Castro, L.A. y Solís-Ferrer, H.E., El cambio de paradigma de la industria a través de la reingeniería de procesos. AlfaPublicaciones, 4(1.1), pp. 293-310, 2022. DOI: https://doi.org/10.33262/ap.v4i1.1.160

[32] Real-Pérez, G.L., Hidalgo-Ávila, A.A. y Ramos-Alfonso, Y., La carga física de los trabajadores: estrategia administrativa en la mejora de procesos. Eca Sinergia, 6(1), pp. 101-118, 2015. DOI: https://doi.org/10.33936/eca_sinergia.v6i1.254.

[33] Mu, R.P., Lin, J., Chi, K.W., and Wang, T., Trends, practices and policy suggestions of innovation-driven digital transformation of social services. Bulletin of Chinese Academy of Sciences, 37(9), pp. 1259-1269, 2022. DOI: https://doi.org/10.16418/j.issn.1000-3045.20220615002.

[34] Fuentes-Gómez, L., González-Álvarez, R., Parrado-Hernández, C.A. y Gálvez-Pereira, K.Y., Evaluación de la calidad percibida de servicios en restaurante a la carta. Universidad y Sociedad, [en línea]. 12(4), pp. 179-191, 2020. Disponible en: https://rus.ucf.edu.cu/index.php/rus/article/view/1629
[35] Abarca-Sánchez, S.A. y Ramos-Alfonso, Y., Análisis de tiempos en el envasado de leche condensada en Industria Láctea Ecuatoriana. Ingeniería Industrial, [en línea]. 43(4), pp. 1-16, 2022. Disponible en: https://rii.cujae.edu.cu/index.php/revistaind/article/view/1199
[36] Acosta.Prieto, J.L., Monzón-Alfaro, Y, Cepero-González, S. y Tito-Reyes, A., Análisis del ciclo de servicio en el proceso de venta de excursiones de una agencia de viajes. Retos Turísticos, 21(1), art. e-4753, 2022.

Y. Ramos-Alfonso, is professor and researcher of the Industrial Engineering career, of the Faculty of Mathematics, Physics and Chemistry of the Technical University of Manabí, Ecuador. She was a professor, head of the degree program at the University of Matanzas, Cuba, until 2019, where she also served as head of the authorized doctoral Area of Industrial Engineering. She is BSc. Eng. in Industrial Engineer, MSC. in Business Administration: mention in Production and Services Management; Dr. in Technical Sciences from the University of Matanzas. She has won awards for his contribution to doctoral training. Her research interests include quality, process management, human factor engineering and education in general terms.
ORCID: 0000-0001-8383-1245

A.B Ruiz-Cedeño, is a professor and researcher at the Technical University of Manabí, Ecuador.
ORCID: 0000-0001-8170-5624

A. Sánchez-Briones, is a professor and researcher at the Technical University of Manabí, Ecuador. She is coordinator of the Master of Business Administration.
ORCID: 0000-0002-8004-3291

N. Sablón-Cossío, is a professor and researcher at the Postgraduate Institute at the Technical University of Manabí, Portoviejo, Ecuador. She is BSc. Eng. in Industrial Engineering from the University of Matanzas, Ecuador. She also graduated with a MBA and a Dr. in Science, Industrial Technical Engineering. All these studies carried out in Cuba. She has published several magazines and conference papers. Dr. Sablón has carried out a research project on supply chains in Mexico, Cuba and Ecuador. She has the National Prize for the result of Scientific Research of the Cuban Academy of Sciences. Her research interests include management, business, logistics, operations management, supply chain, value chain, and circular supply chain.
ORCID: 0000-0002-6691-0037

DYNA
http://dyna.medellin.unal.edu.co/

UNIVERSIDAD NACIONAL DE COLOMBIA

Analytical procedure for calculating impulsive responses on floor systems under human walking

Omar Caballero-Garatachea [a], A. Gustavo Ayala-Milián [b], Gelacio Juárez-Luna [c] & Marco A. Escamilla-García [a]

[a] *Instituto de Ciencias Básicas e Ingeniería, Universidad Autónoma del Estado de Hidalgo, Mineral de la Reforma, Hidalgo, México. omar_caballero@uaeh.edu.mx, marco_escamilla@uaeh.edu.mx*
[b] *Instituto de Ingeniería, Universidad Nacional Autónoma de México, Ciudad Universitaria, Ciudad de México, México. GayalaM@iingen.unam.mx*
[c] *Departamento de Materiales, Universidad Autónoma Metropolitana, Unidad Azcapotzalco, Ciudad de México, México. gjl@azc.uam.mx*

Received: October 1st, 2023. Received in revised form: April 15th, 2024. Accepted: April 22th, 2024.

Abstract
Human walking is an activity which generates impulsive responses on floors systems with fundamental frequency higher than 10 Hz. In the literature, there are procedures based on extensive polynomial functions to calculate impulsive responses on floor systems under human walking. However, the prediction of this type of human activity in the development of analytical procedures is still complex. Because of that, it is necessary to provide alternatives of human walking simulation and dynamic response analysis of the floor system. Considering this, a practical procedure based on the use of a simple harmonic function is proposed to calculate the impulsive response of the floor system, which is validated with a numerical-experimental study consisting of a concrete slab supported on beams subjected to a person's walking. According to the obtained results, it is demonstrated that the proposed procedure provides reasonably approximate results.

Keywords: analytical procedure; reinforced concrete; floor vibration; human walking.

Procedimiento analítico para el cálculo de respuestas impulsivas en sistemas de piso ante el caminar humano

Resumen
El caminar humano es una actividad que genera respuestas impulsivas en sistemas de piso con frecuencia fundamental mayor que 10 Hz. En la literatura se han propuesto procedimientos analíticos basados en funciones polinomiales extensas para calcular respuestas impulsivas en losas ante el caminar humano. Sin embargo, la predicción de este tipo de actividad humana en el desarrollo de procedimientos analíticos aún es compleja. Por tal razón, es necesario proporcionar alternativas de simulación del caminar humano y análisis de la respuesta dinámica del sistema de piso. Considerando lo anterior, se propone un procedimiento práctico basado en el uso de una función armónica simple para calcular la respuesta impulsiva del sistema de piso, el cual se valida con un estudio numérico-experimental de una losa de concreto reforzado apoyada sobre vigas sometida al caminar de una persona. De los resultados obtenidos, se demuestra que el procedimiento propuesto proporciona resultados razonablemente aproximados.

Palabras clave: procedimiento analítico; concreto reforzado; vibración de losa; caminar humano

1 Introduction

The vibration analysis of floor systems under human walking depends on the determination of parameters such as the fundamental frequency and the damping ratio of the floor as well as the magnitude and characterization of the human-induced force. The human walking is simulated as the sum of different harmonics functions, whose frequency values are approximately 1.6 to 9.0 Hz. These functions are associated to Dynamic Load Factors (DLFs) to define the magnitud of the acting force.

Human walking is frequently the dominant type of human-induced excitation activity in residential and office buildings [1,2]. In accordance with [3], the calculation of the vibration of a floor system under human walking mainly depends on its classification: low- or high-frequency floor.

How to cite: Caballero-Garatachea, O., Ayala-Milián, A.G., Juárez-Luna, G., and Escamilla-García, M.A., Analytical procedure for calculating impulsive responses on floor systems under human walking. DYNA, 91(232), pp. 86-94, April - June, 2024.

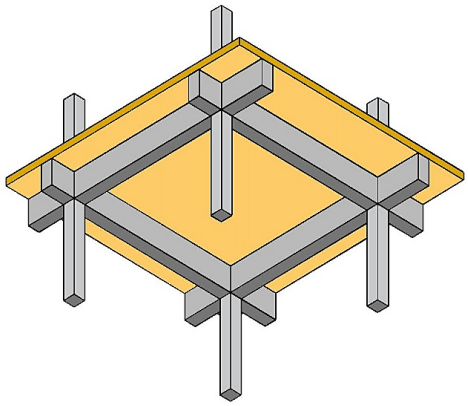

Figure 1. RC two-way slab supported on beams.
Source: The authors

Low-frequency floors are characterized by having a fundamental frequency lower than 9-10 Hz and exhibit a resonance response due to walking activity. On the other hand, the high-frequency floors have at least one responsive natural frequency higher than 9-10 Hz, where the floor system exhibits a sequence of impulses from a person walking [4]. In the analysis of high frequency floors, human walking generates transient responses, which are calculated with based on the use of single footfalls, as shown in Fig. 2a. This criterion provides satisfactory results in the analysis of this type of floor systems as proven in the literature. However, considering that human walking is still an activity of complex prediction, it is necessary to provide other criteria to simulate it adequately. Because of that, this work suggests the hypothesis that a simple harmonic load can potentially predict the impulse response of a high frequency floor under human walking. Thus, an analytical procedure is proposed to calculate the dynamic response of this type of floor system.

Considering the need to use a high frequency floor for the purposes of this work, an existing RC two-way slab supported on beams is analysed for its vibration analysis under human walking. This type of floor system is constituted by significantly rigid structural elements [5,6], as shown in Fig. 1, so it is adequate to generate impulsive responses and to validate, the proposed analytical solution.

1.1 Modelling of human walking on floor systems

1.1.1. Introduction

The human activity of walking is a phenomenon commonly represented by time-domain deterministic force models, which consist of simulating the induced load either with individual footfalls or footfall overlapping, as shown in Fig. 2. The first load function, shown in Fig. 2a, simulates the force induced from the heel to toe and it is considered as a practical function for the calculation of impulse responses on high frequency floors [4,8-10]. The development of this function is based on a polynomial expression, which depends on variables such as the step frequency, person´s weight and contact duration. The second load consists of the summation of forces, as shown in Fig. 2b, where it is observed that both feet generate slightly higher induced loads than the single footfall. In general, these types of excitation have been studied for many years [11] because of the uncertainties that still exist in walking parameters such as weight, step frequency, walking speed and so on. However, their use can provide reasonable results when it is applied for the vibration analysis of floor systems.

Considering that hypothetically a simple harmonic load can generate a realistic human induced-load on the vibration analysis of high frequency floors, a time domain force model was studied to simulate this condition. In this work, the expression proposed by [12] is considered for such analysis, which simulates the vertical dynamic force induced by a pedestrian F(t) and it is expressed as:

$$F(t) = P\,[1 + \Sigma\alpha_i cos(2\pi i f_s t + \emptyset_i)] \quad (1)$$

where P is the weight of a person (N), i is a harmonic multiple of the step frequency, f_s is the step frequency (Hz), ϕ_i is the phase shift (rad) and α_i is the Fourier coefficient for the *ith* harmonic force usually known as dynamic load factor (DLF). Given that the higher harmonics have little contribution in the excitation of the floor system [4], only the first harmonic was considered in the eq. (1), where the action produced by both feet is modelled in a simplified way.

1.1.2. Dynamic load factor

The Dynamic Load Factors (DLFs) are the key to generate an accurate force model and are defined as the ratio of the force amplitude of each harmonic to the weight of the person. Based on Fourier decomposition, several studies were carried out to quantify this parameter, which is the basis to define the periodic human induced force. Based on the literature review carried out by [11] and Zivanović et al. [13], it is observed that authors such as [14-19] provide different values of DLFs to predict adequately the process of human walking. In this work some coefficients were evaluated to accomplish this condition.

1.2 Calculation of the dynamic response of high frequency floors under human walking

To determine the dynamic response of a high frequency floor there are procedures such as Ungar and White [8], Wyatt [9], and Willford *et al*. [10], which are mainly based on the analysis of a single degree-of-freedom system (SDOF) subjected to a footfall as source of excitation. These

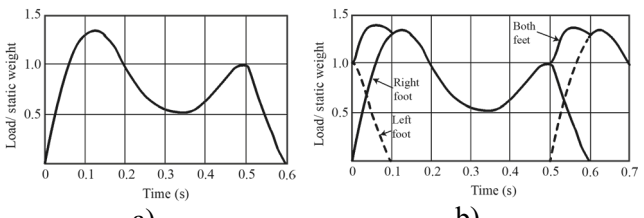

Figure 2. Forcing function resulting from footfalls during walking with a pacing rate of 2 Hz: a) force from single footfall and b) force from footfall overlap
Source: Baumann and Bachmann [7]

procedures do not consider the use of harmonic functions to simulate the dynamic force induced by a pedestrian, it is because mainly the response is not influenced by high harmonics. According to [4] the method proposed by [10] provides best results in the calculation of impulsive responses on floor systems; this method is derived from statistical studies on a SDOF system in terms of velocity, from which an expression to simulate the human induce-load was proposed:

$$I_{eff} = 54\frac{f_s^{1.43}}{f_n^{1.30}} \quad (2)$$

where I_{eff} is called effective impulse, so the velocity of the floor system is calculated with the following expression:

$$v(t) = \mu_i \mu_j \frac{I_{eff}}{M_{\text{mod}}} \quad (3)$$

where M_{mod} is the modal mass of the floor system. μ_i and μ_j are the mode shape ordinates, which correspond to the point *i* where the impulse is applied and the point *j* where the response is measured [10]. As observed, this method does not consider variables such as the weight of the person, damping ratio and the modal stiffness are neglected during the analysis process, so the author´s point of view is to consider these variables in order to improve the prediction of the source of excitation.

Harmonic loads are used on low frequency floors, while impulse loads are used on high frequency floors. It is worth mentioning that in certain circumstances, the classification of the floor system is no reliable when selecting a force model [11]. For instance, when the floor develops a fundamental frequency close to 9-10 Hz, it can develop either resonant or transient responses, so the selection of the force model is no accurate. Because of that, it is feasible to evaluate the applicability of a harmonic load to simulate the human walking on high frequency floors.

In general, the prediction of human walking activity on floor systems is still significantly imprecise and complex, so it is necessary to provide recommendations or alternatives of modelling and simulation to improve it. In this work, a single harmonic function to simulate the force induced by a pedestrian on a high frequency floor is proposed. According to this, an analytical procedure for the calculation of the acceleration of this type of floor system is provided. This procedure is based on a developed closed-form solution, which is derived from the equation of motion of a SDOF system.

2 Proposed method for the calculation of impulsive responses on high frequency floors

2.1 Harmonic force model

Unlike the methods [8–10], where a footfall function is used for modelling a person walking on the high frequency floor, a single harmonic load is proposed. In this case, the eq. (1) is used as a basis for this purpose. Considering the contribution of both feet as the action generating the maximum dynamic response, the lowest harmonic from eq. (1) is used, so the force model is expressed as:

$$F(t) = P + P\alpha_i cos(2\pi i f_s t) \quad (4)$$

which hypothetically generates an impulsive response on the floor system. As observed in Fig. 3, each maximum is associated to the induced load by the heel and toes while the minimum induced load is generated by the sole of the foot. Unlike the function shown in Fig. 2a, the proposed function starts with a maximum applied force at t=0 s, *i.e.*, the maximum response occurs immediately after rest. As observed, the magnitude of eq. (4) depends not only on the value of *P* but also on the value of the DLF α_i corresponding to the lowest harmonic, so in this work, some values of α_i were taken from the literature to evaluate its level of accuracy in the human walking simulation.

2.2 Calculation of the dynamic response of the floor system

In this section, an analytical procedure for the vibration analysis of RC two-way slabs under human walking is proposed. Considering that a floor system has distributed mass and stiffness and therefore can be defined by an infinite number of degrees of freedom, a single degree of freedom model was proposed in order to simplify the analysis. The dynamic load given by eq. (4) was taken as source excitation, where only the lowest harmonic generates the demands of dynamic response on the floor system.

Due to the maximum amplitudes of motion of a floor system are developed at the center of the slab, the analytical procedure is developed to describe the dynamic response of the floor system at this point. In the simplified SDOF equivalent model, the modal mass and stiffness are equivalent to a percentage of the mass and stiffness of the whole slab, the modal damping is a ratio of the critical damping for the fundamental mode. The excitation load is a cosine function to model a person when walking at the midspan of the slab as shown in Fig. 4. From eq. (1), the equation of motion of the system under the influence of viscous damping and the external force is as shown in eq. (5). In this equation, the summation of the load *P* and the weight of the floor are in equilibrium with the force generated by the stiffness of the slab, so only the harmonic contribution is considered in eq. (5).

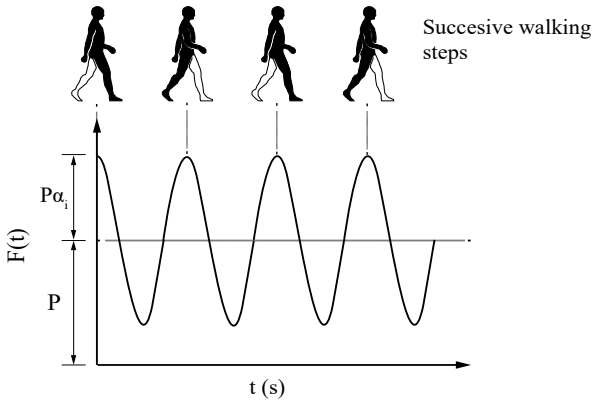

Figure 3. Proposed harmonic load to simulate the human walking
Source: The authors

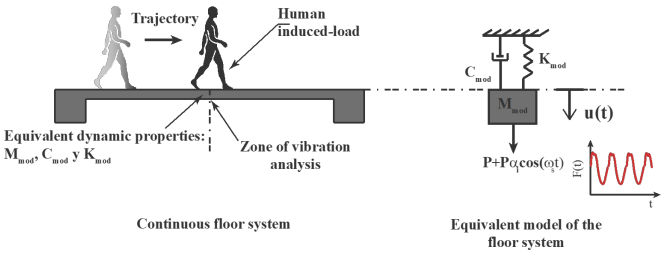

Figure 4. Single degree of freedom system for the vibration analysis of RC two-way slab under human walking.
Source: The authors

$$M_{\text{mod}}\ddot{u} + C_{\text{mod}}\dot{u} + K_{\text{mod}}u = P_o \cos\omega_s t \tag{5}$$

where c_{mod} is the damping and $P_o=P\alpha_i$ in accordance with eq. (5). Dividing both sides of the equation by M_{mod} gives:

$$\ddot{u} + 2\xi\omega_n\dot{u} + \omega_n^2 u = \frac{P_o}{M_{\text{mod}}}\cos\omega_s t \tag{6}$$

The general solution of eq. (6) consists of sum of the complementary solution $u_h(t)$ plus the particular solution $u_p(t)$.

$$u(t) = u_h(t) + u_p(t) \tag{7}$$

the general solution of the underdamped system is given by:

$$u_h(t) = exp(-\xi\omega_n t)\,(A cos\omega_D t + B sin\omega_D t) \tag{8}$$

where

$$\omega_D = \omega_n\sqrt{(1-\xi^2)} \tag{9}$$

ω_n is the fundamental natural frequency of the floor system, ω_D is the damped natural frequency and A and B are constants. The particular solution for u_p(t) is of the form:

$$u_p(t) = C sin\omega_s t + D cos\omega_s t \tag{10}$$

where ω_s is the excitation frequency, which is defined as $\omega_s=2\pi f_s$ in accordance with eq. (4); C and D are constants. Considering that the general solution is the sum of both complementary and particular solutions, the equation predicting the displacement of the SDOF system is:

$$\begin{aligned} u(t) = {} & exp(-\xi\omega_n t)(A cos\omega_D t + B sin\omega_D t) \\ & + C sin\omega_s t + D cos\omega_s t \end{aligned} \tag{11}$$

Deriving eq. (11) the dynamic response of the model can be represented in terms of velocity, as follows:

$$\begin{aligned} du/dt = {} & -exp(-\xi\omega_n t)(A\omega_D sen\omega_D t - B\omega_D cos\omega_D t) \\ & - D\omega_s sen\omega_s t + C\omega_s cos\omega_s t \\ & - \xi\omega_n exp(-\xi\omega_n t)(A cos\omega_D t \\ & + B sin\omega_D t) \end{aligned} \tag{12}$$

Deriving twice eq. (11), the dynamic response of the equivalent system can be represented in terms of acceleration:

$$\begin{aligned} d^2u/dt^2 = {} & exp(-\xi\omega_n t)[(2A\omega_D\xi\omega_n + B\xi^2\omega_n^2 \\ & - B\omega_D^2) sen(\omega_D t) + (A\xi^2\omega_n^2 \\ & - 2B\omega_D\xi\omega_n - A\omega_D^2) cos(\omega_D t)] \\ & - [C\omega_s^2 sen(\omega_s t) + D\omega_s^2 cos(\omega_s t)] \end{aligned} \tag{13}$$

Eqs. (11), (12) and (13) represent the analytical procedure to calculate the dynamic response of the floor system. Using the undetermined coefficient method to calculate the constants C and D, eq. (10) is derived and substituted in eq. (6) in such a way that:

$$\begin{aligned} & [(1-\omega_s^2/(\omega_n^2))C - (2\xi\omega_s/\omega_n)D] sen\omega_s t + [(1 \\ & - \omega_s^2/(\omega_n^2))D \\ & + (2\xi\omega_s/\omega_n)C] cos\omega_s t \\ & = P_o/k_{mod} cos\omega_s t \end{aligned} \tag{14}$$

Solving eq. (14) through the system of equations (15), the values of C and D are computed, as shown in eqs. (16) and (17). As observed, C and D correspond to the particular solution, which mainly involves the relation between the excitation frequency and the natural frequency of the floor system.

$$\begin{bmatrix} \left(1-\frac{\omega_s^2}{\omega_n^2}\right) & -\left(2\xi\frac{\omega_s}{\omega_n}\right) \\ \left(2\xi\frac{\omega_s}{\omega_n}\right) & \left(1-\frac{\omega_s^2}{\omega_n^2}\right) \end{bmatrix} \begin{bmatrix} C \\ D \end{bmatrix} = \begin{bmatrix} 0 \\ \frac{P_o}{k_{\text{mod}}} \end{bmatrix} \tag{15}$$

$$\begin{aligned} C = {} & P_o/k_{mod}(2\xi\omega_s/\omega_n)/([1-(\omega_s/\omega_n)^2]^2 \\ & + [2\xi\omega_s/\omega_n]^2) \end{aligned} \tag{16}$$

$$\begin{aligned} D = {} & P_o/k_{mod}[1-(\omega_s/\omega_n)^2]/([1-(\omega_s/\omega_n)^2]^2 \\ & + [2\xi\omega_s/\omega_n]^2) \end{aligned} \tag{17}$$

Taking into account the initial conditions $u(0)$ and $u'(0)$ in eqs. (11) and (12), respectively, the coefficients A and B are defined as shown in eqs. (18) and (19), which depend on the initial conditions and the values of C and D:

$$u(0) = A + D \quad therefore \quad A = u(0) - D \tag{18}$$

$$u'(0) = B\omega_D + C\omega_s - \xi\omega_n A \quad therefore$$

$$B = (u'(0) + \xi\omega_n u(0) - \xi\omega_n D - C\omega_s)/\omega_D \tag{19}$$

As observed, constants A, B, C and D depends on the slab properties, the characteristics of the load excitation and the initial conditions of the problem. It is worth mentioning that, the analytical procedure proposed in this work is based on the analysis of an equivalent SDOF. All the parameters involved in the phenomenon are included, *i.e*, there are no simplifications in the development of the analytical formulation. The proposed analytical procedure is calibrated with numerical and experimental results where the acceleration is the comparison parameter. An existing office building two-way slab supported on edge beams subjected to

a person walking was used as main reference for the comparative study.

3 Experimental program

A two-way RC slab supported on edge beams, which is part of a three-story RC moment frame structure and is used as office building, was tested. This structure is located in the Autonomous Metropolitan University, Mexico City. The vibration testing was carried out at the first-story for the slab panel shown in Fig. 5. This panel is divided into two parts by a lightweight partition wall, the first part is an office area while the second one is a hallway, as shown in Figs. 6 and 7. The slab thickness was 0.13 m for the whole floor system. The dimensions of the slab panel were 6.20 m x 5.60 m. The width for all beams was 0.25 m. The depth for the beam T-01 was 0.60 m while the depth for the beam T-02 was 0.45 m.

The reinforced concrete slab is constituted of reinforcing steel bars with nominal yield strength of f_y=420 MPa and plain concrete with a compressive strength of f´c=45.10 MPa and a density of W=2400 kg/m^3. The modulus of elasticity was computed from eq. (20), in accordance with the Mexico City Building Code for the design of concrete structures NTCC-17 [20], whose value is E_{cc}=29134 MPa. The floor system supports superimposed dead loads, which are summarized in Table 1.

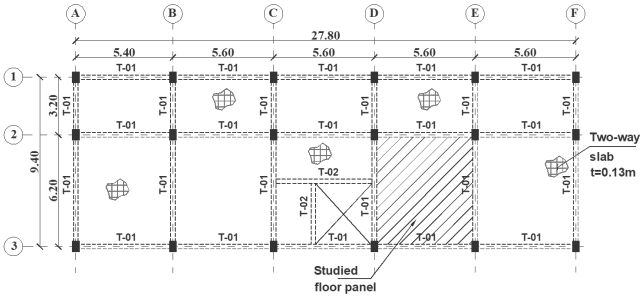

Figure 5. Two-way slab panel tested in the experimental program
Source: The authors

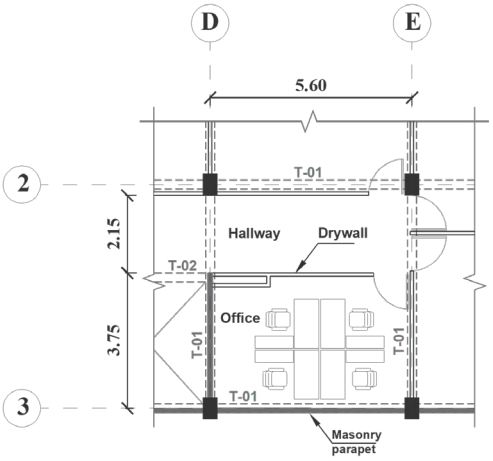

Figure 6. Slab panel having mixed occupancies, office area combined with a hallway
Source: The authors

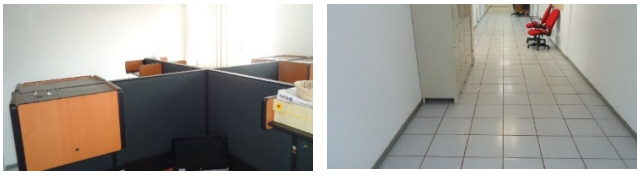

Zona de oficinas **Zona de pasillo**

Figure 7. Characteristics of the slab panel for human walking tests: a) office area and b) hallway
Source: The authors

$$E_{cc} = 2700\sqrt{f'c} + 11000 \quad (20)$$

Table 1.
Superimposed dead loads on the office slabs

Load type	Magnitude (kN/m^2)
Service instalations	0.2
Suspended ceilings	0.2
Ceramic tile	0.2
Furniture and drywall partitions	0.5
Total load	0.11

Source: The authors

3.1 Equipment

Three uniaxial acceleration sensors were used to measure the vertical dynamic response of the slab panel. The accelerations were recorded with a sample rate of 512 Hz. The first sensor (S_1) was installed at the centre of the slab for monitoring the maximum modal amplitude while the two sensors S_2 and S_3 were installed at two supporting beams with the aim of evaluating their contribution in the development of the fundamental mode shape of the panel, as well as the level of acceleration at these points, as shown in Fig. 8. A signal processing equipment, which is a portable spectrum analyzer model SIG-LAB 20-42 [21], was used for data processing. Subsequently, an algorithm was implemented in Matlab V2017 [22] for calculating dynamic responses from either time domain or frequency domain approach.

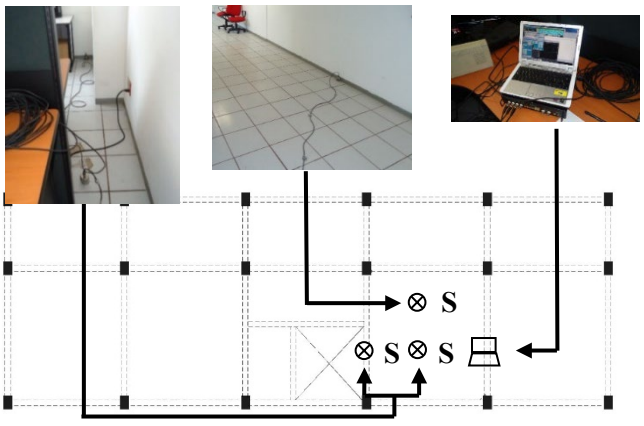

Figure 8. Instrumentation plan to perform experimental measurements
Source: The authors

3.2 Free vibration test

Free vibration tests were performed through ambient vibration measurements (*i.e*, wind, traffic noise, different levels of ground motion, etc.). The acceleration records were carried out with a time window of 300 s, as shown in Fig. 9, where it is observed that the maximum accelerations were recorded by the sensor S_1, while the sensors S_2 and S_3 recorded low values of this parameter. Power Spectral Density (PSD) analyses were performed to identify the f_n of the floor panel.

PSD graphs were calculated for each sensor, where f_n was defined by the peak values in the bandwith labelled B as shown in Fig. 10; according to this, f_n is equal to 14.06 Hz, whose amplitude of motion is graphically described in Fig.

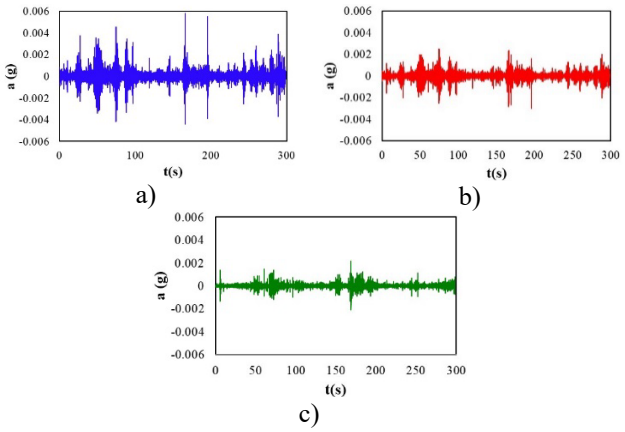

Figure 9. Acceleration records from sensors: a) S_1, b) S_2 and c) S_3
Source: The authors

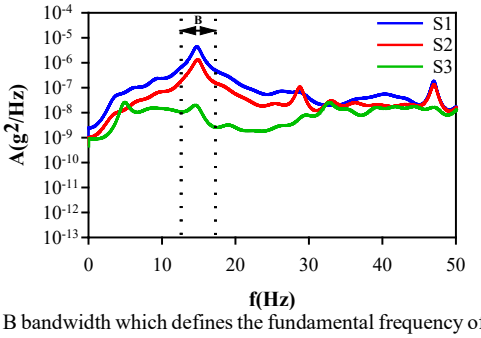

Figure 10. B bandwidth which defines the fundamental frequency of the two-way RC slab panel
Source: The authors

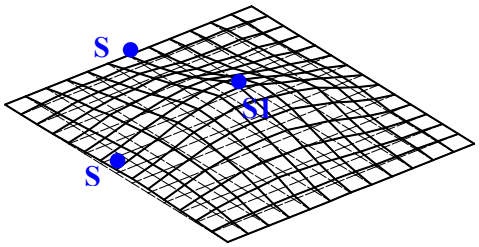

Figure 11. Fundamental mode shape of the slab panel determined experimentally by ambient vibration tests.
Source: The authors

11. It is worth mentioning that the floor system has other defined frecuencies of vibration that may be attributed to either high frequency mode shapes developed in the floor or an electrical feedback initiated by the electrical current source during the test, however, in this work f_n was the variable of interest.

3.3 Forced vibration tests

A forced vibration test was carried out with a person walking on the two-way RC slab panel. The weight of the person was 952 N with a step frequency of 2.0 Hz approximately, which is calculated with an average value determined from steps measurements in walking situation. The person walked in a predefined path as shown in Fig. 12b, which represents a typical walking trajectory on the floor system during its useful life.

Fifteen measurements were carried out for determining the maximum dynamic response of the slab panel. Two measurements were taken from all of them, which are shown in Figs. 13 and 14. These measurements correspond to the recorded accelerations at the midspan of the slab (see Figs. 13a and 14a), where the maximum and minimum peak accelerations recorded were 12.16 and 10.52 cm/s^2,

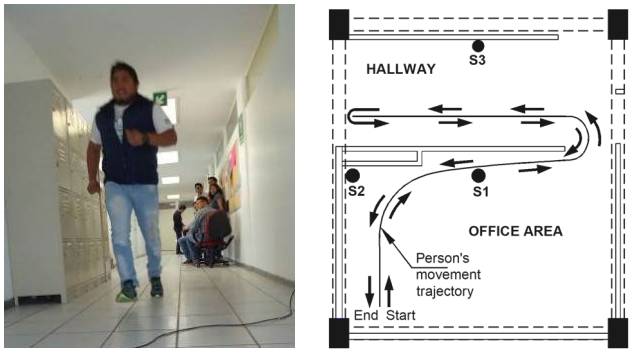

Figure 12. Walking test performed on the two-way reinforced concrete slab panel in an office building: a) one person walking and b) walking trajectory.
Source: The authors

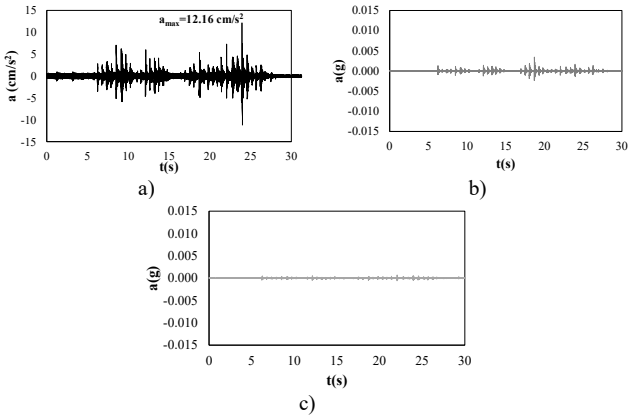

Figure 13. Measure 1 – Accelerations recorded on the floor system with sensors: a) S1, b) S2 and c) S3
Source: The authors

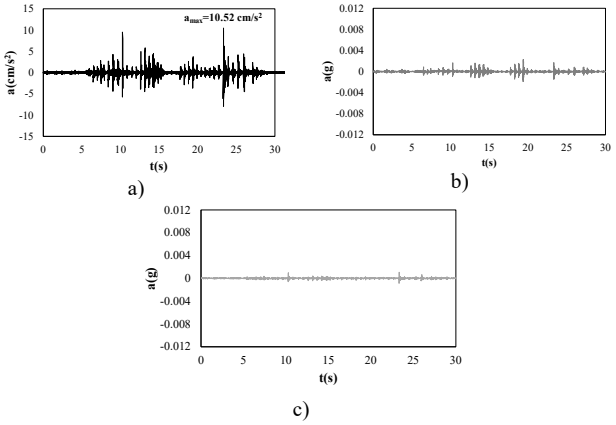

Figure 14. Acceleration records of forced vibration test from sensor S_1: a) measure 1 and b) measure 2
Source: The authors

respectively. On the other hand, the accelerations recorded at the beams by sensors S2 and S3 are significantly low, which means that their contribution in the maximum acceleration of the floor panel can be neglected. Considering the above, the experimental results represent a reference to validate the procedure developed in this work.

4 Numerical modelling

4.1 Mesh convergence study

A numerical simulation of the tested specimen was carried out in the software MIDAS V18 program [23]. Due to the influence of mesh size in the calculation of parameters such as the fundamental frequency and acceleration, an assessment of the meshing strategy is provided. It consists of the analysis of square slabs whose lengths were 4 m and 8 m, respectively; they were modelled with 3D-shell elements. The reinforced concrete elements were modelled as isotropic linear elastic material with a compressive strength f´c=30 MPa and elastic modulus E=24350 MPa. The boundary conditions for each model were simply supported and clamped. These models were subjected to a dynamic load, which is the harmonic function derived from the eq. (4); this force model was applied at midspan using the following parameter values: P= 97 kg, α_i= 0.5, f_s= 2 Hz, i=1. Ratios of natural frequency and acceleration related to the number of elements per side were calculated respectively, where it is seen that 8 elements per side is the minimum to have accurate results for the frequency ratio and 4 elements per side for the peak acceleration ratio. To assure accuracy, 20 elements per panel side were used for meshing the floor systems.

4.2 Fundamental natural frequency

According to the meshing criteria defined above, the test specimen shown in Fig. 5 was modelled to determine its dynamical properties, which were compared with those reported analytically and experimentally. The numerical model was developed with 4-node 3D-shell elements for slabs and 2-node 3D-beam elements for beams. The

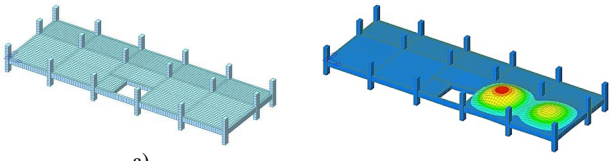

Figure 15. Numerical model of the floor system: a) undeformed model and b) fundamental mode shape of the studied panel
Source: The authors

reinforced concrete elements were modelled as isotropic linear elastic material due to the slabs were under small loads and displacements. The characteristics of the developed model as well as the calculation of its dynamic properties are described below.

Fundamental natural frequency was computed with [23], where the direct method of Lanczos eigen solver was used as the simulation platform. Taking into account the dead loads from the bare structure and the superimposed loads summarized in Table 1, the calculated fundamental natural frequency of the studied panel was 14.78 Hz, with a fundamental mode shape as shown in Fig. 15. The comparison between the numerical and the experimental results gives a difference of 4.9 %.

5 Results and comparisons

A comparative study between analytical, numerical and experimental results was carried out to evaluate the proposed analytical procedure for the calculation of the maximum peak acceleration of a two-way RC slab under a human-induced load. Considering that the test specimen is used as a floor of offices, a value of damping ratio of 0.05 was proposed from the literature [24]. A dynamic analysis was performed to calculate the peak acceleration at the midspan of the slab panel, which consists of solving the equation of motion at each instant of time; in this analysis the value of damping was associated to the minimum and maximum values of frequency of the floor system. Given that the walking load used in eq. (4) depends mainly on the value of DLF, different values of this parameter taken from [14,15,17-19] to evaluate its level of approximation, the values of DLF were 0.257, 0.370, 0.4, 0.5 and 0.431, respectively. Thus, the numerical results are summarized in Table 2.

To calculate the acceleration with eq. (13), the dynamic properties of the slab panel were computed from the numerical model shown in section 4, so f_s, f_n and M_{mod} of the slab panel were 2.0 Hz, 14.78 Hz and 5.57 kg-s^2/cm, respectively. The modal mass was calculated with the expression $M_{mod}= \Sigma\delta_k \times M_k$, where δ_k is the vertical deflection at node k (normalised to the maximum deflection) and M_k is the mass of the floor represented at node k [24]. Thus, k_{mod} was calculated from the basic equation to calculate the fundamental frequency of a SDOF system, $k_{mod}=(2\pi f_n)^2 M_{mod}$ and whose value is 471 kN/cm. Therefore, the values of the coefficients A, B, C and D were calculated. As observed in Table 2, the use of different DLFs generate a variation in the calculation of the vertical acceleration, where the coefficients given by [18] and [14] generate the highest and lowest

dynamic responses, respectively, while [15,17,19] generate similar values of the dynamic response.

The analytical results are similar to those reported numerically and experimentally at t=0 s, while the numerical results are slightly higher than those calculated analytically and experimentally, it is attributed to that the use of mathematical force models often generates an overestimation of the floor vibration response [25]. As shown in Table 2, the analytical and numerical results are higher than 10% when using the DFL given by [18]. [14] generates the lowest results, while [15,17] and [19] generate differences from 3 to 12% with respect to the experimental measurements. Although, the coefficients given by [15,17,19] provide satisfactory results in the calculation of the dynamic response of the floor system, the coefficient given by [17] generates the best results, as shown in Fig. 16.

According to Fig. 16, the analytical dynamic response calculated with eq. (13) is slightly higher than the numerical and experimental results for the zone of decay range, *i.e*, between t=0 s and 0.50 s. It can be attributed to the fact that the value of the damping ratio was taken as 0.05 in the analyses; this value can be higher when the person is on the floor system [26] reducing the amplitudes of oscillation. It should be note that growth of acceleration occurs approximately at t=0.60 and t=1.2 s during the test, it is due to the development of high-harmonic excitations acting on the floor system. These amplitudes are not predicted by the analytical solution, because the first part of the closed form solution in eq. (13) only describes decay.

Table 2.
Analytical, numerical and experimental results considering the use of different dynamic load factors given by different authors

Author(s)	Maximum acceleration (cm/s^2)			
	Eq. (13)	FEA method	Exp. 1	Exp. 2
Rainer *et al*. [18]	13.78	17.14		
Blanchard *et al*. [14]	7.08	8.81		
Schulze [15]	10.19	12.68	12.16	10.52
Bachmann *et al*. [17]	11.02	13.71		
Young [19]	11.86	14.75		

Source: The authors

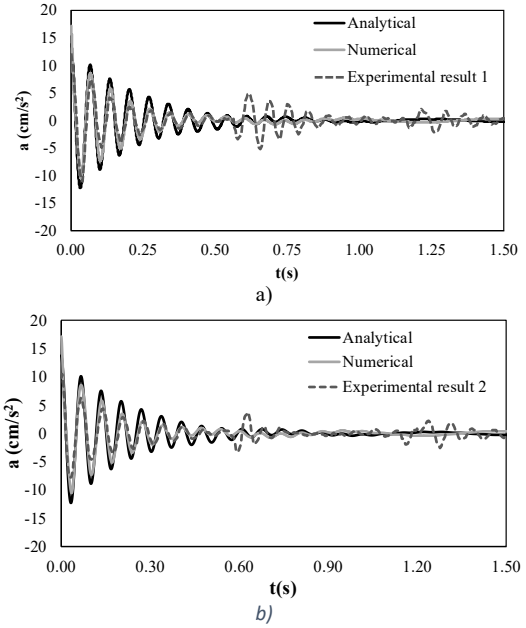

Figure 16. Analytical and numerical accelerations calculated with αi=0.4 [17] and compared with the experimental measurements: a) 1 and b) 2
Source: The authors

6 Conclusions

An assessment of a walking force model and the development and validation of an analytical procedure for the vibration analysis of high frequency floors under human walking is carried out. The study consists of evaluating and assessing the applicability of a simple harmonic load in the calculation of the impulsive response of a high frequency floor. The proposed procedure consists of solving the equation of motion of a SDOF subjected to a cosine load representative of human walking. Subsequently, a numerical-experimental study of a two-way RC slab subjected to human walking was conducted to evaluate their dynamic response. The results obtained were compared with those calculated analytically. In the experimental-numerical study, the accelerations in supporting beams were very low. Because of that, their contribution was not presented in this work. The variable of interest was the dynamic response at the midspan of the RC slab panel.

Using a concentrated load for modelling the human walking on the slab is enough to simulate the effect of a pedestrian on the zone of maximum modal amplitude. The DLFs influence considerably in the calculation of the acceleration of the slab, in the case of this work the DLFs given by [15,17] and [19] contribute to a reasonably prediction of the human induced-load on the floor system. According to this, it is concluded that the use of a cosine function for modelling the human walking has a certain scope of application in the calculation of impulsive responses on the floor system, since the simple harmonic function can predict reasonably the induced force by the heel and toe during the walking process as the force model used by [10].

The developed expression to calculate the dynamic response of the floor system was based on parameters of practical calculation such as modal mass, modal stiffness and damping ratio. The calculation of these parameters corresponds to the fundamental mode shape, whose maximum amplitude occurs at the midspan. M_{mod} and f_n were calculated from the numerical model in order to evaluate the accuracy of the proposed analytical expression as better as possible. It is worth mentioning that, although the method proposed by [10] is based on neglecting some variables in the calculation of the dynamic response of the floor system, the procedure proposed in this work involves more variables of analysis, which can provide advantages in the study of the phenomenon.

Declaration of competing interest

The authors declare that they have no known competing financial interests or personal relationships that could have appeared to influence the work reported in this paper.

Acknowledgement

The authors wish to express their gratitude for the financial support from the General Direction of Academic Personnel and the Institute of Engineering of the National Autonomous University of Mexico. The first and last authors express their gratitude for the support given by the Autonomous University of the State of Hidalgo. The third author acknowledges the support given by the Metropolitan Autonomous University and the academic licences given by Midas Information Technology.

References

[1] Pavic, A., and Reynolds, P., Vibration serviceability of long-span concrete building floors. Part 2: review of mathematical modelling approaches. Shock Vib Dig, 34, pp. 279-297, 2002.
[2] Griffin, M.J., Handbook of human vibration, 1st ed., Elsevier Science, London, UK, 2012.
[3] Racic, V., Pavic, A., and Brownjohn, J.M.W., Experimental identification and analytical modelling of human walking forces: literature review. J Sound Vib, 326, pp. 1-49, 2009. DOI: https://doi.org/10.1016/j.jsv.2009.04.020
[4] Middleton, C.J., and Brownjohn, J.M.V., Response of high frequency floors: a literature review. Eng Struct, 32, pp. 337-352, 2010. DOI: https://doi.org/10.1016/j.engstruct.2009.11.003
[5] Caballero, O. y Juárez, G., Estudio de las variables que influyen en el control de la frecuencia natural de vibración en losas de concreto reforzado. En: XX Congreso Nacional de Ingeniería Estructural. Mérida, Yucatán, México, 2016, pp. 1-13.
[6] Juárez, G. y Caballero, O., Variables que influyen en la frecuencia natural de losas macizas de CR apoyadas en dos direcciones, Revista Internacional de Ingeniería de Estructuras, 25, pp. 561-579, 2020. DOI: https://doi.org/10.24133/riie.v25i4.1863
[7] Baumann, K., and Bachmann, H., Durch Menschen verursachte dynamische Lasten und deren Auswirkungen auf Balkentragwerke (Man-induced dynamic forces and the response of beam structures). Versuchsbericht Nr.7501- 3, Zurich, Birkhäuser Verlag Basel, Institut für Baustatik und Konstruktion, ETH, 1988.
[8] Ungar, E.E., and White, R.W., Footfall-induced vibrations of floors supporting sensitive equipment, Journal of Sound and Vibration, 13, pp. 10-13, 1979. DOI: https://doi.org/10.1121/1.2004124.
[9] Wyatt, T.A., Design guide on the vibration of floors. The Steel Construction Institute, 1989, pp. 1-43. DOI: https://doi.org/10.13140/RG.2.2.29342.95048
[10] Willford, M., Young, P., and Field, C., Predicting footfall-induced vibration: Part 1., in: Proceedings of the Institution of Civil Engineers-Structures and Buildings, 160, pp. 65-72, 2007. DOI: https://doi.org/10.1680/stbu.2007.160.2.65
[11] Younis, A., Avci, O., Hussein, M., Davis, B., and Reynolds, P., Dynamic forces induced by a single pedestrian: a literature review. Appl Mech Rev, 69, pp. 1-17, 2017. DOI: https://doi.org/10.1115/1.4036327.
[12] Allen, D.E., and Murray, T.M., Design criterion for vibrations due to walking, Engineering Journal, AISC, 30, pp. 117-129, 1993.
[13] Živanović, S., Pavic, A., and Reynolds, P., Vibration serviceability of footbridges under human-induced excitation: a literature review. J. Sound Vib., 279(1), pp. 1-74, 2005. DOI: https://doi.org/10.1016/j.jsv.2004.01.019.
[14] Blanchard, J., Davies, B.L., and Smith, J.W., Design criteria and analysis for dynamic loading of footbridges. Symposium on dynamic behaviour of bridges at the transport and road research laboratory: Crowthorne, Berkshire, UK, pp. 90-106, 1977.
[15] Schulze, H., Dynamic effects of the live load on footbridges. Signal und Schiene 24(2), pp. 91-93 and 24(3), pp. 143-147, 1980.
[16] Bachmann, H., and Ammann, W., Vibrations in structures: induced by man and machines. IABSE, Zurich, Switzerland, 1987.
[17] Bachmann, H., Ammann, W.J., Deischl, F., et al, Vibration problems in structures. Birkhäuser, Basel, Switzerland,1995.
[18] Rainer, J.H., Pernica, G., and Allen, D.E., Dynamic loading and response of footbridges. Can J Civ Eng, 15(1), pp. 66-71, 1988. DOI: https://doi.org/10.1139/l88-007
[19] Young, P., Improved floor vibration prediction methodologies. Arup vibration seminar on engineering structural vibration. Current developments in research and practice, London, 2001. DOI: https://doi.org/10.1117/12.615417.
[20] Reglamento de Construcciones para el Distrito Federal. Gaceta Oficial de la Ciudad de México, Normas Técnicas Complementarias para el Diseño y Construcción de Estructuras de Concreto (NTCC-17), México, 2017.
[21] Spectral Dynamics Inc., SIGLAB Manuals, User's Guide, 2001.
[22] MATLAB, R2017b. Natick, Massachusetts: The MathWorks Inc. 2017.
[23] Midas Information Technology Co. Ltd, MIDAS/GEN, General Structural Design System, MIDAS/Gen Ver. 18, 2018.
[24] Feldmann, M., Heinemeyer, C., and Lukić, M., Human-induced vibration of steel structures (Hivoss), European Commission, Directorate-General for Research and Innovation, 2007. DOI: https://data.europa.eu/doi/10.2777/79056.
[25] Brownjohn, J.M.W., Energy dissipation from vibrating floor slabs due to human - structure interaction. Shock Vib, 8(6), pp. 315-323, 2001. DOI: https://doi.org/10.1155/2001/454139.
[26] Brownjohn, J.M.W., Pavic, A., and Omenzetter, P., a spectral density approach for modelling continuous vertical forces on pedestrian structures due to walking, Can. J. Civ. Eng., 31(1), pp. 65-77, 2004. DOI: https://doi.org/10.1139/l03-072

O. Caballero-Garatachea, received his PhD. in Structural Engineering, from the Metropolitan Autonomous University, Campus Azcapotzalco (UAM-A), Mexico. He is currently a research professor at the Autonomous University of the State of Hidalgo, Mexico. His areas of interest include structural dynamics, vibration and analytical formulation of structures idealized as continuous systems.
ORCID: 0000-0001-6927-9888

A.G. Ayala-Milián, received his PhD. in Structural Engineering from the University of Southampton. He is a research professor in the Institute of Engineering (IINGEN-UNAM). His areas of interest include the development of finite elements in structural engineering and seismic design methodologies of buildings based on concepts of performance and resilience.
ORCID: 0000-0002-6777-3273

G. Juárez-Luna, received his PhD. in Structural Engineering from the National Autonomous University of Mexico (UNAM). He is a research professor in the Metropolitan Autonomous University, Campus Azcapotzalco (UAM-A). His areas of interest are mainly the development of finite elements for predicting the behavior of structures in progressive collapse.
ORCID: 0000-0002-1971-5802

M.A. Escamilla-García, received his PhD. in Structural Engineering from the National Autonomous University of Mexico (UNAM). He is an associate professor in the Faculty of Engineering (UNAM). He is currently a research professor at the Autonomous University of the State of Hidalgo. His research work is aimed at developing Approximate Procedures for assessment and seismic design, evaluation of the vulnerability and resilience of structures, structural health.
ORCID: 0000-0001-5276-4369

DYNA
http://dyna.medellin.unal.edu.co/

UNIVERSIDAD NACIONAL DE COLOMBIA

Financial inclusion in Puebla, Mexico: a socioeconomic and spatial econometric analysis

Martín Neri-Suárez [a], José Gonzalo Ramírez-Rosas [a], María Elibeth Morales-Illescas [b] & Felipe Machorro-Ramos [a]

[a] *Ingeniería Financiera, Universidad Politécnica de Puebla, Puebla, México. martin.neri@uppuebla.edu.mx, jose.ramirez@uppuebla.edu.mx, felipe.machorro465@uppuebla.edu.mx*
[b] *Ingeniería en Tecnologías de la Información, Universidad Politécnica de Puebla, Puebla, México. maria.morales@uppuebla.edu.mx*

Received: October 4th, 2023. Received in revised form: May 3rd, 2024. Accepted: May 15th, 2024.

Abstract
This study examines financial inclusion in 217 municipalities in the state of Puebla, Mexico, using statistical analysis and the Moran Index to assess geographic and socioeconomic factors. It was found that 124 municipalities had at least one financial institution, and a cluster of five municipalities showed a high density of these services. In contrast, 93 municipalities lacked financial institutions, and eight of them were in areas with high financial exclusion. The results reveal that municipalities with a higher economically active population and a lower educational lag have better financial inclusion. No significant differences were observed in the poverty levels between municipalities with and without financial inclusion. These findings underscore the need for specific public policies and emphasize the importance of considering the geographic dimension in planning financial inclusion.

Keywords: economic development; financial exclusion; financial institutions; Mexican municipalities; poverty.

Inclusión financiera en Puebla, México: un análisis socioeconómico y econométrico espacial

Resumen
Este estudio examina la inclusión financiera en 217 municipios del estado de Puebla, México, utilizando análisis estadísticos y el índice de Moran para evaluar factores geográficos y socioeconómicos. Se identificó que 124 municipios tienen al menos un establecimiento financiero, y un clúster de cinco municipios mostró una alta densidad de estos servicios. En contraste, 93 municipios carecen de instituciones financieras, y ocho de ellos se encuentran en áreas de alta exclusión financiera. Los resultados revelan que los municipios con una mayor población económicamente activa y menores niveles de rezago educativo tienden a tener mejor inclusión financiera. No se observaron diferencias significativas en los niveles de pobreza entre los municipios con y sin inclusión financiera. Estos hallazgos subrayan la necesidad de políticas públicas específicas y enfatizan la importancia de considerar la dimensión geográfica en la planificación de la inclusión financiera.

Palabras clave: desarrollo económico; exclusión financiera; instituciones financieras; municipios mexicanos; pobreza.

1 Introduction

Financial inclusion is defined as affordable and useful access to a wide range of financial services that cater to a variety of needs, from transactions and payments to savings and credit for both individuals and businesses [1]. Financial inclusion has emerged as a critical factor for economic and social development, particularly in developing countries. This is a multidimensional concept that encompasses access, use, and quality of financial services. These aspects are critical for developing effective public policies that can overcome various barriers to financial inclusion [2]. Regarding access, variables such as financial service availability and accessibility are studied [3]. This approach can be divided into demographic and geographic variables, such as the distance to the nearest bank branch or the number

How to cite: Neri-Suárez, M., Ramírez-Rosas, J.G., Morales-Illescas, M.E., and Machorro-Ramos, F., Financial inclusion in Puebla, Mexico: a socioeconomic and spatial econometric analysis. DYNA, 91(232), pp. 95-102, April - June, 2024.

of bank branches per capita [4]. Internationally, about half of adults in developing countries have a bank account. However, significant disparities in access to financial services persist [5]. In Latin America, countries such as Brazil, Chile, and Uruguay have made considerable progress, but Mexico continues to face significant obstacles in financial inclusion. Specifically, Mexico is grouped with Argentina, Colombia, and Peru as nations with low levels of financial inclusion, characterized by a high proportion of individuals outside the formal financial system [6]. According to data from the National Survey of Financial Inclusion (ENIF) of 2021 [7], 67.8% of the Mexican population has at least one formal financial product. The study of financial inclusion has garnered interest at the subnational level to understand regional disparities in access to and use of financial services. For instance, in countries like India and South Africa, district or provincial-level data have been used to examine financial inclusion [8,9]. In Latin America, subnational research has explored how variations in economic and social development between regions can influence financial inclusion. Studies conducted in Brazil and Colombia have used state and municipal level data to investigate the correlation between financial inclusion and variables, such as income, education, and employment [10]. In Mexico, the 2023 study by [4] highlights the variability in financial inclusion levels among different municipalities, emphasizing the need for public policies that adapt to the particular characteristics of each area. This challenge remains despite implementing the National Financial Inclusion Policy 2020-2024, which addresses multiple key dimensions of financial inclusion: enhancing access to the financial system, effective use of financial services, development of financial skills, and user empowerment [11]. This longitudinal study uses a quantitative approach to examine financial inclusion in the municipalities of the state of Puebla. The research is descriptive and comparative, focusing on three key aspects: the classification of municipalities by their level of financial inclusion, the variation and spatial distribution of the density of financial institutions between 2021 and 2023, and their correlation with socio-economic variables, such as population, employment, poverty, and education. It is noteworthy that the method employed in this study differs from prior approaches by incorporating a spatial component in the analysis, which is often missing in research using multivariate techniques [4,12]. The findings could provide a solid foundation for designing future public policies, particularly in areas with limited or no financial infrastructure.

2 Materials and methods

2.1 Study area

Puebla State is situated in the central-eastern region of Mexico, divided administratively into 217 municipalities and covering an area of 34,306 square kilometers. With its high population density and developed transportation infrastructure, Puebla is among the top eleven states in the country conducive to economic activity. It has 10,127 kilometers of roads, 1,057.2 kilometers of railways, a national and international airport, and five airstrips. These infrastructure elements facilitate the movement of people and goods, essential for economic development and financial inclusion.

2.2 Acquisition and categorization of information on financial institutions

We examined the 217 municipalities in the state of Puebla and divided them into two groups: municipalities with financial inclusion and municipalities with financial exclusion. This classification was made based on the presence or absence of financial institutions in each municipality, using data from the National Statistical Directory of Economic Units of Mexico for the year 2021 [13]. A municipality was deemed to have financial exclusion if it lacked any financial institution from development banks, credit auxiliary organizations, insurance and finance institutions, or credit institutions. On the other hand, a municipality was classified as financially included if it had at least one type of financial institution, including at least one ATM. This classification enables a geographical assessment of access to financial services at the municipal level. It provides a geospatial framework for analyzing the relationship between financial inclusion and other key socioeconomic variables in the state of Puebla.

2.3 Data analysis

Initially, a descriptive analysis was conducted focusing on five socioeconomic variables corresponding to the year 2020 at the municipal level. The variables analyzed include the total population per municipality, the Economically Active Population (EAP), and the percentage of the population with educational lag [14]; the percentage of the population in poverty conditions [15]; and the degree of marginalization [16]. Additionally, a 'Density' variable was created to quantify per capita access to financial services in each municipality, using data from the National Statistical Directory of Economic Units [13]. This variable was calculated for the years 2021 and 2023 and was generated by the ratio between the number of existing financial institutions and the total population in each municipality (Table 1). The approach used provides a fair comparison regarding the availability of financial services among different municipalities. This metric was used to examine how the presence of financial institutions in 2021 relates to the socioeconomic variables of 2020. It is important to note that no comparisons of socioeconomic data with the density of financial institutions were made for the year 2023. The main reason for this omission is the lack of updated socioeconomic data that would allow for accurate comparison of that year. For the statistical analysis, version 2023.06.0 of RStudio was used.

2.4 Normality test

To determine whether the data for each variable were normally distributed, a Shapiro-Wilk test was conducted for each variable in each group. The Shapiro-Wilk test is a statistical test used to test the null hypothesis that a sample is from a normal distribution. It was decided that if the p-value of the Shapiro-Wilk test was greater than 0.05, the data would be considered normally distributed.

Table 1.
Definition of Socioeconomic Variables

Variable	Measurement Scale (Value)	Description
Population	Total population per municipality	Individuals over 18 years old per municipality
Economically Active Population (EAP)	Number of Economically Active Population per municipality	Individuals over 12 years old who have or are seeking employment
Education	Percentage of the population with educational lag	Individuals 15 years and older who cannot read or write
Poverty	Percentage of the population in poverty per municipality	Individuals suffering from at least one social deprivation (access to services, education, food, healthcare, housing) and having a monthly income below the poverty line (approximately 76.41 USD at 2020 prices).
Marginalization	Classified into five categories: Very Low (1), Low (2), Medium (3), High (4), or Very High (5)	A measure of the deprivations suffered by the population, resulting from lack of access to education, residence in inadequate housing, insufficient monetary income
Financial Institutions in 2021 and 2023	Number of financial institutions per municipality in 2021 and 2023	Physical establishments of Credit Auxiliary Organizations, Credit Institutions, Insurance and Finance Institutions, and Development Banks.
Density	Density of financial institutions per 1,000 inhabitants in 2021 and 2023	Number of financial institutions per 1,000 residents calculated by dividing total number financial establishments by total population multiplying result by1000

Source: own elaboration based on information from INEGI (2020, 2023) [13,14], CONEVAL (2021) [15] and CONAPO (2023) [16].

2.5 Comparison tests between groups

To compare the differences between the two groups of municipalities, comparison tests were performed for each variable. For variables that are normally distributed, a student's t-Test was used. For variables that are not normally distributed, a Mann-Whitney U test was used. The student's t-Test is a parametric test that compares the means of two independent groups to determine if they are significantly different. The Mann-Whitney U test is a nonparametric test that compares the distributions of two independent groups to determine if they are significantly different. A 95% confidence level was used for all tests, so we reject the null hypothesis (that there is no difference between the groups) if the p-value is less than 0.05. This analysis provides a detailed insight into the differences between municipalities with financial inclusion and those with financial exclusion in terms of EAP, Poverty Level, Educational Lag, and Degree of Marginalization.

2.6 Distribution of financial institutions between 2021 and 2023

Besides comparing municipalities with financial inclusion and exclusion, the study also analyzed the distribution of the Density of Financial Institutions per 1,000 inhabitants in 2021 and 2023. For 2023, new branches of Banco Bienestar, categorized under Development Banking, were added to the database. This addition is relevant because of Banco Bienestar's role in Mexican government policy aimed at improving the accessibility and conditions of banking services. To assess the data distribution, a Shapiro-Wilk normality test was conducted for each variable. Since the data were not normally distributed, a Wilcoxon test for related samples was used instead of a student's t-Test to compare the density of Financial Institutions in 2021 and 2023. This analysis allowed us to determine whether there are significant differences in the density of these establishments between the two years.

2.7 Spatial econometric analysis

In addition to the descriptive and comparative analyses, a geostatistical analysis of the spatial distribution of Financial Institutions for the years 2021 and 2023 was also conducted. This analysis aimed to identify spatial patterns and areas of high and low density of Financial Institutions. For this purpose, the Moran Index was used, a measure that evaluates spatial autocorrelation in the data. The Moran Index can range between -1 and +1, where a value close to +1 shows strong positive spatial correlation (i.e., nearby areas have similar values), a value close to -1 indicates strong negative spatial correlation (i.e., nearby areas have different values), and a value close to 0 indicates no spatial correlation. The calculation of the Moran Index was performed using the variables 'Density of Financial Institutions for the year 2021 and the year 2023.' The results of the Moran Index provide a quantitative measure of the spatial distribution of Financial Institutions and can help identify areas of interest for future interventions to improve financial inclusion. Geostatistical analyses were performed using GeoDa software version 1.16 [17]. The results of this comparison provide a dynamic view of how financial inclusion in Puebla has changed over a two-year period, which is crucial for understanding the trends and patterns of financial inclusion in the state.

3 Results and discussion

3.1 Spatial distribution of financial inclusion in Puebla

The state of Puebla is comprised of 217 municipalities, which were classified in terms of financial inclusion and exclusion. A total of 124 municipalities were identified with financial inclusion, defined as those with at least one type of financial establishment available to their residents. In contrast, 93 municipalities were identified as falling into the category of financial exclusion, characterized by the total absence of financial institutions by 2021. With the integration of Mexican government development banking in 2023, this was reduced to 85 municipalities without financial services (Fig. 1-a, b).

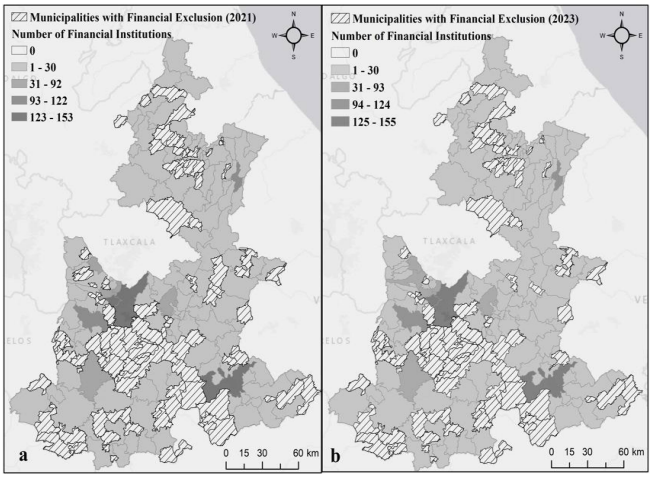

Figure 1. Classification of municipalities in the state of Puebla by financial inclusion and exclusion in 2021 (a) and 2023 (b).
Source: own elaboration based on information from INEGI (2023) [13].

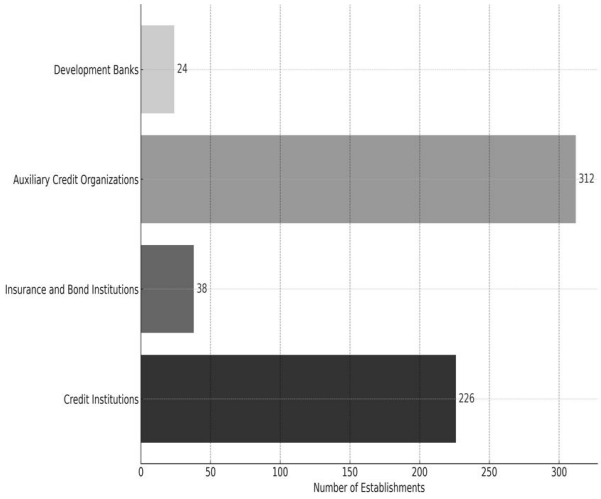

Figure 2. Type and number of financial institutions found in the 124 municipalities with financial inclusion in 2021.
Source: own elaboration based on information from INEGI (2023) [13].

Municipalities with financial inclusion have financial services where credit auxiliary organizations predominate. These include general deposit warehouses, financial leasing companies, financial factoring companies, and savings and loan societies. In second place are credit institutions, which are dedicated to receiving public deposits and granting loans to individuals or companies, charging an interest rate for the use of money. Some examples are private banks, multiple-purpose financial companies, and credit unions [11]. Insurance and finance institutions, as well as Development Banking, are present in third and fourth place, respectively (Fig. 2).

3.2 Changes in the density and spatial distribution of financial institutions (2021-2023)

Between 2021 and 2023, the municipalities studied experienced a statistically significant change in the average density of financial institutions. Specifically, the average density increased from 0.19 in 2021 to 0.22 in 2023 (Fig. 3), suggesting that there is one financial institution for every 4,545 inhabitants. These findings are consistent with previous research that emphasizes the importance of physical access to financial institutions in reducing financial exclusion [5,18,19]. However, it should be noted that an increase in establishment density does not automatically ensure improved financial inclusion [20]. In fact, financial inclusion is a multifaceted phenomenon that can also be influenced by the adoption of financial technologies [21,22]. Therefore, although the increase in the density of banking establishments represents a positive step forward, additional strategies are needed to address other factors affecting financial inclusion.

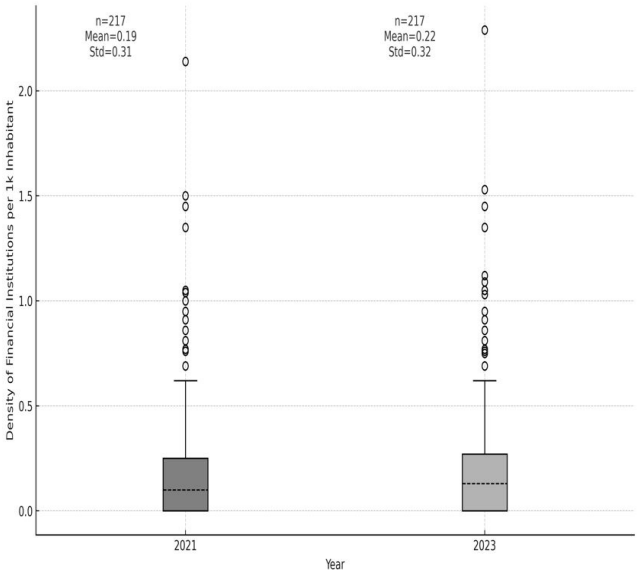

Figure 2. Statistically significant difference in the average density of financial institutions between 2021 and 2023, based on a Wilcoxon test for related samples with a confidence level of 95% ($p = 2.37\times10^{-9}$).
Source: own creation using R software.

The analysis using the Moran Index for the density of financial institutions per thousand inhabitants in 2021 yielded a value of 0.109. This indicates a relatively weak but statistically significant spatial correlation, confirmed by a z-value of 2.6367 at a 95% confidence level. This value suggests a trend toward the clustering of financial institutions in five municipalities, with high-high density values (Fig. 4-A). Specifically, a notable concentration was observed in the municipalities of Coronango, next to the state capital, as well as in San José Chiapa, Oriental, and Rafael Lara Grajales, which are part of the region hosting a significant industrial conglomerate in the automotive sector. In contrast, a cluster of eight municipalities with high financial exclusion was identified, with low-low density values (Fig. 4-a). This means that there are no financial institutions within these eight municipalities or in their surrounding areas. In 2023, the Moran Index registered a value of 0.111, signifying a statistically significant but weak spatial correlation, as

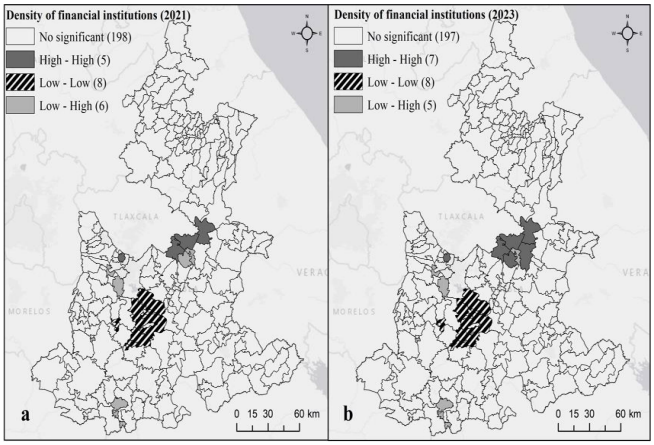

Figure 4. Spatial distribution of the density of financial institutions in the State of Puebla for the years 2021 and 2023. The Moran Index of 0.109 and Z-value of 2.6367 show a significant spatial clustering of financial institutions at a 95% confidence level.
Source: own creation using R software.

confirmed by a z-value of 2.6982 at a 95% confidence level. This data suggests an expanded clustering of seven municipalities with high-high density values, notably incorporating San Salvador el Seco and Soltepec because of their closeness to other high-density areas (Fig. 4-b). Conversely, the cluster of eight municipalities characterized by high financial exclusion remained unchanged. Although the average density of financial institutions rose between 2021 and 2023, the spatial analysis reveals a persistent clustering pattern that favors financially inclusive municipalities while disadvantaging those with financial exclusion. These observations align with prior studies linking urbanization and economic development to increased financial inclusion [2,23].

3.3 Socioeconomic analysis of financial inclusion at the municipal level

The results of the Shapiro-Wilk test for each variable in municipalities with financial inclusion and municipalities with financial exclusion indicate that most of the variables do not follow a normal distribution. The exception is the "Education" variable, which follows a normal distribution in both groups (Table 2).

Table 2.
Normality tests for the socioeconomic variables for the year 2020

Variable	Financial Inclusion (p-value)	Financial Exclusion (p-value)
Population	5.20×10^{-56}	1.32×10^{-10}
Economically Active Population (EAP)	5.27×10^{-23}	3.17×10^{-11}
Education	0.491	0.449
Poverty	4.54×10^{-04}	0.024
Degree of Marginalization	3.70×10^{-07}	5.93×10^{-08}

Note: p-values are from the Shapiro-Wilk normality test. P-values less than 0.05 indicate a rejection of the null hypothesis that the data are normally distributed.
Source: own creation using R software.

Table 3.
Comparison of socioeconomic characteristics between municipalities with Financial Inclusion and Financial Exclusion in 2021: means (x), standard deviations (σ) and results of Mann-Whitney U and Student's t-Tests.

Variable	Financial Inclusion (n=124)	Financial Exclusion (n=93)	Statistical Test	p-value
Population	x = 32106.97; σ= 112832.18	x = 4817.29; σ= 4514.54	Mann-Whitney U Test	7.82×10^{-19}*
Economically Active Population (EAP)	x= 23378.20; σ= 79833.61	x= 3217.43; σ= 3479.96	Mann-Whitney U Test	1.76×10^{-18}*
Education	x= 26.72; σ= 8.14	x= 30.68; σ =7.55	T-Test	3.20×10^{-04}*
Degree of Marginalization	x= 2.82; σ=1.12	x= 3.34; σ=0.94	Mann-Whitney U Test	3.67×10^{-04}*
Poverty	x=75.21; σ = 11.19	x= 77.61; σ = 10.14	Mann-Whitney U Test	0.13

Note: * indicates statistical significance at the α = 0.05 level.
Source: own creation using R software.

3.4 Socioeconomic variables and financial inclusion at the municipal level

The findings of this study underscore significant differences in the levels of financial inclusion between municipalities in relation to the Economically Active Population (EAP) and Educational Gap. Specifically, municipalities with better financial inclusion demonstrated higher EAP, lower Educational Gap and a lower degree of marginalization. These results were corroborated using the Mann-Whitney U test for EAP and Student's t-Test for Educational Gap (Table 3).

These findings are consistent with previous research that underscores the importance of educational level in financial inclusion. Martinez et al. [24] found that individuals with secondary or tertiary educational levels are more likely to use financial instruments compared to those who only have primary education. This correlation between educational level and financial inclusion has also been documented in international contexts, such as in China [25], and across a diverse set of countries [2]. Our study expands on this literature by providing empirical evidence that these trends hold at the municipal level. Municipalities with lower educational lag tend to have better financial inclusion, suggesting that policies aimed at improving educational levels could have a positive collateral impact on financial inclusion. Furthermore, the positive correlation found between the Economically Active Population (EAP) and financial inclusion highlights the importance of employment and economic activity in promoting financial inclusion. This relationship is consistent with previous research suggesting that an increase in individual income is associated with a higher likelihood of using financial instruments [24]. Contrary to what might be expected, this study found no statistically significant differences in the level of poverty between municipalities with financial inclusion and those with financial exclusion, according to the results of the Mann-Whitney test (Table 3). This result is interesting because it contrasts with the commonly accepted notion that

poverty is a key determinant of financial exclusion [26]. Other studies emphasize the crucial role of financial inclusion in socioeconomic development and poverty reduction [27,28]. Such studies argue that financial inclusion contributes to poverty reduction by facilitating the distribution of consumption over time, the acquisition of assets, investments, and improvements in income levels. Along these lines, previous studies in other contexts, such as in India [29], have also shown that poverty-related variables are not always reliable predictors of financial inclusion. However, the absence of a statistically significant relationship between poverty and financial inclusion in our findings suggests that there may be other mediating or moderating factors at play, which could vary at the regional or municipal level. In fact, previous research has identified variables such as access to information technology, local infrastructure, and government policies as factors that could have a significant impact on financial inclusion [30,31]. Our results show significant differences in the degree of marginalization between municipalities with financial inclusion and those with financial exclusion (Table 3). This finding suggests that the degree of marginalization could be another key factor affecting financial inclusion at the municipal level. Marginalization, which is often related to limited access to basic services and economic opportunities, could be both a cause and an effect of financial exclusion. Therefore, strategies to improve financial inclusion should consider a multidimensional approach that addresses both marginalization and these other key factors. Thus, while our research does not invalidate the importance of financial inclusion for economic development and poverty reduction, it adds a layer of complexity to the debate. The need for additional research examining these potential mediating or moderating factors at the local level to provide a more complete understanding of how and when financial inclusion effectively contributes to poverty reduction becomes apparent.

3.5 Implications for areas of financial exclusion

We identified eight municipalities with notable financial exclusion. This result is worrisome, but is consistent with previous studies showing a positive correlation between the level of development and access to financial services [32]. It is evident that the inhabitants of these municipalities face significant challenges in terms of access to financial services. These areas often experience a vicious cycle: the absence of financial services can hinder economic development, subsequently reducing the demand for such services and discouraging new providers. [33]. Residents of these municipalities may face significant challenges in accessing basic financial services. The importance of the spatial dimension in the study of financial inclusion has also been highlighted in the literature [4,34]. The results suggest specific policies may be necessary to address these areas of financial exclusion, as a one-size-fits-all solution is unlikely to be effective given the diversity of factors influencing financial inclusion [35].

4 Conclusion

The central aim of this study was to analyze the state of financial inclusion in the municipalities of the state of Puebla, Mexico, during the period from 2021 to 2023. Among the most significant findings is that municipalities with higher levels of Economically Active Population (EAP) and lower levels of Educational Lag tend to have better financial inclusion. It is noteworthy that no significant differences were found in poverty levels between municipalities with and without financial inclusion.

Likewise, a significant increase in the per capita density of financial institutions was identified for 2023. However, our spatial analysis, supported by the Moran Index, revealed a weak but statistically significant spatial correlation in the density of financial institutions for both 2021 and 2023. This pattern suggests a concentration of financial services in municipalities that already have financial services, while others continue to face high financial exclusion. These findings are consistent with previous research and underscore the importance of considering geography in financial inclusion strategies.

The outcomes regarding concentration and financial exclusion emphasize the need for nuanced and specific policy approaches for different geographical areas. Given that financial exclusion persists, despite the overall increase in the density of financial institutions, it is evident that these areas of financial exclusion may require specific policies to increase the availability of financial services.

Moreover, these results highlight the importance of considering the spatial dimension in the study of financial inclusion. The lack of financial institutions in a municipality, especially if it is surrounded by areas with low density, can limit economic development and, consequently, decrease the demand for these services, discouraging the entry of financial service providers into the market.

These results have important implications for public policy and banking practice in the country. For example, mapping municipalities according to their degree of financial inclusion could serve as a valuable tool for resource allocation and the formulation of government policies. The relationship between the EAP and financial inclusion underscores the need for policies that encourage employment and economic activity to improve access to financial services. However, it is crucial to recognize some limitations of the study. First, the research focuses on a single state in Mexico, which could limit the generalizability of the findings. Second, although the longitudinal nature of the study provides the basis for exploring causal relationships, the presence of unobserved or uncontrolled variables may limit the ability to establish these relationships definitively. Third, the absence of a significant correlation between poverty and financial inclusion could be because of factors not examined in this study, suggesting the need for future research to explore these aspects.

In this regard, it is recommended that future studies

expand the geographical scope of the research, employ longitudinal designs, and explore other potential factors that may influence financial inclusion. This study contributes to the existing literature by offering new perspectives and data that may be useful for researchers, practitioners, and decision-makers in financial inclusion. Additionally, it raises new questions and challenges that could be the focus of future research in this field.

References

[1] World Bank, Financial inclusion overview. [Online]. 2002. [Accessed: Aug. 10th of 2023]. Available at: https://www.worldbank.org/en/topic/financialinclusion/overview

[2] Allen, F., Demirguc-Kunt, A., Klapper, L., and Martinez-Peria, M.S., The foundations of financial inclusion: understanding ownership and use of formal accounts. Journal of Financial Intermediation, 27, pp. 1-30, 2016. DOI: https://doi.org/10.1016/J.JFI.2015.12.003

[3] Beck, T., Demirguc-Kunt, A., and Honohan, P., Access to financial services: measurement, impact, and policies. The World Bank Research Observer, 24(1), pp. 119-145, 2009. DOI: https://doi.org/10.1093/wbro/lkn008

[4] Dircio-Palacios-Macedo, M., Cruz-García, P., Hernández-Trillo, F., and Tortosa-Ausina, E., Constructing a financial inclusion index for Mexican municipalities. Finance Research Letters, 52, art. 103368, 2023. DOI: https://doi.org/10.1016/j.frl.2022.103368

[5] Demirgüç-Kunt, A., Klapper, L., Singer, D., and Ansar, S., The Global Findex Database 2021: financial inclusion, digital payments, and resilience in the age of COVID-19. [Online]. 2022. [Accessed: Aug. 3rd of 2023]. Available at: https://www.worldbank.org/en/publication/globalfindex#sec5

[6] Orazi, S., Martínez, L.B., y Vigier, H.P., La inclusión financiera en América Latina y Europa. Ensayos de Economía, 29(55), art. 79425, 2019. DOI: https://doi.org/10.15446/ede.v29n55.79425

[7] Comisión Nacional Bancaria y de Valores (CNBV) and Instituto Nacional de Estadística y Geografía (INEGI), Encuesta Nacional de Inclusión Financiera. [Online]. 2021. [Accessed: Aug. 03rd of 2023]. Available at: https://www.inegi.org.mx/programas/enif/2021/#informacion_general

[8] Chakravarty, S.R., and Pal, R., Financial inclusion in India: an axiomatic approach. Journal of Policy Modeling, 35(5), 2013. DOI: https://doi.org/10.1016/j.jpolmod.2012.12.007

[9] Mhlanga, D., Dunga, S.H., and Moloi, T., Understanding the drivers of financial inclusion in South Africa. Journal of Economic and Financial Sciences, 14(1), 2021. DOI: https://doi.org/10.4102/jef.v14i1.594

[10] Camara, N., and Tuesta, D., Measuring financial inclusion: a muldimensional index. SSRN Electronic Journal, 14(26), art. 4616, 2014. DOI: https://doi.org/10.2139/ssrn.2634616

[11] CNBV, Política Nacional de Inclusión Financiera. Comisión Nacional Bancaria y de Valores. Gobierno de México. [Online]. 2023. [Accessed: Aug. 04th of 2023]. Available at: https://www.gob.mx/cnbv

[12] Pérez-Akaki, P., y Fonseca-Soto, M.D.R., Análisis espacial de la inclusión financiera y su relación con el nivel de pobreza en los municipios mexicanos. Revista Mexicana de Economía y Finanzas, 12(1), pp. 43-62, 2017. DOI: https://doi.org/10.21919/remef.v12i1.13

[13] INEGI, Directorio Estadístico Nacional de Unidades Económicas: DENUE Interactivo. [Online]. 2023. [Accessed: Aug. 21th of 2023]. Available at: https://www.inegi.org.mx/app/mapa/denue/default.aspx

[14] INEGI, Censo de Población y Vivienda. [Online]. 2020. [Accessed: Aug. 22th of 2023]. Available at: https://www.inegi.org.mx/programas/ccpv/2020/

[15] CONEVAL, Pobreza a nivel municipio 2010-2020. [Online]. 2021. [Accessed: Aug. 10th of 2023]. Available at: https://www.coneval.org.mx/Medicion/Paginas/Pobreza-municipio-2010-2020.aspx

[16] CONAPO, Índices de marginación 2020. [Online]. 2021. [Accessed: Aug. 10th of 2023]. Available at: https://www.gob.mx/conapo/documentos/indices-de-marginacion-2020-284372

[17] Anselin, L., Syabri, I., and Youngihn, K., GeoDa: an introduction to spatial data analysis - exploratory data analysis (1) - Univariate and bivariate analysis. Geographical Analysis, 38(1), pp. 5-22, 2005. DOI: https://doi.org/10.1111/j.0016-7363.2005.00671.x

[18] Karlan, D., and Morduch, J., Access to finance. Handbook of Development Economics, 5(C), pp. 4703-4784, 2010. DOI: https://doi.org/10.1016/B978-0-444-52944-2.00009-4

[19] Suri, T., and Jack, W., The long-run poverty and gender impacts of mobile money. Science, 354(6317), art. 5309, 2016. DOI: https://doi.org/10.1126/science.aah5309

[20] Frost, J., Gambacorta, L., Huang, Y., Song-Shin, H., and Zbinden, P., BigTech and the changing structure of financial intermediation. Economic Policy, 34(100), art. 003, 2019. DOI: https://doi.org/10.1093/EPOLIC/EIAA003

[21] Arner, D.W., Buckley, R.P., and Zetzsche, D.A., Fintech for financial inclusion: a framework for digital financial transformation. SSRN Entrepreneurship & Finance eJournal, art. 5287, 2018. DOI: https://doi.org/10.2139/ssrn.3245287

[22] Bala, S., and Singhal, P., Digital financial inclusion through FinTech. In: Gender Perspectives on Industry 4.0 and the Impact of Technology on Mainstreaming Female Employment, IGI Global, 2022, pp. 77-90. DOI: https://doi.org/10.4018/978-1-7998-8594-8.ch004

[23] Sarma, M., and Pais, J., Financial inclusion and development. Journal of International Development, 23(5), art. 1698, 2011. DOI: https://doi.org/10.1002/jid.1698

[24] Martinez, L.B., Guercio, M.B., Orazi, S., y Vigier, H., Instrumentos financieros claves para la inclusión financiera en América Latina. Revista Finanzas y Política Económica, 14(1), pp. 17-47, 2022. DOI: https://doi.org/10.14718/revfinanzpolitecon.v14.n1.2022.2

[25] Fungáčová, Z., and Weill, L., Understanding financial inclusion in China. China Economic Review, 34, pp. 196-206, 2015. DOI: https://doi.org/10.1016/J.CHIECO.2014.12.004

[26] Demirguc-Kunt, A., Klapper, L., Singer, D., Ansar, S., and Hess, J., The Global Findex Database 2017: measuring financial inclusion and the fintech revolution. [Online]. 2018. [Accessed: Aug. 11th of 2023]. Available at: http://hdl.handle.net/10986/29510

[27] Andrade, G., De Olloqui, F., y Herrera, D., Inclusión financiera en América Latina y el Caribe. Coyuntura actual y desafíos para los próximos años. Banco Interamericano de Desarrollo, 2015. DOI: https://doi.org/10.18235/0000030

[28] Cihák, M., Demirgüç-Kunt, A., Feyen, E., and Levine, R., Benchmarking financial systems around the world. The World Bank. [Online]. 2012. [Accessed: Aug. 10th of 2023]. Available at: http://documents.worldbank.org/curated/en/868131468326381955/Benchmarking-financial-systems-around-the-world

[29] Burgess, R., and Pande, R., Do rural banks matter? Evidence from the Indian social banking experiment. American Economic Review, 95(3), pp. 780-795, 2005. DOI: https://doi.org/10.1257/0002828054201242

[30] Beck, T., Demirguc-Kunt, A., and Martinez-Peria, M.S., Reaching out: access to and use of banking services across countries. Journal of Financial Economics, 85(1), pp. 234-266, 2007. DOI: https://doi.org/10.1016/J.JFINECO.2006.07.002

[31] Koomson, I., Villano, R.A., and Hadley, D., Effect of financial inclusion on poverty and vulnerability to poverty: evidence using a multidimensional measure of financial inclusion. Social Indicators Research, 149(2), pp. 613-639, 2020. DOI: https://doi.org/10.1007/s11205-019-02263-0

[32] Zins, A., and Weill, L., The determinants of financial inclusion in Africa. Review of Development Finance, 6(1), pp. 46-57, 2016. DOI: https://doi.org/10.1016/j.rdf.2016.05.001

[33] Saha, S.K., and Qin, J., Financial inclusion and poverty alleviation: an empirical examination. Economic Change and Restructuring, 56(1), pp. 409-440, 2023. DOI: https://doi.org/10.1007/s10644-022-09428-x

[34] Mylonidis, N., Chletsos, M., and Barbagianni, V., Financial exclusion in the USA: looking beyond demographics. Journal of Financial Stability, 40, pp. 144-158, 2019. DOI: https://doi.org/10.1016/J.JFS.2017.09.004

[35] Ouma, S.A., Odongo, T.M., and Were, M., Mobile financial services and financial inclusion: Is it a boon for savings mobilization? Review of Development Finance, 7(1), pp. 29-35, 2017. DOI: https://doi.org/10.1016/J.RDF.2017.01.001

M. Neri-Suárez, received his BSc. in Engineering with a focus on Natural Resources Management in 2011 from the Mesoamerican Polytechnic University, and earned his MSc in Regional Development in 2014 and his PhD in Regional Development in 2022, both from the Graduate College, Puebla Campus. He has served as a professor of financial engineering at the Polytechnic University of Puebla since 2014. His research interests include: financial inclusion, spatial econometrics, regional development and the economic valuation of natural resources. He is recognized by the National System of Researchers (SNI Conahcyt).
ORCID: 0000-0003-1828-8906

J.G. Ramirez-Rosas, received his BSc. in Public Accounting and Auditing, with a focus area in Financial Management, in 2010. MSc. in Taxation in 2012. MSc. in Organizational Management in 2014, and PhD in Management in 2018. He is currently pursuing an MSc degree in Systems Engineering and Intelligent Computing. He has been a full-time professor in financial engineering at the Polytechnic University of Puebla since 2017. His work has centered around management and value chain in SMEs. He is recognized by the National System of Researchers (SNI Conahcyt).
ORCID: 0000-0003-0664-3843

M.E. Morales-Illescas, received her associate degree in Computer Science with a focus on Telematics and Computer Networks from the Technological University of Puebla in 2005. BSc. Engineering in Computer Science from the Polytechnic University of Puebla in 2012, and an MSc. in Educational Technology from the Popular Autonomous University of the State of Puebla in 2018. She has served as a professor in information technologies and financial engineering at the Polytechnic University of Puebla for 9 years. Her main research focus is Linear Programming for Financial Optimization.
ORCID: 0009-0005-7163-518X

F. Machorro-Ramos, received the BSc. in Business Administration in 2003, earned the MSc in Administrative Sciences in 2005 from the Universidad Veracruzana, and PhD in Economics-Administrative Sciences in 2013 from the Universidad Autónoma del Estado de México. From 2005 to 2022, he worked for various institutions including Instituto Tecnológico Superior de Tierra Blanca, Universidad Católica del Norte de Chile and Universidad de las Américas Puebla. He is currently a professor in the Financial Engineering Department at the Polytechnic University of Puebla. His research interests include: intellectual capital, organizational performance in universities, econometrics, and impact of organized crime on economic growth. He is recognized by the National System of Researchers (SNI Conahcyt).
ORCID: 0000-0002-8910-1347

DYNA
http://dyna.medellin.unal.edu.co/

UNIVERSIDAD NACIONAL DE COLOMBIA

Determine velocity of fluid in curved micro channels fabricated with 3d printing (SLA)

Nícolas Esparza-Proaño & Víctor H. Cabrera-Moreta

Departament of Mechanical Engineering, Universidad Politécnica Salesiana, Quito, Ecuador. nesparza@est.ups.edu.ec, vcabrera@est.ups.ec

Received: March 5th, 2023. Received in revised form: May 3th, 2024. Accepted: May 15th, 2024.

Abstract
The study investigated fluid dynamics in curved microchannels, exploring 3D printing parameters, channel geometry, and fluid properties, crucial for applications in medicine and energy. It highlighted the importance of microfluidics in handling small samples and enabling rapid analysis, stressing the need for precise measurement techniques to validate fluid velocity. Using 3D printing for microchannel design illustrated their utility, with microscopy aiding flow behavior comprehension. The research aimed to validate fluid velocity, covering technology analysis, microdevice design, fabrication, and measurement methodologies. It successfully fabricated microdevices confirming fluid movement via capillarity, revealing the relationship between channel radius and flow velocity. Distinct flow velocity patterns were observed, vital for design optimization. The study affirmed capillary flow as a spontaneous phenomenon, with fluid velocity variations along curved microchannels consistent with mass conservation principles in incompressible flows.

Keywords: microchannels; curved; 3D printing; SLA; microfluidics; fluid; velocity; validation; microscopy; design; applications.

Determinación de la velocidad de fluido en micro canales curvos fabricados con impresión 3D (SLA)

Resumen
El estudio investigó el movimiento de fluidos en microcanales curvados, centrándose en la fabricación mediante impresión 3D (SLA). El artículo analiza la geometría del canal, las propiedades del fluido y la microfluídica en el dispositivo. El objetivo principal fue determinar la velocidad del fluido en estos microcanales curvos mediante manufactura aditiva (SLA). Los resultados del estudio permitieron la fabricación de microdispositivos que validaron el movimiento del fluido por capilaridad, resaltando la relación entre el radio del canal y la velocidad del flujo. Se observaron patrones característicos en la velocidad del flujo, fundamentales para la optimización de diseños en diversas aplicaciones. En resumen, se confirmó el flujo capilar como un fenómeno de absorción espontánea de líquidos, evidenciando la variación de la velocidad del fluido a lo largo de los microcanales curvados, en consonancia con el principio de conservación de masa en flujos incompresibles.

Palabras clave: micro canales; curvo; impresión 3D; SLA; micro fluidos; fluidos; velocidad; validación; microscopía; diseño; aplicaciones.

1 Introduction

The study of fluid velocity in curved microchannels fabricated by 3D printing (SLA) is a relatively new area of research with great potential for applications in various fields. The rationale for this study is based on the need to better understand flow patterns in curved microchannels, which can contribute to the design and optimization of microfluidic systems for biomedical, chemical, and diagnostic applications. In addition, this research may be a precursor to the development of more efficient and accurate microfluidic devices, which in turn could have a significant impact in fields such as medicine, biotechnology, and life sciences.

The focus of the research is on understanding the effect of velocity enhancement in curved sections, specifically in microdevices with curved channels fabricated by 3D printing (SLA). The importance of this study is justified by gaining a

How to cite: Esparza-Proaño, N., and Cabrera-Moreta, V.H., Determine velocity of fluid in curved micro channels fabricated with 3d printing (SLA). DYNA, 91(232), pp. 103-111, April - June, 2024.

better understanding of flow patterns in curved microchannels, which can contribute to the design and optimization of microfluidic systems for biomedical, chemical, and diagnostic applications.

In this study, microdevices with curved channels will be designed and fabricated by 3D printing (SLA) to validate fluid movement by capillarity. The current status of 3D printing (SLA) technology in microchannels with different geometries will be analyzed, a methodology for the fabrication and measurement of fluid in the proposed devices will be established, and the flow velocity measurements obtained in the curved channels will be evaluated.

The research is expected to provide valuable information on fluid behavior in curved microchannels, which can contribute to the design and optimization of microfluidic systems for various applications.

In recent years, the need to understand the effect of velocity enhancement in curved sections, specifically in microdevices with curved channels fabricated by 3D printing (SLA), has become apparent. This research seeks to highlight the relevance of understanding the influence of curved channel radius on fluid velocity, which is crucial for various applications in engineering, materials science, and bioengineering. The rationale is based on the importance of gaining a better understanding of flow patterns in curved microchannels, which can contribute to the design and optimization of microfluidic systems for biomedical, chemical, and diagnostic applications. In addition, this research can lay the foundation for the development of more efficient and accurate microfluidic devices, which in turn could have a significant impact in fields such as medicine and biotechnology.

The proposed research is based on the need to develop an effective methodology to measure and validate flow velocity in curved channels of microdevices fabricated by 3D printing (SLA). Accurate velocity measurement is essential in a variety of applications, such as microfluidics, biotechnology, and nanotechnology. Capillarity has been proposed as a promising technique to solve this challenge in microscopic, curved channels, and 3D printing (SLA) offers the ability to fabricate complex geometries. This research seeks to combine these two technologies to provide a solution that will significantly contribute to the design and development of more efficient and accurate fluidic microdevices in various fields of application.

2 Methodology

2.1 Measurement of fluid velocity in curved microchannels

The study of fluid velocity in curved microchannels fabricated by 3D printing (SLA) is a novel area of research with vast potential for diverse applications. The rationale for this study lies in the need to understand flow patterns in curved microchannels to optimize microfluidic systems applicable in biomedicine, chemistry and diagnostics. This work may be a precursor in the development of more efficient microfluidic devices, impacting areas such as medicine and biotechnology [1-4].

2.2 Measurement techniques

Commonly employed techniques include direct visualization of flow by microscopy, and velocity measurement with particle velocimeter (PIV) or laser Doppler anemometer (LDA). Microscopy allows observation of fluid dynamics, while PIV and LDA measure velocity through moving particles or reflected light, providing accurate data for system design and optimization [3, 5-7].

2.3 Curved microchannel design

Commonly employed techniques include direct visualization of flow by microscopy, and velocity measurement with particle velocimeter (PIV) or laser Doppler anemometer (LDA). Microscopy allows observation of fluid dynamics, while PIV and LDA measure velocity through moving particles or reflected light, providing accurate data for system design and optimization [8-11]. Fig. 1 shows an example of curved channel device.

2.4 Volume and radio calculation

The calculation of volume and radius in curved microchannels is crucial to understand the flow behavior. Volumes were calculated for different radius (4 mm, 6 mm, 8 mm), fundamental to evaluate the efficiency of the system. Figs. 2, 3 and 4 shows the design devices with radius variation along the channel.

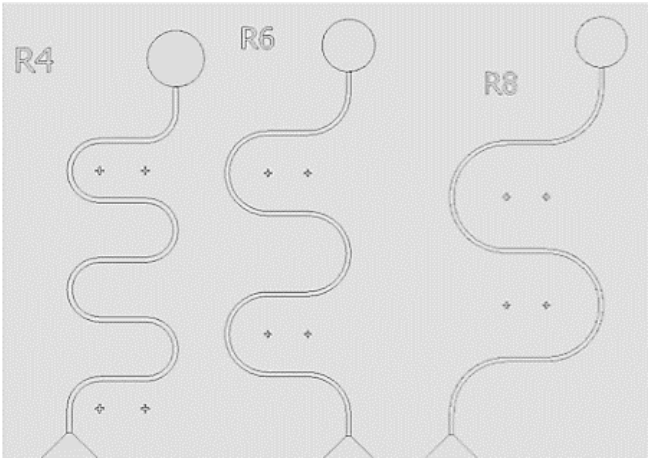

Figure 1. Prototypes designed with radio 4, 6 and 8 mm.
Source: The authors

Volume 4 mm

$$V_{1\,r4} = (5.576mm)(0.65mm)(0.5mm)(5)$$
$$V_1 = 9.061mm^3$$
$$V_{2\,r4} = \pi((4mm)^2 - (3.38mm)^2)(0.5mm)(2.5)$$
$$V_2 = 17.37mm^3$$
$$V_{3\,r4} = (3mm)(0.65mm)(0.5mm)(2)$$
$$V_3 = 1.95mm^3$$
$$V_{TOTAL\,r4} = (9.061 + 17.37 + 1.95)mm^3$$
$$V_{TOTAL\,r4} = 28.3856mm^3$$

Radio deposit 4 mm

$$r = \sqrt{\frac{28.3856mm^3}{\pi(0.7mm)}}$$
$$r = 3.5927mm$$

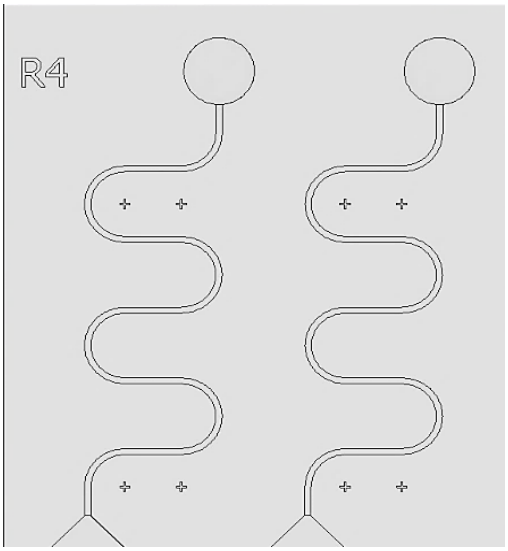

Figure 2. Prototype designed with 4 mm radio of curvature.
Source: The authors

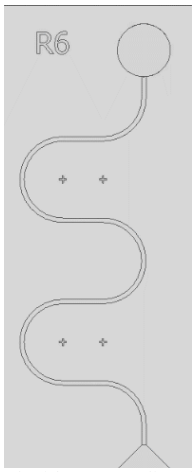

Figure 3. Prototype designed with 6 mm radio of curvature.
Source: The authors

Volume 6 mm

$$V_{1\,r6} = (5.614mm)(0.65mm)(0.5mm)(4)$$
$$V_1 = 7.2982mm^3$$

$$V_{2\,r6} = \pi((6mm)^2 - (5.38mm)^2)(0.5mm)(2)$$
$$V_2 = 22.1658mm^3$$

$$V_{3\,r6} = (3mm)(0.65mm)(0.5mm)(2)$$
$$V_3 = 1.95mm^3$$

$$V_{TOTAL\,r6} = (7.2982 + 22.1658 + 1.95)mm^3$$
$$V_{TOTAL\,r6} = 31.414mm^3$$

Radio deposit 6 mm

$$r = \sqrt{\frac{31.414mm^3}{\pi(0.7mm)}}$$
$$r = 3.7795mm$$

Volume 8 mm

$$V_{1\,r8} = (5.62mm)(0.65mm)(0.5mm)(3)$$
$$V_1 = 5.4795mm^3$$

$$V_{2\,r8} = \pi((8mm)^2 - (7.38mm)^2)(0.5mm)(1.5)$$
$$V_2 = 22.4677mm^3$$

$$V_{3\,r8} = (3mm)(0.65mm)(0.5mm)(2)$$
$$V_3 = 1.95mm^3$$

$$V_{TOTAL\,r8} = (5.4795 + 22.4677 + 1.95)mm^3$$
$$V_{TOTAL\,r6} = 29.8972mm^3$$

Radio deposit 8 mm

$$r = \sqrt{\frac{29.8972mm^3}{\pi(0.7mm)}}$$
$$r = 3.6872mm$$

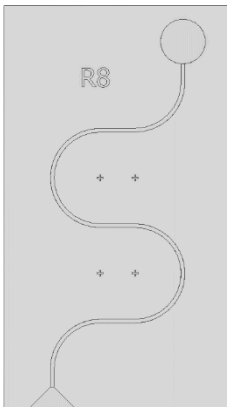

Figure 4. Prototype designed with 8 mm radio of curvature.
Source: The authors

2.5 Data Processing

The calculation of the channel length and Reynolds number is vital for understanding fluid flow. The channel length was calculated considering displacement and capillarity. The Reynolds number, essential to characterize the flow, was obtained by considering the average volumetric flow rate and the viscosity of the fluid. This analysis provides a detailed understanding of fluid behavior in curved microchannels, essential for the accurate and efficient design of microfluidic devices.

Displacement calculation. The displacement of a body is defined as the difference between its final position (xi) and its initial position (xf). In simple terms, the displacement represents the total amount that the body has moved from its initial position (xi) to its final position (xf) [12].

The formula for calculating the displacement is as

follows:

$$\Delta x = xf - xi \quad (1)$$

Calculation of the displacement magnitude. The magnitude of the displacement vector is defined as the length or size of the vector and is calculated by the square root of the sum of the squares of its direction elements. This measure is essential for a complete understanding of the vector, as it provides information about its size regardless of its direction. This concept is fundamental to vector analysis and is used in a variety of scientific and technical fields to characterize the motion and position of objects in space [13].

$$\Delta r = \sqrt{(xf - xi)^2 + (yf - yi)^2} \quad (2)$$

Where:

x and y are the components of the displacement in the horizontal and vertical directions, respectively.

Displacement magnitude summation. The magnitude of the displacement vector is defined as the length or size of the vector and is calculated by the square root of the sum of the squares of its direction elements. This measure is essential for a complete understanding of the vector, as it provides information about its size regardless of its direction. This concept is fundamental to vector analysis and is used in a variety of scientific and technical fields to characterize the motion and position of objects in space.

$$\Sigma_{i=o}^{n} \Delta r \quad (3)$$

Calculation of capillarity in microchannels. Capillary force plays a crucial role in the operation of microfluidic devices as it is generated by the interaction between the fluid and the microchannel material. This force, derived from the nature of the fluid and the properties of the channel, gives rise to phenomena such as capillary penetration in microchannels of finite and rectangular shapes, which directly impacts the accuracy of capillary measurements [3]. Furthermore, capillary force can be employed to control and manipulate fluids at the micro-scale, which is essential in applications such as cancer detection and cell separation [15]. In summary, understanding the influence of capillary force in microchannels is critical for the development and implementation of microfluidic technologies in various scientific fields and technological applications. Fig. 5 illustrates a diagram of drop over an hydrophilic surfase.

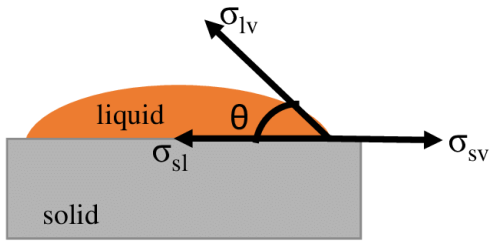

Figure 5. Illustrative diagram representing the contact angle of a fluid drop on a solid surface. [16].
Source: Rupp et al., 2014.

$$Pc = -\Upsilon\left(\frac{\cos\theta b + \cos\theta t}{d} + \frac{\cos\theta l + \cos\theta r}{w}\right) \quad (4)$$

Pc >0 Opposed to flow
Pc<0 Spontaneous wick
Where:
Pc: represents the capillary pressure [Pa]
Υ: is the surface tension of the fluid (N/m)
w: channel width (m)
d: channel height (m)
θb: back contact angle
θt: upper contact angle
θl: left contact angle
θr: right contact angle

Reynolds number calculation. The Reynolds number (Re) is a dimensionless parameter used to relate inertial forces to viscous forces, which allows determining the flow regime in which a system is found, either laminar or turbulent. In microfluidic devices with rectangular cross section, the calculation of the Reynolds number is performed considering the average volumetric flow rate of the device [17].

The Reynolds number is fundamental to characterize the flow behavior in microchannels, being that for low values of Re (Re < 2000) laminar flow prevails, while for higher values, the flow can become turbulent [18]. This characterization is essential to understand and predict the behavior of fluids in microfluidic devices, which significantly influences the design and efficiency of such devices [19], [20].

$$\mathrm{Re} = \frac{\rho V L}{\mu} \quad (5)$$

Where:
ρ: represents the density of the fluid $\left(\frac{kg}{m^3}\right)$
V: linear velocity of the fluid (m/s)
L: characteristic length (m)
μ: dynamic viscosity of the fluid(m^2/s)

3 Results and discussion

The design and printing of three prototypes including a curved microchannel were carried out, considering different curvature radii of 4, 6 and 8 mm. These prototypes were fabricated using a 3D printer by the stereolithographic process (SLA) in order to evaluate the behavior of the fluid and determine how these curvature radii affect its velocity. For each device, 5 tests were performed on each channel, resulting in a total of 15 tests.

3.1 Schematic diagram of the cross section of the devices

The main dimensions of the microchannels are a channel width of 620 µm (Fig. 6) and a depth of 500 µm (Fig. 6). In addition, both the reservoir and outlet have a slope of 200 µm, which prevents the fluid from leaking.

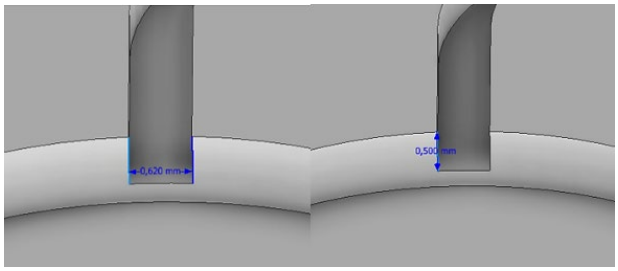

Figure 6. Width of the designed channel - Depth of the designed channel
Source: The authors

Table 1.
Overall dimensions of curved micro channels with r4, r6 and r8.

Dimension	Units	r4	r6	r8
Channel width	(mm)	0.620	0.620	0.620
Channel depth	(mm)	0.500	0.500	0.500
Length	(mm)	71	76	69
Tank radius	(mm)	3.514	3.713	3.613

Source: The authors

3.2 Overall dimensions of the devices

The main dimensions of the curved microchannels designed are expressed in millimeters (mm) and are detailed in Table 1.

3.3 Graphical analysis

The designed geometry of the microdevice with curved channels is divided into blocks graphically and the data is tabulated as a function of the channel length, considering the geometry of the device.

Fig. 7 shows the division into blocks of the microdevice of r4, r6 and r8, with a total of 6 blocks, 5 blocks and 4 blocks respectively, due to the curves present in the channels, which are identified by colors.

3.4 Data Statistics

In the case of the histogram of the curved microdevice with a radius of 4 mm, it is observed that the highest number of velocities is concentrated in the range of 0.0 - 1.3 mm/s, with a mesokurtic curve indicating a wide range of velocities and a slight positive asymmetry. The velocity distribution shows that it stops at the crests (Fig. 8). In the histograms of the curved microdevices with radii of 6 mm and 8 mm, it can be seen that the highest number of velocities are concentrated in the middle sections respectively. The leptokurtic curve indicates that the velocity values are concentrated around their mean, with a positive skewness where the smaller velocity data are concentrated towards the right of the distribution (Fig. 8). For velocity analysis, separation into sections was performed considering changes in channel geometry and total microchannel length."

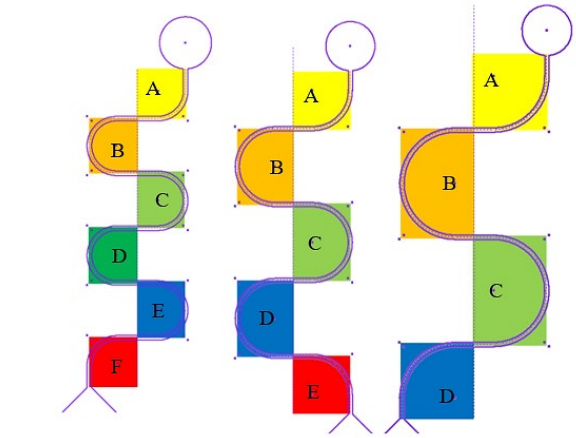

Figure 7. Division of blocks in micro device design with radius 4,6 and 8mm.
Source: The authors

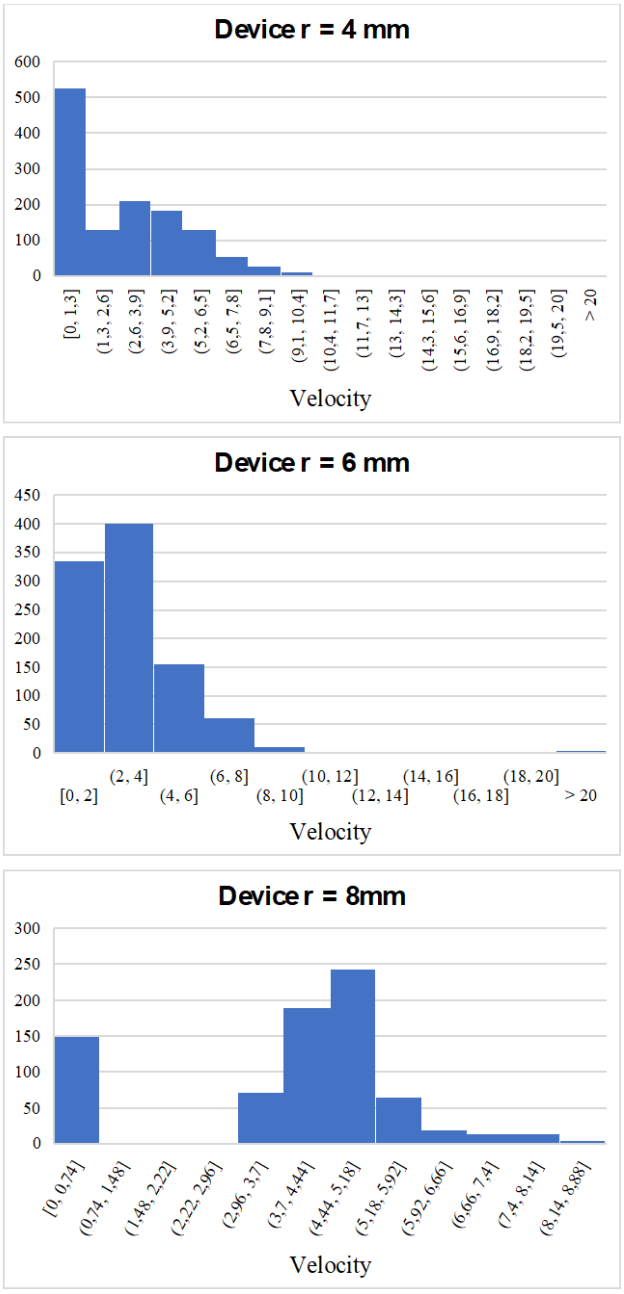

Figure 8. Velocity histograms (mm/s) radio 4, 6 and 8 mm.
Source: The authors

Velocity and Length in Microdevices. Fig. 9 present the velocity and length scatter plots for the three devices, divided into sections according to the device geometry and velocity changes in the microchannels. These graphical representations allow visualizing the relationship between fluid velocity and channel length in different sections of the microdevices, which facilitates the analysis of the flow behavior along its path.

Figs. 9, 10 and 11 show the characteristic behavior of the flow velocity in curved microchannels fabricated with 3D printing. A velocity peak in the curve followed by a decrease in the straight line is highlighted. This phenomenon is attributed to the centrifugal force generated when the fluid changes direction in the curve, which causes a displacement towards the inner wall of the channel. As a result, the contact between the fluid and the inner wall is less than with the outer wall, allowing faster fluid flow in the bend. In contrast, in the straight, the centrifugal force decreases, and the fluid again has contact with both channel walls, which increases friction and causes a decrease in flow velocity. This behavior is crucial in curved microchannel applications in microelectronic, biomedical and nanotechnology systems, where flow velocity is a critical factor that can influence system performance.

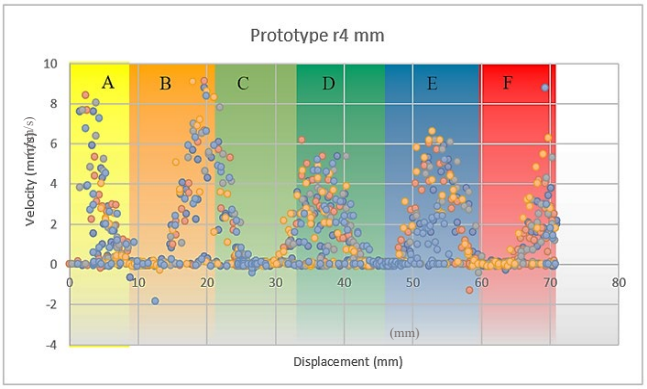

Figure 9. Graph of velocity as a function of length for a device with a radius of 4 mm.
Source: The authors

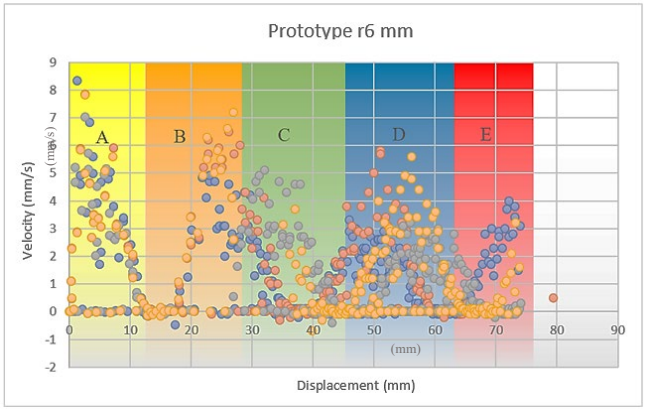

Figure 10. Graph of velocity as a function of length for a device with a radius of 6 mm.
Source: The authors

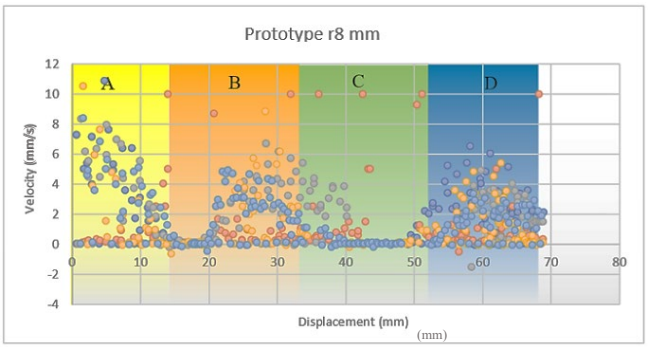

Figure 11. Graph of velocity as a function of length for a device with a radius of 8 mm.
Source: The authors

Calculation of the capillarity of the micro devices. The capillary force measured in the devices is -302.9633 Pa, which reflects the phenomenon of capillary flow, characterized by the spontaneous absorption of liquids in narrow spaces without the intervention of external forces. This process is influenced by cohesion and adhesion forces, which are fundamental to capillarity and the absorption of liquids in such spaces. Cohesion forces operate between the molecules of the liquid, while adhesion forces act between the molecules of the liquid and the walls of the container. These interactions determine the ability of a liquid to move through narrow spaces, such as microchannels, and are essential for understanding and controlling capillary and absorption phenomena in these environments. Accurate measurement of capillary force provides crucial information for the design and optimization of microfluidic devices, especially in applications that require precise liquid handling at the microscopic scale, such as in biomedicine, nanotechnology and other engineering fields.

$$Pc = -\Upsilon\left(\frac{\cos\theta b + \cos\theta t}{d} + \frac{\cos\theta l + \cos\theta r}{w}\right)$$

$$Pc = -0.0728\left(\frac{\cos 65 + \cos 65}{0.0005} + \frac{\cos 40 + \cos 40}{0.000620}\right)$$

$$Pc = -302.9633$$

$$Pc < 0$$

Calculation of Reynolds Number. The fluid motion in the microchannels was characterized by determining the Reynolds number, which was found to be less than 2000 in the three devices analyzed. This result suggests a laminar flow regime, where viscous forces are predominant over inertial forces. The Reynolds number (Re) is a crucial dimensionless parameter that describes the relationship between inertia and viscous forces in a given flow. In the case of Re values below 2000, as observed in this investigation, a laminar flow characterized by a smooth and orderly distribution of the fluid in the microchannels is established. The predominance of laminar flow in these devices is of great importance for various microfluidic applications, especially those requiring controlled and uniform fluid transport, such as in medical diagnostic systems, chemical analysis and

biomedical applications in general. This finding underscores the importance of understanding and characterizing fluid behavior in microchannels for the effective design and development of microfluidic devices in various application areas.

$$\mathrm{Re} = \frac{\rho V L}{\mu}$$

$$L = \frac{4ab}{2(a+b)}$$

$$L = \frac{4\big((0.0005)(0.000620)\big)m^2}{2\big((0.0005)+(0.000620)\big)m}$$

$$L = 5.5357x10^{-4}m$$

$$\mathrm{Re}_{radio4} = \frac{(1000)(0.00267)(5.5357x10^{-4})}{1x10^{-3}}$$

$$\mathrm{Re}_{radio4} = 1.4780$$

$$\mathrm{Re}_{radio6} = \frac{(1000)(0.00242)(5.5357x10^{-4})}{1x10^{-3}}$$

$$\mathrm{Re}_{radio6} = 1.3396$$

$$\mathrm{Re}_{radio8} = \frac{(1000)(0.00438)(5.5357x10^{-4})}{1x10^{-3}}$$

$$\mathrm{Re}_{radio8} = 2.4246$$

Block velocity. Figs. 12, 13 and 14, showing the velocity variation in the different sections (Fig. 7), established for the analysis of the designed geometry of the microdevice with curved channels. Microchannels with curvatures present distinctive hydrodynamic characteristics, and the examination of the velocities per section provides detailed information on the flow distribution along the channel. This evaluation is crucial for understanding flow behavior at various sections, which in turn facilitates informed decision making in the design and implementation of curved microchannels. This analytical approach allows the identification of specific flow patterns, such as changes in velocity and pressure, in different parts of the curved channel.

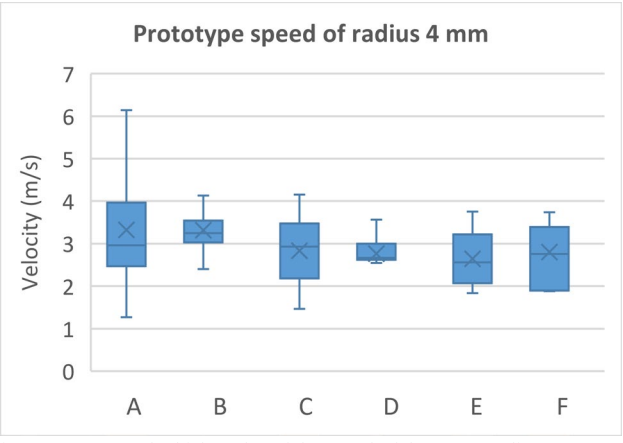

Figure 12. Box and whisker plot of the speed of the 4 mm radio prototype. Source: The authors

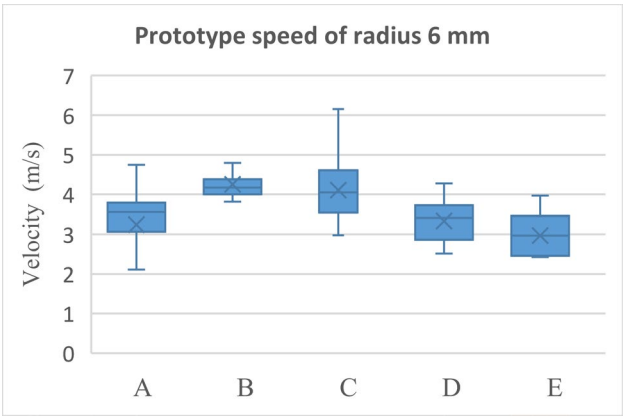

Figure 13. Box and whisker plot of the speed of the 6 mm radio prototype. Source: The authors

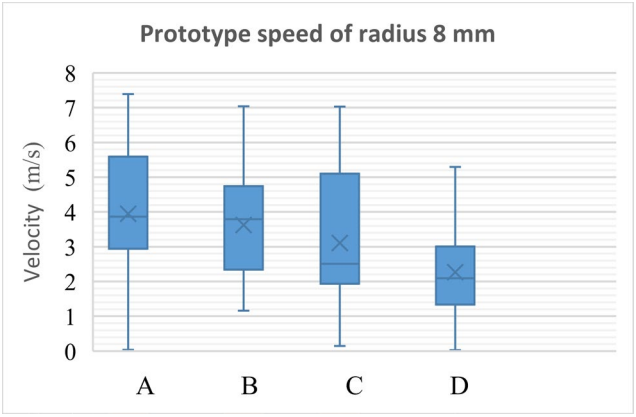

Figure 14. Box and whisker plot of the speed of the 8 mm radio prototype. Source: The authors

By understanding how velocity varies along the channel, microchannel designs can be optimized to ensure uniform and controlled flow, which is essential for numerous applications in fields such as microfluidics, biomedical engineering and nanotechnology. The information obtained from this sectional velocity analysis provides a solid basis for decision making in the design and optimization of curved microchannels, thus contributing to the advancement and continuous improvement of microfluidic systems in a variety of applications.

Figs. 12, 13 and 14 show the variation of velocities in curved microchannels, influenced by the geometrical configuration of the channel, such as its curvature and cross section, which impact the velocity distribution along the channel. This variation can be affected by several factors, such as channel geometry, Reynolds number, fluid inlet conditions and capillarity. A specific trend is observed in the microdevices with curved channels, where at the beginning of the curvatures the velocity decreases, and as the trajectory progresses, it tends to increase again. The velocity data in the three devices show a positive asymmetry, indicating that they are concentrated towards the top with a more uniform distribution, especially near the center of the box. This distribution suggests that the

data are symmetrical, with peaks of velocities in the curves and a reduction in the straight segments of the channel. These findings provide valuable information on the velocity distribution in curved microchannels, contributing to a better understanding of the flow behavior in these devices and to the optimization of their design for various applications in microfluidics and related fields.

4 Conclusions

A micro device with curved channels was designed and fabricated using 3D printing (SLA) to explore fluid movement via capillarity in circular devices. The aim of the study was to evaluate the behavior of the liquid through channels of varying geometries manufactured by additive manufacturing. Currently, there is extensive research in this field due to the versatility and novelty of the technology. Total fabrication process time for each device took approximately 74 minutes, including printing (50 minutes), cleaning (12 minutes), and curing (12 minutes).

Flow velocity tests conducted in the curved channels revealed average velocities of 0.00267 m/s, 0.00242 m/s, and 0.00438 m/s for devices with radii of 4 mm, 6 mm, and 8 mm, respectively. These results demonstrate that larger radii correspond to higher velocities.

To characterize fluid movement within the microchannels, the Reynolds number was calculated for radii of 4 mm, 6 mm, and 8 mm, yielding values of 1.4780, 1.3396, and 2.4246, respectively. These values indicate that all three devices exhibit laminar flow regimes, where viscous forces dominate over inertial forces, as the Reynolds numbers are less than 2000.

Depict the velocity behavior in curved microchannels, showing a distinctive peak followed by deceleration. This phenomenon is attributed to reduced friction along the inner wall during curvature, allowing for acceleration, whereas the straight sections experience greater wall contact and subsequent friction, leading to velocity reduction. Understanding this behavior is crucial for optimizing microchannel designs across various applications, from microelectronics to biomedicine and nanotechnology, where flow velocity significantly influences system performance and effectiveness.

Theoretical capillary force of the microdevices was evaluated to be -302.9633 Pa, signifying spontaneous liquid absorption in narrow spaces without external force assistance, influenced by cohesive and adhesive forces between liquid molecules and container walls.

Variation in fluid velocity along the curved microchannel is reflected in the average velocities obtained: 2.81952 mm/s for the 4 mm radius device, 3.21872 mm/s for the 6 mm device, and 4.15311 mm/s for the 8 mm device. These data align with the expected effect of increasing the curved section in an incompressible flow, adhering to the principle of conservation of mass, where an increase in cross-sectional area results in decreased velocity and vice versa.

References

[1] Rodríguez, E., Tecnología microfluídica para el control ambiental. Fieras de la Ingeniería. [ONLINE]. Accessed: Dec. 04, 2023. [Online]. Available at: https://web.archive.org/web/20131018020809/http://www.fierasdelaingenieria.com/tecnologia-microfluidica-para-el-control-ambiental/

[2] Hurtado-De Mendoza, A., Estudio de la generación de emulsiones en micro fluidos mediante simulación numérica, Nov. 2017.

[3] Sun, B., Jiang, J., Shi, N., and Xu, W., Application of microfluidics technology in chemical engineering for enhanced safety, Process Safety Progress, 35(4), pp. 365–373, 2016. DOI: https://doi.org/10.1002/PRS.11801.

[4] Méndez, M. de O.J.L., Formación de microcápsulas para envío de farmacos a partir de emulsiones usando dispositivos microfluidicos, Tesis, Dr. Instituto de Física y Matemáticas, Universidad Michoacana de San Nicolás de Hidalgo, Morelia, Mexico, 2018, 134 P.

[5] González-Esparza, D., Diseño, modelado y fabricación de un microsistema fluídico para la separación de células tumorales. Tesis MSc. Facultad de Ingeniería de la Construcción y el Hábitat, Universidad Veracruzana, Veracruz, Mexico, 2021, 53 P.

[6] Innofocus Photonics Technology, Microfluidos - Tecnología fotónica de Innofocus. [Online]. [Accessed: December 03rd of 2023]. Available at: https://innofocus.com.au/es/microfluidic/

[7] Rubio, C. and Enfedaque, A., Una tecnología mejora la eficacia de los dispositivos de análisis de microfluidos, Tesis de grado. Universitat Autònoma de Barcelona – UAB, Barcelona, España. [Online]. [Accessed: December 03rd of 2023]. Available at: https://www.uab.cat/web/sala-de-prensa/detalle-noticia/una-tecnologia-innovadora-mejora-la-eficacia-de-los-dispositivos-de-analisis-de-microfluidos-1345667994339.html?noticiaid=1345702820392

[8] Choi, H.J., Lee, J.H., and Jeong, O.C., Pneumatically driven microfluidic platform for micro-particle concentration, Journal of Visualized Experiments, 2022(180), art. 63301, 2022. DOI: https://doi.org/10.3791/63301

[9] Pena-Oyarzún, C.E., Estudio de la influencia de la forma de sección de los microcanales en un disipador de calor, Tesis de Grado, Facultad de Ciencias Físicas y Matemáticas Departamento de Ingeniería Mecánica, Universidad de Chile, Santiago de Chile, Chile, 2021.

[10] Garrido, A.L. and Pérez-Caballero, D.C., Fabricación con láseres ultrarrápidos de dispositivos microfluídicos, Tesis de Grado, Escuela Técnica Superior de Ingenieros Industriales, Universidad Politécnica de Madrid, Madrid, España, 2018, 76 P.

[11] Barraza-Sandoval, M.B., Reduccion de arrastre en superficies biomimeticas superhidrofobicas via impresión 3D, Tesis Dr., Facultad de Ciencias Físicas y Matemáticas, Universidad de Chile, Santiago de Chile, Chile, 2021, 106 P.

[12] Academia Balderix, "▷ Desplazamiento (física). [online]. [Accessed: January 08th of 2024]. Available at: https://www.ingenierizando.com/cinematica/desplazamiento-fisica/

[13] Cuemath, Magnitude of a Vector - Formula, How to Find? Length of Vector. [Online]. [Accessed: January 08th of 2024]. Available at: https://www.cuemath.com/magnitude-of-a-vector-formula/

[14] Elizalde, E., Llenado capilar de microcanales y estructuras nanoporosas, Tesis Dr., Instituto de Física del Litoral, Facultad

de Ingeniería Química, Universidad Nacional del Litoral, Santa Fe, Argentina, 2017, 166 P.
[15] Sósol-Fernández, R.E., Marín-Lizárraga, V.M., Rosales-Cruzaley, B.H., y Lapizco-Encinas, B.H., Analisis de celulas en dispositivos microfluidicos, Revista Mexicana de Ingeniería Química, 11(2), pp. 227-248, 2012. [Online]. Available at: http://www.scielo.org.mx/scielo.php?script=sci_arttext&pid=S1665-27382012000200003&lng=es&nrm=iso
[16] Rupp, F. et al., A review on the wettability of dental implant surfaces I: theoretical and experimental aspects, Acta Biomaterialia, 10(7), pp. 2894–2906, 2014. DOI: https://doi.org/10.1016/j.actbio.2014.02.040.
[17] González-Suárez, A.M., Dispositivo microfluídico para la generación de una curva estándar de forma automática para un inmunoensayo, Tesis MSc., Centro de Investigación y de Estudios Avanzados del Instituto Politécnico Nacional, Unidad Monterrey, Monterrey, Mexico, 2015, 107 P.
[18] Vilchis, P., Fabricación de un dispositivo microfluídico para el estudio de fluidos complejos, 2011.
[19] s.a., Canales. Flujo en Superficie Libre, Departamento de Hidráulica e Hidrología Canales, Facultad de Ingeniería Civil, Universidad Nacional de Ingeniería, Lima, Perú, 2018.
[20] Çengel, Y.A. and Cimbala, J.M., Fluid mechanics: fundamentals and applications, 2014, 300 P.

N. Esparza-Proaño, is a Mechanical Engineering student at the Universidad Politécnica Salesiana with a keen interest in microfluidics, actively participates in extracurricular activities. Dedicated to academic excellence and social responsibility, embodying the university values of integrity, empathy, and leadership.
ORCID: 0009-0001-6273-3774

V.H. Cabrera–Moreta, is principal professor at the Universidad Politécnica Salesiana brings over 8 years of educational expertise. Currently pursuing a PhD. in Mechanical, Fluidics, and Aeronautics at the Universidad Politécnica de Cataluña, Spain, focusing on mechanical design, innovation, entrepreneurship, and micro manufacturing expertise.
ORCID: 0000-0001-9482-5705

DYNA
http://dyna.medellin.unal.edu.co/

UNIVERSIDAD NACIONAL DE COLOMBIA

Study of mental workload in public administration managers

Yilena Cuello-Cuello, Juan Lázaro Acosta-Prieto, Edian Dueñas-Reyes, Joaquín García-Dihigo & Zoe Domínguez-Gómez

University of Matanzas, Matanzas, Cuba, yilena.cuello@gmail.com, acostaprietojuanlazaro@gmail.com, eithan@nauta.cu, joaquin.garcia@umcc.cu, zoedg57@gmail.com

Received: January 22th, 2024. Received in revised form: April 29th, 2024. Accepted: May 16th, 2024.

Abstract
The present research is carried out in the Municipal Administration with the objective of studying the behavior of the mental workload in the work places. The procedure used consists of three stages: preparation, experiments and results. The indicators selected for the study are: Simple Reaction Time, Complex Reaction Time, Discrimination Threshold, Depth Perception and Yoshitake Test are selected. SPSS software is used or the statistical analysis of the data, EndNote as a bibliographic manager and VOSviewer for its graphical representation. An Ishikawa Diagram is used to determine the causes that provoke mental fatigue during the working day in the individuals studied. As a result, out of the 12 workers studied, 6 presented extreme risk, 5 a worrying level and 1 a moderate level of mental workload. A proposal of measures to prevent and reduce the effect of mental workload is elaborated.

Keywords: cognitive capacity; mental workload; cognitive demands; psychophysiological indicators; psychological indicators.

Estudio de carga mental de trabajo en directores de la administración pública

Resumen
En la Administración Municipal se realiza la presente investigación que tiene como objetivo: estudiar el comportamiento de la carga mental de los puestos de trabajo. El procedimiento consta de tres etapas: preparatoria, experimental y resultados. Son seleccionados los indicadores Tiempo de Reacción Simple, Tiempo de Reacción Complejo, Umbral de Discriminación, Percepción de Profundidad y Prueba de Yoshitake. Para el análisis estadístico de los datos se emplea el software SPSS, como gestor bibliográfico el EndNote y el VOSviewer para su representación gráfica. Se realiza un Diagrama de ishikawa que determina cuales son las causas que les provocan fatiga mental durante la jornada laboral a los individuos estudiados. Como resultado de 12 trabajadores estudiados, 6 presentaron riesgo extremo, 5 un nivel preocupante y 1 un nivel moderado de carga mental de trabajo. Se elabora una propuesta de medidas para prevenir y reducir el efecto de la carga mental de trabajo.

Palabras clave: capacidad cognitiva; carga mental; demandas cognitivas; indicadores psicofisiológicos; indicadores psicológicos.

1 Introduction

The period between 1760 and 1830 was known as the First Industrial Revolution. The introduction of equipment brought about new forms of work organization. These changes led to a decrease in physical effort, but increased vigilance and control by the worker [1].

In recent years, technological development has led to an increase in automation processes and has provided a cognitive development due to the impact on mental processes [2-3]. This series of events have evidently brought about changes in the workforce as workers with greater resources and cognitive abilities are increasingly required [4-5]. The demands for skilled workers have grown [6]. The slogan that "the substitution of physical effort for mental effort favors the health of the worker in all circumstances" is only valid when it is limited to cognitive abilities. Hence the emergence of Cognitive Ergonomics.

Ergonomics, according to [7] is the scientific study of the relationship between man and his work environment. Its

How to cite: Cuello-Cuello, Y., Acosta-Prieto, J.L., Dueñas-Reyes, E., García-Dihigo, J., and Domínguez-Gómez, Z., Study of mental workload in public administration managers . DYNA, 91(232), pp. 112-120, April - June, 2024.

assignment is that of designing machines, tools and the way work is carried out, in order to keep the work pressure on the body to a minimum.

Mental workload cannot be so easily measured, not to mention the psychosocial workloads and their consequences [8].

The cognitive demands of the job, according to [9], are defined by the degree of pressure or mobilization and intellectual effort that the worker must face in the performance of his tasks. Another important definition is the term cognitive abilities of the individual, which according to [10] can be defined as those skills and processes of the mind necessary to perform a given task. Task characteristics, such as memory and attention demands, time pressures and work pace, as well as the functions to be performed, the degree of autonomy, and the interaction with other workers, can be cited [11].

The imbalance between task demands and workers' capabilities can lead to mental work overload or underload [12]. Overload reaches situations in which the worker is subjected to more demands than he/she is able to bear, which translates into mental fatigue, while mental underload occurs in jobs with few tasks and few cognitive demands (qualitative underload) or simple tasks with sufficient time for their execution (quantitative underload), which translates into underutilization of the individual's mental capacities [13-14]. The mental load will always be the result of the cognitive demands of the task, the cognitive capacity of the participants and the circumstances in which it is performed [15].

When a worker faces a continuous overload, it can affect both his performance and his health.

There is a close relationship between mental overwork and the appearance of diseases among which the following stand out: obesity, cardiovascular disorders, arterial hypertension, atherosclerosis, diabetes mellitus, dyslipidemia, digestive disorders, asthma, psychiatric disorders, cancer and the much mentioned stress [16].

There are several technical standards dedicated to mental work, although ISO 10075 is the best known, there are also other interesting standards that contemplate ergonomic design principles on machine safety, incorporating recommendations to minimize mental workload. Decree 1477 aims at regulating the promotion of mental health and the prevention of mental problems and disorders in the workplace [17].

The Mexican Official Standard NOM-035-STPS-2018, is a protective standard in labor matters that has three commitments: to identify and prevent psychosocial risk factors and to evaluate the work environment [18]. Among them is also found the ISO 45003:2021 standard that helps build a positive work environment that can help improve organizational resilience, and increase performance and productivity, the standard takes in how to recognize psychosocial risks that can affect workers [19].

There are several objective models for the evaluation of cognitive demand in the workplace, which include variables related to mental workload, such as: LEST, Job Profile, Ergonomic Job Analysis Method (EWA), INSHT Psychosocial Factors Method, ANACT Method, ESCAM, Tabulated Method, NASA-TLX, and SWAT. It is important to point out that the criteria used by the global methods are valid mainly for low or unskilled jobs, that is, monotonous, repetitive jobs with little work content. These methods assess the capacity and incidence of the cognitive demand on the person, but with a subjective perspective. Since they are psychological tools, they let us obtain an assessment of people on the level of mental load experienced during the performance of a task, assuming that this assessment is related to the objective demands of the task, hence the importance of using quantitative indicators [20].

There are indicators of mental workload in the individual that are grouped into 4 levels: biomolecular, physiological, psychological and psychophysiological. They have been experimentally determined based on the reactions of the individual to an excess load.

In Cuban companies the worker is susceptible to suffer health damage because there is no adequate relationship between knowledge and the cognitive demands of the job, there is no autonomy, or the physical or material conditions are not adequate [21]. A company under stressful work conditions will have its productive results affected, and will be less competitive in the market. These aspects can be observed in the following consequences: higher absenteeism, less dedication to work, higher staff turnover, failures in performance and productivity, increase in unsafe activities and accidents, more complaints from customers, failures in the recruitment of new employees, legal problems, and deterioration of the company's image in the public [22].

Cuba is currently developing different transformations aimed at achieving compliance with a national decentralization strategy as part of the process of updating the Cuban economic model. Many decentralization and territorial development experiences fail due to insufficient territorial capacities and knowledge gaps, since this is a multidimensional process that includes economic, social, environmental and institutional development [23]. Territorial development cannot advance without the development of capacities, which leads to an increase in the cognitive demand for jobs.

These cognitive resources invested in the carrying out of an activity have an influence on the health of workers, so it is necessary to identify the ergonomic risks of a cognitive nature associated with it, allowing training on its control and prevention, and thus improving the working conditions of the personnel [24].

There is a need to have a procedure to evaluate the mental workload and take into account the cognitive demand and capabilities of the individual. This would help make decisions regarding the workplace, the selection of personnel to work in it, its redesign to reduce health effects due to the high cognitive demands it may present, guarantee the quality of the activity performed by organizing the work to be developed and establishing a balance between demand and cognitive capacity, thus reducing the margins of error and therefore the economic losses and the level of occupational accidents, and also enabling greater productivity in the workplace.

Cuba has the need for this national decentralization strategy. Provincial and municipal governments should assume a more leading role in promoting sustainable

territorial development, particularly with the objective of achieving economic and food self-sustainability.

The Municipal Administration is located within the Municipal Government and will be our object of study, since it is necessary to know its current situation in this context, if the current tasks they perform have an impact on the health of their workers in order to propose possible solutions to help the decentralization process, which implies a greater cognitive demand in the workplaces. There is a lack of assessment procedures or tools so that it is necessary to use a quantitative criterion to define the cognitive demands or requirements of the job, the worker's capabilities and achieve a balance between the two in terms of mental workload.

Objectives

To carry out a study on the behavior of the mental workload of the positions in the Municipal Administration.

2 Materials and methods

Based on the study of the existing procedures for the evaluation of mental work both in the international and national context done by the authors: [25-26-27] the design of the procedure to evaluate the mental workload of jobs is shown in Fig. 1.

Among the novelties of the proposed procedure are found the criteria applied for the selection of jobs with higher cognitive demands, the selection of indicators to determine the individual's cognitive abilities, the application of the modified human error method to evaluate the cognitive demands of the job, the individual analysis of the behavior of the indicators for each worker and the collective analysis by position.

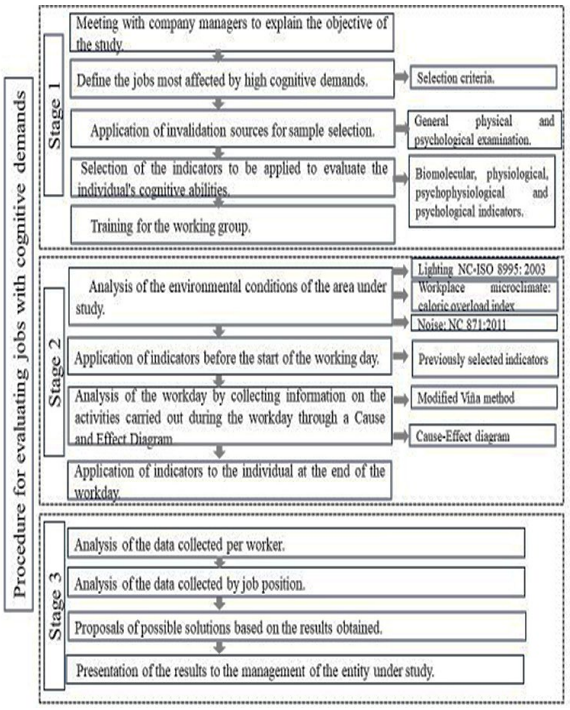

Figure 1. Proposed procedure for assessing mental workload.
Source: The Authors.

Description of Stage I of the proposed procedure

Step 1. Meeting with company managers to explain the objective of the study.

Step 2. Defining the jobs most affected by high cognitive demands.

The inclusion criteria used for the selection of the jobs under study are taken from the bibliography consulted. Below are the ones that were considered: information processing (decisions between several possible modes of action), responsibility (for the health and safety of others), duration and time profile of the activity (working hours, breaks), task content (control, planning, execution, evaluation), competitiveness (the possibility of professional growth), the need to travel for work requirements, environmental conditions (lighting, noise, climatic conditions), dealing with the public or customers, exposure to risks, mental effort of the individual.

The objective of the research is explained to the selected workplaces and the consent of each worker is obtained for the study and to guarantee the confidentiality of the data they provide.

Step 3. Application of invalidation sources for sample selection.

For the selection of the sample, a general physical examination is applied as an exclusion criterion that guarantees the health status of the individuals participating in the research. Below they are the criteria to be taken into account:

- *General physical examination*

All applicants who present any disorder of cardiovascular functioning, chronic or acute disease at the time of the experience is eliminated from the experience.

Step 4. Selection of the indicators to be applied to evaluate the individual's cognitive abilities.

For the selection of the biomolecular, physiological, psychological and psychophysiological indicators, a series of criteria analyzed in the bibliography consulted were taken into account in order to adjust the study to the real and existing conditions in the entity. The selected criteria were: presentation of the equipment, degree of mobility, response only to mental demands, ease of experimental control, ease of normal development of the activity, adjustment to the conditions of the research, temporal resolution, spatial resolution, portability, and cost.

Step 5. Training for the work group.

A working group is trained, which must be formed by experts in the subject.

Description of Stage II of the proposed procedure

Step 1. Analysis of the environmental conditions of the area under study.

Lighting, noise and microclimatic conditions are taken into account, thus analyzing whether they affect the presence of mental workload.

Step 2. Application of indicators before the start of the working day.

Step 3. Analysis of the workday by collecting information on the activities carried out during the workday through a Cause-Effect Diagram.

Step 4. Application of indicators to the individual at the end of the workday.

Table 1.
Level of mental workload according to the number of indicators that vary as expected.

Number of indicators	Level of mental workload	Indications
X ≥ 3	Extreme	May present health problems, if their situation persists over time it may be chronic so immediate intervention is necessary and measures to change their situation must be implemented.
X = 2	Worrisome	It is necessary to intervene in the short term and apply measures to improve the situation.
X = 1	Moderate	Keep the worker under observation and apply measures so that the mental workload does not increase.

Source: The Authors.

Description of Stage III of the proposed procedure

Step 1. Analysis of the data collected per worker.

The statistical processing of the data for the psychophysiological indicators is carried out in SPSS Statistics 22 software. The 10 measurements collected are shown in a table per indicator before and after the workday per individual, as well as their average.

The Kolmogorov-Smirnov test is used to demonstrate the normality of the data. If it follows a normal distribution, the parametric Student's t-test is applied and if it does not follow a normal distribution, the nonparametric test of signs is applied to analyze paired samples and define if there are significant differences between before and after.

The number of indicators that had significant differences between before and after the workday for each worker and that comply with the premise of mental workload are analyzed.

Table 1 shows the level of mental workload taken into account according to the number of indicators that vary as expected. The proposed interpretation is the result of a series of investigations that the authors developed [9,20,25].

Step 2. Analysis of the data collected by job position.

In this step, the behavior of the measurements is analyzed by job position; to achieve this, the sample is divided according to the job position occupied. An analysis of the variation of the selected indicators is performed by subtracting the average measurement after the workday from the average measurement before the workday for each of the individuals.

In order to compare which job is more mentally burdened, a radial graph is proposed for a better understanding of the variation of the indicators.

Step 3. Proposals of possible solutions based on the results obtained.

For this purpose, the measures that were devised include the prevention of mental fatigue in jobs with high cognitive demand, taking into account the results obtained in the application of the Cause-Effect Diagram.

Step 4. Presentation of the results to the management of the entity under study.

3 Results and discussion

Fig. 2 shows the bibliometric map created in the VOSviewer software, based on the co-occurrence of keywords, which shows the keywords that most stand out in the bibliography used.

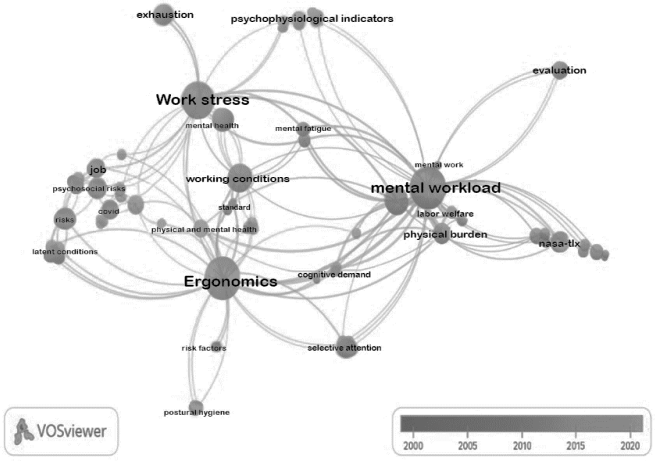

Figure 2. Co-occurrence of keywords in articles related to mental workload assessment models.
Source: The Authors.

An analysis of this bibliometric map showed that the terms that stood out the most were mental workload and mental workload assessment, which demonstrated that the vast majority of studies and research in the field of Cognitive Ergonomics are focused on this topic, due to its importance and that it has become a central focus of analysis and prevention.

A meeting was held with the Mayor and the Director of the Cadres, these people were taken as experts because they have extensive knowledge of each job. The job positions that were considered to have the greatest cognitive demands were those of Mayor, Program Coordinators and Municipal Managers based on the inclusion criterion declared in step 2 of stage 1 of the proposed procedure.

The sources of invalidation were applied to the individuals occupying the posts with the highest cognitive demands previously selected. The group under study consisted of 4 Program Coordinators and 12 Municipal Directors.

The study population consisted of 16 workers in the Municipal Administration Council of Cárdenas. Taking into account that 4 of them were not in a position to be sampled (two of them due to recent illness and the other two because they were in the fulfillment of larger functions during the time that the research was developed), it was then decided to carry out the experimental design with the remaining 12 workers (representing 75% of the total population) and they were considered the maximum possible sample. Three of them are Program Coordinators and nine are Municipal Directors.

With this sample, we achieved a representation of the most influential positions in the municipality due to the capacity and impact that each one of them has at the time of making decisions.

These indicators were used because they had the greatest impact due to the advantages they provide and their easy development. They are the following:

- *Psychophysiological indicators:* Simple Reaction Time

(TRS), Complex Reaction Time (TRC), Tactile Discrimination Threshold (UDT) and Depth Perception (PP).

The TRS and TRC increase when the activity requires a considerable mental load and consequently fatigue is greater. The TRC are longer than the TRS for habitual stimuli, the only disadvantage is that the level of precision and accuracy of the individual is put at stake when having to recognize different stimuli, which may affect the excessive increase in the variation of the TRC between before and after the development of an activity with cognitive demands.

PP increases the distance of alignment perception in view of mental load when measuring the distance to an object based primarily on the process within the person's brain through the exploitation of parallax in motion.

The UDT tends to decrease under mental load and increases the minimum distance at which two stimuli are independently distinguished. It is evident that there is a significant decrease in the acuity of touch when there is an overload of the visual analyzer. It does not happen under the absence of cognitive demands.

- *Psychological indicator:* The Yoshitake test that allows determining the subjective feeling of fatigue presented by the person from the classification of its 30 questions and whether it is caused by physical demands, mental demands or mixed demands.

These tests are dynamic and of quick application, therefore, the normal development of the working day is not interrupted at the time the information is being collected, which facilitates the realization of studies on the analysis of the presence of mental fatigue.

The bio molecular and physiological indicators presented have some disadvantages, among which stand out their enormous implementation requirements which are invasive and require high technology. In field research their application is complicated because special conditions are required and they receive poor acceptance from the subjects who participate in the evaluation, so it is considered that there are not conditions for the application of the indicators in the object of study.

The work group was trained, attaining the experience needed for the measurements of the selected indicators before and after the working day. The work group is formed by 4 students that are members of the science group of Cognitive Ergonomics at the University of Matanzas and the leader of the science group, Eng. Juan Lázaro Acosta Prieto, who were previously linked to the methodology and manipulation of the instruments.

In the workplaces under study the tasks were not carried out in closed physical spaces, but each worker throughout his work day has a dynamic work that does not allow him to stay so long. These workplaces were not exposed to noise levels, there were no lighting problems and none of them were exposed to extreme weather conditions so the environmental conditions are not of concern for the study.

The first measurement of indicators was carried out before starting the work day. A room was provided in the Municipal Administration building and a student per indicator was assigned, so that the measurements were carried out in a circuit, in a dynamic and pleasant way so that the individuals did not feel indisposed by the experience and when the evaluation of their indicators was completed, they retired to their work area.

A meeting was held with the Program Coordinators and Municipal Managers to determine the possible causes that could lead to mental fatigue in their work process. The causes raised by these workers are defined as follows:

- Misuse of productive reserves during the workday.
- Inadequate design of training processes.
- Misuse of productive reserves during the workday.

For a better understanding, Fig. 3 is presented below, which is a Cause-Effect Diagram in which the causes and sub-causes that caused mental fatigue in the Program Coordinators and Municipal Managers are related.

The second measurement of indicators was carried out at the end of the workday, repeating the same measurement process carried out in the morning.

Analysis of the data collected per worker.

When analyzing the 10 measurements per individual at the beginning and end of the workday using the Kolmogorov-Smirnov test for the psychophysiological indicators: TRS, TRC, UDT and PP, it was demonstrated that all the data come from a normal distribution by accepting the null hypothesis with a significance level of 0.05.

The existence of significant differences in paired samples in the TRS, TRC, UDT and PP indicators was analyzed by means of the parametric t-student test, which showed that 0.25%, 41.66%, 75% and 66.67% of the individuals rejected the null hypothesis with a significance level of 0.05 in each of these indicators respectively, so it can be asserted that there are significant differences for this group of individuals between the measurements taken "before" and "after".

Table 2 shows the average values before (B) and after (A) of the 10 measurements per worker in the psychophysiological indicators: TRS, TRC, UDT and PP.

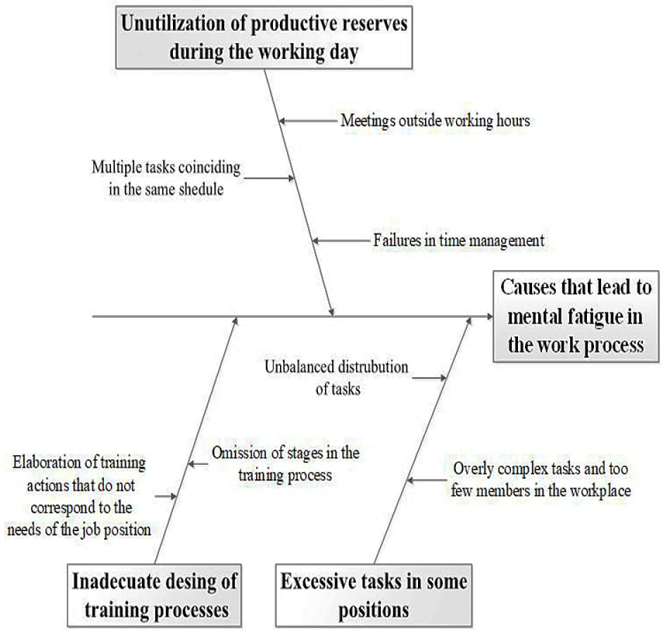

Figure 3. Cause-Effect Diagram of the causes and subcauses that provoked mental fatigue in the Program Coordinators and Municipal Managers. Source: The Authors.

Table 2.
Average values of the psychophysiological indicators used.

No.	Measurement of indicators							
	TRS (s)		TRC (s)		UDT (cm)		PP (cm)	
	B	A	B	A	B	A	B	A
1.	1,08	1,13	1,16	1,23	3,2	4,88	0,33	0,69
2.	0,98	1,37	0,97	1,03	2,61	2,65	2,63	2,76
3.	0,36	1,34	0,44	1,19	1,7	2,35	0,32	1,22
4.	0,43	0,59	0,52	0,7	5,32	5,54	0,38	0,74
5.	0,53	0,99	0,64	1,18	0,76	1,58	0,76	1,41
6.	0,37	0,99	0,44	1,19	0,68	1,53	0,45	0,69
7.	0,46	0,77	0,56	0,92	3,09	3,38	0,73	1,13
8.	0,72	0,64	0,66	1,3	3,09	5,32	0,53	0,79
9.	0,67	0,77	0,81	0,92	2,19	2,39	0,29	1,12
10.	0,6	0,67	0,8	0,72	2,16	2,41	1,17	2,96
11.	0,55	1,09	0,86	0,77	1,3	1,12	2,14	2,4
12.	1,14	1,3	0,55	1,09	3,06	3,28	3,5	3,13

Source: The Authors.

Table 3.
Coefficient of variation values of the sample under study.

Indicators	TRS		TRC		UDT		PP	
	B	A	B	A	B	A	B	A
Coefficient of variation	0.41	0.29	0.31	0.21	0.53	0.49	0.97	0.59

Source: The Authors.

- *Psychological indicator*

The test was applied as a psychological indicator to the group under study at the beginning of the workday and moments after finishing it.

Before starting the workday, 41.67% of the individuals experienced subjective feelings of fatigue with physical-mental demands and 58.33% did not experience subjective feelings of fatigue. At the end of the working day 58.33% of the individuals experienced subjective feelings of fatigue with physical-mental demands, 8.33% physical demands and 8.33% mental demands and 25% did not experience subjective feelings of fatigue.

The symptoms felt were: drowsiness by 66.67%, heaviness in the head, tiredness in the body and incorrect positions by 58.33% and suffering from headache, standing restlessness and suffering from headache was the 50%.

The symptoms presented by individuals with an incidence higher than 50% at the end of the working day were: drowsiness (66.67%), heaviness in the head, tiredness in the body and incorrect positions (58.33%), and suffering from headache, restlessness when standing and headache (50%).

Table 3 summarizes the behavior of the coefficient of variation of the sample under study, which takes into account the relationship between the standard deviation and the average of the psychophysiological indicators used before and after the workday. As Table 3 shows, there was a homogeneous behavior in the TRS an TRC indicators, therefore the average was representative for the population, while in the UDT and PP indicators the average was not a representative value for the set of data obtained.

Fig. 4 shows the number of indicators that suffered significant differences between before and after the workday for each worker and that comply with the mental workload premise.

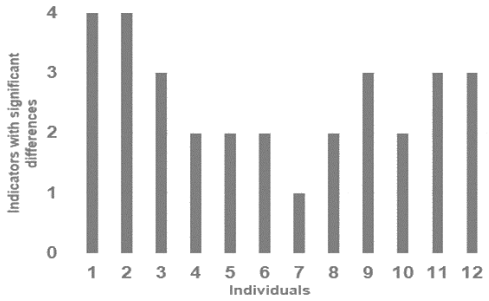

Figure 4. Number of indicators with significant differences in each worker.
Source: The Authors.

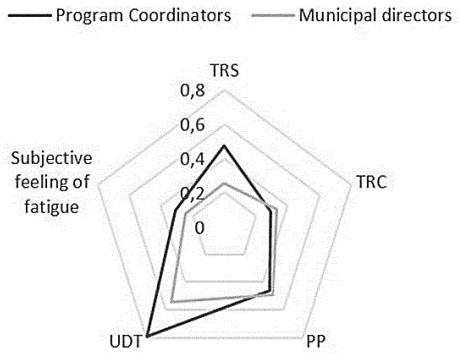

Figure 5. Behavior of the variations of the selected indicators for Program Coordinators and Municipal Managers.
Source: The Authors.

Of the sample studied, 6 individuals presented the expected behavior in the presence of a level of mental fatigue during the workday, with significant variations in the results in at least 60% of the indicators; that is, 3 or more indicators affected, so they suffered from an extreme level of mental workload and there is a risk to their health, if their situation persists over time it may become chronic, so immediate intervention is necessary and measures to change their situation must be applied.

Five workers showed a worrying level of mental workload, with 40% of the indicators showing the expected behavior in the presence of mental fatigue, that is 2. So it is necessary to intervene in the short term and apply measures to improve their situation.

Of the total sample, 1 worker suffered significant differences in only one indicator, so his mental workload is moderate, although the results do not show a high level of concern.

Analysis of the data collected by job position.

In this analysis, the sample was divided according to the job position they occupy and two groups were formed: Program Coordinators and Municipal Managers.

Fig. 5 summarizes the behavior of the variations experienced by both positions.

Fig. 3 shows that the position of Program Coordinator presented a greater variation in the indicators than that of Municipal Directors, which indicates that they have a greater mental workload.

In order to improve the competencies of the personnel of the Municipal Administration and to be able to obtain better results in the decentralization process that implies greater cognitive demands in the jobs, a set of measures were proposed to the entity as shown in Table 4, which are possible solutions based on the results obtained.

A meeting was held with the Intendant, the Director of the Cadre and all the workers to whom the indicators were applied. The results of the research were presented and the need for the entity to commit itself to comply with the proposed measures in order to obtain better results in the decentralization process, which implies greater cognitive demands in the jobs, was raised.

The similarity of preceding studies by other researchers such as [19,28,29] is corroborated.

The first studies conducted by [28] evaluated 60 subjects using psychophysio-logical tests including tactile discrimination threshold and TRS. They exposed healthy subjects to various conditions that demanded mental effort; tactile thresholds decreased their receptive function in the face of greater mental effort with higher values at the end of the task. In the TRS there is a significant difference between before and after, since the values of the measurement gradually increase at the end of the task in the face of high mental demands.

Table 4.
Proposed possible solutions based on the results obtained.

No.	Problem detected	Measures
1	Inadequate design of training processes.	Design a training system for managers in conjunction with the Government-University to increase their competencies. The following topics are addressed in the trainings: Government Structure, Territorial Strategic Development, Socio Demographic Dimension, Territorial and Urban Reorganization, Development and Budget Strategies, Decentralization of competencies, Citizen Participation and Communication, Prevention and Social Attention, Government Management based on Science and Innovation, Practical Activity with Municipal Strategy, Foreign Trade and Foreign Investment, Food Sovereignty, Commercialization and Nutritional Education in Cuba and Sustainable Urban Development.
2	Excess of tasks in some jobs.	The need to sanction the proposed structure by the Municipal Administration was ratified, which had been previously approved by the Provincial and Municipal Directorates and the Municipal Group as well as prior consultation with the PCC (Communist Party), the MININT (Ministry of Home Affairs) and the FAR (Revolutionary Armed Forces) of the territory. The position of Program Coordinator is now called Vice Mayor and the number was increased to 6 and the number of Municipal Directors is increased to 14.
3	Unutilization of productive reserves during the workday.	With the implementation of the new structure, the redistribution of programs is carried out by each Program Coordinator, who are now named Vice-Intendants. The Municipal Administration also received training on Decree 72/2022 "On the organizational structures in the municipal administrations of the People's Power", which establishes the functions of the municipal directors as of the implementation of the decentralization process. A series of training were held with the Mayor and the Council of the Municipal Administration for the development of an adequate work plan to optimize work time within the working day.

Source: The Authors.

Very similar results have been described by [19] who studied the level of mental workload of the professors of the Public Administration degree course of the Escuela Superior Politécnica Agropecuaria de Manabí guided by Carvalho's methodology which is one of those taken into account when designing the procedure shown in the present research. It uses the simple reaction time, complex reaction time and the Subjective Feelings of Fatigue survey as indicators. These measurements were taken at the beginning and end of the working day as proposed in the present procedure. The results show that during administrative hours they maintain the same level of concentration and at the end of the lessons four out of six teachers had a decrease in their attention and have a high level of mental workload. The Subjective Feeling of Fatigue Test showed that 85% of the teachers felt tiredness in the body and legs at the end of their working day, 57% wanted to go to bed, 43% felt tired when talking and straying of attention.

In the research carried out by [29] similar results were found, since he evaluated the behavior of indicators related to mental workload in Industrial Engineering students of the University of Matanzas. He created two sample groups under the assumption of presence and absence of mental workload and evaluated the selected indicators before and after the development of the experimental activity. Among the indicators applied are found: Tactile Discrimination Threshold, Depth Perception, Simple Reaction Time and Yoshitake Test. In depth perception, 43.75% of the individuals who were not exposed to mental workload presented an increase in the values of the measurements at the end of the task and 92.1% of the individuals subjected to the test comply with the premise that when exposed to mental work the PP tends to increase. In the tactile discrimination threshold, the results were 75% and 92.1% for the two sample groups. In simple reaction time, values of 62.5% and 89.47% were obtained, respectively. The application of the Yoshitake test showed that 47% felt heaviness in the head, 73.68% felt confused and dazed, 60.53% felt tired eyesight and were anxious, 52.63% stated that they lose patience easily under cognitively demanding situations.

The results of these investigations coincide with the results in the positions of Municipal Directors and Program Coordinators in such a way that when faced with the cognitive demands of the job, the abovementioned indicators increase their values. In conclusion, in all the investigations these indicators reflect mental fatigue with the fusion of activities, time and demand in the tasks that these people perform daily. This generates a high level of mental load and there is a high degree of wear and tear that affects their physical and psychological state.

The novelty of this procedure is that it is carried out with managers in the Municipal Administration where no studies

of this type had been carried out before. It also permits comparing how this study is similar to others that involve the behavior of the indicators in order to give it greater validity for future research.

This study is of great importance since there is a tendency in the workplaces to increase cognitive demands and therefore there is a greater incidence of mental work; so it is necessary to establish mechanisms to follow up the behavior of workers and create workplaces that guarantee quality of life and prevent risks and occupational diseases related to mental work.

4 Conclusions

1. The procedure for the development of the research consists of three stages: Stage I Preparation, where the work position under study is selected and the sample is selected from the joint application of a general physical and psychological examination. Stage II Experimentation, where indicators are applied before and after the end of the working day and Stage III Results, where an analysis is offered by individuals and positions, the results are interpreted and a solution is proposed.
2. The hypothesis test for the comparison of paired samples, according to the T-Student test, shows that there are significant differences in 91.67% of individuals in TRS, 83.33% in TRC, and 91.67% of individuals have significant differences in PP and UDT.
3. Out of the sample studied, 6 individuals had the expected behavior in the presence of a level of mental fatigue during the working day, 5 workers had a disturbing level of mental workload and 1 worker presented a moderate level as he underwent significant differences in only one indicator, where the position with the highest impact is that of Program Coordinators.
4. At the end of the working day, 75% of the individuals experienced a subjective feeling of fatigue. The symptoms they presented with an incidence of more than 50% at the end of the working day were: drowsiness, heaviness in the head, tiredness in the body, incorrect positions, headaches and getting restless when standing up.
5. An analysis was made of the behavior of the variations of the selected indicators and the position of Program Coordinator presented a greater variation in the indicators than that of Municipal Directors, which indicates that they have a greater mental workload.
6. Measures are proposed to improve the existing conditions in each work position and to benefit the company's health.

References

[1] Vega-Ruíz, M.L. ¿El trabajo es salud?. Archivos de Prevención de Riesgos Laborales, 23(4), pp. 410-414, 2020. DOI: https://doi.org/10.12961/aprl.2020.23.04.01

[2] Litardo-Velásquez, C.A., Díaz-Caballero, J.R., and Perero-Espinoza, G.A., La ergonomía en la prevención de problemas de salud en los trabajadores y su impacto social, Revista Cubana de Ingeniería, [en línea]. 10(2), pp. 3-15, 2019. Disponible en: https://rci.cujae.edu.cu/index.php/rci/article/view/720

[3] Sandoval, O.G.V., Alendes, A.M.H., Mendoza, J.C., Cabanillas, P.E.S., Bonifacio, H.C.M., and Sixto, V.V.C., Meaningful learning in the context of the pandemic. A systematic review, Horizontes Revista de Investigación en Ciencias de la Educación, 6(23), pp. 458-465, 2022. DOI: https://doi.org/10.33996/revistahorizontes.v6i23.348

[4] Charles, R.L. and Nixon, J., Measuring mental workload using physiological measures: a systematic review, Applied Ergonomics, 74, pp. 221-232, 2019. DOI: https://doi.org/10.1016/j.apergo.2018.08.028

[5] Tellez-Bedoya, C.A., and Tellez-Bedoya, C., Retos de la salud mental para la cuarta revolución industrial en las empresas de Colombia, Tendencias, 23(2), pp. 329-355, 2022. DOI: https://doi.org/10.22267/rtend.222302.211

[6] Rojas-Romero, R., Valdés-González, H., and Reyes-Bozo, L., Digital transformation: opportunity or threat to employability?, Revista Facultad de Ingeniería, 30(56), art. 13297, 2021. DOI: https://doi.org/10.19053/01 211129.v30.n56.2021.13297

[7] Torres, Y., y Rodríguez, Y., Surgimiento y evolución de la ergonomía como disciplina: reflexiones sobre la escuela de los factores humanos y la escuela de la ergonomía de la actividad, Revista Facultad Nacional de Salud Pública, 39(2), e342868, 2021. DOI: https://doi.org/10.17533/udea.rfnsp.e342868

[8] Ormaza-Murillo, M.P., Zambrano-Rivera, A.D., Zamora-Napa, S.C., Parra-Ferié, C., and Félix-López, M., Carga mental de profesores de la Escuela Superior Politécnica Agropecuaria de Manabí, Ingeniería Industrial, [en línea]. 40(1), pp. 3-13, 2019. Disponible en: https://scielo.sld.cu/scielo.php?pid=S1815-59362019000100003&script=sci_arttext&tlng=en

[9] Acosta-Prieto, J.L, García-Dihigo, J., Cuello-Cuello, Y., Almeda-Barrios, Y., and Ulloa-Felipe, A.B., Application of indicators associated with mental fatigue in sanitary personnel from Heroes del Moncada Polyclinic in Cárdenas municipality, Cuba. DYNA, 90(226), pp. 107-114, 2023. DOI: https://doi.org/10.15446/dyna.v90n226.106638

[10] Jiménez-Arias, M.S., y Soto-Gutiérrez, Y., Envejecimiento saludable basado en el fortalecimiento de las capacidades cognitivas y el reforzamiento de prácticas saludables de un grupo de personas adultas mayores, Población y Salud en Mesoamérica. [en línea]. 17(2), pp. 255-275, 2019. Disponible en: https://www.scielo.sa.cr/scielo.php?pid=S1659-02012020000100255&script=sci_arttext

[11] Jeffri, N.F.S., and Rambli, D.R.A., A review of augmented reality systems and their effects on mental workload and task performance, Heliyon, 7(3), pp. e06277, 2021. DOI: https://doi.org/10.1016/j.heliyon.2021.e06277

[12] Durán-Coronado, A.A., Maldonado-Macías, A.A., Barajas-Bustillos, M.A., and Hernández-Arellano, J.L., Análisis cognitivos de carga mental e identificación del error humano para mejorar la experiencia de usuario. Ciencia UAT, 14(1), pp. 71-84, 2019. DOI: https://doi.org/10.29059/cienciauat.v14i1.1173

[13] Dehais, F., Lafont, A., Roy, R., and Fairclough, S., A neuroergonomics approach to mental workload, engagement and human performance, Frontiers in Neuroscience, 14(268), art. 0268, 2020. https://doi.org/10.3389/fnins.2020.00268

[14] Gallardo-Gallardo, M.I., Herrán-Peñafiel, J.W., y Carrera-Viver, G.J., Carga mental y desempeño laboral en los trabajadores de una empresa industrial, Revista Científica Retos de la Ciencia, [en línea]. 3(6), pp. 26-44, 2019. Disponible en: https://retosdelaciencia.com/Revistas/index.php/retos/article/view/263

[15] Rivera-Rojas, F., Ceballos-Vásquez, P. y Vílchez-Barboza, V., Carga mental y la calidad de vida relacionada con salud en trabajadores Oncológicos, Revista Salud Uninorte, 36(3), pp. 545-557, 2020. DOI: https://doi.org/10.14482/sun.36.3.616.99

[16] Cobiellas-Carballo, L.I., Anazco-Hernández, A., y Góngora-Gómez, O., Estrés académico y depresión mental en estudiantes de primer año de medicina, Educación Médica Superior, [en línea]. 34(2), 2020. Disponible en: https://scielo.sld.cu/scielo.php?pid=S0864-21412020000200015&script=sci_arttext&tlng=pt

[17] Bezerra-de Mello, M.C.M., Cantor-Cultiva, I.C. y Ferreira, L.P., Panorama de tres países latinoamericanos en problemas de voz

relacionados con condiciones de trabajo, CoDAS, 33(5), pp. e20200304, 2021. DOI: https://doi.org/10.1590/2317-1782/20202020304
[18] Duarte-Castillo, S.M. y Vega-Campos, M.Á., Perspectivas y retos de la NOM-035-STPS-2018 para la atención de riesgos psicosociales y la promoción de entornos organizacionales favorables en México, Trascender, Contabilidad y Gestión, 6(17), pp. 48-86, 2021. DOI: https://doi.org/10.36791/tcg.v0i17.101
[19] Vera-Ávila, C.A., Rodríguez-Rojas, Y.L., y Hernández-Cruz, H.W., Medición del desempeño del sistema de gestión de seguridad y salud en el trabajo: revisión sistemática de literatura, Revista CEA, 8(18), pp. e2052, 2022. DOI: https://doi.org/10.22430/issn.2422-3182
[20] Acosta-Prieto, J.L., Cuello-Cuello, Y., García-Dihigo, J. and Almeda-Barrios, Y., Models for mental workload assessment: a systematic review, Revista San Gregorio, 1(55), pp. 158-180, 2023. DOI: https://doi.org/10.36097/rsan.v1i55.2272
[21] Hernández-Gracia, T.J. y Carrión-García, M.D.L Á., Riesgos laborales de tipo psicosocial y desgaste psíquico en trabajadores de una administración pública mexicana, Revista Salud Uninorte, 37(3), pp. 628-646, 2021. DOI: https://doi.org/10.14482/sun.37.3.613.62
[22] Cruz-Zuñiga, N., Alonso-Castillo, M.M., Armendáriz-García, N.A., and Lima-Rodríguez, J.S., Clima laboral, estrés laboral y consumo de alcohol en trabajadores de la industria. Una revisión sistemática, Revista Española de Salud Pública, [en línea]. 95, e202104057, 2022. Disponible en: https://www.scielosp.org/article/resp/2021.v95/e202104057/es/
[23] Canel-Bermúdez, M.D. and Delgado-Fernández, M., Gestión del gobierno orientado a la innovación: contexto y caracterización del modelo, Revista Universidad y Sociedad, [en línea]. 13(1), pp. 6-16, 2021. Disponible en: https://scielo.sld.cu/scielo.php?script=sci_arttext&pid=S2218-36202021000100006b
[24] Sarmiento-Reyes, Y.R. y Delgado-Fernández, M., Dimensiones y variables de competitividad para un mejor desempeño empresarial, Cofín Habana, [en línea]. 15(2), 2021. Disponible en: https://scielo.sld.cu/scielo.php?pid=S2310-340X2020000300409&script=sci_abstract&tlng=pt
[25] Acosta-Prieto, J.L., Tecnología para la gestión de carga mental en puestos de trabajo con demandas cognitivas. Aplicación en entidades cubanas. Disertacion, Doctoral, Facultad de Ciencias Técnicas, Universidad de Matanzas, Cuba, [en línea]. 2023. Disponible en: https://rein.umcc.cu/handle/123456789/2188
[26] Catalá-Rivero, R.C. Estudio de valoración del trabajo mental en los coordinadores de rampa de la UEB aeropuerto Juan Gualberto Gómez Tesis de Grados MSc., Facultad de Ingeniería Industrial, Universidad de Matanzas, Cuba, [en línea]. 2023. Disponible en: https://rein.umcc.cu/handle/123456789/2327
[27] Martínez-García, L.L. Propuesta de procedimiento para evaluar puestos de trabajo con elevada demanda cognitiva en el Ministerio de Trabajo, Municipio Cárdenas. Tesis de Grado, Facultad de Ingeniería Industrial, Universidad de Matanzas, Cuba, [en línea]. 2021. Disponible en: https://rein.umcc.cu/handle/123456789/938
[28] Almirall, P., Santander, J., y Vergara, A. La variabilidad de la frecuencia cardiaca como indicador del nivel de activación ante el esfuerzo mental, Revista Cubana de Higiene y Epidemiología, [en línea]. 33(1), pp. 3-4, 1995. Disponible en: https://scielo.sld.cu/scielo.php?script=sci_arttext&pid=S1561-30031995000100002
[29] Acosta-Prieto, J.L. Valoración del comportamiento de indicadores relacionados con la carga mental en estudiantes de Ingeniería Industrial de la Universidad de Matanzas. Tesis de Grado, Facultad de Ingeniería Industrial, Universidad de Matanzas, Cuba, 2019.

Y. Cuello-Cuello, is BSc. Eng in Industrial Engineer since 2021, from the University of Matanzas, Cuba. He belongs to the Cognitive Ergonomics Scientific Group, where he has developed theoretical and practical research on mental work. She is studying for a master's degree in Ergonomics and Occupational Safety and Health. She is currently a professor at the University of Matanzas.
https://orcid.org/0000-0003-4589-8670

J.L. Acosta-Prieto, is BSc. Eng. in Industrial Engineer from the University of Matanzas, Cuba, graduated with a degree and scientific merit award. MSc. in Ergonomics and Occupational Health and Safety and MBA Service Management module. PhD in Technical Sciences of Industrial Engineering in the research line of Cognitive Ergonomics. In 2021 he obtained the CITMA National Award as a student researcher, in 2021 the Seal of Future Shapers. In 2020 he was Vice-Dean of the Faculty of Business Sciences of the University of Matanzas, from 2021-2023 Director of the Municipal University Center of Cárdenas and from 2023-present Director of Research and Postgraduate Studies of the University of Matanzas.
ORCID: 0000-0003-1390-2380

E. Dueñas-Reyes, is BSc. Eng. in Industrial Engineer in 2020, from the University of Matanzas, Cuba. Worked as Math teacher since 2018 in the same university. MSc. in Business Administration in 2023.
ORCID: 0000-0002-6332-0752

J. García-Dihigo, is BSc. Eng. in Industrial Engineer. PhD in Technical Sciences in 1988 and PhD in Sciences in 2017. He has taught different subjects related to occupational risk prevention, ergonomics and environment. He is a full professor at the University of Matanzas, Cuba. He has published 63 articles in journals from different countries, 17 of them indexed in group 1 and group 2 databases. He has participated in 103 national and international events in different Latin American countries. He is a methodologist of the Rector's Office of the University of Matanzas where he is in charge of the International Center of Havana, which is an auditing and consulting company. He has been tutor of 10 Doctors in Technical Sciences and 80 Masters in different branches of science.
ORCID: 0000-0002-8791-5830

Z. Domínguez-Gómez, is MBA. Consulting professor at the University of Matanzas, Cuba. Director of the Language Center of the University of Matanzas. Her areas of expertise are ELT and teacher training. She has authored and co-authored some articles and papers on foreign language teaching and teacher training.
ORCID: 0000-0003-1914-2597

DYNA
http://dyna.medellin.unal.edu.co/

UNIVERSIDAD NACIONAL DE COLOMBIA

Herramienta computacional para diseño y optimización de tratamientos squeeze de inhibición de incrustaciones

Carolina Leon-Vanegas [a], Diego Armando Vargas-Silva [b], Farid Bernardo Cortes-Correa [a] & Hernando Buendía-Lombana [b]

[a] Universidad Nacional de Colombia, Sede Medellín, Facultad de Minas, Departamento de Procesos y Energía, Medellín, Colombia. carolina.leonva@ecopetrol.com.co, fbcortes@unal.edu.co
[b] Escuela de Ingeniería de Petróleos, Universidad Industrial de Santander, Colombia. diego.vargas4@correo.uis.edu.co, hernandobuendia@hotmail.com

Received: February 29th, 2024. Received in revised form: May 6th, 2024. Accepted: May 21st, 2024.

Abstract
Physicochemical studies of water show that there is currently an encrusting trend in 24 oil fields in Colombia. This implies that the water has a tendency to precipitate different scales, mainly calcium carbonate and barium sulfate. Emerging the need to implement tools that allow avoiding or delaying precipitation and deposition, through the design and optimization of squeeze treatments. Therefore, a mathematical model applicable to sandstone formations was selected, which was validated for linear and radial flow through literature, laboratory and field, allowing to estimate the distribution of the inhibitor along the plug during adsorption, and its subsequent related release with the desorption phenomenon. This methodology was analyzed under conditions of pressure and flow rates present in the field, allowing the prediction of the useful life of the treatment to be estimated, and the effect of the injected pore volumes and production flow rate on the duration of treatment, concluding that high flow rates have a negative effect on the duration of squeeze treatments. Furthermore, the designed tool allows modeling of adsorption and desorption of inhibitors and constitutes a significant contribution to the prevention of damage to the formation caused by inorganic scales, since there is currently no free software for this purpose.

Keywords: computational tool; squeeze; numerical modelling; adsorption; desorption; scales; formation damage

Computational tool for design and optimization of scale inhibitor squeeze treatments

Resumen
Estudios fisicoquímicos de aguas evidencian que actualmente existe una tendencia incrustante en 24 Campos Petroleros de Colombia. Esto implica que el agua tiene tendencia a precipitar diferentes escamas, principalmente carbonato de calcio y sulfato de bario, surgiendo la necesidad de implementar herramientas para evitar o retardar la precipitación y depositación, mediante el diseño y optimización de tratamientos squeeze. Por tanto, se seleccionó un modelo matemático aplicable a formaciones de areniscas, el cual se validó para flujo lineal y radial mediante literatura, laboratorio y campo, permitiendo estimar la distribución del inhibidor a lo largo del plug durante la adsorción, y su posterior liberación relacionada con el fenómeno de desorción. Dicha metodología se validó en condiciones de presión y caudales en campo, permitiendo estimar la predicción de la vida útil del tratamiento, y se analiza el efecto de los volúmenes porosos inyectados, y caudal de producción sobre la duración del tratamiento, concluyendo que los caudales altos presentan un efecto negativo sobre la duración de los tratamientos squeeze. Además, la herramienta diseñada, permite modelamiento de adsorción y desorción de inhibidores y constituye un aporte significativo para la prevención del daño a la formación ocasionado por escamas inorgánicas, ya que actualmente no se cuenta con software comercial para este propósito.

Palabras clave: herramienta computacional; squeeze; modelamiento numérico; adsorción; desorción; escamas; daño a la formación.

1 Introducción

La formación de incrustaciones o escamas inorgánicas constituye un grave problema para la industria del petróleo y gas, durante la producción de los fluidos del pozo. Las incrustaciones pueden depositarse sobre cualquier superficie,

How to cite: Leon-Vanegas, C., Vargas-Silva, D.A., Cortes-Correa, F.B. and Buendía-Lombana, H., Computational tool for design and optimization of scale inhibitor squeeze treatments. DYNA, 91(232), pp. 121-130, April - June, 2024.

formando una capa cada vez más gruesa, debido al crecimiento continuo de los cristales por adsorción de iones, sobre las imperfecciones de los mismos, ocasionando obstrucción en los canales de flujo del medio poroso o en los pozos, causando daño a la formación y pérdida de productividad, principalmente por reducción de la permeabilidad [1]. Por lo anterior, investigaciones previas han caracterizado este fenómeno estudiando las causas de arrastre, precipitación e impacto en la producción [2].

Además del medio poroso, también se pueden depositar sobre los equipos de superficie causando su mal funcionamiento, o pueden aparecer en cualquier parte a lo largo de los tubos de producción, reduciendo el diámetro interno y bloqueando el flujo; e incluso pueden formarse en las plantas de tratamiento [3]. Lo que lleva a la industria a proponer soluciones de prevención y mitigación, ya sea enfoca a equipos y tuberías [4] o a tratamientos en la cara de pozo para mejorar la permeabilidad [5]

Como consecuencia de la precipitación y posterior depositación, el flujo se reduce a tal punto que puede producirse el abandono del pozo. Adicionalmente, a pesar de la utilización de técnicas de remoción y tratamientos de inhibición, se presentan problemas de taponamiento por depositación de escamas minerales, una vez que se alcanza la Concentración Mínima de Inhibidor (MIC), lo cual significa pérdidas de producción mensual de hasta 1500 Barriles (bbl). Por lo tanto, los costos por la formación de incrustaciones son muy significativos, y la solución a estos problemas le cuesta a la industria cientos de millones de dólares por año en términos de mantenimiento y pérdidas de producción cuando se deja de extraer crudo [6]. Debido a lo anterior, surge la necesidad de plantear modelamientos numéricos para entender estos fenómenos de daño a la formación, no solo por escamas sino también por migración de finos y su respectivo escalado a yacimiento, permitiendo estudiar el efecto que este tipo de daño genera sobre la producción, sentando las bases para el uso de estos modelos a escala de yacimiento [7]. El presente documento incluye un estudio enfocado a condiciones de laboratorio y condiciones de campo, abarcando el ámbito conceptual y numérico, con el fin de plantear una herramienta computacional, la cual, luego de ser validada con datos reales, permite predecir la durabilidad de los tratamientos de inhibición en campo y, por tanto, se puede saber en cuanto tiempo debe realizarse un nuevo tratamiento squeeze, evitando los costos asociados a la depositación y remoción de incrustaciones

2 Metodología

2.1 Modelamiento de los fenómenos adsorción y desorción a condiciones de laboratorio

En la Fig. 1, se observa el diagrama esquemático de una prueba coreflood. Estas pruebas de laboratorio se realizan con el objetivo de simular un tratamiento químico squeeze en yacimiento, siendo una herramienta vital para el entendimiento de los mecanismos que controlan la interacción roca – inhibidor.

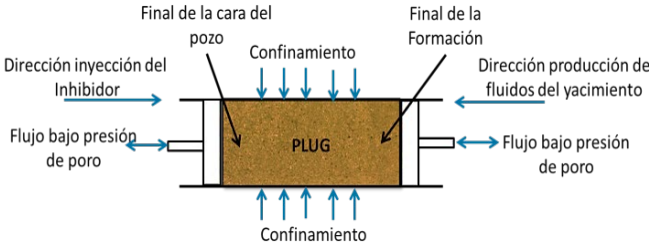

Figura 1; Representación Esquemática de una prueba de coreflood
Fuente: Elaboración propia

El desplazamiento ilustrado (Fig. 1), puede ser analizado mediante un modelo matemático que describe el proceso de adsorción/desorción en laboratorio (ec. 1) [8]

$$\frac{\partial C}{\partial t} = D\left(\frac{\partial^2 C}{\partial x^2}\right) - V\frac{\partial C}{\partial x} - \frac{\rho}{\Phi}\left(\frac{\partial \Gamma}{\partial t}\right) \quad (1)$$

Donde C es la concentración del inhibidor en la fase móvil (g/L o mg/cm3), Γ es el nivel de adsorción (mg/g), D es el coeficiente de dispersión (cm2/s), V la velocidad superficial (cm/s), ϕ la porosidad, ρ la densidad de la roca (g/cm3), x la distancia (cm) y t el tiempo. Debido a la dificultad para medir la dispersión física D, algunos autores consideran este término nulo [8]. En equilibrio, cuando los efectos cinéticos son secundarios, es decir, la tasa de adsorción es muy rápida comparada con la tasa de flujo de fluido, el nivel de adsorción (Γ) permanece constante, solo depende de la concentración del inhibidor (Ec. (2)).

$$-\frac{\rho}{\Phi}\left(\frac{\partial \Gamma}{\partial t}\right) = -\frac{\rho}{\Phi}\left(\frac{\partial \Gamma}{\partial C}\right)\left(\frac{\partial C}{\partial t}\right) \quad (2)$$

Una forma analítica utilizada para describir el nivel de adsorción como función de la concentración son las isotermas de adsorción de Freundlich (Ec. (3)) [9]:

$$\Gamma = k * C^{ni} \quad (3)$$

Como se mencionó anteriormente, Γ representa el nivel de adsorción, C la concentración de la solución, y la forma de la isoterma es gobernada por los parámetros k y ni determinados de manera experimental. El término ∂Γ/∂C de la ec. (2) es el gradiente de la isoterma de adsorción a la concentración C. Teniendo en cuenta las suposiciones anteriores, el modelo matemático para representar el fenómeno de adsorción se muestra en la ec. (4).

$$\frac{\partial C}{\partial t} = -\frac{V}{1 + \frac{\rho}{\Phi}\left(\frac{\partial \Gamma}{\partial C}\right)}\left(\frac{\partial C}{\partial x}\right) \quad (4)$$

La ec. anterior no tiene solución analítica simple, por lo tanto, se debe solucionar mediante aproximaciones numéricas, en este caso diferencias finitas (ec. (5)) donde los superíndices hacen referencia al tiempo y los subíndices hacen referencia al espacio. A continuación, se muestran las aproximaciones de la primera derivada con respecto al tiempo y la distancia.

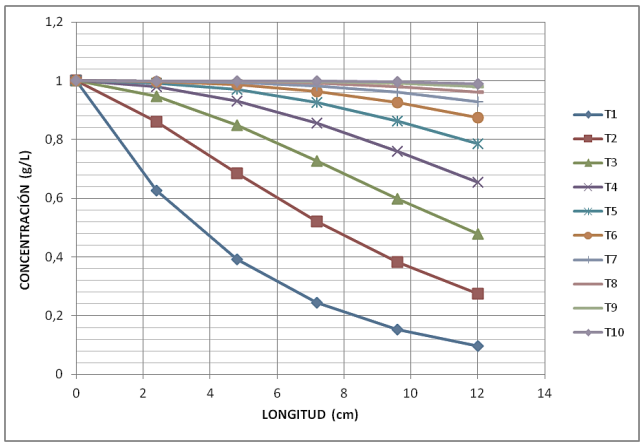

Figure 2. Concentración del inhibidor en función de la distancia para diferentes tiempos
Fuente: Elaboración propia

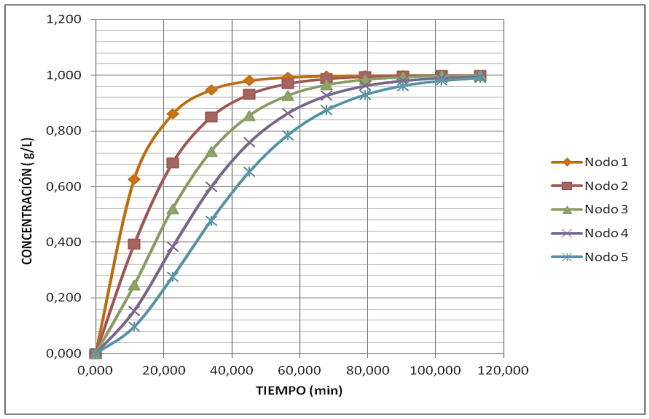

Figura 3: Concentración del inhibidor en del tiempo para diferentes nodos
Fuente: Elaboración propia

$$\frac{\partial C}{\partial t} = \frac{C_i^{n+1} - C_i^n}{\Delta t} \quad y \quad \frac{\partial C}{\partial x} = \frac{C_i^{n+1} - C_{i-1}^{n+1}}{\Delta x} \tag{5}$$

Existen tres formas de solucionar estas aproximaciones: implícita, explícita y una combinación entre estas (Crank–Nicolson). Para el caso de estudio se utilizó la forma implícita, se construyeron las respectivas matrices para un modelo 1D y mediante Excel se generó la inversa y su respectiva solución para distintos tiempos iniciando en cero (0) y finalizando hasta el tiempo necesario para que la concentración se acerque a cero (0), los resultados se evidencian en la Fig. 2

La Fig. 2 corresponde al fenómeno de adsorción, donde se observa la concentración del inhibidor en función de la longitud del plug para distintos tiempos. Para el tiempo 1 la concentración del inhibidor cae drásticamente al pasar por la roca, debido a que el fluido que tiene la muestra inicialmente es solo salmuera (no hay inhibidor en el plug para el tiempo cero). Para los tiempos posteriores, la concentración del inhibidor en la fase móvil se mantiene debido a que la roca ya tiene fluido con inhibidor, por lo tanto, la concentración a la salida de la muestra es cercana a la inicial.

En la Fig. 3 se puede observar el aumento de concentración de inhibidor en cada Δx del plug, que para efectos prácticos serán llamados Nodos, como función del tiempo. Estas curvas representan la concentración de inhibidor que es retenida en la roca, mediante adsorción del inhibidor sobre la superficie de los granos, debido a interacciones electrostáticas y de Van der Waals entre las moléculas del inhibidor y los minerales de la roca [10-12].

Posterior al proceso de inyección del inhibidor en la muestra, se realiza un contraflujo para simular la producción del pozo. En esta parte de la prueba se analiza la desorción, la cual consiste en la liberación del inhibidor que fue adsorbido en la etapa anterior. Durante la desorción el nivel de adsorción (Γ) varía con el tiempo mediante la ec. (6).

$$\left(\frac{\partial \Gamma}{\partial t}\right)_c = r(\Gamma_{eq}(c) - \Gamma) \tag{6}$$

Donde el término $\Gamma_{eq}(c)$ se expresa mediante la isoterma de Freundlich y r es la tasa de desorción. El fenómeno de desorción puede ser representado mediante las ecuaciones (1) y (6), teniendo en cuenta que se considera nulo el valor del coeficiente de dispersión y por lo tanto no se incluye. Para solucionar la ec. (6) se utiliza una aproximación numérica que representa el nivel de adsorción en función del tiempo como se muestra en la ec. (7).

$$\frac{\partial \Gamma}{\partial t} = \frac{\Gamma_i^{n+1} - \Gamma_i^n}{\Delta t} \tag{7}$$

A partir de las ecuaciones (1) y (2), y las aproximaciones numéricas (5) y (6) se obtiene un sistema de dos ecuaciones con dos incógnitas, mediante el cual se solucionan las ecuaciones con métodos iterativos multivariables, para realizar el modelamiento de la desorción del inhibidor en flujo lineal (a nivel de laboratorio).

En la Fig. 4 se representa gráficamente el fenómeno de desorción, mediante la variación de la concentración del inhibidor en función de los volúmenes porosos de agua producida. Cabe resaltar que el nodo 3 corresponde a la salida

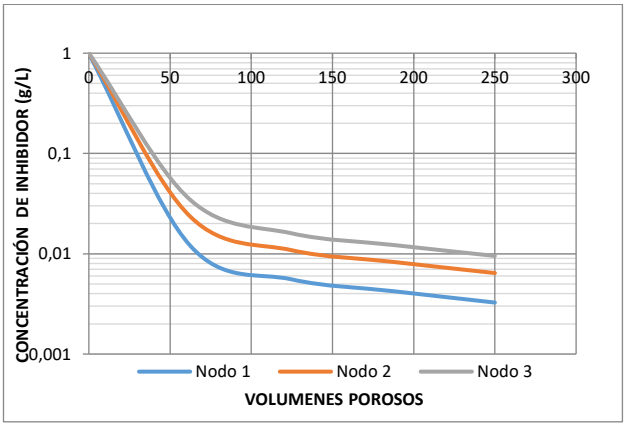

Figura 4 Modelamiento de la desorción de inhibidor durante una prueba coreflood (Residuales de Inhibidor para flujo lineal).
Fuente: Elaboración propia

del plug y por lo tanto representa la concentración en la cara del pozo. Se puede observar que luego de producir 250 volúmenes porosos, la concentración del inhibidor a la salida del plug es aprox. 0,01 g/L (10 ppm). Esta concentración es importante ya que, según el tipo de inhibidor se determina si aún evita la formación de escamas, o si se debe realizar una nueva inyección del tratamiento.

A nivel experimental es necesario desplazar agua de formación en sentido de producción, hasta llegar a la Concentración Mínima de Inhibidor (MIC), ya que por debajo de este valor el inhibidor no es efectivo para evitar la depositación de incrustaciones y por tanto debe realizarse nuevamente un tratamiento Squeeze.

2.2 Modelamiento de los fenómenos adsorción y desorción en campo

En la Fig. 5 se observa el esquema de un tratamiento Squeeze en campo.

El tratamiento realizado en campo, tiene el mismo principio teórico de la prueba de laboratorio. La ec. (8) representa esta prueba, en unidades de campo.

$$\frac{\partial C}{\partial t} = -\frac{\beta}{r}\frac{\partial C}{\partial r} - \frac{(1-\Phi)}{\Phi * S_w}\left(\frac{\partial \Gamma}{\partial t}\right) \tag{8}$$

Donde el término β está representado por ec. (9)

$$\beta = \frac{Q}{2\pi h \Phi S_w} \tag{9}$$

Utilizando las ecuaciones (6) y (8), y las aproximaciones (5) y (7) se soluciona el modelo mediante métodos numéricos multivariables obteniendo resultados de desorción. En la Fig. 6 se observa el fenómeno de desorción en campo, mostrando la concentración remanente del inhibidor en el agua producida durante determinado tiempo. Esta concentración es de gran importancia pues determina si el tratamiento aun es efectivo, para este caso con una concentración inicial de 1 g/L y un caudal de 400 Barriles Por Día (BPD) después de 200 días, existía una concentración de 24.8 ppm (0.0248 g/L).

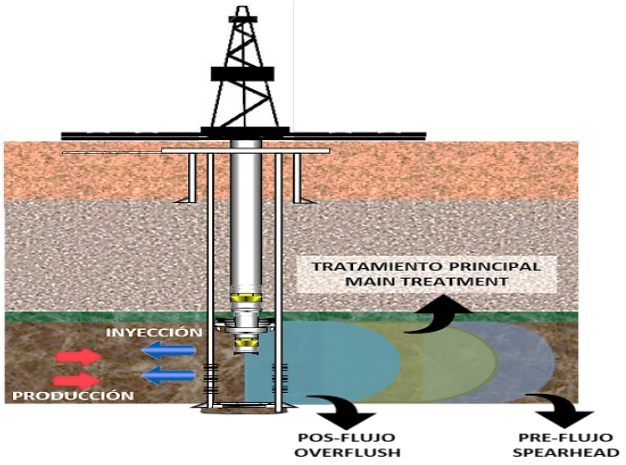

Figura 5: Esquema gráfico de un Tratamiento "Squeeze"
Fuente: Elaboración propia

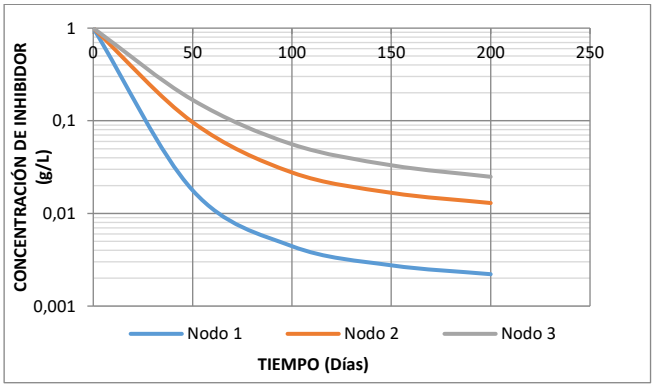

Figura 6: Modelamiento de la desorción de inhibidor a nivel de campo (Residuales de inhibidor para flujo radial).
Fuente: Elaboración propia

El modelo también permite simular la distribución areal de la concentración del inhibidor en campo, y la variación de concentración en función de la distancia al pozo, para cada etapa del tratamiento squeeze. Para el caso del pre-flujo se observan en la Figs. 7 y 8.

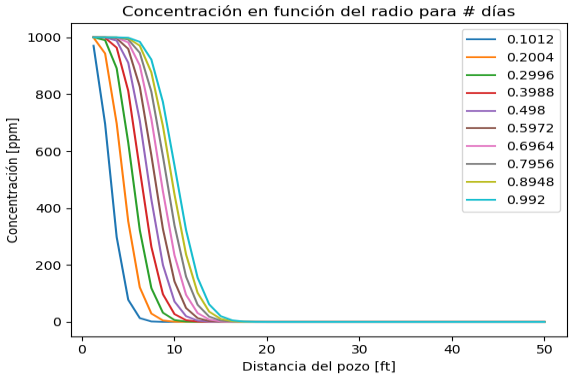

Figura 7: Variación de la concentración de Inhibidor en función de la distancia al pozo (etapa de pre-flujo)
Fuente: Elaboración propia

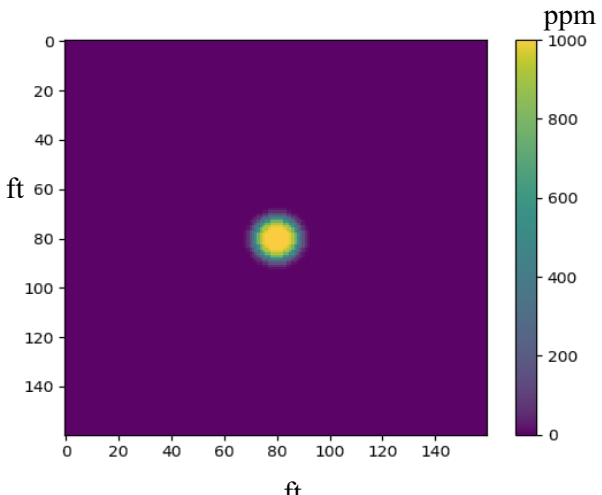

Figura 8: Distribución areal de la concentración de inhibidor durante la etapa de Pre-flujo, (distancias en ft)
Fuente: Elaboración propia

De acuerdo con el diagrama sobre el plano de la Fig. 8, se puede observar la variación de la concentración del inhibidor en el pozo al inicio de la inyección (Máxima concentración) y a determinada distancia del pozo cuando la concentración es cero, mediante la barra de color rojo a azul. Finalizado el tiempo de inyección de pre-flujo la concentración de inhibidor en la cara del pozo es de 1000 ppm.

Luego del pre-flujo, se procede a inyectar el tratamiento, en la Figura se observa la variación de concentración de inhibidor en el pozo al inicio de la inyección del tratamiento. Posteriormente la concentración de inhibidor en todo el pozo es de 100000 ppm, lo cual está representado por el circulo de color amarillo. Así mismo, mediante la Figs. 7 y 9 se puede monitorear la concentración de inhibidor alrededor del pozo, para diferentes días.

Para la siguiente etapa, en la Fig. 11 se puede observar el efecto de la inyección del overflush, desplazando el tratamiento de inhibición inyectado previamente para ubicarlo lo más lejos posible del pozo con el propósito de obtener el mayor tiempo de vida del tratamiento squeeze.

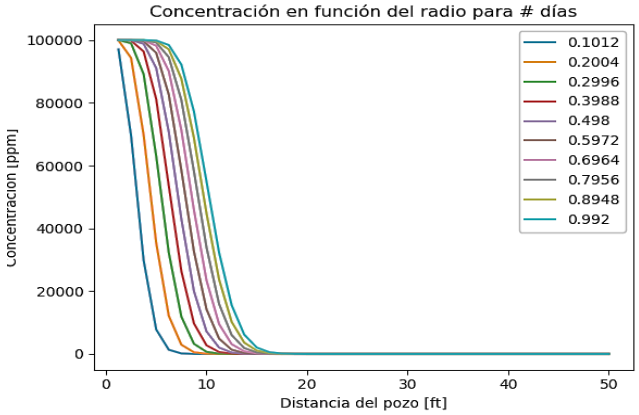

Figura 9: Variación de la concentración de Inhibidor en función de la distancia al pozo (etapa de tratamiento)
Fuente: Elaboración propia

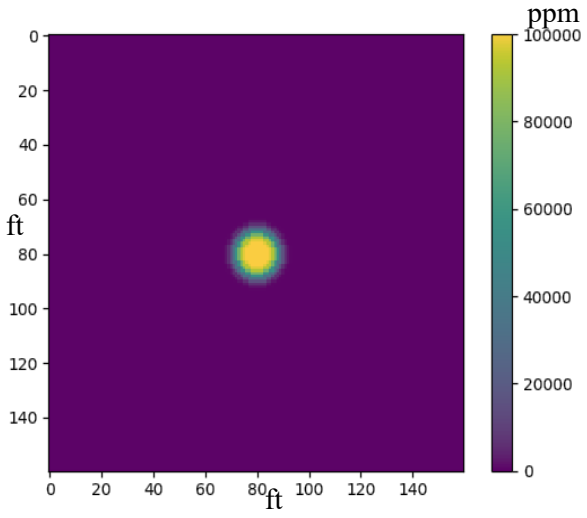

Figura 10: Distribución areal de la concentración de inhibidor durante la etapa de Tratamiento
Fuente: Elaboración propia

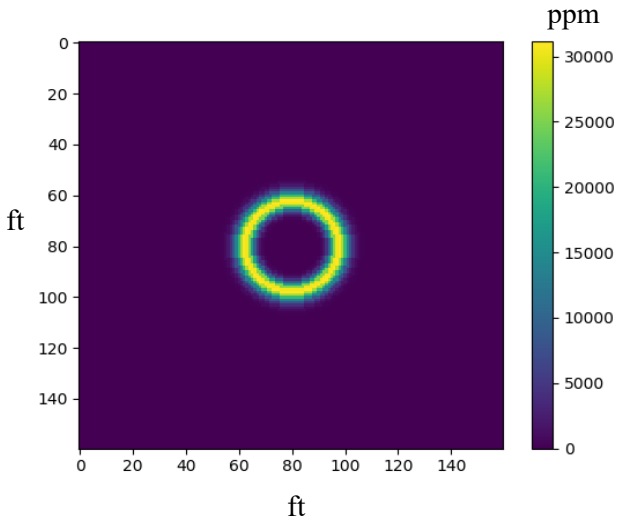

Figura 11: Concentración de Inhibidor después de la inyección de Overflush
Fuente: Elaboración propia

Así mismo, en la Fig. 12 se puede monitorear la concentración del inhibidor alrededor del pozo (radial), evidenciando que, para cualquier tiempo, la concentración de inhibidor aumenta a medida que la distancia al pozo se hace mayor, hasta un valor máximo y posteriormente disminuye hasta llegar a cero.

En la Fig. 13 se pueden observar la variación de concentración en el tiempo, para cada nodo a determinada distancia del pozo. Finalmente, se inicia la desorción, en las Figs. 14 y 15 se evidencia la concentración de inhibidor en el agua de formación después de 500 días de producción. Para este caso, la concentración de inhibidor es de aproximadamente 0.3 ppm

Estas simulaciones son muy importantes, ya que el monitoreo de la concentración a través del tiempo permite evitar la depositación de escamas en la formación y cara del pozo. Es de resaltar que en la Fig. 15 se hace la comparación con un modelo conceptual realizado en ECLIPSE con el fin de soporta el modelo numérico y darle mayor veracidad, antes de pasar a la etapa de optimización y comparación con campo.

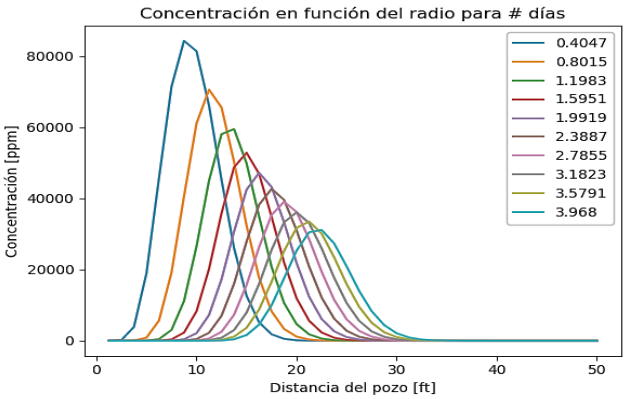

Figura 12: Variación de la concentración de Inhibidor en función de la distancia al pozo (etapa de overflush)
Fuente: Elaboración propia

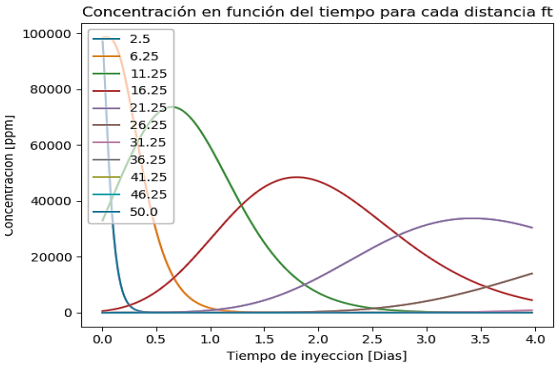

Figura 13: Variación de la concentración de inhibidor en función del tiempo de inyección
Fuente: Elaboración propia

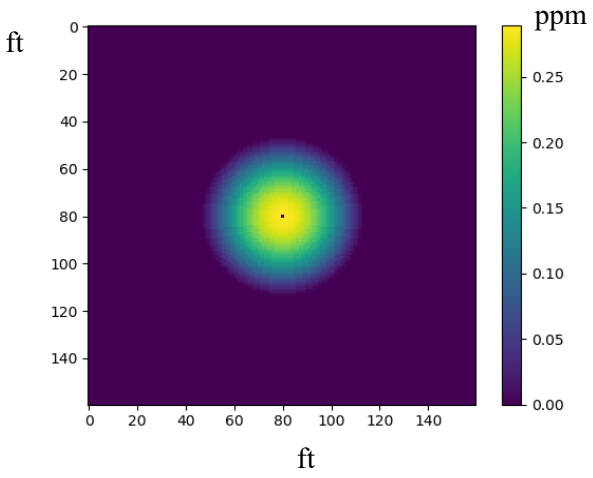

Figura 14: a) Distribución areal de la concentración de inhibidor durante la etapa de Desorción, b) Vista superior de la etapa de desorción
Fuente: Elaboración propia

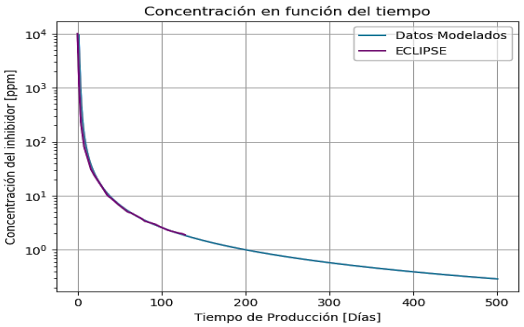

Figura 1: Curva de Desorción del inhibidor
Fuente: Elaboración propia

3 Resultados

3.1 Optimización de tratamientos squeeze mediante la herramienta computacional construida

La principal aplicación del modelo consiste en la posibilidad de realizar optimización de tratamientos de inhibición, mediante la evaluación de parámetros operacionales como el caudal de producción, la cantidad de inhibidor a inyectar, o la concentración del tratamiento de inhibición. De esta manera se puede determinar el valor apropiado de volúmenes porosos que deben ser inyectados, para alcanzar la saturación total de la roca. Con respecto al caudal de producción, es posible determinar el efecto del cambio en la tasa de producción de un pozo, sobre la duración de un tratamiento squeeze para inhibición de incrustaciones. Así mismo, se pueden realizar simulaciones para diferentes concentraciones de inhibidor, con el propósito de determinar la concentración optima que permita mayor durabilidad del tratamiento de inhibición. Adicionalmente, es posible conocer el comportamiento de un inhibidor previo a la inyección en campo, a partir pruebas realizadas en laboratorio a condiciones de yacimiento.

3.2 Impacto del volumen de inhibidor inyectado en la adsorción

Para este análisis consideramos un plug de porosidad 20%, longitud 12 cm y radio 1.5 cm. La variable a analizar son los volúmenes porosos inyectados a un caudal de 1.5 cm3/min, para diferentes concentraciones iniciales de inhibidor. En la Fig. 16, se representa la concentración del inhibidor a la salida del plug en función de los volúmenes porosos inyectados, para dos concentraciones de inhibidor 1 g/L y 3 g/L. De acuerdo con el diagrama, hay un número de volúmenes porosos en los cuales se alcanza la concentración máxima en la fase móvil (se satura la muestra); lo cual, permite establecer un máximo de volúmenes porosos a inyectar durante un tratamiento de inhibición a escala de laboratorio, que es fundamental para definir de manera óptima el volumen de inhibidor a emplear a condiciones reales de campo, evitando sobrecostos y logrando tratar toda la región de interés.

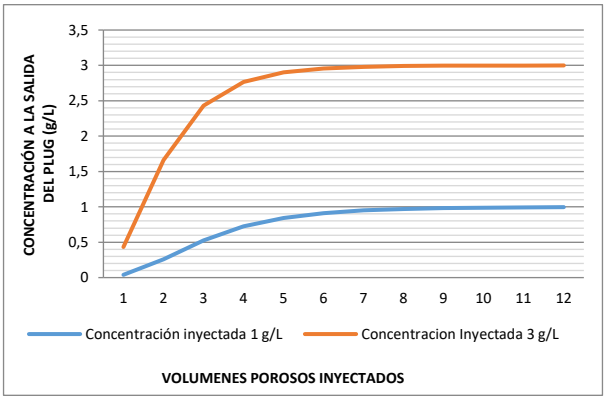

Figura 2: Efecto de los volúmenes porosos inyectados
Fuente: Elaboración propia

3.3 Impacto del caudal de producción sobre la desorción del tratamiento de inhibición

En la Fig. 17, se observa que para un caudal de 100 BPD el tratamiento tiene una mayor duración, comparado con el caudal de 200 BPD, y este dura más comparado con el de 300

BPD; sin embargo, para caudales superiores a 400 BPD se obtienen tiempos de vida similares del tratamiento químico, lo que significa que a estos caudales baja al mínimo la concentración del inhibidor.

4 Validación y discusión

El modelo se validó utilizando algoritmos escritos en el lenguaje de programación de Python, para flujo lineal y radial con datos de literatura, laboratorio, y campo. En las Figs. 18 y 19 se encuentra la comparación entre los datos simulados y los reportados en literatura, para pruebas coreflood con muestras sintéticas. La validación con datos de laboratorio se realizó mediante pruebas de desplazamiento con plugs de campos colombianos como: Acaé, Cusiana, y Cupiagua.

En las Figs. 20 a 23 se encuentran las simulaciones y datos experimentales para muestras de roca de los campos mencionados, y en la Fig. 24 se presenta una de las simulaciones realizadas para un pozo de campo Cusiana.

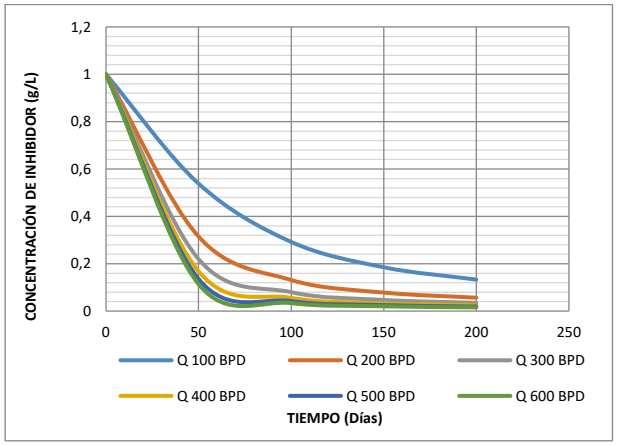

Figura 17: Efecto del caudal sobre la duración del tratamiento squeeze.
Fuente: Elaboración propia

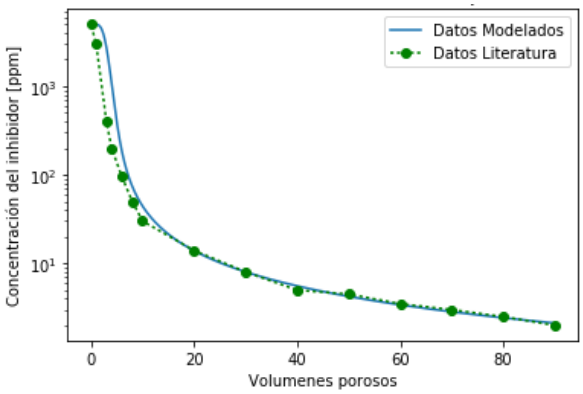

Figura 18: Validación del modelo para flujo lineal con datos de literatura Muestra Sintética # A
Fuente: Elaboración propia

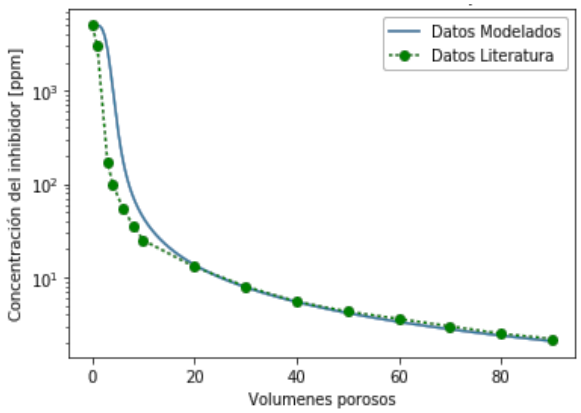

Figura 19: Validación del modelo para flujo lineal con datos de literatura Muestra Sintética # B
Fuente: Elaboración propia

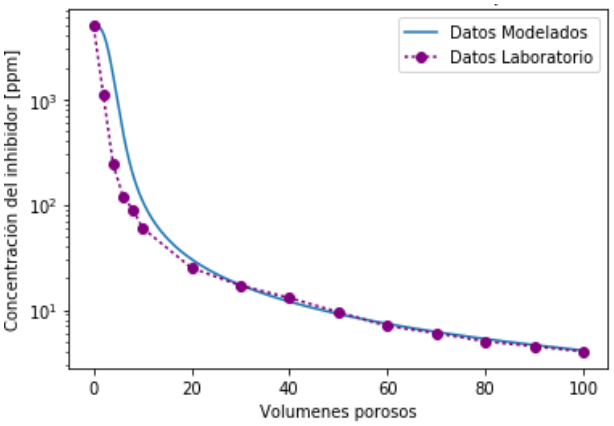

Figura 20: Validación del modelo para flujo lineal con plug de Acaé (Pf. 10630')
Fuente: Elaboración propia

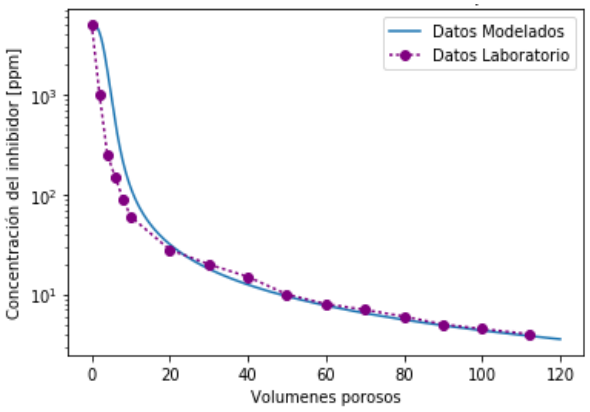

Figura 21: Validación del modelo para flujo lineal con plug de Acaé (Pf. 10633')
Fuente: Elaboración propia

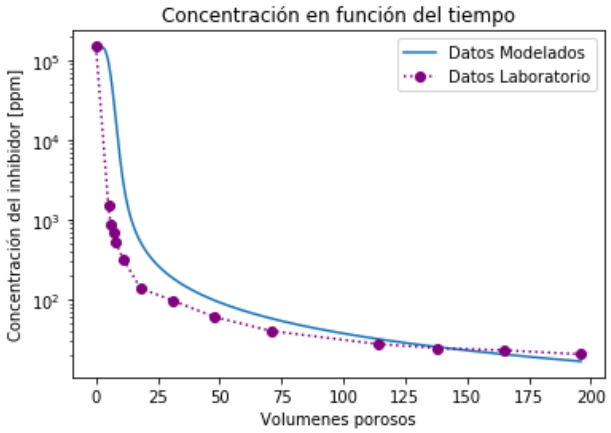

Figura 22: Validación del modelo para flujo lineal con plug de Cusiana (Pf. 16455,3)
Fuente: Elaboración propia

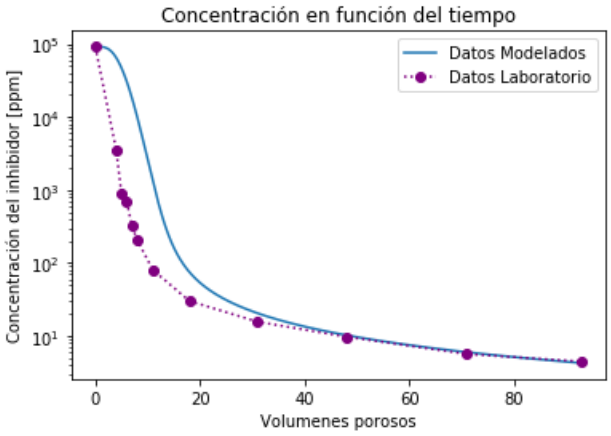

Figura 23: Validación del modelo para flujo lineal con plug de Cupiagua (Pf. 13801,17)
Fuente: Elaboración propia

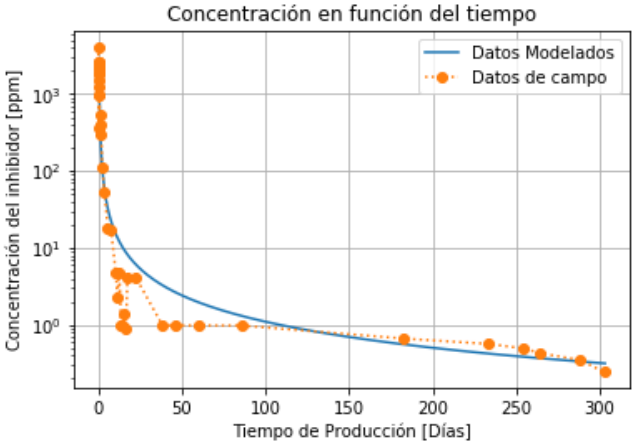

Figura 24: Validación del modelo para flujo radial con datos de Campo Cusiana
Fuente: Elaboración propia

Adicionalmente se realizaron validaciones de la herramienta computacional utilizando simuladores de yacimientos como Eclipse y Squeeze, variando como parámetro el corte de agua de los pozos desde 10 hasta 90% [13-16].

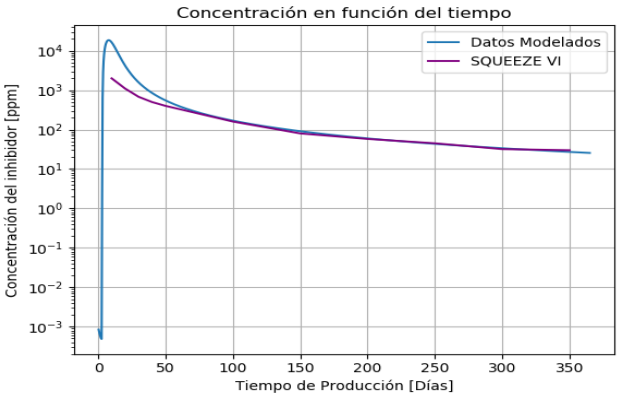

Figura 25: Datos modelados en la Herramienta Vs. Squeeze VI (Cw = 10 %)
Fuente: Elaboración propia

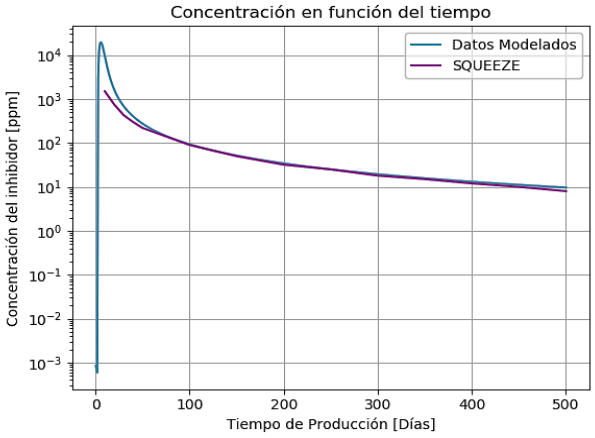

Figura 26: Datos modelados en la Herramienta Vs. Squeeze (Cw =15%)
Fuente: Elaboración propia

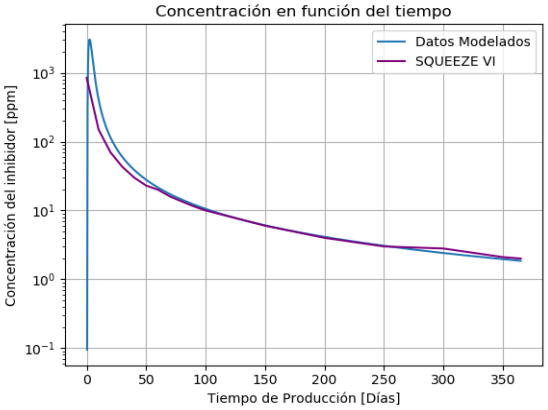

Figura 27: Datos modelados en la Herramienta Vs. Squeeze VI (Cw =55%)
Fuente: Elaboración propia

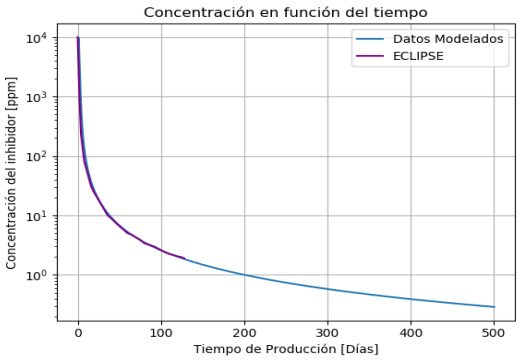

Figura 28: Datos modelados en la Herramienta Vs. Eclipse (Cw=70%)
Fuente: Elaboración propia

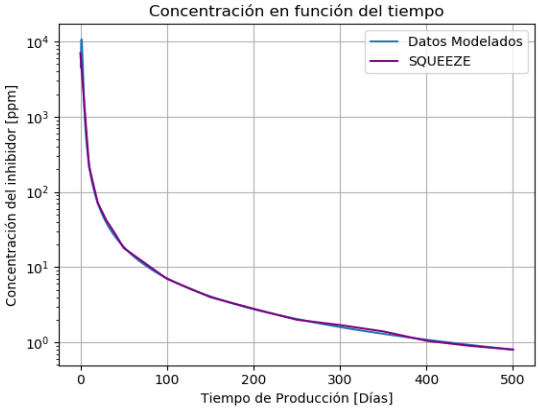

Figura 29: Datos modelados en la Herramienta Vs. Squeeze (Cw=87%)
Fuente: Elaboración propia

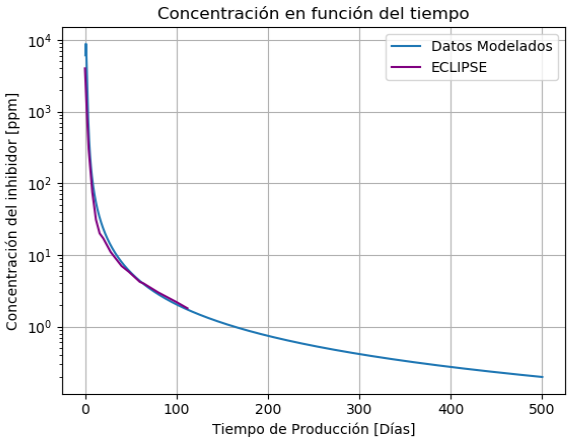

Figura 30: Datos modelados en la Herramienta Vs. Eclipse (Cw=90%)
Fuente: Elaboración propia

En las Figs. 25, a 30, se presenta la comparación de los simuladores, lo cual sumado a las validaciones con datos de laboratorio y campo se puede concluir que la herramienta computacional diseñada es precisa y puede ser usada en predicciones para otros campos. Así mismo, es posible evidenciar que el corte de agua influye en gran medida, un ejemplo de ello se detalla en la Fig. 30 con un corte de agua de 90%, el inhibidor está por debajo de 1 ppm en 350 días, mientras que en la Fig. 25 para los mismos 350 días, la concentración aun es cercana a 50 ppm

5 Conclusiones

La herramienta computacional es de gran importancia para la prevención de la formación de incrustaciones, ya que permite predecir la durabilidad de los tratamientos de inhibición en campo y, por tanto, se puede saber en cuanto tiempo debe realizarse un nuevo tratamiento squeeze, evitando los costos asociados a la depositación y remoción de incrustaciones.

La herramienta computacional para modelamiento de adsorción y desorción de inhibidores constituye un aporte significativo para la prevención del daño a la formación ocasionado por escamas inorgánicas, ya que actualmente no se cuenta con software comercial para este propósito.

La implementación de esta herramienta permitirá realizar optimización de tratamientos de inhibición aplicados en campo, a partir de pruebas de desplazamiento realizadas en laboratorio, o residuales de inhibición obtenidos de tratamientos squeeze previos.

Los resultados del modelamiento del fenómeno de desorción en laboratorio y campo permiten monitorear la concentración de un inhibidor en el agua de producción, y así determinar la vida útil del tratamiento químico.

El modelo presentado es fundamental para el correcto diseño de un tratamiento squeeze, ya que permite evaluar parámetros operacionales como tasa de inyección, caudal de producción, cantidad de inhibidor a inyectar y concentración optima del tratamiento.

Mediante la utilización de la herramienta es posible conocer el comportamiento de interacción roca – inhibidor en yacimientos de areniscas, a partir de pruebas realizadas en laboratorio a condiciones de yacimiento.

La herramienta computacional permite determinar el valor apropiado de volúmenes porosos que deben ser inyectados, para alcanzar la saturación total de la roca, evitando sobrecostos y logrando tratar toda la región de interés.

Al realizar simulaciones se determinó el impacto del caudal de producción sobre la desorción del inhibidor, encontrando que caudales altos presentan un efecto negativo sobre la duración de los tratamientos squeeze.

Referencias

[1] Civan, F. Non-isothermal Permeability Impairment by Fines Migration and Deposition in Porous Media including Dispersive Transport. Transp Porous Med 85, 233–258, 2010 doi: https://doi.org/10.1007/s11242-010-9557-0

[2] Gruesbeck, C., and R. E. Collins. "Entrainment and Deposition of Fine Particles in Porous Media." SPE J. 22, 1982. doi: https://doi.org/10.2118/8430-PA

[3] KELLAND, Malcolm A. “Effect of Various Cations on the Formation of Calcium Carbonate and Barium Sulfate Scale with and without Scale Inhibitors”. En: I&EC Research. p. 5852-5861, 2011. doi: https://doi.org/10.1021/ie2003494

[4] Enyi, G. C., Nasr, G. G., Nourian, A., El Kamkhi, M. A., & Burby, M. L. Removal of scales in petroleum production tubing utilising high

pressure atomisers. In ICLASS 2012, 12th Triennial International Conference on Liquid Atomization and Spray Systems. Institute for Liquid Atomization and Spray Systems-Europe, 2012 Disponible en: http://usir.salford.ac.uk/id/eprint/59503

[5] Taheri-Shakib, J., Naderi, H., Salimidelshad, Y. et al. Using ultrasonic as a new approach for elimination of inorganic scales (NaCl): an experimental study. J Petrol Explor Prod Technol 8, 553–564, 2018 https://doi.org/10.1007/s13202-017-0369-4

[6] JINES, Jose Luis. "Uso del tubo de diálisis en el diseño de tratamiento antiescala en el pozo SA 110 del campo sacha en distrito amazónico ecuatoriano". Trabajo de grado previo a la obtención del Título de: Ingeniero en Petróleo. Escuela Superior Politécnica del litoral. Facultad de Ingeniería en Ciencias de la Tierra, 186 p. 2010.

[7] Zabala Romero, R. D. Modelo fenomenológico para escalar a yacimiento el impacto sobre producción de hidrocarburos del daño de formación por migración de finos. Revista Fuentes, El reventón energético, 14(1), 103–114 2016 https://doi.org/10.18273/revfue.v14n1-2016009

[8] Sorbie, K.S., Yuan, Ming Dong, Todd, A.C., and R.M.S. Wat. "The Modelling and Design of Scale Inhibitor Squeeze Treatments in Complex Reservoirs." Paper presented at the SPE International Symposium on Oilfield Chemistry, Anaheim, California, 1991. doi: https://doi.org/10.2118/21024-MS

[9] Moreno-Enriquez, A.; Vargas-Silva, D.; Gambús-Ordaz, M.; Calderón-Carrillo, Z.; Robles-Albarracín, E. Evaluación del volumen de gas original in situ en yacimientos no convencionales tipo gas-shale mediante múltiples modelos a nivel mundial y su analogía a una formación colombiana. Boletín de Geología, 44(2), 109-123, 2022. https://doi.org/10.18273/revbol.v44n2-2022005

[10] ALBRIGHT, F. L., Albright's Chemical Engineering Handbook. Boca Raton, FL: CRC Press. (2009).

[11] Jordan, M.M., Sorbie, K.S., Griffin, P., Hennessey, S., Hourston, K.E., and P. Waterhouse. "Scale Inhibitor Adsorption/Desorption vs. Precipitation: The Potential for Extending Squeeze Life While Minimising Formation Damage." Paper presented at the SPE European Formation Damage Conference, The Hague, Netherlands, 1995 doi: https://doi.org/10.2118/30106-MS

[12] Yuan, Ming Dong, Sorbie, K.S., Todd, A.C., Atkinson, L.M., Riley, Helen, and Stuart Gurden. "The Modelling of Adsorption and Precipitation Scale Inhibitor Squeeze Treatments in North Sea Fields." Paper presented at the SPE International Symposium on Oilfield Chemistry, New Orleans, Louisiana, 1993 doi: https://doi.org/10.2118/25163-MS

[13] Vazquez, Oscar, Mackay, Eric James, and Kenneth S. Sorbie. "Development of a Non-Aqueous Scale Inhibitor Squeeze Simulator." Paper presented at the SPE International Oilfield Scale Symposium, Aberdeen, UK, 2006. doi: https://doi.org/10.2118/100521-MS

[14] Vazquez, O., Mackay, E., Sorbie, K., and M. Jordan. "Impact of Mutual Solvent Preflush on Scale Squeeze Treatments: Extended Squeeze Lifetime and Improved Well Clean-up Time." Paper presented at the 8th European Formation Damage Conference, Scheveningen, The Netherlands, 2009. doi: https://doi.org/10.2118/121857-MS

[15] Vazquez, O., Mackay, E. J., and K. S. Sorbie. "Modelling of Non-Aqueous and Aqueous Scale Inhibitor Squeeze Treatments." Paper presented at the International Symposium on Oilfield Chemistry, Houston, Texas, U.S.A., 2007. doi: https://doi.org/10.2118/106422-MS

[16] Rakhimov, A.. , Vazquez, O.. , Sorbie, K. S., and E. J. Mackay. "Impact of Fluid Distribution on Scale Inhibitor Squeeze Treatments in Pattern Floods and Fractured Wells." Paper presented at the SPE EUROPEC/EAGE Annual Conference and Exhibition, Barcelona, Spain, 2010. doi: https://doi.org/10.2118/131724-MS

C. Leon-Vanegas, MSc. en Ingeniería de Petróleos, pertenece al Grupo de investigación en fenómenos de superficie, Departamento de Procesos y Energía, Facultad de Minas, Universidad Nacional de Colombia Sede Medellín. Profesional con conocimientos en daño a la formación, estimulación, análisis petrofísicos, modelamiento de procesos y mejoramiento de productividad. Con experiencia en: tratamientos de inhibición, fluidos de control de pozo, y fluidos de estimulación. Experiencia en formulación, gestión y liderazgo de proyectos. Manejo de software especializado de yacimientos para simulación.
ORCID: 0009-0009-1670-2350.

D.A Vargas-Silva, es Ingeniero de Petróleos, MSc. en Geofísica y candidato a Doctor en Ingeniería Química de la Universidad Industrial de Santander, Colombia. Con experiencia en presión de poro mediante modelamiento de cuencas 1D, 2D y 3D, aplicado al Valle Medio del Magdalena (VMM) y Piedemonte. Modelando el fenómeno de pérdidas de fluido de perforación en yacimientos naturalmente fracturados y diseño de software. Actualmente se desempeña como docente de las escuelas de Ingeniería de Petróleos y Física.
ORCID: 0000-0001-6593-1664

F.B Cortes-Correa, es profesor titular y director del grupo Fenómenos de Superficie -Michael Polanyi de la Facultad de Minas, Universidad Nacional de Colombia, sede Medellín. Dr. en Sistemas Energéticos de la Universidad Nacional de Colombia, sede Medellín. Su investigación se centra en fenómeno de adsorción, materiales nanoportados y síntesis de nanomateriales; sus artículos han aparecido en Fuel, Energy and Fuels, Petroleum Science, entre otros.
ORCID: 0000-0003-1207-3859

H. Buendía-Lombana, es Químico, Modelamiento de Procesos Hidrocarburos (GMPH), Escuela de Ingeniería de Petróleos, Universidad Industrial de Santander, Colombia.
ORCID: 0000-0003-0006-7275

DYNA
http://dyna.medellin.unal.edu.co/

UNIVERSIDAD NACIONAL DE COLOMBIA

Forest fire risk zoning for the metropolitan region of Curitiba, Paraná, Brazil

Heitor Renan Ferreira, Antonio Carlos Batista, Alexandre França Tetto & Daniela Biondi

Federal University of Paraná, Forest Engineering Department, Curitiba-PR, Brasil. bmheitorf@gmail.com, batistaufpr@gmail.com, tetto@ufpr.br, dbiondi@ufpr.br

Received: December 12th, 2023. Received in revised form: May 16th, 2024. Accepted: May 20th, 2024.

Abstract
Forest fires are becoming increasingly frequent throughout the globe, influencing socioeconomic and environmental aspects and endangering ecosystems and life. The forest fire risk zoning is an auxiliary tool for elaborating and implementing preventive policies. The present study aims to execute the forest fire risk zoning for the metropolitan region of Curitiba, Paraná, Brazil, testing its efficiency through the relationship with geolocated fires that occurred from 2011 to 2016. Thematic maps were made through information related to demographic density, road system, land use and cover, slope, orientation and altimetry of the terrain. The efficiency of the proposed zoning, 45.8% and 44.0% of the geolocated fires that occurred in the study area in the period 2011 to 2016 were present in areas considered with "very high" and "high" risk, respectively, demonstrating that the proposed zoning can be used to develop prevention policies for the metropolitan region of Curitiba.

Keywords: wildfire; urban-rural interface; wildland-urban interface; fire hazard; fire prediction.

Zonificación del riesgo de incendios forestales para la región metropolitana de Curitiba, Paraná, Brasil

Resumen
Los incendios forestales son cada vez más frecuentes en todo el planeta, influyendo en aspectos socioeconómicos y ambientales, poniendo en peligro los ecosistemas y la vida. La zonificación de riesgo de incendios forestales es una herramienta auxiliar para la elaboración e implementación de políticas preventivas. El presente estudio tiene como objetivo ejecutar la zonificación de riesgo de incendios forestales para la región metropolitana de Curitiba, Paraná, Brasil, probando su eficiencia a través de la relación con incendios geolocalizados ocurridos en el período de 2011 a 2016. Se realizaron mapas temáticos a través de información relacionada con los factores demográficos. densidad, sistema vial, uso y cobertura del suelo, pendiente, orientación y altimetría del terreno. De la eficiencia de la zonificación propuesta, el 45,8% y el 44,0% de los incendios geolocalizados ocurridos en el área de estudio en el periodo 2011 al 2016 estuvieron presentes en áreas consideradas con riesgo "muy alto" y "alto", respectivamente, demostrando que la zonificación propuesta La zonificación se puede utilizar para desarrollar políticas de prevención para la región metropolitana de Curitiba.

Palabras clave: incendio forestal; interfaz urbano-rural; interfaz urbano-forestal; peligro de incendio; predicción de incendios.

1 Introduction

Increasingly, forest fires have impacted different regions of the Earth, directly and indirectly affecting socio-economic and environmental aspects, as well as flora, fauna, soil, and atmospheric air [5,16,24,25].

The latest report released by the Intergovernmental Panel on Climate Change (IPCC) points out that the forecast is for an increase in average land temperature, which may cause, among other adversities, water deficit in many regions, which in turn makes the environment prone to higher numbers of events related to forest fires.

Forest fire risk zoning is an auxiliary tool for the elaboration and execution of preventive policies. The

How to cite: Ferreira, H.R., Batista, A.C., Tetto, A.F., and Biondi, D., Forest fire risk zoning for the metropolitan region of Curitiba, Paraná, Brazil. DYNA, 91(232), pp. 131-138, April - June, 2024.

government can use it to train its personnel and allocate resources, minimizing possible future losses.

The occurrence and propagation of forest fires are mainly influenced by the combustible material's quantity, type, arrangement, humidity, climatic conditions, topography, and vegetation type [24]. Fire risk maps integrate this information into their composition through a geographic information system [4].

In fire planning, the development of regional fire risk maps presents greater accuracy and efficiency than maps produced at larger scales [4].

With the advancement of geospatial programming techniques, several initiatives have been developed for automatic systems for calculating the risk of fires in vegetation. Despite considering variables with slight variation in a short time, such as topography and land use and cover, these systems can monitor daily changes in meteorological variables.

The Curitiba metropolitan region has extensive vegetation areas, including rural properties with agropastoral activities, remnants of native vegetation, and urban lots with vegetation. According to Ferreira [10], from 2011 to 2016, the metropolitan region of Curitiba presented 5,472 records of forest fires, with a burned area of approximately 2,271.45 ha, evidencing the problem caused by this event for the region.

With the increasing evolution of anthropic activities in the metropolitan region of Curitiba, involving the expansion of urban areas towards rural areas, there is a tendency to increase events related to fires in vegetation, directly and indirectly influencing society, leading it to the closest conviviality with fire.

The present study aims to execute the forest fire risk zoning for the metropolitan region of Curitiba, evaluating its efficiency when compared to the registered and geolocated fires from 2011 to 2016 in the study area.

2 Materials and methods

2.1 Study area

The study area comprises 29 municipalities in the Metropolitan Region of Curitiba (MRC). The MRC has a total area of 16,579.58 km² and is located in the eastern part of the state of Paraná, in Brazil's southern region. In 2017, the estimated population was 3,592,465 inhabitants. Its UTM center coordinates are 22S N 7,186,559 m and E 673,674 m [13].

Fig. 1 shows the list of municipalities presents in MRC and its location.

The metropolitan region of Curitiba is located in a region of the Cfb and Cfa climate. Cfb is a temperate climate, without dry season, with fresh versions and Cfa is a subtropical climate, without dry season, with fresh summers and frosts uncommon [3, 17].

Regarding the original vegetation, the study area is part of a phytogeographic region bordering natural fields and Araucaria Forest, including Dense Ombrophilous Forest areas to the north and east of the study area, integrating the Atlantic Forest biome [17].

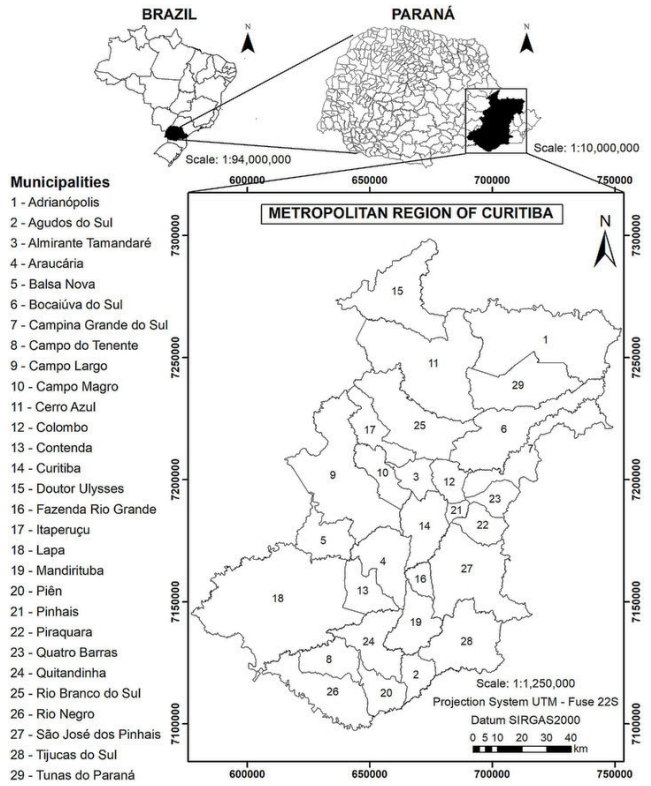

Figure 1. Location of the municipalities presents in the metropolitan region of Curitiba.
Source: The authors.

2.2 Fire risk zoning and research variables

For the preparation of the forest fire risk zoning in the metropolitan region of Curitiba, a superposition of thematic maps was performed according to a weighting model based on the adaptation of the methodologies used by Oliveira [19], Batista et al. [4] and Kovalsyki et al. [15]. These authors used coefficients ranging from 0 to 5 to classify the variables of interest, with subsequent insertion in the equation proposed in their research.

The thematic maps were divided into two groups: fire risk map according to human influence and fire risk map according to environmental factors.

The fire risk map, according to human influence, comprised the demographic density and the road system. There are indications that the anthropic presence is the primary causal agent in the metropolitan region of Curitiba [10,11], not differing from other urbanized regions and presenting areas of wildland-urban interface around the globe. Due to the human presence as a causal agent, different authors, such as Ho et al. [12] and Batista et al. [4] proposed to act with demographic density in risk analysis.

Also, Batista et al. [4], Ferraz and Vettorazzi [9], Kovalsyki et al. [15], Salas and Chuvieco [22], Ribeiro et al. [20], Ho et al. [12], Koproski et al. [14], Mota et al. [18] and Yathish et al. [26] worked with the influence of roads as a risk agent for fires, since highways are related to the anthropogenic presence in the environment.

The fire risk map, according to environmental factors,

was based on land cover and use, slope, altimetry, and terrain orientation.

The cover and use of the soil demonstrate the importance of risk zoning because it presents the presence or absence of vegetation, as well as the different types of this, and may present greater or lesser danger of ignition and propagation, such as more excellent flammability of conifers when compared to various hardwoods [4,24].

Regarding topography, uphill areas tend to have a faster spread of fire than sloping areas, a factor related to convective phenomena, radiation, and conduction [24].

Regarding the orientation of the slopes, in the Southern Hemisphere, there is a higher incidence of the sun's rays on the faces facing north, followed by the west face, demonstrating that both faces receive a more significant amount of energy than the other ones [4,20,24].

Finally, altimetry demonstrates that low elevations present more extended fire risk stations than high elevations. Also, the mountain tops and valley bottoms present different burning conditions during the day because there is a difference in wind currents and temperature and humidity in both locations. Valley funds have higher fire propagation potential during the day, and mountain tops have the most significant potential at night [4].

2.3 Fire risk zoning and research variables

The demographic density map was elaborate with Brazilian Institute of Geography and Statistics (IBGE) information in the 2010 demographic census [6], using the census sector delimited by this organization. Each census sector presents the number of inhabitants in a variable area, thus obtaining the demographic density by sector.

The road system influence map was realized using the information from the Department of Highways of Paraná [7]. A buffer of 1,000 m radius of the center of the road was carried out, thus characterizing the area under the influence.

Table 1 presents the classification of demographic density and distribution of the road system according to Batista et al. [4].

2.4 Fire risk map according to environmental factors

The risk map according to land cover and use was realized using the information contained in collection 5.0 of the year 2016 of the Annual Mapping Project of Land Cover and Use in Brazil [2], which uses satellite images and a data structure linking different variables for mapping the country's land cover and use. Subsequently, a risk classification was performed based on the variables described in the mapping obtained based on the studies of Batista et al. [4] and Kovalsyki et al. [15] (Table 2).

Table 1.
Classification of the variables that compose the risk map according to human influence.

Demographic density		
Inhabitants per km²	**Risk**	**Coefficient**
Up to 40.00	low	1
40.01 - 60.00	moderate	2
60.01 - 80.00	high	3
80.01 - 100.00	very high	4
Above 100.00	extreme	5
Distribution of the road system		
Class	**Risk**	**Coefficient**
With influence	yes	1
Without influence	no	0

Source: The authors.

Table 2.
Land cover and use classification for fire risk map according to environmental factors.

Classification	Risk	Coefficient
Water	null	0
Urban infrastructure Other non vegetated areas Mining	low	1
Natural forest	high	3
Mosaic agricultura and pasture Agriculture Pasture	very high	4
Grassland	extreme	5

Source: The authors.

Table 3.
Topography classification for fire risk map according to environmental factors.

Variable	Classification	Risk	Coefficient
Slope	Up to 15%	low	1
	16% - 25%	moderate	2
	26% - 35%	high	3
	36% - 45%	very high	4
	≥ 46%	extreme	5
Altimetry	Até 600.00 m	extreme	5
	600.01 m – 900.00 m	very high	4
	900.01 m – 1,200.00 m	high	3
	1,200.01 m – 1,500.00 m	moderate	2
	Above 1,500.00 m	low	1
Orientation	112,51° - 247,50°/(SE/S/SW)	low	1
	67,51° - 112,50°/(E)	moderate	2
	22,51° - 67,50°/(NE)	high	3
	247,51° - 337,50°/(NW/W)	very high	4
	337,51° - 22,50°/(N)	extreme	5

Source: The authors.

Urban infrastructure, other non-vegetated areas, and mining were considered as having a "low" danger because of the existence of vacant lots in these areas that may have vegetation fire, making the classification "null" unfeasible since some areas with vegetation were not covered by the spatial resolution used by MAPBIOMAS (30 m).

To obtain the thematic maps of fire risk according to altimetry, slope, and terrain orientation, images of the Satellite Alos Palsar, with a spatial ratio of 12.5 meters, using the digital elevation model. The slope of the terrain was obtained through the tool "slope" and the orientation of the terrain by the tool "aspect", both present in version 10.5 of the ArcGIS software. The recommendations of Batista et al. [4] were followed for the classification (table 3).

After making the thematic maps by counting pixels of the raster-type files in each class, the area occupied in each risk classification was calculated.

2.5 Integration of thematic maps

To complete the thematic maps, the "raster calculator" tool of Arcgis software version 10.5 was used, thus relating

the coefficients found in the pixels of each thematic map.

The weighting model used was adapted from Oliveira [14] and Kovalsyki et al. [15]:

$$FFRZ = (0{,}655 \times DD + 0{,}655 \times RS) + [(0{,}29 \times S\% + 0{,}11 \times OE + 0{,}1 \times AL) + (0{,}8 \times LCU)] \quad (1)$$

Where:
DD = Demographic density.
RS = Road system.
S% = Slope.
OE = Orientation.
AL = Altimetry.
LCU = Land cover and use.

The weighting model used is indicated for the elaboration of forest fire risk zoning in the state of Paraná. It presents similarities in the variables used, as well as presents climatic conditions similar to the study area.

Six classification classes were obtained for forest fire risk zoning, distributed according to the classification method "natural break" of the software ArcGis.

Table 4 presents the classification of the fire risk zoning and the values of each class.

To evaluate the effectiveness of the proposed risk zoning, the forest fires geolocalized in the study area from 2011 to 2016 were used using the Ferreira [10] database.

By relating the geolocation points of the forest fires with the proposed zoning classification, we can verify the number of points per class and, consequently, the percentage of concentration of fires in relation to risk zoning.

3 Results

Fig. 2A and 2B present the fire risk maps according to demographic density and road system, respectively.

The risk map, according to demographic density, showed that 14,284.47 km² (86.1%) of the study area has a "low" risk. The "moderate" risk occupied the area of 606.42 km² (3.7%), the "high" area of 232.3 km² (1.4%), the "very high" area of 194.92 km² (1.2%), and the "extreme" risk the area of 1,261.33 km² (7.6%).

It was observed that the regions with the highest risk comprise the urbanized municipal areas, especially Curitiba. As you move away from the urban area towards peripheral areas, there is a decrease in risk, as the demographic density is lower in rural areas.

The risk map, according to the road system, showed that 2,396.43 km² (14.5%) of the study area is under the influence of highways, while the area without influence was 14,183.22 km² (85.5%). The municipalities with a more significant extension of highways will, therefore, have a larger area under the influence, providing greater circulation of vehicles and anthropic presence.

Table 4.
Risk classes for the proposed zoning.

Class	Risk
0.0	null
1.35 - 3.15	low
3.16 - 4.52	moderate
4.53 - 5.36	high
5.37 - 6.49	very high
> 6.5	extreme

Source: The authors.

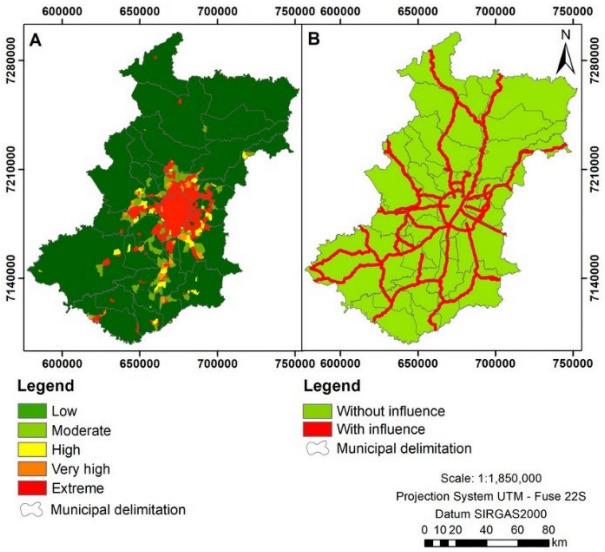

Figure 2. Fire risk map for metropolitan region of Curitiba according to: A) Demographic density; B) Road system.
Source: The authors.

Figs. 3A, 3B, 3C, and 3D presented the fire risk maps according to the land cover and use, slope, orientation, and altimetry.

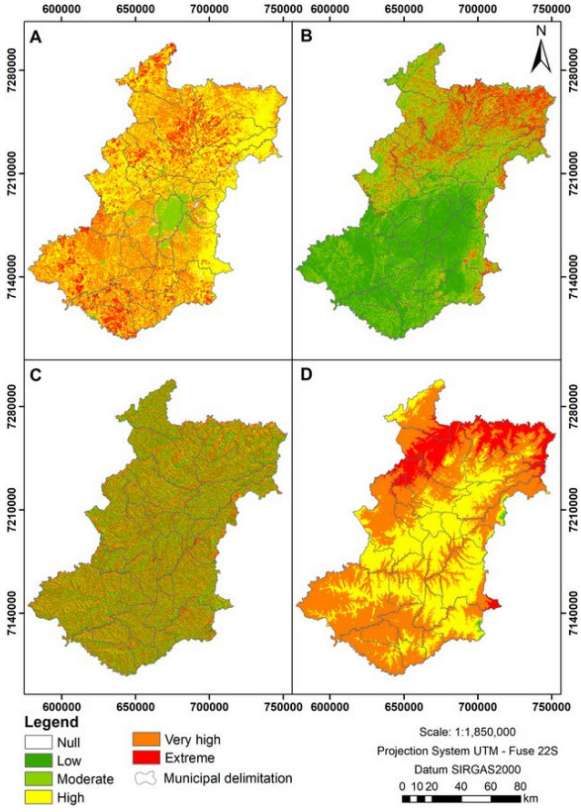

Figure 3. Fire risk map for metropolitan region of Curitiba according to: A) Land cover and use; B) Slope; C) Orientation; and D) Altimetry.
Source: The authors.

Table 5.
Area that the fire risk classification occupied in fire risk map according to land cover and use.

Risk	Land cover and use	
	Area (km²)	%
Null	80.67	0.5
Low	704.82	4.3
Moderate	-	-
High	8,654.96	52.2
Very high	5,181.45	31.2
Extreme	1,957.68	11.8
Total	**16,579.58**	**100**

Source: The authors.

Table 6.
Area that the fire risk classification occupied in fire risk map according to slope and orientation.

Risk	Slope		Orientation	
	Area (km²)	%	Area (km²)	%
Null	-	-	-	-
Low	7,823.94	47.2	6,058.02	36.5
Moderate	3,552.72	21.4	1,966.91	11.9
High	2,231.20	13.5	2,061.39	12.4
Very high	1,516.11	9.1	4,182.62	25.2
Extreme	1,455.62	8.8	2,310.64	13.9
Total	**16,579.58**	**100**	**16,579.58**	**100**

Source: The authors.

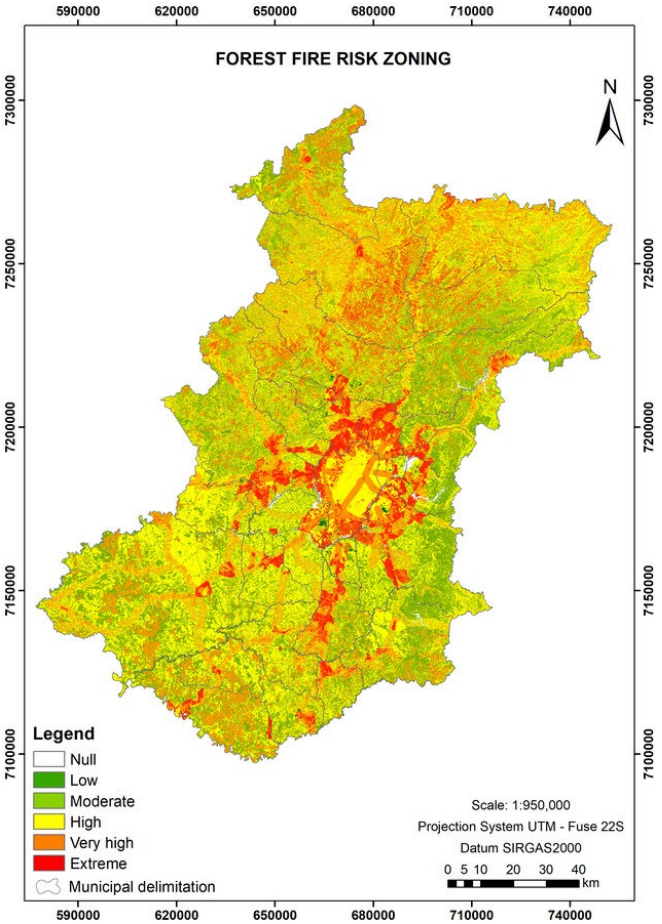

Figure 4. Forest fire risk zoning for metropolitan region of Curitiba.
Source: The authors.

Table 7.
Relationship of forest fire geolocation from 2011 to 2016 with the proposed risk zoning.

Classification FFRZ	Forest fire geolocalization (2011-2016)	
	n°	%
Low	36	0.8
Moderate	28	0.6
High	1,915	44.0
Very high	1,994	45.8
Extreme	381	8.8
Total	**4,354**	**100**

Source: Ferreira [10] and the authors.

There were small divergences between the values available with the MAPBIOMAS files (table in .xls format and raster file), so we chose to use the calculated values of the pixels of the raster file using the ArcGis software.

Table 5 and 6 shows the area that the fire risk classification occupied in each variable.

For the risk map according to land cover and use, the "high" class presented the largest dimensions in the study area (8,654.96 km² - 52.2%). It was found that urbanized regions present mostly areas with "low" risk, as they refer to urban structures. The other regions showed variations according to land cover and use.

Regarding slope, it is observed that most of the study area (7,823.94 km² - 47.2%) is present in the classification of "low" risk. The same occurred for the orientation variable, which presented in the same classification an area of 6,058.02 km² (36.5%). The variable altimetry presented the class "very high" (8,521.31 km² - 51.4%) in most of the study area.

Fig. 4 presents the forest fire risk zoning for the study area.

The result of the thematic maps integralization indicated that 6,946.39 km² (41.9%) of the study area presented the "high" risk classification, followed by 4,575.5 km² (27.6%) of "moderate" risk and 3,744.29 km² (22.6%) of "very high" risk. Furthermore, the "extreme" risk occupied the area of 1,192.74 km² (7.2%), the "null" risk the area of 80.67 km² (0.5%) and the "low" risk the area of 39.99 km² (0.2%).

Table 7 demonstrates the relationship with the risk classes found in the present study.

Regarding the efficiency of the proposed zoning, 45.8% and 44.0% of the geolocated fires that occurred in the study area in the period 2011 to 2016 were present in areas considered with "very high" and "high" risk, respectively.

4 Discussion

Regarding the risk classification according to demographic density, Batista et al. [4] find that 77.14% of the area of the state of Paraná is present in the "low" risk classification. In the state of Santa Catarina, contiguous to Paraná, Ho et al. [12] observe that population density is classified as "low" risk in 65.9% of the analyzed area for the scenario from 2010 to 2020. Both studies corroborate the present research since rural areas have a more significant extension in the national territory.

To Kudremukh National Park, Yathish et al. [26] verify a high relationship between occurrences of forest fires and human activities, including highways. Ajin et al. [1] observe

that anthropogenic factors are the most relevant for forest fires in their study area (Idukki Wildlife Sanctuary). Tetto et al. [25] recommend in their study in the Irati National Forest that the areas with the highest flow of people should have a greater intensity of preventive activities.

Batista et al. [4] observed that for the state of Paraná, the value of 15.18% of areas with an influence of the road system is similar to that found in the present study since it is the same state. In Santa Catarina, Ho et al. [12] verified that 2.39% of the state was under the influence of the road system, a value lower than the present study.

In the fire risk map according to land cover and use, it is verified that for the state of Paraná, Batista et al. [4] identify that 34.03% of the study area has an "extreme" risk classification, with values decreasing to the "low" risk. Possibly, the difference in the scale of analysis of the metropolitan region of Curitiba, compared to the state of Paraná, shows that because there is more urbanization in the MRC, there will consequently be a more evident "low" risk classification. Furthermore, the MRC predominates natural forest and agricultural activities compared to rural formations and forest plantations, reducing the presence of the "extreme" risk classification.

Mota et al. [18] verify that for the state of Mato Grosso, Brazil, the existing particularities of the Cerrado biome increase the ignition potential. Kovalsyki et al. [15] verify that land cover and use present 94.5% of the area of Vila Velha State Park in risk classes equal to or above "high," a value similar to that found in the present study despite the specificities and phytophysiognomy of their study area. For the state of Santa Catarina, Ho et al. [12] observe that the most frequent risk class is "high", occupying 41.33% of the state area, followed by the "extreme" risk class with 38.34%, differing from the present study.

Regarding slope, different studies located in the state of Paraná present high percentages of "low" risk, as verified by Ribeiro et al. [20], Koproski et al. [14], and Kovalsyki et al. [15] (99.3%, 83.76% and 72.1% respectively). In Santa Catarina, Ho et al. [12] found a value of 49.3% for the "low" risk classification, lower than the other studies, demonstrating a greater slope and, consequently greater possibility for the propagation of fire in this state.

The orientation with the "low" risk classification is also predominant in the studies: Kovalsyki [15], which has a value of 44.4% coverage; Batista et al. [4], which also has the "low" hazard class as the most prevalent for the state of Paraná, with a value of 32.80%; and Ho et al. [12], which has 39.14% in the same class. Koproski et al. [14] found that 43.23% of their study area was classified as "very high", demonstrating a higher rate of incident radiation than the other studies.

Regarding altimetry, the different studies were analyzed to corroborate the present study regarding the predominance of a higher-risk class. Kovalsyki et al. [15] show that 74.7% of their study area has a "very high" class, followed also by Koproski et al. [14] with 95.29% coverage of their area and Ho et al. [12] that show the value of 94.59% covered by the "very high" and "extreme" risk classes. Ribeiro et al. [20] verified that 87.6% of their study area is classified as "high". The primary justification for the similarity of the results is that the different studies were performed in the southern region of Brazil, which consequently presents a predominance of areas with higher altitudes.

The forest fire risk zoning proposed in the present study indicates that the border areas between the municipalities tend to show the "extreme" risk, demonstrating the problem in these regions commonly characterized by wildland-urban interface areas.

There is difficulty characterizing areas of wildland-urban interface related to forest fires in the Brazilian scope, but although incipient, the subject has gained strength in the scientific environment. Although there are different classifications around the globe, local specificities should be considered.

Different studies use similar models of integrating thematic maps in the present research. Batista et al. [4] used three different integration models for the state of Paraná. The authors present in their study the predominance of "moderate" risk in one model and the "extreme" and "high" risks in the other two subsequent models, thus demonstrating the variability of the result based on the information used for integration, as well as on the weights assigned in the weighting model.

Sá et al. [21] used different methods of integrating thematic maps and suggested testing different weights in other studies. Using a distinct weighting model, Mota et al. [18] verify that in Mato Grosso, 55.06% of the area is present from the upper to extreme classes. In contrast, for Kovalsyki et al. [15], the class range is 58.2%, and for Eugenio et al. [8] presents 75% for the state of Espirito Santo. These values are higher than in the present study, but there is a distinction in the variables and weights that make up the integralization model used.

Companies, both public and private, employ various methodologies for automating fire risk classification. A notable example is proposed by the National Institute of Space Research (INPE). According to Setzer et al. [23] this methodology is based on the meteorological principle that the longer a specific area goes without rain, the higher its risk of vegetation burning. Additionally, INPE's model incorporates additional variables such as vegetation type, maximum daily temperature readings, minimum relative air humidity levels, topographic elevation, magnitude of latitude, the presence of fires in close proximity to evaluate fire risks more precisely.

The automation of fire risk classification evolves the methodology presented in this study by incorporating variables with daily variability related to vegetation fires.

Comparations between research that used different methodologies and study areas do not present as much effectiveness as testing the very efficiency of the proposed zoning. Thus, by demonstrating the predominance of fires that occurred from 2011 to 2016 in "very high" and "high" risk classifications, it is verified that the proposed zoning is satisfactory for the study area.

5 Conclusion

Based on the results obtained, we concluded that:

- The integration of the different thematic maps generating the forest fire risk zoning for the metropolitan region of Curitiba presented a satisfactory efficiency,

being able to be used for the management of prevention politics, aiming at the minimization of the damages caused by the fires.

- It is recommended to evaluate the optimization of forest fire risk zoning incorporating meteorological variables and urban characteristics since there are variables not covered by this and another manuscript that may present greater refinement and consequently better efficiency in future risk zoning.

References

[1] Ajin, R.S., Loghin, A.M., Jacob, M.K., Vinod, P.G., and Krishnamurthy, R.R., The risk assessment study of potential forest fire in Idukki Wildlife Sanctuary using RS and GIS techniques. International Journal of Advanced Earth Science and Engineering, [online]. 5(1), pp. 308-318, 2016. Available at: https://cloudjl.com/index.php/EarthScience/issue/view/47/39

[2] Annual Mapping Project of Land Cover and Use in Brazil (MAPBIOMAS). Coleção 5.0 da Série Anual de Mapas de Cobertura e Uso de Solo do Brasil [Online]. 2020. [date of reference May 10th of 2020]. Available at: https://mapbiomas.org/

[3] Alvares, C.A., Stape, J.L., Sentelhas, P.C., Gonçalves, J.L.M., and Spavorek, G., Köppen's climate classification map for Brazil. Meteorologische Zeitschrift, 22(6), pp. 711-728, 2013. DOI: https://doi.org/10.1127/0941-2948/2013/0507

[4] Batista A.C., Oliveira, D.S., e Soares, R.V., Zoneamento de risco de incêndios florestais para o estado do Paraná. Curitiba, Brasil, FUPEF, 2002, 86 P.

[5] Bowman, D.M.J.S., Balch, J., Artaxo, P., Bond, W.J., Cochrane, M.A., D'Antonio, C.M., Defries, R., Johnston, F.H., Keeley, J.E., Krawchuk, M.A., Kull, C.A., Mack, M., Moritz, M.A., Pyne, S., Roos, C.I., Scott A.C., Sodhi N.S., and Swetnam T.W., The human dimension of fire regimes on Earth. Journal of Biogeography, 38(12), pp. 2223-2236, 2011. DOI: https://doi.org/10.1111/j.1365-2699.2011.02595.x

[6] Brazilian Institute of Geography and Statistics (IBGE). Censo 2010, [online]. 2010. [date of reference March 21st of 2020]. Available at: https://censo2010.ibge.gov.br/resultados.html

[7] Department of Highways of Paraná. Malha rodoviária, 2020. [date of reference June 20th of 2020]. Available at: http://www.der.pr.gov.br/Pagina/Malha-Rodoviaria

[8] Eugenio, F.C., Santos, A.R., Fiedler, N.C., Ribeiro, G.A., Silva, A.G., Santos, A.B., Paneto, G.G., and Schettino, V.R., Applying GIS to develop a model for forest fire risk: a case study in Espírito Santo, Brazil. Journal of Environmental Management, 173, pp. 65-71, 2016. DOI: https://doi.org/10.1016/j.jenvman.2016.02.021

[9] Ferraz, S.F.B., e Vettorazzi, C.A., Mapeamento de risco de incêndios florestais por meio de sistema de informações geográficas (SIG). Scientia Forestalis, 26(53), pp. 39-48, 1998.

[10] Ferreira, H.R., Análise das ocorrências de incêndios em vegetação na região metropolitana de Curitiba-PR, no período de 2011 a 2016. Dissertação MSc. Engenharia Florestal, Brasil, Universidade Federal do Paraná, Brazil, 2021, 137 P.

[11] Ferreira, H.R., Batista, A.C., Tetto, A.F., Kovalsyki, B., e dos Santos, J.F.L., Incêndios em vegetação em conjunto com outros materiais combustíveis na interface urbano-rural de Curitiba-PR. BIOFIX Scientific Journal, 5(1), pp. 108-113, 2020. DOI: https://doi.org/10.5380/biofix.v5i1.67832

[12] Ho, T.L., Batista, A.C., and Tetto, A.F. Forest fire risk forecast for the state of Santa Catarina due to climate changes. Floresta, 47(4), pp. 427-436, 2017. DOI: https://doi.org/10.5380/rf.v47i4.50877

[13] Institute of Land, Cartography and Geography of Paraná. Relatório de cálculo de área dos municípios do estado do Paraná - ano 2019, [online]. 2019. [date of reference June 10th of 2020]. Available at: http://www.itcg.pr.gov.br/arquivos/File/Dados_2019/RELATORIO_DE_CALCULO_DE_AREA_DOS_MUNICIPIOS_DO_PARANA2019.pdf

[14] Koproski, L.P., Ferreira, M.P., Goldammer, J.G., e Batista, A.C., Modelo de zoneamento de risco de incêndios para unidades de conservação brasileiras: o caso do Parque Estadual do Cerrado (PR). Floresta, 41(3), pp. 551-562, 2011. DOI: https://doi.org/10.5380/rf.v41i3.24049

[15] Kovalsyki, B., Batista, A.C., Tetto, A.F., Sousa, N.J., Carmo, M.R.B., and Soares, R.V., Forest fire risk zoning for the Vila Velha State Park and its surroundings (Ponta Grossa, Paraná). Floresta, 50(4), pp. 1818-1826, 2020. DOI: https://doi.org/10.5380/rf.v50i4.65974

[16] Lourenço, L., Fernandes, S., Bento-Gonçalves, A., Castro, A., Nunes, A., e Vieira, A., Causas de incêndios florestais em Portugal continental. Análise estatística da investigação efetuada no último quindénio (1996 a 2010). Cadernos de Geografia, 30/31, pp. 61-80, 2012. DOI: https://doi.org/10.14195/0871-1623_31_7

[17] Maack, R., Geografia física do Estado do Paraná. Ponta Grossa, Brasil, UEPG, 2012, 526 P.

[18] Mota, P.H.S., Rocha, S.J.S.S., Castro, N.L.M., Marcatti, G.E., França, L,C,J., Schettini, B.L.S., Villanova, P,H., Santos, H,T., and Santos, A,R., Forest fire hazard zoning in Mato Grosso State, Brazil. Land Use Policy, 88, art. 104206, 2019. DOI: https://doi.org/10.1016/j.landusepol.2019.104206

[19] Oliveira, D.S., Zoneamento de risco de incêndios em povoamentos florestais no norte de Santa Catarina. Dissertação Tesis MSc. em Ciências Florestais, Universidade Federal do Paraná, Brasil, 2002, 124 P.

[20] Ribeiro, L., Koproski, L.P., Stolle, L., Lingnau, C., Soares, R.V., e Batista, A.C., Zoneamento de risco de incêndios florestais para a fazenda experimental do Canguiri, Pinhais (PR). Floresta, 38(3), pp. 561-572, 2008. DOI: https://doi.org/10.5380/rf.v38i3.12430

[21] Sá, A., Nero, M., Tavares-Júnior, J., Candeias, A., e Nobrega, R., Comparação e validação da modelagem espacial de riscos de incendios considerando diferentes métodos de predição. Bulletin of Geodetic Sciences, 23(4), pp. 556-577, 2017. DOI: https://doi.org/10.1590/s1982-21702017000400037

[22] Salas, J., and Chuvieco, E., Geographic information systems for wildland fire risk mapping. Wildfire, 3(2), pp. 7-13, 1994.

[23] Setzer, A.W., Sismanoglu, R.A., e Santos, J.G.M., Método do cálculo do risco de fogo do Programa do Instituto Nacional de Pesquisas Espaciais (INPE) - Versão 11, [online]. 2019. [date of reference May 18th of 2024]. Available at: http://mtc-m21c.sid.inpe.br/col/sid.inpe.br/mtc-m21c/2019/11.21.11.03/doc/publicacao.pdf

[24] Soares, R.V., Batista, A.C., e Tetto, A.F., Incêndios florestais: controle, efeitos e uso do fogo. Curitiba, Brasil, 2017, 255 P.

[25] Tetto, A.F., Batista, A.C., Soares, R.V. Zoneamento de risco de incêndios florestais para a Floresta Nacional de Irati, estado do Paraná, Brasil. Scientia Forestalis, 40(94), pp. 259-265, 2012.

[26] Yathish, H., Athira, K.V., Preethi, K., Pruthviraj, U., and Shetty, A., A Comparative analysis of forest fire risk zone mapping methods with expert knowledge. Journal of the Indian Society Remote Sensing, 47(12), pp. 2047-2060, 2019. DOI: https://doi.org/10.1007/s12524-019-01047-w

H.R. Ferreira, is a Forestry Technician in 2008 from the Colégio Florestal Estadual Presidente Costa e Silva, Brazil. BSc. Eng. in Forestry Engineer in 2017, from the Federal University of Paraná (UFPR) Brazil, and BSc. Eng. in Occupational Safety Engineer on 2021, from the UNIFACEAR. Sp. in Forest Fire Prevention in 2021, from the UFPR and a MSc. in Nature Conservation in 2021, from the Postgraduate Program in Forestry Engineering at UFPR, Brazil. He has been a doctoral candidate in the area of Nature Conservation through the Postgraduate Program in Forestry Engineering at UFPR, where he has dedicated himself to academic research related to fires in vegetation located in wildland-urban interface areas, acting as an ad hoc reviewer of journals. He has experience carrying out different works in the forestry area and currently holds the position of forestry engineer at Itaipu Binacional with the Protected Areas Division (MARP.CD).
ORCID: 0000-0002-9433-6757

A.C. Batista, graduated in 1979, MSc. in 1984 and Dr. in Forestry Engineering in 1995 from the Federal University of Paraná, Brazil. He is currently a full professor at the Federal University of Paraná. He has experience in the area of Forest Resources and Forest Engineering, with an emphasis on forest protection and meteorology and forest climatology,

working mainly on the following topics: preventing and combating forest fires, fire behavior, fire effects, controlled burning, microclimate, urban climate and urban-rural interface (WUI). He is a professor at the Postgraduate Program in Forestry Engineering at the Federal University of Paraná and the Postgraduate Program in Forestry and Environmental Sciences at the Federal University of Tocantins. Since April 2016, he has been editor-in-chief of Revista Floresta. He is currently the Coordinator of the Postgraduate Program in Forestry Engineering at the Federal University of Paraná (mandate 07/11/2023-06/11/2025).
ORCID: 0000-0001-5929-3838

A.F. Tetto, is BSc Eng. in Forestry Engineering in 1997from the Federal University of Paraná, Brazil. He specializes in preventing and combating forest fires, with a MSc. and Dr. in Nature Conservation. He served as coordinator of the undergraduate course in Forestry Engineering (2012 to 2014), as Financial Director of FUPEF (Fundação de Pesquisas Florestais do Paraná) (2014 to 2016) and Administrative Director (2019 to 2020). He is currently the financial director of FUPEF, coordinator of the specialization course in preventing and combating forest fires, and associate professor of the Forest Engineering course at UFPR in the disciplines of forest fires, meteorology, and forest climatology and management of wild areas for graduation, and fire ecology, forest microclimatology and management of protected natural areas for postgraduate studies. He works in research with an emphasis on forest fire prevention, microclimatology, and management of conservation units.
ORCID: 0000-0003-2251-964X

D. Biondi, is BSc Eng. in Forestry Engineering from the Federal Rural University of Pernambuco, Brazil. MSc. and Dr. in Forestry Engineering from the Federal University of Paraná. She is currently a full professor at the Federal University of Paraná. She has experience in teaching (undergraduate and postgraduate), research, and extension in the area of forest resources and forestry engineering, with an emphasis on nature conservation. Since August 2014, she has been editor-in-chief of the Journal of the Brazilian Society of Urban Arborization and Deputy Editor of Revista Floresta since July 2016. She coordinates the UFPR Landscaping Laboratory. He has been a Scientific Productivity Fellow at CNPq since 2007. She is currently a member of the Interinstitutional Working Committee of the Public Ministry of Paraná to analyze the Municipal Urban Afforestation Plans of the State of Paraná.
ORCID: 0000-0003-0532-7363

DYNA
http://dyna.medellin.unal.edu.co/

UNIVERSIDAD NACIONAL DE COLOMBIA

Reactivation of three test benches of high, medium and low power electric generators for hydraulic energy conversion

Mairim Hortensia Márquez-Romance, Adriana Mercedes Márquez-Romance, Bettys Farías -De Márquez, Edilberto Guevara-Pérez & Sergio Alejandro Pérez-Pacheco

Centro de Investigaciones Hidrológicas y Ambientales, Universidad de Carabobo, Carabobo, Venezuela. mmarquer@uc.edu.ve, ammarquez@uc.edu.ve, bfarias@uc.edu.ve, eguevara@uc.edu.ve, sperez@uc.edu.ve

Received: February 21th, 2024. Received in revised form: May 30th, 2024. Accepted: June 5th, 2024.

Abstract
This paper deals with the reactivation of three test benches of high, medium and low power electric generators for hydraulic energy conversion in the University of Carabobo Hydraulic Laboratory. The method involves three stages: i) Description of three high, medium and low power electric generators for hydraulic energy conversion, ii) Rehabilitation of three high, medium and low power electric generators for hydraulic energy conversion and iii) Evaluation of performance indexes of high, medium and low power electric generators for hydraulic conversion. The results indicate that for the low power electric generator, the position angle of the distributor blades is an experimental factor that has a significant effect on the response variables studied. With respect to the medium and high power electric generators, the most influential factor on operation and power generation is the flow supplied.

Keywords: Francis turbine; Kaplan turbine; Pelton turbine; power electric generators; turbomachinery.

Reactivación de tres bancos de pruebas de generadores eléctricos de alta, media y baja potencia para conversión de energía hidráulica

Resumen
El presente trabajo trata sobre la reactivación de tres bancos de pruebas de generadores eléctricos de alta, media y baja potencia para conversión de energía hidráulica en el Laboratorio de Hidráulica de la Universidad de Carabobo. El método involucra tres etapas: i) Descripción de tres generadores eléctricos de alta, media y baja potencia para conversión de energía hidráulica, ii) Rehabilitación de generadores eléctricos de alta, media y baja potencia para conversión de energía hidráulica y iii) Evaluación de índices de desempeño de generadores eléctricos de alta, media y baja potencia para conversión de energía hidráulica. Los resultados indican que para el generador eléctrico de baja potencia, el ángulo de posición de las palas del distribuidor es el factor experimental que tiene un efecto significativo en las variables de respuesta estudiadas. Con respecto a los generadores eléctricos de media y alta potencia, el factor que más influye en el funcionamiento y generación de energía es el caudal suministrado.

Palabras clave: Turbina Kaplan; turbina Pelton; turbina Francis; generadores eléctricos de potencia; turbomaquinaria.

1 Introduction

In Venezuela, where the main source of electrical energy is of water origin, representing approximately 60% of the country's total production [1], it is essential to educate the population regarding the generation and saving this resource and implementing plans for the use of any alternative source that contributes preserve the environment and life on the planet [2].

Venezuela is constitutionally and internationally committed to developing technologies that work with clean or renewable energy. For this reason, the State at the energy level has set the following goals: Raise awareness of the rational and efficient use of electricity; improve the distribution, maintenance and generation of the national electricity system; complete the hydroelectric plants already started; working on new low, medium and high generation

How to cite: Márquez-Romance, M.H., Márquez-Romance, A.M., Farías -De Márquez, B., Guevara-Pérez, E. and Pérez-Pacheco, S.A., Reactivation of three test benches of high, medium and low power electric generators for hydraulic energy conversion. DYNA, 91(232), pp. 139-148, April - June, 2024.

electrical projects, as well as investing in educational programs, research, modernization of laboratories, among others [2].

In the Elías Sánchez Díaz hydraulics laboratory, of the School of Civil Engineering of the University of Carabobo, there are three (3) turbine benches that were inoperative for more than 40 years, due to lack of economic resources for their maintenance. The reactivation of these turbine banks corresponded to the project N° 2014000418 supported by the National Fund for Science, Innovation and Technology attached to the Ministry of Popular Power for Science and Technology, through which students attached to the Center for Hydrological and Environmental Research of the University of Carabobo (CIHAM-UC, by its acronym in Spanish) and belonging to the Schools of Mechanical, Electrical and Civil Engineering of the University of Carabobo developed special works to obtain the academic degree and contribute to the reactivation of the benches of low, medium and high power electric generators for conversion of hydraulic energy in the Hydraulic Laboratory of the University of Carabobo., managing to fulfill the purpose satisfactorily [3].

This investigation has as objectives: i) Description of three high, medium and low power electric generators for hydraulic energy conversion, ii) Rehabilitation of three high, medium and low power electric generators for hydraulic energy conversion and iii) Evaluation of performance indexes of high, medium and low power electric generators for hydraulic conversion.

2 Materials and methods

2.1 Description of low power electric generator bench for hydraulic energy conversion

In the schematic diagram shown in Fig. 1, the water required for the operation of the low power electric generator bench (Kaplan turbine), is supplied through line L1 and is controlled by valve (V1), both are located in the top of the flow stabilization tower (FST). The flow stabilization tower contains a flow vertical line (Ld), which is open to the atmosphere and is used to release air masses trapped in the ductwork during filling and testing on the Kaplan turbine bench.

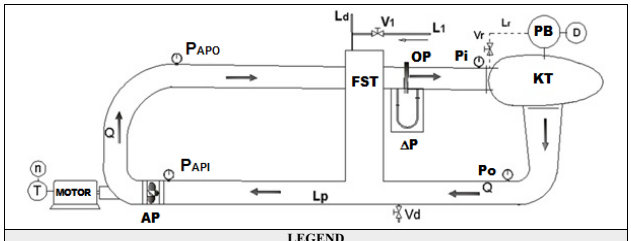

LEGEND	
KT: Kaplan turbine	**T:** Engine torque meter
FST: Flow stabilization tower	**n:** Engine tachometer
AP: Axial flow pump	**L_P:** Fiberglass main duct in Ø 12 "
PB: Prony brake on the KT	**L_1:** Water supply line to the KT test bench
PBD: Prony brake dynamometer	**L_d:** Air release device
ΔP: Mercury piezometer	**L_r:** Cooling line of PB
OP: Orifice plate	**V_r:** Cooling valve of PB
Pi: Inlet pressure gauge of the KT	**V_1:** Fill valve of KT test bench
Po: Outlet pressure gauge of the KT	**V_d:** Drain valve of KT test bench
P_{APO}: Axial pump outlet pressure gauge	**Q:** Water flow of the KT test bench
P_{API}: Axial pump inlet pressure gauge	**motor:** motor driving to the AP

Figure 1. Schematic diagram of the low power electric generator test bench (Kaplan turbine) at the Hydraulic Laboratory of the University of Carabobo. Source: Own elaboration. Adapted from [4].

2.2 Description of medium power electric generator bench for hydraulic energy conversion

The test bench of the medium power electric generator (Francis Turbine) is provided with a common water recirculation system with that of the high-power electric generator (Fig. 2). For the execution of the different tests on the Francis turbine, valves V1 and V3 must be kept open, while valves V2 and V4 must be kept closed. The Francis turbine has a built-in motor-generator (G), being controlled from a control panel, in which the voltage and current consumed or produced during the test can be observed. Pump B transfers the energy to the water (Fig. 2), making it flow to the pipeline system or network through lines L1, L2, L3, and L4. The water acquires a suitable pressure and height to carry out the different tests on the turbines. The pump is fed by tank T1, which must be 80% full before starting the pump. The main ten components that make up the Francis turbine are shown in Fig. 3, which involve [4]: 1) spiral chamber, 2) turbine suction tube, 3) turbine inlet tube, 4) torsion gauge, 5) motor-generator, 6) governor transmission box, 7) tachometer, 8) hydraulic governor, 9) Fink type distributor and 10) electrical connection.

2.3 Description of high-power electric generator bench for hydraulic energy conversion

Fig. 4 shows the Pelton turbine components that directly intervene in the transformation of hydraulic energy into mechanical energy, including the following [4]: 1) Impeller or Wheel, 2) Casing, 3) Lance, 4) Mouthpiece, among others.

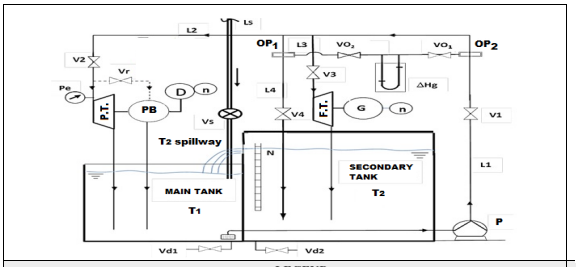

LEGEND:	
PT: Pelton turbine test bench	***L_s :*** Line for supplying water to the bench
FT: Francis turbine test bench	***L_4:*** System discharge line
B: Centrifugal pump	***D:*** Dynamometer to measure the torque of the shaft of the KT
OP_1: Orifice plate to measure pressure drop in line L4.	***V_1, V_2, V_3, V_4:*** Valve that controls the filling of t bench
OP_2: Orifice plate to measure pressure drop in line L1.	***Vr:*** Water cooling valve for the Prony Brake.
ΔHg: Mercury piezometer of the system	***N:*** Tank level T_2
Pe: Pressure gauge at the inlet of the Pelton Turbine.	***T:*** Engine torque meter
PB: Device to measure the power to the axis type brake Prony	***L_r:*** Prony Brake Water Cooling Line
Spillway : T_2 tank spillway	***G:*** Francis turbine generator
L_1 : Pump discharge line.	***Vs:*** Tank fill control valve T2
L_2, L_3: Water adduction lines to turbines	***Vd_1, Vd_2:*** Drain valve for tanks T1 and T2.
T_1: Main tank that feeds the pump	***n:*** Tachometer to measure R.P.M. the motor.
T_2: Tanque de descarga de la turbina Francis.	

Figure 2. Schematic diagram of the test benches of the high (Pelton turbine) and medium (Francis turbine) power electric generators at the Hydraulic Laboratory of the University of Carabobo.
Source: Own elaboration. Adapted from [4].

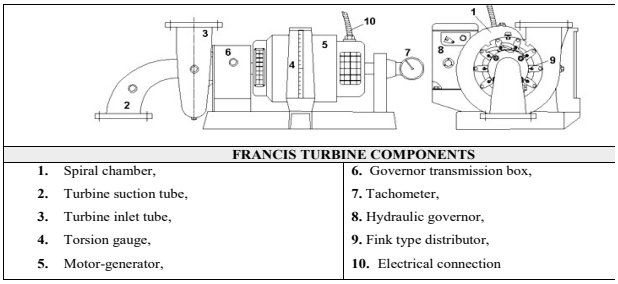

FRANCIS TURBINE COMPONENTS	
1. Spiral chamber,	**6.** Governor transmission box,
2. Turbine suction tube,	**7.** Tachometer,
3. Turbine inlet tube,	**8.** Hydraulic governor,
4. Torsion gauge,	**9.** Fink type distributor,
5. Motor-generator,	**10.** Electrical connection

Figure 3. Francis turbine components in the test bench.
Source: Own elaboration. Adapted from [4].

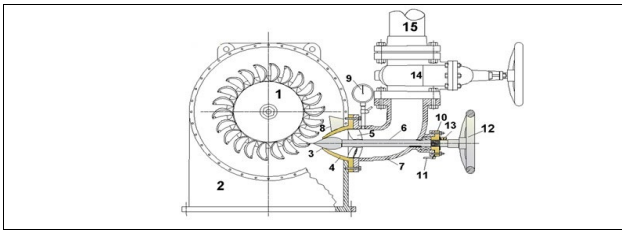

PELTON TURBINE COMPONENTS	
1. Impeller or Wheel	**9.** Bourdon pressure gauge,
2. Casing,	**10.** Brake nozzle,
3. Spear,	**11.** Bypass for packing drain,
4. Nozzle,	**12.** Spear rod flywheel,
5. Spear rod guide cross,	**13.** Nozzle opening guide,
6. Spear rod,	**14.** Flow regulating valve to the Pelton turbine,
7. Distributor,	**15.** System piping.
1. Fixed deflector,	

Figure 4. Pelton Gilkes 5961 turbine components from the test bench of the University of Carabobo (UC) Hydraulic Laboratory.
Source: Own elaboration. Adapted from [4]

2.4 Rehabilitation of three high, medium and low power electric generators for hydraulic energy conversion

The rehabilitation stages involved to carry out restoration and improvement actions of four systems are [4]: 1) electric power supply system for turbine benches, 2) water supply system for turbine benches, 3) Kaplan turbine test bench and 4) Pelton and Francis turbine test benches.

Electric power supply system for three turbine benches

Rehabilitation of electric power supply system for turbine benches involved the following actions: 1) Installation of a new NAB 412 board to embed three-phase 100 A breakers. The purpose of the new panel located within the laboratory area is to allow the turbine benches to be deactivated rapidly and safely in the event of a failure. 2) Installation of a circuit of ten (10) single-phase outlets for use in supplying the electronic instrumentation for monitoring and control foreseen in the practices in the turbine banks. This circuit was connected to the main board of the laboratory

Water supply system for three turbine benches

The water supply system for the benches of Pelton and Francis turbines required the installation of a plastic pipe complement of diameter 2" for feeding the benches (Fig. 5). With regard to the Kaplan turbine test bench, the complement that is installed towards the Kaplan turbine bench must be connected at the top of the stabilizer tower, which is where the inlet to the pipeline of this test bench is located (Fig. 8).

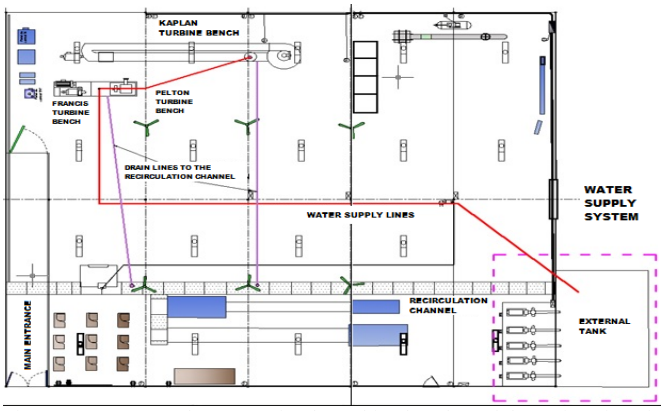

Figure 5. Water supply system for the turbine benches of the University of Carabobo (UC) Hydraulic Laboratory.
Source: Own elaboration. Adapted from [4]

2.4.1 Rehabilitation of low power electric generator bench for hydraulic energy conversion involved the following maintenances [4-5]:

Maintenance and electrical tests in the control panel and motor unit of the turbine bench.

a) Mechanical maintenance of the pumping unit (axial pump), based on the following three aspects: presence of sulfation of connections of iron inside the pump, binding of pump shaft and propeller and unleveling of the motor-pump shaft.
b) General maintenance of the bank ductwork, supported in three observations made in the diagnostic stage: hardened and cracked connection gaskets and presence of hydraulic leaks in the joints.
c) Kaplan turbine mechanical maintenance, which involves to correct the following actions: turbine shaft, distributor, connecting rod and crank binding, presence of iron sulfate inside the turbine, and absence of components or parts of the turbine.
d) Replacement and incorporation of control and measurement instruments: pressure gauges, hoses, valves and other components in the Kaplan turbine bench. The following needs were detected in the diagnostic stage: absence of dynamometer, wire, hoses and valves, need to install pressure gauges on the orifice plate and requirements for a sight glass on the flow stabilization tower.
e) Maintenance of the orifice plate, taps, valve and placement of the piezometric bench, it was found disconnection of the water-air piezometric bank from the ductwork that presents the orifice plate, and occlusion of connections for pressure measurement and valves.
f) Placement of water supply and drain control pipes and valves in the bank. This maintenance is required due to the water supply and drain pipe to the bank has been dismantled.
g) Installation of sight glass in the stabilization tower: it was found that the water level inside the stabilizer cannot be observed.
h) Establishment of the pressure range of the manometers and vacuum meters that will be used in the bench, the

existing pressure gauge on the bench has a range (0-160 psi), which is not adequate to what is expected at the turbine output (-5 to 5 psi) and the pressure gauges and vacuum gauges are required on the pump and turbine.

2.4.2 Rehabilitation of medium power electric generator bench for hydraulic energy conversion.

The test bench is divided into four subsystems involving [4,6-7]:

a) Water storage subsystem: The tank walls were found to be corroded due to exposure to the environment without any protection. Corroded material and paint removal is required on all walls with two coats of anticorrosive and one coat of enamel paint. In addition, the water level meter showed occlusion of the viewing tube due to sediment remaining in the system.
b) Flow distribution subsystem: Four gate valves were found to be clogged in the gate stroke due to corrosion inside the valve, creating an inability to regulate flow, requiring internal cleaning and external anti-corrosion and enamel coating.

The centrifugal water distribution pump presented high electricity consumption, melted supply cables to the pump, and a defective breaker, due to a possible short circuit, requiring replacement by a centrifugal pump with similar working conditions, replacement of the cables with new ones and greater caliber and replacement of the breaker with a new one of 30 A per line.

The manifold presented fracture in one of the union supports due to deterioration of the PVC part because of the exhaustion of its useful life and time in disuse, causing water leaks in the fitting, requiring its replacement of connections.

The mercury piezometer presented malfunction of the selector valves due to corrosion and deterioration caused by disuse, making it impossible to select between one or the other orifice plate, requiring the replacement of the system by a simple valve arrangement. As well as, malfunction at the time of the flow measurement, due to a low level of mercury in the reservoir, obtaining erroneous flow readings, requiring replacement of the mercury.

Orifice plates showed an absence of hoses, spigot connectors and clamps, making it impossible to connect the plates with the piezometer, requiring new hoses, spigot connections and clamps.

a) Francis turbine subsystem, a fractured stationary mechanical seal was found causing malfunction and handling that caused water to leak between the motor-generator and the turbine, requiring the manufacture of the mechanical seal with the original sample. The mechanical seals were embedded in the mating surface of the rotary mechanical seal due to time in disuse and exposure to the environment, creating water leaks between the motor-generator and the turbine, requiring lapping of the mating surface.

There was friction between the impeller and the volute case wear ring due to deformation of the impeller and wear ring surfaces, requiring machining of both parts on a lathe.

The dynamometer did not function due to the deterioration of the mercury reservoir seal, which made it impossible to read the braking force of the Francis turbine, requiring the manufacture of the seal.

Generator presented malfunction due to time in disuse and exposure to the environment, causing an impossibility of generating electrical energy which could lead to other failures, in addition to preventing the measurement of the force to the turbine brake, requiring replacement of the output wiring of the generator with direct connection to voltmeter and ammeter.

A faulty breaker was found in the control panel, due to a possible short circuit, causing the impossibility of energizing the control panel and resistance bench, requiring its replacement.

The control panel showed a defective motor-generator selector cylinder, requiring a new key manufacture.

The control panel had a faulty voltmeter and ammeter, making it impossible to read the voltage and current generated, requiring replacement with new devices.

a) Pelton turbine subsystem, this subsystem is part of the same test bench, sharing the subsystems of water storage and flow distribution and will be described in the next subsection.

2.4.3 Rehabilitation of high-power electric generator bench for hydraulic energy conversion.

Rehabilitation of high-power electric generator bench for hydraulic energy conversion consisted in the maintenance of three components involving [6-7]:

a) Rear bearing presented noise when rotating due to metal-metal friction, finding a rear bearing in poor condition that caused the staggered rotation of the turbine, requiring the replacement of the bearing with a new one.
b) Pressure gauge presented a malfunction that caused damage to the internal components due to the inability to measure the pressure at the turbine inlet, requiring replacement with a new pressure gauge.
c) Dynamometer, there was no dynamometer, which made it impossible to measure the braking force of the turbine, requiring the installation of a new dynamometer (clock-type scale 0-200 kgf).

2.5 Evaluation of performance indexes of high, medium and low power electric generators for hydraulic conversion

2.5.1 Evaluation of performance indexes of low power electric generator bench for hydraulic energy conversion

The experimental test design for the Kaplan Turbine system is a multilevel factorial design where there are three experimental factors and five response variables (Table 1). The experimental factors (Table 1) are comprised of the opening angle of the distributor blades which is defined by nine levels which are 1 in, 1 1/8 in, 1 1/4 in, 1 3/8 in, 1 1/2 in, 1 5/8 in, 1 3/4 in, 1 7/8 in, 2 in; the position angle of the impeller blades which has nine levels that are -5 °, 0 °, 5 °, 10 °, 15 °, 20 °, 25 °, 30 °, 35 ° and the rotation speed of the axis of the Kaplan turbine featuring six levels of studies which are 200 rpm, 400 rpm, 600 rpm, 800 rpm, 1000 rpm and 1200 rpm. For a total of combinations in the factors equal to $9 \; x \; 9 \; x \; 6 = 486$ tests.

Table 1.
Experimental factors of the design of experimental tests in the Kaplan turbine from the test bench of the University of Carabobo (UC) Hydraulic Laboratory.

Experimental factors	Number of Levels	Levels	Unit
Position angle of the distributor blades (X)	9	1, 1 1/8, 1 1/4, 1 3/8, 1 1/2, 1 5/8, 1 3/4, 1 7/8, 2	in
Angle of impeller blade position (ϕ)	9	-5, 0, 5, 10, 15, 20, 25, 30, 35	◦
Rotation speed of the Kaplan turbine shaft (N)	6	200, 400, 600, 800, 1000, 1200	rpm

Source: Adapted from [2].

Table 2.
Experimental factors of the design of experimental tests in the Francis turbine from the test bench of the University of Carabobo (UC) Hydraulic Laboratory.

Number of Levels	Levels	Unit
10	11,36; 17,03; 22,71; 28,39; 34,07; 39,74; 45,42; 51,10; 56,78; 62,45; (50, 75, 100, 125, 150, 175, 200, 225, 250, 275)	[m^3/h], (gpm)
2	50%, 100%	

Source: Adapted from [7].

2.5.2 *Evaluation of performance indexes of medium power electric generator bench for hydraulic energy conversion*

The design of the experimental tests of the Francis turbine system is shown in Table 2; where two (2) experimental factors are observed [7]: 1) Inlet flow (m^3/h) and 2) Distributor opening. For a total of combinations in the factors equal to 10 x 2 = 20 tests.

2.5.3 *Evaluation of performance indexes of high-power electric generator bench for hydraulic energy conversion*

The design of the experimental tests of the Pelton Turbine System is shown in Table 3; where three (3) experimental factors are observed [7]: 1) Inlet Flow (m^3 / h), 2) Punch Travel and 3) Rotation Speed (rpm). The first is tested on four levels. The second is tested on five levels. The third is tested on nine levels respectively. For a total of combinations in the factors equal to 4 x 5 x 9 = 180 tests

Table 3.
Experimental factors of the design of experimental tests in the Pelton turbine from the test bench of the University of Carabobo (UC) Hydraulic Laboratory.

Experimental factors	Number of Levels	Levels	Unit
Inlet flow	4	11,36; 22,71; 34,07; 45,42; (50, 100, 150, 200)	[m^3/h] (gpm)
Punch Travel	5	0.2, 0.4, 0.6, 0.8, 1	
Rotation speed of the Pelton turbine shaft (N)	9	400, 500, 600, 700, 800, 900, 1000, 1100, 1200	(rpm)

Source: Adapted from [7]

2.5.4 *Elaboration of the operating curves for the representation of the variables involved in the Kaplan Turbine, Francis Turbine and Pelton Turbine systems of the UC-Hydraulic Laboratory*

For the elaboration of the characteristic curves of the operation of the Kaplan turbine, Francis turbine and Pelton turbine systems of the UC-Hydraulic Laboratory [7], the data obtained from the experimental tests were processed; which implied estimating the response variables that represent the operation of a hydraulic machine, such as: a) Generated power, b) Efficiency, c) Net available head, among others. Each of these response variables were plotted with respect to the experimental factors controlled or set during the tests, such as: Kaplan and Francis turbines: a) the distributor opening, and b) flow through the turbine. Pelton turbine: a) rotation speed, b) punch stroke and c) flow through the turbine. In this way, a trend curve for the operation of turbine systems is obtained for each combination of these factors.

3 Results and discussion

3.1 Operating curves to represent the variables involved in the Kaplan turbine system of the UC-Hydraulic Laboratory

The operating curves of the Kaplan Turbine where the output variables of the system are shown in Fig 6, being obtained by applying the design of the experimental tests.

Figs. 6-8 represent the characteristic curves of the Kaplan turbine for opening angles of the impeller blades of -5º (Fig. 6) and 25º (Fig. 8). It can be seen that the curves have efficiencies of up to 65%. At opening angles of the impeller blades of 25º (Fig. 8), the system works more efficiently than with an opening of -5º to lower degrees of distributor opening. For instance, for a blade opening angle of -5º (Fig. 6), the performance hills for rotational speeds below 1200 rpm reach a distributor angle of 2 in, being significantly different from a 25º opening (Fig. 8) at the same rotational speed of the turbine shaft, where efficiencies are lower for a 1 1/2 in. distributor opening.

In Fig. 8h, which represents the curves at an angle of 0º (Fig. 6) for opening of the impeller blades, hills were obtained up to 95% of efficiency associated to 1200 rpm. The efficiencies vary between distributor opening angles of 1 3/4 in and 1 1/4 in, in which flow rates between 900 gpm and 1300 gpm are fed instead for a 30º impeller angle (Fig. 8h), reaching performances up to 95% at rotation speed of 1200 rpm and lower where it is appreciated that the performance hills are between 2 in and 1 1/2 in and these efficiencies are obtained for flow rates varying between 1250 gpm and 1600 gpm. Graphically, it is observed that for lower angles of the distributor at 0º, the system is more efficient than with an angle of 30º for opening of the impeller blades.

The curves with opening angles of the impeller of 10º (Fig. 7), 15º (Fig. 7e) and 20º (Fig. 7f) have efficiency hills of up to 80%, the curves at 10º and 15º (Fig.7) have very similar hills, however the difference is more notable for the curve of 80% performance since it could be observed that at lower flow rates of 1200 gpm at 15º (Fig. 7) this performance

is not obtained, instead at 10º it varies between 1300 gpm and 1100 gpm being able to observe graphically how the curve closes due to that the values at this performance do not reach the line with a 2 in manifold angle opening. It should be noted that at higher turning speeds and lower distributor opening the system with an opening of 20º is more efficient than with openings of 10º and 15º (Fig. 7).

When analyzing the curves at 5º opening of the impeller (Fig. 6c), it is observed that the performance hills start and end at an distributor opening of 2 in, unlike the curves at 35º (Fig. 8i) where all the performance hills were evaluated at a rotation speed of 1200 rpm, it is graphically observed that they do not reach 1 3/4 in. This is why it is concluded that at 35º (Fig. 8) the system behaves more efficiently than with an opening of 5º (Fig. 6).

3.2 Operating curves to represent the variables involved in the Francis turbine system of the UC-Hydraulic Laboratory

The results of the operation of the Francis turbine system of the UC-Hydraulic Laboratory are described through the following four variables [7]: 1) Generated Electric Power, 2) Net head delivered by the fluid to the turbine, 3) Rotation speed, and 4) Efficiency of the turbine. These variables are studied with respect to the experimental factors controlled during the tests carried out on the turbine, which are the inlet flow rate and the opening of the inlet distributor.

Flow rate against rotation speed of the Francis turbine system of the UC-Hydraulic Laboratory.

Fig. 9a shows the increase in the speed of rotation with increasing the input flow to the turbine, two curves are shown in the same graph, and each one corresponds to an opening value of the input distributor. The increase in the rotation speed is generated because the higher the input flow, the greater the energy that is provided to the turbine and this converts it into motive energy.

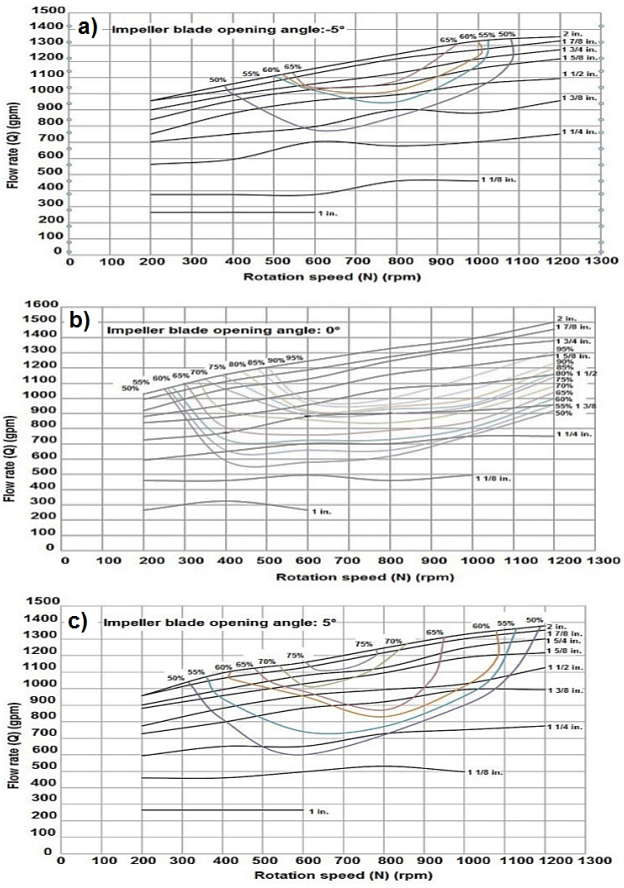

Figure 6. Kaplan turbine characteristic curve for impeller blade position angles of a) -5º, b) 0 ° and c) 5 ° from the test bench of the University of Carabobo (UC) Hydraulic Laboratory.
Source: Adapted from [5].

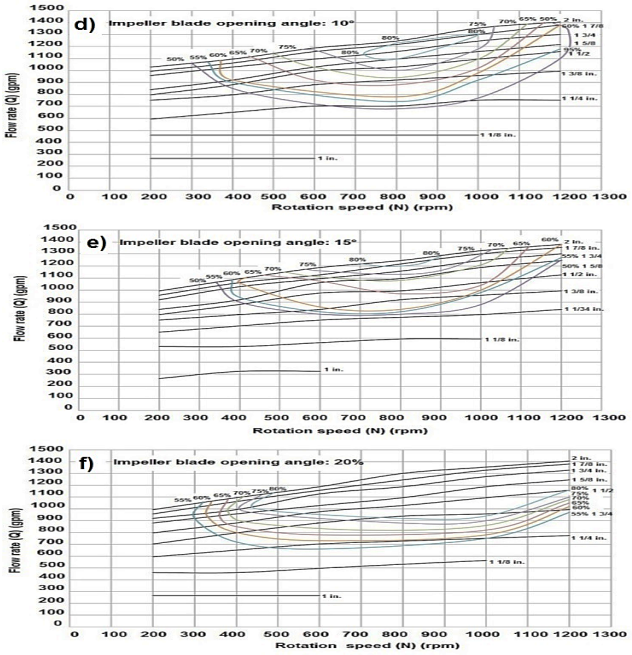

Figure 7. Kaplan turbine characteristic curve for impeller blade position angles of d) 10º, e) 15° and f) 20° from the test bench of the University of Carabobo (UC) Hydraulic Laboratory.
Source: Adapted from [5]

Flow rate against net head of the Francis turbine system of the UC-Hydraulic Laboratory.

Fig. 9b shows the variation of the net charge supplied to the turbine depending on the inlet flow and the position of the turbine distributor. It can be seen that the higher the flow rates, the greater the net load that is generated due to the fact that having a greater volume of fluid circulating through the same area increases the inlet pressures and the fluid velocities. In addition, it can also be seen that for a smaller opening of the distributor, a greater load can be obtained because the inlet is restricted, which causes an increase in the speed and inlet pressure of the fluid.

Flow rate against electrical power generated by the Francis turbine system of the UC-Hydraulic Laboratory.

In Fig. 6c, it can see the increase in electrical power with respect to the flow, this occurs since, as mentioned before, the higher the input flow, the greater the net load is delivered to the turbine, which produces an increase in useful power that the turbine can generate. In the case of the Francis turbine

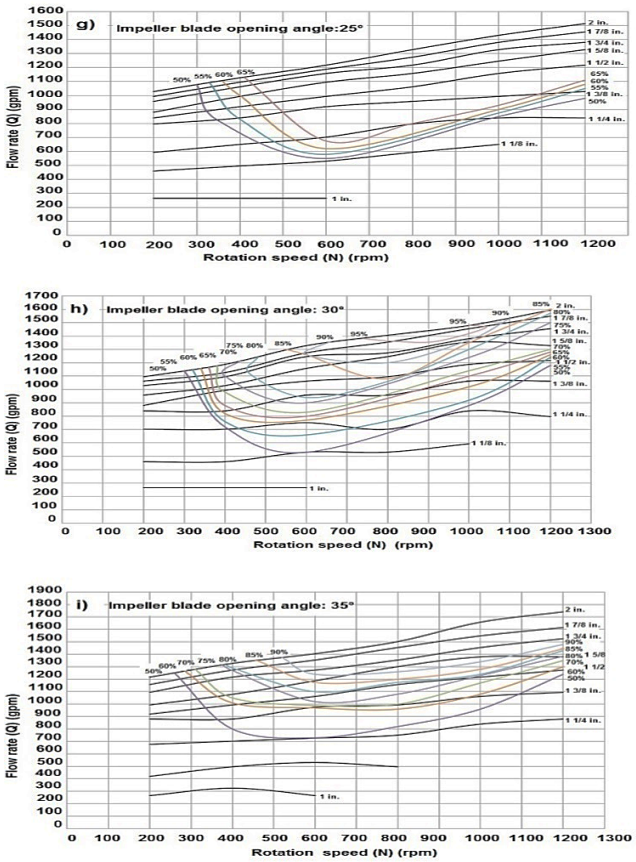

Figure 8. Kaplan turbine characteristic curve for impeller blade position angles of g) 25.º, h) 30° and i) 35° from the test bench of the University of Carabobo (UC) Hydraulic Laboratory.
Source: Adapted from [5].

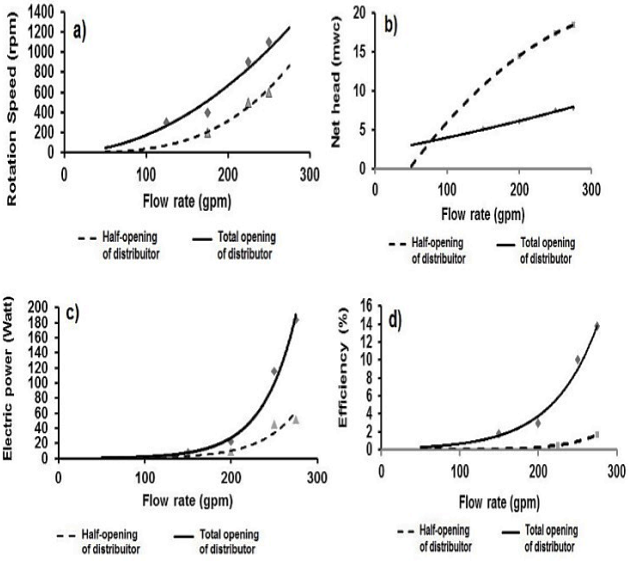

Figure 9. a) Flow against rotational speed curves obtained in Francis turbine test bench. Hydraulic Laboratory - University of Carabobo, b) Flow rate against net head obtained in Francis turbine test bench. Hydraulic Laboratory - University of Carabobo, c) Flow rate against electric power obtained in Francis turbine test bench. Hydraulic Laboratory - University of Carabobo, d) Flow rate against efficiency obtained in Francis turbine test bench. Hydraulic Laboratory - University of Carabobo.
Source: Adapted from [7]

system of the UC-Hydraulic Laboratory, this useful power is directly translated into electrical power thanks to the generator and the electrical panel that it has attached to it.

Flow rate against efficiency obtained from Francis turbine system of the UC-Hydraulic Laboratory

Fig. 9d shows the efficiency with respect to the inlet flow of the Francis turbine system of the test bench of the UC-Hydraulic Laboratory. The graph shows that for higher inlet flows the turbine efficiency tends to increase.

3.3 Operating curves to represent the variables involved in the Pelton turbine system of the UC-Hydraulic Laboratory

The variables that describe the operation of the Pelton turbine system of the UC-Hydraulic Laboratory are [7]: the generated brake power, the net load delivered by the fluid to the turbine and the efficiency obtained from the turbine. Each of these factors is studied with respect to the variables that can be controlled during the test, such as the stroke of the punch, the speed of rotation of the turbine and the input flow to the turbine.

- Flow rate against rotation speed of the Pelton turbine system of the UC-Hydraulic Laboratory

In Fig. 10a, the variation of the rotation speed with respect to the increase in the input flow to the turbine can be observed. This is congruent with the theoretical operation of a turbine which indicates, as it has been studied before, that the higher the inlet flow and the head of the water, the more energy is delivered to the turbine, which is transformed into mechanical energy in the form of angular velocity in the shaft coupled to the turbine rotor.

- Flow rate against net head curve of the Pelton turbine system of the UC-Hydraulic Laboratory.

Fig. 10b shows how the net head available for the action of the turbine increases depending on the increase in the input flow of the turbine. Likewise, it can be observed that for longer strokes of the punch it is possible to obtain data at higher flow rates, which results in curves with less steep slopes. This graph is made only with the data of the tests in which there is a turning speed of 400 rpm, because this is the speed at which for each combination of the different levels of flow and punch stroke it is possible to obtain enough net load points to generate a curve.

- Rotation speed against brake power curves of the Pelton turbine system of the UC-Hydraulic Laboratory.

In Fig. 10c-10f, it can be seen how the power on the Pelton turbine shaft varies depending on the speed of its rotation, likewise the powers obtained and the amount of data collected depending on the flow that is supplied can be compared to the turbine, it is evident that for a higher flow there is the possibility of turning the turbine at higher revolutions and applying a greater brake force on the shaft, this translates into greater power on the turbine shaft even for longer punch strokes those that can be placed at lower flow rates.

- Rotation speed against efficiency of the Pelton turbine system of the UC-Hydraulic Laboratory.

In Fig. 11g-11i, the curves are presented in which it can be observed how the efficiency varies according to the rotation speed of the turbine depending on the different inlet injector openings and the different inlet flow rates with which they were taken the data of the experiment. It is important to note that just as for higher flows a greater brake power is obtained, the efficiency also tends to increase with the increase of the flow that circulates through the turbine.

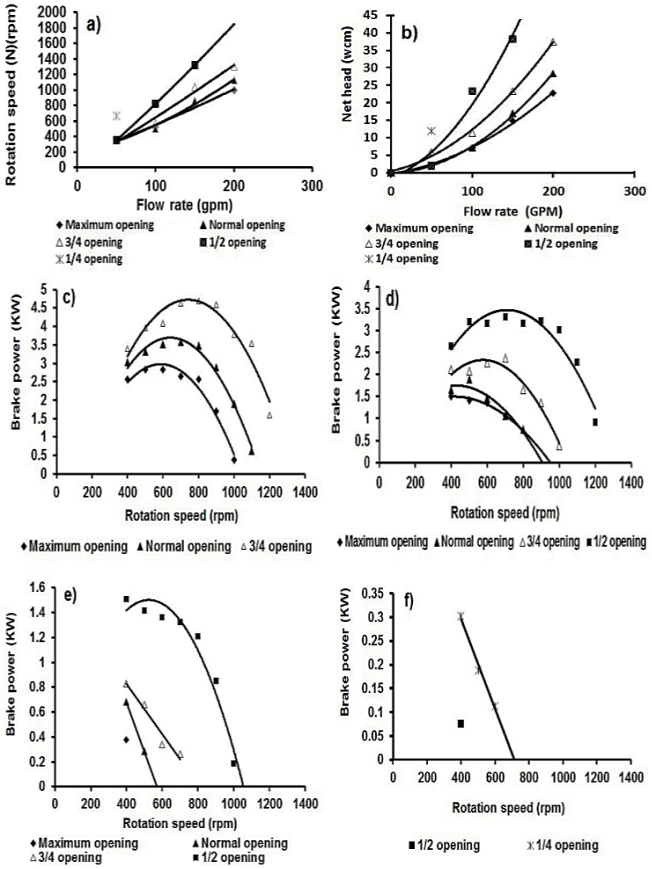

Figure 10. a) Flow rate against rotation speed of the Pelton turbine system of the UC-Hydraulic Laboratory, b) Flow rate against net head curve of the Pelton turbine system of the UC-Hydraulic Laboratory, c) Rotation speed against brake power under a flow rate of 200 gpm, d) Rotation speed against brake power under a flow rate of 150 gpm, e) Rotation speed against brake power under a flow rate of 100 gpm, f) Rotation speed against brake power under a flow rate of 50 gpm.
Source: Adapted from [6-7]

4 Discussion

Kaplan turbine test bench in the current study gave operating results similar to the Kaplan turbine test bench used to implement laboratory test in the "Escuela Superior Politécnica de Chimborazo", Ecuador. In the Kaplan turbine bench operated under the following conditions: rotation speed varied between 405 and 1680 rpm, net head between 1.37 x 10^{-3} and 3.05 x 10^{-2} mwh (meters of water head), flow rate between 1759.39 to 1866.22 gpm, and generated power between 1.34 and 1.45 KW and total efficiencies between 8 and 15 % [8].

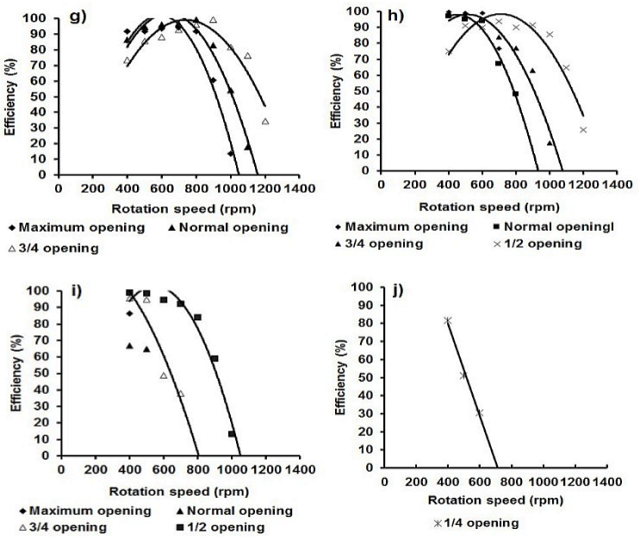

Figure 11. g) Rotation speed against efficiency under a flow rate of 200 gpm, h) Rotation speed against efficiency under a flow rate of 150 gpm, i) Rotation speed against efficiency under a flow rate of 100 gpm, j) Rotation speed against efficiency under a flow rate of 50 gpm.
Source: Adapted from [6-7]

From the current experience to reactivate three hydraulic turbine test benches, prospective studies were produced to project micro hydroelectric generation plants advised by CIHAM-UC. The purpose of the studies was to analyze the hydroelectric potential of Pao Cachinche (PC-WR) (Carabobo-Cojedes States) [9], Pao Las Balsas (PLB-WR) (Cojedes State) [10], Dos Cerritos (DC-WR) (Lara State) [11], and El Pueblito (EP-WR) (Guárico State) water reservoirs [12] used for supplying uses for human consumption and agricultural development. The descriptive statistical analysis carried out on the water elevation variable showed that the PC-WR, PLB-WR and EP-WR did not reach critical water levels during the period 2005-2015. DC-WR presented steady values during the period 1988-2013; where the variables associated to area and volume had a decrease in recent years, without compromising the operating levels of the reservoir. Through the study carried out, it was determined that the design flow would be approximately 1 m3/s according to the criteria used for its selection, taking ecological expenditure as a reference. The design power varied between 73.39 KW and 73.88 KW respectively, corresponding to the selection range of the Francis turbine.

5 Conclusions

The determination of the operating characteristics of the Kaplan turbine allowed us to know which are the parameters that influence the behavior of this type of turbine and establish the ranges in which each parameter operates in the Kaplan Turbine system belonging to the "Elías Sánchez Díaz" from the School of Civil Engineering of the University of Carabobo. The multilevel factorial design was used in the design of experimental tests for the Kaplan turbine system, managing to study the different levels that each experimental factor has through all possible combinations of the levels of each factor; by making use of this design, it was possible to

obtain the influence of each factor on the response variables, determining that the position angle of the distributor blades as an experimental factor has a greater effect on the response variables studied.

The results of the design of the experimental tests have made it possible to know the conditions that influence the operation of each turbine and establish the regulation ranges of each parameter in the Francis turbine and Pelton turbine systems belonging to the "Elías Sánchez Díaz" hydraulic laboratory of the University of Carabobo. The factorial design has led to 7 experimental tests on the Francis Turbine System and 65 experimental tests on the Pelton turbine system. In both turbines, the most influential factor on operation and power generation is the flow supplied; which varies in the first system varies between 100 and 275 gpm; in the second system between 50 and 250 gpm.

Experiences to the laboratory scale about the reactivation of three test benches of hydraulic generators will be useful to develop projects on micro hydroelectric generation plants. The feasibility of projects on micro-plants for hydraulic energy conversion has been analyzed by CIHAM-UC using the framework of the water reservoirs /WR) for human consumption located in the northern region of the Bolivarian Republic of Venezuela, evaluating their hydroelectric potential. The water reservoirs included to Pao Cachinche (PC-WR) (Carabobo-Cojedes States), Pao Las Balsas (PLB-WR) (Cojedes State), Dos Cerritos (DC-WR) (Lara State) and El Pueblito (EP-WR) (Guárico State) water reservoirs used for supplying uses for human consumption and agricultural development. Based on this analysis, it was determined that the design flow would be approximately 1 m^3/s according to the criteria used for its selection, taking ecological flow rate as a reference. The design power varied between 73.39 KW and 73.88 KW respectively, corresponding to the selection range of the Francis turbine.

Data availability

The data that supports the findings of this study are available in the institutional repository of the University of Carabobo through of the following approved bachelor theses: [4-8,10-12].

Acknowledgements

This research was funded by the National Fund for Science, Technology and Innovation, belonging to the Ministry of Popular Power for Science and Technology, Venezuela.

References

[1] Ministerio del Poder Popular para la Energía Eléctrica (MPPEE). MPPEE homologa metodología de cálculos de indicadores para mitigar los efectos del cambio climático. Prensa. [en línea]. 2024. Disponible en: http://mppee.gob.ve/?p=87464

[2] Observatorio Regional de Planificación para el Desarrollo de América latina y el Caribe. Plan de la Patria 2109-2025 de Venezuela. [en línea]. 2024. Disponible en: https://observatorioplanificacion.cepal.org/es/planes/plan-de-la-patria-2019-2025-de-venezuela

[3] Márquez, A., Final Technical Report. Project No. 2014000418: Reactivation of three test benches for high, medium and low power electric generators for the conversion of hydraulic energy, Elías Sánchez Díaz Hydraulic Laboratory, University of Carabobo, Venezuela. [en línea]. 2018. Disponible en: http://riuc.bc.uc.edu.ve/handle/123456789/8453

[4] Márquez, A.M., and Salazar-Reyes, I.A., Proposal for the reactivation of the Kaplan, Pelton and Francis turbine banks in the "Elías Sánchez Díaz" Hydraulics Laboratory, Bachelor's thesis. School of Civil Engineering, University of Carabobo, Venezuela, [online]. 2016. Available at: https://riuc.bc.uc.edu.ve/handle/123456789/8438

[5] Márquez, A.M, García, J., and Pacheco, M., Evaluation of the operation of the Kaplan turbine system in the "Elías Sánchez Díaz" Hydraulics Laboratory, Bachelor's thesis. School of Civil Engineering, University of Carabobo, Venezuela, [online]. 2015. Available at: https://riuc.bc.uc.edu.ve/handle/123456789/8441

[6] Márquez, A.M., Martínez, I., and Uzcátegui, J., Rehabilitation of the Francis-Pelton turbine system of the Hydraulics Laboratory, Bachelor's thesis. School of Civil Engineering, University of Carabobo, Venezuela, [online]. 2016. Available at: https://riuc.bc.uc.edu.ve/handle/123456789/8437

[7] Márquez, A.M, and Cachinca, J., Evaluation of the operation of the Francis turbine and Pelton turbine systems of the Hydraulics Laboratory, Bachelor's thesis. School of Civil Engineering, University of Carabobo, Venezuela, [online]. 2016. Available at: https://riuc.bc.uc.edu.ve/handle/123456789/8440.

[8] López-García, C.G., and Puma-Riofrío, J.I., Repowering of the Kaplan axial flow turbine test bench of the Hydraulic Turbomachinery Laboratory of the Faculty of Mechanics. Undergraduate thesis. "Escuela Superior Politécnica de Chimborazo", Ecuador, 2022.

[9] Márquez, A., Guevara-Rodríguez, O.J., and Linares-Sepúlveda, J.A., Analysis of the hydroenergetic capacity of the Pao Cachinche reservoir. Bachelor's thesis. School of Civil Engineering, University of Carabobo, Venezuela, [online]. 2016. Available at: http://riuc.bc.uc.edu.ve/handle/123456789/8445

[10] Márquez, A., González, N., and Hoyle, M., Analysis of the hydroenergetic capacity of the Pao la balsa reservoir, Cojedes state. Bachelor's thesis. School of Civil Engineering, University of Carabobo, Venezuela, [online]. 2016. Available at: http://riuc.bc.uc.edu.ve/handle.net/123456789/8444

[11] Márquez, A., Rebolledo, M., and González, C., Analysis of the hydroenergy capacity of the reservoirs of the Lara State. Bachelor's thesis. School of Civil Engineering, University of Carabobo, Venezuela, 2016.

[12] Márquez, A., Anderi-Matos, A.R., and Caspe-Moyeja, A.E., Analysis of the hydroenergetic capacity in the reservoirs of the Unare River basin located between the Guárico and Anzoátegui states. Bachelor's thesis. School of Civil Engineering, University of Carabobo, Venezuela, [online]. 2016. Available at: http://www.riuc.bc.uc.edu.ve/handle/123456789/7118

M.H. Márquez-Romance, was born in Venezuela, in 1977. She is BSc. Eng. in Electrical Engineering in 2000 from the UC. MSc. in Instrumentation in 2005, from the Central University of Venezuela. She is PhD student in Instrumentation at Central University of Venezuela. Since 2003, she is professor in School of Basic Studies at UC Engineering Faculty, teaching Physics I, Physics II, Physics Laboratory I, Physics Laboratory II. Since 2002, she was a professor at Jose Antonio Páez University, teaching Control Theory and Sensors and Data Acquisition. She is author of three books. She is member of CIHAM-UC.
ORCID: 0009-0000-9406-5611

A.M. Márquez-Romance, was born in Venezuela, in 1976. She She is BSc. Eng. in Civil Engineering in 1999, MSc. in Environmental Engineering in 2006 and PhD. in Engineering in 2011, all of them form the University of Carabobo (UC), Venezuela. From 2002 to the present, she is professor in School of Civil Engineering. From 2006, she is member and co-founder of the Center for Hydrological and Environmental Research (CIHAM-UC) belonging to UC. From 2013 to the present, she is member and coordinator of UC master program on environmental engineering.
ORCID: 0000-0003-1305-5759

B.E. Farías-De Márquez, was born in Venezuela in 1961. She is aggregate professor of Civil and Environmental Engineering at the University of Carabobo (UC), Venezuela. She is active researcher at Center for Environmental and Hydrological Research of the UC. From 2014 to the present, she is an active professor at Civil Engineering School of the UC. Since 1986, she holds a BSc. Eng. in Civil Engineer from UC and a MSc. in Environmental Engineering. Since 2023, she reached her PhD degree in Environmental Engineering at the UC.
ORCID: 0000-0002-7737-2545

E. Guevara-Pérez, was born in Peru, 1943. He received BSc. Eng. in Agricultural Engineering, in 1968, mention in water resources achieved from the National Agrarian University, Peru. MSc. in Agricultural Engineering in 1970, focused on irrigation and drainage engineering developed in Justus Liebig University, Federal Republic of Germany. PhD. in Water Resources Planning in 1972, from the Christian Albrecht University, Federal Republic of Germany. Sp. in Irrigation and Drainage Engineering and Saline Soils in 1972, from the German Foundation for Developing Countries. Federal Republic of Germany in 1993, the Postdoctoral degree (Visiting Professor) in Colorado State University USA
ORCID: 0000-0003-2813-2147

S.A. Pérez-Pacheco, He is BSc. Eng. in Chemical Engineer in 1980, from the Universidad Simón Bolívar, Venezuela. Postgraduate in Applied Sciences, in 1989, from the University of Sherbrooke, Quebec, Canada, PhD in Chemical Engineering in 2000, from the University of Sherbrooke. Quebec, Canada, and Post doctorate in 2003 from the same University. Full-time professor at the University of Carabobo, Faculty of Engineering, School of Chemical Engineering (1981-2007), currently retired full professor. Founder of Research Unit in Process Engineering, and dedicated to research in area of modeling and simulation of chemical and environmental processes. Honorary member of Center for Hydrological and Environmental Research (CIHAM).
ORCID: 0000-0001-6957-7287

DYNA
http://dyna.medellin.unal.edu.co/

UNIVERSIDAD NACIONAL DE COLOMBIA

Susceptibility to moisture damage in asphalt mixes with blast furnace dust as aggregate

Ricardo Ochoa-Díaz [a], Gloria Elizabeth Grimaldo-León [b] & Carlos Hernando Higuera-Sandoval [a]

[a] *Grupo de Investigación y Desarrollo en Infraestructura Vial, Universidad Pedagógica y Tecnológica de Colombia, Tunja, Colombia. ricardo.ochoa@uptc.edu.co, carlos.higuera@uptc.edu.co*
[b] *Grupo de Investigación en Logística, Operaciones, Gestión y Calidad, Universidad de Boyacá, Tunja, Colombia. gegrimaldo@uniboyaca.edu.co*

Received: January 31th, 2024. Received in revised form: May 29th, 2024. Accepted: June 7th, 2024.

Abstract
One of the ongoing challenges in engineering is mitigating the degradation of road infrastructure caused by water in asphalt mixes. This study aims to assess the impact of blast furnace dust, a byproduct of the steel manufacturing process, on moisture-induced damage in asphalt mixes. Three asphalt mixes were developed following the Marshall methodology: one comprising conventional crushed aggregates, while the others substituted 50% and 100% of the conventional fine aggregate with blast furnace dust. Material characterization procedures and chemical analysis of the blast furnace dust were conducted. Once compliance with the specified material requirements was verified and analyzed, water susceptibility was evaluated through an indirect tensile test across various void content levels. Similarly, leveraging the Superpave gyratory compactor, several compaction indices were determined to estimate the compaction behavior of each mix. Based on the findings, the inclusion of blast furnace dust in an asphalt mix proved satisfactory due to its contributions in enhancing tensile strength, consequently leading to a reduction in moisture-induced damage within the asphalt mix, as well as exhibiting improved compaction behavior. Additionally, this utilization contributed to diminishing the environmental impact linked to the steel production process, where substantial quantities of this residue accumulate.

Keywords: asphalt mixture; blast furnace dust; energy of compaction; moisture susceptibility; recycling.

Susceptibilidad al daño por humedad en mezclas asfálticas con polvo de alto horno como agregado

Resumen
Uno de los desafíos constantes que enfrenta la ingeniería es reducir el deterioro de la infraestructura vial debido al agua en las mezclas asfálticas. La presente investigación busca evaluar la incidencia del polvo de horno alto, un subproducto del proceso del acero, en el daño por humedad en las mezclas asfálticas. Se diseñaron tres mezclas asfálticas bajo la metodología Marshall: una está compuesta por agregados convencionales triturados, las otras sustituyendo el 50% y 100% del agregado fino convencional por polvo de horno alto. Se llevaron a cabo los procedimientos de caracterización de materiales respectivos y la caracterización química del polvo de horno alto. Una vez verificado y analizado el cumplimiento de los requisitos establecidos para los materiales, se evaluó la susceptibilidad al agua utilizando una prueba de tracción indirecta para diferentes contenidos de vacíos. Del mismo modo, y aprovechando el compactador giratorio Superpave, se determinaron algunos índices de compactación y así se estimó el comportamiento de compactación de cada mezcla. Basándose en los resultados, el uso del polvo de horno alto en una mezcla asfáltica es satisfactorio debido a sus contribuciones para mejorar la resistencia a la tracción, lo que resultó en una reducción del daño por humedad en la mezcla asfáltica, así como un mejor comportamiento en la compactación. Además, se contribuyó a reducir el impacto ambiental causado por el proceso del acero, donde se acumulan grandes cantidades de este residuo.

Palabras clave: mezcla asfáltica; polvo de alto horno; energía de compactación; susceptibilidad a la humedad; reciclaje.

1 Introduction

The integral steelmaking process starts from exploiting raw materials: limestone, coal and, of course, iron ore. These materials reach primary manufacturing and undergo their first transformation. Coal is distilled in the coking plant to convert it into coke; the fines (iron, limestone, and coke) are transformed to a suitable granulometry in the sinter plant, and

How to cite: Ochoa-Díaz, R., Grimaldo-León, G.E., and Higuera-Sandoval, C.H., Susceptibility to moisture damage in asphalt mixes with blast furnace dust as aggregate. DYNA, 91(232), pp. 149-158, April - June, 2024..

all the materials for the manufacture of pig iron are melted in the blast furnace. Next, the pig iron is transformed into steel, and the rolling phase transforms the steel into the final finished product.

Throughout the process, waste is generated; in the case of the blast furnace, dust, sludge and slag. Blast furnace slag (BFS) is generated by the segregation of impurities and is composed of calcium, aluminum, silicates, and oxides of silicon and magnesium [1]. Blast furnace dust (BFD) is a waste with very little use; it contains iron, carbon and low amounts of magnesium, silicon, aluminum and calcium [2]. BFD is produced during the cleaning of gases produced in the manufacture of pig iron. The approximate production of BFD is from 7 to 45 kg per ton of pig iron [1].

Today, sustainability and environmental factors are important in pavement production and construction, and materials have come under investigation. Therefore, research regarding BFD as a partial or complete substitute for fine aggregate in an asphalt mix, and evaluation of damage by humidity, is proposed.

One of the most frequent damages in asphalt pavements is caused by the effect of water, especially in high rainfall areas [3]. This phenomenon is associated with the asphalt cement's cohesion, and the adhesion between the aggregate and the asphalt cement [4]. To somewhat mitigate this problem, it is necessary to look for alternative materials that improve the performance of asphalt mixes.

Our result analysis follows the different stages of this research. The first part included the physical characterization of the materials used: stone aggregates, blast furnace dust and asphalt cement. Second, BFD components and texture were identified. Lastly, the dosage of the materials, the design process for the proposed mixtures and the performance of the susceptibility test to humidity damage for different percentages of voids were reviewed.

Figure 1. Blast furmace dust
Source: the authors.

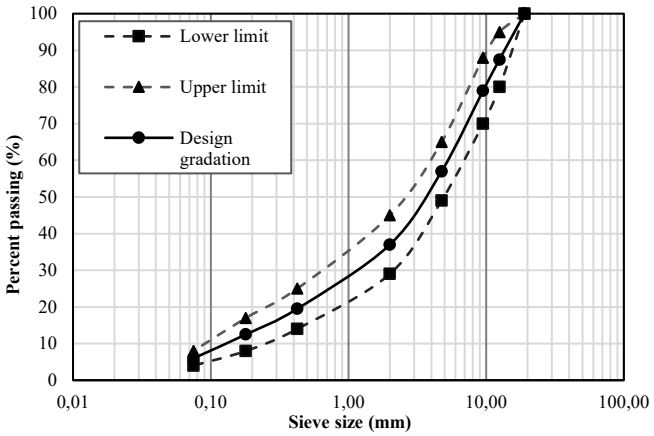

Figure 2. Working gradation for mixtures type MCD-19 according to article 450-13 INVIAS
Source: the authors.

2 Materials and methodology

Mixture design was carried out under the Marshall method with its specific procedures. Three asphalt mixes were designed: the first (M-0) was made with conventional natural aggregates (gravel and sand); in the second (M-50), 50% of the fine aggregate was replaced by BFD; and in the third (M-100), 100% of its fine aggregate was replaced by BFD. The Superpave Gyratory Compactor was used for compaction.

2.1 Materials

Two companies located in the department of Boyacá (Colombia) supplied the research materials. Triturados Paz de Río supplied the natural stone materials, and the steel company Votorantim-Paz de Río S.A. provided the BFD, Fig. 1. As a binder, 80-100 penetration asphalt cement was used according to the classification of Article 410-13 of the general road construction specifications INVIAS [5]. The physical and mechanical properties of the aggregates and asphalt cement are shown in Tables 1 and 2. Mixtures were designed under the grading curve of a hot-dense mix MDC-19, Fig. 2 for research analysis [6].

The BFD was included in the granulometry in the range of passing sieve No. 4 and retained on sieve No. 200. This distribution maintains the sizes for the MDC-19 mix. The dosage of the aggregates was sampled by volume for the different mixtures, and the dosage of the asphalt binder was sampled by weight [7], accounting for the difference in mass between the sand and the BFD.

The X-ray fluorescence (XRF) technique was performed using a Rigaku Primus II sequential spectrometer with a rhodium tube and a 30-micron beryllium window to know the BFD's chemical composition. Likewise, to know the BFD phases, X-ray diffraction (XRD) analysis was performed. The test was carried out with the Panalytical equipment, model Empyrean, equipped with a copper tube, using the Bragg - Brentano optical configuration, and with a high-speed, solid-state detector for data acquisition called PIXEL 3D 2x2. We worked at an acceleration voltage of 45 kV, a current intensity of 40 mA, and with a sweep angle (2θ) from 6.0996° to 81.98096°. This test is based on the relationship between the intensities of the diffraction peaks of a defined mineralogical phase. Fig. 3 shows the XRD spectrum of the BFD used in the investigation.

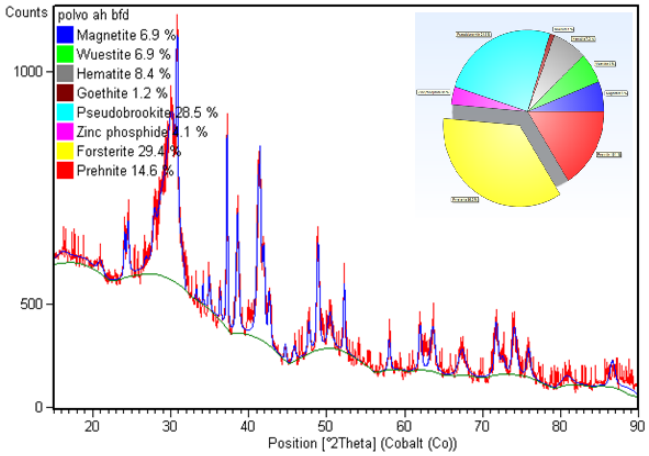

Figure 3. XRD spectrum result of the tested BFD
Source: the authors.

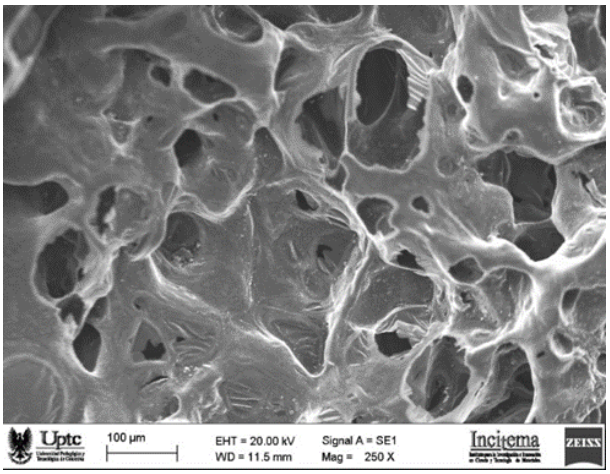

Figure 4. SEM micrograph of the BFD
Source: the authors.

In addition, the BFD particles were subjected to microscopic examination to characterize their shape and surface texture. The examination was performed with the Leo 410 scanning electron microscope (SEM), with a chamber vacuum of 9.85E-5 Torr, filament current of 1.2 nA, and anode voltage of 15 kV.

Fig. 4 presents an SEM micrograph of BFD at a scale of 250X, which presents pores and a rough texture with rounded edges. A strong adhesion bond with asphalt cement can be attributed to these characteristics of texture and roughness [8-9].

BFD analysis shows compounds rich in iron and magnesium. The BFD had iron hydroxides ($Fe(OH)_2$), evidencing water exposure with its ongoing reaction. There are also forsterite-type magnesium silicates (Mg2SiO4) generated at high temperatures, which present calcium and aluminum silicates such as prehnite ($Ca_2Al(Si_3Al)O_{10}(OH)_2$), Goethite ($\alpha$-$Fe_3$+O(OH)) which is formed under oxidizing conditions as a product of the weathering of iron-bearing minerals.

According to Table 3, BFD's main chemical component is Fe_2O_3 with 77.50%, followed by SiO_2 (5.50%), and CaO (4.95%). In the sand, as expected, the main component is SiO_2 at 88.70%, Fe_2O_3 at only 0.99%, and CaO at 0.46%. In the gravel-type coarse aggregate, the main constituents are CaO (63.40%), SiO_2 (16.60%), and Al_2O_3 (9.30%). Regarding the BFD's volumetric expansion, it can be asserted that this material has a low probability of having expansive characteristics due to the low content of CaO and MgO [10-12].

Table 1.
Basic physical properties of the aggregates used

Test	BFD			Specification	Standard
	Course	Fine	Fine		
Loss Angeles Abrasion (%)	20	-	-	<25	ASTM C 131
Degradation (Micro-Deval) (%)	19.4	-	-	<25	ASTM D 6928
Mechanical strength, 10% fine (kN)	122.7	-	-	>110	SABS Meth 842
Fractured particles (%)	94.1	-	-	>85	ASTM D 5821
Plasticity index (%)	-	NP	NP	NP	ASTM D 4318
Sand equivalent (%)	-	70	93.8	>50	ASTM D 2919
Bulk specific gravity	2.62	2.71	2.36	-	ASTM C 127/128
Absorption (%)	1.2	3.1	5.6	-	

Source: The authors

Table 2.
Basic properties of asphalt cement

Properties	Measured values	Specification	Standard
Penetration at 25°C (0.1 mm)	83.5	80 - 100	ASTM D 5-97
Ductility, 5 cm/min, 25°C (cm)	102	>100	ASTM D 113
Softening point (°C)	46.0	>45	ASTM D 36
Flashpoint (°C)	266	>230	ASTM D 92
Viscosity at 60°C (P)	1490	>1000	ASTM D 2171

Source: The authors

Table 3.
Chemical composition of aggregates in XRF

Component	Gravel	Sand	BFD
	% in weight		
MgO	3.80	1.60	1.00
Al_2O_3	9.30	7.30	3.60
SiO_2	16.60	88.70	5.50
P_2O_5	-	-	0.20
CaO	63.40	0.46	4.95
MnO	0.17	-	3.32
Fe_2O_3	3.04	0.99	77.50
Others	3.63	1.00	0.90

Source: The authors

The CaO/SiO_2 ratio establishes the alkalinity level of the material. Alkalinity is classified into three grades [13]: low (<1.8), intermediate (1.8-2.5), and high (>2.5) alkalinity. Intermediate or high alkalinities define a good affinity between the aggregate and the asphalt binder [14][15]. The coarse aggregate presents a ratio of 3.8, which indicates a good affinity. The BFD's CaO/SiO_2 ratio is 0.9; in the sand, it is 0.005. Therefore, BFD has a better affinity with asphalt cement.

It is not imperative that the results obtained through XRF and XRD analyzes necessarily coincide. These techniques provide different perspectives on the sample and rely on different principles to obtain their data. While XRF is used to identify the elemental composition of the sample and quantify the concentration of the elements present, XRD is used to reveal the crystal structure of the sample.

The XRF data support the presence of Fe_2O_3 identified by XRD as iron hydroxides and goethite. The XRF data also indicate the presence of other elements such as SiO_2, CaO and Al_2O_3, which are consistent with the silicates, calcium and aluminum identified by XRD. The XRD and XRF results provide complementary and coherent information about the BFD material, supporting the presence of specific compounds and their chemical composition.

2.2 Methodology

2.2.1 Compaction indices

The Superpave gyratory compactor (SGC) is a laboratory device that simulates the compaction process on a large scale, considering factors such as temperature, density, and stiffness. This allows for a more accurate measurement of compaction and a more consistent production of high-quality asphalt mixes.

Considering that, in this investigation the specimens were compacted with the SGC, the compaction curves were drawn, depending on the voids with air (%Av) and the percentage of the theoretical maximum specific gravity (%G_{mm}) against the number of turns. (N). Since the voids with air and the level of compaction influence the behavior of the asphalt mix, the studied mixes were analyzed, calculating the following indices:

Compaction energy index (CEI)

The compaction energy index (CEI) is the area under the compaction curve (number of gyrations Vs. % G_{mm}) from gyration number eight to the gyration in which 92% of G_{mm} is reached, as shown in Figure 5 (in the Results and Discussion section to follow), which represents the compaction carried out during the construction of the asphalt folder. It is taken from gyration eight to simulate the compaction carried out by the paver during the process of spreading the mix, and 92% of G_{mm} is the approximate density (Av = 8%) at the end of the construction process and giving the service to the transit [16]. The CEI can be calculated with eq. (1)[17].

$$CEI = \sum_{N=8}^{N\ 92\%} \%G_{mm} \quad (1)$$

Where:
CEI = compaction energy index
N92% = number of gyrations 92% of maximum theorical density
%G_{mm} = percent of maximum theorical density.

Traffic compaction index (TCI)

This index is defined as the area under the compaction curve (number of gyrations Vs. % G_{mm}) from 92% of G_{mm} through 96% of G_{mm} (Av=4%) [16][18] and up to the end of the compaction curve in Figure 5. The pavement continues to compact under vehicle loads, and, according to construction and design specifications, it is required that the mix be compacted to 96% G_{mm} (Av = 4%). The TCI evaluates the compaction to which the mix is subjected after the pavement is put into service and that is caused by the loads of the vehicles. The TCI is calculated with eq. (2) [17].

$$TCI = \sum_{N\ 92\%}^{N96\%\ y\ End\ cc} \%G_{mm} \quad (2)$$

Where:
TCI = traffic compaction Index
N92% = number of gyrations 92% of maximum theorical density
N96% = number of gyrations 96% of maximum theorical density and maximum compaction
%G_{mm} = percent of maximum theorical density.

Mix stability index (MSI)

This index is defined as the area under the compaction curve (number of gyrations Vs. % Air Voids) from turn number eight to the turn in which 8% Air voids in the mix is reached (92% of G_{mm}) [19] as shown in Figure 6 (In the Results and Discussion section to follow). This index indicates the energy used in the compaction process of the asphalt layer during construction. Av = 8% is used, considering that during the construction process the mixture will remain with that percentage of voids (92% of the G_{mm}). The MSI is calculated with eq. (3) [17].

$$MSI = \sum_{N=8}^{N\ 8\%\ Av} \%Av \quad (3)$$

Where:
MSI = mix stability index

N8% Av= number of gyrations 8% of air voids
%Av = Air voids.

Mix resistance index (MRI)

The mix resistance Index is the area under the compaction curve (number of gyrations vs. % Air Voids) from the gyrations where 8% air voids are reached (Air Voids after the construction process is finished) passing through the gyrations where 4% Air Voids are reached and up to the end of the compaction curve [19] as seen in Figure 6. This index indicates the ability to withstand compaction under the action of vehicle loads during the pavement's service life. The MRI is calculated using eq. (4) [17].

$$MRI = \sum_{N8\%\ Av}^{N\ 4\%\ Av\ y\ end\ CC} \%Av \quad (4)$$

Where:
MSI = Mix resistance index
N8%Av = number of gyrations 8% of Air Voids,
N4% = number of gyrations 4% of Air Voids and maximum compaction
%Av = Air Voids.

In this study the compaction indices were determined for the different percentages of Air voids. That is, 4, 6, 8 and 10% (96, 94, 92 and 90 % G_{mm}).

2.2.2 Moisture damage susceptibility test

Various methods are found in the literature to assess how susceptible an asphalt mix is in the presence of water. In this study, the tensile strength ratio (TSR) method was used, for which the description in the ASTM D4867/D4867M-96 standard was considered, and which consisted of the preparation of six Marshall-type cylindrical specimens for each type of mixture, which are compacted until obtaining a percentage of air voids of 7±1%. The test tubes produced are divided into two groups: a group of three test tubes are conditioned (as defined below), and the other group is kept dry throughout the test process. Conditioning consists of bringing the specimens to partial saturation until obtaining a saturation between 55% and 80%. Finally, before the tensile specimens fail, all the specimens are placed in a water bath at 25 ℃ for two hours [20].

In accordance with the standards, the test is carried out at a controlled deformation rate at a load speed of 50 mm/min (2 in./min). The average tensile strength of the conditioned specimens (Stm) is compared with the average tensile strength of the unconditioned specimens (Std). The tensile strength in each case is calculated with eq. (5), and the resistance ratio (TSR) between the conditioned and unconditioned specimens is expressed with eq. (6).

$$S_t = \frac{2000 * P}{\pi * t * D} \quad (5)$$

$$TSR = \frac{S_{tm}}{S_{td}} * 100 \quad (6)$$

Where:
St = tensile strength in kPa
P = maximum load in N
t = specimen thickness in mm
D = specimen diameter in mm.

In this study and to evaluate the incidence of BFD as a fine aggregate in asphalt mixes, the test was carried out with groups of specimens and with a variation of the percentage of voids of air with 4%, 6%, 8%, and 10% in each type of mix.

3 Results and discussions

3.1 Design of the mixtures

3.1.1 Preliminary design

Table 4 contains the Marshall design parameters for each mixture. There was a variation in the optimum asphalt content; in the base mix M-0, it was 5.4%, and in the mixes with BFD, they were 7.2% for mix M-50 and 7.9% for mix M-100. This increase can be attributed to the characteristics of shape and texture found in the BFD and the percentage of absorption found for this material.

The stabilities for mixtures M-0, M-50 and M-100 were 13,500 N, 12,100 N, and 11,200 N, respectively, which met the requirements specified. M-50, made by substituting 50% of the fine aggregate with BFD, presented a 10% lower stability concerning the base mix but 34% higher concerning the minimum specified stability. M-100, made by substituting 100% of the fine aggregate with BFD, was the least stable of the mixes, yet still 24% higher than the minimum required. The decreased stability of these mixtures can be attributed to the higher asphalt cement content since a thicker asphalt cement film appears surrounding the aggregates. The flow obtained for the mixtures under study presented very similar values and complied with the established requirements.

The durability of the asphalt surface layer is a function of the void content, given that the fewer voids, the lower its permeability. But a very low void content can cause exudation of the asphalt cement. The foregoing allows us to specify that the studied mixtures presented an adequate void content that guarantees good behavior. The voids with air in the mixtures presented similar values, 4.67%, 4.92%, and 4.99%, respectively. On the other hand, VMA values slightly increased in BFD mixtures by 15.80% in M-1, 17.36% in M-50, and 19.37% in M-100. The slight increase in this parameter can be attributed to the increase in the asphalt cement content in each mixture. This increase represents more available space to accommodate the effective volume of asphalt, which is favorable since the thicker the asphalt cement film that covers the aggregate particles, the more durable the mix will be. In addition, if VAM is too low, the mix may suffer durability and dry appearance problems, and if VAM is too high, the mix may present stability problems [21].

Table 4.
Values for the Marshall design for each mixture

Marshall Test	Unit	Value			Criteria
		M-0	M-50	M-100	
Asphalt content (by weight)	%	5.4	7.2	7.9	-
Specific gravity bulk (G_{mb})	g/cm^3	2.39	2.25	2.11	-
Stability	N	13500	12100	11200	9000
Flow	mm	3.35	3.21	3.16	2.0 – 3.5
Ratio: stability/flow	kN/mm	4.03	3.77	3.54	3.0 - 6.0
Voids with air (Av)	%	4.67	4.92	4.99	4.0 – 6.0
Voids in mineral aggregates (VAM)	%	15.80	17.36	19.37	>15.0
Asphalt-filled voids (VFA)	%	70.30	71.44	73.52	65 - 75

Source: the authors

Similarly, VFA values increased in BFD mixtures, 70.30%, 71.44%, and 73.52%, respectively. The higher VFA in BFD mixtures can be attributed to the chemical composition and its rough and porous microtexture. This can be beneficial for asphalt concrete since there will be greater adherence between the aggregate and the asphalt, resulting in greater durability.

3.1.2 Compaction indices

The compaction of an asphalt layer is important for its performance during its useful life, the level of compaction has a direct relationship with the air voids. A mix with high air content can have subsequent compaction due to vehicle loads and a mix with low air content can lead to problems such as exudation and premature deterioration of the asphalt layer [17].

The compaction graphs (number of gyrations Vs. % G_{mm}) prepared with the SGC data for the analyzed mixtures and the illustration of the CEI and TCI indices are shown in Figure 5 a and b.

The M-0 mix with the gyration number eight of the SGC reached 86.2% of G_{mm}, while the M-50 mix for the same number of gyrations reached 85.5% of G G_{mm}. Likewise, to reach 92% of G_{mm} (Av=8%), the M-0 mix needed 32 gyrations of SGC and the M-50 mix needed 42 gyrations, from which the CEI values for each mix result. In the case of TCI, the M-0 mix needed 95 gyrations to reach 96% of the G_{mm} (Av=4%) and the M-50 mix needed 104 gyrations. Likewise, the maximum density in the SGC, the M-0 mixture was obtained at 115 gyrations for a percentage of voids with air of 3.61% and the M-50 mixture with 120 gyrations, a percentage of voids of 3.51% was obtained, as illustrated in Fig. 5a.

On the other hand, the M-100 mix in gyration number eight reached 87.3% of the G_{mm}, while to reach 92% of the G_{mm} (Av=8%) it needed 37 gyrations, to reach 96% of the G_{mm} (Av=4 %), 105 gyrations were necessary, and at 125 gyrations the maximum density was obtained (Av=3.53%) as shown in Fig. 5b.

To determine the MSI and MRI indices, the compaction graphs (number of gyrations Vs. % Av) were prepared as seen in Fig. 6, which illustrates the concept of these indices. Fig. 6a shows the comparison of the indices of the base mix (M-0) and the M-50; in the same way, Fig. 6b illustrates the difference of the indices of the base mix (M-0) and the M-100.

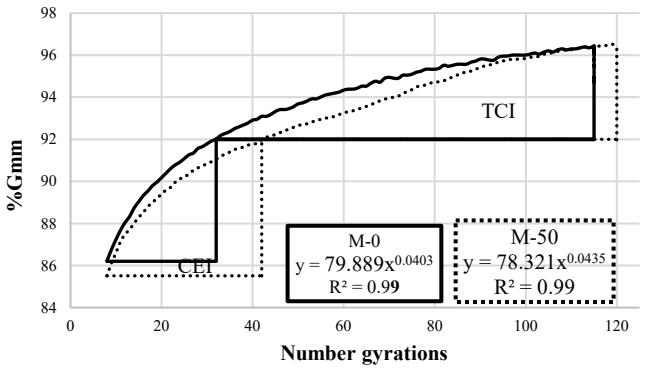

(a)

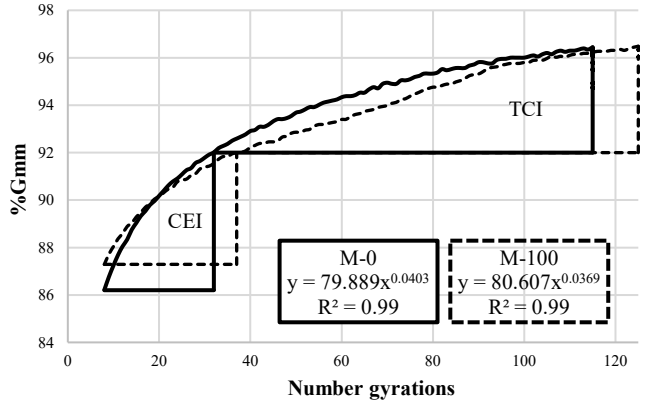

(b)

Figure 5. Compaction curves and comparison of CEI and TCI
Source: the authors.

Table 5 presents the numerical results of each index. A low CEI indicates a better workability in the mix, but a value that is too low means a tender mix that should be avoided [16] and higher CEI values indicate that they require more energy to be compacted during the construction process, that is, a greater number of roller passes. On the other hand, a high TCI is preferable in asphalt mixtures due to its ability to support more vehicle loads and prolong its useful life; it requires more compaction to achieve 4% voids with air [17]. An ideal asphalt mix would be one that has a low CEI and high TCI, which would be easier to compact during construction and difficult to compact under traffic loads.

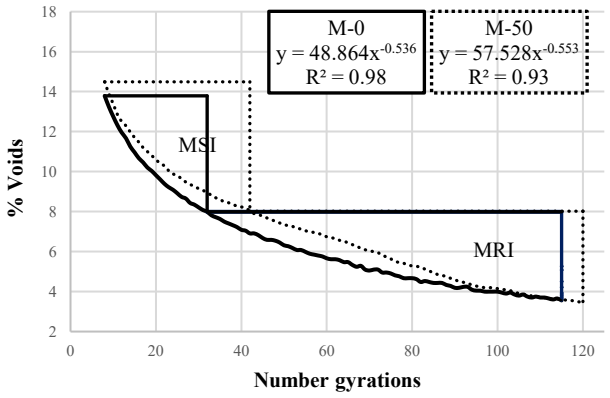

(a)

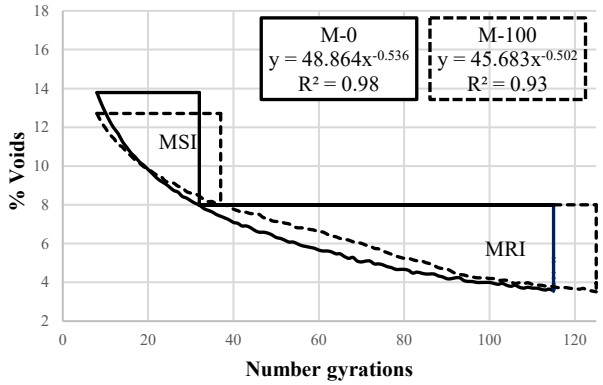

(b)

Figure 6. Compaction curves and comparison of MSI and MRI
Source: the authors.

In the same way, it is desirable that the MSI values are low, since this makes the mix more workable and easier to compact. On the other hand, it is recommended to have high MRI values, since this increases the resistance to compaction due to vehicle loads and provides adequate resistance to rutting [19].

Therefore, the ideal mixture would be the M-0 mixture since it presents the lowest CEI value and the highest TCI value. However, of the mixtures with the incorporation of BFD as an aggregate, the one that offers the best characteristics, according to the indices, is the M-100 mixture; which can be attributed to the presence of BFD as a fine aggregate, due to the greater affinity that this material has with asphalt cement. The M-50 mixture would require more compaction energy during its construction and would more easily reach 4% air voids due to compaction caused by traffic. In the same way, the results of MSI and MRI lead us to the same diagnosis.

Table 5.
Compaction index values

Índex	M-0	M-50	M-100
CEI: N=8; 92%G_{mm}	2246	3142	2707
TCI: 92%G_{mm}; 96%G_{mm}	6039	5936	6878
TCI: 92%G_{mm}; end. C.C.	7962	7473	7772
MSI: N=8; Av=8%	254	358	293
MRI: Av=8%; Av=4%	361	368	407
MRI: Av=8%; end. C.C.	438	426	427

Source: the authors

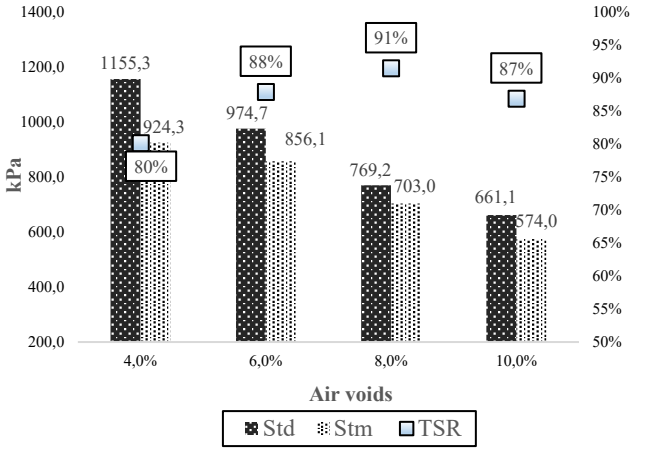

Figure 7. TSR results for mixture M-0
Source: the authors.

However, according to the compaction indices of the three mixtures analyzed, these do not present a considerable difference, which indicates that the compaction process, during construction and after putting the pavement into service, will have adequate behavior.

3.2 Moisture damage analysis

According to most specifications, the tensile strength ratio (TSR) must be greater than 80% to guarantee that the asphalt mix will not be further affected by the presence of water.

Fig. 7 shows the tensile strength values of the conditioned and unconditioned specimens, as well as the variation for each percentage of voids with air in the conventional M-0 mixture. As expected, the tensile strength of the conditioned specimens is lower than those obtained in the unconditioned ones, and the tensile strength decreases at a higher percentage of voids. However, the indirect TSR for all cases meets the minimum requirement of 80%, finding the highest value for 8% voids with air.

Fig. 8 shows the results of the mixture tensile strength test, where 50% of the fine aggregate was replaced by BFD (M-50). Similarly, the higher the void percentage, the greater the decrease in tensile strength in conditioned and unconditioned specimens. However, the variation is not as great as in the M-0 mix. Likewise, the TSR values in all cases meet the minimum defined requirement of 80%, although values higher than those shown in the M-1 mixture were found. Similarly, the highest TSR value occurs with 8% voids with air. This behavior can be attributed to the improved affinity between BFD and asphalt and the increased absorption percentage in BFD according to its texture and porosity.

On the other hand, an improvement is observed in the tensile strength of the conditioned specimens for 6.0%, 8.0% and 10.0% voids with air, to the values found in the M-0 mixture, as well as in the tensile strength of the unconditioned specimens for 8.0% and 10.0%. Thus, the partial substitution of the fine aggregate with BFD improves mix performance. These results can be attributed to the improved affinity of BFD, which forms a stronger bond with asphalt cement in the presence of water, which makes BFD a favorable material in the asphalt mix.

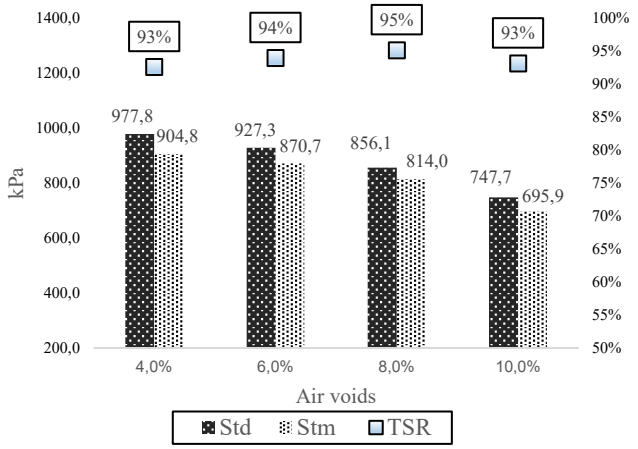

Figure 8. TSR results for mixture M-50
Source: the authors.

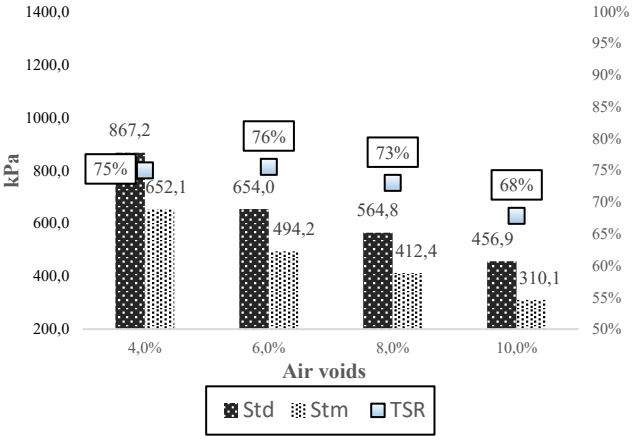

Figure 9. TSR results for mixture M-100
Source: the authors.

Fig. 9 shows M-100 performance. The tensile strength decreased considerably, compared to M-0 and M-50, both for the conditioned and unconditioned test pieces for all void percentages. In none of the cases is the minimum requirement of 80% in the TSR value met. The mixture with 100% BFD as fine aggregate did not show satisfactory resistance to moisture damage. The highest TSR value was found for 6.0% air voids, with a value of 76%. These results can be justified due to the higher content of asphalt cement, where the cohesive force of the asphalt is reduced, causing a decrease in mix rigidity [22,23].

The TSR of the designed mixtures and for each percentage of voids with air are shown in Fig. 10. The behavior of the base mix M-0 increases up to 8% voids with air; for 10% voids with air, the TSR value decreases by four percentage points regarding the value obtained for 8%. For the M-50 mix, there was an increase in the TRS values in all the percentages of voids with air compared to the base mix. However, in M-2, TSR behavior for the different percentages of voids with air is almost linear. It does not show great variation as the voids with air increase. The lowest TRS values were found in M-100 with decreases as the percentage of voids with air increases. The results of the tests indicate that using BFD aggregate in a percentage of up to 50% is favorable for the manufacture of asphalt mixes to be used as a wearing course.

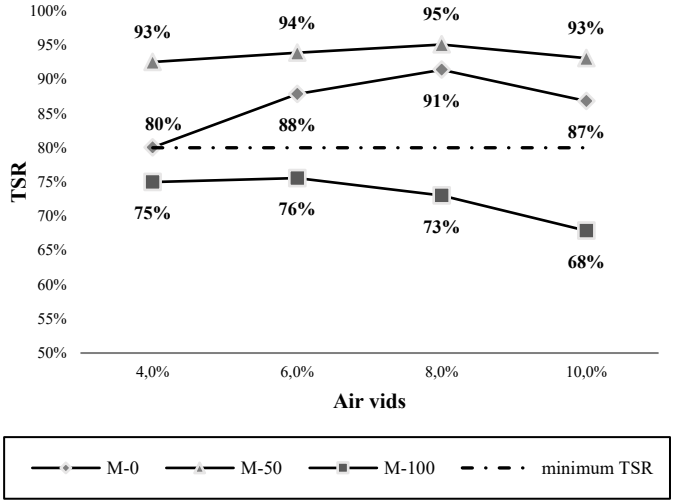

Figure 10. Influence of the BFD aggregate on the tensile strength ratio (TSR)
Source: the authors

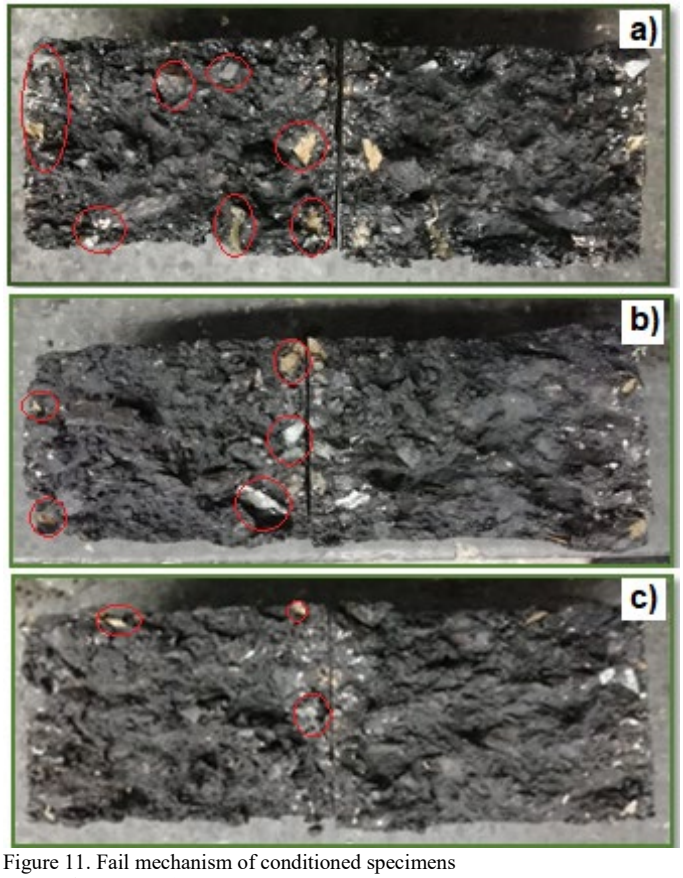

Figure 11. Fail mechanism of conditioned specimens
a) M-0, b) M-50 y c) M-100
Source: the authors.

The visual inspection of the tested specimens that presented the highest TSR value for each type of mixture indicated that the unconditioned specimens failed regarding the course aggregate rupture in all the mixtures studied, while the conditioned ones, for M-0, showed a failure surface due to loss of adhesion and weakening of the aggregate-asphalt union, Fig. 11a.

In the case of the conditioned test tubes of the M-50 mix, Fig. 11b, there was a smaller failure surface associated with a loss of adhesion between the aggregate and the asphalt and the greater failure surface was related to a reduction in asphalt cohesive force. Fig. 11c shows the conditioned specimen of the M-100 mix. There are few aggregates without an asphalt coating, which indicates that the failure due to adhesion loss decreased remarkably and the largest surface presents a black color, which indicates the loss in the cohesive strength of the asphalt [24][25].

4 Conclusions

After the analysis of the compaction indices using the Superpave gyratory compactor, it can be concluded that the results obtained indicate that there is no considerable difference in the three evaluated mixes, M-0, M-50, and M-100. This suggests that, in terms of compaction, all the mixtures meet the required standards and have a similar behavior in terms of their density and structure. However, it is important to consider that this result only refers to the compaction index and that other properties and characteristics of the mixtures may vary and should be evaluated separately.

To analyze the incidence of BFD, the fine aggregate was partially and totally replaced in the studied mixtures. The Marshall design determined that the optimum content of asphalt binder in mixtures with BFD is greater than the asphalt necessary to obtain the best characteristics in the M-0 mixture. The M-50 mix increased by only 1.8% compared to the base mix. Similarly, the M-100 mixture achieved an increase of 2.5%. These results are supported by the BFD's surface texture and higher absorption compared to sand.

The physical-mechanical behavior of the mixtures with partial and total fine aggregate replacement with BFD is acceptable. The mixes meet all the Marshall design parameters required in the specifications. Therefore, the incorporation of BFD in asphalt mixes for pavements does not impair their performance. On the contrary, it helps in the use of industrial waste, contributing to the environmental impact and the sustainable development of materials for pavements.

According to our results, BFD additions of up to 50% in asphalt mixtures improve the behavior against moisture damage in rolling layers for pavements. Tensile strength values increase. Therefore, the TSR values improve. The use of a higher BFD percentage would be possible by incorporating additives that improve asphalt cohesion.

The behavior of voids with air turned out as expected: as the void percentage increased, the mixtures showed greater damage to moisture. An optimal value of 8% voids with air is presented since it achieved the highest TSR values. However, when BFD totally replaced the fine aggregate, the mixture failed to meet the minimum recommended TSR.

Blast furnace dust (BFD), the material implemented in this research, offers optimal characteristics for use as fine aggregate in mixtures for asphalt concrete and increases aggregate-asphalt cohesion. A disadvantage in the use of this material is the increase in the asphalt cement content, which makes the mixtures more expensive, which can be compensated in the long run with greater durability and resistance to moisture damage.

The implementation of BFD as a fine aggregate in asphalt mixes contributes to having more environmentally friendly asphalt mixes considering that waste generated by the steel industry is repurposed, which would otherwise accumulate in storage yards, and the exploitation of non-renewable conventional aggregates is reduced.

Acknowledgements

The authors thank José Manuel Sierra, director of the laboratory of materials and pavements of the school of Transport and Road Engineering of the UPTC. also, to *INCITEMA* for the collaboration in carrying out the chemical characterization tests. To the companies: *Votorantin-Acerías Paz del Río S.A*, *Triturados Paz del Rio S.A.* and *Incoasfaltos S.A.S.*, for the supply of materials.

References

[1] Lobato, N.C.C., Villegas, E.A., and Mansur,M.B., Management of solid wastes from steelmaking and galvanizing processes: a brief review, Resour. Conserv. Recycl., 102, pp. 49–57, 2015. DOI: https://doi.org/10.1016/j.resconrec.2015.05.025.

[2] Hu,T., Sun,T., Kou, J., Geng, C., Wang, X., and Chen, C., Recovering titanium and iron by co-reduction roasting of seaside titanomagnetite and blast furnace dust, Int. J. Miner. Process., 165, pp. 28–33, 2017. DOI: https://doi.org/10.1016/j.minpro.2017.06.003.

[3] Reyes, F.A. y Figueroa, A.S., Análisis de la susceptibilidad al daño por humedad de una mezcla asfáltica a partir del ensayo mist y del programa ipas 2d ®, Rev. Infraestruct. Vial - LanammeUCR, 17, (2215–3705), pp. 31–39, 2016.

[4] Hernández, R., Limón, P., Sandoval, I. y Cremades, I., Análisis de la susceptibilidad a la humedad de varios tipos de mezclas asfálticas mediante el módulo dinámico, in Expo-Asfalto 2017.

[5] C. Instituto Nacional de Vías, Art. 410-13 Suministro de Cemento Asfáltico, Bogotá, 2022.

[6] INVIAS, Artículo 450-22 Mezclas asfálticas en caliente de gradación continua, Bogotá, 2022.

[7] Asmerican Society for Testing and Materials, ASTM D6927-15 Standard test method for Marshall stability and flow of asphalt mixtures, Philadelphia, [Online]. 2015. Available at: https://doi.org/10.1520/D6927-15.

[8] Kehagia, F., Skid resistance performance of asphalt wearing courses with electric arc furnace slag aggregates, Waste Manag. Res., 27, (3), pp. 288–294, 2009. DOI: https://doi.org/10.1177/0734242X08092025.

[9] Xie, J., Chen, J., Wu, S., Lin, J., and Wei, W., Performance characteristics of asphalt mixture with basic oxygen furnace slag, Constr. Build. Mater., 38, pp. 796–803, 2013. DOI: https://doi.org/10.1016/j.conbuildmat.2012.09.056.

[10] Sorlini, S., Sanzeni, A., and Rondi, L., Reuse of steel slag in bituminous paving mixtures, J. Hazard. Mater., (209–210), pp. 84–91, 2012. DOI: https://doi.org/10.1016/j.jhazmat.2011.12.066.

[11] Ameri, M., Hesami, S., and Goli, H., Laboratory evaluation of warm mix asphalt mixtures containing electric arc furnace (EAF) steel slag, Constr. Build. Mater., 49, pp. 611–617, 2013. DOI: https://doi.org/10.1016/j.conbuildmat.2013.08.034.

[12] Wang, G., Determination of the expansion force of coarse steel slag aggregate, Constr. Build. Mater., 24, (10), pp. 1961–1966, 2010. DOI: https://doi.org/10.1016/j.conbuildmat.2010.04.004.

[13] Chen, Z., Wu, S., Wen, J., Zhao, M., Yi, M., and Wan, J., Utilization of gneiss coarse aggregate and steel slag fine aggregate in asphalt mixture, Constr. Build. Mater., 93, pp. 911–918, 2015. DOI: https://doi.org/10.1016/j.conbuildmat.2015.05.070.
[14] Xie, J., Wu, S., Lin, J., Cai, J., Chen, Z., and Wei, W., Recycling of basic oxygen furnace slag in asphalt mixture: Material characterization & moisture damage investigation, Constr. Build. Mater., 36, pp. 467–474, 2012. DOI: https://doi.org/10.1016/j.conbuildmat.2012.06.023.
[15] Hesami, S., Ameri, M., Goli, H., and Akbari, A., Laboratory investigation of moisture susceptibility of warm-mix asphalt mixtures containing steel slag aggregates, Int. J. Pavement Eng., 16, (8), pp. 745–759, 2015. DOI: https://doi.org/10.1080/10298436.2014.953502.
[16] Fatin, A., and Mahmoud, F., Wisconsin highway research program using the gyratory compactor to measure mechanical stability of asphalt mixtures, October, 2004.
[17] Tedla, T.A., Singh, D., and Showkat, B., Effects of air voids on comprehensive laboratory performance of cold mix containing recycled asphalt pavement, Constr. Build. Mater., 368, (November), 2022, art. 130416, 2023. DOI: https://doi.org/10.1016/j.conbuildmat.2023.130416.
[18] Kim, Y., Im, S., and Lee, D.H., Impacts of curing time and moisture content on engineering properties of cold in-place recycling mixtures using foamed or emulsified asphalt, J. Mater. Civ. Eng., 23, (5), pp. 542–553, 2011. DOI: https://doi.org/10.1061/(ASCE)MT.1943-5533.0000209.
[19] Delrio-Prat, M., Vega-Zamanillo, A., Castro-Fresno, D., and Calzada-Pérez, M.Á., Energy consumption during compaction with a Gyratory Intensive Compactor Tester. Estimation models, Constr. Build. Mater., 25, (2), pp. 979–986, 2011. DOI: https://doi.org/10.1016/j.conbuildmat.2010.06.083.
[20] ASTM D 4867/D4867M, Standard Test Method for Effect of Moisture on Asphalt Concrete Paving Mixtures 1, Annu. B. Am. Soc. Test. Mater. ASTM Stand., pp. 1–5, 2006. DOI: https://doi.org/10.1520/D4867.
[21] Garnica, A.P., Flores, F.M., y Alamilla, D.H., Caracterización geomecánica de mezclas asfálticas, Inst. Mex. del Transp., (267), 2005, 105 P.
[22] Ling, C., Hanz A., and Bahia, H., Measuring moisture susceptibility of Cold Mix Asphalt with a modified boiling test based on digital imaging, Constr. Build. Mater., (105), pp. 391–399, 2016. DOI: https://doi.org/10.1016/j.conbuildmat.2015.12.093.
[23] Cucalon, L.G., Yin, F.A., Martin, E., Arambula, E., Estakhri, C., and Park, E.S., Evaluation of moisture susceptibility minimization strategies for warm-mix asphalt: case study, J. Mater. Civ. Eng., 28, (2,) 2016. DOI: https://doi.org/10.1061/(asce)mt.1943-5533.0001383.
[24] Figueroa, A.S., and Reyes, F.A., Influence of water in asphalt binders and its impact on stripping of asphalt mixtures, Mater. Sci. Eng., [Online]. 2012. Available at: https://www.semanticscholar.org/paper/A-5-EE-278-INFLUENCE-OF-WATER-IN-ASPHALT-BINDERS-ON-Figueroa-Reyes/f17e186e277650836e0ad14893b7610fd87694eb
[25] Chaturabong, P., and Bahia, H.U., Effect of moisture on the cohesion of asphalt mastic ond bonding with surface of aggregates, Road Mater. Pavement Des., 19, pp. 741–753, 2018. DOI: https://doi.org/10.1080/14680629.2016.1267659.

R. Ochoa-Díaz, is BSc. in Transportation and Roads Engineer and MSc. degree in Road Infrastructure, both from the Universidad Pedagógica y Tecnológica de Colombia, Tunja, Colombia. And PhD. in Engineering and Materials Science at the Universidad Pedagógica y Tecnológica de Colombia. He is professor with professional, academic and research experience in the area of pavements and new materials. He is active researcher of the road infrastructure research and development group, Grinfravial, at the School of Transportation and Roads Engineering the Universidad Pedagógica y Tecnológica de Colombia.
ORCID: 0000-0003-1151-7884

G.E. Grimaldo-León, is BSc. in Industrial Production Engineer from the Universidad Francisco de Paula Santander. MBA in Business Management from the Universidad Autónoma de Bucaramanga. She is research professor at the Universidad de Boyacá in the area of business management and researcher of the LOGyCA research group at the Universidad de Boyacá.
ORCID: 0000-0002-8211-4305

C.H. Higuera-Sandoval, is BSc. in Transportation and Roads Engineer and from the Universidad Pedagógica y Tecnológica de Colombia, Tunja, Colombia. And Master in Land Road Engineering from the Universidad del Cauca He is professor with professional, academic and research experience in the area of pavements. He is active researcher of the road infrastructure research and development group, Grinfravial, at the School of Transportation and Roads Engineering the Universidad Pedagógica y Tecnológica de Colombia.
ORCID: 0000-0003-1333-2517

DYNA
http://dyna.medellin.unal.edu.co/

UNIVERSIDAD NACIONAL DE COLOMBIA

Estado del arte y nueva variable de estado para diagnosticar la excentricidad en generadores sincrónicos

Pablo Tomás Herrera-Basabe & Oreste Hernández-Areu

Facultad de Ingeniería Eléctrica, Centro de Investigaciones y Pruebas Electroenergéticas, Universidad Tecnológica de La Habana, Cuba.
pablotohe@electrica.cujae.edu.cu, orestesh@electrica.cujae.edu.cu

Received: December 13th, 2023. Received in revised form: May 15th, 2024. Accepted: June 14th, 2024.

Resumen
La excentricidad en los generadores sincrónicos de polos salientes (GSPS) es un modo de fallo que requiere de una atención particular producto a su posible consecuencia catastrófica. Para diagnosticarla, los especialistas se han centrado en el espectro de frecuencia de la corriente del estator, obtenido por la Transformada Rápida de Fourier (FFT). Otras técnicas como el análisis de la corriente en transitorios, el flujo y las vibraciones, han probado ser fuentes de información valiosa.
La publicación persigue ilustrar el estado del arte sobre el diagnóstico de la excentricidad en los GSPS y propone una nueva variable de estado para el diagnóstico de este modo de fallo con el activo en servicio. Como resultado del trabajo sobre la tecnología y la investigación teórica realizada, se concluye que es posible diagnosticar la excentricidad del generador eléctrico a partir del comportamiento de la corriente por el neutro de la máquina en operación.

Palabras Claves: diagnóstico a máquinas eléctricas; grupos electrógenos; generador sincrónico.

State of the art and new state variable to diagnose eccentricity in synchronous generators

Abstract
Eccentricity in salient poles synchronous generators (SPSG) is a failure mode that requires particular attention due to its possible catastrophic consequence. To diagnose it, specialists have focused on the frequency spectrum of the stator current, obtained from the Fast Fourier Transform (FFT). Other techniques, such as transient current analysis, flux and vibration have proven to be valuable sources of information.
The paper aims to illustrate the state of the art on the diagnosis of eccentricity in SPSG and proposes a new state variable for the diagnosis of this failure mode with the asset in service. As a result of the work on the technology and the theoretical research carried out, it is concluded that it is possible to diagnose the eccentricity of the electric generator from the behavior of the neutral current of the machine in operation.

Keywords: diagnosis to the electrical machines; generator set; synchronous generator.

1 Introducción

1.1 Actualidad de los sistemas de generación distribuida

El término generación distribuida no tiene un consenso en el campo científico internacional, abarcando diferentes definiciones tales como la planteada por [1], donde expone que es: la generación de electricidad producidas por plantas pequeñas (menor a 10 MW), con capacidad suficiente para interconectarse al sistema eléctrico, considerando su propósito, ubicación, capacidad nominal, nivel de tensión y características de la zona a servir.

De igual modo, [2] explica que es la generación de energía eléctrica con fines de autoabastecimiento y acoplada a la red de distribución. En cambio, [3] relaciona las definiciones abordadas por instituciones internacionales,

How to cite: Herrera-Basabe, P.T., and Hernández-Areu, O., Estado del arte y nueva variable de estado para diagnosticar la excentricidad en generadores sincrónicos DYNA, 91(232), pp. 159-165, April - June, 2024..

como: IEEE (Institute of Electrical and Electronic Engineers por sus siglas en inglés), que la define como las centrales de generación, acopladas al sistema eléctrico a través de un punto de conexión común, mientras que el CIGRE (Conseil Intemational des Grands Réseaux Électriques, por sus siglas en francés), amplía que son centrales generadoras no gestionada su operación centralmente, con capacidades entre 50 y 100 MW. Del mismo modo el US. DOE (United States Department of Energy) y el EPRI (Electric Power Research Institute), sostienen que la Generación Distribuida, estás constituidas por plantas generadoras con capacidades que varían entre 1 kW hasta 50 MW[1].

En consecuencia, con las definiciones anteriores, se puede definir la generación distribuida como el conjunto de plantas de generación eléctrica descentralizadas, aisladas o interconectadas a un sistema eléctrico, con fines de autoconsumo o públicos, contribuyendo al incremento de la confiabilidad y la eficiencia del sistema y la calidad del servicio al consumidor final, siguiendo las regulaciones establecidas por el país.

1.2 Contexto mundial

El mundo moderno trabaja en la optimización de los recursos técnico, económicos y humanos, así como la reducción del impacto medioambiental, para ello, se diversifican las tecnologías de generación, abandonando, en muchos casos las antiguas, grandes y costosas plantas de generación de electricidad para reorientar los esfuerzos hacia la generación distribuida con vista a disminuir los costos de inversiones y hacer resilientes las decisiones para expandir el servicio eléctrico a una mayoría. Se plantea que con la implementación de la generación distribuida se reducen los costos asociados a las pérdidas por conceptos de trasmisión y distribución en un 5 al 10 % de la energía generada [1].

Por otro lado, existen países pobres, donde la generación distribuida es la única forma de disfrute del servicio eléctrico, accediendo a este, unas pocas horas al día durante todo el año para el consumo doméstico y en ocasiones, solo como parte de servicios básicos de vida, como en abastos de agua, y centros de socialización entre otros.

En América Latina, se han expandido las formas flexibles de generación distribuida diversificando las tecnologías de generación, con fuentes convencionales y renovables de energías. Actualmente, el empleo de grupos electrógenos como una de las formas de generación distribuida, ha sido utilizada para incrementar la capacidad generadora, a partir de las bondades de la tecnología como su fácil operación, su bajo costo de inversión y de operación en comparación con las grandes centrales termoeléctricas. Con la implementación de instalaciones generadoras con grupos electrógenos, se ha llevado el servicio eléctrico a lugares remotos, donde las inversiones en infraestructuras eléctricas son un obstáculo para mejorar la calidad de vida de la población.

2 Desarrollo

2.1 Fallas más significativas en los generadores eléctricos de polos salientes

Basado en los reportes técnico emitidos por IEEE y EPRI, los fallos de mayor ocurrencia en los generadores sincrónicos de polos salientes son los de excentricidad, cortocircuitos y circuitos abiertos, siendo los de excentricidad los que más prevalecen al ser un síntoma de daños en los rodamientos de apoyo del eje del rotor.

Por este motivo, minimizar este modo de fallo es un reto vital para garantizar la confiabilidad del activo y la estabilidad en la producción de energía eléctrica de las plantas generadoras y con ello la salud del sistema eléctrico.

2.2 Diagnóstico de excentricidades en máquinas eléctricas rotatorias

Según reportes de IEEE y EPRI; el modo de fallo por excentricidad del conjunto estator-rotor es una de las fallas más críticas porque causa daños irreversibles al generador sincrónico. Provocan alteraciones en las características de operación, tales como: aumento de los armónicos de tensión y corriente, reducción de la eficiencia, aumento de la temperatura, y del par pulsante, entre otras [4].

Se plantea que las excentricidades aparecen cuando el entrehierro no es uniforme, teniendo un origen multifactorial. Además, el incremento en la excentricidad a niveles fuera de los rangos admitidos, puede conllevar al daño catastrófico del conjunto estator – rotor y en consecuencia la parada imprevista de la máquina, conjuntamente con costosas reparaciones [6].

2.3 ¿Qué es la excentricidad del entrehierro?

La bibliografía técnica expone tres tipos principales de excentricidades: las estáticas, las dinámicas y las mixtas [4, 7, 8].

Excentricidad estática. Es la condición en la que la menor distancia entre el rotor y el estator de la máquina permanece fija en el espacio. En este estado, existe una coincidencia entre el eje de giro del rotor y su eje geométrico, no siendo así con el eje geométrico del estator. Las causas más comunes de este modo de fallo son: la ovalidad del núcleo del estator o el desalineamiento del rotor en el estator, como consecuencia de una incorrecta fijación o el deterioro de los rodamientos que soportan el eje del rotor, deformación de sus fijaciones en las tapas que sostienen los rodamientos, tolerancias excesivas, etc.

Excentricidad dinámica. Se produce cuando la longitud de mínimo entrehierro no permanece fija en el espacio. En esta condición, existe coincidencia del eje geométrico del estator y el eje de rotación del rotor, no así con el eje geométrico del rotor. Se destacan como causas fundamentales de este modo de fallo: el desalineamiento en

[1] Ramos, E., La generación distribuida: El camino hacia la producción descentralizada de electricidad y pautas para su reglamentación. Forseti. Revista de derecho, 2020, (p.9).

el montaje de los rodamientos, el desgaste de estos y las resonancias a velocidades críticas, etc.

Excentricidad mixta. Constituye el modo de fallo más común en las máquinas eléctricas rotatorias, donde se combinar ambas excentricidades.

2.4 Métodos actuales utilizados en el diagnóstico de excentricidades

En la actualidad existen varios métodos para el diagnóstico de excentricidades en las máquinas eléctricas rotatorias. Estos se han enfocado más en el diagnóstico de los motores de inducción, no siendo así en los generadores sincrónicos [9]. Entre estos métodos, están los métodos invasivos y los no invasivos. Los invasivos consisten en crear formas de acceso al interior de la máquina, para acceder a los parámetros de comportamiento que intervienen en la excentricidad. Los no invasivos, son aquellos que no requieren del acceso al interior de la máquina para su diagnóstico y, por ende, sacar la máquina de servicio.

Para el diagnóstico de este modo de fallo en la máquina eléctrica rotatoria, los especialistas en la industria habitualmente han centrado la atención en encontrar el espectro de frecuencia de la corriente del estator, mediante la Transformada Rápida de Fourier (FFT), identificando el nivel de excentricidad a partir de la amplitud de dichos armónicos. También se destacan como otras técnicas empleadas, el análisis de la corriente en transitorio, el análisis de flujo y el análisis de las vibraciones, los cuales han demostrado ser eficaces. Se recomienda para mejor precisión en el diagnóstico, integrar las diferentes técnicas y métodos entre sí. Los métodos de análisis de las corrientes y flujo de dispersión son técnicas muy versátiles para aplicaciones complejas o de difícil acceso, en donde la instrumentación para realizar la medida de vibraciones u otro aparato de diagnóstico no sea posible emplear [6].

Aunque la mayoría de las investigaciones relacionadas con el diagnóstico de este modo de fallo en las máquinas eléctricas rotatorias, tratan sobre su aplicación en los motores de inducción, la literatura científica actualizada aporta gran volumen de información sobre este modo de fallo en generadores. Como novedad, los diagnósticos modernos requieren, no solo, la discriminación entre un estado de la máquina sana y uno defectuoso, sino también, la identificación confiable y la estimación del nivel de gravedad de la falla, que permita la planificación de las acciones de mantenimiento y del servicio [10].

2.4.1 Monitoreo de la densidad del flujo magnético.

En un generador sano y con el entrehierro simétrico, la densidad de flujo es uniforme. La falla de excentricidad, conduce a un entrehierro asimétrico, trayendo consigo la distorsión en la densidad de flujo magnético. El monitoreo del flujo del entrehierro es uno de los métodos invasivos que se ha utilizado para investigar la ocurrencia de fallas de excentricidad en el generador sincrónico. Para ello, se inserta en la ranura del estator, un sensor llamado sonda de flujo o bobina de búsqueda [4].

Una forma más económica para monitorear la densidad de flujo magnético del entrehierro, es a través de la tensión terminal de la máquina, al no requerir de la introducción de sensores en el estator, ya que esta variable tiene relación directa con la distorsión del patrón de flujo magnético causado por una falla de excentricidad. Sin embargo, existen otros factores que distorsionan el flujo magnético del entrehierro, como son los armónicos debidos a la estructura sincrónica del generador, el cortocircuito de barras del estator o del devanado del rotor y la rotura de la barra de amortiguación de los polos del rotor. En consecuencia, la señal del flujo magnético del entrehierro, no es efectiva para la detección de fallas de excentricidad, debido que no constituye un método ventajoso para distinguir el tipo y la gravedad de la falla de excentricidad en el generador sincrónico [4].

2.4.2 Monitoreos de las corrientes del estator

En la investigación realizada por [4], se exhibe que el 85% de las fallas de excentricidad dinámica en el generador sincrónico de polo saliente, provoca el aumento de la magnitud de los armónicos de corrientes del estator y aunque el incremento en los armónicos 3^{ero}, 17^{mo} y 19^{no}, se ha utilizado como índice para la detección del fallo, este indicador no ha sido una herramienta suficiente para la detección de fallos por excentricidad, ya que estos armónicos existen inherentemente en señales de la máquina sincrónica debido a su estructura. También, los componentes de armónicos en los sistemas de potencias causados por cargas no lineales son similares a los armónicos mencionados anteriormente.

El uso de este método se basa en el análisis del espectro de frecuencia de las corrientes de fases del estator, mediante la Transformada Rápida de Fourier. Como inconveniente de este método está que su sensibilidad es bastante baja, y para percibir cambios apreciables, se requiere un alto grado de excentricidad en la máquina [11].

2.4.3 Monitoreo de la tensión del estator

A través de la tensión de fase del estator del generador sincrónico, se puede detectar un fallo de excentricidad, ya que la asimetría estimula armónicos de alto orden en esta variable. El armónico de orden 21^{ero}, se ha utilizado como índice para el diagnóstico de fallas de excentricidad y aunque este índice tiene una alta sensibilidad ante fallas de excentricidad, puede verse afectado por el ruido. También los armónicos de tensión de fase como 3^{ero}, 5^{to}, 13^{ero}, 17^{mo} y 19^{no}, han sido utilizados como índices para el diagnóstico de excentricidad, sin embargo, la forma del estator, las ranuras del rotor, la saliencia del polo del rotor y la conexión en serie o en paralelo del devanado del estator, también tienen efecto sobre los armónicos mencionados [4].

2.4.4 Monitoreo del flujo de eje y tensión de eje

En una máquina ideal, el flujo que interactúa con todos

los pares de polos es idéntico. Cuando el activo se encuentra bajo el efecto de una falla de excentricidad, se pierde la simetría del entrehierro y en consecuencia se afecta el flujo magnético en el rotor. Esta variable se conoce como flujo de eje de la máquina. El rango de tensiones inducidas en el eje varía desde unos mV hasta cientos de mV en correspondencia con la potencia de la máquina.

Los resultados experimentales demuestran, que la falla de excentricidad genera tensión en el eje y su magnitud tiene relación directa con la gravedad de la falla de excentricidad. Aunque los armónicos 5to, 6to y 8vo de tensiones en el eje, se han utilizado como índices de falla de excentricidad, hay muchos factores que conducen a una densidad de flujo magnético desequilibrado del entrehierro y generan tensión en el eje. El flujo magnético del eje existe en una máquina sincrónica sana debido al hueco de soldadura y la forma que hacen que el núcleo del estator se convierta en asimétrico [4].

2.4.5 Crítica a los métodos presentados

En concordancia con lo analizado y resumido en [4], los métodos propuestos presentan desventajas que afectan su uso para la detección de fallos de excentricidad.

a) El monitoreo de la densidad del flujo magnético es un método invasivo costoso, que requiere de la existencia de la sonda de flujo insertada dentro de la ranura del estator de la máquina, por lo que no es aplicable al generador que esté funcionando.
b) El monitoreo de los armónicos de corriente del estator del generador no resulta eficaz para diagnosticar el fallo de excentricidad cuando se encuentra en presencia de cargas no lineales. Aunque, variaciones temporales del vector espacial de corriente del estator, son una medida apropiada para el reconocimiento del tipo de fallo de excentricidad, la severidad de la falla no puede ser estimada por este indicador.
c) El monitoreo a través del contenido de armónicos de la tensión de fase en el generador sincrónico se ve afectado bajo carga no lineal, así como también en condiciones de carga nominal, debido al aumento de los niveles de ruido. Por otro lado, los armónicos pares de la frecuencia fundamental en el devanado del campo del excitador, también aparecen en presencia de otras fallas como cortocircuito y falla de barra rota del amortiguador.
d) El monitoreo de la tensión de eje y el flujo de eje son métodos invasivos que requieren para su implementación de equipos sensibles, además, este método no permite reconocer el tipo de fallo por excentricidad ni su severidad.

2.5 Métodos empleados para el modelado de los generadores sincrónicos en general

Los generadores sincrónicos son modelados generalmente mediante el empleo de cuatro métodos: Modelo dq0, Enfoque de función de bobinado (WFA), Modelo de dominio de fase (PDM) y Método de Elementos Finitos (FEM). Siendo el primero el más simple de los métodos, aplicable solamente para condiciones de simetría y balanceado de la máquina, lo que lo hace una herramienta útil para predecir el comportamiento en un generador sano, no así para la detección de fallas graves que generen condiciones de asimetría en el sistema electromagnético de esta [9].

Debido a las inconveniencias del Modelo dq0 para la modelación de fallas internas en la máquina sincrónica, los modelos de fallas generalmente se derivan en el dominio de fase, donde las ecuaciones de tensión y flujo inducido se desarrollan directamente en la referencia de fase fija sin transformación de coordenadas. Este método centra su clave de éxito en el cálculo preciso de la inductancia del devanado defectuoso para modelar el fallo interno de la máquina sincrónica. La complejidad que implica el cálculo de estas inductancias en las máquinas sincrónicas de polos salientes, fundamentalmente en máquinas con muchas bobinas tanto en el devanado del estator como del rotor, impide la generalización de este modelo [12].

La falla interna en el generador sincrónico, ha sido modelada en [12] basada en la WFA, en esta se brinda un nuevo procedimiento de estimación de la inductancia, la cual integra todos los armónicos espaciales en la modelación de fallas. Con el empleo del método WFA, se pueden modelar las diferentes condiciones de fallos de la máquina eléctrica. Esta técnica requiere para su aplicación, asumir que se desprecia el efecto de las ranuras del estator, la histéresis magnética y además la saturación del hierro [9]. Estos supuestos, simplifican el método, pero se aleja del estado real de máquina.

El método de mayor precisión empleado en la modelación de los fallos en su etapa inicial en la máquina eléctrica es el Método de Elementos Finitos (FEM) [11], el cual requiere de procesos computacionales complejos, pero modela la máquina más próxima a la realidad, por esta razón este método es utilizado para validar otros métodos cuando no es posible realizarlo directamente en la máquina o el costo del experimento es elevado [9]. Independientemente de su exactitud, el mayor inconveniente del método es que demanda información detallada de la geometría constructiva de la máquina [7].

Además de los cuatro métodos fundamentales antes mencionados, son utilizados el Método Híbrido [13] y el Método de Enfoque de Función de Bobinado Modificado (MWFA) [14]. Todos estos métodos poseen ventajas y desventajas en su aplicación [9], los cuales son resumidos en la Tabla 1.

2.6 Modelos más empleados para el caso de generadores sincrónicos de polos salientes

En [5], se plantea que las fallas por excentricidad en los generadores sincrónicos de polos salientes han sido modeladas por diferentes vías, una de ellas es utilizando el Método Función del Devanado (WFM, por sus siglas en inglés de Winding Function Method), para las fallas de excentricidad dinámica. Considera el efecto de la saturación, empleando la modelación para el cálculo del campo magnético del entrehierro, el Método de los Elementos

Tabla 1.
Breve Resumen de Varios Métodos de Modelado de los Generadores Sincrónicos.

Métodos	Aplicaciones	Ventajas	Desventajas
dq0	• Sistemas simétricos. • Fallos severos del devanado del estator. • Fallas de excentricidad.	• Simple. • Operaciones computacionales rápidas.	• No aplicable en condiciones de fallas. • Supone distribución sinusoidal de las magnitudes eléctricas. • No tiene en cuenta el efecto de los armónicos espaciales. • No considera la saturación.
WFA	• Sistemas asimétricos. • Fallos menores y severos del devanado del estator.	• Preciso. • Sensible para entrehierro uniforme.	• Tiempo prolongado de operaciones computacionales.
Híbrido	• Sistemas simétricos y asimétricos. • Condiciones de estados estable. • Fallos menores del devanado del estator.	• Más preciso que el WFA. • Más simple que el WFA.	• Tiempo moderado de operaciones computacionales.
PDM	• Fallas internas y a tierra del devanado del estator. • Condiciones transitorias.	• Precisión. • Independencia de la distribución del bobinado. • Considera el efecto de la saturación.	• Más complejo que el dq0. • Mayor tiempo de operaciones computacionales.
MWFA	• WFA extendido. • Falla de fase a tierra. • Excentricidad dinámica del rotor. • Excentricidad mixta. • Todo tipo de fallas.	• Adecuado para entrehierros no uniformes • Predice el funcionamiento del estado transitorio y el estado estable. • Independiente de la distribución del bobinado. • Considera la saturación. • Considera el efecto de todos los armónicos espaciales y temporales.	• Complejidad. • Alto tiempo computacional.
FEM	• Optimización de máquinas eléctricas. • Validación de métodos de modelado. • Comprobación de parámetros eléctricos en diversas condiciones.	• Alta precisión. • Modelación de todas las condiciones.	• Tiempo. • Necesita computadoras potentes. • Complejidad.

Fuente. Traducida por el autor de Mostafaei, M. and Faiz, J. 2021

Finitos, el cual requiere complejas operaciones de cálculos, en comparación con el método analítico, que es menos exacto pero su resultado es aceptado para la estimación del flujo magnético del entrehierro.

Por otro lado, en [15], se dice que, para la simulación de una falla de excentricidad estática en el generador sincrónico de polo saliente, se emplea el Análisis de Elementos Finitos. En la investigación, se consideran diferentes severidades de la falla de excentricidad estática y se muestra su efecto sobre la densidad de flujo, la tensión y la corriente y se compara con el generador saludable. Como resultado se observa un patrón asimétrico del flujo magnético del entrehierro en el generador defectuoso, generando armónicos en las señales de flujo y tensión. Para la detección de la excentricidad estática, se prefiere el índice en función de la señal de tensión sin carga.

Del mismo modo en [16], se modela un generador sincrónico de polo saliente, pero en este caso para el estudio de la falla de excentricidad dinámica, donde son estudiados los estados de funcionamiento del generador desde vacío hasta plena carga bajo la falla de excentricidad dinámica y comparado con una máquina saludable. El aumento del grado de excentricidad bajo carga lineal en comparación con el caso sin carga se investiga en función del índice total de distorsión de armónico (THD), verificando los resultados experimentalmente.

3 Propuesta de variables de estado para el diagnóstico de la excentricidad

3.1 Corriente por el neutro del generador

La corriente por el neutro del generador puede originarse como consecuencia de anomalías externas, tales como asimetrías en la carga, el rápido aumento de las cargas no lineales e introducción de especificaciones erróneas y/o instalación de la puesta a tierra del neutro de la máquina. También pueden encontrar su origen en causas internas asociadas a las condiciones constructivas del generador como la excentricidad, entrehierros, etc.; fallas eléctricas como los cortocircuitos en los devanados, entre espiras, a tierra, etc.

Esto trae como consecuencia la aparición de corrientes de secuencia positiva, negativa y cero de orden del armónico fundamental, que producen efectos indeseados en la máquina [17].

La forma de onda preponderante de la corriente en el neutro del generador es de tercera armónica, con niveles moderados de la componente fundamental. Además, debido a las diferencias constructivas de las máquinas, aun cuando estas sean de igual capacidad y el mismo fabricante, estos valores son diferentes.

Con el monitoreo del comportamiento de la tendencia en los armónicos de la corriente por el neutro, puede diagnosticarse el desbalance electromagnético de la máquina, ya que variaciones de origen mecánico o eléctrico, repercuten en este indicador [18].

La componente de tercera armónica de la corriente en el neutro del generador, es dependiente de las condiciones de carga de este, por lo que, para carga máxima, alcanza su valor máximo. Debido a ello, esta variable no es efectiva para el diagnóstico de la excentricidad durante la operación del activo, ya que se vería afectada por las fluctuaciones de la carga durante la operación de la máquina complejizando el diagnóstico. En cambio, la componente fundamental de la corriente por el neutro, no se modifica con la carga, manteniéndose invariable durante su operación, esto hace que sea una variable que aporte información del grado de excentricidad de la máquina [18].

En los sistemas ideales, donde la máquina se considera perfectamente balanceada, la corriente que circula por el neutro del generador es cero, no comportándose así en la realidad, donde siempre existe circulando un nivel de corriente por el neutro que se encuentra entre el 5 y el 10% de la corriente nominal de la máquina [19][2]. La ventaja principal del uso de esta variable para el diagnóstico de la excentricidad del generador, es que no se ve afectada por las variaciones que experimente la carga. Además, si no se manifiestan afectaciones en el balance electromagnético de la máquina, entonces la magnitud de la armónica fundamental de la corriente por el neutro, se mantiene invariable en el tiempo [18]. Por otro lado, constituye un método no invasivo que requiere de costos bajos para su implementación, con un apreciable fin práctico.

3.2 Grado de excentricidad del entrehierro

Este parámetro se verifica como parte de la rutina de mantenimiento del generador eléctrico del grupo electrógeno Hyundai 9H25/33 en el programa de trabajo previsto en las 24000 hora según la matriz de mantenimiento existente en el procedimiento F-PM-11-062 [20]. El proceso de medición está completamente detallado en la instrucción F-IM-11-169[3] del manual de procedimientos e instrucciones de la Empresa de Mantenimientos a Grupos electrógenos de Fuel Oil (EMGEF). El objetivo que se persigue, es verificar el estado de simetría del entrehierro con el paso del tiempo de operación del activo. La medición se realiza con el equipo fuera de servicio, por lo que hay que interrumpir el proceso de producción para su realización.

4 Conclusiones

En la investigación teórica realizada sobre el estado del arte del diagnóstico de la excentricidad en los generadores sincrónicos, se demuestra que los métodos presentados tienen inconvenientes que limitan su uso en las centrales de la generación distribuida en operación.

Para modelar el generador sincrónico más próximo a su desempeño real, es recomendable el empleo del Método de Elementos Finitos, aun cuando demanda un alto nivel de datos característicos de la máquina y trabajo computacional.

Se determina que la componente fundamental de la corriente por el neutro del generador es una variable de estado de diagnóstico que se encuentra directamente relacionada con la deformación del campo electromagnético en la máquina rotatoria y en consecuencias brinda información del grado de excentricidad de esta.

Bibliografia

[1] Muñoz-Vizhñay, J.P., Rojas-Moncayo, M.V., y Barreto-Calle, C.R., Incentivo a la generación distribuida en el Ecuador. Ingenius. Revista de Ciencia y Tecnología (19), pp. 60-68, 2018. ISSN: 1390-650X 1390-860X.

[2] Navarrete, H.G. y García, A.A., Análisis del marco legal de la generación distribuida en América Latina y Nicaragua, para la incorporación de aparatos de medición inteligente. Nexo Revista Científica, 33(01), pp. 51-68, 2020, ISSN-e: 1995-9516.

[3] Ramos, E., La generación distribuida: el camino hacia la producción descentralizada de electricidad y pautas para su reglamentación. Forseti. Revista de Derecho, 8(11), pp. 07-35, 2020, ISSN 2312-3583.

[4] Ehya, H., Sadeghi, I., and Faiz, J., Online condition monitoring of large synchronous generator under eccentricity fault. In: 12th IEEE Conference on Industrial Electronics and Applications (ICIEA), 2017, ISBN: 1509061614.

[5] Sadeghi, I., Ehya, H., and Faiz, J., Analytic method for eccentricity fault diagnosis in salient-pole synchronous generators. In: 2017 International Conference on Optimization of Electrical and Electronic Equipment (OPTIM) & 2017 Intl Aegean Conference on Electrical Machines and Power Electronics (ACEMP), IEEE, 2017., ISBN: 1509044892.

[6] Castro-Coronado, H., Aplicabilidad de la técnica predictiva de análisis de dispersión de flujo para la detección de fallos electromecánicos en máquinas síncronas, 2020.

[7] Terron-Santiago, C., Martinez-Roman, J., Puche-Panadero, R., Sapena-Bano, A., Burriel-Valencia, J., and Pineda-Sanchez, M., Analytical model of eccentric induction machines using the conformal winding tensor approach. Sensors, 22(9), art. 3150, 2022. DOI: https://doi.org/10.3390/s22093150

[8] Pal, R.S.C., and Mohanty, A.R., A simplified dynamical model of mixed eccentricity fault in a three-phase induction motor. IEEE Transactions on Industrial Electronics, 68(5), pp. 4341-4350, 2020. DOI: https://doi.org/10.1109/TIE.2020.2987274.

[9] Mostafaei, M., and Faiz, J., An overview of various faults detection methods in synchronous generators. IET Electric Power Applications, 15(4), pp. 391-404, 2021. DOI: https://doi.org/10.1109/TPEL.2019.2892142

[2] (...). What should be borne in mind is that air-gap eccentricity exists even in a healthy motor, but within a permissible limit depending on the motor construction; e.g., 10 % eccentricity is often acceptable for a healthy motor. There is often an intrinsic static eccentricity. Manufacturers usually try to reduce the eccentricity level as much as possible (to under 5 %).

[3] Extraído de la matriz de mantenimiento del procedimiento F-PM-11-062.

[10] Gyftakis, K.N., et al., Diagnosis of static eccentricity in 3-phase synchronous machines using a pseudo zero-sequence current. Energies, 12(13), art. 2476, 2019. DOI: https://doi.org/10.3390/en12132476
[11] Ehya, H., et al., Static and dynamic eccentricity fault diagnosis of large salient pole synchronous generators by means of external magnetic field. IET Electric Power Applications, 15(7), pp. 890-902, 2021. DOI: https://doi.org/10.1049/elp2.12068
[12] Tu, X., et al., A new model of synchronous machine internal faults based on winding distribution. IEEE Transactions on Industrial electronics, 53(6), pp. 1818-1828, 2006. DOI: https://doi.org/10.1109/TIE.2006.885125
[13] Nadarajan, S., et al., Hybrid model for wound-rotor synchronous generator to detect and diagnose turn-to-turn short-circuit fault in stator windings. IEEE Transactions on Industrial Electronics, 62(3), pp. 1888-1900, 2014. DOI: https://doi.org/10.1109/TIE.2014.2370931
[14] Al-Nuaim, N.A. and Toliyat, H., A novel method for modeling dynamic air-gap eccentricity in synchronous machines based on modified winding function theory. IEEE Transactions on energy conversion, 13(2), pp. 156-162, 1998. DOI: https://doi.org/10.1109/60.678979
[15] Toufighian, S.M., Faiz, J., and Erfani-Nik, A., Static eccentricity fault detection in salient and non-salient synchronous generators using harmonic components. In: 12th Power Electronics, Drive Systems, and Technologies Conference (PEDSTC). 2021. IEEE. DOI: https://doi.org/10.1109/PEDSTC52094.2021.9405971
[16] Ehya, H., Faiz, J., and Abu-Elhaija, W., Detailed performance analysis of salient pole synchronous generator under dynamic eccentricity fault. In: IEEE Conference Jordan, 2014. DOI: https://doi.org/10.1109/TMAG.2011.2105498.
[17] Díaz Martínez, H.J., et al., Minimización de los efectos causados por desequilibrio de carga y armónicos, mediante la variación de la puesta a tierra del neutro del devanado del estator en turbogeneradores, 2019.
[18] Martínez, R.C., et al., Diagnóstico de generadores de potencia a través del Sistema de Monitoreo en Línea, AnGeL, 2017. DOI: https://doi.org/10.4067/S0718-07642016000200003
[19] Salah, A.A., Dorrell, D.G., and Guo, Y., A review of the monitoring and damping unbalanced magnetic pull in induction machines due to rotor eccentricity. IEEE Transactions on Industry Applications, 55(3), pp. 2569-2580, 2019. DOI: https://doi.org/10.1109/TIA.2019.2892359
[20] EMGEF, Procedimiento para la ejecución del mantenimiento preventivo planificado del generador modelo HSR7-719-8P Hyundai 2.5 MW, versión G2 y G3. Revisión de los transformadores de fuerza tipo TMP 25000/115, TMP 12500/34.5 y MT 0292., in F-PM-11-062. 2011, 4 P.

P.T. Herrera-Basabe, recibió el título en Ingeniería Eléctrica en 1997. Durante su vida laboral se ha desemeñado en áreas del diseño y explotación de los sitemás eléctricos soterrados y centrales de generación con tubinas a gas y grupos eléctrógenos a fuel oil. De 1997 a 2018 trabajó para empresas de ingeniería y servicios de la Unión Eléctrica de Cuba, Se desepeñó como inspector de pruebas en fábricas para la adquisicón de los grúpos eléctrógenos a Fuel Oil de1.7 MW y 2.5 MW, además de brindar servicios de asesoría técnica en el extranjero en esta tecnología. De 2020 a 2022 trabajó como consultor internacional del proyecto Eléctrico SE4All de PNUD Guinea Ecuatorial. Se encuentra actualmente laborando como profesor de la facultad de ingeniería eléctrica de la Universidad Tecnológica de la Habana (CUJAE) y en proceso de formación doctoral. Sus intereses de investigación incluyen: simulación, modelado y diagnóstico de fallos por excentricidad en generadores sincrónicos de grupos electrógenos.
ORCID: 0009-0001-3884-7245

O. Hernández-Areu, recibió el título en Ingeniería Eléctrica en 1981, el grado de Dr. en Ciencias Técnicas en 1995. Es director del Centro de Investigaciones Pruebas Electroenergéticas (CIPEL). Facultad de Ingeniería Eléctrica, Universidad Tecnológica de la Habana "José Antonio Echevarría" CUJAE. Se desempeña como profesor e investigador en Ingeniería Eléctrica en; diseño, pruebas, modelación y diagnóstico de transformadores y máquinas eléctricas.
ORCID: 0000-0002-2672-239X

DYNA
http://dyna.medellin.unal.edu.co/

UNIVERSIDAD NACIONAL DE COLOMBIA

Caracterización de los residuos textiles posindustria en Bogotá

Juan Carlos Robles-Camargo, Paula Tatiana Hincapié-Corredor & Luisa Fernanda Ariza-Murillo

Facultad de Ingenierías, Universidad de América, Bogotá, Colombia. Juan.robles@profesores.uamerica.edu.co, paula.hincapie2@estudiantes.uamerica.edu.co, luisa.ariza@estudiantes.uamerica.edu.co

Received: December 20th, 2023. Received in revised form: May 16th, 2024. Accepted: May 31th, 2024.

Resumen
El aumento en el consumo de prendas de vestir año a año genera una creciente demanda de materias primas y, por tanto, grandes cantidades de residual del proceso textil y confección con impacto a nivel ambiental en el componente aire, tierra y agua. La investigación precisa la cantidad de residuo generado por 7 empresas de Bogotá D.C durante el Q1 del año en curso previo conocimiento de sus procesos productivos por medio de observación directa que permitió categorizar el residuo textil por actividad en Hilatura (4.106,4 kg), Lavado y teñido de telas (10.500 m3), Confección (1.203 kg), Remate prenda (511 kg), No especificado (50 kg) y Otros (2,76 kg), encontrándose que la Licra (12% - 407 kg), Algodón perchado (10% - 343,57 kg) y el Rayón (9,7% - 340 kg) son los materiales con mayor generación de residuos.

Palabras clave: residuos; textil; posindustria; economía circular; logística inversa.

Characterization of post-industry textile waste in Bogotá

Abstract
The increase in clothing consumption year after year generates a growing demand for raw materials and, therefore, large quantities of waste from the textile and manufacturing process with an environmental impact on the air, land and water component. The research specifies the amount of waste generated by 7 companies in Bogotá D.C during Q1 of the current year, prior knowledge of their production processes through direct observation that allowed the textile waste to be categorized by activity in Spinning (4,106.4 kg), Washing and treatment of fabrics (10,500 m3), Clothing (1,203 kg), Garment finishing (511 kg), Unspecified (50 kg) and Others (2.76 kg), finding that Lycra (12% - 407 kg), Cotton (10% - 343.57 kg) and Rayon (9.7% - 340 kg) are the materials with the highest waste generation.

Key words: waste; textile; post-industry; circular economy; reverse logistics.

1 Introducción

De acuerdo con la base de datos RUES de Confecámaras Colombia al 01 de julio de 2021, de las 12.712 empresas activas asociadas a actividades del sector textil como preparación, hilatura, tejeduría y acabados, las microempresas representan el 89,6% del entorno económico, seguido por pequeñas (7,5%), medianas (2,3%) hasta las grandes empresas (0,6%) que cuentan con una fuerza laboral de 1,8 millones de trabajadores [1]. Para el 2021 hubo un incremento del 20,9% en el número de empresas activas respecto al 2020, en el que se registraron 10.512 de estas. En su desagregación por ciudad al 2021 se tiene que en Bogotá se concentra gran parte del tejido productivo con 4.120 empresas, seguido de Antioquía con 2.478 y el Valle del Cauca con 939 empresas [2].

Bogotá habría sido al 2020 la segunda ciudad de Latinoamérica con mayor inversión en moda, ascendiendo a US$260 millones según el estudio "Sector de la moda" de la EAE Business School, antecedida por Ciudad de México con US$426 millones.

El consumo en moda al interior del país alcanzó $27,7 billones en 2021, 21% más que en 2020 y 5% más que en 2019 a partir de datos de Inexmoda. Esto convierte al sector en protagonista de la economía local y en referente de su resistencia a la crisis en época de pandemia. Sobre las exportaciones de textiles y confecciones se presentó un crecimiento acumulado de enero a diciembre de 2021- US$2.534 millones un 27% más que el mismo período de 2020, razón por la que el presidente de Inexmoda, Carlos Botero se declara entusiasta con las proyecciones de crecimiento económico del sector, la canasta de

How to cite: Robles-Camargo, J.C., Hincapié-Corredor, P.T., and Ariza-Murillo, L.F., Caracterización de los residuos textiles posindustria en Bogotá. DYNA, 91(232), pp. 166-171, April - June, 2024.

la moda representó al 2022 un 3,3% del gasto de los hogares, acercándose al 3,6% de la participación prepandemia de enero de 2020, siendo de gran importancia para las exportaciones del país. Por otro lado, la tendencia de consumo de las ventas online señala que el calzado representa el 25% del total de ventas en internet, seguido del textil hogar con 19,3%. Finalmente, el mercado de ropa de segunda mano representa para Bogotá el 40% de las compras de ropa usada, seguido de Medellín con un 23%, Barranquilla, 22%, Cali y Bucaramanga 15% cada una [3].

Sin embargo, este tan mencionado crecimiento aumenta el impacto ambiental que genera dicha actividad económica, llegándose a disponer más de 147.000 toneladas de textiles en el relleno Sanitario Doña Juana [UAESP, 2021] [3-8]. Por otro lado, las estadísticas de la Fundación Ellen MacArthur publicadas por el Banco Mundial señalan que se necesitan 10.000 litros de agua para la producción de 1 kilo de algodón y 387.000 millones de litros anuales en la producción textil.

De ahí que en la investigación se haya buscado obtener información sobre la generación del residuo textil pre consumo en Bogotá de manera aplicada, entiéndase residuo como el material que se desecha a lo largo del proceso productivo. Se consultaron 45 empresas, de las cuáles facilitaron el levantamiento de la data 7, el proceso consistió en visitarlas o agendar reuniones virtuales según disponibilidad, generalmente era el líder del proceso quien tomaba la vocería para guiar el recorrido y describir sus actividades [9]. El 82% de las empresas que se abstuvo de participar en la investigación manifestaba no poder compartir dichos datos por confidencialidad a pesar de ofrecer la firma de un acuerdo para trabajar de manera anónima, no tener tiempo o directamente no tener interés en participar, la colaboración del 18% restante permitió obtener los siguientes resultados [10-12].

1.1 Marco teórico

El sector textil se dedica a la producción de fibras, hilados y tejidos para la confección de prendas de vestir y artículos para el hogar. Esta industria es una de las más importantes en el mundo, actualmente constituye un importante centro de ingresos, en especial en los países de desarrollo.

En consecuencia, es importante mirar alternativas que promuevan el aumento de la productividad del sector con énfasis en disminuir el impacto ambiental a través del uso de los remanentes de materia que se generan en el proceso productivo.

Sin embargo, actualmente en Colombia no hay datos caracterizados de los desechos generados en la industria textil y que faciliten el desarrollo de modelos económicos verdes alineados a los ODS facilitando la reinserción de los mismos en el proceso productivo de la industria en cuestión.

Para ello, se analizarán algunos conceptos de economía circular y logística inversa, orientados a satisfacer esta problemática, limitando la misma a la caracterización de los residuos posindustrial y su importancia en los procesos de economía circular.

1.1.1 Sector textil

El término industria textil ha evolucionado abarcando diferentes procesos como el tufting anudado de alfombras y el enfurtido, desde su definición inicial basada en el tejido de las telas a partir de fibras textiles. [6]

Entre 2002 y 2016, 1.277 establecimientos industriales que se dedicaban a la elaboración de los productos finales de la cadena Productos Textiles, los cuales representaron el 15,3% del total de establecimientos industriales registrados en la EAM. Al observar la dinámica de crecimiento del número de establecimientos de la cadena se evidencia una tendencia de crecimiento constante con una tasa de crecimiento promedio anual del 1,6%. [13-17]

1.1.2 Cadena productiva

La cadena productiva que también es llamada la cadena de valor es un conjunto de fuerzas que intervienen en procesos productivos enfocados en convertir la materia prima en producción final y comercialización hasta llegar al consumidor final.

La cadena productiva es definida en como un conjunto de fuerzas, que generan actividades económicas que generan inversiones, están siendo asociadas a la capacidad productiva de los sectores que producen insumos para línea. [18]

Igualmente, Kaplinsky - (2000) definió la cadena productiva desde tres enfoques diferentes 1. Desplazar las etapas que comprenden el suministro de bienes y servicios del consumidor, prestando más atención a las etapas como la comercialización y la distribución, es decir prestando más atención a las etapas “intangibles” 2. Recoger los flujos de información, validando que muchas veces las vinculaciones entre empresas no siempre están en condiciones que implican competencia o igualdad de competencias y conocimientos. 3. Identificar las actividades de alto rendimiento son la clave para comprender la apropiación de la producción [19]

Finalmente, el DANE (2012) define La cadena productiva de Productos Textiles describe el proceso productivo que inicia con la fabricación de fibras de todo tipo de material, continúa con la fabricación de hilados y tejidos para finalizar con la elaboración de los siguientes tipos de bienes por parte de las empresas manufactureras de Colombia: prendas de vestir (camisas, pantalones, abrigos, ropa interior elaboradas en todo tipo de fibras textiles); otros productos de materiales textiles (alfombras, cordelería, empaque de material textil); y otro tipo de prendas de vestir.[20]

1.2 Recuperación de valor

Es la selección y retiro del residuo sólido para someterlo a un proceso de reaprovechamiento en el que se le convierta en materia prima provechosa en la fabricación de nuevos productos. [21] Así mismo, la valorización es el aprovechamiento del recurso contenido en el residuo y engloba todo procedimiento que posibilite su manejo. [22] Relacionado a la obtención de beneficio económico una vez el producto recuperado es devuelto al mercado o reintegrado al proceso productivo. [23]

2 Método

La investigación desarrollada fue de carácter cuantitativo con un alcance de tipo descriptivo, usando la observación directa del proceso productivo a través de una muestra de 7

empresas del sector textil-confección de la ciudad de Bogotá.

Para ello, el proceso investigativo se dividió en 3 fases presentadas a continuación:

2.1 Fase exploratoria

Identificación de las fuentes de información primarias y secundarias como sustento teórico del proyecto. Esto permite visualizar no solo el grado de implementación de la logística inversa en el sector textil sino su futuro aplicativo, por tanto, el acercamiento a la industria permitirá describir de manera generalizada sus procesos operativos, la generación de residuos y las oportunidades de aprovechamiento.

2.2 Fase descriptiva

Una vez se ha realizado el acercamiento práctico al sector, se procede a la agrupación del residuo generado de acuerdo con sus características fisicoquímicas ubicando estrategias de gestión enmarcadas en el flujo inverso de la cadena de suministro de estas organizaciones.

2.3 Fase de análisis

Una vez se han categorizado los residuos, se evaluará su impacto ambiental y nivel de priorización mediante una matriz técnica a partir de la que identificarán planes de acción que minimicen el grado de incidencia de esta operación en su área de influencia.

3 Resultados

Entre el material registrado de las 7 empresas investigadas, al Q1-2023 se tienen 3510,9 kg en tela, 4.106,40 kg de hilo poliéster, 10.500 m3 de agua en vertimientos por agua residuales, así como 2,76 kg en material complementario como cartón, plástico y papel periódico, gran importancia para la investigación pues dan luz sobre otra arista a considerar en la medición del impacto ambiental del sector. Esto a su vez representa 144.109 unidades que se encuentran activas en el mercado por las empresas 1 a 6 cuya actividad económica es la fabricación de prendas.

En cuanto a tela, la Licra compuesta por 82% Nylon-18% Elastano (407 kg), algodón perchado 100% Poliéster (343,57 kg) y el Rayón como una fibra celulósica semisintética (340 kg) son los tres residuos que se generan en mayor volumen mientras el tipo Teddy 20% Poliéster- 80% Poliamida (5,40 kg), Entretela (algodón 100% blanco con termoadhesivo plástico) y la Franela (50% algodón – 50% Poliéster) son el sobrante menos popular.

La Fig.1 muestra la cantidad de residuo en kg por tipo de tela que emplearon las empresas durante el Q1. Se tiene desde lica, pasando por lana sintética hasta franela.

3.1 Residual por actividad de la tela

El material remanente se categoriza en tres procesos macro concentrados netamente en la tela: residual del corte, confección de la prenda o remate, por empresa. A partir de estos hallazgos es que se medirá su impacto ambiental en los factores: tierra, agua y suelo.

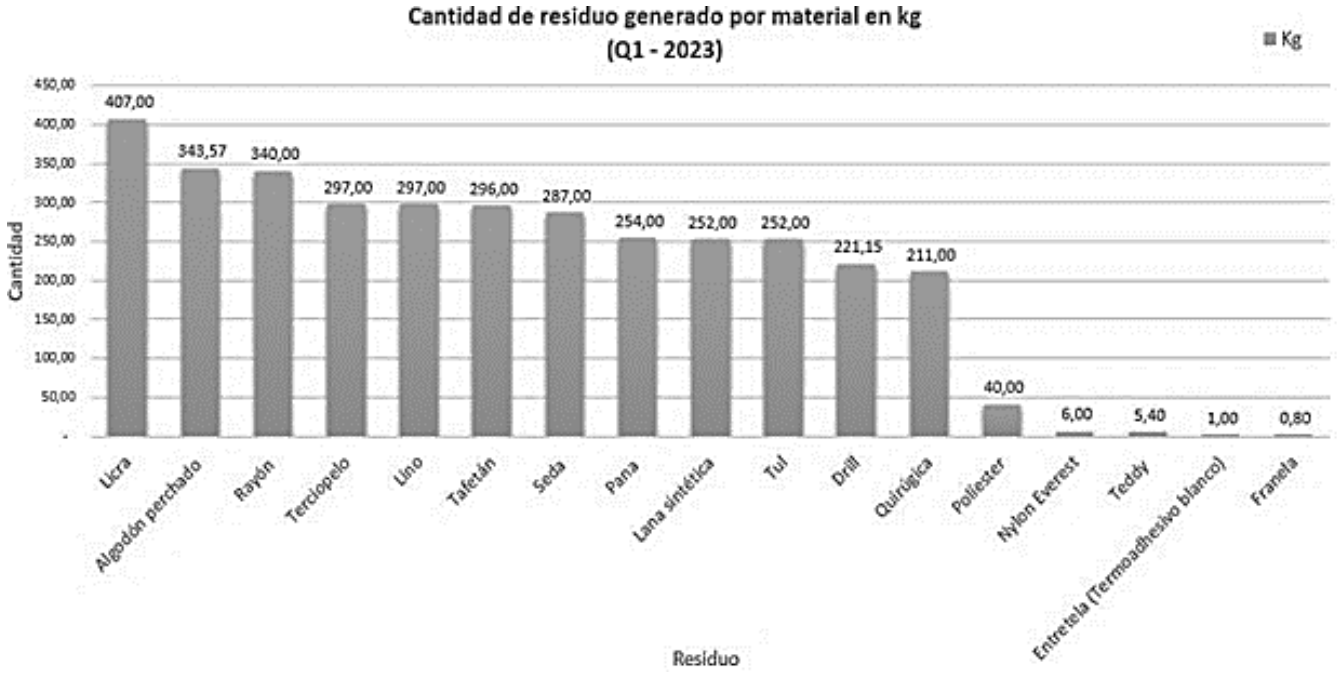

Figura 1. Cantidad de residuos generados por material en kg durante el Q1 del 2023
Fuente Elaboración propia

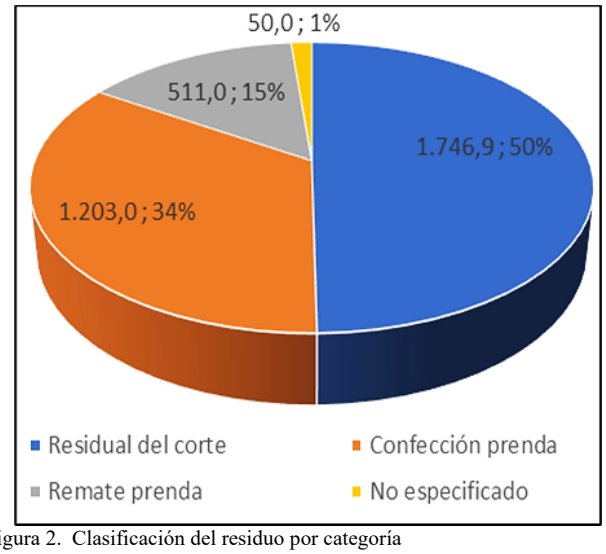

Figura 2. Clasificación del residuo por categoría
Fuente Elaboración propia

La Fig. 2 muestra las cuatro actividades primarias en las que se clasificó el residuo para facilitar la interpretación de resultados.

Hablar de cada uno de los procesos anteriores, es importante para el sector textil, ya que no se puede prescindir de ninguno de ellos por la naturaleza del proceso, además de la intervención de cada uno de los operarios. De allí, que el análisis de cada uno de los procesos, cobra mayor importancia en este tipo de estudios.

Por tanto, es imperativo el hecho que: durante el proceso creativo … se asume un rol que puede ser, cortar las telas, hilvanar las piezas, coser y bordar, aplicar accesorios y realizar las terminaciones de la pieza (bordes y amarras). Sumado a este trabajo de orden manual, se encuentra todo un quehacer de gestión del colectivo, el cual posibilita la realización de todas las actividades programadas por las empresas. [25]

La Tabla 1 relaciona por empresa y actividad ejecutada el remanente del proceso en kg, esta permitirá focalizar esfuerzos en cuanto generación de estrategias de mitigación del impacto ambiental.

En la Tabla 2, se relaciona la información suministrada por las pequeñas empresas (#1, #2, #3, #4 y #6) y la mediana empresa (#5) para un total de 3.510,9 kg de residual de tela, conformado por retazos de largo variable y fibra de hilo, sumado a los 2,76 kg de Otros como papel periódico, tubos base para hilo de plástico y cartón, así como bolsas plásticas donde vienen empacados los rollos de tela. La gran empresa (#6: Lafayette) genera en su actividad de Hilatura 4.106,4 kg de residual de hilo texturizado en Polyester y en la de lavado y teñido de telas 10.500 m3 durante el Q1, la cantidad de residuo es equiparable a la magnitud de su operación, sin embargo, para que no genere mayor dispersión de los datos se presenta su información en ítems aparte.

Tabla 1.
Cantidad de residuo generado en kg por actividad

	Revisar	Actividad	kg
Empresa 1	Residual del corte	Eliminar orillo	10
	Residual del corte	Cortar tela	24
Empresa 2	Confección prenda	Unir hombros	0,01
	Confección prenda	Pegar manga	0,01
	Confección prenda	Cerrar costado - Unir capota	12
	Confección prenda	Pegar puños y pretina	0,3
	Confección prenda	Coser delantero/posterior	0,1
	Confección prenda	Pegar portañuela	0,05
Empresa 3	Residual del corte	Cortar peluche	5,4
	Remate prenda	Pulir cobija	1
	Residual del corte	Cortar algodón perchado	3
	Residual del corte	Eliminar orillo	4
	Confección prenda	Unir hombros	0,06
	Confección prenda	Pegar manga	0,03
	Confección prenda	Cerrar costado - Unir capota	0,06
	Confección prenda	Pegar puños y pretina	0,09
Empresa 4	Residual del corte	Cortar tela	0,5
	Confección prenda	Pegar cuello	0,3
	*		10
Empresa 5	Residual del corte		1700
	Confección prenda		1190
	Remate prenda		510
Empresa 6	**		40
		Total	**3510,9**

*El remanente total del segundo proceso chaqueta con forro interno es un acumulado del proceso completo, no se obtuvo un dato aproximado por actividad.
**La empresa #6 suministra únicamente un aproximado del total de residuos generados durante el Q1.
Ambos datos se agruparán en la categoría "No especificado", mientras los 4.106,4 kg de hilo Poliéster se condensa en la categoría Hilatura, agua residual 10.500 m3 en Vertidos y el material complementario 2,76 kg en Otros.

Fuente Elaboración propia

Tabla 2.
Resumen de la clasificación residual por actividad

Actividad	Valor - Unidad
Residual del corte	1.746,9 kg – 50%
Confección prenda	1.203,0 kg – 34%
Remate prenda	511,0 kg – 15%
No especificado	50 kg – 1%
Total	**3510,9 - 100%**
+ Otros	2,76 kg
+ Lavado y teñido de telas	Vertidos 10.500 m^3
+ Hilatura	4.106,4 kg

Fuente Elaboración propia

La Tabla 2 se refiere a la representación porcentual del residual por actividad respecto al total generado.

El residual del corte como el conjunto de actividades que generan el 50% - 1.746,9 kg del remanente de las 6/7 empresas, seguido de la confección de prenda 34% - 1.203,0 kg, el Remate de la prenda 15% - 511,0 kg y el material no especificado 50 kg-1%.

Las acciones o planes de mejora que se desarrollen deben apuntar a minimizar el residual del corte sobre todo en la eliminación del orillo, este es el remate natural que impide el tejido se deshilache pero que debe ser retirado para que no aparezca en el producto terminado; adicional está el corte de la prenda de acuerdo con los moldes, el residuo proviene de los espacios entre cada parte de la prenda, un aspecto común según indicaron los encargados del proceso de las empresas #1, #3 y #4 es la necesidad de dejar al menos 5 mm entre los trazos para que la cuchilla de la tijera o máquina eléctrica pueda operar sin trabas y sin desviarse del trazado preestablecido.

En cuanto a la confección de la prenda, el uso de la fileteadora para rematar el borde del tejido evitando se deshilache la costura genera el desperdicio, esta es una actividad clave como punto de control de calidad de las empresas ya que hilos que se suelten o costura poco resistente a tirones pueden ser motivo de inconformidad por parte del cliente. El remate de la prenda relaciona el pulido de sus costuras, de esta forma se evita el deshilache del margen de la costura, estabiliza y mantiene la forma aportando mayor resistencia al uso y lavado [22-24] e involucra el uso de tijeras y rematadores; ambas categorías relacionan también el material No especificado.

4 Conclusiones

El acceso a información de los procesos de hilatura, lavado y teñido, corte, confección y remate de la prenda permitió identificar que durante el Q1 se generaron en Bogotá residuos sólidos como hilo Poliéster 4.106,40 kg, el vertimiento de 10.500 m^3 de agua con una concentración en mg/L de entre otras, Aluminio < 0,01, Cloruros 675 y Mercurio < 0,001, 3.510,9 kg en tela compuesta en mayor medida por Licra (12% - 407 kg), Algodón perchado (10% - 343,57 kg) y Rayón (9,7% - 340 kg) junto a 2,76 kg de material requerido para completar el proceso de fabricación como cartón, plástico y papel periódico.

En cuanto a la cantidad de residuos generados en kg (7.620,06) por actividad de acuerdo con el total estimado, el 54% corresponde a hilatura, 23% al residual del corte, el 16% a confección, 7% al remate de la prenda, 1% no especificado y el 0,04% corresponde a otros (material complementario).

Dicho material se traduce en 144.109 unidades fabricadas por 6 de las 7 empresas. Ahora bien, por medio de la matriz de Leopold [26] se realizó un análisis del impacto ambiental que produce cada uno de los residuos asumiendo dos factores: A. Características físicas y químicas y B. Factor residual con el parámetro de referencia 100 puntos y evaluación del componente como negativo o positivo, obteniendo así, un impacto negativo del residual de la actividad económica de las 7 empresas expresado de la siguiente manera: 1) en el componente suelo se tiene una calificación de - 306 puntos. 2) en el componente agua -235 puntos y 3). En el componente aire -245 puntos., superando las 100 unidades de referencia, esto debido al alto volumen generado y a la falta de estrategias de gestión del remanente.

Conocer esta información permitirá dimensionar la cantidad de residuos que se producen y las actividades en las que se generaron para focalizar los planes de mitigación basados en las oportunidades de recuperación y aprovechamiento.

La logística inversa despierta cada vez mayor interés en el sector textil, con las empresas identificando los flujos inversos en sus procesos de producción buscando un futuro sostenible para sus organizaciones. Un ejemplo de esto son los casos de éxito de empresas que implementan el reciclaje, refabricación, canibalización y restauración con ventajas no solo ambientales sino de reducción de costos de operación, mejora en la clasificación de los residuos generados, y aprovechando los mismos como materia prima para nuevas prendas de textiles.

Referencias

[1] El sector Textil-Confección aporta una quinta parte del empleo manufacturero en Colombia. Fashion Network [En línea]. [Acceso: octubre 31, 2022] Disponible en: https://pe.fashionnetwork.com/news/El-sector-textil-confeccion-aporta-una-quinta-parte-del-empleo-manufacturero-en-colombia,886741.html

[2] Terminaciones de costuras, Seam Pedia. Dic. 2020. [En línea]. [Acceso: Junio 22, 2022]. Disponible en: https://seampedia.com/terminaciones-de-costuras/.

[3] Fuentes-Ibarra, L.F. Debate de control político sector textil, Mincomercio. pp. 1–89, 2021.

[4] Diario La República. Consumo de moda en Colombia cerró ventas por $27,7 billones el año pasado. 2022. [En línea]. Disponible en: https://www.larepublica.co/empresas/consumo-de-moda-en-colombia-cerro-ventas-por-27-7-billones-el-ano-pasado-3316367

[5] La gran apuesta de Bogotá para disminuir residuos textiles, Red Moda Circular. [En línea]. [Acceso: Junio 22 ,2022]. Disponible en: https://bogota.gov.co/mi-ciudad/ambiente/red-moda-circular-como-disminuir-los-residuos-textiles-en-bogota

[6] Bonnati, A. y. Gabarrell, X., Conceptos generales sobre residuos, 2008. [En línea]. [Acceso: Agosto 10, 2022]. Disponible: https://docplayer.es/18497834-Capitulo-7-conceptos-generales-sobre-residuos.html

[7] Gómez, R., Correa, A. y Vásquez, L., Logística inversa, un enfoque con responsabilidad. Criterio Libre. 10(16), pp. 143-158, 2012. DOI: https://doi.org/10.18041/1900-0642/criteriolibre.2012v10n16.1167

[8] Arostegui, J., La cadena de suministro en la industria textil: el impacto de los distribuidores y tendencias hacia una cadena más sostenible. Tesis de grado., Facultad de Economía y Empresa. Universidad del País Vasco, España, 2021. [En línea]. [Acceso: Agosto 15, 2022]. Disponible en: https://addi.ehu.es/bitstream/handle/10810/55281/TFG_JoneAresteguiZorrilla.pdf?sequence=5&isAllowed=y

[9] Council of Supply Chain Management Professionals (CSCMP). CSCMP Supply Chain Management Definitions and Glossary. 2013. [En línea]. [Acceso: Agosto 15, 2022]. Disponible en: https://cscmp.org/CSCMP/CSCMP/Educate/SCM_Definitions_and_Glossary_of_Terms.aspx

[10] Calvente, A., El concepto moderno de sustentabilidad. UAIS Sustentabilidad. 2007. [En línea]. [Acceso: Agosto 20, 2022]. Disponible en: https://hopelchen.tecnm.mx/principal/sylabus/fpdb/recursos/r76250.PDF

[11] Enka, Quienes Somos. [En línea]. [Acceso: Septiembre 12, 2022]. Disponible en: https://www.enka.com.co/la-empresa/quienes-somos/

[12] El empaque.com. Apropet: el nuevo nombre del reciclaje de PET post consumo en Colombia. 2016. [En línea]. [Acceso: Septiembre 16, 2022]. Disponible en:

https://www.elempaque.com/es/noticias/apropet-el-nuevo-nombre-del-reciclaje-de-pet-post-consumo-en-colombia
[13] Chi, B., Tipos de terminaciones de costuras.2020. [En línea]. [Acceso: Noviembre 12, 2022]. Disponible en: https://seampedia.com/terminaciones-de-costuras/
[14] Sánchez, A., El mercado del fast fashion en Colombia tiene una expectativa de crecimiento del 9%. MODA. 2019. [En línea]. [Acceso: junio 23, 2022]. Disponible en: https://www.larepublica.co/empresas/el-mercado-del-fast-fashion-en-colombia-tiene-una-expectativa-de-crecimiento-de-9-2915829
[15] Ramírez, L., Red Moda Circular: la gran apuesta de Bogotá para disminuir residuos textiles. Secretaria de ambiente. 2022. [En línea]. [Acceso: junio 24, 2022]. Disponible en: https://bogota.gov.co/mi-ciudad/ambiente/red-moda-circular-como-disminuir-los-residuos-textiles-enbogota#:~:text=%C2%BFQu%C3%A9%20es%20y%20qu%C3%A9%20beneficios,contaminaci%C3%B3n%20textil%20en%20la%20ciudad.
[16] Carreño-Rojas, L., ¿A dónde va a parar la ropa en Colombia? ECONOMÍA. 2022. [En línea]. [Acceso: Junio 23, 2022]. Disponible en: https://www.elespectador.com/economia/a-donde-va-a-parar-la-ropa-en-colombia/.
[17] Acosta, S.N. y Velandia, D.F., Metodología para la aplicación de economía circular y logística inversa en el algodón para la industria textil en Bogotá. Tesis pre., Facultad de Ingenierías, Fundación Universidad de América, Bogotá, Colombia, 2022 [En línea]. [Acceso: Junio 28, 2022]. Disponible:http://repository.uamerica.edu.co/bitstream/20.500.11839/8812/1/3161311-2022-1-II.pdf
[18] Chicaiza-Pedraza, L.T. and Robles-Camargo, J.C., Proposal for a circular economy for the recovery of value from fruit waste in packaging manufacturing. DYNA. 88(217), pp. 140-149, 2021. DOI: https://doi.org/10.15446/dyna.v88n217.91850
[19] Gómez, M.C., Economía circular: una contribución a la competitividad dentro de la industria textil colombiana, Tesis de grado, Facultad de Economia, Fundación Universidad de América, Bogotá, Colombia, 2021. [En línea]. [Acceso: Noviembre 22, 2022]. Disponible en: https://repository.uamerica.edu.co/bitstream/20.500.11839/8333/1/2162182-2021-1-EC.pdf
[20] Tena, A., Cuando la ropa destruye el planeta. 2019. [En línea]. [Acceso: Noviembre 21, 2022]. Disponible en: https://www.publico.es/sociedad/industria-textil-vivir-vestir-ropa-destruye-planeta.html
[21] Gómez, L., A dónde va a parar la ropa que se bota a la basura?. 2018. [En línea]. [Acceso: Noviembre 21, 2022]. Disponible en: https://www.eltiempo.com/archivo/documento/CMS-15636476
[22] González, P., Soto, D. y Mora, A., Sector textil colombiano y su influencia en la economía del país. 2018. [en línea]. [Acceso: octubre 21, 2022]. Disponible en: https://journal.poligran.edu.co/index.php/puntodevista/article/view/1118/844
[23] Espinel, P., Aparicio, D. y Mora. A., Sector textil colombiano y su influencia en la economía del país. [En línea]. [Acceso: Octubre 18, 2022]. Disponible en: https://journal.poligran.edu.co/index.php/puntodevista/article/view/1118/844
[24] ISO 14006: 2011 Sistemas de gestión ambiental- Directrices para la incorporación del ecodiseño. [En línea]. [Acceso: Octubre 07, 2022]. Disponible en: https://iso.cat/es/norma-iso-14006-ecodiseno/
[25] Barrientos, A., Bordar para incidir: práctica textil artivista del colectivo chileno Memorarte Arpilleras Urbanas. Cuadernos de Antropología Social, (58), pp. 193-218, 2023. DOI: https://doi.org/10.34096/cas.i58.11450
[26] Leopold, L., Procedure for evaluating environmental impact. Geological Survey Circular, Washington, (645), pp. 1-16, 1971.

J.C. Robles-Camargo, Universidad Católica de Colombia, Bogotá, Colombia. PhD en Administración, Sp. en Gerencia Estratégica de Negocios, Innovación de Negocios y docente investigador.
ORCID: 0000-0002-3208-9287
P.T. Hincapié-Corredor, es Ing. Industrial, investigadora de la Fundación Universidad de América, Bogotá, Colombia.
ORCID: 0009-0008-7612-425X

L.F. Ariza-Murillo, es Ingeniera Industrial, investigadora de la Fundación Universidad de América, Bogotá, Colombia.
ORCID: 0009-0000-2613-9383

DYNA
http://dyna.medellin.unal.edu.co/

UNIVERSIDAD NACIONAL DE COLOMBIA

Localización de instalaciones en logística humanitaria: una revisión de la literatura y consideraciones para futuras investigaciones

Miguel Antonio Daza-Moscoso [a], María Fernanda Carnero-Quispe [a] & José Manuel Cárdenas-Medina [a b]

[a] *Departamento de Ingenierías de la Industria y el Ambiente, Universidad Católica San Pablo, Arequipa, Perú. miguel.daza@ucsp.edu.pe, mfcarnero@ucsp.edu.pe*
[b] *Facultad de Ingeniería, Universidad Peruana de Ciencias Aplicadas, Lima, Perú, pcinjcar@upc.edu.pe.*

Received: October 25th, 2023. Received in revised form: February 27th,2024. Accepted: March 12th, 2024

Resumen
La localización de instalaciones en la logística humanitaria es un problema crucial ya afecta directamente a la capacidad de respuesta, eficiencia en la distribución y al rendimiento de las operaciones de ayuda, este problema se caracteriza por la incertidumbre de la información, la velocidad en la reacción, la falta de recursos y la variabilidad del entorno haciendo que se generen nuevos modelos que se puedan ajustar a la realidad. En esta revisión de literatura se analizaron investigaciones publicadas entre los años 2020 y 2022. Con base en los estudios revisados, estos prefieren ajustarse a la realidad utilizando límites de capacidad, modelos estocásticos, ubicaciones no predefinidas, funciones de privación y multiobjetivo en emergencias generadas por desastres naturales. Finalmente se debe de considerar en futuras investigaciones: el tipo de temporalidad de la instalación, el enrutamiento con sus restricciones, el uso de modelos más robustos y el tamaño de las instalaciones.

Palabras clave: logística humanitaria; localización de instalaciones; desastres naturales.

Facility location in humanitarian logistics: a literature review and considerations for future research

Abstract
The location of facilities in humanitarian logistics is a crucial problem as it directly affects the responsiveness, efficiency in distribution and performance of aid operations, this problem is characterized by uncertainty of information, speed of reaction, lack of resources and variability of the environment making it necessary to generate new models that can be adjusted to reality. In this literature review, research published between 2020 and 2022 was analyzed. Based on the studies reviewed, they prefer to adjust to reality using capacity limits, stochastic models, non-predefined locations, deprivation and multi-objective functions in emergencies generated by natural disasters. Finally, the following should be considered in future research: the type of temporality of the facility, the routing with its restrictions, the use of more robust models and the size of the facilities.

Keywords: humanitarian logistics; facility location; natural disasters.

1 Introducción

Cada año ocurren alrededor de 376 desastres naturales que afectan a 98.6 millones de personas alrededor del mundo [18], esto hace que la logística humanitaria sea una parte esencial de la gestión de desastres y una de las mejores formas para reducir el tiempo y costo en las operaciones de socorro, esto sucede tanto para países desarrollados como para subdesarrollados, ya que ambos serán afectados por la escasez de recursos básicos [24].

La logística no es una tarea sencilla en caso de desastres; ya que se caracteriza por un aumento considerable en la incertidumbre y complejidad de la situación post desastre, haciendo que el 80% del éxito de los esfuerzos dependan de la logística humanitaria [25]. Estas actividades son vitales especialmente en las primeras 72 horas posteriores al desastre natural [5].

How to cite: Daza-Moscoso, M.A., Carnero-Quispe, M.F. and Cárdenas-Medina, J.M., Localización de instalaciones en logística humanitaria: una revisión de la literatura y consideraciones para futuras investigaciones. DYNA, 91(232), pp. 172-180, April - June, 2024.

La localización de instalaciones consiste en seleccionar el lugar ideal para ubicar cierta instalación. Esta es una tarea importante en la logística humanitaria ya afecta directamente en la capacidad de respuesta a los desastres [1] y al rendimiento de las operaciones de ayuda [27]. Cumple distintas funciones en la logística humanitaria, en el nivel estratégico, se determina la localización de las instalaciones y su capacidad, en el nivel operativo, se asignan los costos ya sean logísticos o de privación [1], por lo tanto, es de suma importancia considerar en la planificación y operación de la logística humanitaria.

El ciclo de gestión de desastre comprende las fases de mitigación, preparación, respuesta y recuperación [6]. Las dos primeras fases se realizan antes del desastre con el fin de reducir posibles impactos económicos, sociales y físicos. Algunas de las operaciones que se realizan son simulacros, reposicionamiento de suministros de emergencia y la creación de leyes [10]. Las otras fases se realizan después del desastre, cuyo objetivo es disminuir el sufrimiento de las personas [5], estas operaciones incluyen la búsqueda y el transporte de equipo de rescate, personal y los materiales necesarios para la evaluación del impacto y las reparaciones [11]. El presente artículo evalúa la operación de localización de instalaciones que puede realizarse en la fase de preparación y respuesta [2].

Las instalaciones se pueden dividir en permanentes y temporales, la localización de las instalaciones temporales por lo general se realiza en fase de respuesta, después del desastre; se abren y cierran durante un periodo de tiempo. Sus principales objetivos son minimizar la distancia de desplazamiento, la demanda insatisfecha y el costo [19], mientras que las instalaciones permanentes suelen ubicarse en la etapa de preparación donde su función es poder brindar los recursos cuando ocurra el desastre, esto incluye almacenes, hospitales y cadenas de suministro [39], estas instalaciones son componentes críticos para la etapa de preparación y estas requieren una planificación a largo plazo [1].

La decisión de la localización de una instalación puede afectar al desempeño de las operaciones de socorro debido a que el número de las instalaciones y su localización afectan directamente al tiempo acción y a los costos incurridos, limitando la capacidad de respuesta [1], poniendo en peligro la seguridad del personal y de las víctimas del desastre [21]. Una localización correcta puede mejorar la eficiencia en la cadena de suministros, reducir costos, además de garantizar la cercanía a las áreas afectadas y la correcta disposición de los servicios a las personas [20].

Los principales desafíos son la existencia de la complejidad y la incertidumbre que existe para satisfacer la demanda, controlar los costos asociados a la apertura y mantenimiento de las instalaciones de manera eficiente y efectiva [1]. También existen condiciones geográficas y el tamaño de los lugares que no permiten que todos sean una opción viable para las instalaciones. Además, estas condiciones pueden afectar a la infraestructura existente como el bloqueo de carreteras y puentes que pueden limitar considerablemente el transporte hacia las áreas afectadas [42].

Mientras que las principales restricciones utilizadas para la resolución de este problema son las restricciones de capacidad, restricciones de distancia, restricciones de demanda y restricciones de asignación. La restricción de capacidad limita la cantidad de recursos que puede tener una instalación. Las restricciones de distancia limitan la distancia entre la instalación y las víctimas de la emergencia. Las restricciones de demanda limitan la cantidad de personas que se pueden atender por cada instalación. La restricción de asignación determina dónde se pueden ubicar las instalaciones y la distribución de los recursos [33].

Para superar estos retos, se utilizan sistemas de información geográfica (SIG) que permiten identificar las áreas afectadas y posibles ubicaciones [7] además proporciona información topográfica, climática, de la infraestructura y rastrear el movimientos de los suministros y del personal, lo que puede mejorar la capacidad de respuesta, como en la investigación de Ming, J., Richard, J. P. P., & Zhu, J. (2021) [21] donde utilizaron SIG para poder reubicar estaciones de bomberos, además se considera otros factores como el tiempo de respuesta y condiciones de tráfico. Sin embargo, no todas las organizaciones disponen de acceso a tecnologías como SIG y aunque las tengan tienen que saber cómo usar esa información en entornos complejos y cambiantes [38]. También se utilizan los costos de privación, el valor económico del sufrimiento de las personas [32], si estos no se consideran correctamente no se podrá garantizar los resultados del modelo generando mayores costos, duplicación de esfuerzo y desperdicio de recursos, debido a que en muchos casos estos costos representan más del 50% de los costos totales debido al aumento del sufrimiento de las personas [5]. Esta es una de las principales diferencias con la localización de instalaciones de la logística comercial, ya que busca beneficiar a las víctimas, pero también aumenta la dificultad [42] en la formulación del proyecto y el desarrollo de métodos apropiados de optimización [5].

Así mismo, es importante utilizar algoritmos heurísticos dado que permiten tener soluciones cercanas a la óptima en un tiempo menor a algoritmos exactos [14], por lo general la mayoría de investigadores considera modelos multiobjetivo que contienen criterios monetarios y no monetarios [29].

Las funciones objetivo de los modelos incluyen costos logísticos como el transporte o apertura de la instalación, y los costos de privación. En la investigación de Loree y Aros-Vera (2018) [18] donde realizaron un modelo matemático para determinar la localización de puntos de distribución y la asignación de bienes de ayuda humanitaria se considera el costo social (costo logístico y privación) haciendo que tengan un impacto en la víctima, el valor óptimo de instalaciones y su impacto en el costo social, este modelo puede satisfacer cualquier punto de la demanda mientras tenga la capacidad disponible.

Algunos modelos como el de Nikhil Patel y Sandeep Trivedi durante la pandemia del COVID-19 [28] consideran la cantidad de población, cantidad de ubicaciones candidatas, la distancia máxima entre los pacientes y el hospital, la cantidad de pacientes y de ser necesario el cómo agruparlos para su atención, mientras que otros consideran posibles fallas en la red, eficiencia, eficacia y equidad para medir el rendimiento del sistema proporcionando soluciones equitativas y sostenibles en términos de costo, además se utilizó optimización robusta distribucional (DRO) para superar las limitaciones generadas por el método basado en

escenarios con el fin de poder tener una eficiencia computacional adecuada [16].

Cotes y Cantillo [5] propusieron un modelo de localización de instalaciones para el preposionamiento de suministros en situaciones de desastre. El objetivo del modelo es minimizar los costos sociales globales, que incluyen tanto los costos privados (como los costos de transporte, inventario e instalaciones) como los costos de privación, también se define la cantidad de cada tipo de producto a ser almacenado para atender a las áreas afectadas por el desastre durante la respuesta inicial. El modelo se aplicó con éxito en la región Caribe colombiana, que fue afectada por el fenómeno "La Niña" en el período 2010-2011.

Mohri, Akbarzadeh y Sayed Matin [23] proponen un modelo híbrido para la ubicar instalaciones de emergencia con el objetivo de mejorar la cobertura, este modelo combina el análisis envolvente de datos (DEA) que permite identificar las instalaciones más eficientes y el problema de localización máxima de cobertura (MCLP) que determina el menor número de instalaciones para cubrir una región determinada de tal forma que maximizan la eficiencia en el servicio y la respuesta a la demanda.

Esta investigación está organizada en las siguientes partes: En la segunda parte se describirán los principales criterios que se tomaron para la realización de esta revisión de literatura. En la tercera sección se realizará una descripción de las principales consideraciones que se utilizan en la localización de instalaciones en la logística humanitaria que se encontraron. Finalmente, en la última sección están ubicadas las conclusiones y recomendaciones para futuras investigaciones.

2 Metodología

Para la revisión de literatura se realizó un proceso conformado por tres fases, las cuales tienen como objetivos definir cuáles son las características principales para la revisión de los artículos como el tema principal y calidad de los artículos que se van a leer, definir las partes principales que se tienen para su selección y finalmente poder analizar y clasificar cada artículo según los parámetros que se consideraron (Fig. 1).

Fase 1: Se definen las palabras clave para la búsqueda de investigaciones que son: Facility location, Humanitarian, Disaster, Emergency.

Los artículos escogidos deben pertenecer a una revista con un SJR (SCImago Journal Rank) mayor o igual a Q2, y que no tengan una antigüedad mayor a 3 años (2020-2022), además se utilizó como principal base de datos SCOPUS y para la elección de los artículos, se utilizó la siguiente ecuación:

"TITLE-ABS-KEY ((disaster OR emergency OR humanitarian) AND "facility location") AND PUBYEAR > 2019 AND PUBYEAR < 2024 AND (LIMIT-TO (PUBSTAGE, "final")) AND (LIMIT-TO (DOCTYPE, "ar")) AND (LIMIT-TO (LANGUAGE, "English"))".

Fase 2: Se realizó una lectura de los resúmenes y conclusiones, los cuales cumplen con los requisitos previos se aceptarán además de esos requisitos no se están considerando las investigaciones que hablan de localización

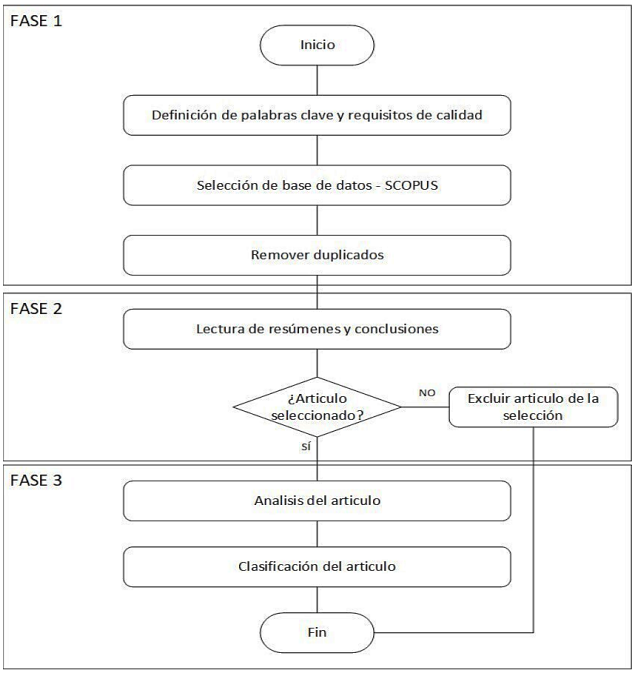

Figura 1. Flujograma de análisis de artículos.
Fuente: Elaboración propia.

de instalaciones movibles como ambulancias, drones, camiones y también la localización de objetos como sirenas o equipos médicos, debido a que requiere un tipo de tratamiento diferente para su movilización en el caso que la localización sea incorrecta a diferencia de una instalación, la cual puede permanecer en una ubicación durante un tiempo determinado o puede ser permanente lo que implica que va a estar en horizonte de tiempo prolongado y en el caso que la instalación sea localizada en un lugar incorrecto su movimiento no tiene una mayor complejidad ya que son objetos y no una instalación como tal y no dependen de variables como la demanda, aunque si pueden tener variables de cobertura. Tampoco se consideraron investigaciones que son revisiones de literatura del tema y artículos que solo hablaban exclusivamente de la instalación o se centraban en la cadena de suministro en el área del desastre, ya que estos artículos en muchos casos no proporcionaban una solución a este problema y solo describen el entorno o la instalación con sus características. También se tomó como característica importante que los artículos se hayan generado modelos matemáticos y técnicas de optimización para poder resolver el problema de localización de instalaciones, también se priorizo los artículos que sus modelos matemáticos buscan una mayor eficiencia a modelos anteriores.

Fase 3: Se realizará un análisis de cada uno de los artículos escogidos de la anterior fase para poder clasificarlos según los campos elegidos (ver Tabla 1), los cuales son:

- Temporalidad: este campo se divide en las instalaciones que son temporales y permanentes.
- Función objetivo que se divide en funciones que consideran variables clásicas y variables de deprivación o ambas.
- Tipo de objetivo, puede ser de un solo objetivo o multiobjetivo.
- Modelo según la certeza de los parámetros puede ser determinístico o estocástico.
- Localización se divide en predefinidos y no definidos.

Tabla 1.
Descripción general de las investigaciones sobre localización de instalaciones en la logística humanitaria de los últimos 3 años.

Referencias	Temporalidad[1]	Función Objetivo[2]	Tipo de Objetivo[3]	Modelo[4]	Localización[5]	Problema[6]	Caso de estudio[7]	Problema de enrutamiento	Etapa[8]	Tipo de desastre[9]	Tipo de instalación[10]
[29]	T	C&P	MT	ST	NP	FC	R	x	R	FL	S
[26]	T	C&P	MT	ST	PR	FC	R		R	CE	DC
[13]	T	C&P	MT	ST	NP	FC	NR	x	R	CV	DC
[31]	P	CL	MT	ST	NP	FC	R		P	FL	EC
[3]	P	C&P	MT	ST	NP	FC	R	x	P&R	EQ	DC
[32]	T	C&P	MT	ST	NP	FC	R		R	EQ	MC
[24]	P	C&P	MT	ST	NP	FC	R		P	ST	DC
[21]	P	C&P	MT	ST	NP	FC	R	x	P	FR	FS
[40]	P	CL	MT	ST	NP	FC	NR		R	GR	WH
[39]	P	C&P	MT	ST	NP	FC	NR		P	GR	GR
[12]	T	C&P	MT	DT	NP	FC	NR		P	GR	EC
[37]	T	DP	SN	ST	NP	UF	R		P	FL	MC
[25]	P	CL	MT	ST	NP	UF	NR		P	GR	MC
[15]	T	CL	SN	ST	NP	FC	R		P&R	CV	WH
[33]	T	C&P	MT	ST	NP	FC	R	x	R	EQ	MC
[7]	T	DP	SN	DT	NP	FC	R		R	EQ	MC
[14]	P	DP	MT	DT	NP	FC	NR		R	TA	TR
[20]	T	C&P	MT	ST	NP	FC	R		P&R	EQ	DC
[27]	T	CL	MT	ST	NP	FC	R		P	EQ	MC
[23]	P	DP	MT	ST	NP	FC	R		P	RC	MC
[36]	T	DP	MT	ST	NP	FC	R		R	CV	EC
[42]	T	C&P	MT	ST	NP	FC	R		P	HR	EC
[9]	T	C&P	MT	ST	NP	FC	R		P&R	EQ	DC
[34]	T	C&P	MT	ST	NP	FC	NR	x	R	GR	GR
[30]	P	CL	MT	ST	NP	FC	R		P	HR	DC
[38]	T	C&P	MT	ST	NP	FC	R		R	FL	WH

[1]: T: T: Temporal, P: Permanente.
[2]: Clásico, DP: Privación, C&P: Clásico y Privación.
[3]: SN: Mono objetivo, MT: Multiobjetivo.
[4]: DT: Determinista, ST: Estocástico.
[5]: NP: No Predefinido, PR: Predefinido.
[6]: UF: Capacidad ilimitada, FC: Capacidad fija.
[7]: R: Real, NR: No Real.
[8]: R: Respuesta, P: Preparación, R&P: Respuesta y Preparación.
[9]: COVID-19, CE: Ciclón, EQ: Terremoto, FR: Incendio, FL: Inundación, GR: General, HR: Huracán, RC: Choques de carretera, ST: Tormenta, TA: Ataque terrorista.
[10]: S: Refugio, DC: Centro de distribución, EC: Centro de emergencia, MC: Centros médicos, GR: General, WH: Almacén, FS: Estación de bomberos, TR: Instalación de respuesta a terroristas.
Fuente: Elaboración propia.

- Problema considera capacidad ilimitada o una capacidad limitada de las instalaciones.
- Etapa, se identifican a cuál etapa del manejo de desastres pertenece la investigación, ya sea en la etapa de preparación (pre desastre) o respuesta (post desastre).
- La investigación considera el problema de enrutamiento.
- La investigación utiliza un caso real o no.
- Tipo desastre que considera el artículo.
- Tipo de instalación se va a instalar

3 Análisis y discusión

Se puede observar que en los últimos 10 años las investigaciones sobre localización de instalaciones en la logística humanitaria han ido creciendo como se refleja en la Fig. 2, de la misma forma el 81% de las investigaciones pertenecen a revistas con un nivel Q1 (Fig. 3), siendo las principales revistas Computers and Industrial Engineering, International Journal of Disaster Risk Reduction, Socio-Economic Planning Sciences y Transportation Research Part E: Logistics and Transportation Review (ver Tabla 2).

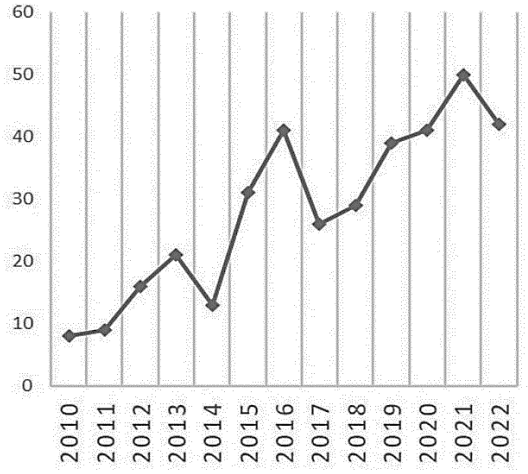

Figura 2. Línea de tendencia de las investigaciones sobre localización de instalaciones en la logística humanitaria.
Fuente: Elaboración propia.

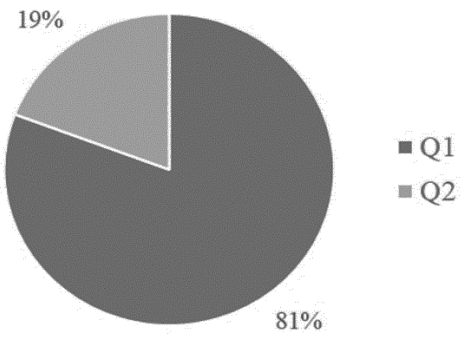

Figura 3. Calificación de las revistas en SCImago.
Fuente: Elaboración propia.

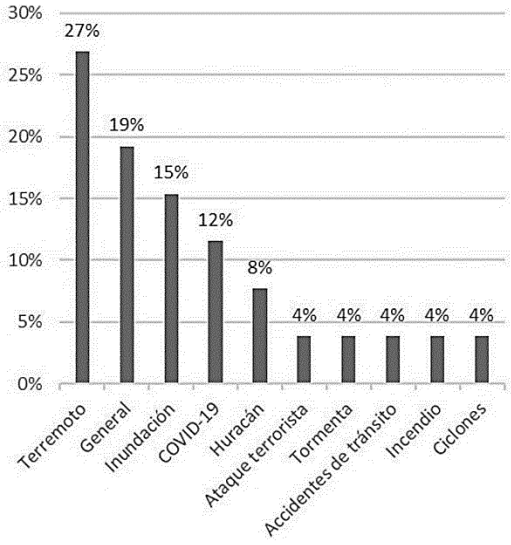

Figura 4. Tipos de desastre.
Fuente: Elaboración propia.

En la Fig. 4 se muestra que la mayoría de los artículos se centra en desastres naturales (74%), entre los cuales están terremotos, inundaciones, tormentas y huracanes, con una menor cantidad están la pandemia, incendios, ataques terroristas y accidentes de tránsito, mientras que las investigaciones sobre desastres genéricos o que no los mencionan son muy escasos (19%). Las investigaciones se están centrando en desastres de inicio rápido como lo pueden ser los terremotos, huracanes e inundaciones siendo el 62% de los artículos. Estas tendencias son debido a que los modelos actuales quieren hacer frente a los desastres naturales que como principal característica que son el tiempo de acción es corto, dentro de las primeras 24 horas [1] donde se busca reducir la pérdida de vidas y de los bienes [37], condiciones para tomar una acción de tiempo real aumentan la dificultad debido a la poca disponibilidad de información y aumentaría el tiempo de solución del problema. Esto hace que las palabras "caso de estudio" sea muy comunes y se tomen en cuenta para la consideración de modelos ya que se prueba su validez con información de pasados desastres.

Tabla 2.
Fuentes a la que pertenecen las investigaciones analizadas

Revista	Cantidad
Computers and Industrial Engineering	**3**
International Journal of Disaster Risk Reduction	**3**
Socio-Economic Planning Sciences	**2**
Transportation Research Part E: Logistics and Transportation Review	**2**
Decision Analytics Journal	**1**
European Journal of Operational Research	**1**
Health Care Management Science	**1**
IEEE Access	**1**
International Journal of Sustainable Transportation	**1**
International Transactions in Operational Research	**1**
Mathematical Problems in Engineering	**1**
Mathematics	**1**
Natural Hazards	**1**
Natural Hazards and Earth System Sciences	**1**
Safety Science	**1**
Science Progress	**1**
Sustainability	**1**
The Asian Journal of Shipping and Logistics	**1**
Transportation Research Part B: Methodological	**1**
Transportation Research Part C: Emerging Technologies	**1**

Fuente: Elaboración propia.

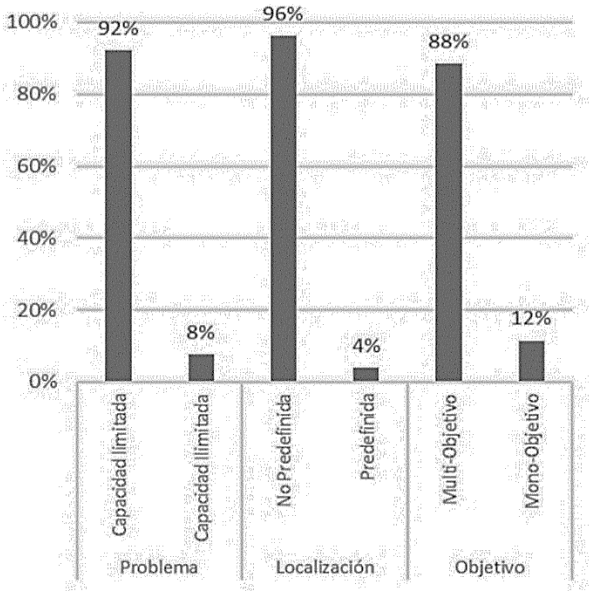

Figura 5. Tipos de modelos según el problema, localización y objetivo.
Fuente: Elaboración propia.

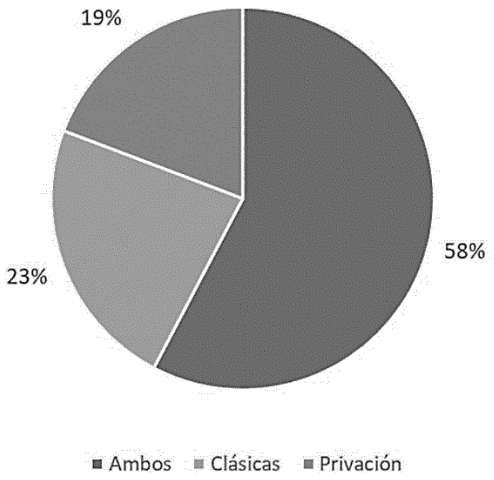

Figura 6. Tipos de variables.
Fuente: Elaboración propia

En los últimos años las investigaciones sobre la localización de instalaciones en la logística humanitaria hacen uso de modelos que contemplen la incertidumbre y la variabilidad de escenarios (Fig. 5) ya sea considerando las diferentes localizaciones de áreas afectadas [31], diferente cantidad de demandas por zonas [3] o zonas más afectadas por un desastre [29] o limitaciones en la capacidad de las instalaciones (Fig. 5), esto se debe a que en la actualidad se busca poder hacer frente a situaciones reales donde datos como la demanda o áreas afectadas no se conocen de antemano, un claro ejemplo de esto es el uso de modelos multiobjetivo antes que los modelos con un solo objetivo como se muestra en la Fig. 5, los cuales en su mayoría consideran la minimización de los costos totales que incluyen costos de apertura de la facilidad, costos de suministro, costo de transporte, entre otros costos que también se utilizan dentro de la logística comercial.

Un ejemplo de esto es la primera función objetivo de la investigación de Praneetpholkrang et al. (2021) [29] tiene como objetivo minimizar el costo total de abrir y operar refugios durante un desastre. Este costo total se compone de tres términos: el costo fijo para abrir los refugios, el costo de transporte para evacuar a las víctimas desde la zona afectada al refugio seleccionado y el costo del servicio, que se refiere al personal necesario para trabajar en los refugios durante el desastre (Eq. 1).

$$Min\ f_1 = \sum_{j \in J} X_j f_j + \alpha \sum_{i \in I} \sum_{j \in J} d_{ij} dY_{ij} h_i + \beta T \sum_{i\, c\, i} \frac{Z_{ij}}{\gamma} \quad (1)$$

Otro ejemplo es el artículo de H. Sun et al. (2021) [33] es la función objetivo que busca minimizar la suma de índice de severidad de la lesión (ISS) de todas las víctimas, incluyendo la penalización de las víctimas leves y graves que no han sido trasladadas, a eso se añade la minimización del costo total que incluye la falta de suministros médicos, costo de construcción de instalaciones temporales, costo de compra de suministros médicos, costo de transporte y contratación de vehículos (Eq. 2).

$$minZ_1 = F^l + F^s + \sum_{i \in I} p^l U_i^l + \sum_{j \in J} p^s U_j^s \quad (2)$$

Como se puede ver en estos dos ejemplos, las funciones objetivo en su mayoría incluyen variables clásicas de funciones objetivo utilizadas en la logística comercial como el costo de apertura de la instalación y a estos costos se están comenzando a considerarse los costos de privación (Fig. 6) que en su mayoría son costos por penalidades ocasionadas por la demanda no satisfecha o costos relacionados con el no bienestar de las personas afectadas y costos de servicio o cobertura, siendo estos de suma importancia porque en una situación de desastre buscan aliviar el sufrimiento de las personas [3] y de no considerarlos podían ocasionar situaciones muy graves como la pérdida de vidas [5], mientras que las otras funciones objetivos consideran sobre todo maximizar o minimizar variables no monetarias como la cobertura [23], bienestar [3], demanda servida [21] o el tiempo de evacuación [29].

De la misma forma se observa un mayor uso de modelos estocásticos (Fig. 7) en los cuales se considera la incertidumbre la cual está presente en una situación de un desastre real. la mayoría de las investigaciones las localizaciones en su mayoría no están predefinidas y estas se pueden clasificar según las localizaciones candidatas que pueden ser en cada punto de los nodos o en lugares como parques, colegios o terrenos disponibles, en el caso de los modelos que consideran ubicaciones predefinidas hacen uso de expertos para definir de antemano la localización de las instalaciones [26], también consideran la falta de información.

Los principales tipos de instalaciones utilizados en la logística humanitaria son centros de distribución, centros médicos, almacenes y refugios, siendo los principales los centros médicos y centros de distribución (ver Fig. 8).

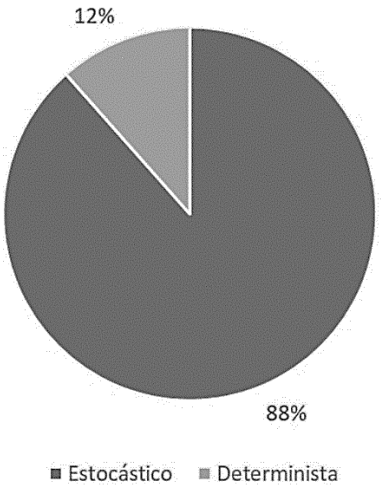

Figura 7. Tipo de modelo.
Fuente: Elaboración propia.

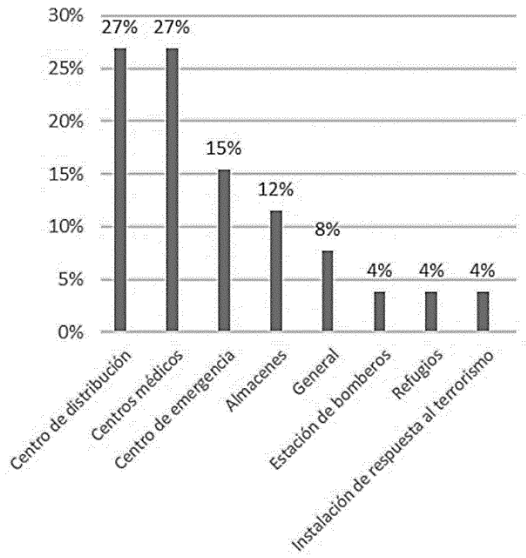

Figura 8. Tipos de localización.
Fuente: Elaboración propia.

Los refugios tienen como principal objetivo reducir el transporte de las víctimas desde la zona del desastre hasta el refugio y servir a la mayor cantidad de víctimas, por lo general se considera que los refugios son temporales y se apertura en la etapa de respuesta, otra consideración son que no siempre el refugio más cercano a la zona de desastre es el más seguro [29]. De la misma forma los centros de distribución buscan reducir el costo de transporte entre los centros de distribución y las personas, para este caso se tienen que determinar la cantidad de bienes que debe de tener cada instalación y su distribución equitativa para todos los afectados, buscando siempre el mayor nivel de satisfacción de las personas. Finalmente, los centros médicos surgen como respuesta a que la capacidad de los hospitales en un desastre no es suficiente [23], por lo cual considerar el transporte o la cercanía de la instalación hacia las víctimas, otro factor sería la condición de las víctimas, cada uno tendrá un diferente grado de severidad unas necesitan una atención más rápida que otros [31].

Entre las principales palabras clave que se encontraron en la revisión fueron "caso de estudio", aplicación, tomador de decisiones, servicio, incertidumbre, personas, riesgo, entre otros términos relacionados con la eficiencia y efectividad, lo que demuestra que los artículos se están enfocando en realizar modelos que se puedan aplicar al mundo real donde la falta de información crea incertidumbre y se busca poder reducir el sufrimiento de las personas asegurando la eficiencia en las operaciones.

4 Conclusiones

4.1 Resumen

Es necesario reconocer la importancia que tiene la localización de instalaciones en situación de emergencia, ya que sin una correcta localización puede generar problemas como retrasos en la entrega, costos más elevados, problemas de seguridad y dificultades en la coordinación. Además, debido a la frecuencia de los desastres naturales y emergencias, es importante encontrar una forma eficiente y efectiva la localización de las instalaciones en estos escenarios.

En los últimos años, la investigaciones sobre la localización de instalaciones en la logística humanitaria es un tema que está cobrando mucho interés, esto se muestra en una mayor cantidad de artículos pertenecientes a revistas con calidad Q1 y el constante esfuerzo por generar modelos que puedan funcionar en condiciones reales donde la información antes y después del desastre es incierta y el tiempo de acción es corto haciendo que se consideren los desastres naturales que ocurrieron como principal fuente de información para los casos de estudio de los artículos, estos artículos se suelen centrarse en la etapa de respuesta a las emergencias, por lo cual utilizan modelos estocásticos con los cuales ayudan a optimizar las decisiones de localización y distribución, donde la localización de las instalaciones no está predefinidas, también hacen uso de funciones multiobjetivo para poder resolver este problema que no solo buscan reducir el costo de apertura o transporte que es común en la logística comercial, además buscan maximizar eficiencia o minimizar el tiempo de respuesta, además en las funciones objetivo se prioriza incluir variables de privación como la demanda satisfecha o la cobertura, estas variables tienen que ser consideradas porque sin ellas no se puede asegurar completamente que se estén reduciendo el sufrimiento de las víctimas y estas en muchos caso sino se consideran pueden generar costos adicionales y posiblemente la pérdida de vidas.

4.2 Consideraciones para futuras investigaciones

- Problema de enrutamiento

Uno de los principales vacíos en las investigaciones es el poco uso de las restricciones en el transporte, esto se puede observar en la Tabla 1, donde los artículos que hacen mención del problema de enrutamiento son menos de la mitad, este factor es muy importante sobre todo en la distribución y localización de las instalaciones debido a que los desastres naturales no solo afectan a los nodos también pueden afectan a las calles algo que es muy común cuando ocurre un desastre [40] o una zona entera, lo cual puede imposibilitar la apertura de las instalaciones debido a la interrupción de servicios esenciales como luz y agua ya que estas fallas vas más allá de las fallas de las instalación y puede ocasionar el cierre de estas [32], un ejemplo de esto son las réplicas de los terremotos, las cuales pueden afectar a instalciones ya desplegadas [9].

Al existir una gran variedad de desastres y peligros es necesario saber dónde se va a ubicar una instalación considerando las condiciones geográficas que condicionan la elección de posibles localizaciones y su relación con la eficiencia en la respuesta a la emergencia [37]. Otro factor para considerar es la fuente de los suministros para la facilidad, esta puede tener una o varias como lo pueden ser varias tiendas para un centro de distribución o un solo almacén de emergencia, ocurre una situación similar a la distribución, las dificultades geográficas o interrupciones en las vías pueden dificultar que la instalación pueda ser suministrada con los materiales necesarios.

- Modelos Robustos

La utilización de modelos estocásticos se ha vuelto casi un estándar para los últimas investigaciones sobre localización de instalaciones en la logística humanitaria debido a que la demanda no está determinada en el mundo real cuando ocurre un desastre y que la demanda no sea conocida afecta a la localización de las instalaciones y al servicio, convirtiendo a los modelos estocásticos en una de las principales herramientas para resolver este tipo de problemas, sin embargo, no todos los desastres naturales ocurren en zonas pequeñas y muchos de estos problemas manejan una gran cantidad de incertidumbre por lo cual muchas veces hay factores que no se consideran, con el fin de poder capturar factores aleatorios se están comenzando a utilizar modelos robustos, debido a que estos modelos pueden hacer frente a la cantidad limitada de información y a las nuevas condiciones o restricciones.

- Instalaciones temporales

Varias de las investigaciones no consideran la temporalidad o no la mencionan directamente, en muchos casos se asume que las instalaciones que se realizan en la etapa de respuesta son temporales mientras los ubicados en la etapa de preparación son permanentes, para la correcta definición del problema es necesario definir qué tipo de temporalidad tendrá la facilidad debido a su relación con otras variables como el tiempo de respuesta que es diferente para cada tipo de facilidad, las instalaciones temporales tienen un tiempo de permanencia en un lugar determinado mientras que las instalaciones permanentes tienen que cumplir funciones específicas en el largo plazo, esto también determina algunas características como el tiempo de instalación, la cobertura y las funciones que pueden cumplir.

- Un solo tipo de facilidad

La mayoría de investigaciones sólo considera un solo tamaño de las instalaciones, en la mayoría de casos la instalación solo depende de la cantidad de recursos que debe de tener y la cobertura que tiene para poder satisfacer su demanda, sin embargo, en una situación real no siempre las instalaciones son de un solo tamaño, esto depende mucho de donde se va a construir la instalación, no es lo mismo construir en una calle que en un colegio o un parque, y que demanda debe cubrir, esto se traduce en los costos totales y el recursos necesarios para su funcionamiento como el tiempo de respuesta o los suministros.

Reconocimiento

Esta investigación forma parte Hito 1 del proyecto "Modelo matemático para la localización de puntos de entrega temporales de bienes de ayuda humanitaria en caso de sismo de gran magnitud para el distrito de Alto Selva Alegre, Arequipa" UCSP-2022-25Años-P36.

Referencias

[1] Balcik, B., and Beamon, B.M., Facility location in humanitarian relief. International Journal of Logistics Research and Applications, 11(2), pp. 101-121, 2008. DOI: https://doi.org/10.1080/13675560701561789.

[2] Boonmee, C., Arimura, M., and Asada, T., Facility location optimization model for emergency humanitarian logistics. International Journal of Disaster Risk Reduction, 24, pp. 485-498, 2017. DOI: https://doi.org/10.1016/j.ijdrr.2017.01.017.

[3] Boostani, A., Jolai, F., and Bozorgi-Amiri, A., Designing a sustainable humanitarian relief logistics model in pre- and postdisaster management. International Journal of Sustainable Transportation, 15(8), pp. 604-620, 2020. DOI: https://doi.org/10.1080/15568318.2020.1773975.

[4] Bozorgi-Amiri, A., and Khorsi, M., A dynamic multi-objective location-routing model for relief logistic planning under uncertainty on demand, travel time, and cost parameters. The International Journal of Advanced Manufacturing Technology, 85(5-8), pp. 1633-1648, 2015. DOI: https://doi.org/10.1007/s00170-015-7923-3.

[5] Cotes, N., and Cantillo, V., Including deprivation costs in facility location models for humanitarian relief logistics. Socio-Economic Planning Sciences, 65, pp. 89-100, 2019. DOI: https://doi.org/10.1016/j.seps.2018.03.002.

[6] Cozzolino, A., Humanitarian logistics and supply chain management. Humanitarian Logistics. Cross-Sector Cooperation in Disaster Relief Management. SpringerBriefs in Business, Ed., 2012, pp. 5-16. DOI: https://doi.org/10.1007/978-3-642-30186-5_2

[7] Gulzari, A., and Tarakci, H., A healthcare location-allocation model with an application of telemedicine for an earthquake response phase. International Journal of Disaster Risk Reduction, 55, art. 102100, 2021. DOI: https://doi.org/10.1016/j.ijdrr.2021.102100.

[8] Gutjahr, W.J., and Fischer, S., Equity and deprivation costs in humanitarian logistics. European Journal of Operational Research, 270(1), pp. 185-197, 2018. DOI: https://doi.org/10.1016/j.ejor.2018.03.019.

[9] Haeri, A., Hosseini-Motlagh, S.M., Samani, M.R.G., and Rezaei, M., A bi-level programming approach for improving relief logistics operations: a real case in Kermanshah earthquake. Computers & Industrial Engineering, 145, art. 106532, 2020. DOI: https://doi.org/10.1016/j.cie.2020.106532.

[10] Holguín-Veras, J., Jaller, M., Van Wassenhove, L.N., Pérez, N. and Wachtendorf, T., On the unique features of post-disaster humanitarian logistics. Journal of Operations Management, 30(7-8), pp. 494-506, 2012. DOI: https://doi.org/10.1016/j.jom.2012.08.003.

[11] Holguín-Veras, J., Pérez, N., Jaller, M., Van Wassenhove, L.N. and Aros-Vera, F., On the appropriate objective function for post-disaster humanitarian logistics models. Journal of Operations Management, 31(5), pp. 262-280, 2013. DOI: https://doi.org/10.1016/j.jom.2013.06.002.

[12] Jiang, Z., and Ouyang, Y., Reliable location of first responder stations for cooperative response to disasters. Transportation Research Part B: Methodological, 149, pp. 20-32, 2021. DOI: https://doi.org/10.1016/j.trb.2021.04.004.

[13] Khodaee, V., Kayvanfar, V., and Haji, A., A humanitarian cold supply chain distribution model with equity consideration: the case of COVID-19 vaccine distribution in the European Union. Decision Analytics Journal, 4, art. 100126. 2022. DOI: https://doi.org/10.1016/j.dajour.2022.100126.

[14] Li, Q., Li, M., Gan, J., and Guo, C., A game-theoretic approach for the location of terror response facilities with both disruption risk and hidden information. International Transactions in Operational Research, 28(4), pp. 1864-1889, 2020. DOI: https://doi.org/10.1111/itor.12900.

[15] Liu, K., Liu, C., Xiang, X., and Tian, Z., Testing facility location and dynamic capacity planning for pandemics with demand uncertainty. European Journal of Operational Research, 304(1), pp. 150-168, 2023. DOI: https://doi.org/10.1016/j.ejor.2021.11.028.

[16] Liu, K., Zhang, H., and Zhang, Z.H., The efficiency, equity and effectiveness of location strategies in humanitarian logistics: a robust chance-constrained approach. Transportation Research Part E: Logistics and Transportation Review, 156, art. 102521, 2021. DOI: https://doi.org/10.1016/j.tre.2021.102521.

[17] Liu, Y., Yuan, Y., Shen, J. and Gao, W., Emergency response facility location in transportation networks: a literature review. Journal of Traffic and Transportation Engineering, 8(2), pp. 153-169, 2021. DOI: https://doi.org/10.1016/j.jtte.2021.03.001.

[18] oree, N., and Aros-Vera, F., Points of distribution location and inventory management model for post-disaster humanitarian logistics.

Transportation Research Part E: Logistics and Transportation Review, 116, pp. 1-24, 2018. DOI: https://doi.org/10.1016/j.tre.2018.05.003.
[19] Maharjan, R., and Hanaoka, S., A multi-actor multi-objective optimization approach for locating temporary logistics hubs during disaster response. Journal of Humanitarian Logistics and Supply Chain Management, 8(1), pp. 2-21, 2018. DOI: https://doi.org/10.1108/jhlscm-08-2017-0040.
[20] Maharjan, R., and Hanaoka, S., A credibility-based multi-objective temporary logistics hub location-allocation model for relief supply and distribution under uncertainty. Socio-Economic Planning Sciences, 70, art. 100727, 2020. DOI: https://doi.org/10.1016/j.seps.2019.07.003.
[21] Ming, J., Richard, J.P.P., and Zhu, J., A facility location and allocation model for cooperative fire services. IEEE Access, 9, pp. 90908-90918. 2021. DOI: https://doi.org/10.1109/access.2021.3091481.
[22] Mishra, M., Singh, S.P., and Gupta, M.P., Two phase algorithm for bi-objective relief distribution location problem. Annals of Operations Research. 2022. DOI: https://doi.org/10.1007/s10479-022-04751-y.
[23] Mohri, S.S., Akbarzadeh, M., and Sayed-Matin, S.H., A Hybrid model for locating new emergency facilities to improve the coverage of the road crashes. Socio-Economic Planning Sciences, 69, art. 100683, 2020. DOI: https://doi.org/10.1016/j.seps.2019.01.005.
[24] Monzón, J., Liberatore, F., and Vitoriano, B., A Mathematical Pre-Disaster Model with Uncertainty and Multiple Criteria for Facility Location and Network Fortification. Mathematics, 8(4), art. 529, 2020. DOI: https://doi.org/10.3390/math8040529.
[25] Mousavi, H., Darestani, S.A., and Azimi, P., An artificial neural network based mathematical model for a stochastic health care facility location problem. Health Care Management Science, 24(3), pp. 499-514. 2021. DOI: https://doi.org/10.1007/s10729-020-09533-1.
[26] Nawazish, M., Padhi, S.S., and Edwin-Cheng, T., Stratified delivery aid plans for humanitarian aid distribution centre selection. Computers & Industrial Engineering, 171, art. 108451, 2022. DOI: https://doi.org/10.1016/j.cie.2022.108451.
[27] Oksuz, M.K., and Satoglu, S.I., A two-stage stochastic model for location planning of temporary medical centers for disaster response. International Journal of Disaster Risk Reduction, 44, art. 101426, 2020. DOI: https://doi.org/10.1016/j.ijdrr.2019.101426.
[28] Patel, N., and Trivedi, S., Choosing optimal locations for temporary health care facilities during health crisis using binary integer programming. Sage Science Review of Applied Machine Learning, [online]. 3(2), pp. 1-20, 2020. Available at: https://journals.sagescience.org/index.php/ssraml/article/view/7.
[29] Praneetpholkrang, P., Huynh, V.N., and Kanjanawattana, S., A multi-objective optimization model for shelter location-allocation in response to humanitarian relief logistics. The Asian Journal of Shipping and Logistics, 37(2), pp. 149-156, 2021. DOI: https://doi.org/10.1016/j.ajsl.2021.01.003.
[30] Shehadeh, K.S., and Tucker, E.L., Stochastic optimization models for location and inventory prepositioning of disaster relief supplies. Transportation Research Part C: Emerging Technologies, 144, art. 103871, 2022. DOI: https://doi.org/10.1016/j.trc.2022.103871.
[31] Shu, J., Lv, W., and Na, Q., Humanitarian relief supply network design: expander graph based approach and a case study of 2013 Flood in Northeast China. Transportation Research Part E: Logistics and Transportation Review, 146, art. 102178, 2021. DOI: https://doi.org/10.1016/j.tre.2020.102178.
[32] Sun, H., Li, J., Wang, T., and Xue, Y., A novel scenario-based robust bi-objective optimization model for humanitarian logistics network under risk of disruptions. Transportation Research Part E: Logistics and Transportation Review, 157, art. 102578, 2022. DOI: https://doi.org/10.1016/j.tre.2021.102578.
[33] Sun, H., Wang, Y., and Xue, Y., A bi-objective robust optimization model for disaster response planning under uncertainties. Computers & Industrial Engineering, 155, art. 107213, 2021. DOI: https://doi.org/10.1016/j.cie.2021.107213.
[34] Sun, Q., and Liu, S., Locating abrupt disaster emergency logistics centres using improved artificial bee colony (IABC) algorithm. Science Progress, 104(2), art. 003685042110162, 2021. DOI: https://doi.org/10.1177/00368504211016205.
[35] Tofighi, S., Torabi, S., and Mansouri, S., Humanitarian logistics network design under mixed uncertainty. European Journal of Operational Research, 250(1), pp. 239-250, 2016. DOI: https://doi.org/10.1016/j.ejor.2015.08.059.
[36] Wang, H., and Ma, X., Research on multiobjective location of urban emergency logistics under major emergencies. Mathematical Problems in Engineering, art. 5577797, 2021, DOI: https://doi.org/10.1155/2021/5577797
[37] Yang, Y., Yin, J., Ye, M., She, D., and Yu, J., Multi-coverage optimal location model for emergency medical service (EMS) facilities under various disaster scenarios: a case study of urban fluvial floods in the Minhang district of Shanghai, China. Natural Hazards and Earth System Sciences, 20(1), pp. 181-195, 2020. DOI: https://doi.org/10.5194/nhess-20-181-2020.
[38] Yeh, C.H., and Chen, Y.R., Location model analysis of flood relief facilities: a case study of the Fazih River floodplain, Taiwan. Natural Hazards, 103(1), pp. 317-327, 2020. DOI: https://doi.org/10.1007/s11069-020-03989-8.
[39] Yu, W., Reachability guarantee-based model for pre-positioning of emergency facilities under uncertain disaster damages. International Journal of Disaster Risk Reduction, 42, art. 101335, 2020. DOI: https://doi.org/10.1016/j.ijdrr.2019.101335.
[40] Yu, W., Pre-disaster location and storage model for emergency commodities considering both randomness and uncertainty. Safety Science, 141, art. 105330, 2021. DOI: https://doi.org/10.1016/j.ssci.2021.105330.
[41] Dönmez, Z., Kara, B.Y., Karsu, Z., and Saldanha-da-Gama, F., Humanitarian facility location under uncertainty: Critical review and future prospects. Omega, 102, art. 102393, 2021. DOI: https://doi.org/10.1016/j.omega.2021.102393.
[42] Zhang, L., and Cui, N., Pre-positioning facility location and resource allocation in humanitarian relief operations considering deprivation costs. Sustainability, 13(8), art. 4141, 2021. DOI: https://doi.org/10.3390/su13084141.

M.A. Daza-Moscoso, es Ing. Industrial de la Universidad Católica San Pablo, Perú.
ORCID: 0000-0003-4720-8311

J.M. Cárdenas Medina, es Dr. en Ingeniería de Producción con énfasis en Gestión de Tecnologías de la Información por la Escola Politécnica de la Universidad de São Paulo, Brasil. Ing. Industrial de la Universidad Nacional de San Agustín de Arequipa, Perú. MSc. en Integración Latinoamericana (Relaciones Internacionales) de la Universidad de São Paulo, Brasil. Director de la carrera de Ingeniería Industrial de EPE de la Universidad Peruana de Ciencias Aplicadas.
ORCID: 0000-0002-2801-3546

M.F. Carnero-Quispe, es Ing. Industrial de la Universidad Católica San Pablo, Perú.
ORCID: 0000-0002-8123-8218

DYNA

DYNA 91 (232), April - June, 2024
is an edition consisting of 100 printed issues
which was finished printing in the month of June of 2024
in Todograficas Ltda. Medellín - Colombia

The cover was printed on Propalcote C1S 250 g,
the interior pages on Propal Beige 90 g.
The fonts used are Times New Roman, Imprint MT Shadow

- Phytoremediation of Methylene Blue and Congo Red by duckweed (Lemna minor)
- Adaptative comfort modeling for a typical non-centrifugal cane sugar processing facility
- The impact of nanotechnology in achieving sustainable design
- Influence of input variables on the unitary deformation experienced in pipes subjected to the action of lateral loads
- Postural physical burden of street vendors in Boyacá, Colombia
- Dashboard for assessing patient flow management in hospital institutions
- Probabilistic weibull reliability of a shaft design subjected to bending and torsion stress
- A reliability model for non-isothermal isotropic damages
- Evaluation and improvement process in quality of service: case studies of restaurants in Manabí
- Analytical procedure for calculating impulsive responses on floor systems under human walking
- Financial inclusion in Puebla, Mexico: a socioeconomic and spatial econometric analysis
- Determine velocity of fluid in curved micro channels fabricated with 3d printing (SLA)
- Study of mental workload in public administration managers
- Computational tool for design and optimization of scale inhibitor squeeze treatments
- Forest fire risk zoning for the metropolitan region of Curitiba, Paraná, Brazil
- Reactivation of three test benches of high, medium and low power electric generators for hydraulic energy conversion
- Susceptibility to moisture damage in asphalt mixes with blast furnace dust as aggregate
- State of the art and new state variable to diagnose eccentricity in synchronous generators
- Characterization of post-industry textile waste in Bogotá
- Facility location in humanitarian logistics: a literature review and considerations for future research

- Fitorremediación de Azul de Metileno y Rojo Congo por lenteja de agua (Lemna minor)
- Modelamiento de confort adaptativo para un trapiche panelero
- El impacto de la nanotecnología en la consecución de un diseño sostenible
- Influencia de las variables de entrada en la deformación unitaria evidenciada en tuberías sometidas a la acción de cargas laterales
- Carga física postural en vendedores ambulantes de Boyacá, Colombia
- Tablero de control para evaluar la gestión de los flujos de pacientes en instituciones hospitalarias
- Confiabilidad probabilística Weibull en el diseño de un eje sometido a esfuerzos de flexión y torsión
- Un modelo de confiabilidad para daños isotrópicos no isotérmicos
- Proceso de evaluación y mejora en la calidad del servicio: caso de estudio restaurantes en Manabí
- Procedimiento analítico para el cálculo de respuestas impulsivas en sistemas de piso ante el caminar humano
- Inclusión financiera en Puebla, México: un análisis socioeconómico y econométrico espacial
- Determinación de la velocidad de fluido en micro canales curvos fabricados con impresión 3D (SLA)
- Estudio de carga mental de trabajo en directores de la administración pública
- Herramienta computacional para diseño y optimización de tratamientos squeeze de inhibición de incrustaciones
- Zonificación del riesgo de incendios forestales para la región metropolitana de Curitiba, Paraná, Brasil
- Reactivación de tres bancos de pruebas de generadores eléctricos de alta, media y baja potencia para conversión de energía hidráulica
- Susceptibilidad al daño por humedad en mezclas asfálticas con polvo de alto horno como agregado
- Estado del arte y nueva variable de estado para diagnosticar la excentricidad en generadores sincrónicos
- Caracterización de los residuos textiles posindustria en Bogotá
- Localización de instalaciones en logística humanitaria: una revisión de la literatura y consideraciones para futuras investigaciones